GENERAL MOTORS CORPORATION

Final Report

SURVEYOR LUNAR ROVING VEHICLE

Phase I — JPL Contract 950657

VOL. II: APPENDIXES

Section II Electronic Subsystems

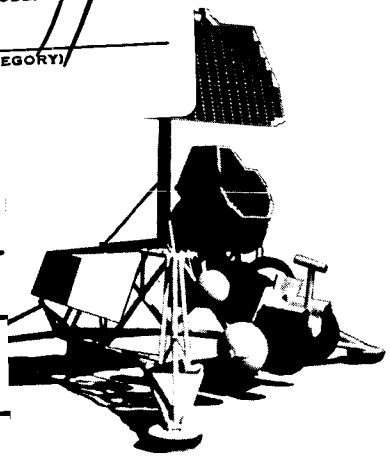

GM DEFENSE RESEARCH LABORATORIES SANTA BARBARA, CALIFORNIA

TR64-26

April 23, 1964

Copy No 034

GENERAL MOTORS CORPORATION

Final Report

SURVEYOR LUNAR ROVING VEHICLE

Phase I — JPL Contract 950657

NAS 7-100

VOL. II: APPENDIXES

Section II Electronic Subsystems

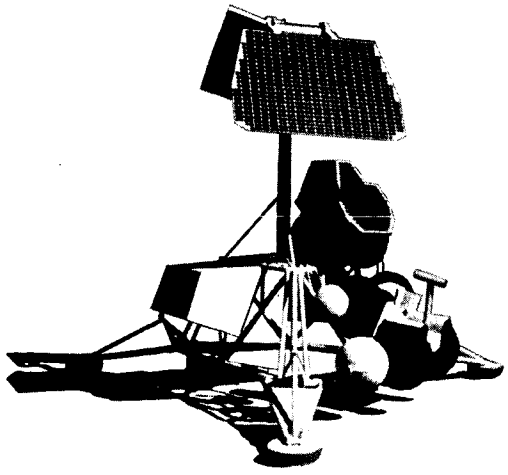

GM DEFENSE RESEARCH LABORATORIES SANTA BARBARA, CALIFORNIA

TR64-26

April 23, 1964

PREFACE

This report is one of a series of reports prepared under JPL Contract No. 950657 by GM Defense Research Laboratories, Santa Barbara, California, and its major subcontractor for electronics, Radio Corporation of America, Astro-Electronics Division, Princeton, New Jersey.

SECTION II

TABLE OF CONTENTS

APPENDIX I

OPERATIONAL GROUND EQUIPMENT

APPENDIX I

OPERATIONAL GROUND EQUIPMENT

A. INTRODUCTION

The Operational Ground Equipment (OGE), as initially conceived, consisted of five units. Four of these units were termed "stations" and the fifth was an automatic unit. The title, along with a brief description of each of these five, follows:

1. Control Station

   Vehicle orders are dispatched from the Control Station to the vehicle. Completion of the instructions is indicated at this station along with a TV presentation taken from the (SLRV) vehicle. The operator(s) who attends this station has at his command an instruction program which is continually being up-dated as the situation requires.

2. Engineering or Diagnostic Station

   The Engineering Station receives telemetry data concerning the status of all monitored components. It is the function of the operator(s) at this station not only to look for failures, but also to sense trends which, if allowed to continue, would result in failures.

3. Navigation Station

   This station receives telemetry data pertinent to vehicle navigation. Navigation pictures are presented at this station and current and future positions of the vehicle accounted for. Program inputs are supplied to the Control Station when necessary.

4. Scientific Station

   The Scientific Station is intended to monitor the execution of scientific experiments and to revise and update the scientific portion of the program. This will probably require a staff to aid in data reduction and interpretation. Extensive use of storage and computing facilities will be required from this station.

5. Data Processing

   This equipment will receive raw data. This data will then be sorted and distributed to the proper station or stations. Also, inputs may be routed through this unit for formatting or integration into the Surveyor command format.

However, as more insight was gained into the workings of the Space Flight Operations Facility (SFOF) and the Deep Space Instrumentation Facilities (DSIF), two facts were noted. First, in planning new missions use should be made, as much as possible, of the existing JPL space facilities. Second, the division of effort at SFOF, which is the space flight control center, is broken out in an almost identical fashion to the task divisions listed above.

The six major areas at SFOF are listed below along with the corresponding SLRV stations.

SFOF	SLRV
Missions Control and Operations Area	Control Station
Flight Path Analysis Area	Navigation Station
Spacecraft Performance Analysis Area	Engineering or Diagnostic Station
Space Science Display and Analysis Area	Scientific Station
Data Processing Area	Data Processing
Video Analysis Area	Video Processing Area (not included above)

For purposes of defining equipment needs in greater detail, it has been assumed in the remainder of this appendix that control would be centered either at SFOF or in a similar control arrangement (not currently in existence) at the DSIF stations. It has further been assumed that a Control Data Console (CDC), in use with the Surveyor, will also be available for SLRV use.

B. OPERATIONAL GROUND EQUIPMENT

A list containing all of the OGE needs is included in this section as Table II. 1-1. This is intended to be a master list (exclusive of data processing needs) and will be updated as more information becomes available. Should the mission be controlled from any of the DSIF's, virtually all of this equipment would have to be considered. However, with SFOF control, a different situation exists. Following this list is a more detailed description of the equipment.

There is now, or planned for early 1966, much equipment at the SFOF which is defined as "mission independent." This equipment (updated as required) is permanently installed and is available for the performance of missions from this facility. Table II. 1-2 lists the known equipment planned or available. Equipment which may be installed for a single project is termed "mission dependent" and must be compatible with SFOF requirements. If the SLRV mission were to be conducted from this installation, full use, as far as is possible, would be made of the existing equipment. The list of Table II. 1-2 does not include computing and data processing or supporting equipment in other areas of the facility, which also would be utilized in the SLRV mission.

Table II. 1-1

MASTER EQUIPMENT LIST

Location	Equipment	Input From	Output To	Function
Video Analysis Station	Video Tape and Storage Unit	DSIF or Microwave Link	Storage	Permanent Record of Raw Video Signals as Received.
	Distortion Measuring Equipment	DSIF or Microwave Link	Distortion Correction Function Generator	To Determine Distortion Present in Incoming Frame of Video.
	Distortion Correction Function Generator	Distortion Meas. Equip.	Film Recorder	To Generate Distortion Correction Signal to Film Recorder.
	Film Recorder	Raw Video and Distortion Corrector	Unit Record Assembler	To Generate a Film From Incoming Video Signal
	Unit Record Assembler	Film Recorder	Data Addition Equip.	To Generate a Document Containing A Film.
	Data Addition Equipment	Unit Record Assembler	Distribution or Library	To Insert Pertinent Telemetry and Computed Information on Unit Record Document.
	Unit Record Library (2)	Data Addition Equip.	Storage	To File Film Documents for Fast Access.

Table II. 1-1

MASTER EQUIPMENT LIST (Continued)

Location	Equipment	Input From	Output To	Function
	Unit Record Handling Equip.	Video Analysis Station	All Video Display Areas	To Provide Access to Video Film Documents as Required.
	Scan Conversion Equipment	DSIF/Recorder	Operator(s)	To Convert Slow Scan TV to Conventional Scan Rates.
	On Line Film Processor	Film Recorder	Operator(s)	Develops Film.
	Format Generator	DSIF	Film Recorder and Scan Conversion Equip.	To Provide Format for Unit Record Assembler.
Navigation	Command Verification Display	Control Station & Buffer/Dist.	Operator(s)	To Display Certain Commands Sent To The SLRV And Verified Commands From Telemetry.
	Telemetry Display	Data Processing	Operator(s)	To Display Certain Telemetered Data Returning From the SLRV.
	Stereo Viewer	Video Analysis Station	Operator(s)	To Provide a Near Real Time SLRV TV Display For Navigational Purposes.
	Planar Viewer	Video Analysis Station	Operator(s)	To Provide a Near Real Time SLRV TV Display For Steering Purposes.

Table II. 1-1

MASTER EQUIPMENT LIST (Continued)

Location	Equipment	Input From	Output To	Function
	Library Recall and Index	Files	Operator(s)	To Provide the Ability to Recall Previous Views for Topographical Checks.
	Candidate Area Display	Scientific Analysis Station	Operator(s)	To Provide Information On Probable Areas for Investigation.
	Ground Track Plotter 30" x 30" (4)	Computer	Operator(s)	To Provide Near Real Time Plot of SLRV Position For Navigation and Transfer Capabilities
	Certification Display	Science Analysis Station	Operator(s)	To Provide Indication of a Certified Landing Point.
	Program Interrupter	Operator(s)	Control Station	To Allow Program Interruption or Modification Under Certain Prescribed Conditions.
	Surface Data Display	Data Processing	Operator(s)	To Provide Near Real Time Soil Property Information for Navigation
	Voice Link	Operator(s)	Operator(s)	To Allow Voice Communication Within/Between DSIF/SFOF.

Table II. 1-1

MASTER EQUIPMENT LIST (Continued)

Location	Equipment	Input From	Output To	Function
Data Processing	Performance Area Data Distributor	CDC/DSIF	Engineering Area	To Sort Out Data Which is Needed at the Engineering Station.
	Scientific Area Data Distributor	DCD/DSIF	Scientific Area	To Sort Out Data Which Is Needed at the Scientific Station.
	Navigation Area Data Distributor	CDC/DSIF	Navigation Area	To Sort Out Data Which Is Needed at the Navigation Station.
	Control Area Data Distributor	CDC/DSIF	Control Area	To Sort Out Data Which Is Needed at the Control Station.
	Command Print Out	Control Station	Hard Copy Record	To Supply a Permanent Record of All Commands Issued During a Mission.
	Telemetry Print Out	CDC/DSIF	Hard Copy Record	To Supply a Permanent Record of All Telemetry (except TV and soil meas.) Received During a Mission.
	Computer Distributor	CDC/DSIF	Computer	To Supply to a Computer That Data Which Requires Computation Before Presentation to the Stations.
	Computer Buffer	Computer	Selected	To Supply to the Stations that Data Which Has Been Processed by the Computer.

Table II. 1-1

MASTER EQUIPMENT LIST (Continued)

Location	Equipment	Input From	Output To	Function
	CDC Formatter	Control Station/SFOF	CDC	To Place Commands into a Format Recognized by the CDC.
	SFOF Buffer/ Distributor	SFOF/CDC	CDC/SFOF	To Route Information to and From DSIF/SFOF.
	Switchboard	All Stations	All Stations	To Provide Voice Communications Between SFOF/DSIF.
Control Station	Command and Verification Display	CDC/Data Processing	Operator(s)	To Display Commands Sent to the SLRV and the Verification Received From Telemetry.
	Telemetry Display	Data Processing	Operator(s)	To Display all Telemetry Data From the SLRV.
	General SLRV Status Display	Performance Station	Operator(s)	To Provide a Gross Picture of the SLRV System Status.
	Stored Command Sequences	Pre-Prepared	Operator(s)	To Provide the Operator(s) with Common Sequences of Commands.
	Command Initiator	Operator(s)	Data Processing	To Provide the Operator(s) With Equipment to Initiate Commands or Sequences of Commands.
	Stereo/Planar View Display	Video Analysis Station	Operator	To Porvide the Operator With a Near Real Time View for Obstacle Detection and Steering.

Table II. 1-1

MASTER EQUIPMENT LIST (Continued)

Location	Equipment	Input From	Output To	Function
	Command Inhibit Equipment	Built-in	N. A.	To Provide Built-in Inhibits to Prevent Commands Which Might Damage the Vehicle or Endanger the Mission.
	Command Lockouts	Operator(s)	N. A.	To Provide the Operator With the Ability to Lockout the Transmission of Commands which Have for Some Reason Become Hostile to the Mission.
	Certification Display	Science Analysis Station	Operator(s)	To Indicate Candidate Landing Point Certification in Terms of Relief and Soil Parameters,
	Surveyor Status Display	Data Processing	Operator(s)	To Display Status of all Surveyor Equipment Necessary for the Completion of the SLRV Mission.
	Program Interrupter and Modifier	Operator(s)	Data Processing	To Act as Center for Program Interruptions from Other Stations.
	Voice Link	Operator(s)	Operator(s)	To Provide Voice Communication Within/Between DSIF/SFOF.
	Plot and Field of View Display #1 (2)	Video Analysis Station	Operator(s)	To Provide a Ground Track Plot and Field of View With Respect to SLRV Heading and Topography in Near Real Time With Transfer Capability.

Table II. 1-1

MASTER EQUIPMENT LIST (Continued)

Location	Equipment	Input From	Output To	Function
	Oriented Stereo/ Planar Display	Video Analysis Station	Operator(s)	To Provide Non-Real Time Display of Selected Planar or Stereo Pairs With Associated Scale Factors. (Recall)
	Plot and Field of View Display #2	Video Analysis Station	Operator(s)	To Provide a Ground Track Plot and Field of View With Respect to Selected SLRV Locations and Headings Together With Topographical Relationship in Non-Real Time. (Recall)
Scientific Analysis Station	Soil Properties Data Recorder	Data Processing	Hard Copy	To Provide a Permanent Record of all Soil Properties Measurements for Accurate Analysis.
	Soil Properties Record	Data Processing	Operator(s)	To Provide Data on a Temporary Basis for Certification of a Potential Landing Point.
	Soil Properties and Relief Certification Transmitter	Operator(s)	Navigation and Control Stations	To Transmit Information that a Potential Landing Point is Acceptable on a Short Term Basis.
	Program Interrupter	Operator(s)	Control Station	To Allow Program Interruption Under Certain Specified Conditions.
	Voice Communications	Operator(s)	Operator(s)	To Allow Voice Communication Within/Between DSIF/SFOF.

Table II. 1-1

MASTER EQUIPMENT LIST (Continued)

Location	Equipment	Input From	Output To	Function
	18 Channel Recorder	Data Processing	Hard Copy	To Record Certain Analog Data for Energy and Mission Profile Analysis.
	Channel Selector	Data Processing	Recorder	To Select Data Which is to be Recorded.
	Library	Data Processing Scientific Anal. Control Station	Hard Copy	To Provide a Library for all Mission Data.
	Stereo 3 Dimensional Plotters (3)	Video Documents	Hard Copy Temporary Record	To Provide a Rapid Plot of Important Topographical Features, Camera Orientation, Frame Coverage Relative to Topography, and Add This Data to Video Documents.
	Command and Verification Display	CDC/Data Processing	Operator(s)	To Provide a Display of Commands Sent to the SLRV and Verification Received from Telemetry.
Engineering Station	Command Verification Display	Command Station & Buffer-Dist.	Operator(s)	To Display Commands Sent to the SLRV and Verification Received From TM.
	Telemetry Display	Data Processing	Operator(s)	To Display Telemetry Data Returning From the SLRV.

Table II. 1-1

MASTER EQUIPMENT LIST (Continued)

Location	Equipment	Input From	Output To	Function
	18 Channel Recorder	Data Processing	Operator(s)	To Record Certain Analog Data On a Continuous Chart.
	Recorder Channel Selector	Data Processing	Recorder	To Allow Selection of Certain Telemetered Functions to be Recorded for Viewing.
	Telemetry Synchronizer	Data Processing	Recorder	To Correlate Recorder Data with Hard Copy Records of the Telemetry.
	Program Interrupter	Operator(s)	Buffer/Dist.	To Allow Interruption of the Program Under Certain Prescribed Conditions.
	Voice Communications	Operator(s)	Operator(s)	To Allow Voice Communications Within and Between DSIF/SFOF.
	Self Check and Calibration	Built-in at All Stations	Operator(s)	To Allow Automatic or Semi-Automatic Calibration and Troubleshooting of All Critical Equipment.
	Station Status	All Stations	Operator(s)	To Monitor Operating Condition of all Stations.

Table II. 1-1

MASTER EQUIPMENT LIST (Continued)

Location	Equipment	Input From	Output To	Function
	Lunar Information Storage	Previous Information	Operator(s)	To Provide Access to Information Concerning the Moon (i. e., Terminator Time, Etc.).
	Surveyor Status	CDC/DSIF	Operator(s)	To Display Information Concerning All Surveyor Bus Equipment Necessary For the Completion of the SLRV Mission.

Table II. 1-2 (a)

MISSION INDEPENDENT EQUIPMENT AT SFOF

Deep Space Instrumentation Facility At SFOF	Spacecraft Performance Analysis Area	Space Science Analysis Area	Missions Control and Operations Areas	Flight Path Analysis Area
DSIF control room at SFOF	Program computer ops. console	7 ft. projection screens (video) (3)	large status boards approx. 40 ft. total (3)	Mid course parameter display 36" x 44"
Milgo plotter 30x30 in.	Axis Spacecraft simulator (3)	Chalk & bulletin boards	30x30 plotter (1)	Target parameter display 36" x 44"
Receive only TTY printers (6)	Analog support desk	Light tables 5 ftx3 ft. (2)	TTY receive only printers (2)	Tracking data display 12 ft.
TTY send-receive keyboards (2)	TV monitors 23 in. (15)	Video-commun. console (1)	Reperforators (2)	Tracking & data analysis consoles (3)
Reperforators (2)	TM display 18 ft. long	Mission independent staff consoles (2)	Adm printers (5)	Orbit determination consoles (3)
cckt-ceiling TV cameras (8)	Subsystem analysis consoles (10)	Spare consoles (4)	SC-3070 printers (2)	Flight path anal. consoles (7)
Adm. Printer (1)	System performance consoles (4)	23 in. TV monitors (30)	Card readers (2)	Trajectory consoles (2)
Remote in/out console	Input/output console (1)	Ops. console (1)	Input/output consoles (2)	Maneuver consoles (2)
Audio commun. console (1)	Adm. printer (1)	SC3070 printer (1)	Operations consoles (7)	Operations console (1)
Operational consoles (3)	Operational console (1)	Adm. printer (1)	11x17 plotter (1)	Input/output console (1)
DSIF Tech info. display 85x32 in.	Data processing & evaluation consoles (3)	Input/output console (1)	Talker-recorder station (2)	Video-commun. console (1)
Chalk (42x48 in.) status boards (3)	Spare consoles (2)	11"x17" plotter (1)	Display control station (2)	TV status display monitors 23 in. (30)
DSIF oper. status display 96x48"	Bulk data distrib. desk (1)	30"x30" plotter (1)	Hard copy TV cameras (9)	Card reader (1)
TV monitors	Video & comm. console (1)	Burroughs card reader (1)	Mgr. consoles (2)	SC3070 printer (1)
Voice communications	SC-3070 printer (1)	Receive only TTY printers (3)		ADM printer (1)
DSIF schedule display 18x84"	Rec. only TTY page printers (4)	Reperforators (3)	Equipment Distribution at SFOF (Pasadena)	11x17 plotter (1)
Bulletin boards 36x56" (2)	Reperforators (2)	Science-sensor display-12 ft. (1)		30x30 plotter (2)
SC-3070 printer (1)	Burroughs card reader (1)	Eng. display sensor - 15 ft. (1)	Ref. EPD 180 JPL Oct. '63.	Key punch (1)
	11x17" X-Y plotter (1)	Hard copy TV cameras (6)		Display-Miss parameters 3x10 1/2 ft.
	30x30" plotter (1)	Video projectors (3)		Display-orbital param. 3x10 1/2 ft.
	SPAA sequence display 18 ft.	Conf. table areas (5)		Rec. only TTY printers(6)
		Moon mosaic		Reperforators (2)
				Large chalk boards (2)
				Hard copy TV cameras (7)

Table II. 1-2 (b)

DSIF RECORDING EQUIPMENT

Goldstone		Johannesburg	Woomera
Echo Site	Pioneer Site		
Direct writing 8 channel Sanborn Mod. 358	Direct writing 8 channel Sanborn Mod. 158	Photographic Oscillograph - 14 chan. Midwest 621	
Photographic 36 chan. Midwest 603	Photographic Oscillograph - 14 chan. Midwest 621	Photographic Oscillograph 36 chan. Midwest 603	
Tape recorder Ampex FR 107 1/2 in. tape	Photographic 36 Chan. Midwest 603	Tape recorder CEC 752 A 1/2 in. tape	SAME AS JOHANNESBURG
Tape Recorder Ampex FR 607 1/2 in. tape	Tape Recorder Ampex FR 107 1/2 in. tape	Tape Recorder CEC 752 A 1/2 in. tape	
Printer H-P 560A	Tape Recorder Ampex FR 607 1/2 in. tape	Printer H-P 560A	
	Printer H-P 560A		

C. SLRV OPERATIONAL SEQUENCE OF EVENTS

Shown in this section is a possible sequence of events which is intended to test the Ground Equipment as it has been proposed.

CODE

- A - Mission Control - SFOF
- B - Communication Center - JPL
- C - Computing Facility - SFOF
- D - DSIF Net Control - SFOF
- E - JPL/HAC Control Center - AMR
- F - Flight Path Analysis - SFOF (Navigation Station)
- G - S/C Performance Analysis - SFOF (Performance Analysis Station)
- H - SFOF
- S/C - Spacecraft
- 11 Goldstone DSIF
- 41 Woomera DSIF
- 42 Canberra DSIF
- 51 Johannesburg DSIF

Prior to Touchdown	To
1. Mission Director requests status of all OGE.	G
2. Performance Analysis reports status of all OGE.	A
3. Mission Director requests status of DSIF/SFOF-SLRV equipment.	11 & H
4. DSIF reports equipment status. SFOF reports equipment status.	A
5. Navigation station requests pre-landing photos from Control Station and alerts Scientific Analysis.	A
6. Control Station starts transmission of pre-landing photo acquisition sequence.	11

7.	Video processing reports reception of pre-landing photos and GMT to be displayed. (Distribution to Scientific Analysis, Navigation Station and Control Area follows).	A
8.	Navigation Station determines "best guess" touchdown point and surveyor orientation.	A

Touchdown

1.	Navigation Station determines "best guess" touchdown point and surveyor orientation.	A
2.	Mission Director announces handover of program to SLRV mission objectives.	H
3.	Control Station sends SLRV "wake up" signal.	SLRV
4.	Performance Analysis starts evaluation of SLRV and Surveyor subsystem status.	H
5.	Performance Analysis reports any unusual condition present in SLRV Surveyor TM data.	H
6.	Navigation requests pre-deployment TV photos.	A
7.	Control Station initiates TV sequence.	SLRV
8.	Video analysis reports photo sequence received, and initiates film processing and distribution.	H
9.	Performance analysis reports preliminary status of TV subsystem.	H

Deployment

10.	Mission director evaluates deployment situation.	H
11.	Mission director requests SLRV deployment.	A
12.	Control Station sends deployment command sequence.	SLRV
13.	Performance Analysis reports any unusual condition in SLRV subsystem status.	H

14.	Navigation Station requests 360° TV sequence.	A
15.	Control Station initiates 360° TV sequence. (Could be part of deployment routine)	SLRV
16.	Video Analysis reports acquisition, processing and distribution of TV sequence.	
17.	Navigation station reports SLRV heading.	A
18.	Performance analysis requests subsystem exercise routines.	A
19.	Control Station starts transmission of locomotion, steering, TV and DIBSI routines.	SLRV
20.	Performance Analysis establishes status of all sub-systems and reports any unusual condition. Also establishes continuous displays (i.e. temperature, pressure, electrical, communication etc.)	H
21.	Scientific Analysis reports "quick look" soil property evaluation.	H
22.	Video Analysis establishes stereo pair photos and distributes. (and repeats on every TV scan).	H
23.	Scientific Analysis initiates topographical profile analysis.	H
24.	Navigation Station establishes a recommended course and heading.	A
25.	Control Station starts transmission of locomotion, TV and steering routines to reach a vantage point.	SLRV
26.	Scientific Analysis reports results of photo examination for candidate landing points.	A & F
27.	Navigation Station provides user areas a ground track plot of SLRV.	

Vantage Point Arrival

28.	Navigation Station reports location of vantage point.	A
29.	Navigation Station defines scan sector and requests TV sequence.	A
30.	Control Station initiates TV sequence in defined scan sector.	SLRV
31.	Video Processing acquires, processes and distributes TV sequence photos.	H
32.	Scientific Analysis reports reports results of preliminary photo examination for candidate landing points.	H
33.	Navigation Station defines scan range.	A
34.	Scientific Analysis reports whether candidate landing point is in scan zone.	H
	IF YES	
35.	Navigation Station reports recommended heading to reach candidate landing point.	A
36.	Control station starts transmission of locomotion, steering and TV sequences to reach candidate landing point.	SLRV
37.	Navigation Station observes ground track plot and reports candidate landing point arrival.	A

Landing Point Arrival

38.	Scientific Analysis requests TV sequence.	A
39.	Navigation Station requests Range and Bearing Sequence and determines location of candidate landing point.	A
40.	Navigation Station defines TV scan sector.	A
41.	Control Station initiates TV sequence and Range and Bearing sequence.	SLRV

42.	Video Processing reports acquisition, processing and distribution of TV photos.	H
43.	Scientific analysis reports "quick look" relief evaluation.	H
44.	Scientific analysis requests Soil Measurement sequence.	A
45.	Control Station initiates DIBSI command sequence.	SLRV
46.	Scientific analysis reports results of "quick look" soil property evaluation.	H
47.	Scientific analysis reports bearing strength and relief certification status.	H
	If Certification Status is YES	
48.	Scientific Analysis requests and control station initiates additional DIBSI and/or TV sequence as required.	SLRV
	If Certification is Still Confirmed	
49.	Navigation Station reports location of landing point and updates ground track plot.	A
50.	Navigation Station reports course and heading to new search area perimeter (preferred and secondary)	A
51.	Control Station initiates locomotion, steering and TV sequences to reach search area perimeter.	SLRV
	Search Area Perimeter Arrival	
52.	Navigation Station reports search area perimeter arrival and requests TV sequence in specified Scan sector.	A
53.	Navigation Station requests Range and Bearing measurement.	A
54.	Control Station starts transmission of TV and Range and Bearing sequences.	SLRV

55.	Navigation Station reports search area perimeter arrival.	A
56.	Video Processing acquires, processes and distributes TV photos.	H
57.	Repeat. 23 through 56. and - as required.	
58.	Performance Analysis reports any unusual occurrence in SLRV, Surveyor and/or SFOF/DSIF status.	H

Charge

59.	Performance Analysis reports forecast of GMT for battery charge.	A
60.	Performance Analysis reports arrival of battery charge time and length of charge required.	H
61.	Navigation Station reports recommended heading for charge.	A
62.	Control Station initiates steering, locomotion and charge sequences.	SLRV
63.	Mission Director announces GMT for resuming operation.	H

Maintenance

64.	Performance analysis initiates routine check and calibration of all OGE equipment.	C
65.	Performance Analysis reports status of OGE, SFOF-DSIF Equipment and maintenance requirements.	A
66.	Routine and emergency maintenance performed.	H
67.	Scientific analysis initiates non-real time photo analysis, mapping and data analysis.	H
68.	Scientific analysis reports corrections to SLRV ground track, landing point locations and soil property analyses.	F

69.	Navigation Analysis updates plots and data on displays as required.	H
70.	Mission Director reports updated mission plan and work schedule.	H
71.	Performance Analysis reports Battery Charge time complete.	H
72.	Mission Director directs "wake up" sequence be transmitted.	A
73.	Control Station starts transmission of "wake up" sequence.	SLRV
74.	Performance Analysis establishes status of all sub-systems and reports predicted work time available.	H
75.	Performance Analysis reports status of all supporting equipment, (DSIF-SFOF-OGE) and reports any unusual condition, also establishes continuous status displays.	H
76.	Navigation Analysis requests TV 360° scan sequence.	A
77.	Control station starts transmission of TV scan sequence.	SLRV
78.	Video analysis reports acquisition processing and distribution of TV photos.	H
79.	Repeat 23 through 56 as required.	

DSIF Maintenance and Time Functions (Ref. JPL TM 32-319)

I. Acquisition Procedures

A.	First time acquisition	5 to 8 min.
B.	Subsequent acquisition	1 to 3 min.

If signal strength approaches receiver threshold, time increases.

C.	Telemetry Synchronization	20 min. max.

-but if errors develop - time increases

D.	Decommutator synchronization depending on bit rates (may be reduced if commutator position is known beforehand)	4 sec to over 2 hours
E.	Antenna Pointing (if angles are known)	1 min average
F.	Receiver Tuning (min. signal 3 to 6 db above receiver threshold.)	1 to 2 min at lunar distances
G.	Telemetry Discriminator Lockup each subcarrier	10 to 20 sec.

II. Testing Checkout and Maintenance

A.	After Equipment is installed and tested, one or two complete network runs	10 hrs. average.
B.	Subsequent routine checks and calibrations.	3 hrs/day
C.	Routine Maintenance	8 hr. period/3 days

COMMON SEQUENCES OF COMMANDS

TV Single Picture

B-36	Stand by mode
B-2	TV on
B-14	SLRV transmitter high power
C-6	Surveyor transmitter wide band
B-7	TV start picture sequence

B-15	SLRV transmitter low power
C-5	Surveyor transmitter narrow band
B-3	TV standby
AND	
B-5	TV step AZ, head CW
OR	
B-6	TV step AZ head CCW
TOTAL -	8 commands - average (assume B-36)

LOCOMOTION - SINGLE STEP

A-1	Locomote forward
AND	TV single picture as above
TOTAL -	9 commands average

RANGE AND BEARING

C-2	Range and Bearing on
C-8	Range measurement
C-9	Bearing measurement
C-10	Stop range and bearing measurement
B-18	Range and bearing measurement off
TOTAL -	5 commands

DIBSI Measurement

Assume:

Standby mode

Steer center

TV - correct azimuth

Execute:

B-25	DIBSI select
B-26	DIBSI deploy
B-2	TV on
B-14	SLRV transmitter high power
C-6	Surveyor transmitter wide band
B-7	TV start picture sequence
B-15	SLRV transmitter low power
C-5	Surveyor narrow band
B-3	TV stand by
B-28	DIBSI start
	Allow "N" impacts
B-29	DIBSI stop
B-2	TV on
B-14	SLRV transmitter high power
C-6	Surveyor transmitter wide band
B-7	TV start picture sequence
B-15	SLRV transmitter low power
C-5	Surveyor narrow band
B-3	TV stand by
B-27	DIBSI retract
AND	Take a TV picture, as above
B-2	
B-14	
C-6	

B-7

B-15

C-5

B-3

AND

Step azimuth head CW or CCW as required

Total average - 30 commands

CHARGE ROUTINE

B-34	Solar panel step up
	Repeat as required, or
B-32	Solar panel deploy
AND	
B-10	Start battery charge
B-4	TV off
B-16	SLRV transmitter off
B-20	VSD's off
B-16	SLRV TM off
C-4	Surveyor transmitter off

TOTAL - 8 commands

WAKE UP ROUTINE

C-3	VHF transmitter on low power	
B-11	Stop battery charge	
B-19	Telemetry on	OR B-36 Standby Mode
B-21	VSD's on	

B-3	TV standby
B-35	Solar panel retract

TOTAL - 2 to 6 commands

D. DIGITAL COMPUTER REQUIREMENTS OF OGE

The digital computer is an integral part of the OGE. It is used to real time process telemetry, commands, DSIF transmitted data and inquiry from OGE stations. It must multi-process scientific problems in non-real time. All data from SLRV is processed by the computer and stored for recall and processing by analysis programs.

All data inputs are entered into the computer via an overlapped data channel (IBM 7288 at SFOF). This data channel has assigned buffers in the memory. When the buffers are full the computer interrupts the program in process and processes input information from the buffer.

SLRV data entering computer consists of

- PCM Telemetry Data at 1100 bits per second
- DIBSI Data - Analog data which is sampled at 10,000 samples per second per channel with two channels being transmitted. Each sample is represented by 10 bits.
- Range and Bearing Data - Each item transmitted separately on an analog channel. 100 samples per second required with 10 bits per sample.
- DSIF Data - From the two DSIF stations data will be transmitted over transmission lines at 600 or 1200 characters per second. Multiple lines will connect each DSIF to SFOF.
- OGE Console Inputs - Commands will be entered into the computer and channeled to SLRV vehicle. Macro commands will be interpreted and command sequences generated for SLRV maneuvers.

PCM Telemetry - Four types of PCM telemetry are normal telemetry, DIBSI, TV ID data and Surveyor data.

Normal PCM telemetry contains the majority of information received on the status of the vehicle. Information measured within each compartment i. e., Axle 1, Axle 2 and Axle 3 is transmitted. These quantities are decommutated, calibrated, converted to engineering units, checked against limits and displayed. Displays are digital, analog and discretes. Warnings are issued to OGE when sensed in telemetry. Predicted problems will be indicated to OGE console for selected items on the basis of extrapolation of data.

DIBSI PCM data will be received along with two analog channels of DIBSI data. It will be decommutated, processed and displayed.

Television pictures will be transmitted along with PCM TV ID data. The ID data will enter the computer and be decommutated, converted to engineering units, image rotation angles computed and be combined with data received over normal PCM data. This data is converted for film recording. An index of TV pictures will be built up in auxiliary memory (IBM 1301 disc. files at SFOF) with cross-indexing for subsequent retrieval of film chips on an inquiry basis from OGE consoles.

The Surveyor vehicle will be transmitting measurements of its status. Selected quantities will be processed for display for SLRV OGE operators.

DIBSI analog data is transmitted over two channels. It is converted from analog to digital and entered into the computer over two sub-channels of the communications channel. The data is calibrated, converted to engineering units and "quick look" processed to evaluate soil properties. Soil properties displays will be channeled to interested OGE consoles. Data will be stored for non-real time analysis. Site certification will be determined from PCM Telemetered Soil Penetration Data and analog force and acceleration data.

Range and Bearing Data will be transmitted in digital form. It will be entered into the computer for calibration and coordinate computation. These will be displayed and used in Navigation Computations.

Commands to SLRV vehicle will be initiated at OGE command console with command subsystem also a part of navigation console for navigation use and back-up. Individual commands and macro commands will be initiated from consoles. Command lockout for hostile command will be incorporated into computer programs.

Individual Command(s) will be initiated by OGE. The computer will receive commands and store until OGE execute signal is received. It will then order the commands into proper sequence and gate the sequence out to command subsystem.

Macro commands will be initiated from OGE and entered into the computer i.e., TV sequence, battery charge sequence, etc. The computer will choose proper command sequence from memory (random access file) and issue sequence to the command subsystem.

Command lockout will be initiated from OGE for commands that have proven hostile to SLRV, i. e., would lead to SLRV failure such as power drain, etc. Command processing by computer program will analyze command sequences for hostile commands and delete or take other appropriate action.

DSIF data will be received from remote stations over data transmission lines. This will consist of SLRV performance data obtained during DSIF operation of vehicle, messages and non real time data when DSIF is not operating vehicle.

DSIF data on vehicle performance received during DSIF SLRV operation will enter the computer over communications systems subchannels. It

will be checked for errors in transmission and processed to display SLRV performance at OGE stations.

DSIF Messages - Informative and inquiry messages will be analyzed and transmitted to proper OGE operators.

DSIF non-real time data can be received during SFOF SLRV operation or other DSIF operation. This data will be multi-processed or stored and processed when computer is available, i. e., during battery charge periods.

OGE stations will be equipped to query the computer for information and initiate computations of special analysis programs. Requests for recall of selected parameter historical data will be processed. Requests for film chips will be analyzed relative to film chip cross index stored in memory.

Special analysis programs will be required which will take historical data and combine it mathematically and provide resultant printout and/or graphical display channeled to OGE operators. These programs will be stored in random access storage and will be executed in a multi-processing mode.

Mission simulation programs to make predictions and monitor mission progress will be required.

Computer outputs will consist of digital and discrete addressable display data channeled to the address and distribution unit which will channel displays to OGE consoles and to the performance station oscillograph recorder; printed outputs on remote printers, graphical outputs on remote plotters and message outputs on remote teletypewriters or inquiry units. Data transmission to DSIF will be generated by the computer.

Displays at GOE consoles will consist of pertinent mission data obtained from computer input data. After processing, data will be tagged with an

address of the display and placed on a single parallel communications system subchannel and sent to the address and distribution subsystem for channeling to proper display unit.

Central SLRV display will be processed the same as 3.7.1 containing all mission progress data. This display will be monitored by TV cameras.

Oscillograph records of selected telemetry signals will be provided to the performance station by the computer via the address and distribution subsystem. The digital data will be converted to analog and combined with time and graphed at slow speed on the oscillograph for performance monitoring.

Remote printers of medium speed for printing output of inquiries and analysis programs will be required. A separate communications system subchannel will be needed for each printer.

Remote plotters are required to provide graphical representation of mission progress, TV coverage, terrain, parameters requested for trend analysis, etc. The computer will generate plotter control information and channel it to proper plotter. It will be necessary to have a communication system subchannel for each plotter.

Message outputs to teletypewriters and inquiry unit typewriters will be generated by the computer as required. This will require low speed communications system subchannels.

Data transmission to remote DSIF stations will be generated by the computer. Data pertinent to DSIF stations will be encoded and channeled through communications system subchannels.

Computing equipment requirements - A digital computer system of high speed with at least four overlapped data channels is required. This would

consist of magnetic tape, random access memory and communication subsystem data channels. Ability to multi-process is required.

SFOF computing facilities meet and exceed those required for SLRV mission. It consists of two IBM 7040 computers and two IBM 7094 computers having shared IBM 1301 disc files and direct data connections between the 7040's and 7094's. The 7040's are used as input and output processers while the 7094 is used for analysis computations.

SFOF Communications channels are multiple IBM 7288 with appropriate subchannels. SLRV mission will require only a portion of one 7288 channel.

SFOF random access memories consist of IBM 1301 disc files for storage of programs, recent history data and cross-index of TV pictures. SFOF facilities are more than sufficient.

DSIF computing facilities will have to perform the functions required for SLRV mission. Presently DSIF has no computing equipment. None is planned for the near future. In order to provide 24-hour SLRV operation digital computers are required. This need not be as complete a facility as SFOF. Non-real time analysis programs would be processed slower.

DSIF computing facility for SLRV would require a computer with the capabilities of an IBM 7044 computer with two tape channels and 1301 disc files. The computer would be used for input-output processing as well as computing.

A communications channel similar to one IBM 7288 with fewer subchannels would suffice.

DSIF random access files would be used, as indicated previously, at SFOF facility.

Programming requirements in support of the SLRV mission.

Programs are required to process all data entering the computer system and to perform analysis of history data. Real time and non-real time programs are required. Use of existing SFOF programs and subroutine will be used wherever possible. DSIF programs will have to perform the same functions.

PCM telemetry processing programs must perform the following functions (Real time)

1. Decommutation of data
2. Calibration and flagging of data
3. Conversion to engineering units
4. Limits check of quantities and issuance of alarms
5. Prediction of impending problems based on recent past history
6. Output to display programs

OGE Output Processer programs are required to channel information to particular OGE equipment.

1. Message switching
2. Generation of curve plotting
3. Preparation of displays
4. Generation of remote printing
5. Issue SLRV command sequence

Inquires to the computer will be analyzed by a computer program and response formulated.

1. Decode inquiry and process with proper program
2. Prepare program for permissible inquiries
3. Search for data to be used in responding to inquiry
4. Code response and transmit

TV ID data is received via PCM and requires special processing programs. (Real time)

1. Prepare output to film recorder
2. Store in random access file
3. Prepare cross-reference index for rapid retrieval

DIBSI Telemetry Processer (Real Time)

1. Calibrate flag and store data
2. DIBSI analysis programs

DSIF Transmission Processing (Real Time)

1. Receive and error check
2. Calibrate and convert to engineering units
3. Process to OGE to indicate status
4. Transmit reduced data to DSIF

Scientific Analysis programs (Non Real Time)

1. Simulation programs
2. Special parametric analysis

Supervisory programs to control multiprocessing. This program could be available at SFOF but would have to be modified for DSIF.

1. Utility programs
2. Data update programs

When the finitely conductive surface is interposed, as in Figure II.2-1b, the system-loss term will be altered to the degree that the first three terms on the right-hand side of Equation (II. 2-12a) are affected. Then

$$L'_{sys} = (L' + \Delta L' + L'' + \Delta L'')_{feed} + (L' + \Delta L' + L'' + \Delta L'')_{VSWR} - (G_t + \Delta G_t + G'_r + \Delta G_r) + 20 \log_{10} d_m + 20 \log_{10} F_{mc} - 27.552 + 20 \log_{10} A \qquad \text{(II.2-13a)}$$

$$= L_{sys} + (\Delta L' + \Delta L'')_{feed} + (\Delta L' + \Delta L'')_{VSWR} - (\Delta G_t + \Delta G_r) + 20 \log_{10} A \qquad \text{(II. 2-13b)}$$

Since the proximity of the conductive surface is a function of terrain characteristics, antenna erectness, antenna height, and temperature, the Δ components of Equation (II.2-13b) are not only a function of the electromagnetic characteristics of the surface, but are dependent upon the mission and terrain in a time-statistical fashion. Some of these variations are statistically independent, while others are highly correlated. Therefore, it is desirable to provide a safety margin, M, to encompass these variations, and Equation (II.2-13b) becomes

$$L'_{sys} = L_{sys} + M + 20 \log_{10} A \qquad \text{(II.2-13c)}$$

The important effect created by the conductive surface is the parameter A, which can be defined by

$$A \equiv \frac{E_{cs}}{E_{fs}} \qquad (\text{where } 2 \geq A \geq 0) \qquad \text{(II.2-14)}$$

The evaluation of A is therefore the primary criterion in the analysis of the lunar propagation. However, as previously indicated, the solution for A is based upon its subdivision into parts, each of which are related to the development of the full lunar propagation model. As the first step in this development, it is common to assume that the intervening conductive surface is smooth and homogeneous, but in addition, is planar as shown in Figure II.2-2. Based upon this model, it will be noted that three paths are available for the signal energy to traverse from the transmitter to the receiver. These paths are: (1) the direct path in which the total path length is r_1 ; (2) the indirect path, where the signal energy is reflected from the surface at the intermediate point 0, and the total path length is r_2 ; (3) the guided path, where the signal energy reaches the surface at many points, and some of the energy is guided along the surface to breakout at the point R to reach the receiving antenna. The latter path is relatively complex to illustrate the condition accurately; however, empirical data indicate this path has an equivalent path length of approximately r_2.

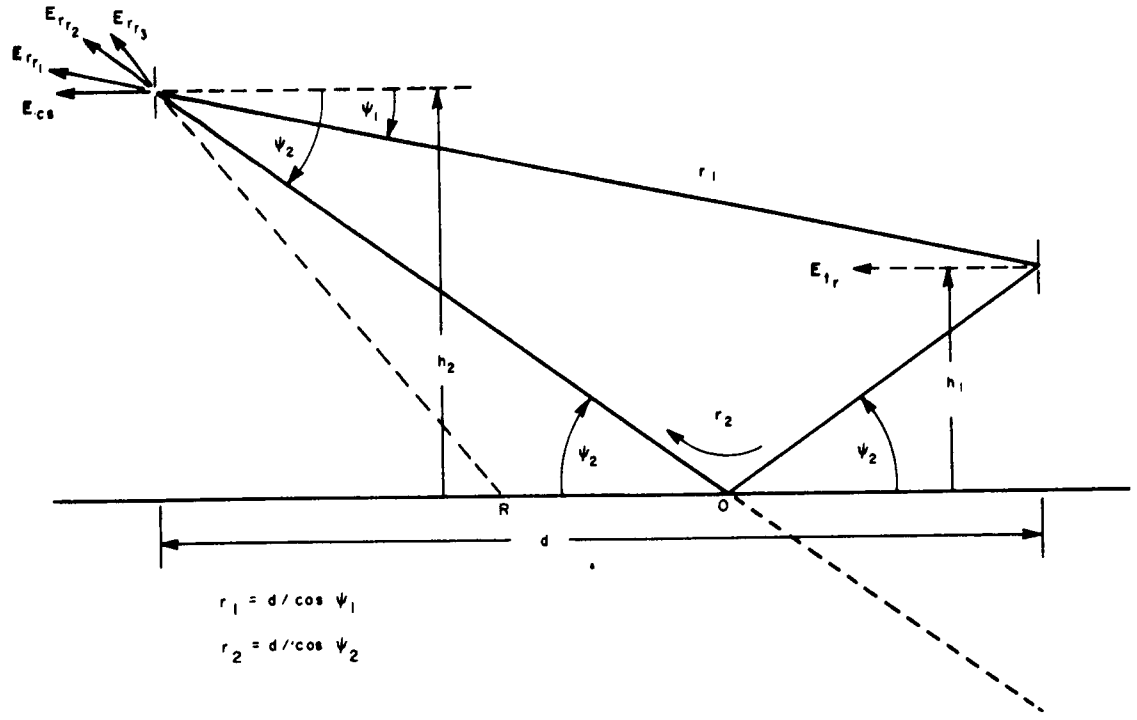

Figure II.2-2. Planar Surface Propagation Model

The signal at the receiver will now be a vectorial combination of the energy arriving by three typical paths. For each path, the vector will have both an amplitude and phase relationship that will be independent of the other paths. The direct path will have an amplitude which decreases as 4π times the path length measured in wavelengths. The phase relationship will be simply the total distance divided by the velocity of propagation. For the second path, the signal level and phase will not only be a factor that r_2 is greater than r_1, but at the point of reflection, not all of the incident energy will be turned along the path of reflection. Some of this energy will enter the interface and be lost to the second path. In addition, a phase transient will be introduced by the reflecting surface. These were pointed out by Equations (II. 2-3), (II. 2-4) and (II. 2-5).

Next it must be noted that the angle of departure at the transmitting antenna differs for each path and is also true for the angle of arrival at the receiving antenna. Due to the directivity characteristics of each antenna, the initial signal amplitude along each path will have a different coupling effect. Kraus (Reference 10) indicates a relatively simple approximation that could be applied on the basis of a thin linear antenna. When this is adjusted to have an equatorial angular reference, the effective far-field intensity can be given by

$$E_{t_{r_a}} \approx E_{t_r} \frac{\cos\left(\frac{\pi}{2}\sin\psi_a\right)}{\cos\psi_a} , \qquad \text{(II. 2-15a)}$$

which can be further modified, if the values of ψ are ≤ 3 degrees, to

$$E_{t_{r_a}} = E_{t_r} \cos \psi_a \qquad \text{(II. 2-15b)}$$

From this background, it is now possible to develop the signal components along each path. For the first two paths,

$$E_{r_{r_1}} = E_{t_r} \cos \psi_1 \left[\frac{1}{4\pi \frac{r_1}{\lambda}} \right] \cos \psi_1 \, e^{j\left(\frac{2\pi r_1}{\lambda} + \gamma_o\right)} \qquad \text{(II. 2-16a)}$$

$$E_{r_{r_2}} = E_{t_r} \cos \psi_2 \left[\frac{1}{4\pi \frac{r_2}{\lambda}} \right] \bar{R} \cos \psi_2 \, e^{j\left(\frac{2\pi r_2}{\lambda} + \gamma_o\right)} \qquad \text{(II. 2-17a)}$$

By selecting a reference time when $\gamma_o = 0$, these become

$$E_{r_{r_1}} = E_{t_r} \frac{\cos^2 \psi_1}{\left(\frac{4\pi}{\lambda}\right)\frac{d}{\cos \psi_1}} \, e^{j\left(\frac{2\pi r_1}{\lambda}\right)}$$

$$= \frac{E_{t_r}}{d\left(\frac{4\pi}{\lambda}\right)} \cos^3 \psi_1 \, e^{j\left(\frac{2\pi r_1}{\lambda}\right)} \qquad \text{(II. 2-16b)}$$

and

$$E_{r_{r_2}} = E_{t_r} \frac{\bar{R} \cos^2 \psi_2}{\left(\frac{4\pi}{\lambda}\right)\frac{d}{\cos \psi_2}} \, e^{j\left(\frac{2\pi r_2}{\lambda}\right)}$$

$$= \frac{E_{t_r}}{d\left(\frac{4\pi}{\lambda}\right)} \bar{R} \cos^3 \psi_2 \, e^{j\left(\frac{2\pi r_2}{\lambda}\right)}, \qquad \text{(II. 2-17b)}$$

which may be defined, in terms E_o at a unit distance, by

$$E_{r_{r_1}} = \frac{E_o}{d} \cos^3 \psi_1 \, e^{j\left(\frac{2\pi r_1}{\lambda}\right)} \qquad \text{(II. 2-16c)}$$

and

$$E_{r_{r_2}} = \frac{E_o}{d} \bar{R} \cos^3 \psi_2 \, e^{j\left(\frac{2\pi r_1}{\lambda}\right)} \qquad \text{(II. 2-17c)}$$

For the third path, the entry and exit points are indefinable. However, it is recognized that at each point of reflection along the surface, energy of the value $(1 - \bar{R})$ will be transferred into the surface. Then, possibly due to inhomogeneity, some of this energy will reappear and travel along the interface. These surface fields could be propagating in all directions, such that a statistical summation could be made at any location, including the point 0. From this hypothesis, the energy intensity due to the third path can be given by

$$E_{r_{r_3}} = E_{t_r} \sum_i \left\{ \frac{\cos\psi_1 \, (1-\bar{R}_i) \cos\psi_1}{\frac{4\pi}{\lambda} f(r_i, h_1, h_2)} \, e^{j \frac{2\pi}{\lambda} f(r_i, h_1, h_2)} \right\}, \qquad \text{(II. 2-18a)}$$

which has been simplified by Norton to the following.

$$E_{r_{r_3}} = E_{t_r} \left\{ \frac{(1-\bar{R}) \cos^2 \psi_2 \, f\,(P, B)}{\frac{4\pi d}{\lambda}} \, e^{j\left(\frac{2\pi r_2}{\lambda} - \theta\right)} \right\} \qquad \text{(II. 2-18b)}$$

and in terms of the field at unit distance

$$E_{r_{r_3}} = \frac{E_o}{d} \left\{ (1-\bar{R}) \cos^2 \psi_2 \, f\,(P, B) \, e^{j\left(\frac{2\pi r_2}{\lambda} - \theta\right)} \right\} \qquad \text{(II. 2-18c)}$$

When Equations (II.2-16c), (II.2-17c), and (II.2-18c) are combined, the total received field intensity

$$E_{cs} = \frac{E_o}{d}\left\{\cos^3\psi_1\, e^{j\left(\frac{2\pi r_1}{\lambda}\right)} + \bar{R}\cos^3\psi_2\, e^{j\left(\frac{2\pi r_2}{\lambda}\right)} + (1-\bar{R})\, f(P, B)\cos^2\psi_2\, e^{j\left(\frac{2\pi r_2}{\lambda}-\theta\right)}\right\} \quad \text{(II.2-19)}$$

which is Norton's expression for the ground-wave field intensity for short distances over a smooth planar surface. The parameters of Equation (II.2-19), other than the geometric relationships given in Figure II.2-2, are

$$\bar{R} = \frac{\left(\frac{q_1+q_2}{2p}\right) e^{j\left(\frac{\pi}{4}-\frac{b}{2}\right)} - 1}{\left(\frac{q_1+q_2}{2p}\right) e^{j\left(\frac{\pi}{4}-\frac{b}{2}\right)} + 1} \quad \text{(II.2-20)}$$

$$p = \frac{\pi r_2}{\lambda}\,|T|^2 \quad \text{(II.2-21)}$$

$$q_{1,2} = \frac{2\pi h_{1,2}}{\lambda}\,|T| \quad \text{(II.2-22)}$$

$$T_{v,h} = \frac{1}{\sqrt{\epsilon_{e,m}}} \quad \text{(II.2-23)}$$

$$\epsilon_e = \frac{\epsilon_o'^2}{\epsilon_o' - \cos^2\psi_2} \quad \text{(II.2-24)}$$

$$\epsilon_m = \frac{1}{\epsilon_o' - \cos^2\psi_2} \quad \text{(II.2-25)}$$

$$\epsilon_o' = \epsilon_{r_2} - j\,60\sigma_2\lambda \quad \text{(II.2-26)}$$

$$P\, e^{jB} = p\left[1 + \frac{q_1+q_2}{2p}\, e^{j\left(\frac{\pi}{4}-\frac{b}{2}\right)}\right]^2 e^{jb} \quad \text{(II.2-27a)}$$

$$\equiv \frac{4p\, e^{jb}}{(1-\bar{R})^2} \quad \text{(II.2-27b)}$$

TR64-26

Thus,

$$|T_v| = \left[\frac{\sqrt{(\epsilon_{r_2} - \cos^2\psi_2)^2 + (60\sigma_2\lambda)^2}}{\epsilon_{r_2}^2 + (60\sigma_2\lambda)^2}\right]^{1/2} \quad \text{(II. 2-28a)}$$

$$|T_h| = \left[\sqrt{(\epsilon_{r_2} - \cos^2\psi_2)^2 + (60\sigma_2\lambda)^2}\right]^{1/2} \quad \text{(II. 2-28b)}$$

and

$$b_v = 2\tan^{-1}\left[\frac{\epsilon_{r_2}}{60\sigma_2\lambda}\right] - \tan^{-1}\left[\frac{\epsilon_{r_2} - \cos^2\psi_2}{60\sigma_2\lambda}\right] \quad \text{(II. 2-29a)}$$

$$b_h = 180 - \tan^{-1}\left[\frac{\epsilon_{r_2} - \cos^2\psi_2}{60\sigma_2\lambda}\right] \quad \text{(II. 2-29b)}$$

From Figure II. 2-2, it can be recognized that the first path is actually the free-space condition. Thus, if it is assumed that there exists conditions where the first two terms of Equation (II. 2-19) predominate over the third term, then by suppressing the third path and substituting Equations (II. 2-19) and (II. 2-16c) into Equation (II. 2-14),

$$A = \frac{\frac{E_o}{d}\left\{\cos^3\psi_1\, e^{j\left(\frac{2\pi r_1}{\lambda}\right)} + \bar{R}\cos^3\psi_2\, e^{j\left(\frac{2\pi r_2}{\lambda}\right)}\right\}}{\frac{E_o}{d}\cos^3\psi_1\, e^{j\left(\frac{2\pi r_1}{\lambda}\right)}} \quad \text{(II. 2-30)}$$

$$= 1 + \bar{R}\,\frac{\cos^3\psi_2}{\cos^3\psi_1}\, e^{j\frac{2\pi}{\lambda}(r_2 - r_1)}$$

Since the $\psi_2 \approx \psi_1$ at low grazing angles, and $R \leq 1$, the maximum value for A is 2, the boundary given with Equation (II. 2-14).

Now, in order to model the component segments which constitute the value for A, it is first assumed that the antenna heights $h_1 = h_2 = 0$. Then, from Equation (II. 2-22), $q_1 = q_2 = 0$. With those introduced into Equation (II. 2-20), the value of $\bar{R}$ is found to be -1, and $r_1 = r_2 = d$, resulting in $\psi_1 = \psi_2 = 0$. By introducing these conditions into

APPENDIX II
COMMUNICATIONS SUBSYSTEM

APPENDIX II
COMMUNICATIONS SUBSYSTEM

A. ANALYSIS OF ELECTROMAGNETIC PROPAGATION BETWEEN THE SURVEYOR BUS AND THE SURVEYOR LUNAR-ROVING VEHICLE

1. General

A solution to the degradation in intensity or density of an electromagnetic field as it is propagated between two terminals can be obtained through the appropriate use of Maxwell's equations. If the propagating medium is homogeneous and continuous, the solution is relatively simple. However, if the propagating medium is not homogeneous, an approach to the solution can be obtained by considering that the total propagation path is the summation of consecutive media, each of which is homogeneous and continuous within its own boundaries, but becomes discontinuous at the boundary of the adjacent media. Thus, Maxwell's equations must be applied in successive fashion to accommodate the interface parameters of the individual media. This now becomes a complex process of accurately defining the location and consitituency of the elementary segments, and is further complicated if the intra-relationship between segments is not time-constant. This situation is common in the modeling for terrestrial terminals, and techniques have been developed to reduce the complexity even though the accuracy of the results are impaired.

When the ray path of the propagated energy passes close to a finitely conductive surface, the electrical characteristics of the elementary segments in that vicinity must be adjusted to account for the characteristics of this surface. For terrestrial terminals, the surface is assumed to be homogeneous, so that the effects introduced to the elementary segments are proportional to the distance they are separated from the conductive surface. However, when the surface is not homogeneous, the effect upon the segments will be different. In the case of the SLRV, due to its dynamic status, the path relationship will be a random time variable. For this type of condition, the assumptions that are usually made tend to normalize the propagation model and provide a margin to accommodate the variations that might be incurred.

Calculations of the effects of propagation across the surface of the moon involve a multitude of parameters which must be considered. Some of these are discussed to illustrate their importance as visualized for similar terrestrial terminals, while others are considered to be negligible in terms of results obtained through other scientific investigations. The usual procedure for handling this type of propagation problem is to assign median values for many of the parameters. Even though empirical

data have shown relatively close comparison to the theoretical data for the terrestrial terminals, it is not realistic to assume that all of the terrestrial experience can be directly extrapolated to the lunar propagation problem. For this reason, it is desirable to establish only those parameters that are considered to be insensitive in the location of analytical saddle points.

As the SLRV explores the surface of the moon, its separation from the Surveyor will be a variable of time. However, it is assumed that the maximum separation will be that dictated by the operational desires of the SLRV and will be limited to approximately 3200 meters. This is a very short range in comparison to distances usually considered for terrestrial conditions. Thus, the usual concept of a "smooth sphere of homogeneous electrical characteristics" can not be looked upon too favorably. For much longer ranges, the localized regions of heterogeneity become smoothed in an average value without introducing large errors. For the moon, this "smoothing" assumption can not be applied, and the path turbulences can be expected to approach 3σ values instead of the normal variance about the mean.

The direction of propagation is immaterial due to the bilateral characteristics of the propagating media. Thus, for purposes of this analysis, the direction has been selected to be from SLRV to Surveyor.

It is further assumed that the total propagational effect is the vertical sum of the individual segment contributions. With this in mind, the analysis of the propagated signals is based upon the consideration of individual effects created by the presence of the lunar surface, in comparison to the signals over a truly "free-space" path. Since the presence of the lunar surface has several reactions, the following discussion of some of these responses is presented in the following paragraphs. A glossary of the terms used in this analysis is presented on page II. 2-30.

Antenna Characteristics

An antenna functions as a launching device to convert electromagnetic energy from conducted to radiated (and vice versa) fields. The efficiency of this device is based upon its ability to make this energy transformation in terms of its insertion loss. However, physical devices, such as the antenna elements, can be expected to have lossy elements that will shift some of the radio-frequency (r-f) energy into the thermal spectrum. These lossy components can be identified as the radiating elements, the feedlines, and the interconnecting and matching elements.

Since the SLRV has an operational requirement for transferring information bi-directionally, duplex techniques must be provided, if the transfer is not simultaneous, or diplex techniques, if simultaneous transfer is required. In this analysis, it is assumed that simultaneous operation will be used, and a diplexer is considered as part of the antenna circuitry. The function of the diplexer is to maintain a proper flow route for

the signal energy, so that the radiating elements of the antenna can be used as a common element. It is further assumed that the operation will be at fixed frequencies, adequately separated in the spectrum such that the diplexer can be fixed tuned with both narrow- and isolated-passband characteristics for each direction.

The characteristic impedance of an antenna is a function of its physical dimensions and its coupling effects to the surrounding environment. In the case of an antenna located close to a finitely conductive surface, the radiation efficiency is affected by the actual clearance and the electromagnetic characteristics of the surrounding surface. For Surveyor antenna, the effective clearance will be dependent upon the attitude reached after landing. However, the SLRV will not be this constant, since it must negotiate terrain obstacles and contours. Therefore, the impedance match of the SLRV antenna (for each of the frequencies used) will be a time variable in terms of the attitude caused by the pitch and roll of the vehicle and the proximity of adjacent terrain as a function of its contouring.

Another factor that can affect the antenna performance is the thermal coefficient of the components as they are subjected to a variable kinetic temperature. The antenna on Surveyor will be subjected to diurnal temperature variations, whereas the SLRV will be subjected to shorter temperature variations.

Finally, the antennas will possess a certain degree of three dimensional directionality. This results in a variation of the antenna transfer efficiency in terms of angular radials along the path of propagation. As a result of the fixed attitude of the Surveyor after landing and the terrain contour negotiated by the SLRV, the antenna transfer characteristics will be a statistical variable in angle from the Surveyor.

Polarization

In the selection of the operating parameters, it is desirable to choose those factors which are most insensitive to the operational conditions. One such parameter is the polarization characteristics of the antennas, which are defined by the relationship of the electric vector with the plane containing the Poynting (ray path) vector incident to and reflective from the finitely conductive surface in proximity to the antenna. Since the electric vector can either maintain a constant relationship with this plane or be in a time rotation, there are several ways to identify the polarity. In the case of constant relationship with the plane, the electric field is considered to be linear, and can be called vertical, if it remains in the propagation plane; or horizontal, if it is normal to the propagation plane. However, when the vector is in time roation, it can be called circular, if the vector amplitude is constant; and elliptical, if the amplitude is time-modulated. For the rotational electric vector, both right- and left-handed directions of rotation are possible (defined in terms of direction of rotation for a slot in the head of a screw such that forwarded motion is dependent upon the cut of the threads along the shank).

Polarity considerations for this propagation analysis are basically confined to either horizontal or vertical directions, due to the effects created by the interface between free space and lunar surface. However, uniform azimuth gain characteristics can be provided with horizontal polarization by the use of multiple dipoles properly oriented and energized. The two specific antennas considered for calculating the propagation losses were a vertical, quarter-wavelength stub with four radials (quadrature displacement) of a quarter wavelength to provide vertical polarization, and two quadrature-displaced, half-wavelength dipoles in a horizontal plane, fed in phase quadrature for the horizontal polarization. The latter type is more commonly known as a horizontal "turnstile" antenna.

Deflection

The amplitude of electromagnetic energy is a function of the impedance relationship between the launching device (antenna) and the surrounding medium. The purpose of the antenna is to provide a highly efficient launch of the electromagnetic ragiation, which it accomplishes by acting as a transformer-matching device between the feedline and the propagating medium. The intrinsic impedance (η) of any medium is expressed as the ratio between the magnitude of the electric vector, E, and that of the magnetic vector, H . This is given by

$$\eta = \frac{E}{H} = \left[\frac{\mu}{\epsilon - j\frac{\sigma}{\omega}}\right]^{1/2} \quad ohms \qquad \text{(II. 2-1)}$$

where the electromagnetic characteristics of the propagating medium are given by its permeability(μ), permittivity(ϵ) , and conductivity(σ) ; while the propagated energy is expressed by

$$\omega = 2\pi f$$

$$= 2\pi \frac{c}{\lambda} \qquad \text{(II-2-2)}$$

Whenever the propagated energy passes across an interface between media of different intrinsic impedance, a mismatch will exist and some energy will be reflected at the interface, while the rest passes into the second medium.

The amplitude and phase of the reflected energy(R) will be related to the grazing angle at the interface and to the intrinsic impedance of each medium, such that

$$R_h e^{j\phi_h} = \frac{\sin\psi_a - (\bar{n}^2 - \cos^2\psi_a)^{1/2}}{\sin\psi_a + (\bar{n}^2 - \cos^2\psi_a)^{1/2}} \qquad \text{(II. 2-3)}$$

for completely horizontally polarized waves, and

$$R_v e^{j\phi_v} = \frac{\bar{n}^2 \sin\psi_a - (\bar{n}^2 - \cos^2\psi_a)^{1/2}}{\bar{n}^2 \sin\psi_a + (\bar{n}^2 - \cos^2\psi_a)^{1/2}} \qquad \text{(II. 2-4)}$$

for completely vertically polarized waves, where $\bar{n}$ is the index of refraction described below, ψ is the grazing angle (complement of the incidence angle), and ϕ is the lag angle due to reflection.

Refraction

As the propagated energy passes across the interface between two media, its path direction will be shifted from the geometrical extrapolation of its direction in the first medium. This change in direction is called refraction and is described by Snell's Law. The index of refraction $(\bar{n})$ of any medium is a measure of the amount of shift that may be expected and is usually normalized in terms of the free space parameters, μ_o, ϵ_o, and σ_o, such that

$$\bar{n} = (\mu_o \epsilon_o)^{-1/2} \left(\mu\epsilon - j \frac{\sigma\mu}{\omega} \right)^{1/2} \qquad \text{(II. 2-5)}$$

or

$$\bar{n}^2 = \frac{\epsilon_{r_2} - j \frac{\sigma_2}{\omega \epsilon_o}}{\epsilon_{r_1}} \qquad \text{(II. 2-6a)}$$

where

$\epsilon_{r_{1,2}}$ is the relative permittivity of the each medium with respect to free space, equal to 1 when the medium is free space,

ϵ_o is the permittivity of free space $= (36\pi \times 10^4)^{-1}$

σ_2 is the conductivity of the second medium in mks, and

ω is $2\pi f$, where f is the frequency of the propagated energy.

Now, the index of refraction for an interface between free space and the conductive surface of the moon can be expressed by

$$\bar{n}^2 = \epsilon_{r_2} - j\,18 \times 10^3 \frac{\sigma_2}{F_{mc}} \qquad \text{(II.2-6b)}$$

$$= \epsilon_{r_2} - j\,60\,\sigma_2\,\lambda \qquad \text{(II.2-6c)}$$

Dispersion

Electromagnetic energy normally travels away from a launching source along radial lines. In the case of an isotropic source in free space, the field density decreases as the square of the distance, measured in wavelengths, of the propagated energy. This action is similar to the radial dispersion of light. However, when the energy passes through the interface between the two media, the surface reflection will introduce a diffusional effect, and the field will be a combination of both the direct and indirect energy paths.

Diffraction

When electromagnetic energy is propagated in close proximity to an "opaque" object, the normally expected shadow region will contain a penumbra instead of a total shadow. The amplitude of the signal density within the penumbra is a function of the angle of depression below grazing and of the electromagnetic composition of the object. Many theories have been postulated to support this relationship, which can be simplified into a descriptive definition.

It was pointed out that some of the incident energy is reflected at the media interface, while the rest is passed across the interface. The ratio of reflected-to-passed energy is dependent upon the index of refraction, which is a function of the surface conductivity and relative permittivity, and the angle of incidence. From Equations (II.2-3) or (II.2-4), it can be seen that the amplitude of the reflected signal becomes zero when the numerator of the right-hand side becomes zero. For either horizontal or vertical polarization, this takes place when $\bar{n}^2$ *is* 1, and from Equation (II.2-6), this would be the case when ϵ_{r_2} equals 1 and σ equals 0.

These conditions would be descriptive of a transparent body. As the value of $\bar{n}^2$ increases, the body passes through translucency into opaqueness. Under any of these conditions, the amount of incident energy which passes through the interface is given by $(1 - \bar{R})$. This energy is then refracted and if the body is not homogeneous, some will be reflected at internal discontinuities. Some of this energy will approach the surface at the critical angle and will be guided along the surface, even though it is not planar.

Thus, some of this energy will appear beyond the geometrical edge of the surface that eclipses the radiant energy. This energy is called the diffraction field.

2. Analytic Methods for Evaluation of Lunar Propagation

Determination of the signal levels anticipated at the receiver terminals is dependent upon the development of a descriptive model for the propagation path across the lunar surface. This problem has been investigated for many years in terms of the description of terrestrial models. These models tend to characterize the propagational effects in terms of the paths over which the energy appears to have traveled. Two such paths have been traditionally used as the major subdivisions, i.e., "sky" and "ground" waves. Each of these have, in turn, separate subdivisions, but since it is anticipated that the lunar environment is practically void of an atmosphere and of an elevated ionosphere, only the major subdivisions of the latter are considered.

Ground waves are divided into "space" and "surface" waves. Space waves are those whose propagation path remains totally within the first medium, while surface waves are those which have negotiated the interface. Thus, the space waves are inclusive of the direct and reflected paths and can be geometrically visualized (ray theory), while the surface waves currently include all methods by which the energy is guided along the surface at the interface.

Since these categories are divisions of convenience, it should not be assumed that the fields are discrete. It is simply a fact that in certain regions, the field due to the space wave is most predominant, while in others it is almost non-existent with respect to that due to the surface wave. Thus, investigations have been performed to develop isolated mathematical descriptions for each of these concepts. In developing these models, certain assumptions have been made to minimize the complexity introduced by the numerous parameters involved. The first of these assumptions has been homogeneity for each medium on either side of the interface. The second is the assumption of a smooth spherical surface in order that the effective radius of curvature can be expressed in wavelengths at the operating frequency. This latter condition developed as the result of the evolution of the mathematical expressions in passing from the optic spectrum, where laboratory demonstration is convenient, to the radio frequency spectrum, where laboratory standardization is different.

The present methods for computing the electromagnetic field at remote locations from a transmitter, when a finitely conductive surface intervenes, are all related to the work of Sommerfeld (Reference 1*). Although this solution (with subsequent modifications) is applicable to the calculations for the SLRV, its mathematical complexity is not suitable for engineering analyses intended to locate a saddle point for many variables. Sommerfeld's solution involves the series of zonal harmonics for which the convergence

*See paragraph 4. for References

is extremely slow under certain conditions. Watson (Reference 2) developed a transformation applicable to the series of zonal harmonics which provided more rapid convergence. This method yielded a series of residues by the use of a complex integral which introduced the application of both Bessel and Hankel functions as part of the integration about the zeroes. More recently, the complexity of the solution was further reduced by van der Pol and Bremmer (Reference 3 and 4) whose application was generally limited to the operational considerations of the broadcase service and its hardware characteristics. Since that time, many have approached the problem of simplifying the calculations.

Analytic Approach

Of the methods available for conveniently calculating the propagation loss between antennas that are in close proximity to a finitely conductive surface, those developed by Bullington, Burrows, or Norton are most frequently referenced. Although these have a common origin - (van der Pol and Bremmer (Reference 5) - they differ in the degree of convenience. Bullington (Reference 6) developed a method utilizing a set of nomographs, but the number of analytic parameters are limited to provide the convenience. Burrows (Reference 7) developed a combination including both nomographs and graphical descriptions which are applicable to additional parameters. However, both approaches tend to restrict their applicability to terrestrial-surface conditions. In contrast, Norton (Reference 8) developed a set of normalized curves with wider application. However, his method utilizes the overlay comparison to derive the variation of field intensity. Neither of these methods permit convenience in an analytical evaluation wherein parametric trades are anticipated to determine performance under preferred situations.

For the specific problem of propagating electromagnetic energy across the surface of the moon, Vogler (Reference 9) has developed a set of curves which do not require the overlay comparison. Unfortunately, the separation range covered by Vogler is beyond the capability of SLRV, and the parametric selection did not consider weight and power restrictions for an unmanned exploration.

Thus, the approach that was used for the SLRV is predominately a by-product of Norton, with some of Vogler's techniques incorporated. The basis for this approach is the recognition that the signal level at the input terminals of the receiver will be materially affected by the introduction of a finitely conductive surface, such that the amount of change can be compared to an unaffected path. Figure II. 2-1 presents the model for the two conditions of propagation: free space and an intervening surface.

For the free space model of Figure II. 2-1, the propagating medium is considered to be both homogeneous and nonconductive. For this case, the system transfer loss (ℓ_{sys}) is

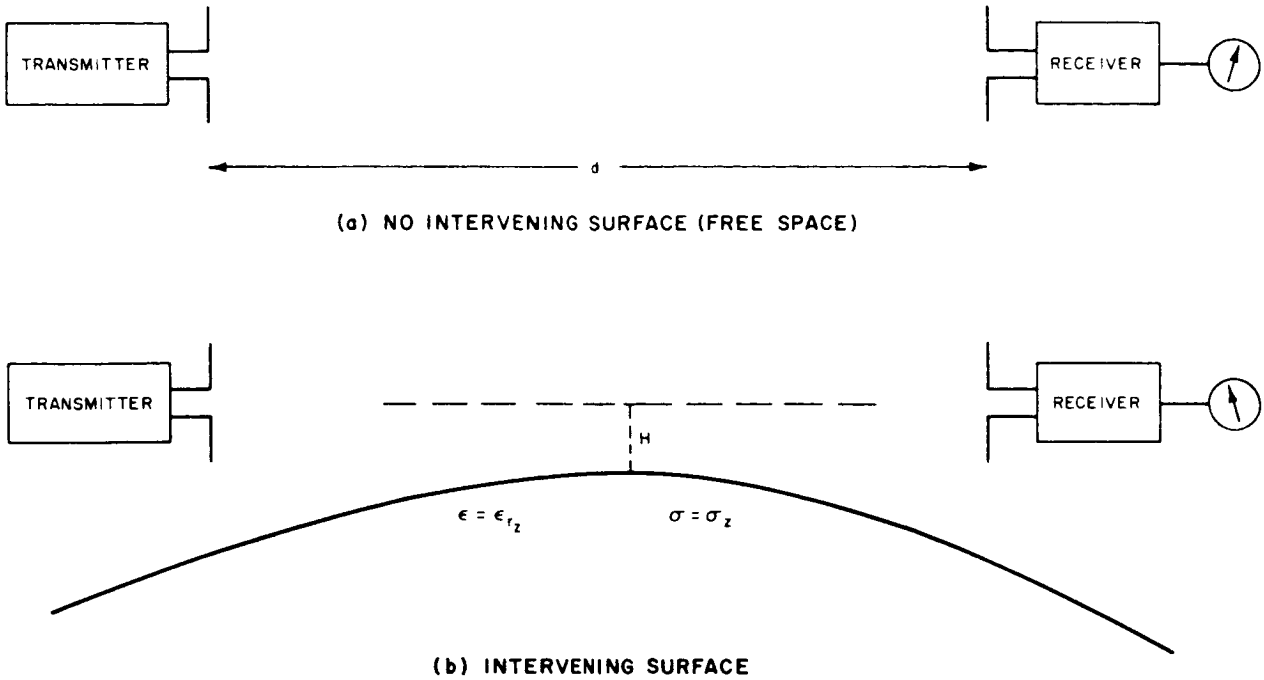

Figure II.2-1. Propagation Path Model

defined as the ratio of the transmitter output power to the available signal power at the receive terminals.

$$\ell_{sys} = \frac{p_t}{p_r}, \tag{II.2-7}$$

which is a dimensionless number frequently expressed in decibels by the following:

$$\begin{aligned} L_{sys} &= 10 \log_{10} p_t - 10 \log_{10} p_r \\ &= p_t - p_r \end{aligned} \tag{II.2-8}$$

Since the transmitter is not connected to the propagating medium in a loss-free manner, some energy will be consumed in this transformation. An identical situation will exist

at the receiver. The radiated fields in the vicinity of each antenna can be expressed in terms of these losses:

$$P_{t_r} = P_t - L'_{feed} - L'_{VSWR} + G_t \qquad \text{(II. 2-9a)}$$

and

$$P_{r_r} = P_r + L''_{feed} + L''_{VSWR} - G_r \qquad \text{(II. 2-9b)}$$

which, when inserted in Equation (II. 2-8), becomes

$$L_{sys} = P_{t_r} - P_{r_r} + (L' + L'')_{feed} + (L' + L'')_{VSWR} - (G_t + G_r) \qquad \text{(II. 2-10)}$$

However, the transmission loss between isotropic antennas is given by

$$L_{trans} = P_{t_r} - P_{r_r} = 20 \log_{10}\left(\frac{4\pi d}{\lambda}\right)$$
$$= 20 \log_{10} d_m + 20 \log_{10} F_{mc} - 27.552 \qquad \text{(II. 2-11)}$$

which when substituted into Equation (II. 2-10) produces

$$L_{sys} = (L' + L'')_{feed} + (L' + L'')_{VSWR} - (G_t + G_r)$$
$$+ 20 \log_{10} d_m + 20 \log_{10} F_{mc} - 27.552 \qquad \text{(II. 2-12a)}$$

or

$$L_{sys} = L_{trans} + C_t + C_r \qquad \text{(II. 2-12b)}$$

Equation (II. 2-19), the first two paths cancel, and the received signal energy is due to the third term, such that, with Equation (II. 2-27b),

$$E_{cs_o} = \frac{E_o}{d} \left\{ 2f(p, b)\, e^{j\left(\frac{2\pi d}{\lambda} - \gamma_o\right)} \right\} \qquad \text{(II. 2-31)}$$

or in an expression of a loss factor,

$$\frac{E_{cs_o}}{E_o\, d} = 2f(p, b)\, e^{j\left(\frac{2\pi d}{\lambda} - \gamma_o\right)} = 2A_o \qquad \text{(II. 2-32)}$$

an evaluation of which is given in Figure II. 2-3, as derived from Norton (Reference 8).

When the antennas are elevated, the nulls of the first two terms of Equation (II. 2-19) are no longer complete, and the field intensity will increase proportionally as long as the third term is not materially affected. This increase in field intensity could be accommodated by the introduction of height-gain factors to Equation (II. 2-32) for each antenna.

Then,

$$\frac{E_{cs_o}}{E_o\, d} = 2A_o\, f(q_1)\, f(q_2) \qquad \text{(II. 2-33)}$$

Height-gain functions have been evaluated by Norton (Reference 8) in terms of q, which can be determined by Equation (II. 2-22), and are shown in Figure II. 2-4. The range of the height values must be such that the value of $2A_o$ is not materially affected. This can be true only as long as $\psi_1 \approx \psi_2 \approx 0$.

This means that $d >> h$.

For conditions of surface electromagnetic properties found on Earth, the values of $|T|$ are relatively large. Thus, for the elevated-antenna and planar-surface condition, the value of p obtained from Equation (II. 2-21), using $r_2 = d$, and the values of q from Equation (II. 2-22) will be found to coincide with the linear portions of the curves in Figures II. 2-3 and II. 2-4. When the value of p is greater than 50, the value of A_o is

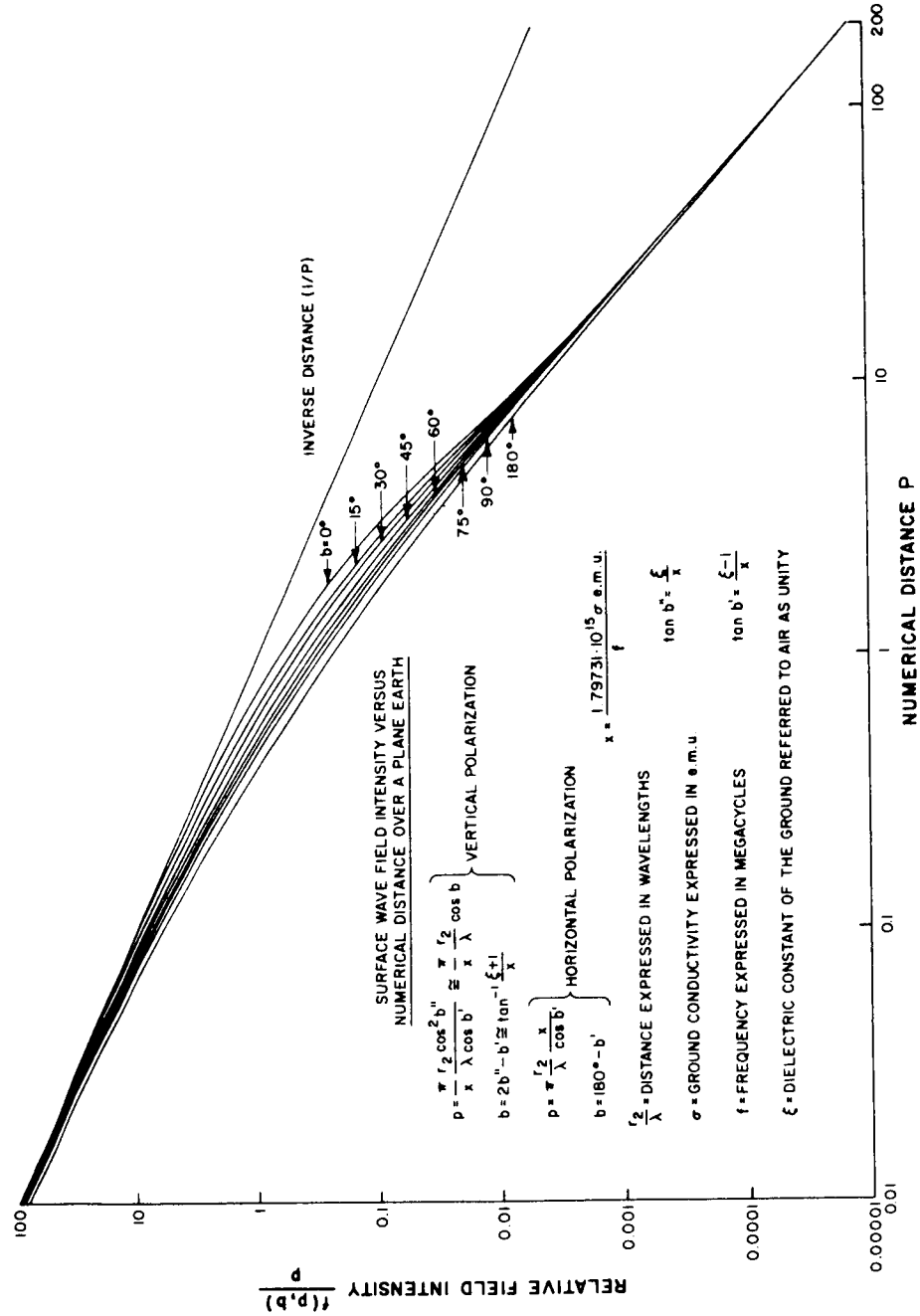

Figure II.2-3. Surface-wave Field Intensity Versus Numerical Distance Over a Plane Earth

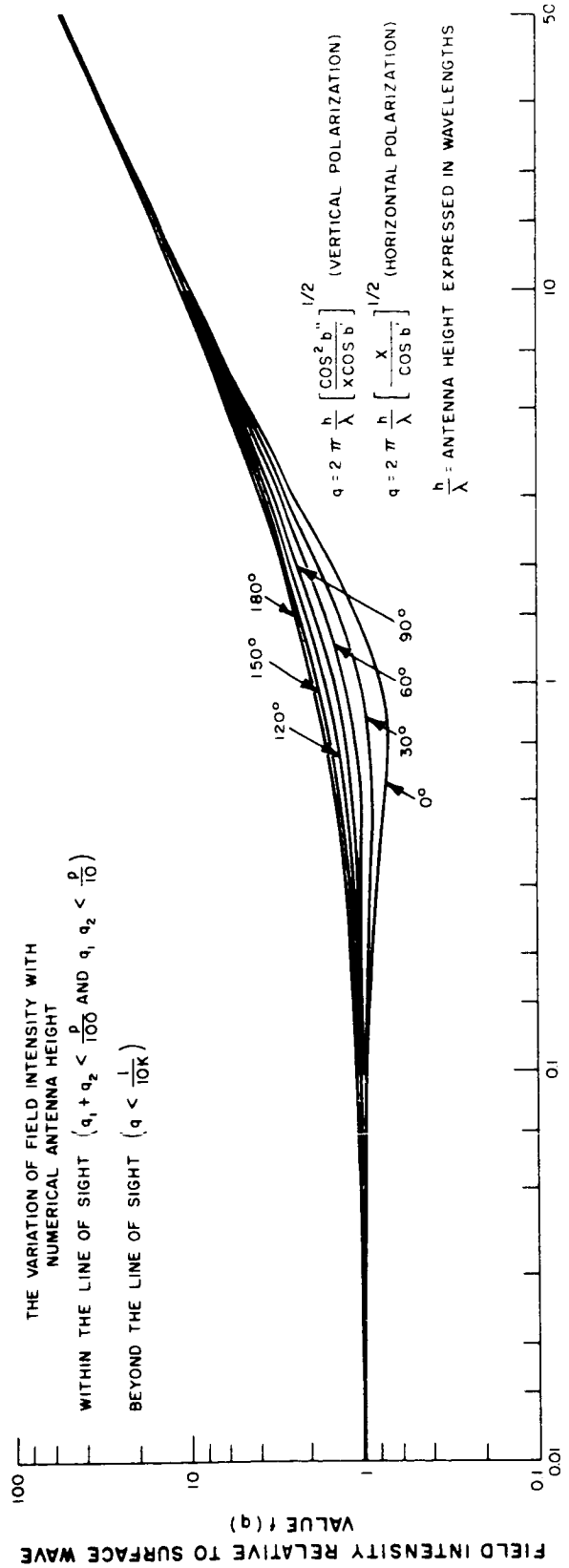

Figure II. 2-4. The Variation of Field Intensity With Numerical Antenna Height for Low Antennas

found to be $1/2p$. Similarly, for the values of q greater than 20, the value of $f(q) = q$. When these are introduced into Equation (II.1-3),

$$\frac{E_{cs_o}}{E_o \sqrt{d}} = 2\left(\frac{1}{2p}\right)(q_1)(q_2) \qquad \text{(II.2-34a)}$$

$$\frac{\left[\frac{2\pi h_1}{\lambda} \angle T\right]\left[\frac{2\pi h_2}{\lambda} \angle T\right]}{\frac{\pi d}{\lambda} \angle T^2} \frac{4\pi h_1 h_2}{\lambda d} \qquad \text{(II.2-34b)}$$

which is the basis for the nomographs developed by Bullington. However, the lunar-surface parameters are such that the antennas under consideration in this analysis would have mean values which range from 0.1 to 1.0 of Bullington's minimum effective values. The error introduced by use of his nomographs would fall within the 3- to 5-db range.

When the value of $d \gg h$, the spherical surface can no longer be approximated by a flat plane. However, another corrective factor could be introduced into Equation (II.2-3) to compensate for the dispersive losses introduced.

$$\frac{E_{cs_o}}{E_o \sqrt{d}} = 2 A_o f(q_1) f(q_2) f(d/a) \qquad \text{(II.2-35)}$$

The shadow factor, $f(d/a)$, is thus the correction that could be introduced by the dispersion factor, D, which would be introduced as $D\bar{R}$ in place of $\bar{R}$ in Equation (II.2-19). The actual value of D is a function of the radius of curvature, antenna heights, total distance, and distance to the reflection point. However, the antenna height in this case is the effective height above a reference plane at the point of reflection, such that the computation of the divergence factor is accomplished by a simultaneous covergence of the selected distance to the reflection point in relationship to the effective antenna height.

In an attempt to avoid this laborious calculation, the technique for computing the shadow factor as presented by Burrows was used. In this case, the effects of the surface electromagnetic properties are only approximated, but since the maximum shadow loss in the range of interest only amounted to about 1.3 db, any errors are considered to be insignificant. Burrows' shadow-factor curve is shown in Figure II.2-5, from which it is seen that the angular distance represented by 3200 meters on the moon is highly insignificant. Actually, over this distance the surface bulge of a smooth sphere

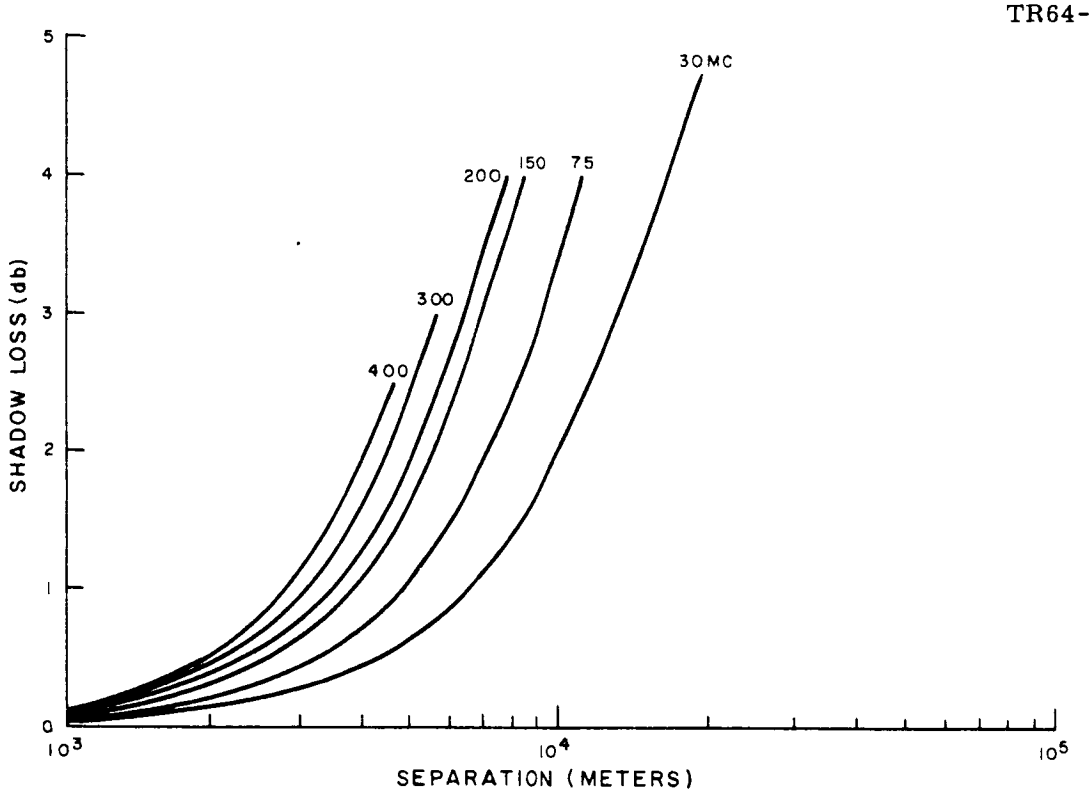

Figure II.2-5. Shadow Factor Loss Due to Spherical Surface

is of the order of 3 meters. It is actually expected that the terrain will produce greater bulges and will be the most predominant factor for the non-planar condition. Under these conditions, Equation (II.2-35) could be expressed as

$$A = \frac{E_{cs_o}}{E_o/d} = 2\,A_o\,f(q_1)\,f(q_2)\,f(d/a)\,f(H/d') \qquad \text{(II.2-36)}$$

Now Equation (II.2-36) can be inserted into Equation (II.2-13c), such that

$$L'_{sys} = L_{sys} + M + 20\log_{10}[2\,A_o\,f(q_1)\,f(q_2)\,f(d/a)\,f(H/d')]$$

$$= L_{sys} + M + 6.02 + 20\log_{10} A_o + F(q_1) + F(q_2) \qquad \text{(II.2-37a)}$$

$$+ F(d/a) + F(H/d') \qquad \text{(II.2-37b)}$$

which can be combined with Equation (II.2-12b), and by rearrangement, becomes

$$L'_{sys} = C_t + C_r + 6.02 + F(q_1) + F(q_2) + F(H/d')$$

$$+ F(d/a) + 20\log_{10} A_o + L_{trans} \qquad \text{(II.2-38)}$$

Equation (II.2-38) presents the propagation losses which can determine the carrier power level at the receiver terminals in terms of the transmitter power output, through application of Equation (II. 2-7) or (II.2-8). However, this is still not a convenient factor for performance evaluation. The performance of a communication link is actually dependent upon the quality of the receiver output. This, however, is a function of the ratio of the receiver input carrier-to-noise power ratio. If the noise power remained constant over the frequency spectrum being investigated, the system loss would be the criterion for evaluation. Since this is not the case, the noise aspect must be investigated.

The input carrier-to-noise ratio at the receiver terminals is a figure of merit which can be expressed by

$$\left(\frac{C}{N}\right)_{in} = \frac{p_r}{k\, t_e\, bw\, f_n} = \frac{p_r}{k\, t_o\, bw\, f_b} \qquad \text{(II.2-39)}$$

or in decibels,

$$\left[\frac{C}{N}\right]_{in} = P_r - K - T_o - BW - F_b \qquad \text{(II.2-40a)}$$

When Equation (II.2-40a) is normalized for a transmitter power output of 1 watt and a receiver predetection-bandwidth of 1 kilocycle per second, then, by applying Equation (II.2-8),

$$\left[\frac{C}{N}\right]_{in} = -L'_{sys} + 204 - 30 - F_b = 174 - L'_{sys} - F_b \qquad \text{(II.2-40b)}$$

However, F_b is frequency sensitive and contains F_n. Figure II.2-6 demonstrates the sensitivity of F_n for certain vacuum tubes. Although these tubes would not necessarily be used for this application, it is expected that the actual noise figure for the receiver will be close to that for the 6J4 tube when referenced to a test temperature of 288.39 degrees K.

The value of F_b can be obtained by the process given by Vogler;

$$f_b = f_e - 1 + f_c + \ell_c (f_t - 1) + \ell_c \ell_t (f_n - 1) \qquad \text{(II.2-41)}$$

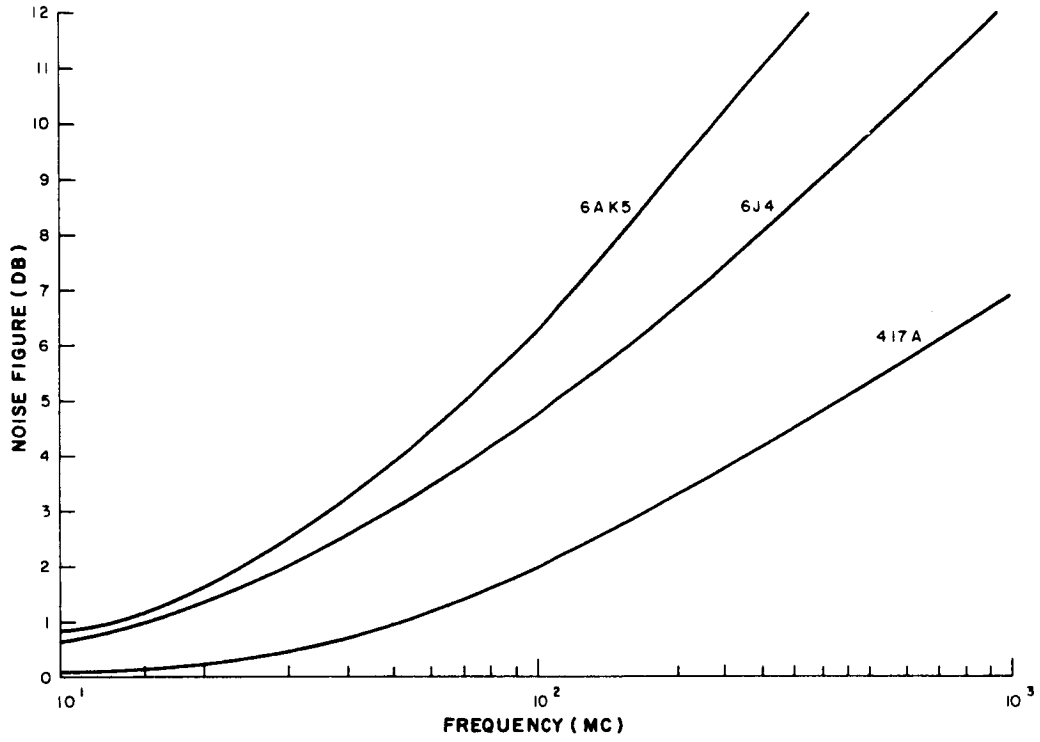

Figure II. 2-6. Typical Noise Figure of Vacuum Tubes

The values of $F_e = 10 \log_{10} f_e$ can be obtained by the relationship of $P_e = 10 \log_{10} k t_b bw$, for which the values of t_b are shown in Figure II. 2-7. Then, by use of the following relationships,

$$f_c = 1 + (\ell_c - 1)(t_c / t_o) \qquad \text{(II. 2-42)}$$

$$f_t = 1 + (\ell_t - 1)(t_t / t_o) \qquad \text{(II. 2-43)}$$

which, when introduced into equation (II. 2-41)

$$f_b = f_e + (\ell_c - 1)(t_c / t_o) + \ell_c (\ell_t - 1)(t_t / t_o) + \ell_t \ell_t (f_n - 1) \qquad \text{(II. 2-44a)}$$

when the value of $t_e = t_t = 463$ degrees K, and $t_o = 288.39$ degrees K, Equation (II. 2-44a) reduces to

$$f_b = f_e + \ell_c \ell_t (f_n + 0.6) - 1.6 \qquad \text{(II. 2-44b)}$$

To evaluate this, it is necessary to at least approximate the loss characteristics of the antenna, feedline, multiplexer, and connectors.

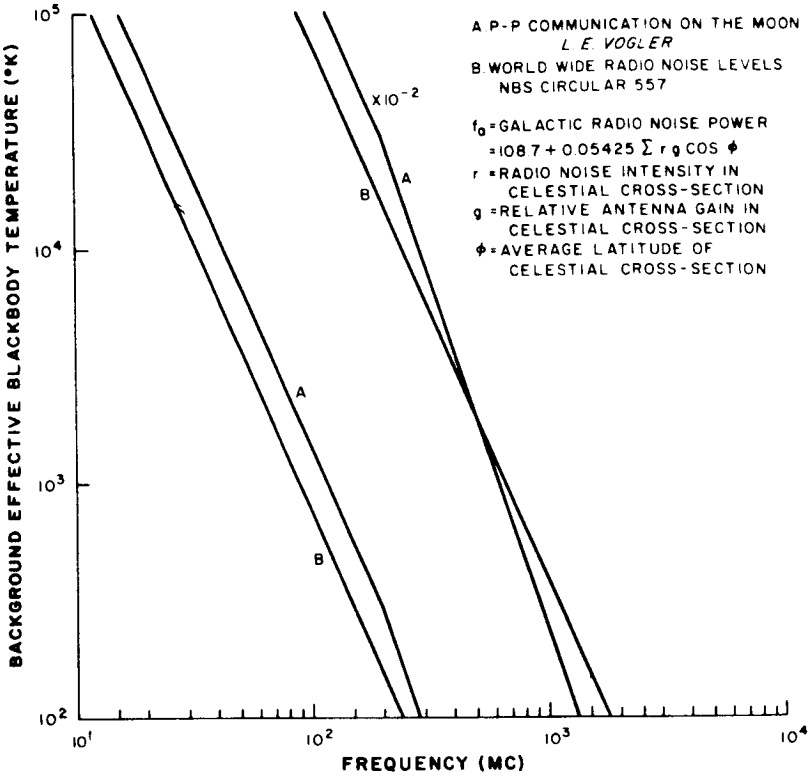

Figure II. 2-7. Background Effective Black Body Temperature

Now, Equations (II. 2-38) and (II. 2-40c) can be combined to give

$$\left[\frac{C}{N}\right]_{1n} = 174 + \left\{[(C_t + C_r) + 6.02 + F(q_1) + F(q_2) - F_b] - F(H/d') \right. \qquad \text{(II. 2-45)}$$

$$\left. - [F(d/a) + 20 \log_{10} A_o + L_{trans}] \right\} - M$$

with the composite lunar-propagation losses exemplified by the quantity in the braces, and tabulated in Table II. 2-1. The value of Equation (II. 2-45) is plotted in Figure II. 2-8 with no margin and for the specific antenna heights of h_1 = 15 meters and h_2 = 3.75 meters, and F (H/d') = 0, the condition for smooth terrain.

The results of the propagation analyses indicate a frequency reference in the region of 140 megacycles per second for the smooth terrain condition. Now, it is necessary to consider variations in surface contour and antenna heights.

To determine the diffraction loss due to terrain irregularity, F (H/d'), a simplified technique utilizing a nomograph from Bullington (Reference 6) was adopted and is shown in Figure II. 2-9. Although the derivation of this nomograph has not been verified, it is assumed that the derivation is related to optical considerations which do not account for the surface constituency. However, typical values are given in Table II. 2-1 for a particular type of hill.

TABLE II. 2-1

COMPOSITE LUNAR PROPAGATION LOSSES

Frequency (mc/s)		30		75		150		200		250		300		400	
Polarization		h	v	h	v	h	v	h	v	h	v	h	v	h	v
Transmitting Antenna		- 0.94	+ 0.80	- 1.05	+ 0.66	- 1.20	+ 0.47	- 1.28	+ 0.36	- 1.35	+ 0.27	- 1.41	+ 0.19	- 1.51	+ 0.02
Receiving Antenna		- 0.53	+ 1.25	- 0.55	+ 1.23	- 0.59	+ 1.20	- 0.62	+ 1.15	- 0.64	+ 1.13	- 0.65	+ 1.11	- 0.69	+ 1.07
Half-Space		+ 6.02	+ 6.02	+ 6.02	+ 6.02	+ 6.02	+ 6.02	+ 6.02	+ 6.02	+ 6.02	+ 6.02	+ 6.02	+ 6.02	+ 6.02	+ 6.02
Height Gain (t)		+ 5.38	+ 4.43	+ 8.39	+ 7.57	+12.43	+11.60	+14.52	+13.70	+16.26	+15.43	+17.73	+16.89	+20.10	+19.28
Height Gain (r)		+14.14	+13.05	+18.94	+18.06	+23.93	+23.08	+26.23	+25.40	+28.08	+27.24	+29.60	+28.79	+32.06	+31.23
Noise Environment		-18.11	-18.13	-10.11	-10.27	- 7.81	- 8.16	- 8.19	- 8.62	- 8.74	- 9.34	- 9.82	-10.44	-10.44	-11.00
Obstacle Diffraction		-16.00	-16.00	-20.00	-20.00	-23.00	-23.00	-24.20	-24.20	-25.00	-25.00	-25.80	-25.80	-26.80	-26.80
Subtotal		-10.04	-10.18	+ 1.64	+ 1.95	+ 9.79	+10.27	+12.48	+13.09	+14.63	+15.40	+16.15	+17.38	+18.74	+19.82
d = 320m	Planar	-33.64	-31.86	-36.62	-35.02	-41.06	-39.38	-43.62	-41.58	-44.88	-46.36	-46.24	-44.66	-48.06	-47.00
	Free Space	-52.09	-52.09	-60.05	-60.05	-66.07	-66.07	-68.57	-68.57	-70.51	-70.51	-72.09	-72.09	-74.59	-74.59
	Total	95.77	94.13	95.03	93.12	97.34	95.18	99.71	97.06	100.76	98.47	102.18	99.37	103.91	101.77
640	Planar	-39.56	-37.64	-42.32	-40.74	-46.73	-45.26	-48.95	-47.29	-50.76	-49.07	-52.26	-50.60	-54.08	-53.02
	Free Space	-58.11	-58.11	-66.07	-66.07	-72.09	-72.09	-74.59	-74.59	-76.53	-76.53	-78.11	-78.11	-80.62	-80.62
	Total	107.71	105.93	106.75	104.86	109.03	107.08	111.06	108.79	112.66	110.20	114.22	111.33	115.96	113.82
960	Shadow	- 0.01	- 0.01	- 0.02	- 0.02	- 0.04	- 0.04	- 0.07	- 0.67	- 0.08	- 0.08	- 0.10	- 0.10	- 0.12	- 0.12
	Planar	-42.84	-40.84	-45.78	-44.26	-50.26	-48.59	-52.48	-50.81	-54.28	-52.60	-55.78	-54.12	-57.60	-56.54
	Free Space	-61.44	-61.44	-69.40	-69.40	-75.42	-75.42	-77.92	-77.92	-79.86	-79.86	-81.44	-81.44	-83.94	-83.94
	Total	114.33	112.47	113.56	111.73	115.93	112.78	117.99	115.71	119.51	117.14	121.17	118.28	122.92	120.78
1280	Shadow	- 0.03	- 0.03	- 0.06	- 0.06	- 0.11	- 0.11	- 0.15	- 0.15	- 0.17	- 0.17	- 0.20	- 0.20	- 0.23	- 0.23
	Planar	-45.24	-43.28	-48.28	-46.50	-52.75	-51.09	-54.97	-53.31	-56.78	-55.09	-58.28	-56.62	-60.10	-59.04
	Free Space	-64.13	-64.13	-72.09	-72.09	-78.11	-78.11	-80.61	-80.61	-82.55	-82.55	-84.13	-84.13	-86.63	-86.63
	Total	119.44	117.62	118.69	116.70	121.18	119.04	123.25	120.98	124.87	122.41	126.46	123.57	128.23	126.08
1600	Shadow	- 0.08	- 0.08	- 0.12	- 0.12	- 0.20	- 0.20	- 0.24	- 0.24	- 0.28	- 0.28	- 0.33	- 0.33	- 0.35	- 0.35
	Planar	-47.17	-45.22	-50.22	-48.52	-54.70	-53.02	-56.92	-55.26	-58.72	-57.04	-60.22	-58.56	-62.04	-60.98
	Free Space	-66.07	-66.07	-74.03	-74.03	-80.05	-80.05	-82.55	-82.55	-84.49	-84.49	-86.07	-86.07	-88.57	-88.57
	Total	123.36	121.56	122.73	120.72	125.16	123.00	127.23	124.96	128.86	126.41	130.47	127.59	132.22	130.08
3200	Shadow	- 0.30	- 0.30	- 0.48	- 0.48	- 0.69	- 0.70	- 0.85	- 0.87	- 0.90	- 0.95	- 0.97	- 1.04	- 1.20	- 1.28
	Planar	-53.19	-51.24	-56.24	-54.54	-60.72	-59.04	-62.94	-61.28	-64.74	-63.06	-66.24	-64.58	-68.06	-67.00
	Free Space	-72.09	-72.09	-80.05	-80.05	-86.07	-86.07	-88.57	-88.57	-90.61	-90.51	-92.09	-92.09	-94.59	-94.59
	Total	135.92	133.81	135.13	133.12	137.69	135.54	139.88	137.63	141.82	139.22	143.15	140.33	145.11	143.05

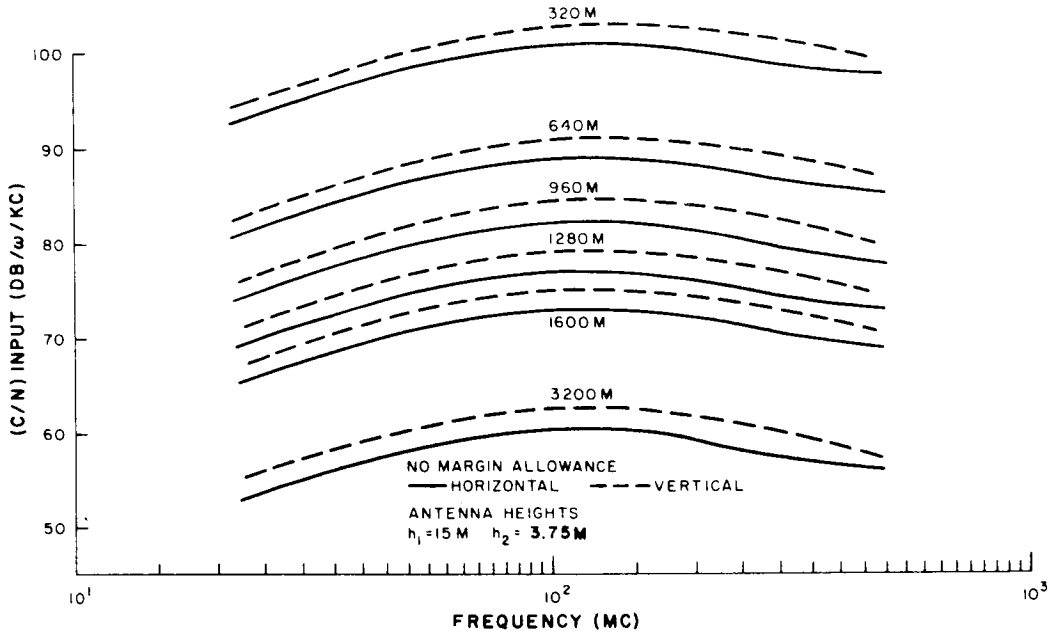

Figure II. 2-8. Lunar Propagation Performance (smooth terrain)

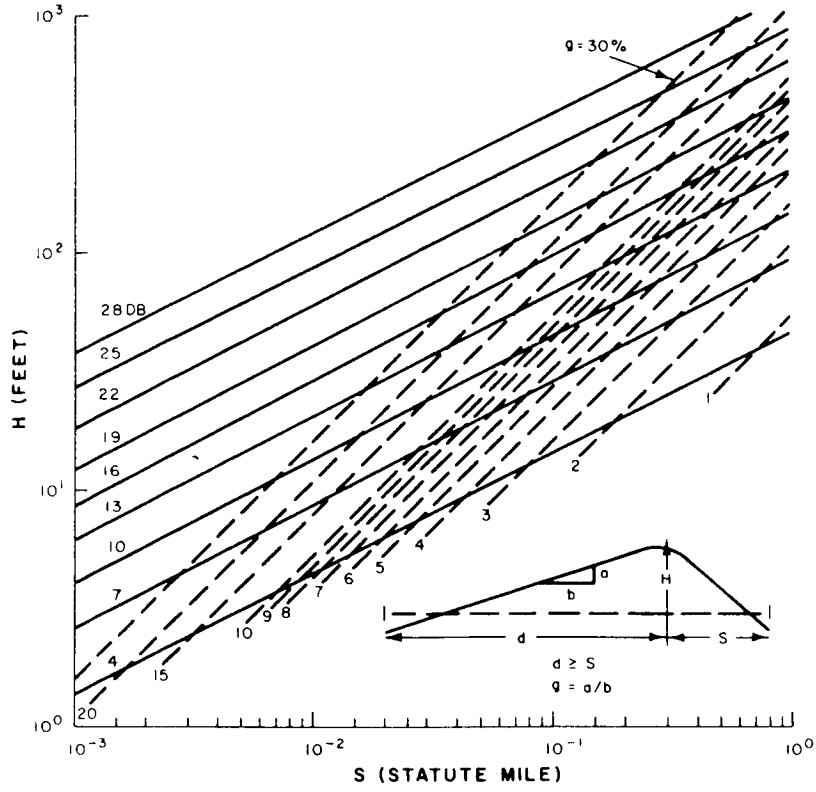

Figure II. 2-9. Obstacle Diffraction Loss (F = 150 mc.)

Variations in height gain for the antennas are shown in Figures II. 2-10 and II. 2-11, where the latter is applicable to the 150-Mc frequency only. However, a change in antenna height is obtained only by changing the length of the feedlines, which affects the values of ℓ_t in Equation (II. -41), and the value of L_{feed} in Equation (II. 2-12a). Since these are physical values, they cannot be introduced until the antenna characteristics are fully determined.

Finally, it is difficult to determine the value to be assigned for M, due to the statistical nature of the variables it should cover. The tolerances to be allocated for M requires additional analysis.

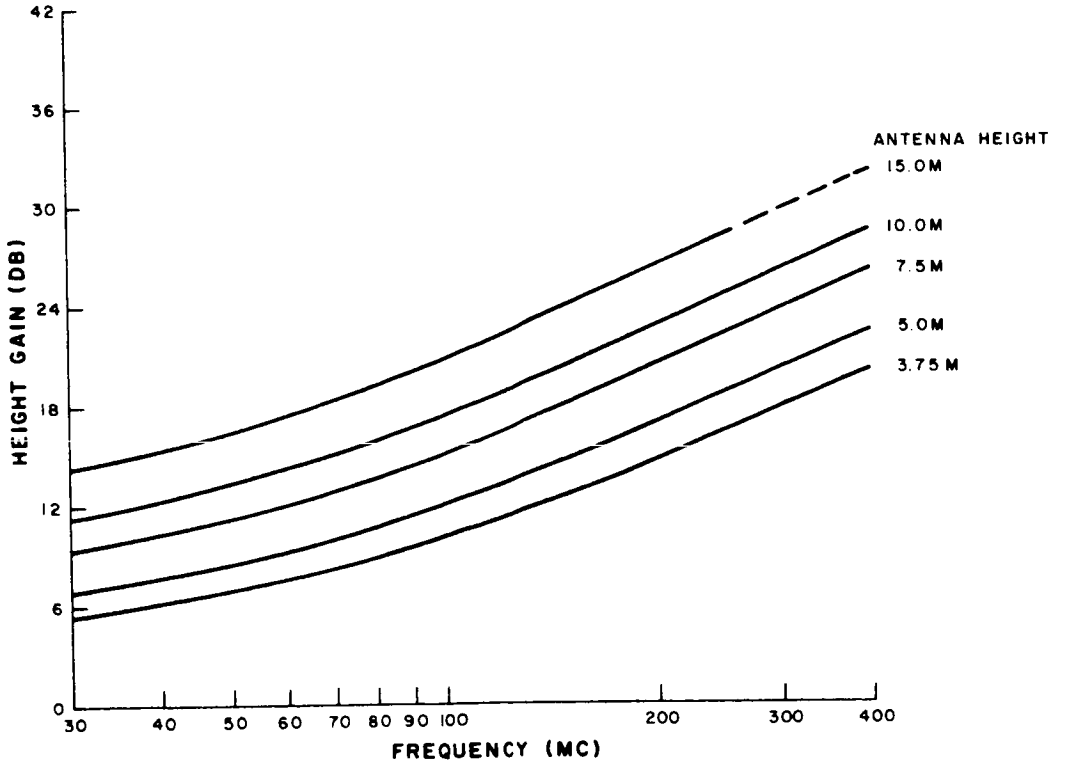

Figure II. 2-10. Height Gain Variations Horizontal Polarization

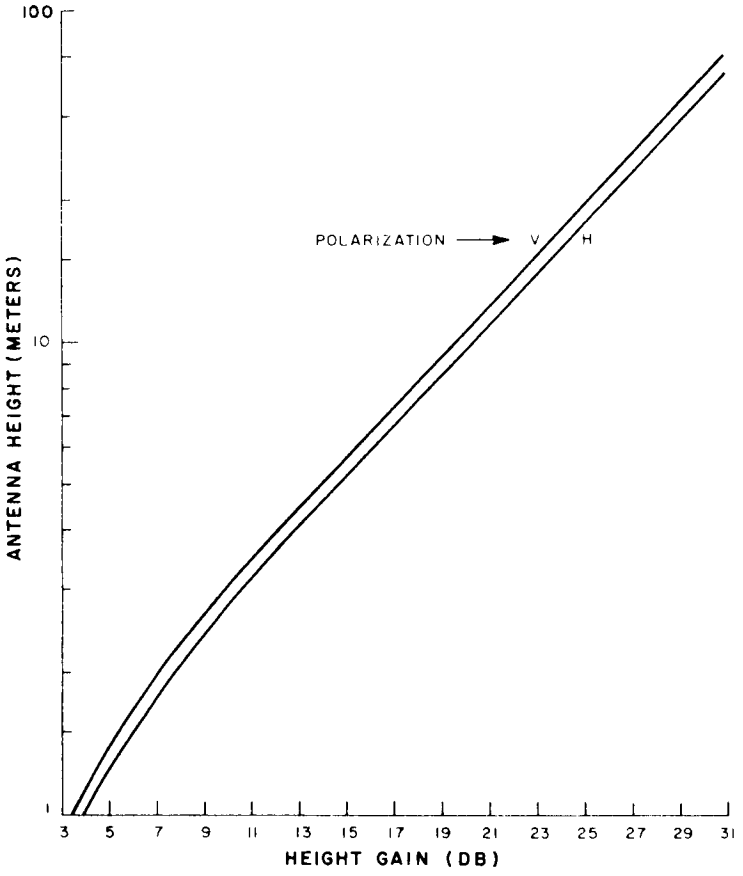

Figure II. 2-11. Antenna Height Gain (150 Mc)

4. References

Sommerfeld, A.

1. Ann. der Phys., vol. 4, no. 28, pp. 665-756; March (1909)
"Uber die Ausbreitung der Wellen der drahtlosen telegraphie,"

11. Jahr. der drahtlosen Tel., vol. 4, p. 157 (1910)
"Ausbreitung der Wellen in der drahtlosen Telegraphie. Einfluss der Bodenbeschaffenheit auf gerichtete and ungerichtete wellenauge."

Watson, G. N.

2. Proc. Roy. Soc. (London), A, vol. 95, pp. 83-99; October 7 (1918)
"The diffraction of electric waves by the earth"

12. Proc. Roy. Soc. (London), A, vol. 95, pp. 546-563; July 15 (1919)
"The transmission of electric waves around the earth"

von der Pol, B. and Bremmer, H.

3. Phil. Mag., vol. 24, pp. 141-176; July (1937), Part I

4. Phil. Mag., vol. 25, pp. 825-864; supplement, November (1937), Part II
"The diffraction of electromagnetic waves from an electrical point source round a finitely conducting sphere, with applications to radiotelegraphy and the theory of the rainbow."

5. Phil. Mag., vol. 25, 817-834; June (1938)
"The propagation of radio waves over a finitely conducting spherical earth"

13. Phil. Mag., vol. 27, pp. 261-275; March (1939)
"Further note on the propagation of radio waves over a finitely conducting spherical earth"

Bullington, K.

6. Proc. I.R.E., vol. 35, no. 10, pp. 1122-1136; October (1947)
"Radio propagation at frequencies above 30 megacycles"

14. Bell Sys. Tech. Jour., vol. 36, no. 3, pp. 593-626; May (1957)
"Radio propagation fundamentals"

Burrows, C. R.

15. Bell Sys. Tech. Jour., vol. 16, no. 1, pp. 45-75; January 1937
"Radio propagation over plane earth - field stength curves"

7. NDRC Summary Technical Report of the Committee on Propagation, Vol. 3; (1945)
"The propagation of radio waves through the standard atmosphere"

Burrows, C. R. and Gray, M. C.

16. Proc. I.R.E., vol. 29, no. 1, pp. 16-24; January 1941
"The effect of the earth's curvature on ground-wave propagation"

10. Kraus, J. D., Antennas, McGraw Hill, New York, 1950

Norton, K. A.

17. Proc. I.R.E., vol. 24, no. 10, pp. 1367-1387; October (1936), Part I
Proc. I.R.E., vol. 25, no. 9, pp. 1203-1236; September (1937), Part II
"The propagation of radio waves over the surface of the earth and in the upper atmosphere"

8. Proc. I.R.E., vol. 29, no. 12, pp. 623-639; December (1941)
"The calculation of ground wave field intensity over a finitely conducting spherical earth"

Vogler, L. E.

9. Jour. of Resea. NBS, vol. 67D, no. 1, pp. 5-21, Jan.-Feb. (1963)
"Point-to-point communication on the moon"

5. Glossary of Terms

a	-	mean equatorial radius of curvature for the spherical surface (1,738 kilometers for the moon)	Equation (II. 2-35)
A	-	propagation-loss factor introduced by the interposition of a finitely conductive, spherical surface	Equation (II. 2-14)
A_o	-	propagation-loss factor introduced by the interposition of a finitely conductive, planar surface	Equation (II. 2-32)
b	-	approximate angular relationship for the surface dissipation factor applicable to zero-height antennas	Equation (II. 2-20)
b_v	-	angular relationship for vertically polarized antennas	Equation (II. 2-29a)
b_h	-	angular relationship for horizontally polarized antennas	Equation (II. 2-29b)
bw	-	predetection bandwidth of the receiver (cycles per second)	Equation (II. 2-39)
B	-	same as b except for finite antenna heights	Equation (II. 2-18b)
BW	-	$10 \log_{10}$ bw	Equation (II. 2-40a)
c	-	velocity of propagation of electromagnetic energy in free space (2.99793×10^8 meters per second)	Equation (II. 2-2)

$C_{r,t}$	- composite gain and loss figure for the antenna in the radial direction of interest with respect to the receiver (transmitter)	Equation (II. 2-12b)
$\left(\frac{C}{N}\right)_{in}$	- carrier-to-noise ratio at the input terminals of the receiver	Equation (II. 2-39)
$\left[\frac{C}{N}\right]_{in}$	- $10 \log_{10} (C/N)_{in}$	Equation (II. 2-40a)
d	- separation between antennas measured along the reference surface (meters)	Equation (II. 2-11)
d'	- separation between the antenna and the peak of a terrain obstacle; measured along the reference surface	Figure (II. 2-9)
E	- intensity of the electric component of the Poynting vector	Equation (II. 2-1)
E_{cs}	- electric-field intensity when a conductive surface is interposed	Equation (II. 2-14)
E_{cs_o}	- electric-field intensity due only to surface-wave propagation	Equation (II. 2-31)
E_{fs}	- electric-field intensity under free-space conditions	Equation (II. 2-14)
E_o	- electric-field intensity at a unit distance from the antenna	Equation (II. 2-16c)
$E_{r_{1,2,3}}$	- electric-field intensity due to propagation along path 1 (2 or 3)	Equation (II. 2-16), (II. 1-17), (II. 2-18)
E_{t_r}	- effective radiated-field intensity at the transmitting antenna	Equation (II. 2-15)
$E_{t_{r_a}}$	- effective radiated-field intensity along a radial from the transmitting antenna	Equation (II. 2-15)
f	- rate of sinusoidal alternative of the electric field as it passes a given point (cycles per second)	Equation (II. 2-2)

f_b	-	noise factor for the composite noise background	Equation (II. 2-39a)
f_c	-	noise factor for the circuit elements of the receiving antenna	Equation (II. 2-42)
f_e	-	noise factor for the portion of the background noise that is external to the antenna	Equation (II. 2-41)
f_n	-	noise factor for the portion of the background noise that is internal to the receiver	Equation (II. 2-39)
f_t	-	noise factor for the transmission facilities between the receiver and the antenna elements	Equation (II. 2-43)
f(d/a)	-	shadow loss factor due to spherical surface	Equation (II. 2-35)
f(H/d')	-	diffraction loss factor due to surface perturbations	Equation (II. 2-36)
$f(q_{1,2})$	-	height gain factor due to non-zero antenna heights	Equation (II. 2-33)
F_b	-	$10 \log_{10} f_b$	Equation (II. 2-40a)
F_e	-	$10 \log_{10} f_e$	
F_{mc}	-	value of f expressed in megacycles per second	Equation (II. 2-11)
F(d/a)	-	$10 \log_{10} f\ (d/a)$	Equation (II. 2-37b)
F(H/d')	-	$10 \log_{10} f\ (H/d')$	Equation (II. 2-37b)
$F(q_{1,2})$	-	$10 \log_{10} f\ (q_{1,2})$	Equation (II. 2-37b)
$G_{r,t}$	-	directionality gain of the receiving (transmitting) antenna in the equatorial plane (decibels)	Equation (II. 2-9)

$h_{1,2}$	- physical height of the maximum current position of the antenna with respect to the reference plane (meters)	Equation (II. 2-22)
H	- physical height of the terrain obstacle above the plane referencing the antenna heights	Equation (II. 2-36)
H	- intensity of the magnetic component of the Poynting vector	Equation (II. 2-1)
i	- term of a series	Equation (II. 2-18a)
j	- imaginary designator ($\sqrt{-1}$)	Equation (II. 2-1)
k	- Boltzmann's constant (1.38×10^{-23} joules/°K)	Equation (II. 2-39)
K	- $10 \log_{10} k$	Equation (II. 2-40)
ℓ_c	- loss factor for the circuit elements of the receiving antenna	Equation (II. 2-41)
ℓ_t	- loss factor for the transmission facilities between the receiver and the antenna elements	Equation (II. 2-41)
ℓ_{sys}	- loss factor for the transmission path between transmitting and receiving antennas	Equation (II. 2-7)
L'_{feed}	- loss figure for the transmission facilities between the transmitter and the antenna elements (decibels)	Equation (II. 2-9a)
L''_{feed}	- $10 \log_{10} \ell_t$	Equation (II. 2-9b)
L_{sys}	- loss figure for the system between the transponder and receiver terminals under free-space conditions (decibels)	Equation (II. 2-8)
L'_{sys}	- loss figure for the system between the transmitter and receiver terminals when a conductive surface is interposed (decibels)	Equation (II. 2-13a)
L'_{vswr}	- loss figure due to impedance mismatch between the transmitter and the propagating medium (decibels)	Equation (II. 2-9a)

L''_{vswr}	- loss figure due to impedance mismatch between the propagating medium and the receiver (decibels)	Equation (II. 2-9b)
M	- safety figure to accommodate statistical variation (decibels)	Equation (II. 2-13c)
$\bar{n}$	- index of refraction at the interface between two media	Equation (II. 2-3)
p	- a "numerical" distance for normalizing to zero height antennas	Equation (II. 2-21)
p_r	- available signal power at the receiver terminals (watts)	Equation (II. 2-7)
p_t	- available signal power at the transmitter terminals (watts)	Equation (II. 2-7)
P	- a "numerical" distance for non-zero antenna heights	Equation (II. 2-18b)
P_r	- $10 \log_{10} p_r$	Equation (II. 2-8)
P_t	- $10 \log_{10} p_t$	Equation (II. 2-8)
P_{r_r}	- available radiated signal power at the receiving antenna (watts)	Equation (II. 2-9b)
P_{t_r}	- available radiated signal power at the transmitting antenna (watts)	Equation (II. 2-9a)
$q_{1,2}$	- a "numerical" height for non-zero height transmitting (receiving) antenna	Equation (II. 2-22)
$r_{1,2}$	- propagation distance for the direct (indirect) path	Equation (II. 2-16a) (II. 1-17a)
$R_{v,h}$ $\rightarrow$	- ratio of the amplitude of the reflected energy to the incident energy for vertical (horizontal) polarization	Equation (II. 2-3) (II. 1-4)
$\bar{R}$	- vector ratio of the reflected energy to the incident energy $(= Re^{j\phi})$	Equation (II. 2-20)

t_b	- ambient background noise temperature (°Kelvin)	
t_o	- reference noise temperature (288.39°K)	Equation (II.2-39)
T_o	- $10 \log_{10} t_o$	
$T_{v,h}$	- numerical function of the surface electromagnetic properties for vertical (horizontal) polarization	Equation (II.2-23)
γ_o	- phase relationship of the carrier frequency at the reference time	Equation (II.2-16a)
Δ	- incremental change of loss elements due to the proximity of the conducting surface	Equation (II.2-13a)
ϵ	- medium relative permittivity	Equation (II.2-1)
$\epsilon_{e,m}$	- complex dielectric factor for an electric (magnetic) moment	Equation (II.2-24) (II.2-25)
ϵ_o	- permittivity of free space $(36\pi \times 10^9)^{-1}$	Equation (II.2-5)
ϵ'_o	- complex dielectric constant for the specific medium	Equation (II.2-26)
$\epsilon_{r_{1,2}}$	- relative permittivity of each medium at the interface with respect to free space	Equation (II.2-6a)
η	- intrinsic impedance of the medium	Equation (II.2-1)
θ	- residual phase delay due to propagation along the interface of the two media	Equation (II.2-18)
λ	- physical distance separating phase fronts of 2π radians differential (meters)	Equation (II.2-2)
μ	- relative permeability of the medium with respect to free space	Equation (II.2-1)
π	- the time taken for a simple harmonic motion to reach its opposite extreme position (3.14159.....)	Equation (II.2-2)

σ	-	conductivity of any medium (mho/meter)	Equation (II. 2-1)
σ_o	-	conductivity of free space	Equation (II. 2-5)
σ_2	-	conductivity of the reflective surface (mho/mtr)	Equation (II. 2-6a)
$\phi_{v,h}$	-	phase delay at the interface due to reflection for a vertical (horizontal) incident wave	Equation (II. 2-3) (II. 2-4)
ψ_α	-	angular relation of the radial propagation direction in the elevation plane	Equation (II. 2-3)
$\psi_{1,2}$	-	angular relation for the direct (indirect) path	Equation (II. 2-16a) (II. -17a)
ω	-	angular rate of rotation of the carrier (radians/second)	Equation (II. 2-1)
t_o	-	equivalent noise temperature (°Kelvin)	Equation (II. 2-39)

B. ANALYSIS OF DIRECT SLRV-TO-EARTH AND EARTH-TO-SLRV COMMUNICATIONS LINKS

1. Introduction

This discussion is primarily an analysis of the direct SLRV-to-Earth communications link, to determine the gain required for S-band antenna to be placed on SLRV, assuming the SLRV S-band transmitter has a power output of 2.5 watts. This value of 2.5 watts is selected as the maximum that could be tolerated from a primary power and weight standpoint.

2. SLRV-to-Earth Link Analysis

Since the Earth DSIF sites may consist of 85-foot-diameter antennas and parametric amplifier combinations (Canberra and Johannesburg), as well as a 210-foot-antenna and maser combination (Goldstone), both cases have been considered in this analysis.

Power Gain and Pointing Loss for DSIF Antennas

The key references used for review of these parameters were:

(1) JPL Space Program Summary 37-19, Vol. III, dated January 1963, titled "DSIF".

(2) JPL Technical Report 32-260, dated July 1962, titled "Constraints in Space Telecommunication Systems."

Reference (1) presents a plot of power gain as a function of surface error for both 85-foot and 210-foot antennas as Figure 1 on page 38 for 2300 Mc and aperture efficiency of 0.75. Reference (2) plots power gain as a function of frequency for 85-foot and 250-foot antennas for rms-surface-error-to-diameter ratios of 1.5×10^{-4} and 2.5×10^{-4}. The curve for a 210-foot antenna was added to this figure, as well as the comparisons of Table II.2-2, observed for the 2300-Mc case.

Accordingly, these references agree within about 0.5 db for the 85-foot case and 1.4 db for the 210-foot case. These values are close enough so it can be argued that the curves should coincide and the differences noted are due to drafting or printing errors. The most significant difference between the two references is contained in the following quotes.

SPS 37-19 states: "It is still considered that the rms surface error for Precision 1 environment should not be allowed to exceed 0.25 inches" (The Precision 1 environment refers to level of wind velocity). Using this 0.25-inch value with Figure 1 of 37-19

TABLE II. 2-2

COMPARISON OF PARAMETERS FOR AN 85-FOOT DISH ANTENNA AND A 210-FOOT DISH ANTENNA, BOTH AT 2300 MC

Antenna	RMS Surface Error to Diameter Ratio	RMS Surface Error (inches)	Gain (db) from Reference	
			SPS 37-19	TR 32-260
85-foot Dish	1.5×10^{-4}	0.153	54	53.6
	2.5×10^{-4}	0.255	53	52.4
210-foot Dish	1.5×10^{-4}	0.378	59	57.6
	2.5×10^{-4}	0.630	51.4	50.0

results in gains of 53 db for the 85-foot dish and 61 db for the 210-foot dish. Note, the 0.25 inch implies a distortion/diameter ratio of 9.9×10^{-5} for the 210-foot dish.

In contrast, TR 32-60 states: ".....a practical gain limit of approximately 60 db is reached due to these factors". (These factors include distortions due to wind and thermal loads, plus gravitational variations across the surface of the dish as it is moved to different positions.)

Even if the more optimistic value of 0.25 inch rms distortion is used, it should be noted that this relates to a 68% probability value (assuming a Gaussian distribution of surface irregularities). This can be restated to say that there is a probability of only 0.68 that the surface error will not exceed this 1σ (or rms) distortion value. Similarly, the probability that the gain will be maintained at 61 db is only 0.68. If it is desirable to use a value of gain which will be met or exceeded with a probability of 0.90, a distortion value of $1.65\ \sigma$, or 0.41-inch, should be used; this corresponds to gains of 58.3 db for the 210-foot dish and 50.4 db for the 85-foot dish. The 59-db value used in the previous analysis corresponds to a surface error (from SPS 37-19) of 0.378 inch or $1.51\ \sigma$ and is equivalent to an 87% probability level. Figure II. 2-12 depicts the data discussed.

Based on the foregoing discussion, it is recommended that the set of gain values given in Table II. 2-3 be used (these are essentially those of SPS 37-19).

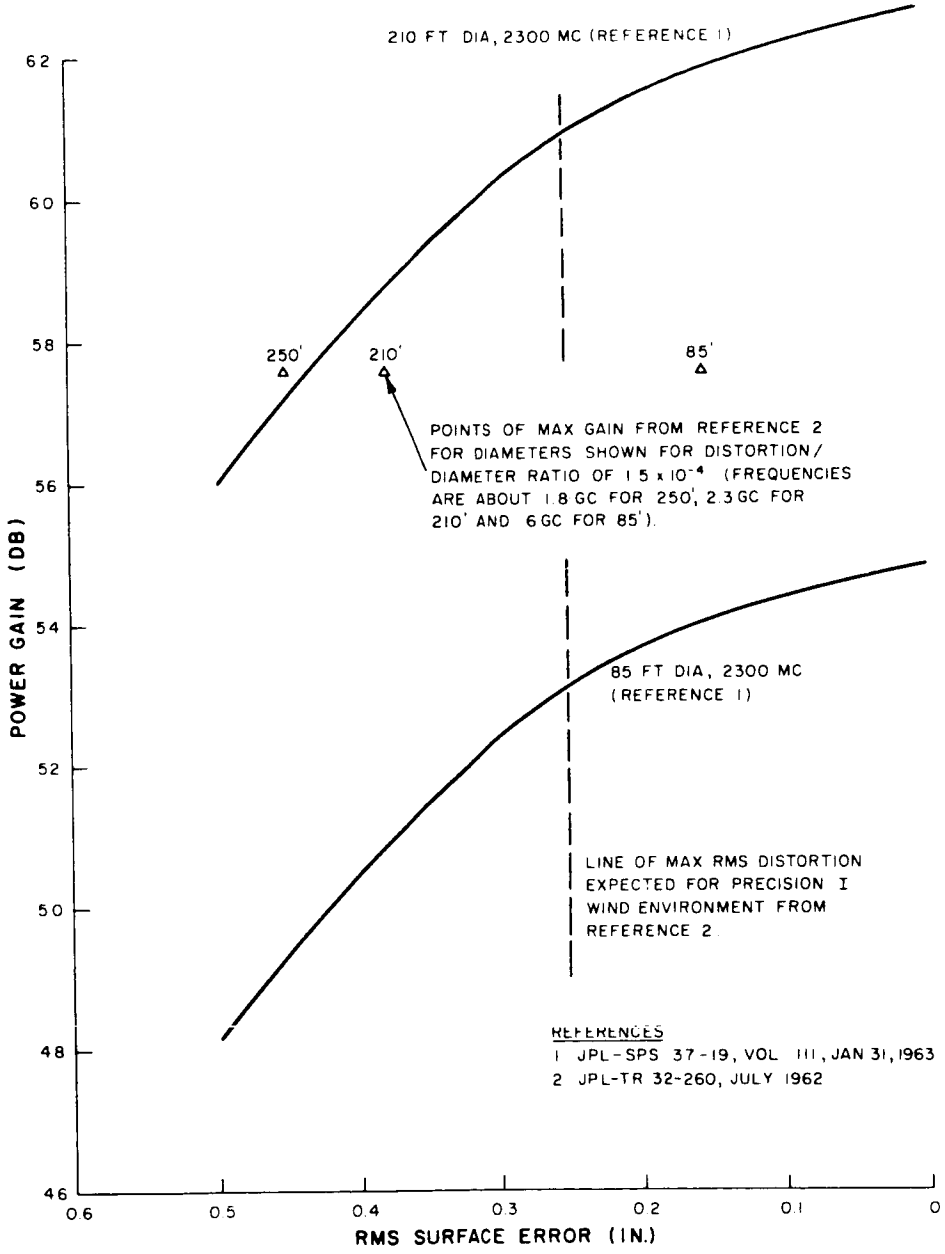

Figure II. 2-12. Antenna Gain vs. Surface Deformations

TABLE II. 2-3

RECOMMENDED SET OF GAIN VALUES FOR USE WITH 85-FOOT AND 210-FOOT DIAMETER DISH ANTENNAS

Probability that Value of Gain will be Achieved	Corresponding Values of Gain (db)	
	85-foot Diameter Dish Antenna	210-foot Diameter Dish Antenna
50% (Mean)	54.6	62.6
68% (1σ)*	53.0	61.0
80% (1.3σ)	52.0	60.0
90% (1.65σ)	50.3	58.3
95% (2σ)	48.0	56.0

*Equivalent to 0.25-inch surface irregularity

Separation of the SLRV and Surveyor vehicles on the surface of the moon is so small relative to the Earth-Moon range that these vehicles may be considered as one point within the 0.5° angle subtended by the moon as viewed from the earth. If gain values of 59 db and 51 db, respectively, are used for the 210-foot and 85-foot cases (probability between 80 and 90%), these correspond to 1-db beamwidths of 0.12° and 0.30°, using the basic 0.75 aperture efficiency value of SPS 37-19. From JPL Surveyor Project Control Document #6, "Surveyor Spacecraft/DSIF System Interface Requirements", July "63, the 1σ tracking accuracy anticipated for the 85-foot dish antenna is 0.14°. Assuming the same relationship-to-beamwidth can be achieved for the 210-foot unit, the pointing error losses would be as given in Table II. 2-4.

TABLE II. 2-4

COMPARISON OF POINTING LOSS OF ANTENNAS FOR VARIOUS DESIRED PERFORMANCE PROBABILITY LEVELS

Desired Performance Probability Level	Corresponding Pointing Loss (db) for Either Antenna
68% ($1\ \sigma$)	0.12 db
80% (1.3σ)	0.22 db
90% (1.65σ)	0.42 db
95% ($2\ \sigma$)	0.80 db

Receiving System Total Effective Noise Temperature

The key references used in review of this T_e parameter were as follows.

(1) JPL "Telecommunication Design Control Tables for Surveyor", dated Oct. 7, 1963.

(2) JPL Surveyor Project Control Document #6 "Surveyor Spacecraft/ DSIF System Interface Requirements" dated July 29, 1963.

(3) "Introduction to Radar Systems" McGraw Hill text authored by M. I. Skalnik.

A review of the data contained in the first two references plus calculations performed per the approaches given in the third reference have resulted in the selection of the following total system effective temperatures.

For Goldstone, where the use of a 210-foot dish antenna with a traveling-wave maser "front end" and parametric mixer is expected, the T_e should be 165°K (mean), with a standard deviation value of 27°K. This is based on the following.

	Mean Temperature	1σ Value
Maser plus circuit losses	55°K	10°K
Antenna temperature (full 3-db beamwidth pointed at moon)	110°K	25°K

This results in the total mean temperature of 165°K with $\sigma_e = \sqrt{\Sigma \sigma_n^2}$ or 27°K.

For the Canberra and Johannesburg sites, where the 85-foot dish antenna will be employed, none of the documents reviewed clarifies whether a maser or parametric amplifier will be used as the RF amplifier. Accordingly, both cases have been included in the following link analysis. The appropriate T_e values are as follows.

Maser RF Amplifier:

The value of T_e here is the same as the value of T_e for the 210-foot case previously discussed, because the entire beamwidth of interest will be pointed at the moon.

Parametric RF Amplifier:

The value of T_e in this case will be 380°K with a 1σ value of 56°K based on the following data.

	Mean Temperature	1 σ Value
Parametric Amplifier plus losses	270°K	50°K
Antenna Temperature	110°K	25°K

Summarizing these data and considering the different probability levels used previously results in the data given in Table II. 2-5.

TABLE II. 2-5

SUMMARY OF PARAMETER DATA FOR TOTAL EFFECTIVE NOISE TEMPERATURE

Desired Performance Probability Level	T_e or Total Receiving System Effective Noise Temp (°K)		Corresponding Noise Figure (db) Related to 290°K	
	Maser	Paramp	Maser	Paramp
50% (mean)	165	380	2.0	3.6
68% (1 σ)	192	436	2.2	4.0
80% (1.3 σ)	200	453	2.3	4.1
90% (1.65 σ)	210	473	2.4	4.2
95% (2 σ)	219	492	2.5	4.3

DSIF Predetection Bandwidth Compatibility

Standard predetection bandwidths to be provided at the DSIF sites for the Surveyor program are 3.3 Mc (3 db), 20 kc (1 db) and 4.4 kc (1 db). Switching between such bandwidths will be accomplished by a CDC operator; the switching time is 10 seconds. The 3.3-Mc bandwidth is appropriate for a 220-kc video bandwidth case, with a modulation index of 3. However, this bandwidth becomes excessive when considering TV video bandwidths in the 20-kc to 80-kc realm. The IF bandwidths of 20-kc and 4.4-kc are obviously too narrow for video information. Accordingly, at least one additional IF would have to be provided if a direct SLRV-to-Earth TV link were included in the final SLRV configuration. (Other new IF's may also be necessary for the DIBSI and telemetry data, but these are not considered here).

This analysis includes the following assumptions which are based on the latest analyses on phase-lock demodulation requirements and TV quality.

(1) The carrier-to-noise ratio (C/N) threshold in a closed-loop noise bandwidth, B_N, is assumed to be 2.3 db, to meet a lock-threshold mean-square phase-error of 0.5 rad^2, with a lock-loss probability of about 5×10^{-3}. For lock-loss probabilities of 10^{-3} and 10^{-4}, the CNR's would have to be 3 db and 4.6 db, respectively.

(2) The SLRV S-band transmitter high-level power output is assumed to be kept at 2.5 watts because of the significant saving in weight and primary power, as contrasted to a 5-watt requirement. (A 2.5-watt unit weighs 4.7 lbs. and requires 25-watts of input power, as contrasted to 9 lbs. and 60 watts for the 5-watt unit). The power level out of the diplexer is assumed to be 2.0 watts.

(3) The DSIF FM demodulator video signal-to-noise ratio (S/N) is assumed to be no less than 27 db (rms/rms); this corresponds to 36 db (p-p/rms) and 24 db (pp/pp), where a crest factor of 4 is used for the latter figure. These values refer to the communications subsystem only, and do not include the consideration of noise in the TV camera and electronics.

(4) Other link parameters are:

- SLRV Antenna: Gain is to be calculated; Polarization is circular.
- Video Bandwidth: Range of 20-kc to 80-kc
- Carrier Frequency: 2295 Mc
- Modulation: FM
- Demodulation: Modulation tracking phase-lock-loop demodulation.
- Space loss: 211.6 db
- Other fixed losses 2 db, with 1 σ value of 0.5 db. (Items included here are microwave antenna cable loss at SLRV, pointing of SLRV antenna, and equipment degradation.)
- Video signal sync-tip energy loss: 2 db
- DSIF antenna gain and pointing loss plus receiving system effective noise temperature: per previous discussion.
- Performance probability levels to be considered: 68% (1 σ), 80% (1.3 σ), and 90% (1.65 σ). The total db margins, as contrasted to the mean (50%) level required for these levels are given in Table II. 2-6.

TABLE II. 2-6

TOTAL MARGINS (DB) FOR PERFORMANCE PROBABILITY LEVELS OF 68%, 80%, AND 90%

Parameter	Margins (db) required for stated performance probability levels		
	68%	80%	90%
Antenna Gain	1.60	2.60	4.30
Pointing Error	0.12	0.22	0.42
Noise Temperature:			
Maser	0.20	0.30	0.40
Paramp	0.40	0.50	0.60
Other Losses	0.50	0.65	0.83
Over-all Margin*	1.70	2.70	4.40

*Over-all margin calculated as square root of sum of squares, with average values of 0.3 db (68%), 0.4 db (80%) and 0.5 db (90%) for maser-paramp noise-figure variations.

To achieve a 27-db (rms/rms) (S/N) for the video output, Robinson shows the following phase-lock-loop parameters and modulation index.

$$\frac{1}{2 f_m} B_N = 10$$

or

$$B_N = 20 f_m$$

$$B_o = 1.06 B_N = 21.2 f_m$$

$$m = 3.8 \text{ and } (SNR) B_N = 2.3 \text{ db}$$

Therefore, if the range from 20 kc to 80-kc is considered for video bandwidths, the range of B is from 400-kc to 1.6-Mc.

The tabulation of link parameters is as shown in Table II.2-7 for the specific cases of 20-kc, 40-kc and 80-kc video bandwidths. It should be noted that a 90% performance level can be achieved with an SLRV antenna gain of only 12.3 db, in the case of the 80-kc bandwidth, the 210-foot antenna, and a maser RF amplifier. However, this SLRV antenna gain requirement increases to 23.9 db for the 85-foot antenna with preamplifier installations. **Figure II.2-13 is a plot of the results given in Table II.2-7 for** masers only.

If a value of P_{ℓ} (lock-loss) of 10^{-4} were required, the antenna gain values would have to be increased by 2.3 db. Further, if it is desirable to consider the initial 220-kc video bandwidth case, the antenna gains given would have to be increased 4.4 db over the 80-kc values, 7.4 db over the 40-kc values, and 10.4 db over the 20-kc values.

Section E of this appendix contains a discussion of the weight and power requirements associated with antennas (and their drive systems) of gains comparable to those given in Table II.2-7. Physical characteristics for the over-all S-band configuration on SLRV (to provide direct Earth-to-SLRV-to-Earth communication are summarized in Section F. The data presented were compared with the data on the other subsystems on SLRV and the results indicated that the direct communications link should be rejected for the 100-pound SLRV.

3. Direct Earth-to-SLRV Link Analysis

This link need be discussed only briefly due to the narrow bandwidth associated with commands, and the high DSIF transmitter powers available. Let us assume the following set of parameters and solve for the receiver IF bandwidth that could be accommodated for commands.

Transmitter Power Output	100 watts
Frequency	2115 mc/s
Modulation	PM
DSIF Antenna Gain (85 ft)	50 db
Receiver Noise Figure	13 db
Noise Temperature (Excluding Receiver)	200° K
Receiver CNR required in IF bandwidth for phase-lock receiver	6 db
Space losses	211 db
SLRV antenna gain	0 db
Other Losses	4 db

TABLE II.2-7

LINK PERFORMANCE SUMMARY FOR THE DIRECT SLRV-TO-EARTH COMMUNICATIONS LINK

Parameter	85-Foot Dish Antenna		210-Foot Dish Antenna
	Maser	Paramp	Maser Only
Mean Value - DSIF Antenna Gain	54.6 db	54.6 db	62.6 db
Mean Effective Noise Temperature	165°K	380°K	165°K
S-Band Xmtr. Output (Incl. Diplexer Loss)	3.0 dbw	3.0 dbw	3.0 dbw
Space Loss	211.6 db	211.6 db	211.6 db
Loop Noise Bandwidth, B_N	20 fm	20 fm	20 fm
Required Threshold in B_N ($10^{-2} < P_\ell < 10^{-3}$)	2.3 db	2.3 db	2.3 db
Receiver Noise Spectral Density (kT)	-206.4 dbw/cps	-202.8 dbw/cps	-206.4 dbw/cps
Receiver Noise (kTB_N for 80-kc f_m case)	-144.4 dbw	-140.8 dbw	-144.4 dbw
Required Input Signal Power (80-kc case)	-142.1 dbw	-138.5 dbw	-142.1 dbw
Other Losses			
(1) Video Sync. Tip	2.0 db	2.0 db	2.0 db
(2) Cabling, SLRV antenna pointing	2.0 db	2.0 db	2.0 db
(3) Statistical Margin (Predominantly DSIF Antenna at:			
68% Performance Level	1.7 db	1.7 db	1.7 db
80% Performance Level	2.7 db	2.7 db	2.7 db
90% Performance Level	4.4 db	4.4 db	4.4 db
Required SLRV Antenna Gain at:			
80 kc			
68% Performance Level	17.6 db	21.2 db	9.6 db
80% Performance Level	18.6 db	22.2 db	10.6 db
90% Performance Level	20.3 db	23.9 db	12.3 db
40 kc			
68% Performance Level	14.6 db	18.2 db	6.6 db
80% Performance Level	15.6 db	19.2 db	7.6 db
90% Performance Level	17.3 db	20.9 db	9.3 db
20 kc			
68% Performance Level	11.6 db	15.2 db	3.6 db
80% Performance Level	12.6 db	16.2 db	4.6 db
90% Performance Level	14.3 db	17.9 db	6.3 db

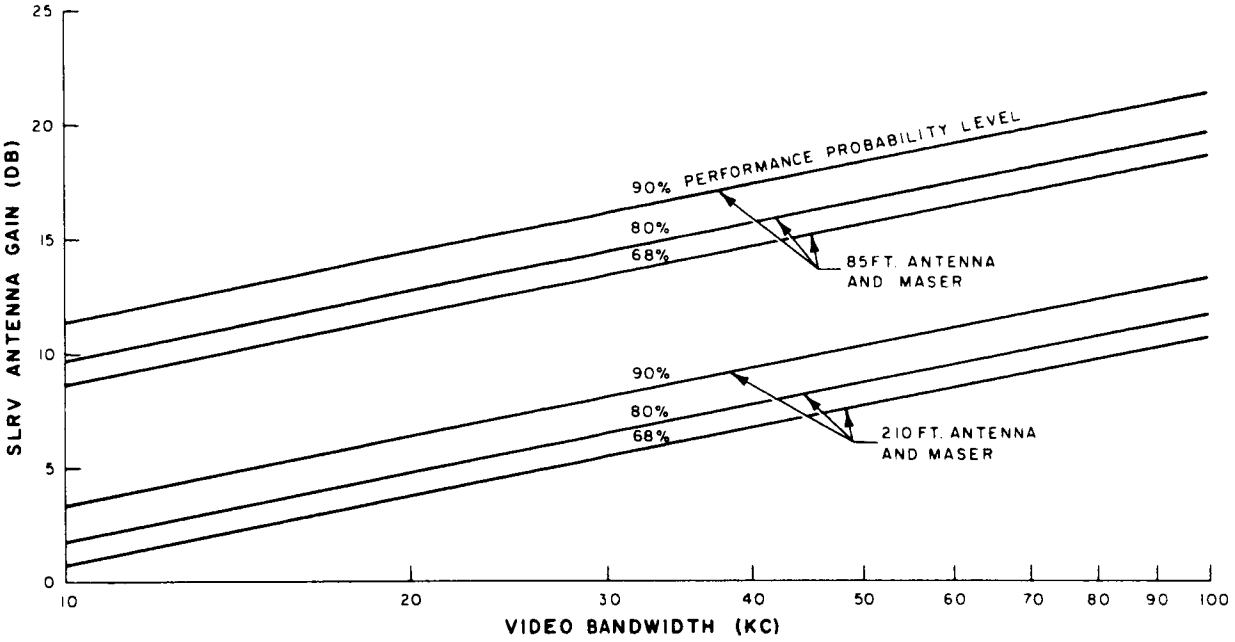

Figure II.2-13. SLRV Antenna Gain vs Video Bandwidth (Direct SLRV/Earth Link)

These parameters result in an IF bandwidth of about 16-kc, adequate for the anticipated command data which consists of split-phase RZ 48 bits/second digital data, carried on a 2.3-kc subcarrier. Use of narrow post-detection filters for the 48-bit/second data will provide commands with a bit-error probability of less than 10^{-6}. Reserve power (up to 10 kw) could be employed at the DSIF transmitter site if desired to provide greater margin.

C. MODULATION AND DEMODULATION INVESTIGATIONS

1. Surveyor-to-SLRV Commands

The Surveyor-to-SLRV link sends a 2.3-kc subcarrier frequency-modulated by 48 bits per second, bi-phase data. This quasi return-to-zero (RZ) data requires twice the bandwidth of non-return-to-zero data. The 48-bit-per-second data rate, with a 3rd-harmonic recovery of the bit-cycle frequency, would require the output low-pass filter to have a 48 x 3 = 144-cps cutoff frequency.

Because Surveyor uses standard IRIG FM-FM channel assignments, the 2.3-kc oscillator may be limited to the standard ± 173-cps deviation, with a modulation index of 5, and a bandwidth limitation on the subcarrier of only about ± 200 cps. A 35-cps response is standard for the 2.3-kc subcarrier, but this may be increased by reducing the deviation. The distortion may be held to a low value if the sum of the deviation and the frequency response does not exceed 200 cps. If the 144-cps response noted above is used for recovering the third harmonic, then the deviation would be only 56 cps. This is inefficient for FM-FM modulation; thus, only the fundamental of the 48-bit-per-second data rate will be recovered. This allows a 200-48 = 152-cps deviation, with a modulation index of 3. Following optimum-detection procedures, a 72-cps, low-pass filter will be required on the output.

From Fig. II. 2-14, a bit-error probability of 10^{-5}, for standard frequency modulation with a modulation index of 3, requires an E/N_o ratio of 19 db. This is equivalent to a carrier-to-noise (C/N) ratio in the subcarrier passband of 400 cps. Thus,

$$(C/N)_{SC} = (E/N_o)/BT$$

Then

$$(C/N)_{SC} = 80/\frac{200}{96} = 40$$

$$= 16\ db$$

This is derived with a carrier deviation by the 2.3 kc from the relation that (see Equation II. 2-46.

$$(C/N)_{sc} = \frac{(D_b)}{(f_a)} \left(\frac{B_{if}}{2b}\right) (C/N)_{if}$$

where, $(C/N)_{if}$ applies to the VHF-FM receiver IF in the SLRV. The receiver IF (B_{if}) must also be wide enough to include the oscillator instability in both the transmitter and the receiver, each of ± 0.005%. At 150 Mc, this amounts to a total of ± 15 kc in the receiver IF.

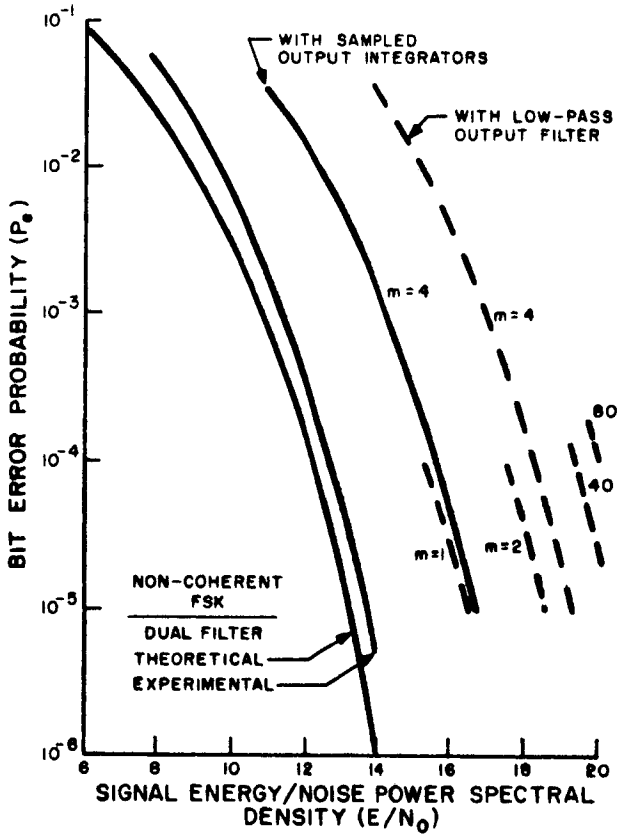

Fig. II. 2-14. Measured Performance of FSK-FM Dual Filter Limiter Discriminator as a Detection Method

It can be shown that for an optimum system with a limiter-discriminator detector, $B_{if} = 2(D_b + f_i)$. A modulation index $(m = D_b/f_a)$ to make best use of the bandwidth imposed by 7,500 cps for f_i would be about 4, which determines $D_b = 4(2.5) = 10$ kc.

Then,

$$B_{if} = 2\,(10 + 15) = 50\ kc$$

and

$$(C/N)_{sc} = 20 \log 4 + 10 \log \frac{50}{0.8} + (C/N)_{if}$$

with a $(C/N)_{if}$ = 12 db,

$$(C/N)_{sc} = 12 + 18.0 + 12 = 42\ db$$

This is far in excess of the required 16 db derived above. By lowering the deviation to about 2 kc to provide 16 db, the receiver IF is lowered to $2(2 + 15) = 34$ kc, or 2/3 the value of 50 kc used above. About 3 db less transmitter power will be permissable.

In summary:

Mod. Index	B_{if} (kc)	$(C/N)_{if}$ (db)
4	50	12
1	34	11

2. SLRV-to-Surveyor Telemetry

The 1100-bits/second telemetry data to be sent is analyzed here for either frequency-modulation of the carrier with an NRZ binary signal, or the "quasi" RZ split-phase binary data of essentially twice the 1100-bit/second rate.

NRZ Binary Data

Assuming a d-c output response is required, the 15-kc total instability of the link (i.e. ±0.005% of carrier at each terminal) imposes a receiver IF passband requirement of:

$$B_{if} = 2\,(f_k + 2\,f_i) = 2\,[\,1100 + 2\,(15)] = 62.2\ kc.$$

With a limiter-discriminator detector and output data filter of

$$f_c = 1100\,(3/4) = 825\ cps,$$

the ratio of B_{if}/f_m equals 19 db. From Fig. II. 2-15, it is seen that a 16-db threshold $(C/N)_T$ is required. The modulation index of the carrier will be

$$m = 1 + 2\,f_i/f_k = 28,$$

and the frequency deviation is 31.1 kc.

Split-Phase Binary Data

The split-phase binary form requires a $B_{if} = 2(2f_k + f_i) = 2(2.2+15) = 34.4$ kc, with an output filter of $f_c = 2200\,(3/4) = 1.65$ kc. Since $B_{if}/f_m = 13$ db in this case, Figure II. 2-15 shows $(C/N)_T = 12$ db. The deviation is 2200 cps.

This latter method using a split-phase waveform saves 4 db in $(C/N)_T$ over the first method, and about 2:1 in bandwidth, for a total improvement of 7 db. However, we should refer to Fig. II. 2-14, which shows the best performance available with limiter-discriminator detection without extra bandwidth for frequency instabilities.

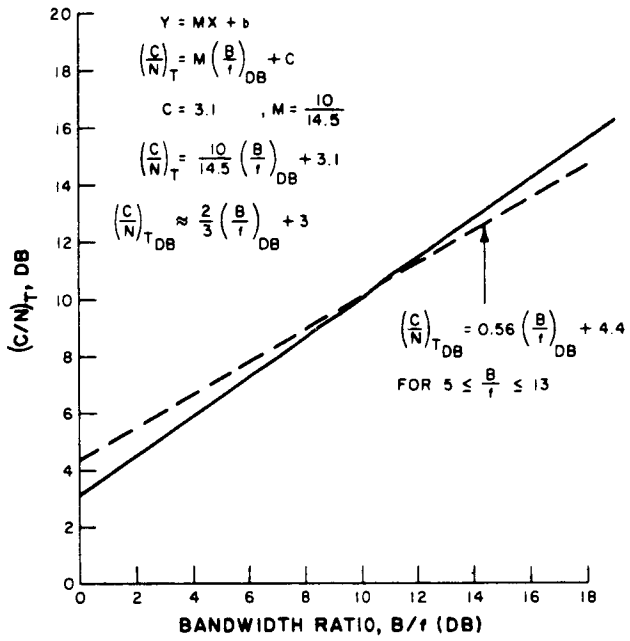

Fig. II. 2-15. Threshold Carrier-to-Noise Ratio versus Bandwidth Ratio

The above 12 db is a noise threshold, but in addition, an E/N_o value of 16.4 db for $m=1$ (low-pass filter output curve) must be available.

From

$$C/N = \left(\frac{E}{N_o}\right)\left(\frac{1}{BT}\right) = \frac{43.5}{34 \times 10^3/2200} \quad ,$$

we obtain $C/N = 4.5\ db$.

Since this is lower than the threshold value of 12 db, a BEP of 10^{-5} will indeed be available at a 12 db $(C/N)_T$ ratio.

Note that, with the minimum bandwidth required for a modulation index of 1 being $2f_k$ (4400 cps), the $(C/N)_T$ would then be 12 less 3, or 9 db. Compared to the 4.5 db derived above, this means that the high instability values for the link cause a 4.5 db penalty.

This 4.5 db inefficiency could be eliminated by coherent detection, which detects on the basis of signal energy and noise density, independent of bandwidth used. However, circuits for this may not be justified because of possible added weight and power requirements.

A summary of the FM limiter-discriminator performance is tabulated below. The split-phase signal is preferred because of the lower bandwidth and C/N ratio required.

Signal Type	Receiver IF Bandwidth	$(C/N)_T$	Output Low-Pass Filter	Mod. Index
NRZ Binary	62.2 KC	16 db	825 cps	28
Split-Phase	34.4 KC	12 db	1.65 KC	1

3. SLRV-to-Surveyor Television

Use of FM permits this signal to be received at the Surveyor with a 27-db rms-signal-to-rms-noise ratio and a modulation index of 2.4. This is equivalent to a 36-db peak-peak-signal-to-rms-noise ratio. The input C/N ratio required in an equivalent AM bandwidth would be 15 db. In a receiver IF passband of $B_{if} = 2f_m(1 + m)$, the C/N ratio would be 15 - 10 log 3.4, or 9.7 db.

If the S/N ratio of the total system including the camera is limited by the transmission link value, then a typical 12-db pre-emphasis gives a theoretical 9 db improvement, with pre-emphasis starting at 18% of the maximum modulating frequency. As noise in the camera chain exceeds or is equal to link noise, then less gain is available from pre-emphasis; e.g., with link and camera noise levels equal (i.e., equal S/N values), the pre-emphasis improvement drops from the 12 mentioned above to only an available maximum of 3 db in the overall S/N ratio.

The use of aperture correction provides maximum optical resolution by the vidicon, raising a 10% line resolution to about 70% resolution at the upper video frequency. The 12 db/octave aperture correction proposed starts at a frequency of about 85 kc. Noise is increased by a factor of about 3.5 over that of the uncorrected response at the upper frequencies. This noise contribution needs to be contained in the noise analysis, and being solely dependent upon the final vidicon performance, an assessment of its noise contribution could not be final at this time. Because it would probably contribute at least 3 db more noise, a 30-db S/N ratio from the vidicon would be reduced to a 27-db aperture correction. Being nearly the same S/N as expected in the link performance, the pre-emphasis gain in S/N would fall in the category of being less than 3 db — most likely only 2 db.

Although some space television cameras have provided 36 to 44 db S/N ratios, it is not necessarily true that the type used for SLRV under the more severe moon environment conditions will provide this measure of surplus S/N. The 36 to 44 db S/N would provide 7 db pre-emphasis gain.

In view of aperture correction imposing an increase of noise and of the probability that the camera S/N will not exceed 35 db, it is concluded that only 2 db pre-emphasis gain will result.

During subsequent camera studies, a greater S/N may be found available, but it is not assumed as probable at this time.

Thus, the present analysis assumes that a 25-db rms-signal-to-rms-noise ratio will be delivered by a flat receiver, and 27 db by pre-emphasis signal processing. Previously, a modulation index of 2.4 was noted as necessary for 27 db. A 25-db S/N requires an index of 1.9 at a C/N_{am} of 14 db. In the receiver IF of $2 f_m (1 + m)$, or $5.8 f_m$, a B/N_{if} of 14 minus 10 log $(1 + m)$ or 9.4 db is required.

The final receiver 27-db S/N_r couples with the camera S/N_c to provide a final S/N_o by the relation:

$$\frac{S}{N_o} = \frac{S/N_r}{\left(\frac{S/N_r}{S/N_c} + 1\right)}$$

Thus, if S/N_c is 27 db, then the combined S/N_o is 24 db. If the $S/N_c = 36$ db(4,000 power ratio) and $S/N_r = 27$ db (500) then,

$$\frac{S}{N_o} = \frac{500}{\left(\frac{500}{4,000} + 1\right)} = 435$$

or

$$\frac{S}{N_o} = 26.4 \text{ db}$$

This example 9-db increase in camera S/N provides a combined performance for all practical purposes equal to the over-all desired value of 27 db. The reverse situation in which a camera S/N of 27 could be compensated for in the same manner by a 9-db increase in transmitter power is not acceptable from weight and power consideration for SLRV.

4. SLRV-to-Surveyor DIBSI Data

Carrier Detection and Multiplex Synthesis

The multiplexing of DIBSI signals includes those force and acceleration signals measured, and also discrete DIBSI engineering data. These are detected in limiter-discriminator detectors as described in the following paragraphs.

First, for a multiplexed baseband signal of a low-pass video signal and one or more bandpass-modulated subcarrier signals, the video signal will be detected with an output mean square S/N ratio of:

$$\left(\frac{S}{N}\right)_1 = 3\left(\frac{D_1}{f}\right)^2 \left(\frac{B_t}{2f_1}\right)\left(\frac{C}{N_t}\right) \qquad \text{(II. 2-46)}$$

The quantities are defined in Figure II. 2-16

A subcarrier at a center frequency of f_a (see Fig. II. 2-17) will be detected with an S/N ratio at the carrier detection output of a passband filter of bandwidth, b, described by:

$$\left(\frac{C}{N}\right)_b = \left(\frac{D_b}{f_a}\right)^2 \left(\frac{B_t}{2b}\right)\left(\frac{C}{N_t}\right) \qquad \text{(II. 2-47)}$$

The ratio of equation II. 2-46 to equation II. 2-47 gives the interesting ratio equation of:

$$\frac{(S/N)_1}{(C/N)_b} = 3\left(\frac{b}{f_1}\right)\left(\frac{D_1}{D_b}\right)^2 \left(\frac{f_a}{f_1}\right)^2 \qquad \text{(II. 2-48)}$$

This equation removes several unknown variables from the analysis, and allows determination of the required carrier deviation ratio of $D_1/D_b = r$. Letting $(S/N)_1/(C/N)_b = p$, then

$$r^2 = \left(\frac{p}{3}\right)\left(\frac{f_1}{b}\right)\left(\frac{f_1}{f_a}\right)^2 \qquad \text{(II. 2-49)}$$

Thus, r may be determined because p is derived from the specified performance, f_1 is known, and b and f_a are derived from basic rules of basebanding the multiplexed signals.

If equation (II. 2-46) is used to derive a modulation index, m_1, for only the video signal, then $B_1 = 2 f_1 (1+m_1)$, and for a required $(S/N)_1$, at a threshold value of $(C/N)_1$, the system for the video signal above is known by the typical FM performance plots presented in para. C. 5 of this appendix.

Use of this value of m_1 and the r value derived by equation (4) establishes the value of the deviation, D_b, of the subcarrier. The following presents a development of this

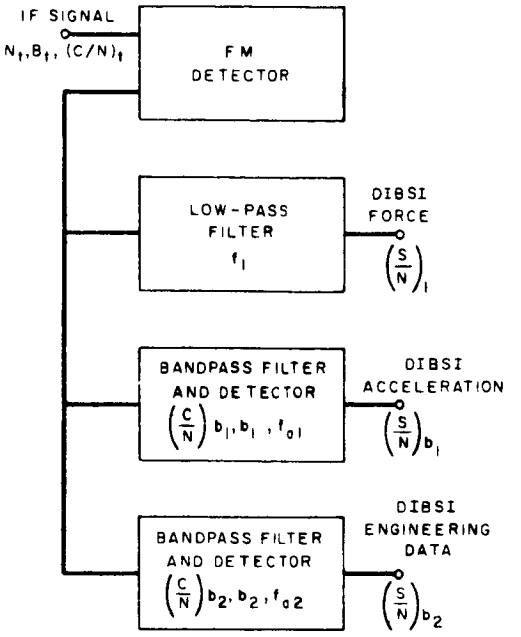

Figure II.2-16. Multiplex and Detection Block Diagram

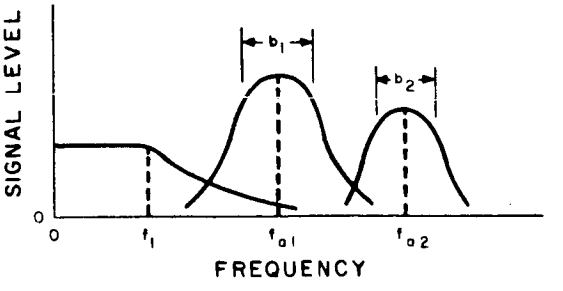

Figure II.2-17. Multiplex Spectrum and Filter

method of iteration to solve FM multiplex problems, and present also a series of design curves by which a rapid solution is possible to the problem of operating at threshold detection for the composite signal, with compatible values of signal deviations.

Design Procedure For Multiplexing Signal

With only the lowest modulating signal at baseband, it will be recovered at a S/N ratio of (standard FM):

$$\left(\frac{S}{N_1}\right) = 3\, m_1^2 \left(\frac{C}{N}\right)_{am} \tag{II. 2-50}$$

$$= 3 \left(\frac{B_1}{2f_1}\right) \left(\frac{D_1}{f_1}\right)^2 \left(\frac{C}{N_1}\right) \tag{II. 2-51}$$

$$= 3 \left(\frac{B_1}{2f_1}\right) \left(m_1^2\right) \left(\frac{C}{N_1}\right)$$

because the N_1 in the IF passband exhibits a flat power spectral density, ratios of bandwidth determine ratio of noise powers; thus,

$$\left(\frac{C}{N_{am}}\right) = \left(\frac{C}{N_1}\right) \left(\frac{N_1}{N_{am}}\right) = \left(\frac{C}{N_1}\right) \left(\frac{B_1}{2f_1}\right) \tag{II. 2-52}$$

where B_1 for practical values of m of wideband FM receivers is

$$B_1 = 2 f_1 (1+m_1) \tag{II. 2-53}$$

in which m_1 is the modulation index.

Substituting (II. 2-52) in (II. 2-51) gives

$$\left(\frac{S}{N_1}\right) = 3 (1 + m_1)\, m_1^2 \left(\frac{C}{N_1}\right) \tag{II. 2-54}$$

By adding a second signal and modulating the carrier to a total deviation of D_t, with a resultant noise bandwidth of

$$B_t = 2 f_t (1 + m_t), \tag{II. 2-55}$$

The signal will be detected to a (S/N) ratio of (equation II. 2-51):

$$\left(\frac{S}{N_1}\right) = 3 \left(\frac{B_t}{2f_1}\right) m_1^2 \left(\frac{C}{N_t}\right) \tag{II. 2-56}$$

Because again, as with equation (II. 2-52),

$$\left(\frac{C}{N_t}\right) = \left(\frac{C}{N_1}\right)\left(\frac{N_1}{C_t}\right) = \left(\frac{C}{N_1}\right)\left(\frac{B_1}{B_t}\right), \qquad \text{(II. 2-57)}$$

equation (II.2-56) becomes,

$$\left(\frac{S}{N_1}\right) = 3\left(\frac{B_t}{2f_1}\right) m_1^2 \left(\frac{C}{N_1}\right)\left(\frac{B_1}{B_t}\right) \qquad \text{(II.2-58)}$$

It is to be noted that the B_t variable would cancel in the equation, but in fact the quantity $\left(\frac{C}{N_1}\right)\left(\frac{B_1}{B_t}\right)$ must equal or exceed a threshold in FM which is determined by the ratio B_t/f_t, in which f_t is the maximum frequency component of the FDM signal. In any event, having chosen a threshold value of C/N_1 for the first signal to derive an acceptable output S/N_1 with an accompanying value of m_1, the extra bandwith reduces the value of C/N_1 to C/N_t. If the added signal is relatively narrowband, the added bandwidth may be slight and the threshold may still be exceeded, in which case a complete optimum system is specified by the addition of the individual deviations and by crosstalk considerations which determines baseband channelization.

However, if the threshold is not exceeded, then a threshold value of C/N_t equal to $(C/N_t)_T$ is chosen higher than $(C/N)(B_1/B_t)$, and is found on Figure II. 2-15 for the derived ratio of B_t/f_t.

This increase of C/N_t will give more output S/N than derived above, so m_1 and m_b may be reduced to m_1' and m_b', to provide the same output S/N with the higher C/N input values for the new higher (C/N_t) threshold value. Then from equation (II. 2-56) adjusted S/N equation with the primed values becomes:

$$\left(\frac{S}{N_1}\right) = 3\left(\frac{B_t'}{2f_1}\right) (m_1')^2 \left(\frac{C}{N_T}\right)_T \qquad \text{(II. 2-59)}$$

which, compared to the same S/N before the adjustment and described by equation (II. 2-58) gives the ratio

$$\frac{S/N_1}{S/N_1} = 1 = \frac{B_t' (m_1')^2 (C/N_t)_T}{B_t m^2{}_1 (C/N_1)(B_1/B_t)} \qquad \text{(II. 2-60)}$$

and from equation (II. 2-53)

$$B_t' = 2 f_t (1 + m_t')$$

and

$$B_t = 2 f_t (1 + m_t) \qquad \text{(II.2-61)}$$

then equation (II. 2-60) may be written:

$$\frac{(1 + m_t) m_1^2}{(1 + m_t') (m_1')^2} = \frac{(C/N_t)}{(C/N_1) (B_1/B_t)} \qquad \text{(II.2-62)}$$

Equation (II. 2-62) provides a correction value, m_1', of the original m_1 value. This final value of m_1' establishes the desired S/N in channel 1, even though another channel has been added. The right side of equation (II. 2-63) in decibels is then equal to a function of m_t and m_1 in decibels. Some simplification may be introduced by determining m_t in terms of m_1 First, let

$$m_t = \frac{D_1 + D_b}{f_a + b/2} \qquad \text{(II.2-63)}$$

and letting $r = D_1/D_b$,

$$m_t = \frac{D_1 (1 + 1/r)}{f_a + b/2} \qquad \text{(II.2-64)}$$

and since $m_1 = D_1/f_1$,

then

$$m_t = m_1 \cdot \frac{1 + 1/r}{(f_a/f_1) + b/2 f_1} \qquad \text{(II.2-65)}$$

By definition,

$$m_t = m_1 F(a) = m_1 \left(\frac{f_1 + f_a \sqrt{3/P} \sqrt{f_1 b}}{f_a + b/2} \right) \qquad \text{(II.2-66)}$$

with

$$r = \sqrt{\frac{f_1}{3b}} \left(\frac{f_1}{f_a} \right)$$

$$F(a) \text{ reduces to } F'(a) = (f_1/f_a) + K\sqrt{b/f_1}, \text{ for } b/2f_a << 1 .$$

This relation is shown in Figure II. 2-18.

Equation (II. 2-62) then becomes:

$$\frac{(1 + F(a)\, m_1)\, m_1^2}{(1 + F(a)\, m_1')\, (m_1')^2} = \frac{(C/N_t)_T}{(C/N_1)\,(B_1/B_t)} \qquad \text{(II. 2-67)}$$

Since the new value of m_1' may be expressed as a fraction of the m_1 value, then let

$$Z = m_1'/m_1 \qquad \text{(II. 2-68)}$$

Equation (II. 2-67) becomes:

$$\frac{1 + F(a)\, m_1)}{(1 + F(a)\, Z\, m_1)\, Z^2} = \frac{(C/N_t)_T}{(C/N_1)\,(B_1/B_t)} \qquad \text{(II. 2-69)}$$

The ratio on the right is known from calculations and Figure II. 2-15. The value of F(a) is computed from equation (II. 2-66) (or Figure II. 2-18), and m_1 is known from calculations. Z is determined from the resulting cubic equation. One solution is to plot the left side of equation (II 2-69) as a function of Z for different values of $F(a)\, m_1$. An inspection of equation (II. 2-69) shows that for values of $F(a)\, m_1$ of unity or smaller, and for likely values of Z between 0.5 and unity, the left side varies as $1/Z^2$. In the limit of large values of $F(a)\, m_1$ of 5 or more, and for Z of 0.5 or less, the left side tends toward $1/Z^3$ Figure II. 2-19 shows the function as a variable of z, with different values of $F(a)\, m_1$. This figure will be used to derive the final value of m_1 in the multiplexing of several or groups of signals, knowing the ratio of the right hand side of equation (II. 2-70).

An alternate approach to the solution of equation (II. 2-69) is to use the empirical formula describing the threshold value of $(C/N_t)_T$ and B/f as shown on Figure II. 2-15. A reasonably accurate expression is derived that

$$\left(\frac{C}{N_t}\right)_{T/db} = \frac{2\,B}{3\,f}\Big|_{db} + 3 \qquad \text{(II. 2-70)}$$

Equation (II. 2-69) then becomes

$$\frac{1 + F(a)\, m_1}{1 + Z\, F(a)\, m_1)\, Z^2} = \frac{\left(\frac{3B_1}{3f_t}\right) + 3}{(C/N_1)\,(B_1/B_t)} \qquad \text{(II. 2-71)}$$

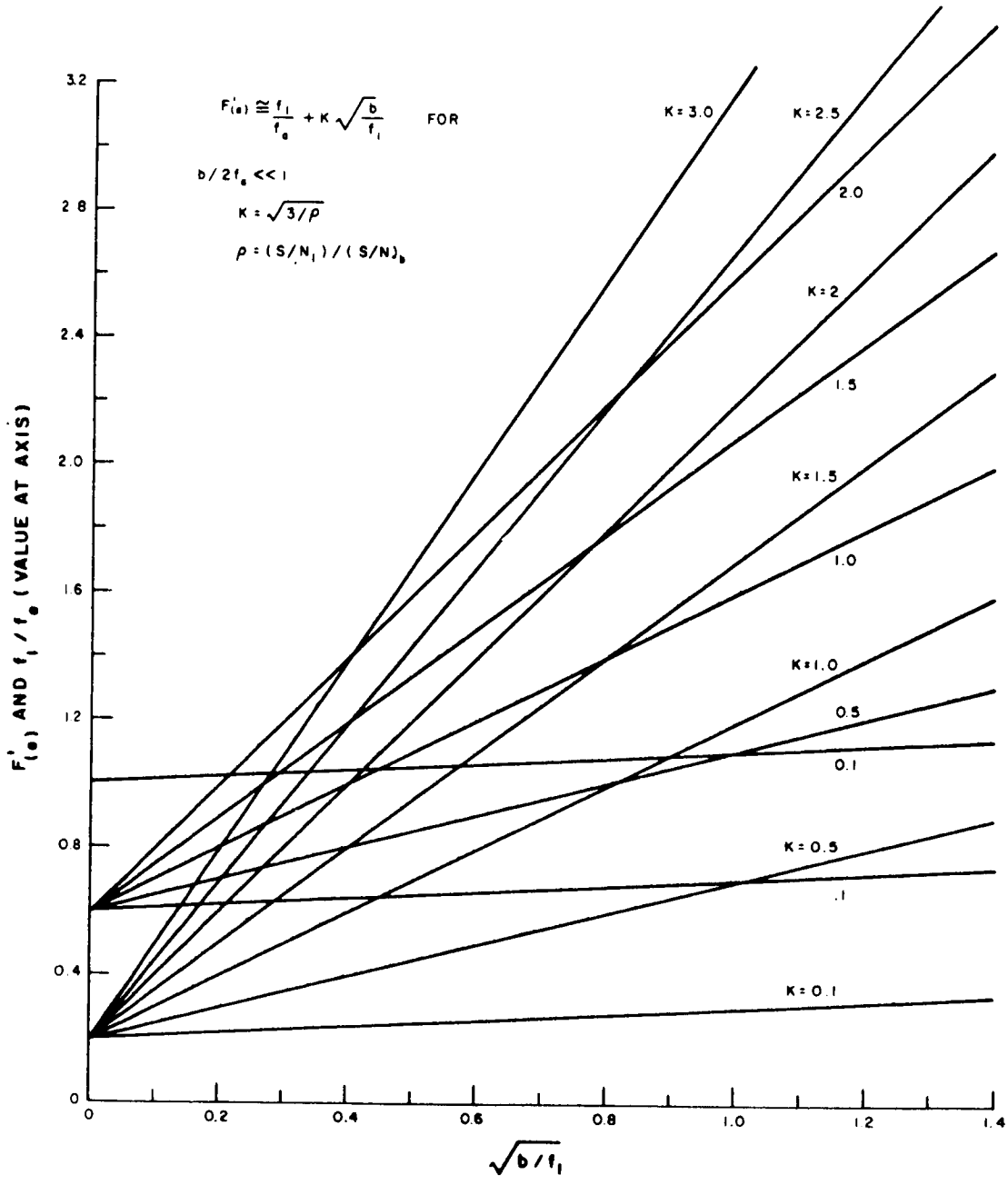

Figure II. 2-18. FM Multiplex Design Chart No. 1

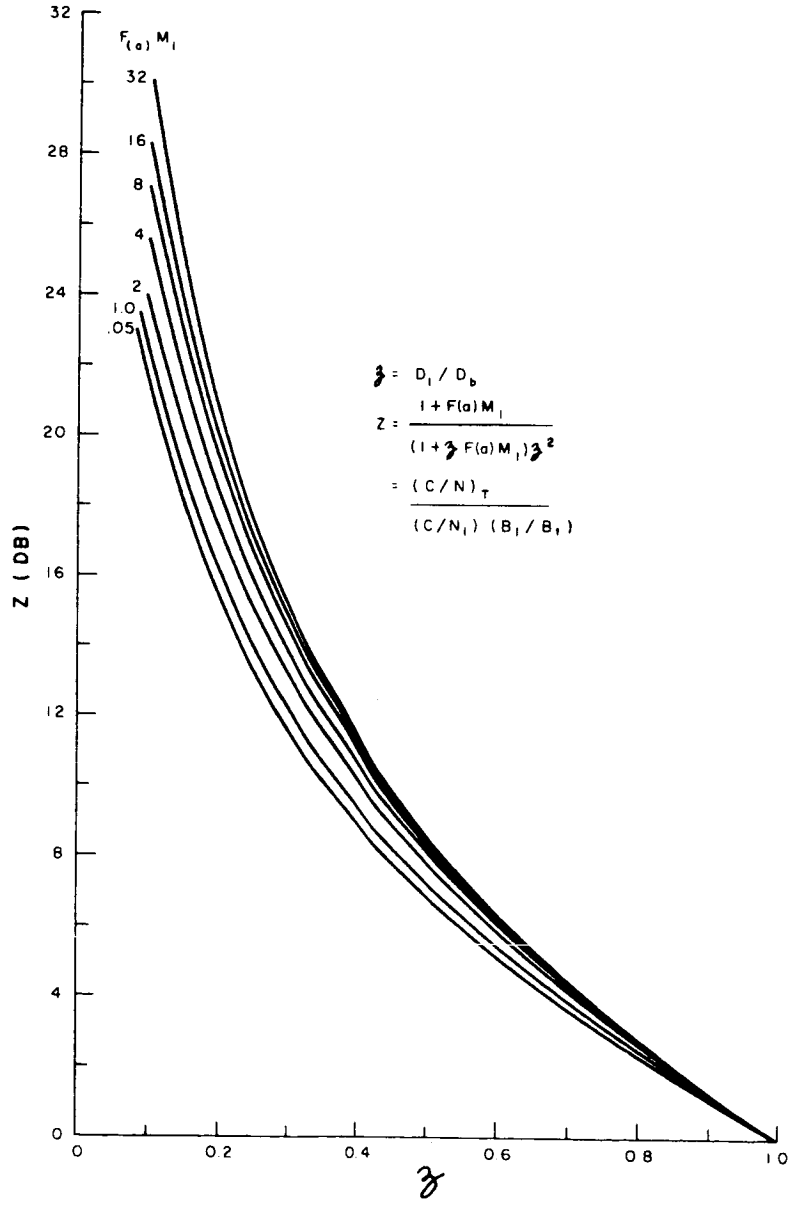

Figure II. 2-19. FM Multiplex Design Chart No. 2

This reduces to:

$$Z^2 (13 + 17 Z F(a) m_t 4_Z{}^2 F(a)^2 m_1{}^2) = 3 (1 + F(a)m_1) (C/N_1) (B_1/B_t)$$

Because this is no more easily solved than equation (II. 2-69), the latter is solved for Figure II. 2-19, because it depicts the physical meaning of the right side of the equation.

AM Basebanding of the Acceleration Signal

First consider only the 2-kc force signal modulating the carrier. According to Figure II. 2-18, the modulation index is optimumly determined for FM to be $8\sqrt{2}$ for a 50-db $S/N(rms/rms)$ ratio, with a C/N_{am} threshold of 24 db. Because $B_1 = 2f_1(1 + m_1)$, then,

$$B_1 = 2 \times 2 (1 + 11.3) = 49.2 \text{ kc}$$

From equation (II. 2-53) the ratio r may be determined for the DIBSI acceleration signal amplitude modulated on an 8-kc carrier. Assume the same S/N of 50 db $(b = 1)$ and $b = 4$kc, then:

$$r^2 = \frac{2}{(3)(4)} \left(\frac{2}{8}\right)^2 = \frac{1}{96}$$

$$\therefore r = 0.102$$

$$\text{or } D_1 = 0.102 D_{b1}$$

The quantity $F(a)$ from equations (II. 2-66) and (II. 2-67) is then

$$F(a) = \frac{1 + 1/r}{f_a/f_1 + b/2 f_1} = \frac{1 + 1/0.102}{8/2 + 4/2(2)}$$

$$= 2.2$$

and with $m_1 = 11.3$, $F_{(a)}m_1 = 2.2(11.3) = 24.9$. To use Figure II. 2-19, the value of Z required is (from equation (II. 2-69) $Z = (C/N_t)_T/(C/N)_1(B_1/B_t)$. The predetection C/N ratio of the force signal is from equation (II. 2-52),

$$\frac{C}{N_{am}} = \left(\frac{C}{N_1}\right)\left(\frac{B_1}{2f_1}\right) = \frac{C}{N_1} (1 + m_1)$$

$$\left.\frac{C}{N_1}\right|_{db} = \left.\frac{C}{N_{am}}\right|_{db} - \left.(1 + m_1)\right|_{db} = 24 - 10 \log 12.3$$

$$= 24 - 10.9 = 13.1 \text{ db}$$

From D_1 and r and

$$D_t = D_1 + D_b = 11.3\ (2) + \frac{11.3(2)}{0.102} = 244\ kc,$$

$$m_t = \frac{244}{10} = 24.4$$

then

$$\frac{B_t}{f_t} = (1 + m_t)^2 = 50.8,\ or\ 17.1\ db$$

and

Fig. II. 2-15 gives $(C/N)_T = 15\ db$

Then

$$\frac{(C/N)_T}{(C/N)_1\ (B_1/B_t)} = 12.1\ db$$

which, on Fig. II. 2-19, shows $Z = 0.39$.

The final carrier deviations are this value times the original, or

$$D_1 = 0.39(22.6) = 8.8\ kc,$$

$$D_{b1} = 0.39\ (22.6)\ (9.8) = 86.5\ kc,$$

$$D_t = 86.5 + 8.8 = 95.3\ kc,$$

and

$$D_t = 2(D_t + f_t) - 2(95.3 + 10) = 211\ kc$$

Other system values for S/N ratios of 40 and 30 db are shown in Table II. 2-8.

FM Subcarrier for Acceleration Signal

The subcarrier should be the lowest frequency that permits acceptably low crosstalk with other channels and simultaneously allows practical filter design for the channels. It is known that a well designed FM receiver with a capture ratio of about 2 db will suppress spurious signals to 50 or 60 db when the spurious signal is less than 2 db of the desired signal. Allowing an 8-db safety margin, the ratio of the FM subcarrier amplitude to the adjacent channel in-band spurious level will be assigned a 10-db value.

TABLE II. 2-8

CHARACTERISTICS OF DIBSI ACCELERATION ON AM SUBCARRIER AT 8 KC AND TELEMETRY SUBCARRIER AT 16 KC

DIBSI Force and Acceleration			Telemetry (BEP = 10^{-5})		Total Dev. (kc)	Surveyor VHF Receiver IF	
Output S/N (db)	Carrier Deviation (kc)		$(C/N)_{sc}$ (db)	Dev. (kc)		Bandwidth B_t (kc)	Threshold $(C/N)_T$, (db)
	Force	Accel.					
50	8.8	86.5	9	1.7	97.0	230.0	12
40	6.2	60.0	9	3.3	69.5	175.0	11
30	2.4	23.3	9	3.9	29.6	95.2	9

Figure II. 2-20 shows a typical arrangement of multiplexing 2 channels. The 10-db value at the edge of the subcarrier channel is made up of the ratio of the two signals, r_1, and the attenuation of the filter, A_f, of the lower channel. The value of r from equation (II. 2-52) can be plotted as a function of f_d; then, for an attenuation rate of A_f, given by the receiver's low channel filter, the 10-db point may be determined. Good filtering is realized with a 36-db/octave attenuation rate.

Without resorting to this full synthesis method, an educated guess of f_a is possible by basing it on (1) a determination of r and (2) a B_{sc} value of $[2 f_b (1 + m_{sc})]$ and a shape factor of 3 for the receiver's bandpass filter. With a 30-db attenuation at $\pm B_{sc}$ from f_a, then $f_{a1} = B_{sc} + f_1$. These are listed in Table II. 2-8 for different S/N ratios.

From equation (II. 2-52),

$$r^2 = \left(\frac{p}{3}\right)\left(\frac{f_1}{b}\right)\left(\frac{f_1}{f_a}\right)^2$$

For an output quality S/N of 50 db,

$$p = (S/N)/(C/N)_{sc} = 50 - 13 \quad 37 \text{ db}$$

$$r^2|_{db} = 37 - 4.8 + 10\,(2/52) + 20 \log\,(2/54)$$

$$r_{50} = 0.295$$

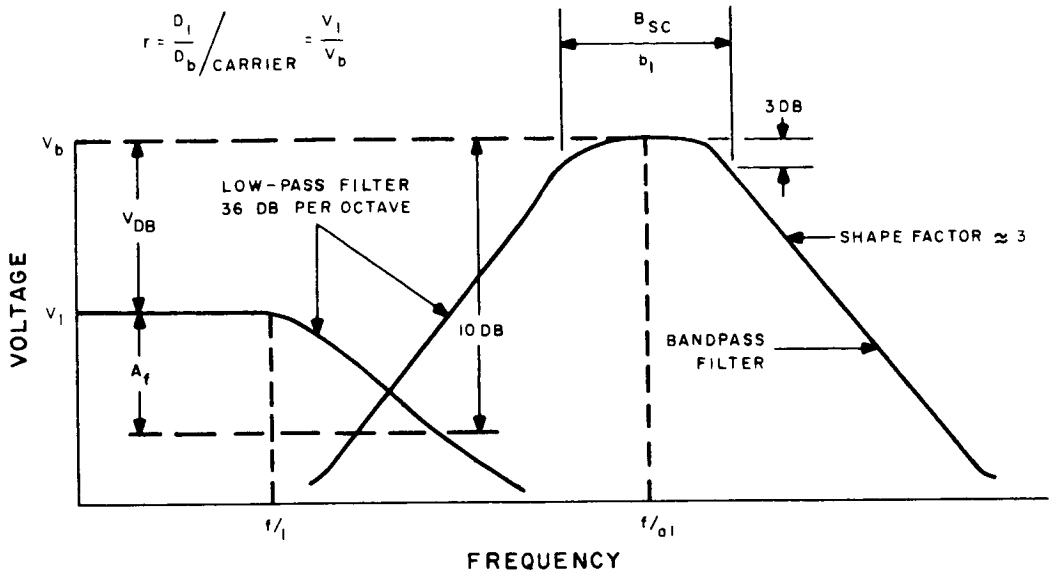

Figure II. 2-20. Typical Arrangement of Multiplexing Two Channels (Multiplex Crosstalk Diagram)

for S/N of 40 and 30 db, respectively, the values of r are:

$$r_{40} = 0.24$$

and

$$r_{30} = 0.23$$

From the analysis of multiplexing without FM subcarriers, the DIBSI force signal is derived to deviate the carrier 22.6 kc. Then the above ratios show the carrier deviation, D_D, by the subcarrier to be as shown on Table II. 2-9. The total deviation, D_t, of the carrier and the Surveyor's receiver bandwidth, B_{if}, are also shown.

The amount of deviation on the subcarrier, corresponding to modulation indices of 12, 7, and 3, for center frequencies 54, 34, and 18 kc is quite large — about ±50%, or about 7.5 times that of standard IRIG. This is attainable from special biased multivibrators or saturable inductance oscillators. Some instability problems and linearity or calibration problems of modulation are present, but may be solved by calibration voltages much as required in any accurate telemetry system.

TABLE II. 2-9

CHARACTERISTICS OF DIBSI ACCELERATION ON FM SUBCARRIER AND TELEMETRY ON FM SUBCARRIER

DIBSI Force and Acceleration			Telemetry Data	Total Dev. (kc)	Surveyor VHF Receiver IF		Subcarrier			
Output S/N (db)	Carrier Deviation (kc)		(BEP = 10^{-5}) $(C/N)_{sc}$ = 9 db Dev. (kc)		Bandwidth	Threshold	Frequencies		Bandwidths	
	Force	Accel.			B_r (kc)	$(C/N)_T$, (db)	Accel. (kc)	Telem. (kc)	Accel. (kc)	Telem. (kc)
50	17.0	57.5	15.5	90.0	356.0	8.0	54	86	52	4
40	7.0	33.5	15.0	56.2	228.4	7.5	34	56	32	4
30	3.7	16.0	6.0	25.7	120.0	7.0	18	32	16	4

Two Examples of Telemetry Addition

(1) With Acceleration as AM Signal at 8 kc:

Put Telemetry at 16 kc with 4 kc bandpass filter. This will be detected in Surveyor with a limiter/discriminator for the subcarrier.

For coherent FSK and detection (assume: BEP = 10^{-5}):

$$E/N_o = 12$$

Reconstituting the data with the third harmonic content ($B = 4$ kc);

$$\left(\frac{C}{N}\right)_{tm} = \left(\frac{E}{N_o}\right)\left(\frac{1}{BT}\right) = 12 \text{ db} - 10 \log 4000 \times \frac{1}{1100} = 6.4 \text{ db}$$

Thus, carrier detection must provide 6.4 db, minimum (7 db will be used in the following calculations), in 4 kc. If a 2-db "relay" noise increase is allowed, then the following system parameters result:

$$\text{For } \left(\frac{S}{N}\right)_1 = 50 \text{ db: } r_{tm} = 5.8 \text{ and } D_{tm} = \frac{D_1}{r} = 3.9 \text{ kc}$$

$$(\text{with } Z = 0.39, \text{ then } D_{tm} = 1.7 \text{ kc})$$

For $\left(\frac{S}{N}\right)_1$ = 40 db: r_{tm} = 1.8 and D_{tm} = 7.8 kc

(with Z = 0.44, then D_{tm} = 3.3 kc)

For $\left(\frac{S}{N}\right)_1$ = 30 db: r_{tm} = 0.62 and D_{tm} = 9.2 kc

(with Z = 0.42, then D_{tm} = 3.9 kc)

These deviations must be added to those derived earlier for the force and acceleration signals. The system results are listed in Table II. 2-8.

(2) With Acceleration as FM Subcarrier Signal:

Place telemetry 6 kc above f_t and use 4 kc bandpass filter as with AM acceleration subcarrier. Then, as in the foregoing example, the following parametric values result.

For $\left(\frac{S}{N}\right)_1$ = 50 db: r_{tm} = 1.11

For $\left(\frac{S}{N}\right)_1$ = 40 db: r_{tm} = 0.513

For $\left(\frac{S}{N}\right)_1$ = 30 db: r_{tm} = 0.3

These, again, must be added to the force and acceleration signals. The system results are shown in Table II. 2-9.

5. Conventional FM, FMFB, and Phase-Lock Detection

Less transmitter power is required now than was needed for earlier typical FM detectors (Foster Seeley, etc.), due to advances in modulation/detection techniques. Considerable analytical effort has been devoted to discovering when the threshold occurs, the parametric effects of the modulation index, the relation of compatible thermal and non-linear noise levels in an optimum system, and the nature and occurrence of the spurious loss of lock in the phase-lock type of detector. Measurements with NASA satellites (Pioneer series and Mariner) have established capability with data type of systems in general, and the Telstar, Relay, and Echo projects have provided quality evaluation of analog signal transmission primarily for frequency-following detectors

(FMFB). Other types of modulation techniques have been compared and one of these performance ratings is shown in Figure II. 2-21. (It should be pointed out that the comparison is made on the basis of transmitter power required for recoverable signal purity.) The increase in spectrum utilization of one system over another is not to be considered a penalty, even though it ranges from 10.5 Mc for digilock modulation to 0.22 Mc for single side-band for a 220-kc video-modulating signal. Recent analysis for Echo and Telstar receivers using FMFB have modified the capability as shown for FMFB and will be developed later along with phase lock (PL) detection. The pulse-code modulated mode shown is for a 5-bit coding (32-level) of differentially coherent (phase-shift keyed) detected video.

Fig. II. 2-22 compares the performances of other detection schemes. The FSK receivers applicable in Fig. II.2-22 are those using dual-filter (matched filter mode) detection of the coherent or non-coherent type, depending upon whether bit phase and coherent integration during the bit is used, or the simple threshold detection level is used at the detector output.

The non-coherent FSK detection methods also include the popular limiter discriminator receiver. Frequency instabilities, f_i, and doppler shift, f_d, are not included; these would broaden the IF and lower the threshold or increase the bit error rate (BEP). The figure represents typical AMR receiver performance, wherein f_i and f_d are compensated for by vernier adjustment of the receiver's injection oscillator to some mixer. Measured performances are shown due to the lack of theory to describe accurately the threshold effects.

The relative merits of these detection techniques are apparent in Figs. II.2-21, 2-22 and 2-23. The conclusion may be drawn that coherent detection is best for data reception. Analog signal quality by FMFB reception is shown in Fig. 2-21 to be better than others, although so far, phase-lock detection is not shown.

The performances of various phase- and frequency-modulation detection systems, which are either FM, FMFB, or PL, are shown in Figure II. 2-23. The plots for FMFB or PL are from Enloe[11], Spilker[12], and Choate[9], and for FM (limiter-discriminator), from Crosby[7] and Stumpers[10]. The input signal-to-noise ratio parameters described by the authors mentioned are normalized in the input signal-to-noise ratio parameter to a ratio at the input that would be found in an equivalent AM IF passband of twice the highest modulating frequency, f_m, i.e., the equivalent a-m signal-to-noise ratio of C/N_{am}. The signal-to-noise ratio in the receiver IF would be $(C/N)_{if} = (2 f_m/B_{if})\, C/N_{am}$. Of most significance is the threshold curve for each detection scheme, because above their threshold values, all detection schemes give the same output signal-to-noise ratio S_o/N_o for a given C/N_{am} by the relation $S_o/N_o = 3m^2\, C/N_{am}$ for power values of the variables. The modulation index value, m, for FM is the ratio D/f_m where D is the peak deviation of the carrier. The deviation in a phase-modulation system is ϕf_m where ϕ is the radian deviation. The equation holds for increasing

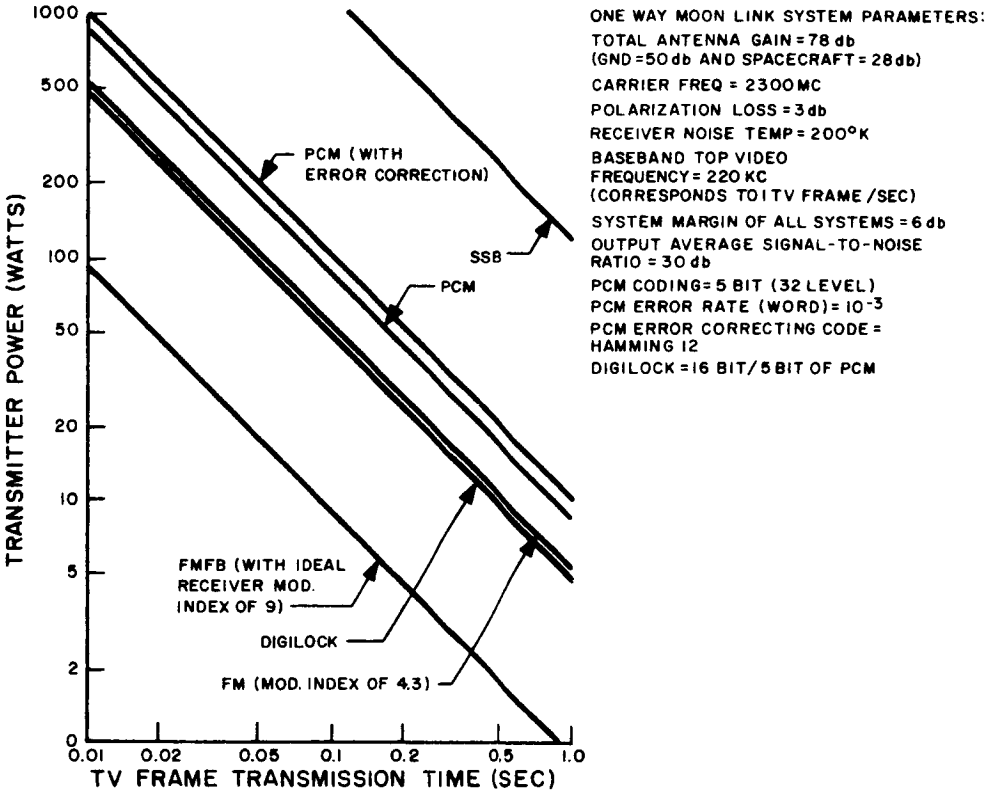

Figure II. 2-21. Performance Ratings for One Type of Modulation Technique

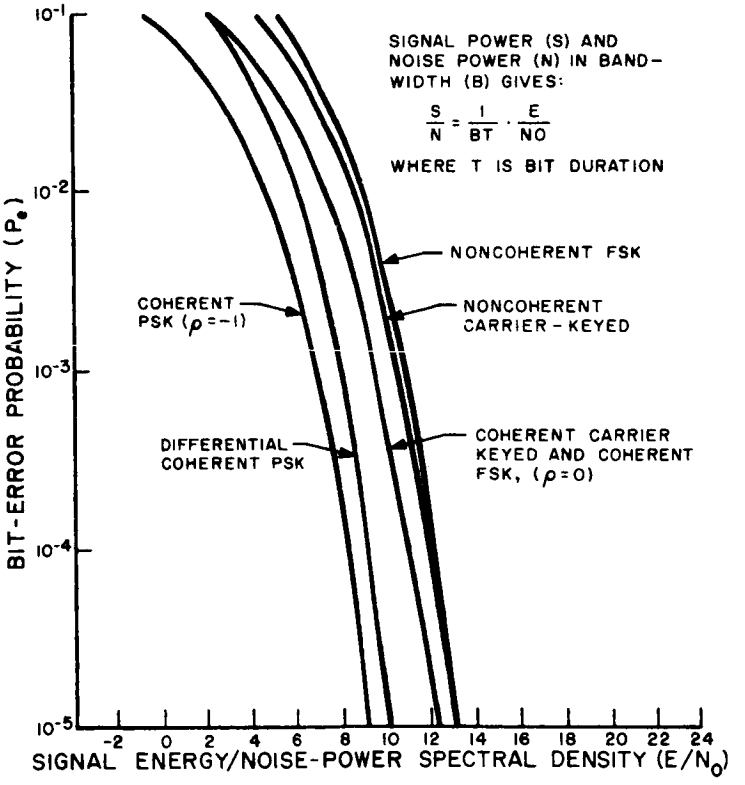

Figure II.2-22. Bit Error Probability Vs. Signal Energy to Noise Power Density Ratio (E/No.)

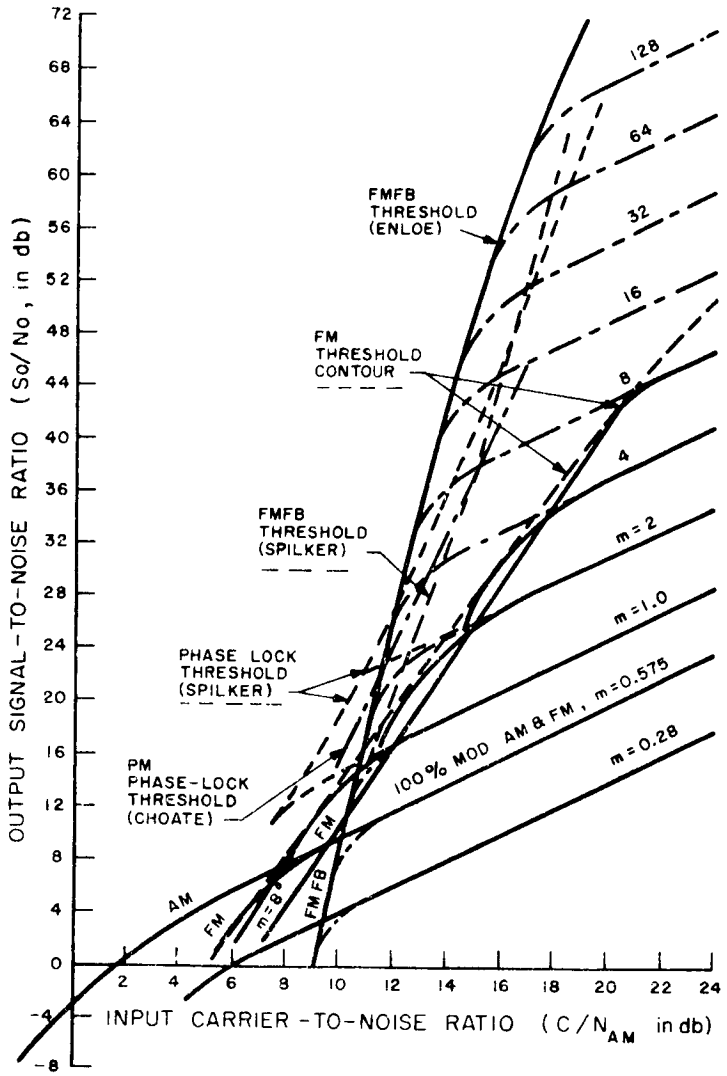

Figure II. 2-23. Performances of Various Phase- and Frequency Modulation Detection Systems

C/N_{am} values until the intermodulation signal-to-noise ratio (non-linearity effects) exerts a leveling influence on the thermal signal-to-noise ratio attainable.

The derivation of Figure II.2-23 shows that all investigators used the same model for the feedback loop, but in some respects differences in interpretation and sophistication appeared between the different analyses. Also, Enloe's paper needed considerable interpretation and extension to derive a performance curve such as the one shown in Figure II. 2-23. Spilker did not use the sophisticated threshold of standard f-m as did Enloe. Spilker and Enloe were close in their values of 0. 1 and 0. 25 for the mean square radians disturbance in the loop at threshold, whereas Choate uses a value of one-radian. To derive a generalized curve, Spilker's analysis was modified to include a threshold value of 7 to 12 db, dependent upon the bandwidth expansion used as shown by Enloe. Choate's model of analysis is used, in which the signal distortion is about

6 db below the thermal noise power in the closed loop at threshold. Most of these changes are reflected in Figure II. 2-23. Finding the different curves were at odds by only a few db (and taking into consideration the relative thoroughness of the different analyses), a set of final curves for threshold values was derived, as shown in Figure II. 2-24. A typical extension beyond the C/N_{am} threshold values is shown for agreement with Choate's work. For completeness, Choate's phase-lock curves for PM are shown as Figure II. 2-25. More recently, Robinson has published curves similar to the above, with different mean square radians of noise values as a variable of a family of curves. A 0.5 radians^2 mean square error is used by Robinson in his final performance for practical systems, even though values of 0.7 and 1.0 are shown in his theoretical deviations. Robinson's results are shown in Figure II. 2-26 (Figure II-A-4 of Robinson's paper) with an additional 0.25 mean square-radian error curve. Develet[22] has used a more elegant model of a phase-lock system which simulates more exactly the non-linear processes involved when distrubance occurs in the loop at threshold. His results are the same as those shown in Figure II. 2-24 except that the same output signal-to-noise ratio is shifted one db lower on the C/N_{am} axis. Develet's solution is based on a signal spectrum approximating a Gaussian spectrum, and may not be directly applicable to other spectrums, although in other analyses this variation in signal distribution has not altered results by more than several db. His evaluation is shown in Figure II. 2-27 with the additional plots of performance possible for 0.5, 0.25, and 0.1 mean-square phase errors.

From Figure II. 2-24 it is clear that, for an output signal-to-noise ratio in the order of 25 to 30 db, either FMFB or PL detectors are 2 to 3 db better than are FM limiter-discriminator detectors. Because PL detectors are of simpler design than FMFB detectors, PL detection is preferred. A reference phase-noise level at thresholds of 0.5 rads^2 (mean square) will be assigned.

A difference in performance attainable with phase-lock detection by Develet and Robinson is obvious, with the least difference of only 1 db for a 0.25 mean square radian error. The largest difference occurs for a one mean square radian error which shows Robinson's evaluation to provide the same output SNR with 4 db less input SNR. At a threshold value of 0.5 mean square radians, the difference is 1.8 db. Because Develet's Analysis also includes the performance attainable with an optimum loop filter, Robinson's curve for one radian squared error is seen to be 1.8 db better than that possible with the optimum filter. Since Develet uses a non-linear model and Robinson does not, Develet appears to be more valid for the large error values. Also, his evaluation for a 0.5 radian squared error is identical to the curve of Figure II. 2-26, which was derived for the same 0.5 mean-square error from previous reports on phase lock performance. Another recent report by Viterbi (23) supports Develet's findings as the exact analysis provided by continuous randomwalk techniques is the same as Develet's up to one radian square error. This is as large as any analysis has allowed the error to be for practical phase lock loops.

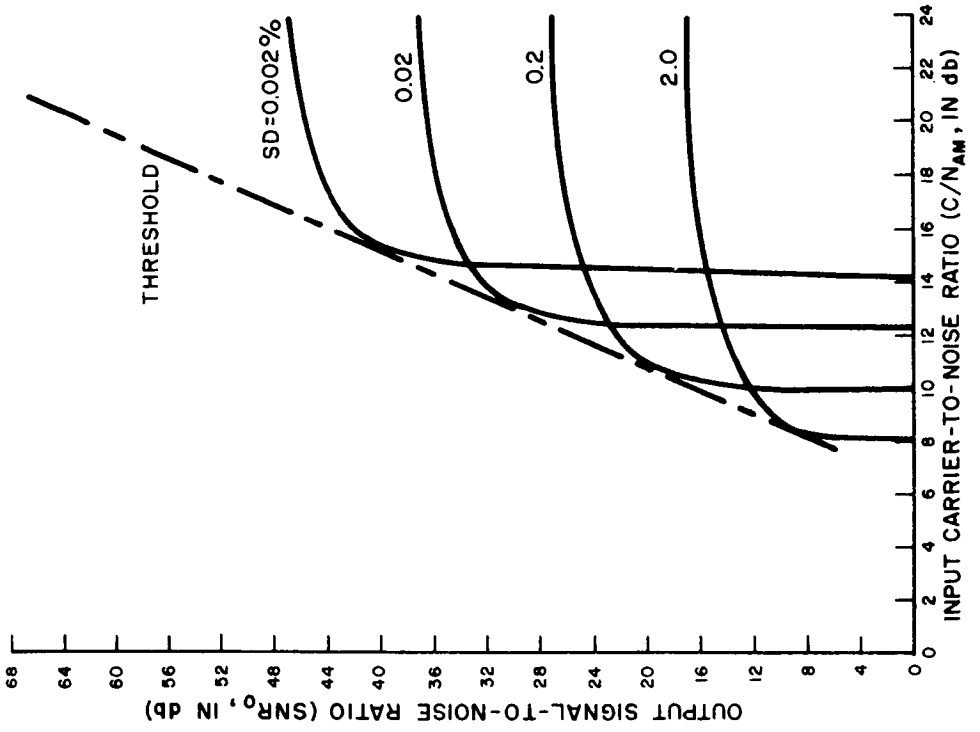

Figure II. 2-25. Choate's Phase-Lock Curves for Phase Modulation

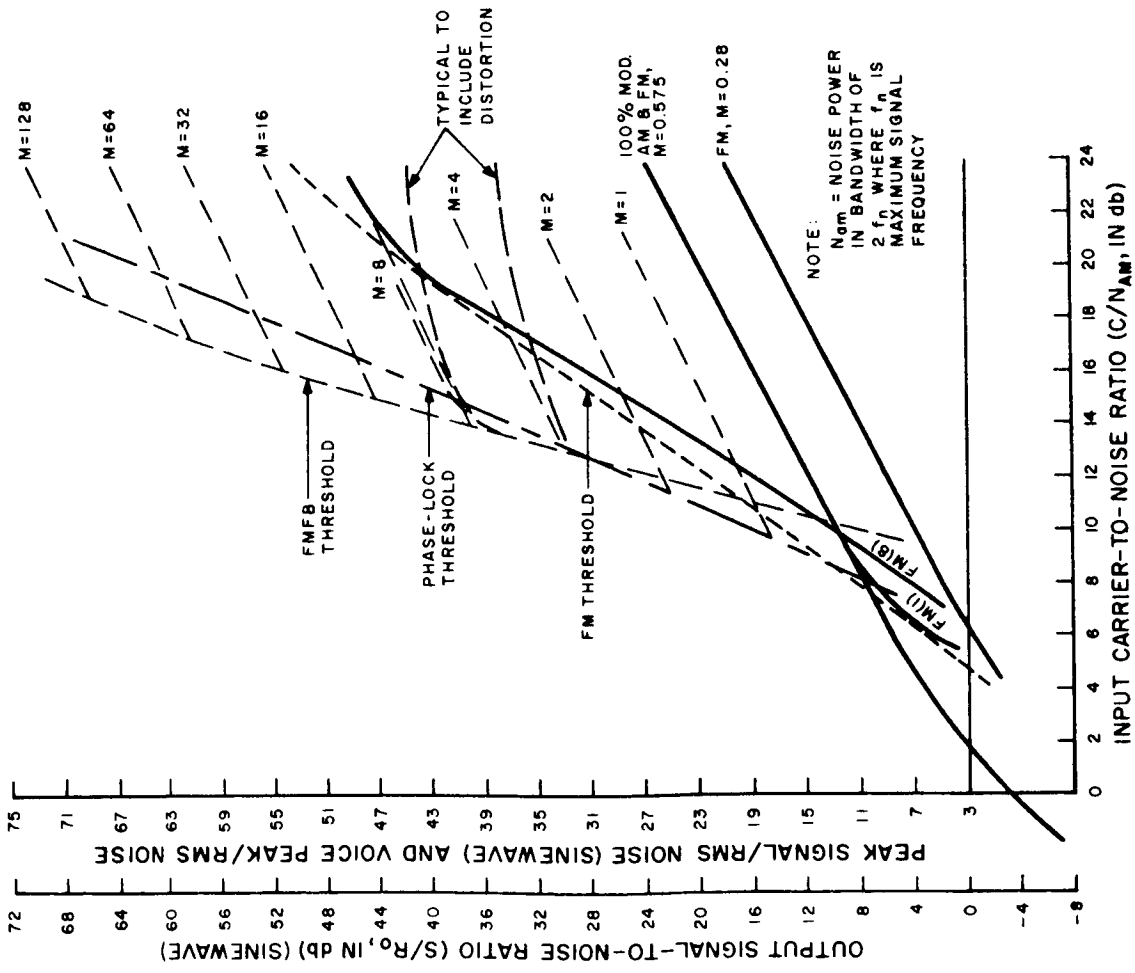

Figure II. 2-24. A Set of Curves Derived for Detection Threshold Values

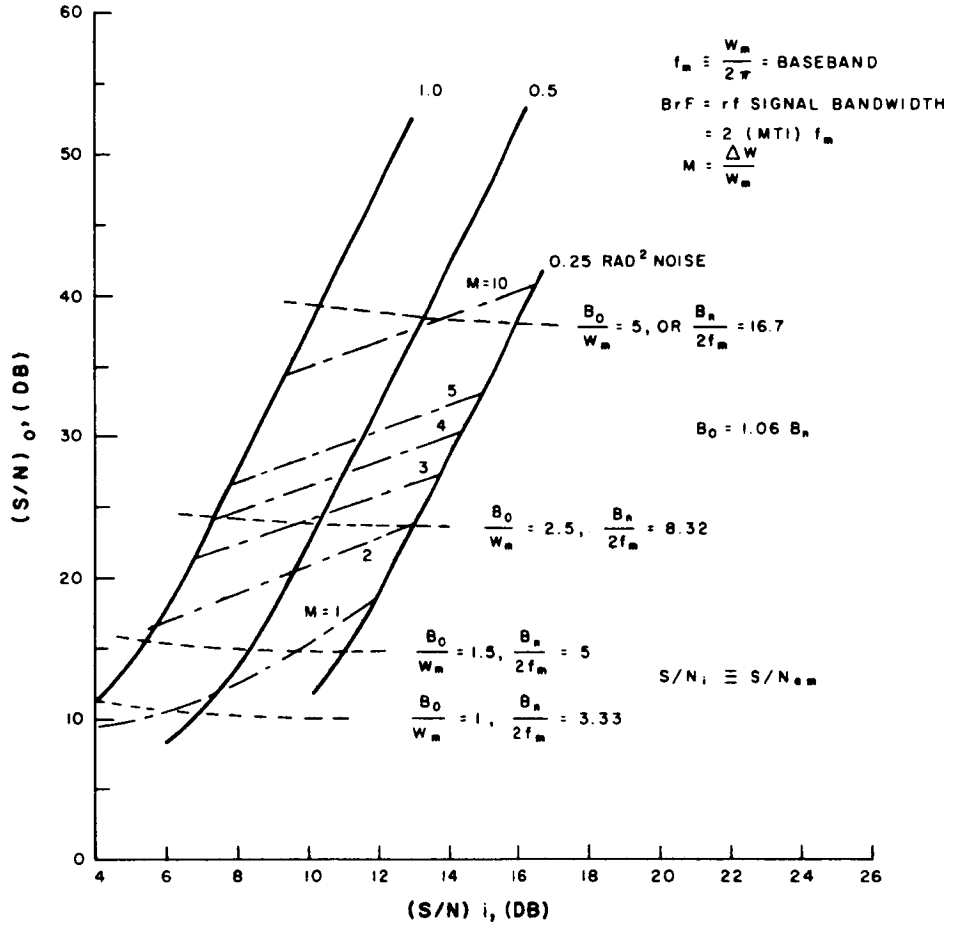

Figure II. 2-26. Phase-Lock Receiver Performance — Robinson

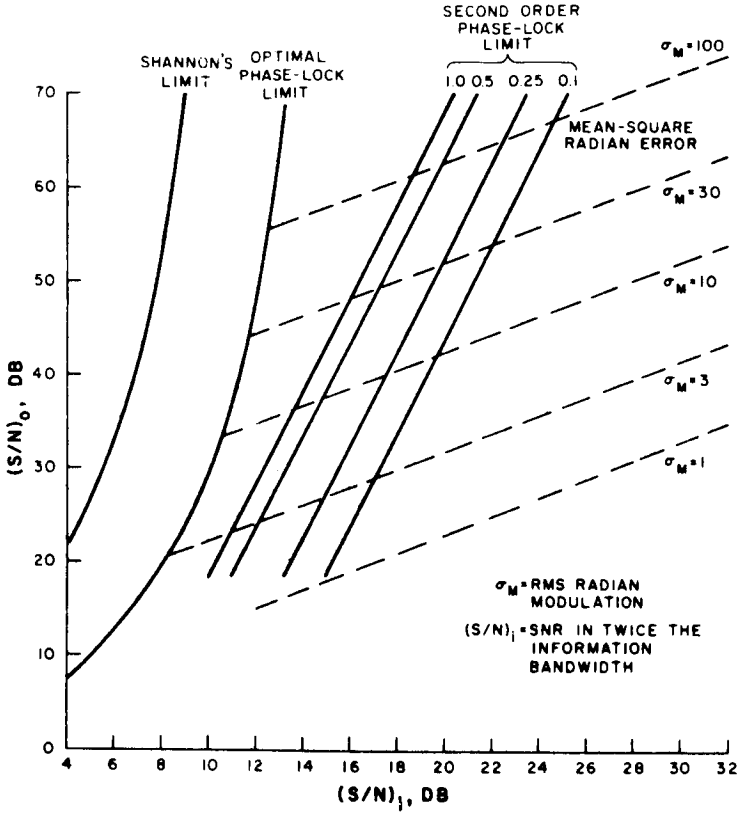

Figure II.2-27. Phase-Lock Receiver Performance — Develet

REFERENCES

(1) Galiardi, R. N; Miller, T; Minimum Power Wideband Communication System for Space Vehicles; 1961 Proc. of Nat'l Telemetry Conference.

(2) McRae, D; Phase Locked Demodulation in Telemetry Receivers, Proc. of 1958 National Telemetry Symposium.

(3) Sink, R. L; The Use of PCM in Data Links with Satellites, Space Vehicles and Long Range Missiles, 1959 Nat'l Sym. on Space Electronics and Telemetry.

(4) Lowton, J. G; Comparison of Binary Data Transmission Systems; Proc. 1958 Conf. on Mil. Electronics, p. 54.

(5) Pierce, J. N; Error Probabilities in Frequency Shift Keying, Masters Degree Thesis, MIT, 1953.

(6) Black, H. S; Modulation Theory, D. Van Nostrand Company, Inc., New York.

(7) Crosby, M. G; Frequency Modulation Noise Characteristics, Proc. IRE, April 1937, pp. 472-514.

(8) Schwartz, M; Information Transmission, Modulation and Noise, McGraw-Hill Book Company, Inc., N. Y. C.

(9) Choate, R. L; Design Techniques for Low-Power Telemetry, Tech Report No. 32-153, Jet Propulsion Laboratory, Calif. Inst. of Tech., March 5, 1962.

(10) Stumpers, F. S. H. M; Theory of Frequency Modulation Noise, Proc. IRE, September 1948, pp. 1081-1092.

(11) Enloe, L. R; Decreasing the Threshold in FM by Frequency Feedback, Proc. IRE, January 1962, pp. 18-30.

(12) Spilker, J. J. Jr; Threshold Comparison of Phase Lock, Frequency-Lock and Maximum-Likelihood Types of FM Discriminators, 1961 Proc. of the IRE Wescon.

(13) Parry, C. A; Optimum Design Considerations for Radio Relays Utilizing the Tropospheric Scotte, Mode of Propagation, Communication and Electronics, March 1960, pp. 71-80.

(14) Robinson, L. M; Tanlock, A Phase-Lock Loop of Extended Tracking Capability, Conf. Proc., Nat'l Winter Conv. Mil. Elec., February 1962.

(15) Frost, W. O; O. B. King; SS-FM; A Frequency Division Telemetry System with High Capacity, Proc. 1959 Nat'l Sym. on Space Electronics and Telemetry, IRE.

(16) Chaffee, J. G; Bell Sys. Tech. Journ., July 1938, pp. 403-437.

(17) Ruthroff, C. L; Bell Sys. Tech. Journ., July 1961, pp. 1149-1157.

(18) Ewen, H. E; A Thermodynamic Analysis of Maser Systems, The Microwave Journal, March 1959.

(19) Hoberg, O. A; Saturn Telemetry and Tracking, Astronautics, February 1962.

(20) Reiger, S; Error Probabilities of Binary Data Transmission Systems in the Presence of Random Noise, 1953 IRE Nat'l Convention Proceedings, Part 8, p. 72.

(21) Robinson, L. M; Interim Report, Apollo Modulation Technique Study, Cislunar Communications, July 1962.

(22) Develet, J. A., Jr; A Threshold Criterion for Phase-Lock Demodulation, Proc. IEEE, February 1963, P. 349.

(23) Viterbi, A. J.; Phase-Locked Loop Dynamics in the Presence of Noise by Fokker-Planck Techniques, Proc. IEEE, December 1963.

D. RANGING AND BEARING INVESTIGATIONS AND ERROR ANALYSES

1. Introduction

This section of Appendix II contains: (1) analyses of the errors to be expected for the techniques selected for determining range (R) and bearing (ϕ) described in para. C.4 of this appendix, and (2) descriptions of other approaches which were studied, but discarded in favor of the selected techniques.

2. Error Analyses

Ranging Error Analysis

There are basically two types of error that are encountered in measuring range: (1) bias (or fixed) errors, that can be minimized or eliminated by calibration, and (2) statistical (random) errors that determine the ultimate accuracy obtainable.

(1) The primary bias errors are:

a. Range Ambiguity

Since the 200-kc tone completes a 360° change of phase every 750 meters (round trip), some sort of "dead reckoning" must be incorporated to determine in which of the five possible range zones SLRV is located. Since the mission is of such a nature that a fairly long time is spent in each zone, it is felt that the ambiguity can be calibrated out quite easily on Earth.

b. Receiver Filter Delay Distortion

It has been shown that the delay distortion inherent in "frequency swept" tuned circuits can be minimized by designing controls over both the slope of the tuned circuit and the bandwidth required.

Baghdady[1] shows that the required bandwidth (B), for low distortion, is given by:

$$B = 2(\Delta\Omega + \nu\omega_m) \qquad \text{(II.2-72)}$$

where

$\Delta\Omega$ is the frequency deviation $\beta\omega_m$;

ω_m is the modulation frequency;

β is the modulation index; and

ν = 5K/2, where K is the sluggishness ratio of the filter.

(1) E. J. Baghdady, "Lectures on Communication System Theory," McGraw Hill, pp. 479-483.

It will be assumed that the bandwidth is determined by a single tuned high-Q circuit, so that

$$K = 1$$

Hence, $\nu = 3$

Other forms of equation 1 are:

$$B = 2(\beta\,\omega_m + 3\omega_m) \quad \text{in radians}$$

$$B = 2(\beta + 3) \quad \text{in cycles per second} \qquad \text{(II.2-73)}$$

A plot of the above formula is shown in Figure II. 2-28. As an example, it can be seen that an IF bandwidth of 2 megacycles per second and a modulation frequency of 200 kilocycles per second requires a modulation index, β, of 2 or less.

If it is desired to determine the required bandwidth in terms of the frequency deviation and β, instead of the modulation frequency and β, equation (II.2-73) can be written as

$$\beta\frac{B}{\omega_m} = 2\left(1 + \frac{3}{\beta}\right) \quad \text{in radians} \qquad \text{(II.2-74)}$$

or

$$\frac{B}{\Delta f} = 2\left(1 + \frac{3}{\beta}\right) \quad \text{in cycles per second} \qquad \text{(II.2-75)}$$

A plot of equation (II.2-75) is shown in Figure II.2-29.

When the modulation index, β, is equal to 2 or less, the bias error due to delay distortion is negligibly small, but can be eliminated by calibration if necessary.

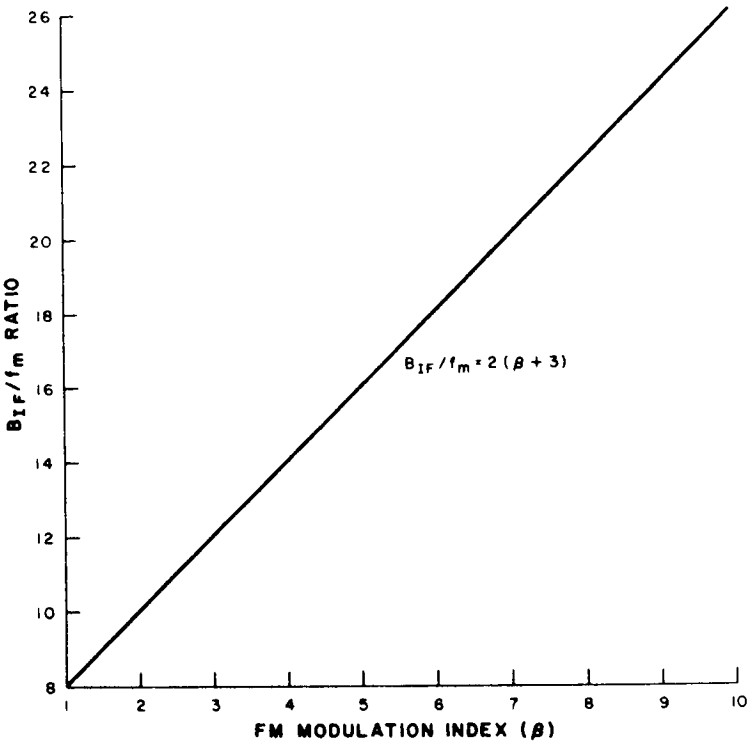

Figure II.2-28. Normalized IF Bandwidth for FM as a Function of f_m and β

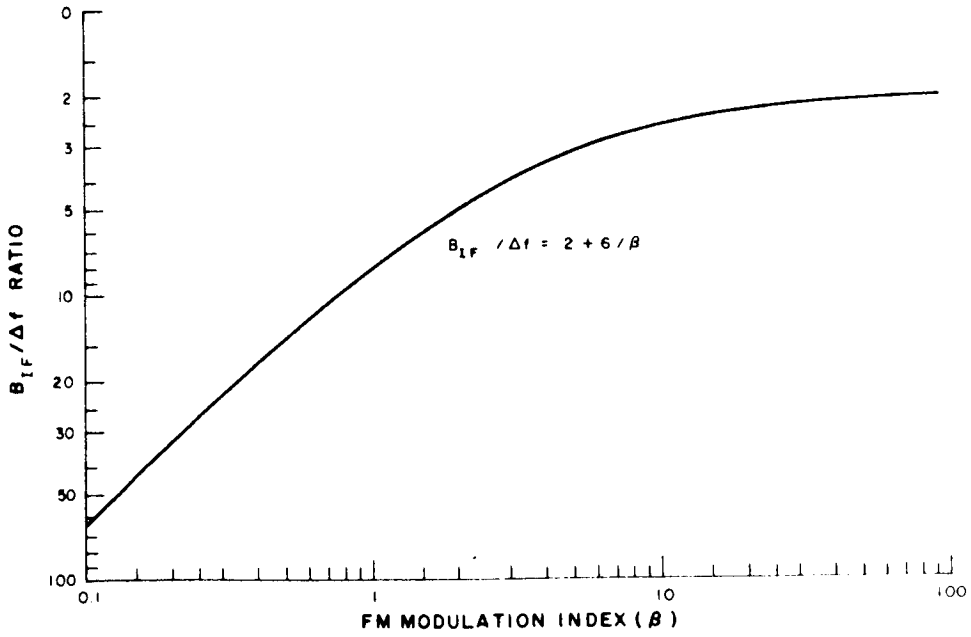

Figure II.2-29. Normalized IF Bandwidth for FM as a Function of Δ f and β

(2) The primary statistical errors are:

a. Signal to Noise

The signal and noise vectors in a narrowband filter can be graphically shown as;

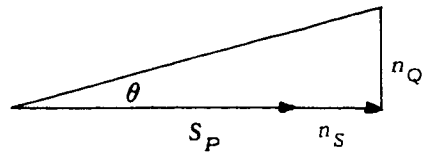

Where: S_p is the peak signal voltage (reference),

n_s is the in-phase rms gaussian noise (1σ),

n_Q is the quadrature rms gaussian noise (1σ), and

θ is the resulting rms phase error (1σ).

Now:
$$\theta = Tan^{-1}\left(\frac{n_Q}{S_p+n_s}\right) \qquad \text{(II.2-76)}$$

and for $S_p >> n_s$,
$\theta < 5^\circ$.

But
$$\theta = \frac{n}{S_p} = \frac{rms\ noise}{peak\ signal} \qquad \text{(II.2-77)}$$

Thus,
$$\theta = \frac{1}{\sqrt{2}\left(\frac{S}{n}\right)_{rms}} \sim \frac{0.7}{\left(\frac{S}{n}\right)_{rms}} \qquad \text{(II.2-78)}$$

A plot of equation (II.2-78) is shown in Figure II. 2-30.

Since the low-pass filter following the digital phase detector on Surveyor can be made arbitrarily small, the random phase error can be reduced to insignificance. However reduction of the bandwidth of the bandpass filter following the FM receiver

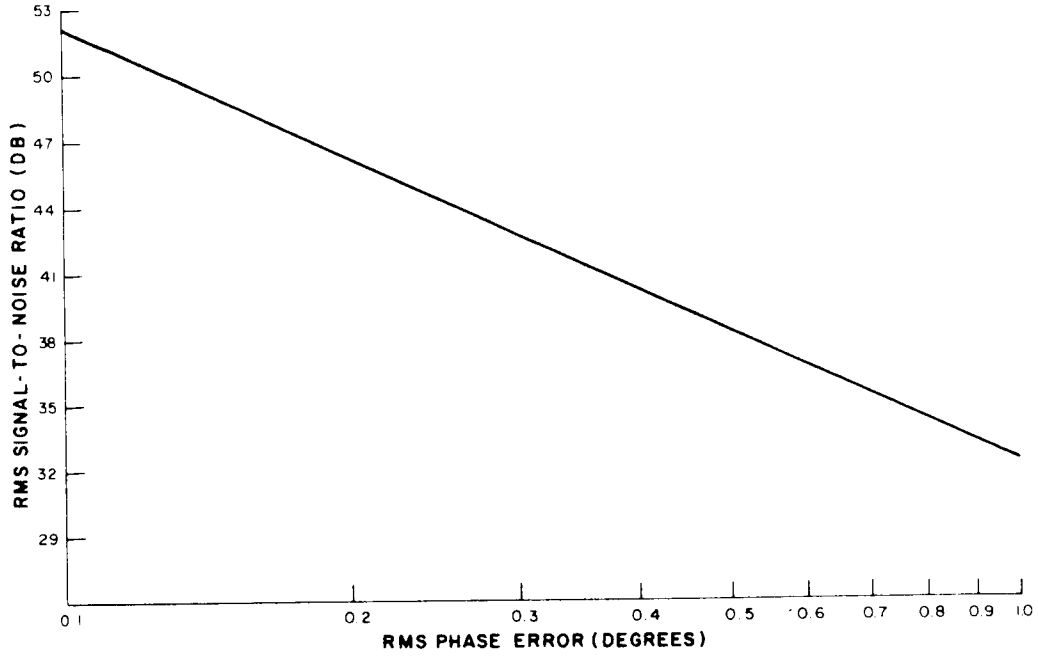

Figure II.2-30. Phase Error Versus Signal/Noise Ratio

on SLRV is limited because of the temperature-stability relationships. Therefore, phase jitter due to a low signal-to-noise ratio will occur here.

Table II.2-10 was derived from Skinner's Threshold curves given by Enloe[2]

TABLE II.2-10

THRESHOLD PERFORMANCE

$\left(\frac{C}{N}\right)$ db	$\left(\frac{S}{n}\right)_0$ db	$\left(\frac{S}{n}\right)_1$ db	$\left(\frac{S}{n}\right)_2$ db
3	13	23	33
6	21	31	41
9	30	40	50
12	35	45	55

(2) Enloe, "Decreasing the Threshold in FM by Frequency Feedback", Proceed, IRE, Jan 1962, p. 27, Figure 9.

Where: $\frac{C}{N}$ is the IF carrier-to-noise ratio in a 2-Mc bandwidth:

$\left(\frac{S}{n}\right)_0$ is the Output signal-to-noise ratio in a LP filter of 200-kc bandwidth;

$\left(\frac{S}{n}\right)_1$ is the Output signal-to-noise ratio in a BP filter of 20-kc bandwidth;

$\left(\frac{S}{n}\right)_2$ is the Output signal-to-noise ratio in a BP filter of 2-kc bandwidth.

The table shows that the output signal-to-noise ratio in the 2-kc bandpass filter is at least 41 db when the input carrier-to-noise ratio is 6 db or greater. This signal-to-noise ratio results in an rms phase error of 0.36 degrees (from Figure II.2-30). A plot of rms phase error versus rms range accuracy for 4 different modulation tones is shown in Figure II. 2-31. The range accuracy for 0.36° phase error is 1.5 meters (200-kc tone).

b. Filter Phase Stability

Another source of random errors is the shift of the center frequency of the 200-kc bandpass filter (on SLRV) with temperature. An analysis of the phase error, θ_e, has been made; the results of this analysis are plotted in Figure II. 2-32. In this figure, ΔT is the change in ambient temperature, the I_i's are the total temperature coefficients of the tuning elements in the filter, and Δf is the resulting shift in the center frequency of the tuned circuit. The resulting phase error is a function of the center frequency shift and the bandwidth of the filter.

For a ΔT is 50°C and an overall temperature coefficient of 40 ppm, the Δf is 200 cycles per second.

For a bandwidth (3 db) of 2-kc, the resulting phase error is 0.15 degree.

The resulting range error is 0.6 meter.

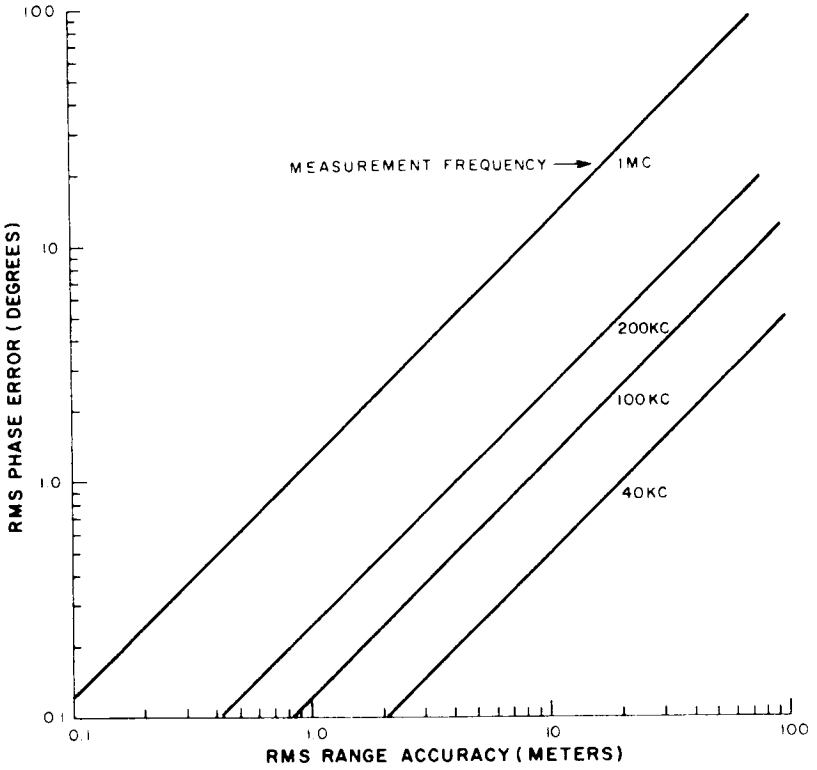

Figure II. 2-31. Phase Vs. Range Error

c. Reference Oscillator Error

The short-term stability (1 to 10 seconds) of the 200-kc crystal oscillator is 2 parts in 10^9, resulting in an rms phase error of 0.14°.

The resulting range error is 0.6 meter.

d. Analog-to-Digital Encoding Error

If the Range data (DC voltage) is routed to the TM section of the Surveyor Telecommunications subsystem for Surveyor/Earth transmission, 10-bit word encoding of this voltage will occur. Since a random error in encoding can occur on the least significant bit, the resulting error is 1 part in 1024. The resultant phase error would be $\frac{360}{1024} = 0.35°$, corresponding to a range error of 1.5 meters.

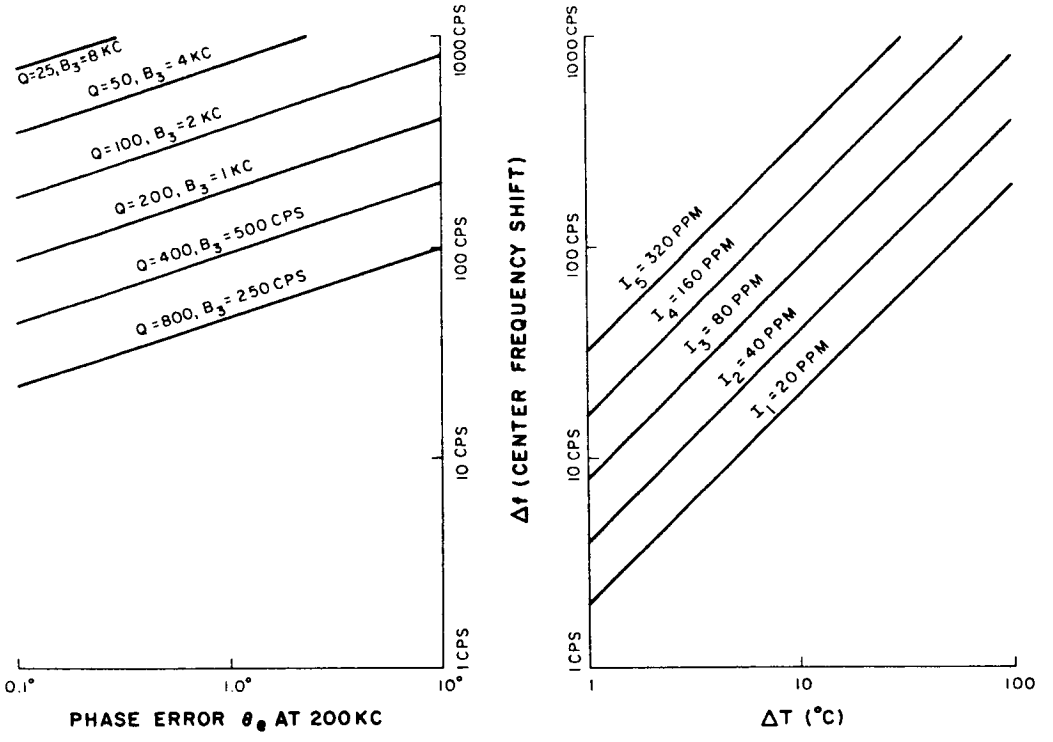

Figure II.2-32. Phase Error Versus ΔT for a Single Tuned Bandpass Filter

e. Rise-Time Error

The rise-time error for the two-stage amplifier-clipper is 0.5 degree.

This represents a range error of 2 meters. This error can be reduced to 0.05° by adding another amplifier-clipper stage.

f. Total RMS Error

The total range error, σ T, is equal to $\sqrt{\sum_{i=1}^{n} \sigma_i^2}$.

$$\therefore \sigma T = \sqrt{(1.5)^2 + (0.6)^2 + (0.6)^2 + (1.5)^2 + (2.0)^2}$$

$$\sigma T = 3.04 \text{ meters, rms.}$$

(Note that this is based on the assumption that encoding via the Surveyor telemetry subsystem is employed. Use of direct

analog modulation on a subcarrier (VCO) would result in greater error because of the magnitude of frequency drift for such VCO's.)

(3) Recommended Modulation

To enhance the received signal-to-noise ratio and to minimize the effects of multipath propagation, frequency modulation with a modulation index of 2 is recommended.

Bearing Error Analysis

(1) The principle bias error is receiver-filter delay distortion. This was analyzed under "Ranging," and can be eliminated by calibrating with an adjustable delay.

(2) The primary statistical errors are:

a. Antenna Pattern

Calibration curves will be derived for each antenna in free-space radiation tests, and again when mounted on Surveyor. However, the residual rms error during actual operations on the moon is estimated at this time to be in the range ±1 to ±2°. This error will be dependent on the SLRV-Surveyor-Moon geometry (i.e., tilt to Surveyor and SLRV antennas, terrain variations, etc.). The more conservative value of ±2° is used for the remainder of this error analysis.

b. Signal to Noise

0.36° (see Ranging error analysis)

c. Filter Phase Stability

0.15° (see Ranging error analysis)

d. Reference Oscillator Error

0.14° (see Ranging error analysis)

e. Analog-to-Digital Encoding Error

0.35° (see Ranging error analysis)

f. Rise-Time Error

0.50° (see Ranging error analysis)

(3) Total RMS Phase Error

$$\sigma_{T_\phi} = \sqrt{2^2 + \overline{0.38}^2 + \overline{0.15}^2 + \overline{0.14}^2 + \overline{0.35}^2 + \overline{0.50}^2}$$

$$\sigma_{T_\phi} = 2.13 \text{ degrees, rms}$$

3. Alternate Techniques Investigated

Ranging

In the selected Pseudo-Noise-Code method of ranging, a noise-like sequence of pulses is transmitted from the DSIF site to Surveyor and then transponded back to DSIF. The return code is cross-correlated with a delayed replica of the code, the delay time being a measure of the range of Surveyor. A second sequence is sent from DSIF to Surveyor to SLRV, then back to Surveyor, than back to DSIF. This second time around provides a measure of the total range from DSIF to SLRV.

Subtraction of the second measurement from the first should result in a measure of the range between Surveyor and SLRV. However, it is felt that the accuracy of such a range calculation will be rather poor because of the presence of lunar perturbations. Russell[3], et al, state that there are 155 periodic terms in the expression of perturbations of the lunar longitude, with coefficients exceeding 0.1° (approx. 200 meters), and more than 500 smaller ones. Moulton[4] analyzes some of the perturbations in his section on Lunar Theory.

At the present writing, there is no known measure of the amplitude of the perturbations that can occur in the 2.6 seconds time difference between the two ranging signals. Since the Earth-to-Moon link is not necessary to measure the range between Surveyor and SLRV, it is felt that the PN code method of ranging should not be used.

An approach which would provide simultaneous processing of a code such as E/S/SLRV/S/E, to avoid the 2.6-second delay between the E/S/E and the E/S/SLRV/S/E separate transmissions, would require complex equipment whose weight and primary power requirements would not be compatible with SLRV mission requirements.

Bearing

In addition to the selected technique of the four-element, two-port antenna and digital phase detector, two alternate

---

(3) Russell-Dugan-Stewart, "Astronomy" Pt. I The Solar System, Ginn & Co. pp. 287-290

(4) F. R. Moulton, "An Introduction to Celestial Mechanics", Second Rev. Edition 12th Printing 1959, The Macmillian Co., pp. 337-365.

techniques were investigated. These were the "Coherent Bearing Indicator" and "Lighthouse" methods. The former method was discarded because it required two antennas on Surveyor and had an inherent ambiguity. The latter approach required a motor to turn a dish antenna, which introduced mechanical problems and greater power consumption than the selected approach. Descriptions of these two approaches follow.

Coherent Bearing Indicator Method

The bearing (azimuth) angle from a base line established through Surveyor and SLRV is directly proportional to the phase difference between two r-f signals derived from a common oscillator. Both signals are compared in a calibrated phase detector. The phase detector produces a d-c voltage that is directly proportional to the cosine of the bearing angle.

Two antennas, spaced 1/4 wavelength apart, are mounted on the Surveyor vehicle. The r-f signals to the antennas are in quadrature (sine - cosine relationship). The resulting radiation pattern is shown in Figure II.2-33 for 0, 90, 180, and 270 degree bearings.

In actuality, one of the signals is sent at one-half the frequency of the other to prevent crosstalk problems in the receiving unit. Upon reception the one-half frequency signal is doubled. The phase angle of the one-half frequency is restored to the correct value when doubling occurs. To simplify the following discussion it will be assumed that both antennas are at the upper frequency.

Because of the 90 degree ($\frac{\lambda}{4}$) phase shift between the signals and the $\frac{\lambda}{4}$ wavelength spacing, the phase difference is 0 degrees on the semi-infinite line (determined by the two antennas) projecting to the right, 180 degrees on the semi-infinite line projecting to the left, 90 degrees up, and 270 degrees down, as shown in Figure II.2-33

The normalized d-c voltage out of a calibrated phase detector for any bearing angle is shown in Figure II.2-34.

A block diagram of the solid-state transmitter is shown in Figure II.2-35. The two antennas (60 mc and 30 mc) are simple whips mounted on the Surveyor at a spacing of $\frac{\lambda}{4}$ (5/4 meters ~ 4 feet); the reference frequency being 60 mc. A block diagram of the solid-state dual-frequency receiver is shown in Figure II.2-36 with the minimum signal levels and stage gains indicated. It is in reality two receivers; one tuned to 60 mc (ω_o) and the other tuned to 30 mc ($\frac{\omega_o}{2}$).

The 30 mc receiver amplifies the 400 microvolt signal up to 4.5 volts (peak). The 30 mc signal is then doubled to 60 mc and the resulting 2.8 volt (peak) signal is used to "gate" the 60 mc phase detector.

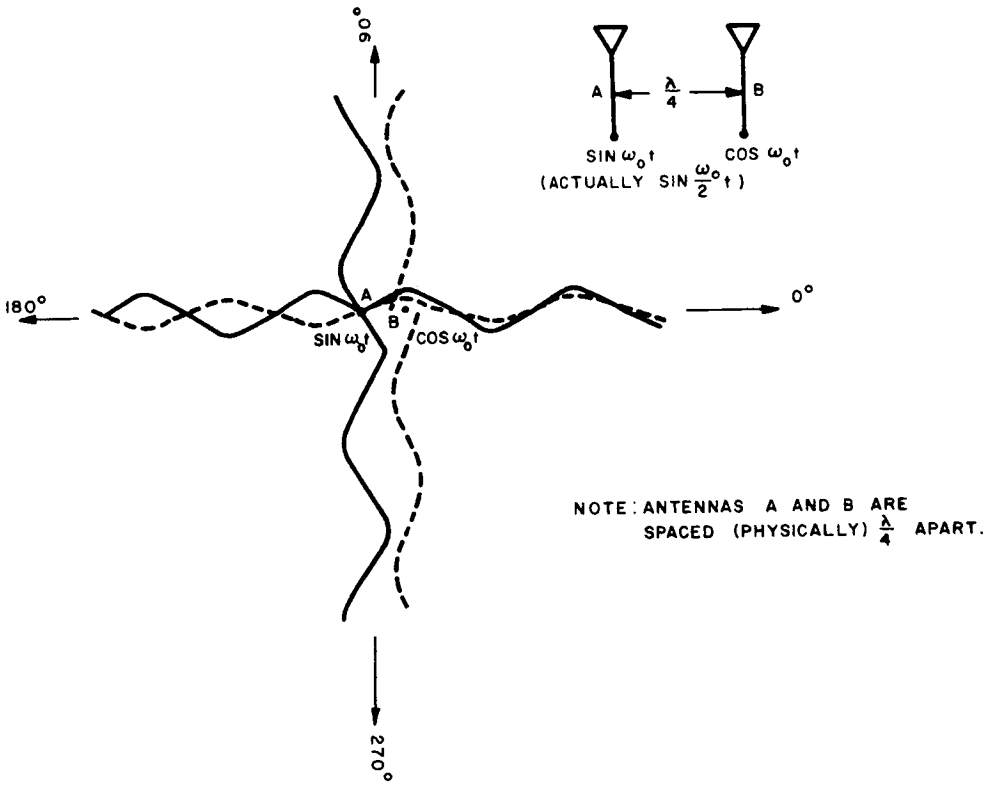

Figure II.2-33. Phase Relationships from the Two Surveyor Mounted Antenna Signals at 0, 90, 180, and 270 Degree Bearings

The other received signal (280 microvolt, 60 Mc, RF carrier) is amplified and limited in the Bearing Channel to 0.28 volt (peak). Constant amplitude voltage to the phase detector, independent of antenna signal strength, is assured by the utilization of solid-state high-frequency limiters. Thus, the output voltage (DC) is only a function of the phase angle between the reference and the bearing signals.

Only one antenna is used to receive both the 30 Mc and the 60 Mc signals. Isolation and matching is accomplished by the incorporation of a 30 Mc RF preselector and a 60 Mc RF preselector, as shown in the Figure II. 2-36.

"Light House" Method

A narrow beam of RF energy (2100 Mc to 2300 Mc) horizontally scans a full 360 degrees at a low rate (10 seconds/360 degrees) in a "Light-House" fashion. When the beam is pointing to a predetermined azimuth angle (due north) a VHF (100 mc to 200 mc) omni-directional (in the horizontal plane) r-f carrier is flashed on for a short time (0.01 second). The time difference between the illumination of the SLRV S-band receiving antenna and the reception of the VHF "flash" is a measure of the bearing of SLRV with respect to the reference line established on Surveyor.

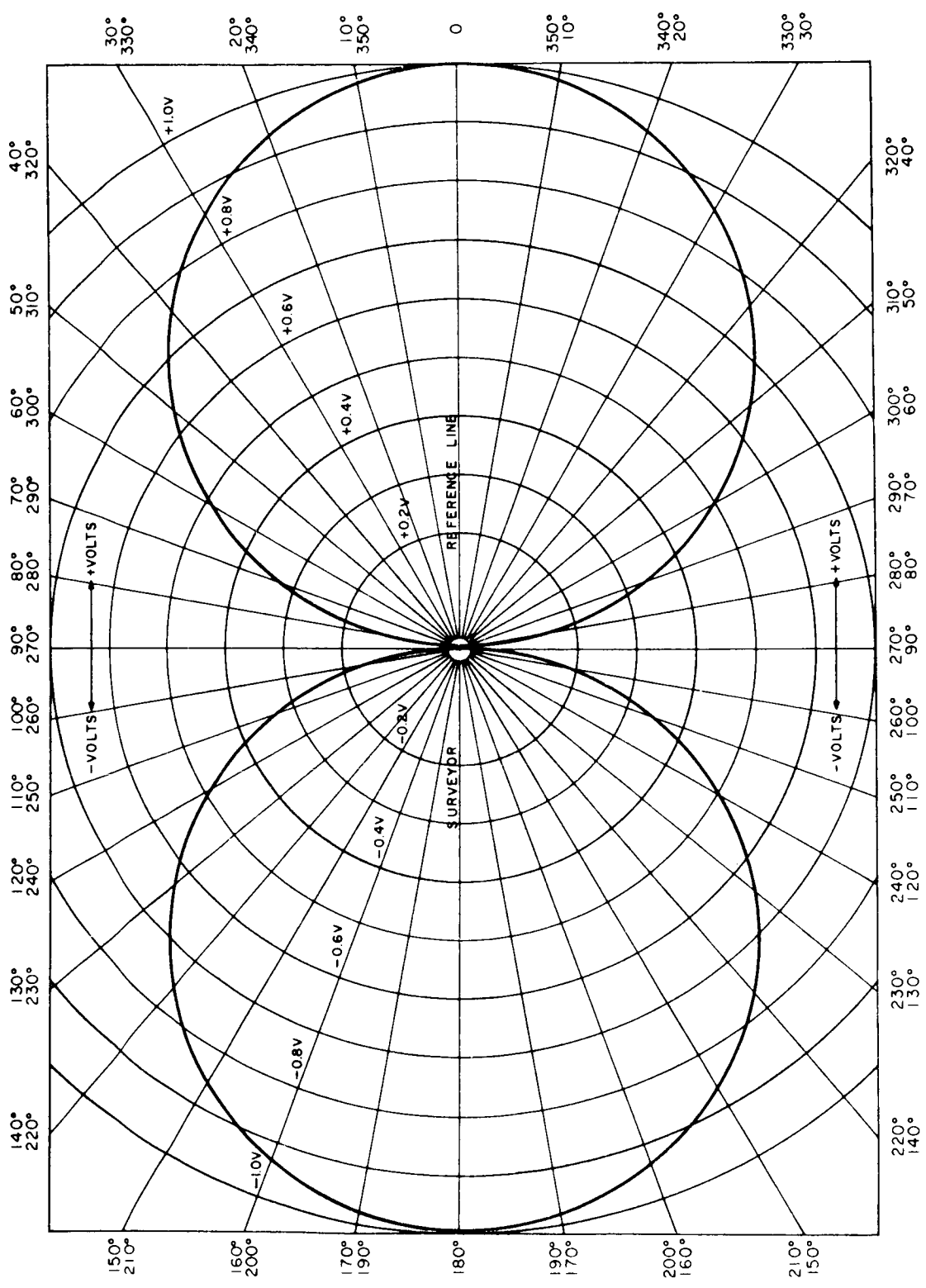

Figure II. 2-34. Normalized d-c Voltage Pattern of a Calibrated Phase Detector

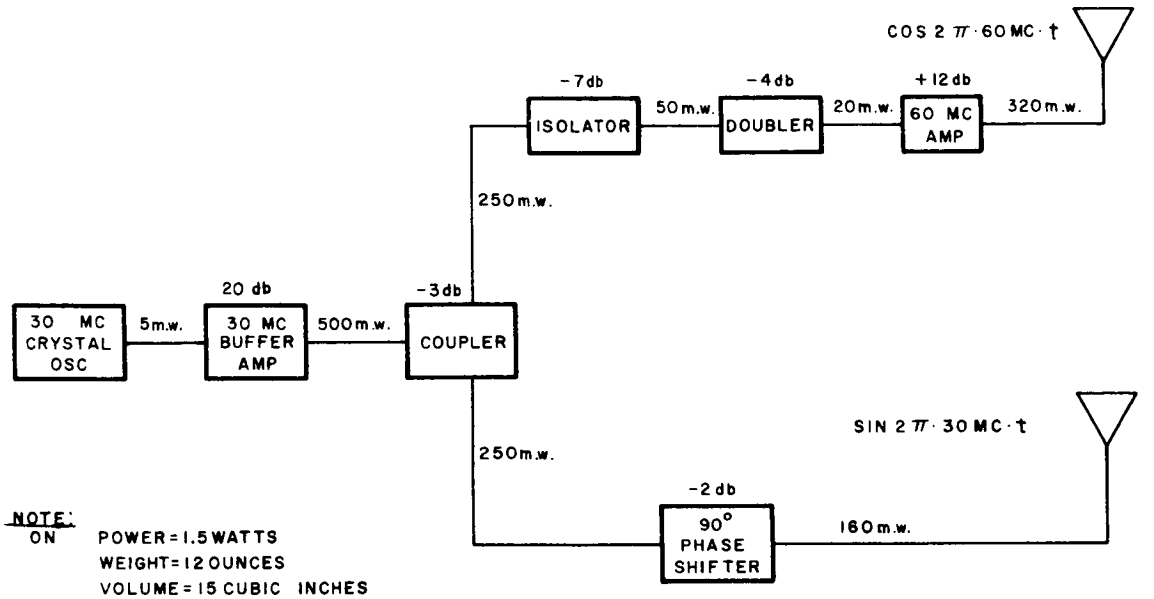

Figure II. 2-35. Bearing Angle Transmitter, Block Diagram

S-band, r-f energy could be fed into a 1-foot diameter, parabolic reflector that is rotating (upon command) in the horizontal plane at a rate of 1 revolution per 10 seconds, (36 degrees/second). At 2300 mc the 3-db beam width of the antenna is about 30 degrees, much too coarse for any practical bearing measurement. This, however, can be improved in the following manner. A predetermined threshold is set in the SLRV S-band receiver. The instant the input signal is large enough to cross the threshold (positive going) two time gates are opened and remain opened until:

a. the VHF omni-directional "flash" crosses its own threshold, closing the first gate. See Figure II. 2-36.

b. The other gate is closed after the received S-band signal falls below the threshold.

The end result is that the two pulses, T_1 seconds wide, and T_2 seconds wide, are sent back to earth via Surveyor for processing.

The processing consists of taking one-half the duration of T_2 and subtracting it from T_1. This results in a true measurement (if the S-band beam is symmetrical about the center line (C.L.), see Figure II. 2-37, of the bearing angle (in units of time) from the Surveyor 0-degree reference line and the SLRV vehicle.

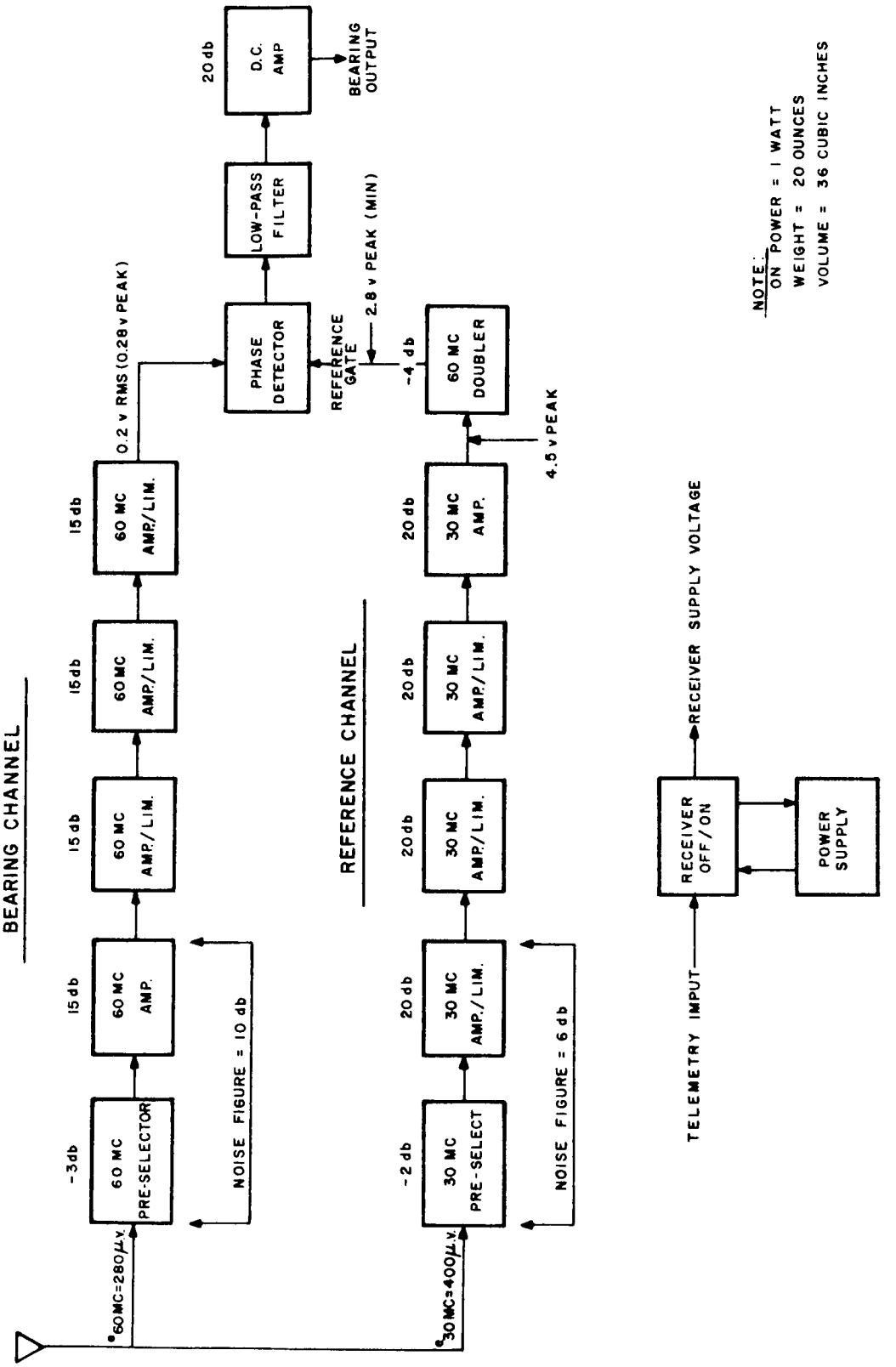

Figure II.2-36. Tentative SLRV Bearing Receiver, Block Diagram

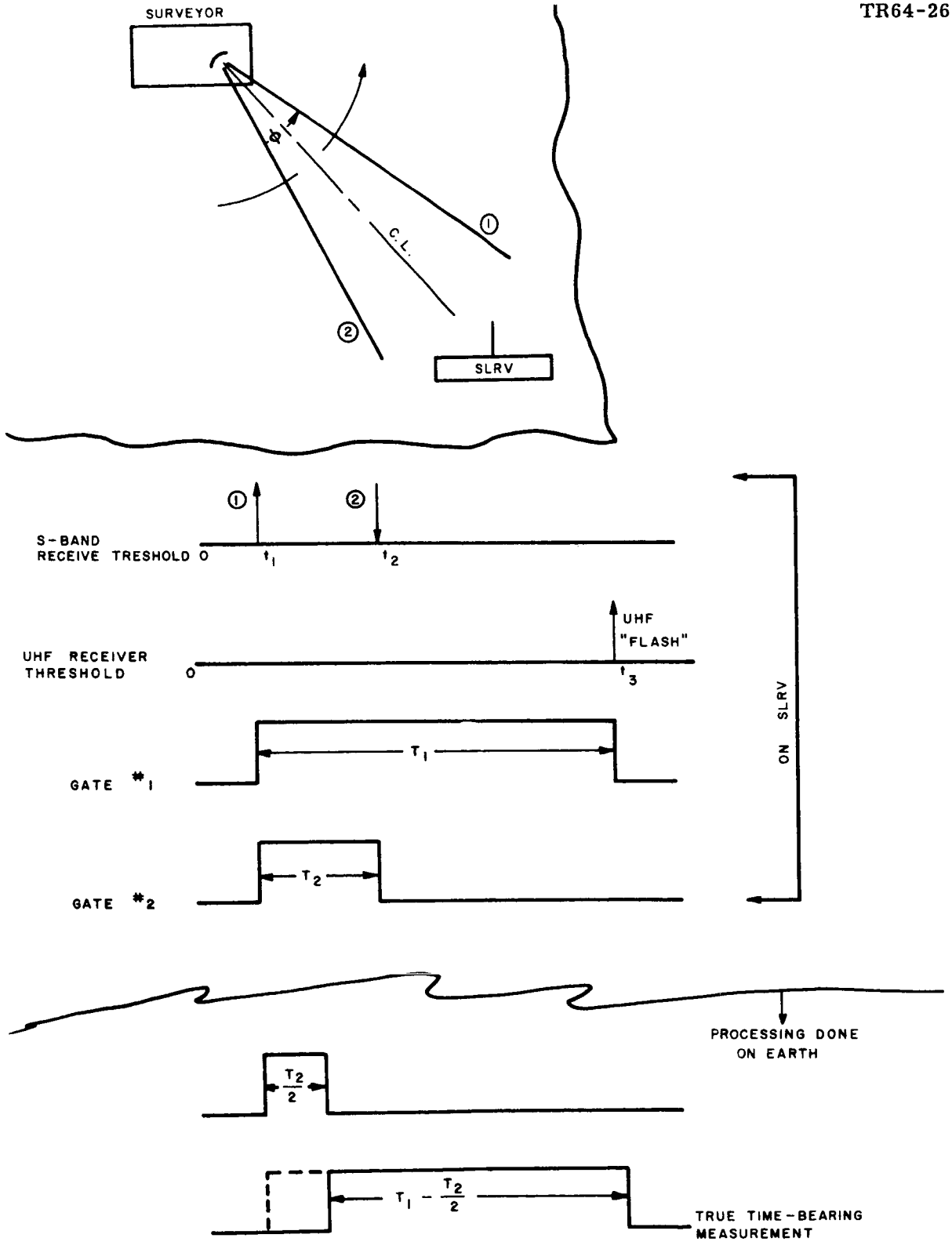

Figure II. 2-37. Light-House Timing Diagram

The S-band r-f energy can be obtained from the existing 10-watt S-band transmitter on board the Surveyor. (The required transmitted power is less than 10 milliwatts.) New equipment need only be a small RF probe (to extract the 10 milliwatts), a rotating coupler, a 12-inch parabolic reflector on a rotating shaft, and a drive motor. The required power is about 1.5 watts (motor drive), and this is only on when commanded from earth.

4. Phase Deviation Analysis for Single-Tuned Circuit

Consider the following parallel tuned circuit,

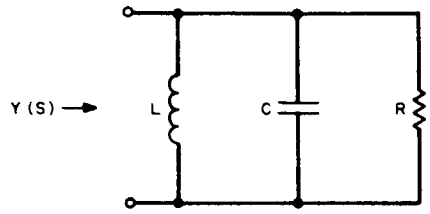

$$Y(S) = \frac{1}{LS} + CS + \frac{1}{R} = \frac{R+RLCS^2+LS}{RLS} \qquad \text{(II.2-79)}$$

$$Z(S) = \left(\frac{1}{C}\right)\left(\frac{S}{S^2 + \frac{S}{RC} + \frac{1}{LC}}\right) \qquad \text{(II.2-80)}$$

Let

$$W_o = \frac{1}{\sqrt{LC}}$$

and

$$Q = \frac{R}{W_o L}$$

Then:

$$\frac{1}{RC} = \frac{1}{QW_o LC} = \frac{W_o^2}{W_o Q} \quad \frac{Wo}{Q}$$

and

$$Z(S) = \left(\frac{1}{C}\right)\frac{S}{S^2 + \frac{W_o S}{Q} + W_o^2} \qquad \text{(II.2-81)}$$

Now let

$$S = jW, \text{ where } j = \sqrt{-1}$$

Then

$$Z(jW) = \left(\frac{1}{C}\right)\left(\frac{jW}{W_o^2 - W^2 + j\frac{W_o}{Q}W}\right) \qquad \text{(II. 2-82)}$$

$$= \left(\frac{1}{C}\right)\frac{W\left[\frac{W_o}{Q}W + j(W_o^2 - W^2)\right]}{(W_o^2 - W^2)^2 + \left(\frac{W_o}{Q}\right)^2 W^2}$$

$$= A(W) + j\,B(W)$$

$$= R(W)\,e^{j\theta}$$

where

$$R(W) = \sqrt{[A(W)]^2 + [B(W)]^2}$$

and

$$\theta = Tan^{-1}\frac{B(W)}{A(W)}$$

Considering only the phase angle θ,

$$\theta = Tan^{-1}\frac{W_o^2 - W^2}{\frac{W_o W}{Q}} \qquad \text{(II. 2-83)}$$

$$= Tan^{-1}\,Q\,\frac{f_o^2 - f^2}{f_o f}\,, \qquad \text{(II. 2-84)}$$

Now, let

$$f = f_o + \Delta f .$$

then,

$$\theta = Tan^{-1} Q \cdot \frac{f_o^2 - (f_o + \Delta f)^2}{f_o (f_o + \Delta f)} \qquad \text{(II. 2-85)}$$

$$= Tan^{-1} \left[- Q \frac{2\Delta f f_o - (\Delta f)^2}{f_o^2 + fo\Delta f} \right]$$

$$= Tan^{-1} \left[- Q \frac{2\frac{\Delta f}{f_o} - \frac{\Delta f^2}{f_o}}{1 + \frac{\Delta f}{f_o}} \right]$$

Let

$$\frac{\Delta f}{f_o} = x$$

then

$$\theta = Tan^{-1} \left[-Q \frac{x\,(2-x)}{1 + x} \right] \qquad \text{(II. 2-86)}$$

and

$$d\theta = \frac{1}{1 + \left[Q \frac{x(2+x)}{1 + x} \right]^2} (-Q) \frac{(2 - 2x)(1 + x) - 2x + x^2}{(1 + x)^2} dx \qquad \text{(II. 2-87)}$$

$$= \frac{(1 + x)^2}{(1 + x)^2 + Q^2 x^2 (2 + x)^2} (-Q) \frac{2 - 2x - x^2}{(1 + x)^2} dx$$

$$= - Q \frac{2 - 2x - x^2}{(1+x)^2 + Q^2 x^2 (2 + x)^2} dx$$

Now, since

$$x \ll 1,$$

$$d\theta \approx - \frac{2Q}{1 + 4Q^2 x^2} \, dx \qquad \text{(II.2-88)}$$

But

$$x = \frac{\Delta f}{f_o},$$

and

$$dx = \frac{1}{f_o} \, d(\Delta f).$$

Therefore:

$$\frac{d\theta}{d(\Delta f)} = \frac{\frac{2}{f_o} Q}{1 + \left(\frac{2Q}{f_o}\right)^2 (\Delta f)^2} \qquad \text{(II.2-89)}$$

Since the 3-db bandwidth, $B_3 = \frac{f_o}{Q}$,

then

$$\frac{d\theta}{d(\Delta f)} = - \frac{\frac{2}{B_3}}{1 + \left(\frac{2}{B_3}\right)^2 (\Delta f)^2} \, . \qquad \text{(II.2-90)}$$

And since

$$\frac{2\Delta f}{B_3} < 1,$$

then

$$\frac{d\theta}{d(\Delta f)} = - \frac{2}{B_3} \left[1 - \left(\frac{2\Delta f}{B_3}\right)^2 + \left(\frac{2\Delta f}{B_3}\right)^4 - \cdots \right] \qquad \text{(II.2-91)}$$

which is approximately

$$\frac{d\vartheta}{d(\Delta f)} = -\frac{2}{B_3}\left[1 - \left(\frac{2\Delta f}{B_3}\right)^2\right], \qquad \text{(II.2-92)}$$

The term, $-\frac{2}{B_3}$, represents the linear phase shift of the network, while the term, $\frac{2}{B_3}\left(\frac{2\Delta f}{B_3}\right)^2$, represents the deviation from linearity.

Letting:

$$\frac{d\theta_e}{d(\Delta f)} = \frac{2}{B_3}\left(\frac{2\Delta f}{B_3}\right)^2 \qquad \text{(II.2-93)}$$

and integrating, we have

$$\theta_e = \frac{8}{3}\left(\frac{\Delta f}{B_3}\right)^3 \quad \text{in radians,} \qquad \text{(II.2-94)}$$

or

$$\theta_e = 152\left(\frac{\Delta f}{B_3}\right)^3 \quad \text{in degrees.} \qquad \text{(II.2-95)}$$

5. Rise-Time Uncertainty

To change the state of the flip-flop, a differential voltage of at least 0.6 volt peak is required, in the case of silicon transistors. This voltage must be obtained in no more than 0.5° of the axis crossing of the 200-kc sine wave. See Figure II.2-38 on the following page.

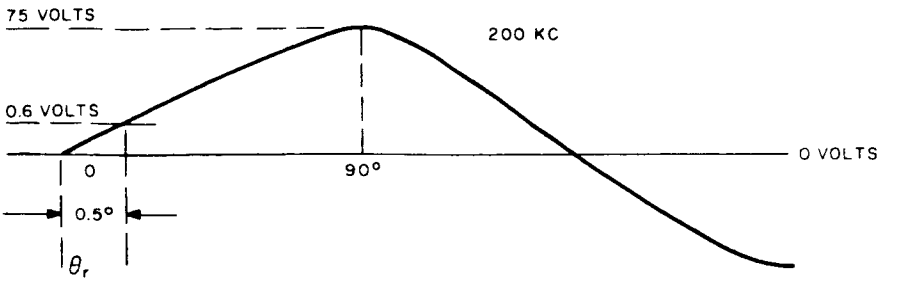

Figure II.2-38

If the sine wave were not altered, the voltage at the peak of the wave (90° angle) would be 75 volts, while the total peak-to-peak signal level would be 150 volts. For the power supply voltages available, complicated circuit design would be required to furnish the 150-volt swing. Care would also have to be taken to prevent "transistor breakdown". A more practical method of obtaining the rise time without excessive voltage levels is shown in Figure II.2-39 and described below.

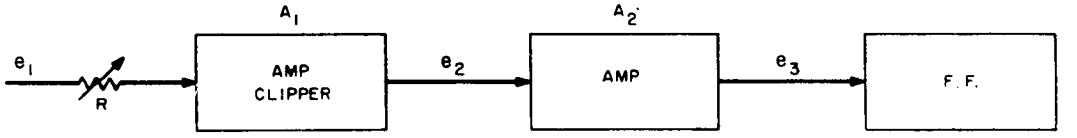

Figure II.2-39

The signal, e_1, is set by R to the maximum input level (A_1) at which linearity can be maintained, i.e. approximately 0.8 volt peak. The signal is amplified by a factor of 10 to 8 volts peak, and then clipped to a level of 0.6 volt by two parallel (reversed) high-speed silicon diodes.

Amplifier A_2 then raises the 0.6-volt e_2 signal to a level of 6 volts peak. It can be seen that if no clipping were performed on the signal, the output voltage, e_3, would be 0.8 x 10 x 10 = 80 volts peak, slightly higher than the 75 volts required in the previous case. However, even though the amplitude has been altered, the rise time is of the required value to produce a phase uncertainty, θ_r, of less than 0.5 degree. This 0.5 degree results in a range uncertainty of 2 meters.

Note: The X10 gain of each A_1 and A_2 represents a good compromise between gain, stability, and impedance levels.

6. Preservation of Bearing Angle Undergoing Frequency Translation

Let the reference signal be:

$$\cos \omega_o t, \tag{II.2-96}$$

and the phase-shifted signal be:

$$\cos (\omega_o t + \phi_o), \tag{II.2-97}$$

and the injection frequency be:

$$\cos (\omega_1 t + \phi_1) . \tag{II.2-98}$$

Mixing (II.2-96) and (II.2-98) we have:

$$\begin{aligned} &\cos \omega_o t \cos (\omega_1 t + \phi_1) \\ &= \tfrac{1}{2} \cos [(\omega_o - \omega_1) t - \phi_1] + \tfrac{1}{2} \cos [(\omega_o + \omega_1) t + \phi_1] . \end{aligned} \tag{II.2-99}$$

Lowpass filtering and normalizing (II.2-99) gives:

$$\cos [\omega_o - \omega_1) t - \phi_1] . \tag{II.2-100}$$

In similar manner, mixing (II.2-97) + (II.2-98) gives:

$$\cos [(\omega_o - \omega_1) t - \phi_1 + \phi_o] \tag{II.2-101}$$

Mixing (II.2-100) and (II.2-101) gives:

$$\begin{aligned} &\cos [(\omega_o - \omega_1) t - \phi_1] \cos [(\omega_o - \omega_1) t - \phi_1 + \phi_o] \\ &= \tfrac{1}{2} \cos \phi_o + \tfrac{1}{2} \cos 2 [(\omega_o - \omega_1) t - \phi_1 + \frac{\phi_o}{2}] \end{aligned}$$

Filtering and normalizing shows that ϕ_o is preserved.

E. ANTENNA INVESTIGATION

1. Antenna Type Studied

The antenna requirements for the Surveyor Lunar Roving Vehicle mission after the vehicle is deployed on the moon can conveniently be discussed relative to three possible communication links:

A. Direct vehicle-to-earth (SLRV/E)

B. Direct earth-to-vehicle (E/SLRV)

C. Communication between SLRV and the Surveyor (SLRV/S).

Link A would be used to send all data from the vehicle to the earth. Link B would be used to send all commands from the earth to the vehicle. Link C would be used for two purposes:

(1) Two-way communication in which the Surveyor would act as a relay station for communication between the earth and the SLRV.

(2) Direction finding or azimuth bearing determination of the SLRV relative to the Surveyor.

The use of Links A and B would make the SLRV relatively independent of the Surveyor, assuming that bearing information can be obtained by some independent means. The full use of Link C, in which the Surveyor acts as a relay station, relieves the vehicle antenna needs to the extent that Link A is not essential. It is likely that Link B will always be necessary, although it may, to some extent, be combined with Link A. Equipping all three links adds some redundancy to the Communication Subsystem.

The vehicle antenna requirements for the three links are as follows[1]:

Link A: SLRV-to-Earth

1. gain (3 db points): range of 10 db to 30 db
2. frequency: 2295 Mc
3. polarization: linear or elliptical
4. bandwidth: 1 percent maximum
5. steering capability: The 3-db beamwidth should preferably encompass Earth at transmission. Since the SLRV will move about on the moon's surface and may negotiate steep slopes up to 70 degrees, techniques and equipment suitable for Earth-sensing and steering of the antenna must be investigated.

(1) F.A. Hartshorne letter, August 27, 1963.

6. mechanical considerations: extremely lightweight (preferably less than one pound) and storable within the available volume for the SLRV.

Link B: Earth-to-SLRV

1. gain: greater than -10 db
2. frequency: 2115 Mc
3. polarization: linear or elliptical
4. bandwidth: 0.5 percent maximum
5. mechanical considerations: same as link A.

Link C: SLRV-to-Surveyor

1. gain: pattern to provide maximum uniform directivity in azimuth plane with minimum degradation to ±20 degrees out of this plane
2. frequencies: (a) range of 30 to 400 Mc
   (b) range of 2100 to 2300 Mc
3. polarization: horizontal or vertical
4. bandwidth: linear variation from 1 Mc to 30 Mc to 5 Mc at 400 Mc (these are maximum values)
5. diplex considerations: antenna may be common for transission and reception
6. heights: approximate antenna heights above local terrain are 15 meters for the Surveyor and 2 to 4 meters on the SLRV.
7. mechanical: same as link A.
8. bearing accuracy: ±5 degrees

Use of Link C at a frequency other than the DSIF one, which is 2100 to 2300 Mc, will require additional antennas on the Surveyor and these, therefore, need to be considered in this study.

Links A and B may be considered to have the same propagation paths, and thus the following angles are pertinent to both:

(1) Location of landing spot on moon:	±60 degree longitude ±10 degree latitude
(2) Lunar libration:	±8 degree longitude ±7 degree latitude
(3) Subtended angle of earth:	2 degrees
(4) Excursion of vehicle axis from local vertical during motion:	±70 degrees

Fig. II.2-40 illustrates the antenna coverage required for the maximum extent of these angles. This amounts to a maximum coverage of 280 degrees and reduces to a minimum of about 160 degrees if the landing spot is at zero degrees latitude and longitude. Presumably a reasonably precise knowledge of the landing spot will be available prior to launch and can be preset into the stabilization system. The mission length will be sufficiently long that the full libration angles will be transversed. These could be pre-programmed as a function of time, however. Thus, in principle only the 70-degree movement of the vehicle relative to local vertical and the 360 degrees in azimuth will need to be corrected for in the antenna pointing. However, a fixed antenna on the vehicle such as for Link B will need to have the 140- to 280-degrees coverage, dependent upon the exact landing spot.

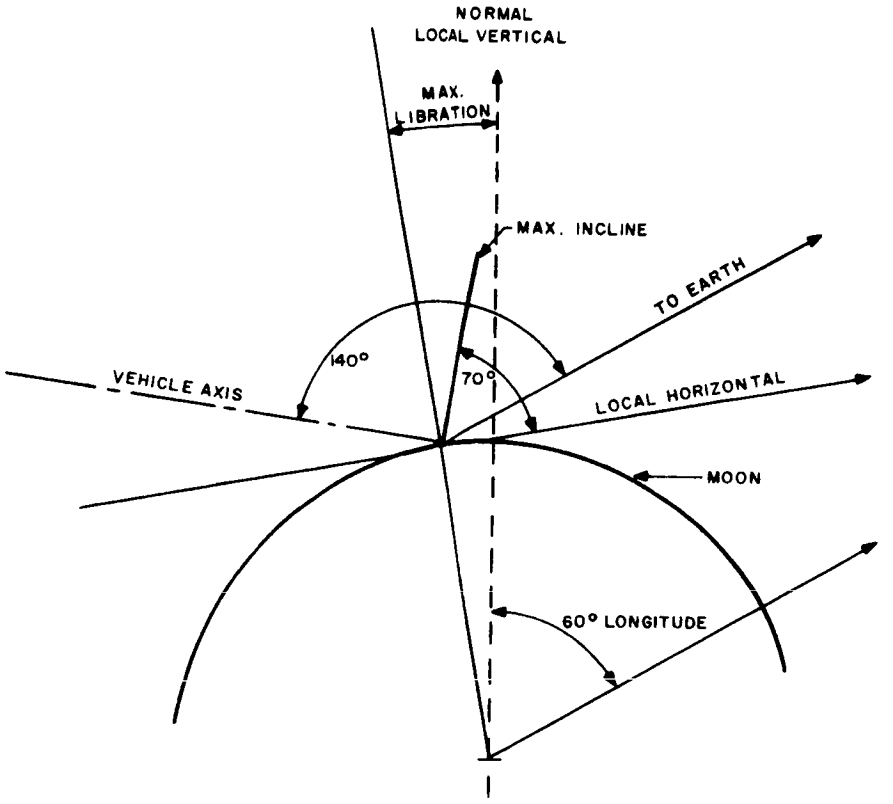

Figure II.2-40. Antenna Coverage Required for Maximum Communications Coverage of 280 Degrees

Conical Dipole

Application: communication between Surveyor and SLRV

Electrical characteristics: omnidirectional azimuth pattern vertical polarization dual-band operation (VHF and S-band)

The geometry of a conical dipole is defined by an angular dimension (the cone-flare angle) and a linear dimension (the cone length). Only the latter of these two parameters is a function of frequency change. A characteristic of the conical dipole is its broadband impedance properties, as shown by the curves of Figure II. 2-41 (a). Another characteristic is the reduction in length at the first resonance. In the example shown, the half-length at first resonance is 45 degrees (or 1/8 wavelength); thus the over-all length is only 1/4 wavelength.

For the first resonance at an arbitrarily chosen VHF frequency of 400 Mc, a flare angle of 50 degrees will give a second resonance at 2295 Mc. The balanced input resistances will then be 40 ohms and 180 ohms, respectively, at the two frequencies. A simple composite matching transformer may then be designed to give an impedance match at both frequencies to a feed line having a characteristic impedance of, say, 200 ohms.

The curves of Fig. II. 2-41 (b) show the elevation patterns of the conical dipole at both frequencies with respect to a linearly polarized isotropic source. The angle θ is measured from the axis of the dipole. The 400 Mc pattern is practically the same as that produced by a half-wave dipole. However, the 2295 Mc pattern is considerably broader, giving approximately isotropic coverage except for small null cones at the poles.

Fig. II. 2-42 shows the conical dipole dimensions and details of one feed method. The lightweight transmission line may be made of three narrow aluminum strips on a mylar ribbon. The center strip is fed against the two outer strips to form a coaxial-type line. The equipotential outer strips join to the truncated tip of the lower cone, and the center strip extends to the tip of the upper cone. The matching transformer may be incorporated in this terminal region.

Advantages:

Simplicity in construction
Small size at VHF (only 1/4 wavelength in height)
Dual-band operation
Very broad elevation-angle coverage at 2.3 kmc.

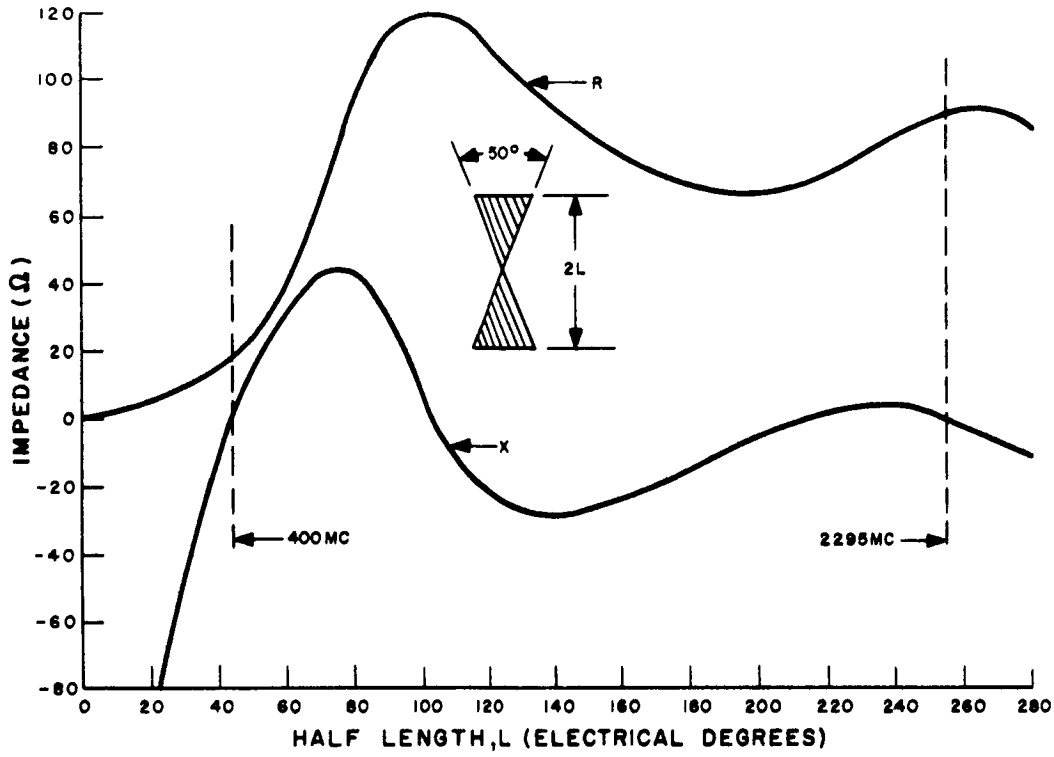

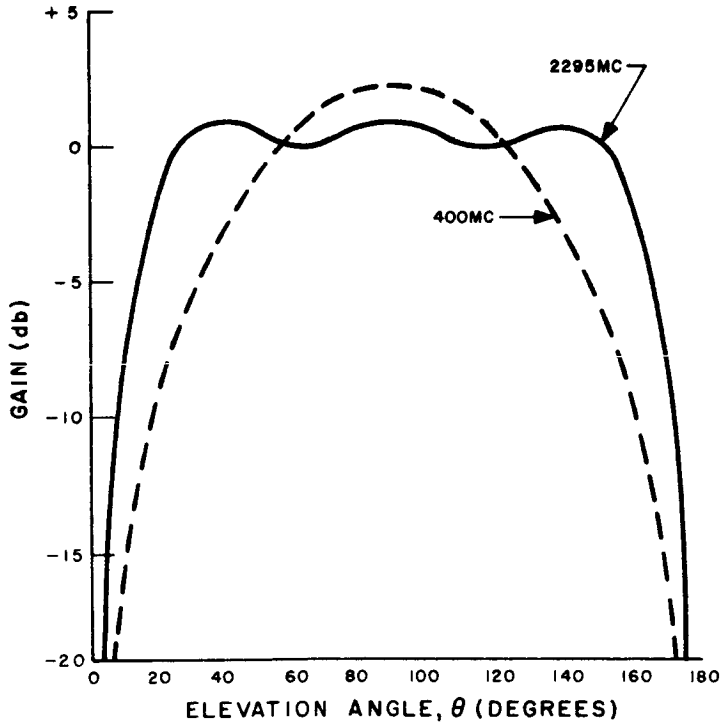

Figure II. 2-41. Impedance and Elevation Patterns of the Conical Dipole Antenna at 400 Mc and 2295 Mc

Turnstile

Application: communication between Surveyor and SLRV and between Earth and SLRV.

Electrical Characteristics: hemispherical coverage, horizontally polarized in azimuth plane ($\theta = 90°$), circularly polarized at pole ($\theta = 0°$).

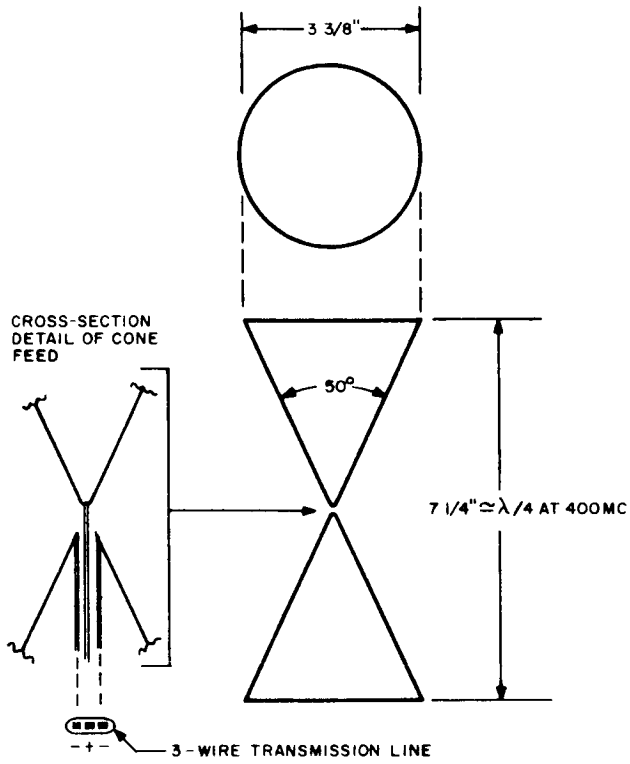

Figure II.2-42. Dual-Band Conical Dipole

The turnstile antenna consists of crossed dipoles fed with equal amplitude voltages in phase quadrature. A perfectly circular pattern is obtained in the plane of the turnstile for very-short dipole elements. The slighly narrower pattern produced by practical half-wave dipoles results in an amplitude variation of 0.9 db in the azimuth plane (Figure II.2-43). The gain figures are relative to a linearly polarized isotropic source.

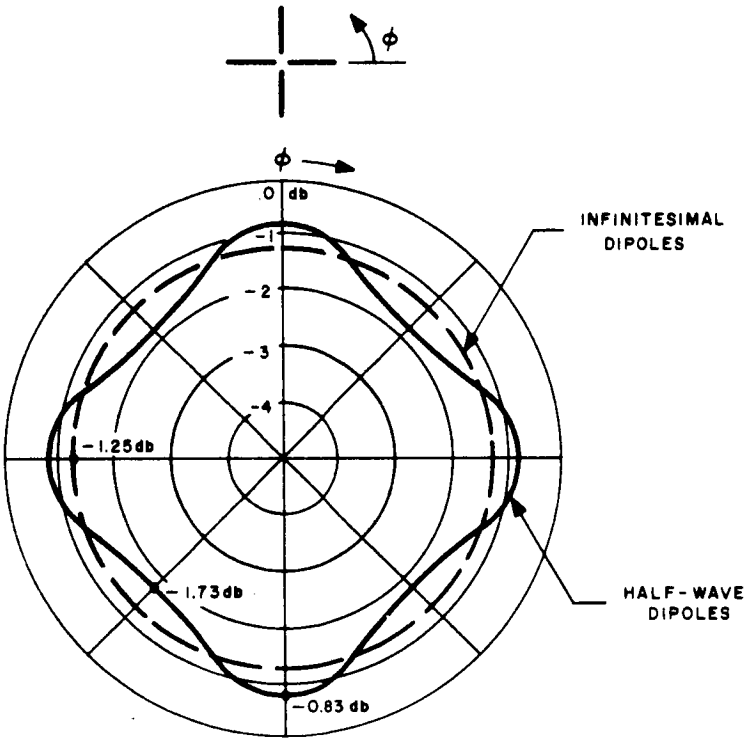

Figure II.2-43. Azimuth Patterns of Turnstile Antennas ($\theta = 90^{o}$)

The curves of Fig. II.2-44 show the signal variation with respect to a circularly polarized source as measured in the elevation plane with circularly polarized antennas. Also plotted is the ellipticity, or axial ratio, indicating that the radiation is circularly polarized at the poles and linearly polarized in the azimuth plane.

For simplicity in calculations, these radiation properties as well as those that follow for other low-gain antennas are based on the use of infinitesimal unit-radiators which produce patterns having rotational symmetry about the $\theta = 0^{o}$ axis. Practical antennas would produce only small departures from these idealized characteristics, as indicated in Figure II.2-43.

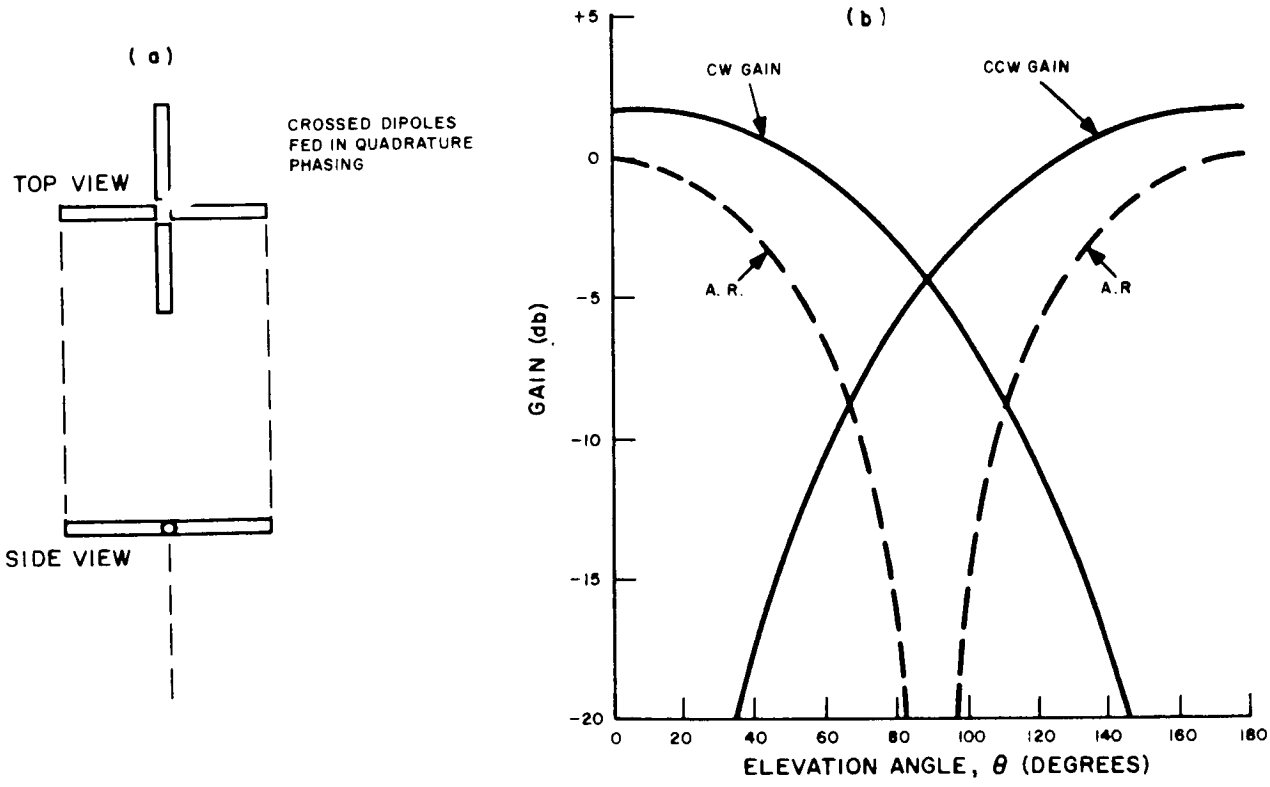

Figure II. 2-44. Signal Variation as Measured with Circularly Polarized Antennas

A closer approximation to these theoretical patterns may be realized by employing crossed radiators made in the form of "fan" or triangular elements (Fig. II. 2-45 (a)). As with the cone, a fan dipole at first resonance is considerably shorter than a half-wave in over-all length; this reduction in length is also accompanied by a broader dipole pattern more closely approximating that of an infinitesimal dipole.

If an unfurlable turnstile antenna with foreshortened fan elements must operate at a lower VHF frequency, one approach would be to print the fans on dielectric sheets hinged at their edges to form a "four-page book," which opens with the sheets locking at right angles.

In the ordinary turnstile having crossed dipoles fed in phase quadrature, each dipole must be matched to obtain the equal power division necessary for a symmetrical azimuth pattern. As the dipoles are shortened below first resonance, the VSWR increases as illustrated in Fig. II. 2-45 (b), and the azimuth pattern becomes bidirectional. An equalizing network, shown in Fig. II. 2-46 (a), may be employed to overcome this problem. This network has two quarter-wave lines branching from the input port to feed the orthogonal dipoles. Two resistors are

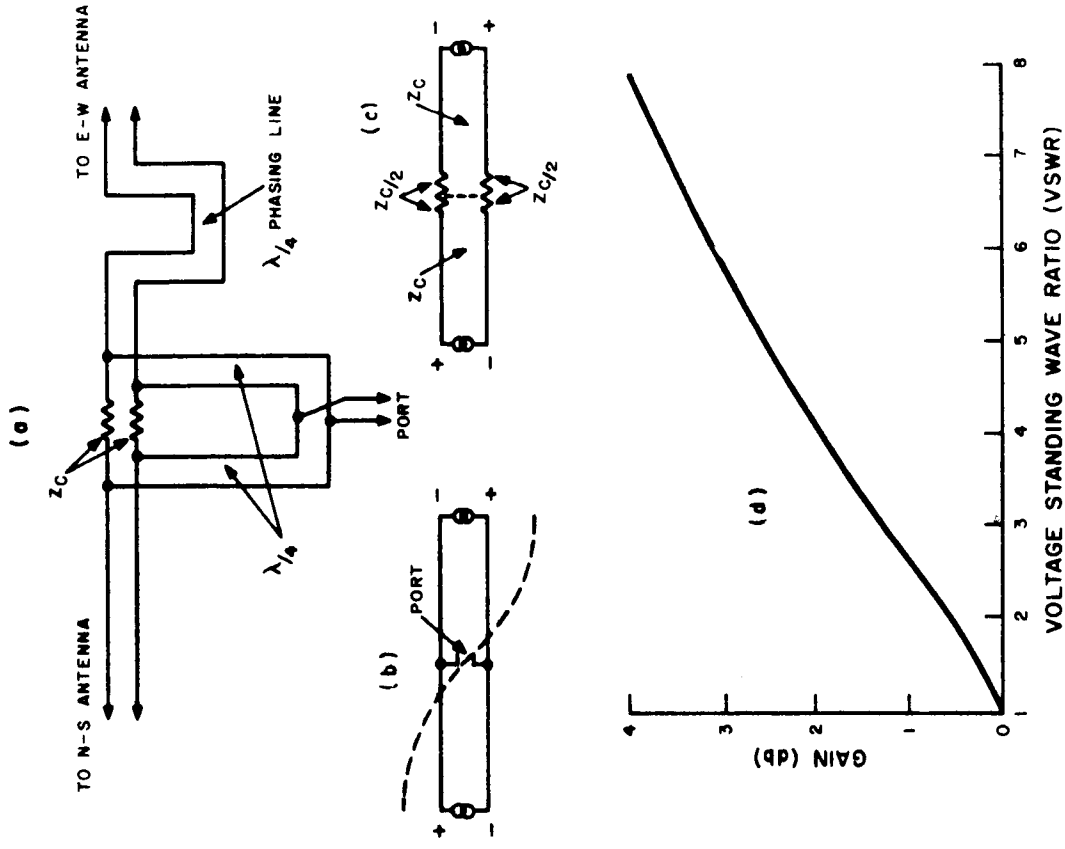

Figure II. 2-46. Reflection Absorption Circuitry

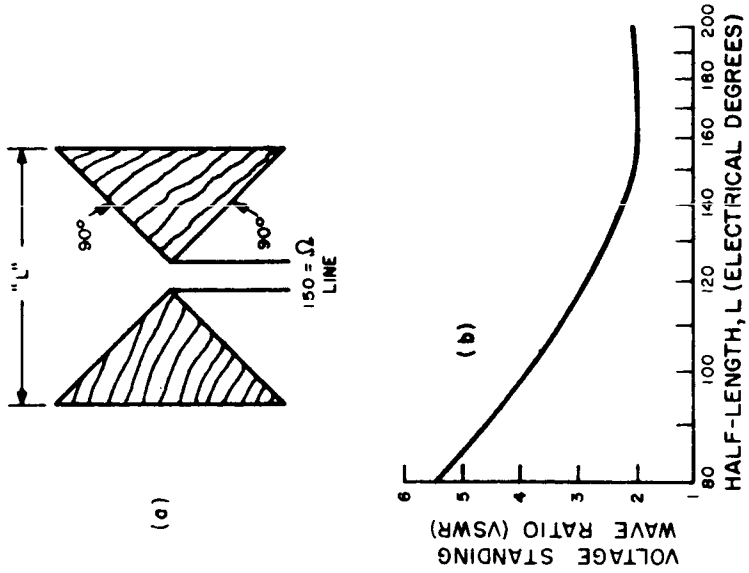

Figure II. 2-45. Fan Dipole Antenna

joined across the quarter-wave lines as indicated. No power is absorbed by the resistors for an incident wave traveling from the input to the dipoles, since no potential is developed across either resistor. If the crossed dipoles are mismatched, however, the two reflected waves will arrive at the resistor terminals out of phase because of the round-trip differential phase lag through the quarter-wave phasing line. These waves, being out of phase, cannot feed into the input (Fig. II. 2-46 (b)), and the reflected power is completely absorbed by the resistors, as illustrated in Fig. II. 2-46 (c). Thus the radiated power of the two dipoles is equal, independent of their mismatch, at the cost of wasted power in the resistors. Fig. II. 2-46 (d) illustrates the relative magnitude of the power lost with respect to the VSWR of the crossed dipoles. It is seen for example, that even a 4:1 VSWR results in only a 2-db loss in power gain.

Array of Four Tilted Dipoles

Application: communication between (1) Surveyor and SLRV, and (2) Earth and SLRV.

Electrical Characteristics: improved hemispherical coverage.

It is noted from Fig. II. 2-43(b) that the turnstile has a 6-db drop in gain from the zenith ($\theta = 0^{\circ}$) to the azimuth plane ($\theta = 90^{\circ}$). An improved hemispherical coverage may be obtained with an array of four tilted dipoles in the form of a square (Fig. II. 2-47 (a)) and fed in progressive phasing. By proper choice of the square dimensions (S) and the dipole tilt angle (α), circular polarization may be produced in the azimuth plane as well as at the zenith. This is illustrated in Figure II. 2-47 (b), which shows the axial ratio characteristic and circularly polarized gains with respect to a circularly polarized isotropic source. It is seen that the coverage for one sense of circular polarization is considerably improved as compared with the simple turnstile, which has identical clockwise and counterclockwise pattern shapes. The desired sense of circular polarization in the upper hemisphere for this array is controlled by the direction of the dipole tilt angles and the sense of the dipole phase excitations. The patterns of Fig. II. 2-47 (b) are produced by a spacing of approximately one-third wavelength between opposite dipole elements. Thus the size of this array is small in terms of wavelengths.

Azimuth Direction Finder

Application: direction finder on Surveyor to locate SLRV in azimuth; communication between Surveyor and SLRV.

Electrical Characteristics: omnidirectional azimuth pattern, vertical polarization azimuth direction finding.

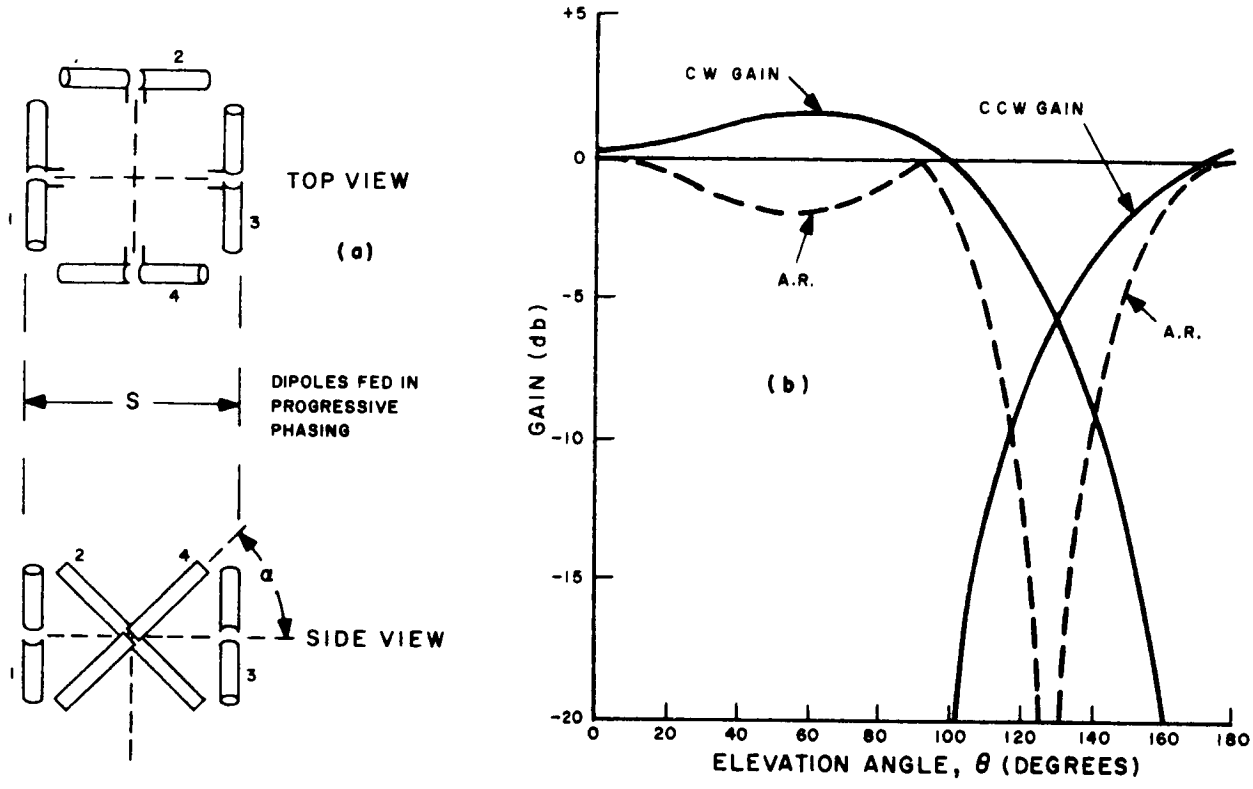

Figure II.2-47. Array of Four Tilted Dipoles

A direction-finding array designed for a typical VHF frequency of 400 Mc is pictured in Fig. II. 2-48 (a). Four equally spaced vertical dipoles are joined by open-wire lines to circuitry at the center of the array. This circuitry, shown in Figure II. 2-48 (b), consists of two square hybrids made of balanced quarter-wave line sections. Signal at the input labeled "o mode" will feed all four dipoles in phase. Signal at the "+1-mode" input will energize the four dipoles in progressive phasing. There will be no cross-coupling between the two inputs.

The radiation patterns produced from power applied at either of the inputs are similar in shape, each being a "doughnut" type essentially omnidirectional in azimuth, with nulls along the vertical axis. However, the far-field phase for the 0-mode input is constant for all azimuth angles, while the phase for the +1-mode input is proportional to the azimuth angle. Therefore, a comparison of the received phase between the two ports gives the azimuth direction of the incoming wave without ambiguity. Either port may also be used for communication.

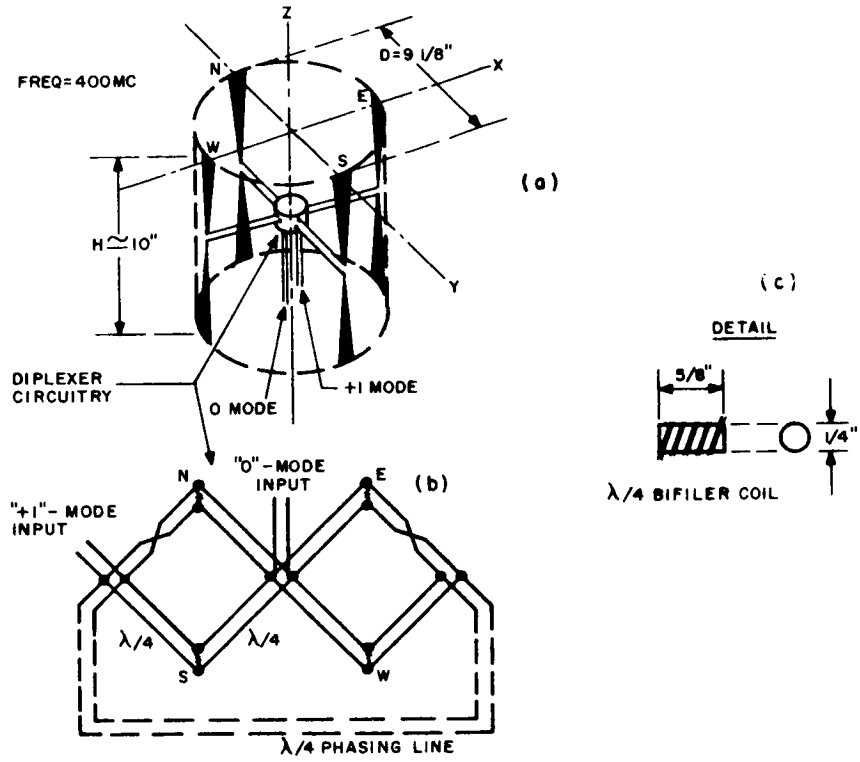

Figure II.2-48. Direction Finder, Four Vertical Dipoles

As the spacing D between opposite dipoles decreases, the azimuth patterns for the two ports become more circular. On the other hand, a reduced spacing increases the impedance-matching problems. A value of D = 0.31λ was chosen for the design of Fig. II.2-48 (a) as a satisfactory compromise. For this spacing the greatest azimuth pattern variations is 1.0 db. This will cause a maximum bearing error of ±3 degrees at azimuth angles of 22.5 degrees, 67.5 degrees, etc. No error occurs at angles of 0, 45, or 90 degrees, etc.

The circuitry of Fig. II. 2-48 (b) may be made in a very compact form by winding the quarter-wave line sections as bifilar coils, as shown in Figure II. 2-48(c). The entire circuitry may then be enclosed within a container about 1.5 inches on a side.

Elevation-Azimuth Direction Finder (Turnstile plus single axial radiator)

Application: direction finder on SLRV to obtain θ, ϕ bearings on circularly polarized signals from Earth; reception of 2.3-kmc command signals from Earth.

Electrical Characteristics: hemispherical coverage; direction-finding in two coordinates (θ, ϕ).

This antenna is a combination of the horizontal turnstile previously described and a single vertical radiator located at the turnstile center. Circularly polarized patterns in the elevation plane for each of these two decoupled components are plotted in Figure II.2-49(a) with respect to a circularly polarized isotropic source. The pattern for the vertical radiator (0-mode) has nulls along the vertical axis ($\theta = 0^{o}$, 180^{o}) and a maximum value in the azimuth plane ($\theta = 90^{o}$). Hence the ratio of the amplitudes for the two ports (plotted in Figure II.2-49(b) is a measure of the bearing from the $\theta = 0^{o}$ axis. The azimuth bearing (ϕ) may also be obtained from a phase comparison between the two ports. Thus, complete bearing information is obtained to control the pointing toward Earth of a high-gain transmitting antenna on the SLRV. Hemispherical coverage is also obtained from the +1-mode port for reception of commands from Earth.

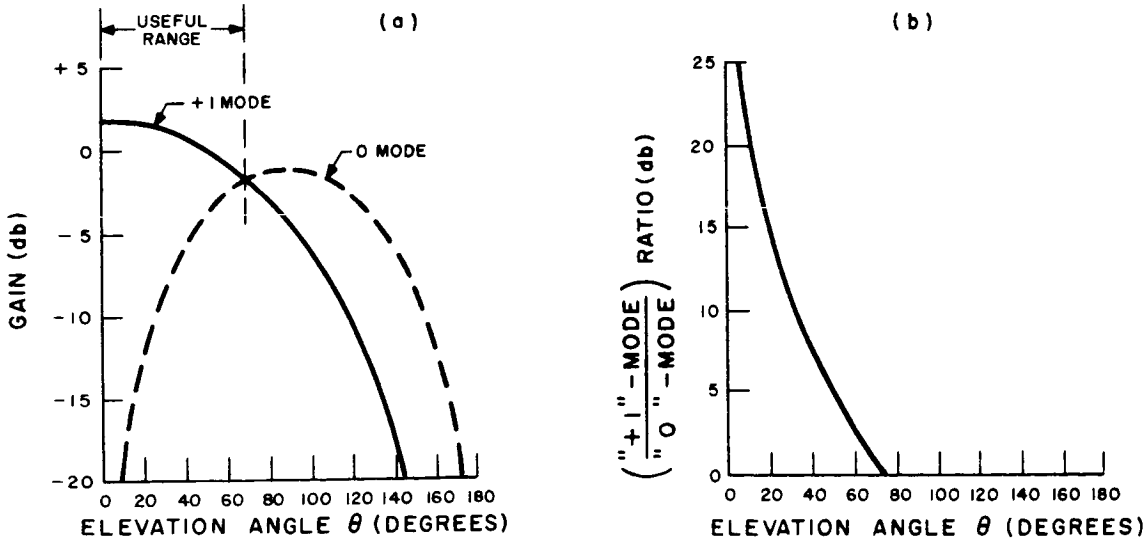

Figure II.2-49. Direction Finder, Turnstile and Single Axial Radiator

Elevation-Azimuth Direction Finder (Array of four tilted dipoles plus a single axial radiator)

Application: improved direction finder on SLRV to obtain θ, ϕ bearings on circularly polarized signals from Earth; improved reception of 2.3 kMc command signals from Earth.

Electrical characteristics: more than hemispherical coverage; direction finding in two coordinates (θ, ϕ).

An improved direction finder may be made by combining an axial radiator (0-mode) with the array of four tilted dipoles (+1-mode) previously described in Fig. II. 2-47. The elevation patterns for circular polarization obtained from the two separate ports are plotted in Figure II.2-50(a) with respect to a circularly polarized isotropic source. Bearings for θ and ϕ are obtained as in the preceding direction finder. On comparing Figure II.2-49(a) and Figure II.2-50(a), it is seen that the broader coverage of the four-dipole array gives an extended useful range for the θ-bearing determination. The amplitude ratio of the signals from the two decoupled ports is plotted in Figure II.2-50(b). The maximum dimension of either of the two direction finders described in Figure II.2-49 and II.2-50 less than 2.5 inches for a design frequency of 2.3 kMc.

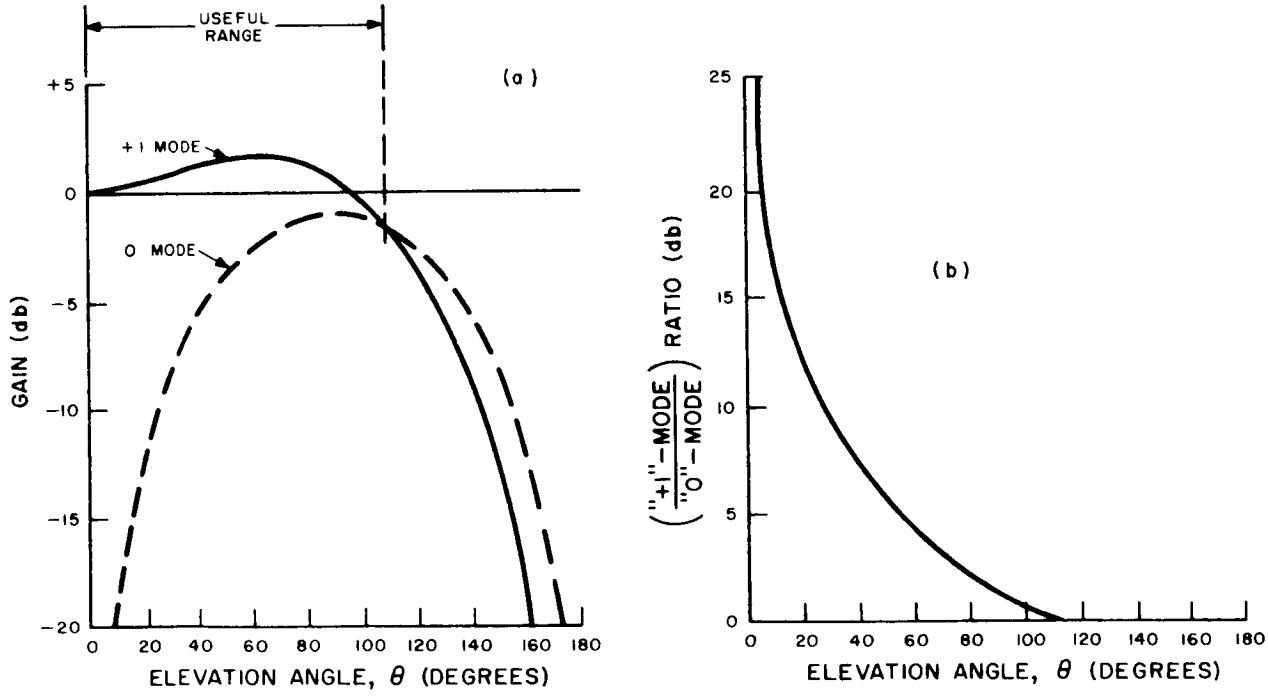

Figure II 2-50. Direction Finder, Array of Four Tilted Dipoles and Single Axial Radiator

Work has now started on determining the effect of ground reflections on the accuracy of the bearing for the various direction finding systems considered. If necessary, a study will be made on modifications of the antenna components to reduce the ground pickup.

Directive Antennas for SLRV, Single Helix

Application: medium-gain SLRV antenna for 2.3-kMc transmission to Earth.

Electrical Characteristics: circular polarization, 14-db gain.

The end-fire helix is a simple, lightweight antenna of moderate gain for transmission of the 2.3-kMc data from the SLRV to Earth. Circular polarization is inherently obtained from this type of antenna. Figure II.2-51 shows the design of a single helix having a gain of 14 db. The spiraled conductor is printed on a thin-wall dielectric cylinder. If it is necessary to unfurl this antenna, the cylinder may be made of a gas-inflated mylar tube. Another technique employs a self-erecting, flexible, foam cylinder to support the spiral. Since the helix is very broad band in both the radiation and impedance characteristics, it is relatively uncritical to minor variations in its geometric dimensions.

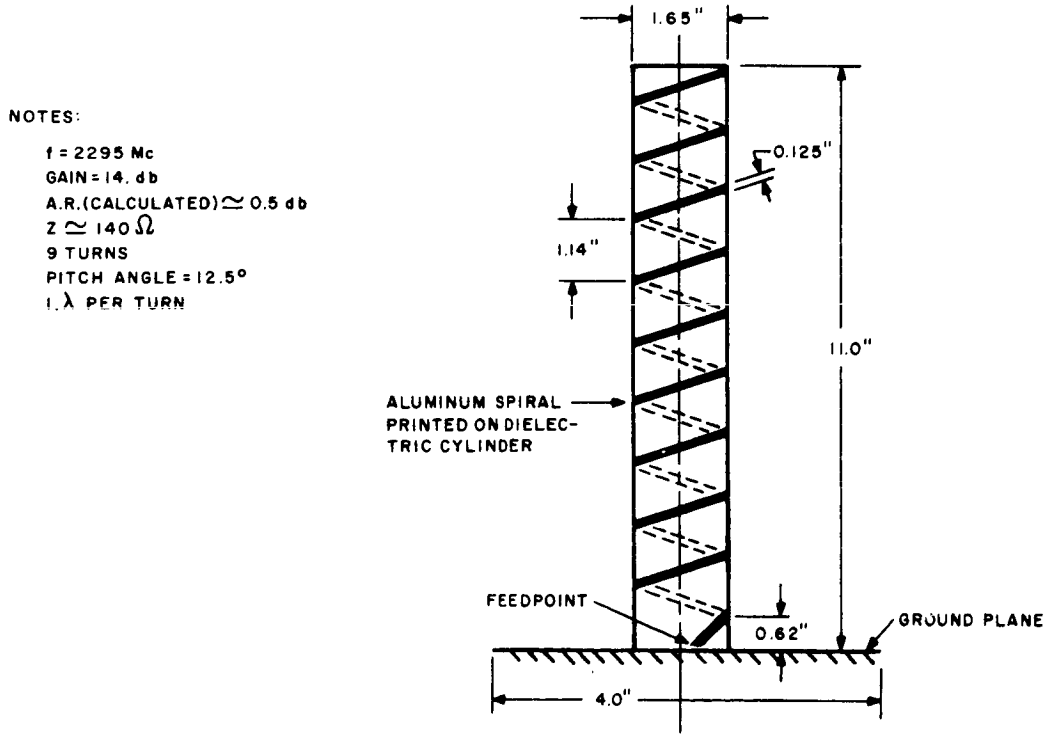

Figure II.2-51. Single-Helix Design

Although increased gain may be obtained by lengthening the helix, mechanical problems of stowage, erection, and pointing makes this unfeasible, and a multiple-helix array is preferable.

Four-Element Helix Array

Application: high-gain SLRV antenna for 2.3-kMc transmission to Earth

Electrical Characteristics: circular polarization, 20 db gain.

A directive antenna having 20-db gain may be formed from four of the helices described in Figure II.2-51. This array is approximately one cubic foot in volume.

For an open-wire transmission line feeder, a simple means may be employed with this array to avoid the use of baluns. One pair of the helices is rotated 180 degrees with respect to the other pair as shown in the front view of Figure II.2-52(a). This rotation introduces a 180-degree phase difference, which is compensated by feeding from a balanced transmission line. Short lengths of strip transmission line join the helix inputs to the open-wire terminals at the center of the array. The relative patterns in the major planes are plotted in Figure II.2-52(b).

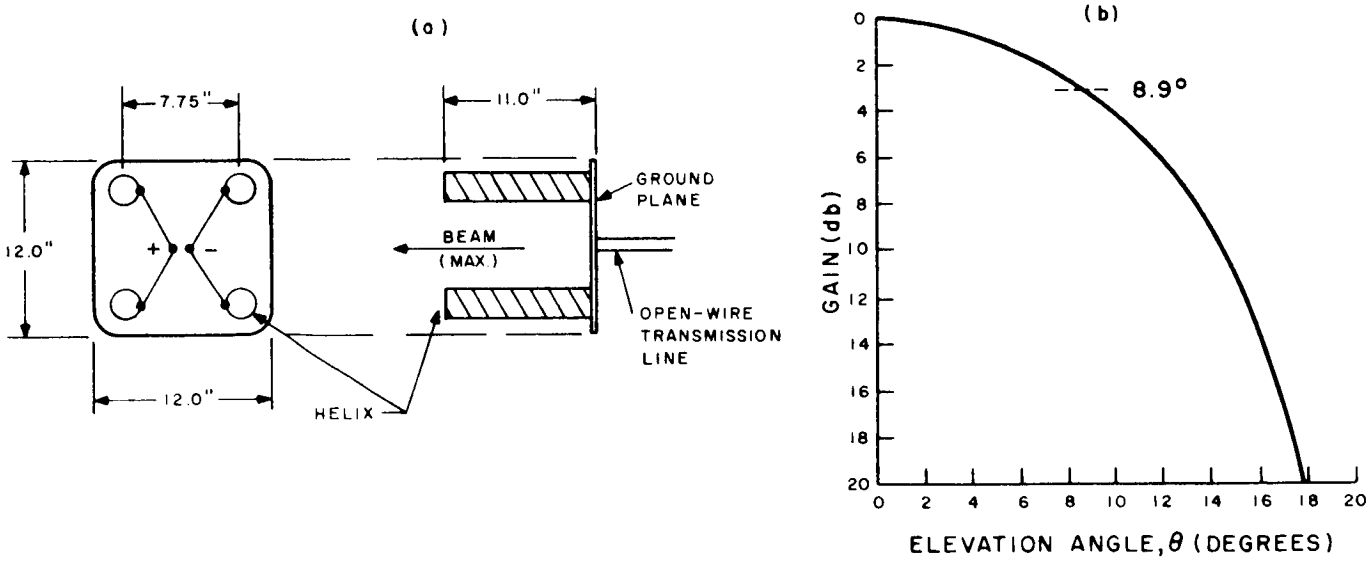

Figure II.2-52. Four-Element Helix Array

The characteristics of other combinations of helices have been studied. For the 11-inch helix unit described in Fig. II.2-51, a summary of the results is given in Table II.2-11.

TABLE II.2-11

CHARACTERISTICS OF VARIOUS COMBINATIONS OF 11-INCH HELICES

Number of 11-Inch Helices	Aperture Size (inches)	Gain (db)
8	18 × 20	23
10	18 × 28	24
14	18 × 35	25
22	31 × 35	27

Another applicable design recently completed at RCA is an array of seven helices on a circular aperture of 16-inch diameter. In this case the helices are 6.7 inches long. Complete data on the antenna design and steering mechanism is available upon request.

Yagi Antenna

Application: as a medium-gain element in a directive array for 2.3-kMc transmission from SLRV to Earth.

Electrical Characteristics: 12-db gain; circular polarization (using crossed Yagi elements).

Circularly polarized directive antennas may also be made of unit elements other than helices. Two possibilities are the "disk-on-rod" end-fire antenna and the Yagi antenna using orthogonal parasitic elements. As these two approaches are basically the same type, only the latter is described here. The linearly polarized Yagi of Figure II.2-53(a), designed for 2.3 kMc, consists of one reflector element and four director elements. Major-plane patterns are plotted in Figure II.2-53(b). For circular polarization, the Yagi suffers a disadvantage as compared to the helix in that a more complicated launcher is required.

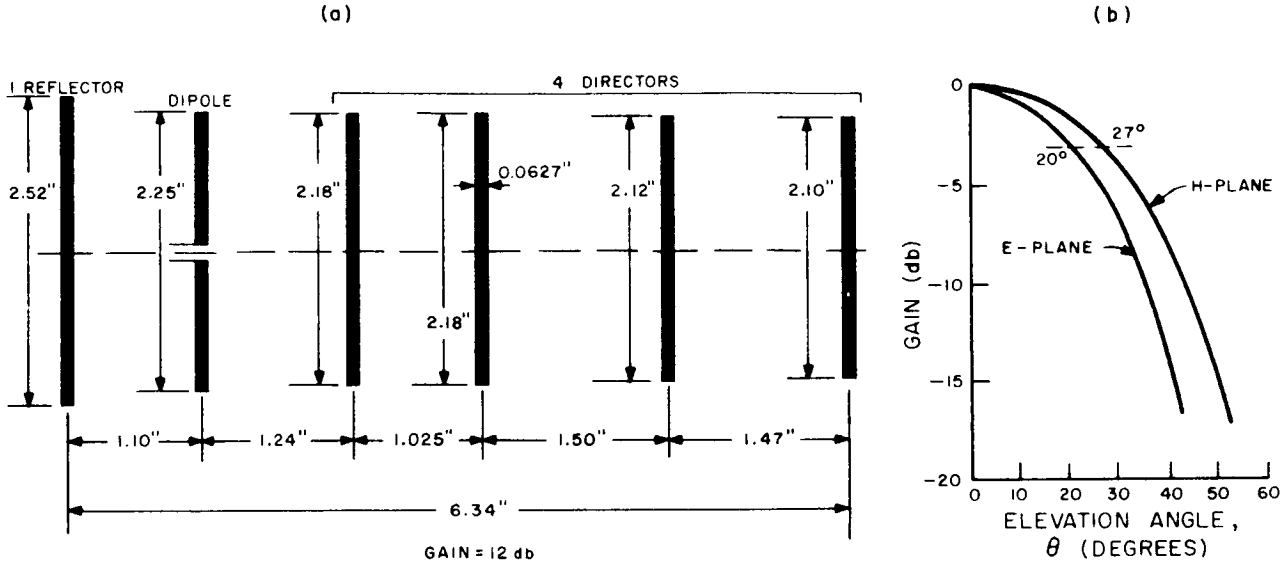

Figure II. 2-53. Yagi Antenna

Rhombic Antenna

Application: medium-gain antenna for 2.3-kMc transmission from SLRV to Earth.

Electrical Characteristics: 13- to 16-db gain; circular polarization; low efficiency.

Some consideration has been given to long wire directive antennas such as the rhombic. Although very inefficient with regard to the space occupied, the rhombic is one of the simplest means to obtain medium gains, particularly if the side-lobe level is not critical. The example illustrated in Figure II.2-54(a) for 2.3 kMc has a gain of 13 db and dimensions of 16 inches in width by 28 inches in length. Two stacked rhombics of this type will give a gain of 16 db. Two linearly polarized sets oriented at right angles and fed in phase quadrature can be employed to obtain circular polarization. A mylar double-cone assembly could be used (Figure II. 2-54(b)) as a simple means to obtain an inflatable rhombic array.

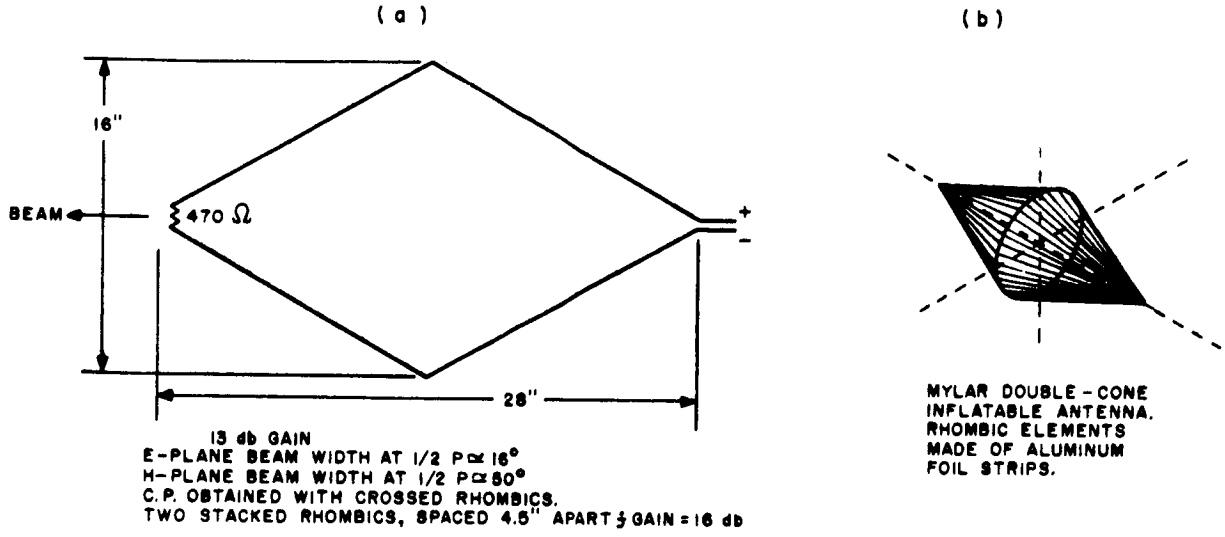

Figure II.2-54. Rhombic Antenna

The Parabola

Application: high-gain antenna for 2.3 kMc transmission from SLRV to Earth.

Electrical Characteristics: circular polarization; low aperture efficiency; simplest distribution system.

The curves of Figure II.2-55 give the beamwidths and gains of a parabolic reflector antenna in terms of the aperture diameter. These data are probably somewhat optimistic at the lower gains because of the increased blockage area of the circularly polarized feed for smaller reflectors. In general, the inherent lower efficiency of parabolas requires an aperture area about twice that of well-designed broadside arrays. A more detailed discussion of the parabola for this particular application is given in the mechanical summary.

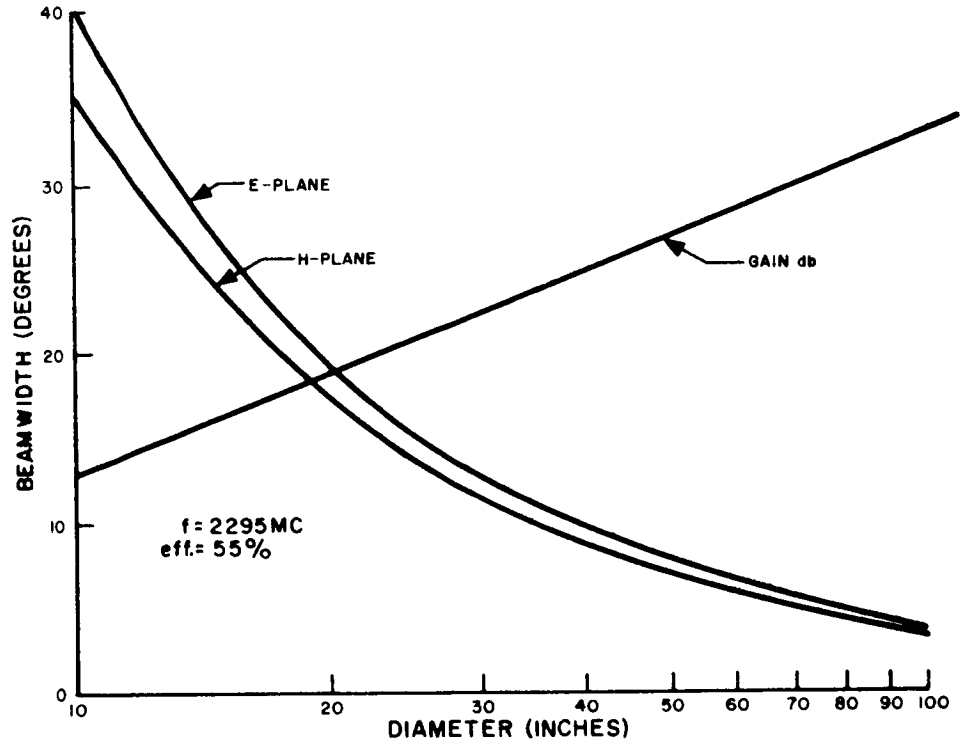

Figure II. 2-55. Parabolic Reflector Antenna

Planar Array

Application: high-gain antenna for 2.3-kMc transmission from SLRV to Earth.

Electrical Characteristics: circular polarization; high gain; high aperture efficiency.

A major objection to the planar array of low-gain elements has been the increased complexity of the distribution network and the large number of unit radiators. Recently, however, study has been started on a printed circuit technique that might possibly reduce these problems to a practical level.

In this system, a number of unit radiators made in the form of crossed slots (Figure II. 2-56) are made in a planar conductive sheet. Each unit radiator is fed, as indicated, from printed circuit strip transmission lines from opposite sides of the sheet to excite orthogonal polarizations. Thus, the radiator is amenable to circularly polarized radiation.

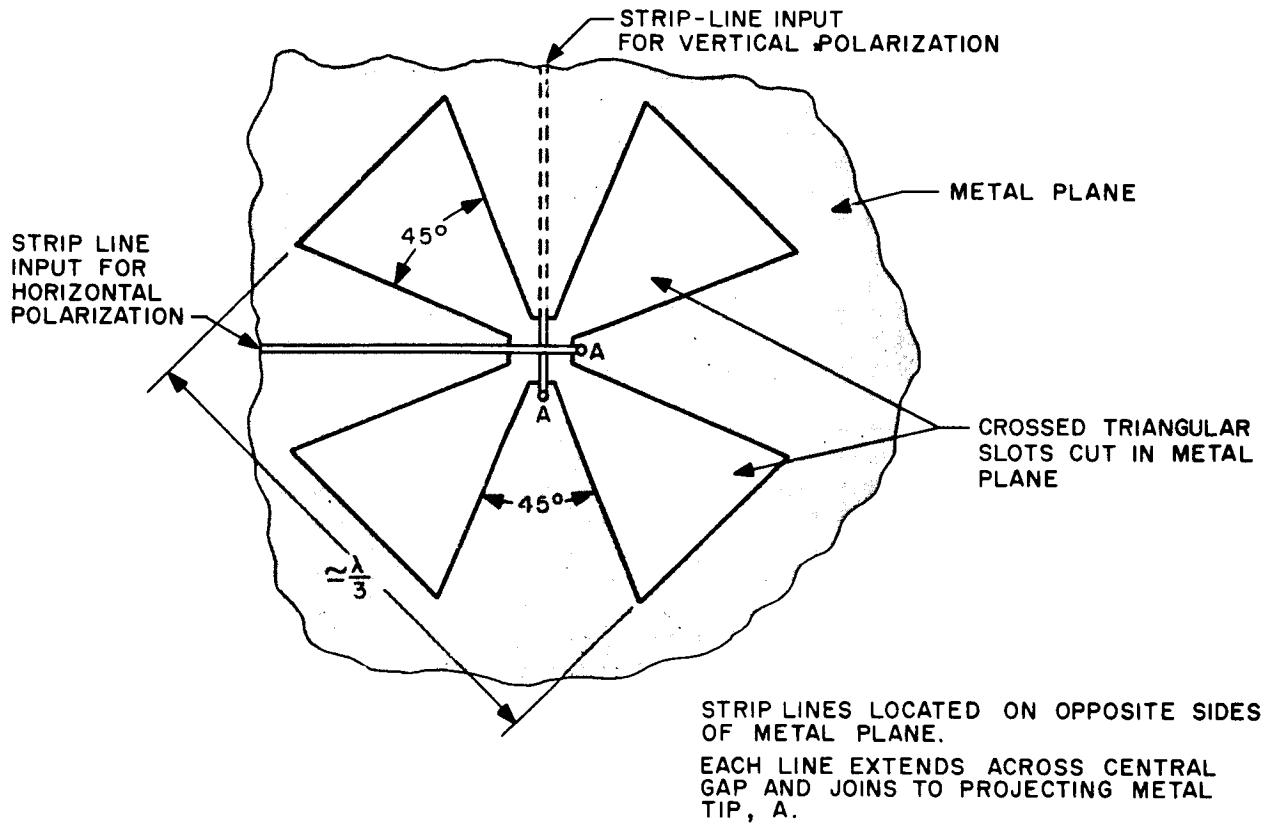

Figure II.2-56. Crossed-Slot Radiator

Corporate networks on either side of the sheet may be made, as indicated in Figure II.2-57(a), to provide equal path lengths to all radiators. Thus, the directive beam is broadside to the sheet at all frequencies. The detail of Figure II.2-57(b) shows one possible method of maintaining impedance-matching throughout the network regardless of the number of unit radiators.

Figure II.2-58 illustrates a section of the array showing the layout of the distribution networks with respect to the crossed slots. Since such an antenna would radiate a bidirectional pattern; another reflector sheet, spaced approximately one-quarter wavelength away, is required to produce a unidirectional pattern.

Table II.2-12 gives some idea of the possible configurations at 2.3 kMc for various gains.

It is possible that such an array could be made as an inflatable assembly of very low weight and relatively high efficiency. Further study on this approach will be made to determine its feasibility for this particular space application.

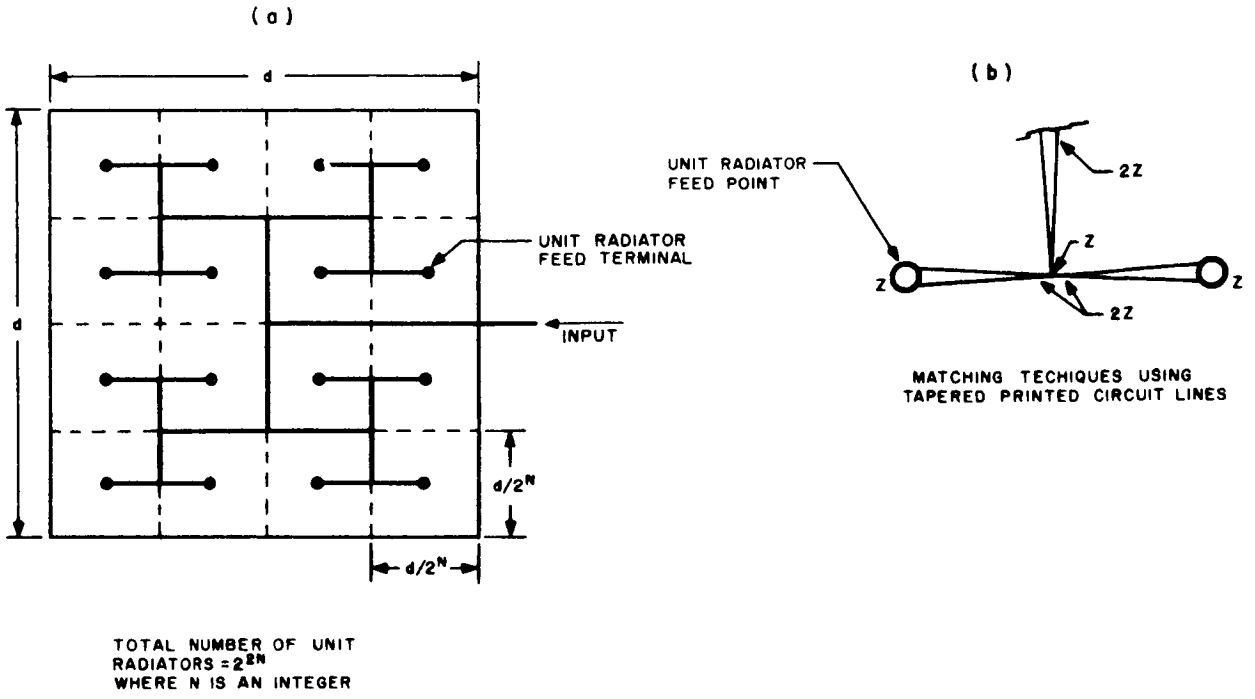

Figure II.2-57. Planar Corporate Network

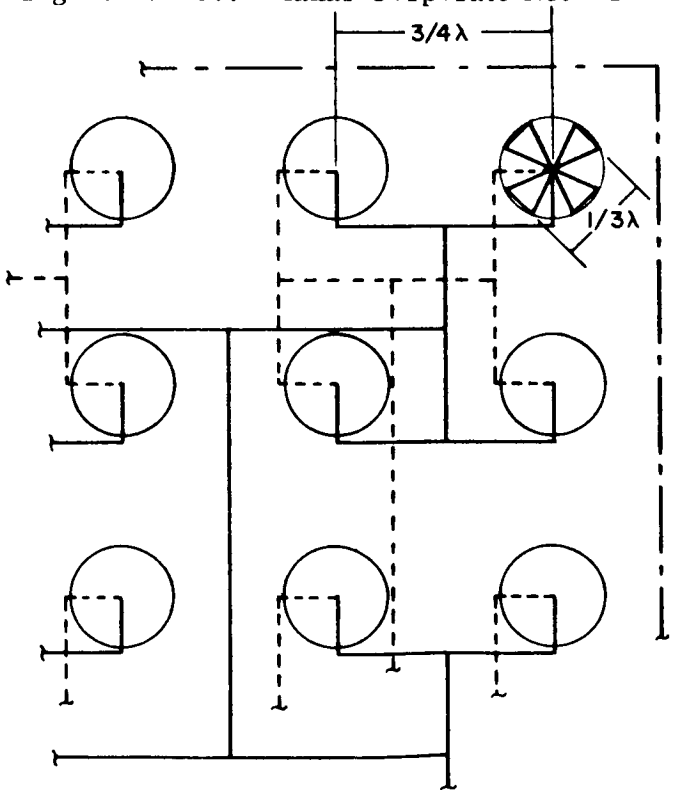

Figure II.2-58. Section of Planar Array, Showing Layout of Distribution Networks with Respect to Crossed Slots

TABLE II. 2-12

POSSIBLE CONFIGURATIONS OF PLANAR ANTENNA ARRAY
(2.3-KMC TRANSMISSION)

Number of Elements	Gain (db)	Side Dimension (inches)
4	13	8
16	19	16
64	25	32
256	31	64

2. **Mechanical and Mounting**

High-Gain Antennas (Link A)

It is assumed that the high-gain antenna must be steerable because of the narrow beamwidth. Investigations into steerable antennas indicates that most of the weight (better than 80 percent) is, from a weight consideration, almost all in the gimbal and servo-drive system. The conclusion may therefore be drawn that any type of compact radiator may be mounted on the gimbal and used.

The compactness is important because the vehicle folds up into the stowage position, and the antenna package must fit the vehicle under these conditions. The linear arrays offer the most performance for the least volume over optical types at this gain. Both types will be discussed below.

Steerable Arrays

Figure II. 2-59 shows one possible arrangement of a steering mechanism that will probably package quite compactly within the folded vehicle. It is an elevation-on-azimuth mount with the elevation axis offset to the side. This results in a height saving, for when the array points at zenith, the elevation mechanism is fully retracted. The unbalanced moment would be less if this axis were located on the center line of the array, but this would necessitate some form of mechanism to retract the whole mount at a considerable weight penalty. The locked axis position is at the zenith, which is the extension of the azimuth axis. This would better be located on the horizon as would be the case with an X-Y mount, but this is not possible without locating the X-Y axes at an elevated position, at the center of the array, as explained above.

The helix array may be collapsed like bed springs if additional clearance is required when the vehicle is folded. Variations in the array may be considered, such as the single-helix or four-helix array or other arrangements within the space limitations.

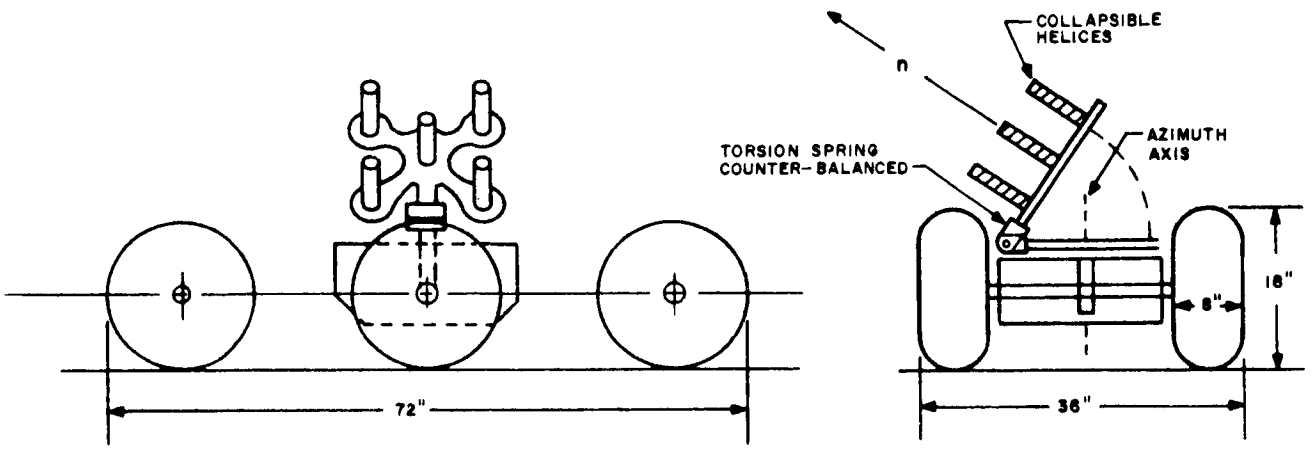

Figure II.2-59. SLRV High-Gain Steerable Antenna

The weight of the entire configuration can be kept to a minimum if the tracking speeds and accelerations are low. Some speed such as 5 degrees per second with an acceleration of 10 degrees per second may be reasonable. Direct-current motors would give the most efficient operation from a power and weight standpoint. The over-all weight of the antenna, gimbal, and drive system would be in the 5- to 8-pound range. It would be difficult to design a system of 5 pounds or less to meet the expected operating requirements. Static power requirements (no signal) would be 1 or 2 watts, and peak power 5 to 10 watts. The duty cycle would be low at the expected operating mode of the SLRV.

Steerable Dishes

The dish must be larger in diameter than the array for equal performance at this gain. Small dishes (4 to 5 λ) tend to be scatterers rather than collimators. If the performance of a 25-inch dish (5 λ) were adequate (assumed) this would mean that it must be folded to meet the stowage requirements. An inflatable or an umbrella system could be used to achieve this end.

To be steerable and for the dish to clear the wheels and structure, a mast would be required at least 12 inches high. The umbrella must be folded up, tilted down parallel to the mast, and the whole assembly laid down flat on the vehicle to be equal in stowage volume to the array. This would involve a prohibitive weight penalty.

No easy way is seen to make a steerable inflatable dish either, since the diameter of the dish represents a penalty that cannot be easily overcome. For these reasons the dish is not as good a solution as the steerable array. If higher gains are required the dish may be the only solution, but weight penalties must be expected.

Low-Gain Antennas

All of the low-gain antennas at S-band are relatively light in weight. The turnstile with a monopole for direction finding will weigh less than one tenth of a pound. If elevation above the vehicle is required the weight will increase, and if a mechanical retracting system is required for vehicle clearance in the stowed position then the weight may be multiplied several times.

A VHF antenna will be heavier, but only by a matter of a few ounces. Probable weight is in the vicinity of a quarter of a pound for this antenna at 400 Mc. The mast will become more complicated and heavier, particularly if mechanical retraction is necessary.

Other configurations with more elements will weigh correspondingly more, although it is believed that most types will represent less than 5 percent of a total Communications Subsystem weight of 10 pounds.

If 30 Mc is selected and/or a higher mast is required, the inflatable self-rigidizing solution proposed by GM-DRL may be the best solution to the weight and stowage problem. In such a case, the dipoles would become part of the inflate.

3. Selected Designs

VHF Antenna for Surveyor

General Description

The antenna array pictured in Figure II.2-60 consists of four vertical dipoles of height H, equally spaced on a circle of radius S. The dipole elements are made of two light-weight wires forming a "Vee" for greater bandwidth. Each dipole is joined by an open wire, balanced transmission line to the feed network at the center of the array. Two transmission lines extend downward from the feed network to the communications and direction-finding equipment

in the surveyor. Inputs to these two decoupled lines produce azimuth patterns which are approximately circular but differ in their far-field phase progressions with azimuth angle. For direction-finding, the azimuth bearing of the incoming wave is a function of the phase difference between signals received at the two network ports. Either port may be employed for the communications link.

Antenna Theory and Design

Theoretically, an infinite number of vertical dipoles arranged in a circular ring array will produce a perfectly circular pattern in the azimuth plane when

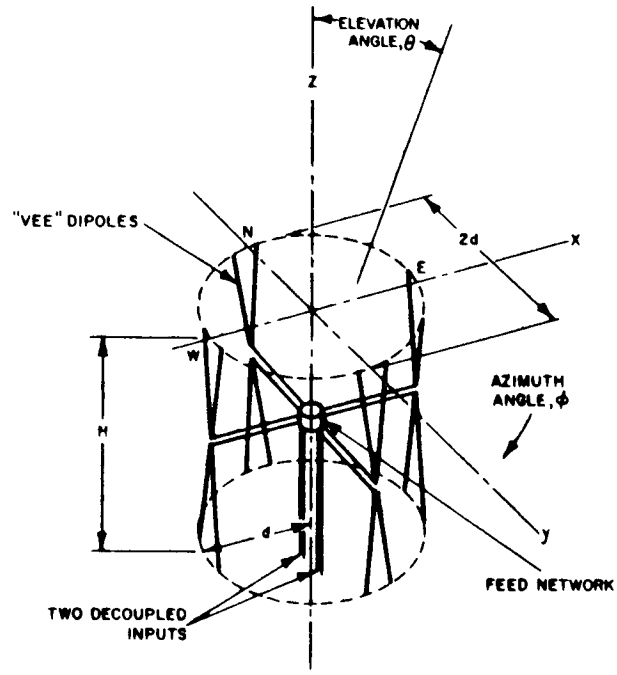

Figure II. 2-60. Communications/Direction-Finding Antenna for Surveyor

the dipoles are fed with equal-amplitude signals having an integral number (H) of complete cycles of phase progression around the circle. Thus, all dipoles are fed in-phase for H = 0, and are phased in proportion to the azimuth angle for H = 1. It is apparent from symmetry that the far-field phase progression in the azimuth plane will vary in the same manner as the ring excitation phasing.

These idealized patterns may be closely approximated by a simple antenna array of only four, equally-spaced dipoles arranged on a very small circle (S⟶0). Such an array, however, falls into the supergain category for the H = 1 mode, resulting in very high Q and poor efficiency. Hence, the radius of the circle must be increased for practical configurations. This increase is accomplished by variations from circularity in the azimuth patterns for both types of mode excitation. Figure II.2-61(a) shows typical departures from circularity for the H = 0 mode as the radius, S, is increased. Similar data for the H = 1 mode are given in Figure II.2-61(b). It is observed that a maximum for one mode occurs at the same azimuth angle as a minimum for the other mode.

The relative field pattern in the azimuth plane for the H = 0 mode is:

$$\cos(kS\cos\phi) + \cos(kS\sin\phi) \qquad \text{(II.2-102)}$$

and for the H = 1 mode:

$$\sin(kS\cos\phi) + j\sin(kS\sin\phi), \qquad \text{(II.2-103)}$$

where

$$k = \frac{2\pi}{\lambda}, \text{ and } \phi \text{ is the azimuth angle.}$$

The circularity of the azimuth pattern may be defined as the ratio of the maximum to the minimum values of field.

From equation (II.2-102) for H = 0,

$$\text{circularity} = \frac{F(\phi = 0°)}{F(\phi = 45°)} = \frac{1 + \cos kS}{2\cos\left(\frac{\sqrt{2}}{2}KS\right)} \qquad \text{(II.2-104)}$$

From equation (II.2-103) for H = 1,

$$\text{circularity} = \frac{F(\phi = 45°)}{F(\phi = 0°)} = \frac{\sqrt{2}\sin\left(\frac{\sqrt{2}}{2}kS\right)}{\sin kS} \qquad \text{(II.2-105)}$$

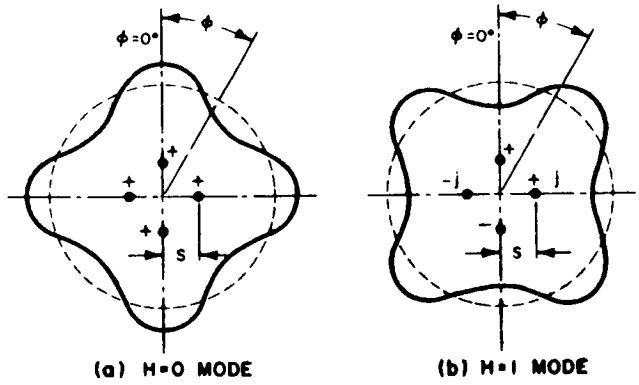

Figure II.2-61. Typical Azimuth Patterns for a Four-Dipole Array with Increased Radius

The circularity ratios (in db) are plotted in Figure II 2-62 as a function of S/λ. It is noted that the H = 0 mode has a more circular azimuth pattern for any value of the radius, S.

The theoretical gains relative to a linearly polarized isotropic source are plotted in Figs. II. 2-63(a) and 2-63(b) for the two mode excitations. These data were calculated by the mutual impedance method for thin-wire, half-wire dipoles, assuming no ohmic losses.

Curves for the resistance and reactance of individual dipoles in the array are plotted in Figure II.2-64 against the circle radius in wavelengths. These curves are for theoretical half-wave dipoles with no ohmic losses, and are presented to illustrate the general type of impedance variation rather than as actual values that might be obtained in practice where the dipole length, shape, and feed termination can introduce considerable variations.

It is seen from Figure II 2-62 that as S approaches zero, the dipole impedance for H = 0 is equal to four times that of a free-space dipole (73.2 + j 42.5 ohms). For H = 1, the dipole impedance approaches zero as S becomes smaller. Hence, too small a radius complicates the impedance matching problems in the network circuitry and increases the ohmic losses.

Next to be considered are the far-field phase variations for the two types of excitation. From equation (II. 2-102) it is seen that the phase is independent of the azimuth angle for the H = 0 mode. From equation (II. 2-103), the phase angle, ψ, is:

$$\psi = \tan^{-1} \frac{\sin (kS \sin \phi)}{\sin (kS \cos \phi)} . \qquad \text{(II.2-106)}$$

Thus, as S approaches zero, the far-field phase angle is the same as the azimuth angle. Also, $\psi = \phi$ for ϕ equal to multiples of 45^{o}, i.e., 0^{o}, 45^{o}, 90^{o}, etc.

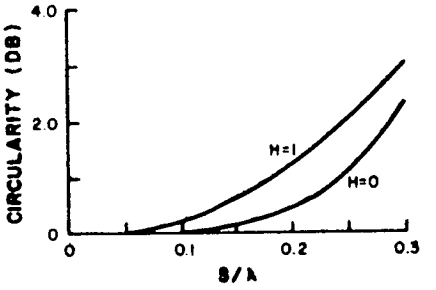

Figure II. 2-62. Azimuth Pattern Circularity

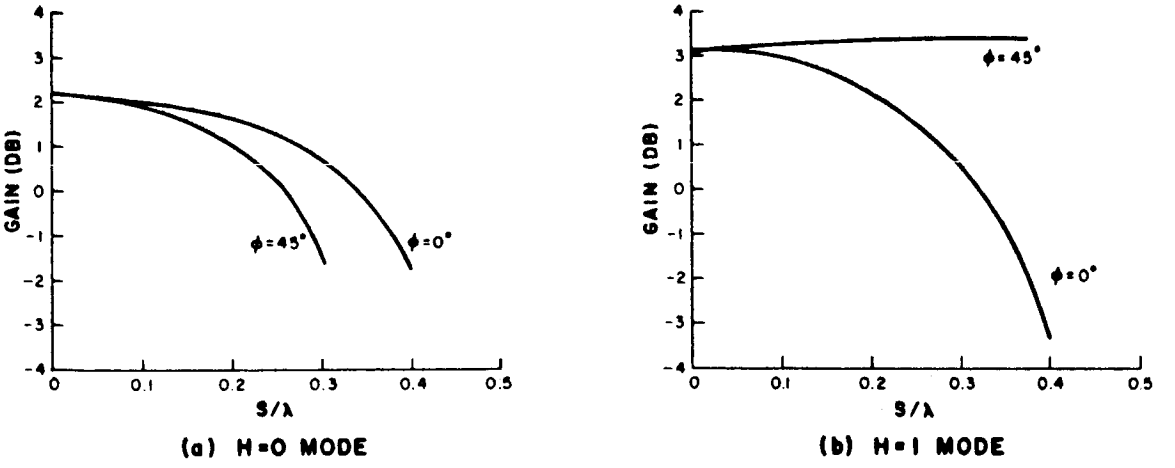

Figure II.2-63. Gain Versus S/λ for the H = 0 and H = 1 Modes

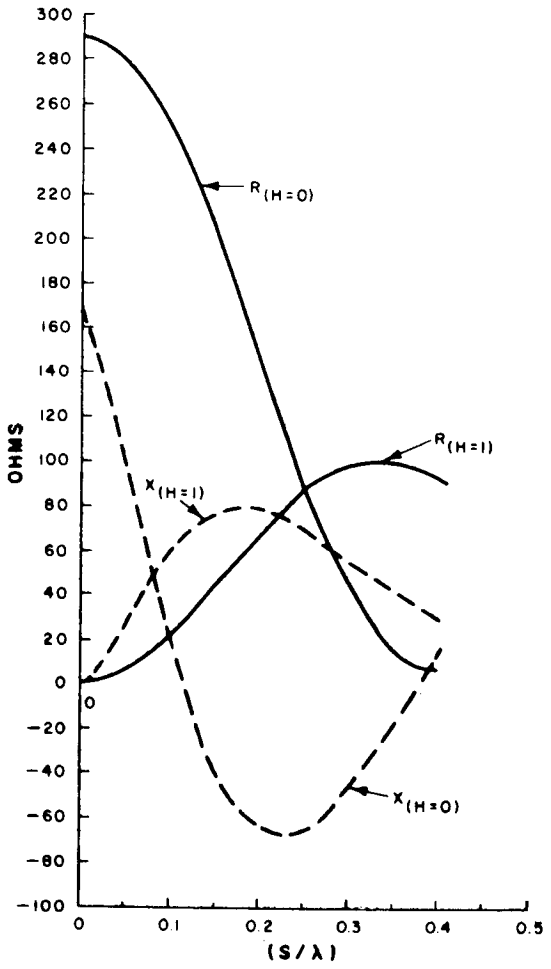

Figure II.2-64. Individual Dipole Impedance

The maximum difference between ψ and ϕ occurs at the intermediate angles of $\phi = 22.5^{o}$, 67.5^{o}, etc., for which

$$\psi = \tan^{-1} \frac{\sin (0.382\ kS)}{\sin (0.923\ kS)} \quad . \tag{II.2-107}$$

This relationship is plotted against the radius, S/λ, in Figure II.2-65. It is to be noted that this difference is not a bearing error, since a calibration curve can be constructed for a given radius to obtain the true bearing.

From a study of the above data, a ring radius of 0.167λ was chosen as a suitable compromise. A calibration curve is given in Figure II.2-66, which relates the correct azimuth bearing to the measured phase difference between the two ports.

Expressions for the relative field patterns in the elevation plane are:

$$\underline{H = 0 \text{ mode}}$$

$$\text{For } \phi = 0^{\circ};\ F = [1 + \cos (kS \sin \theta)]\ D_{\theta} \tag{II.2-108}$$

and

$$\phi = 45°; \quad F = \left[\cos\left(\frac{K\sqrt{2}\,S}{2}\sin\theta\right)\right] D_\theta \qquad \text{(II.2-109)}$$

$\underline{H = 1 \text{ mode}}$

$$\text{For } \phi = 0°; \; F = \left[\sin(kS\sin\theta)\right] D_\theta \qquad \text{(II.2-110)}$$

and

$$\phi = 45°; \quad F = \left[\sin\left(\frac{k\sqrt{2}\,S}{2}\sin\theta\right)\right] D_\theta \qquad \text{(II.2-111)}$$

where D_θ is the relative field pattern of a single dipole element.

Using these expressions, polar elevation patterns for S = 0.167 λ are given in Figures II.2-67 and -68 in db, for the two modes with respect to an isotropic source. This radius is 13.1 inches at the frequency of 150 Mc chosen for the SLRV-to-Surveyor line. The overall height, H, of the dipoles will be approximately three feet at this frequency.

From Figure II.2-62 the azimuth pattern circularity is 0.25 db for the H = 0 mode and 0.75 db for the H = 1 mode. Referring to Figure II.2-63, the H = 0 mode gain is 1.6 db ±0.2 db and the H = 1 mode gain is 2.9 db ±0.4 db.

For the Surveyor-to-SLRV communication link at 120 Mc, the radius, S, is 0.134 λ, giving a H = 0 mode gain of 1.8 db ±0.1 db and a H = 1 mode gain of 3.0 db ±0.2 db.

From previous experience in antenna designs of this type, a bandwidth of at least 5% and a VSWR of 1.2:1 can be obtained for the director-finding array at 150 Mc. An additional matching element at the triplexer output will possible be required to obtain a match at the 120 Mc band.

It is estimated that the phase difference between signals received on the two feed lines will be within ±1.5° of the azimuth bearing angle. This figure includes the distorting effects caused by the Surveyor, but exclude multipath errors due to terrain variations.

Feed Network

The feed network for the two types of mode excitation as first proposed* is drawn in Figure II 2-69(a). This circuitry consists of two square hybrids made of balanced, quarter-wave lines (L). A signal at the H = 0 mode port will feed all four of

*See Paragraph E.

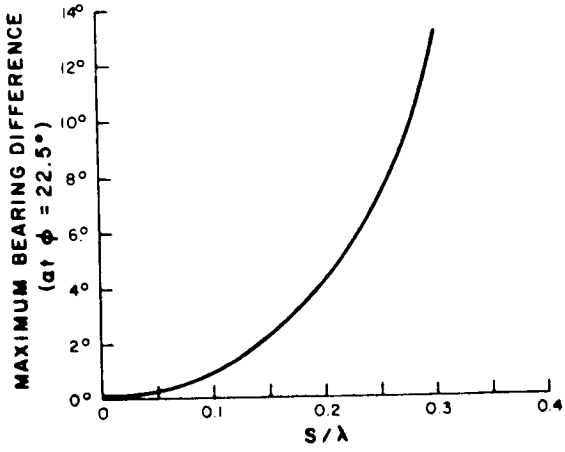

Figure II.2-65. Relationship of Radius to Maximum Bearing Difference

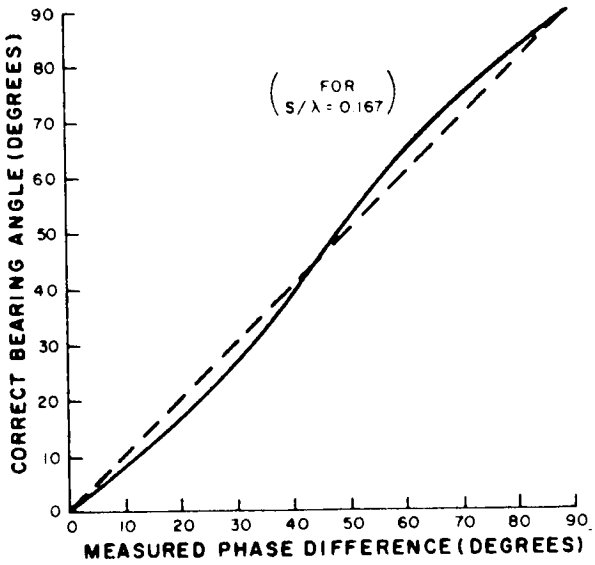

Figure II. 2-66. Calibration Curve Relating Correct Azimuth Bearing to the Measured Phase Difference Between Two Posts

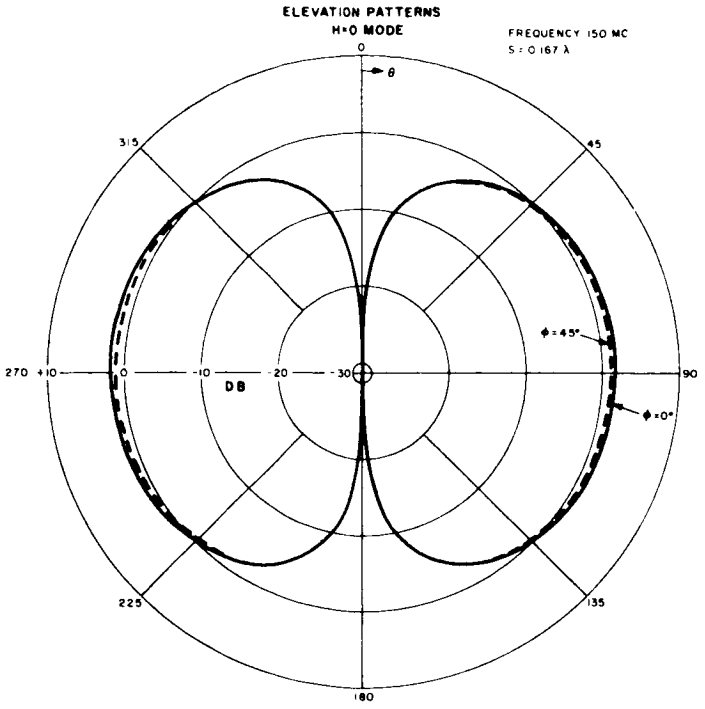

Figure II.2-67. Polar Elevation Pattern for S = 0.167 λ for the H = 0 Mode with Respect to an Isotropic Source

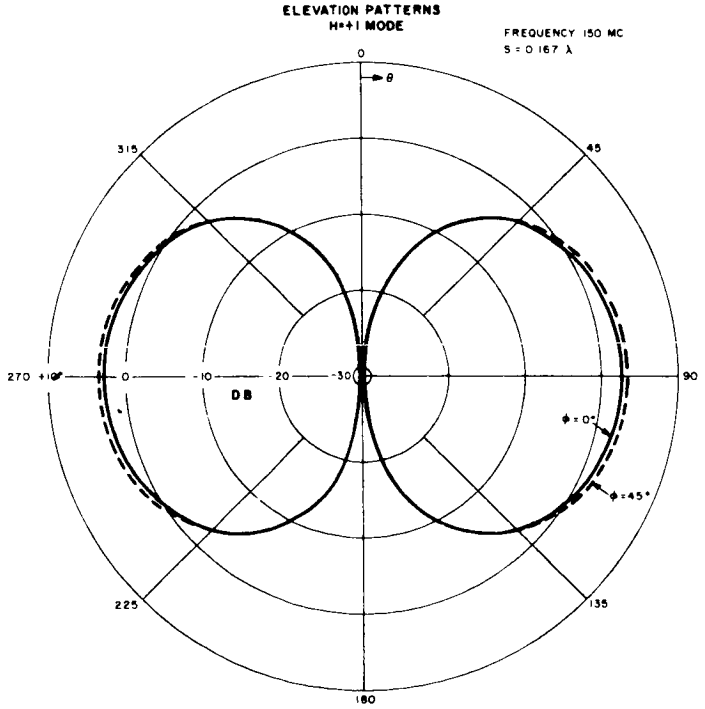

Figure II. 2-68. Polar Elevation Pattern for S = 0.167 λ for the H = 1 Mode with Respect to an Isotropic Source

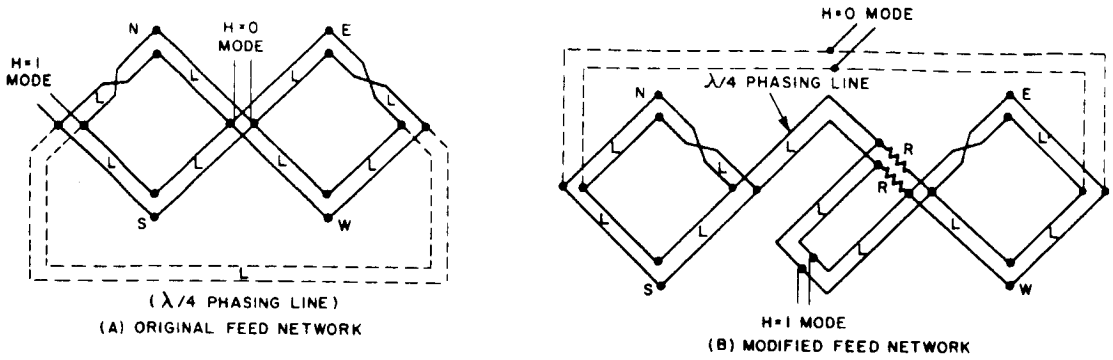

Figure II. 2-69. Feed Networks for Two Types of Mode Excitation

the dipoles (labeled N, S, E, and W) in phase. An input at the H = 1 mode input will energize the four dipoles in quadrature phasing because of the two line transpositions in the hybrids and the quarter-wave phasing line. It is apparent from the circuitry that there will be no cross-coupling between the two ports.

For input at the H = 1 mode port, equal power division to the four dipoles is provided by this network if the dipoles are matched over the desired band of frequencies. Identical mismatches of the four dipoles results in both amplitude and phase distortion of the azimuth pattern. A means for insuring the pattern symmetry independent of the dipole matching is shown in the modified block network of Figure II. 2-69.

In this network, an input at the H = 0 mode port feeds the four dipoles in-phase as before. However, additional quarter-wave elements and resistors have been added to the circuitry. Input power at the H = 1 mode port splits equally through two quarter-wave line sections to the N-S and E-W hybrids. No power is absorbed by the two resistors from this incident wave, since no potential is developed across either resistor when connected as shown. If the dipoles are mismatched, however, the two reflected waves will arrive at the resistor terminals out of phase because of the round-trip differential phase lag through the quarter-wave phasing line. These return waves, being out of phase, cannot feed into the input and the reflected power is completely absorbed by the resistors. Thus, equal powers are radiated by the four dipoles, independent of their mismatch, at the cost of a small amount of power lost in the resistors. The fraction of power lost is equal to the square of the reflection coefficient from the dipoles. For example, a VSWR of 2:1 at the dipoles results in only 0.5 db power lost.

The final choice of the feed network type will depend upon actual impedance bandwidth measurements made on an experimental model of the antenna. The chosen feed network may be made in very compact form by winding the quarter-wave line sections as bifiler coils, which may be enclosed in a small container at the center of the array. An alternative approach would be to join the labeled terminals indicated in Figure II.2-69 directly to the dipole. Thus, two line sections extend from each dipole toward the central region of the array where the eight lines are appropriately joined as diagrammed in this figure. The feasibility of this approach will be determined after further detailed study of the final mechanical design of the array and the particular mechanical system employed for unfurling the dipoles and support arms. It is estimated that the maximum loss in the feed network will be 0.5 db.

Mechanical Design

This antenna (Figure II. 2-70(a)) is estimated to weight one pound, based upon a design using light-weight tubular elements, or beryllium hair-pin springs.

The folding and method of construction of the elements would be governed in part by the type of mast, and method of folding or stowing the mast. For example, the elements might have to fold into a short length if a telescoping mast were required, but might easily be made of spring-loaded hinged or semi-rigid members if a whip type mast is selected. Any of these possible designs for a compact folding antenna should fall within the estimated weight of one pound.

In one concept of the antenna it will be folded in two planes, flat against a mast. (Figure II.2-70(b)). The folding is accomplished by spring loading the elements, and spring loading a pair of parallel linkage support arms for each of the four pairs of elements (Figure II.2-70(c)). In the stowed position, the antenna is held by a ring. As the mast extends the elements are pulled free of the restraining ring, and pops open into position.

There are other possibilities for folding, one of which is to make the elements and support arms of spring wire and spring tape, coiled up in the stowed position. When released, all would spring into position. The choice of method, not to be limited to the above suggestions, should result from a more detailed study and design effort in subsequent phases, when more is known about the compatibility requirements.

Locating this antenna on Surveyor is a real problem, as it must clear the high-gain antenna and solar panels and be located at an adequate height for good DF and gain characteristics. A long telescoping mast from the vehicle landing gear or structure will be heavy. No easy way is seen to mount it on the present mast, since the VHF mast will interfere with the linkages for the array and solar panel. However, this is the best location, if a way can be found to avoid the difficulty mentioned. This results in a short light mast that will raise the antenna well above the vehicle. However, rotation of the main mast may also rotate the VHF antenna.

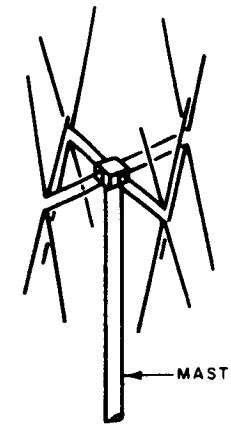

(a) VHF ANTENNA OBLIQUE VIEW

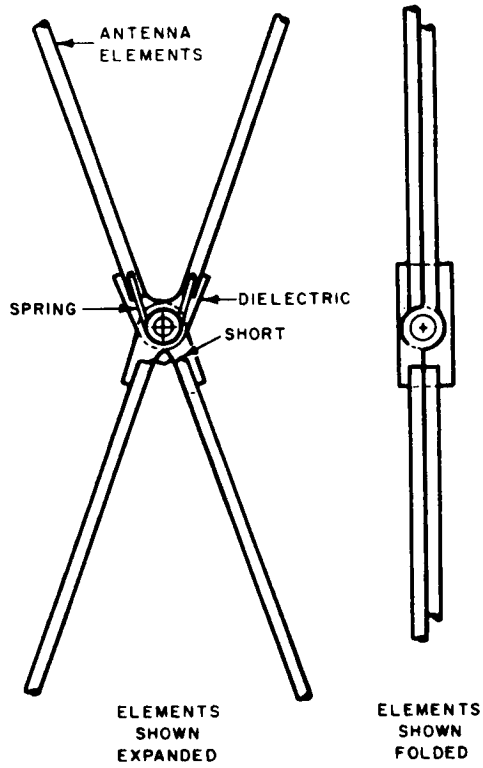

(c) DETAIL OF CENTER JOINT

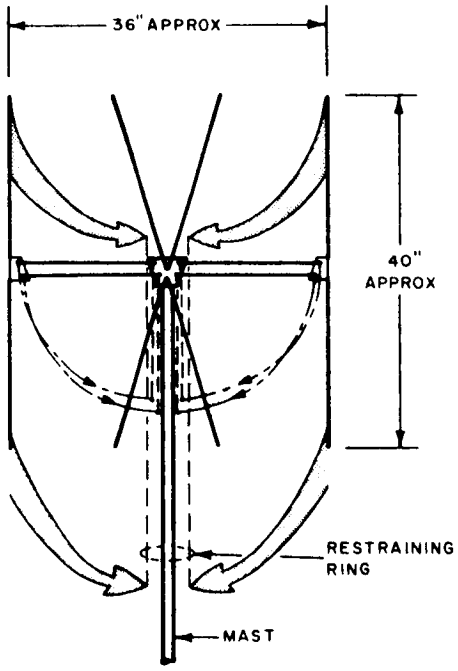

(b) ANTENNA FOLDING METHOD

Figure II.2-70. Mechanical Design of the Proposed VHF Antenna for Surveyor

The lightest solution would be to locate the VHF antenna around the main mast below the solar panel and array. But this cuts the height above the lunar surface approximately in half, with obvious disadvantages.

For a mechanism, the cold-gas telescoping mast is one solution. The mast and mechanism weights of the Radiation Detector and Geophysical Experiment booms, as used on Surveyor, will give an approximation of the weight for the VHF antenna mast. If the VHF antenna could be located on the main mast and erected by the same cold-gas mechanism, some weight could be saved. This might be accomplished if the VHF mast were to telescope within the main mast. A STEM* device might also be used to extend the VHF antenna and form the mast. A small D.C. driving motor would be required, (or a spring motor) to unwind the device.

No decision has been made on the construction of the two transmission lines to the VHF antenna. A pair of open wire lines is attractive from a loss standpoint and would be light. However, they will be difficult to coil and keep in proper relation to each other. A pair of printed lines on a thin mylar film tube would be light. A coiled plastic spring might be used to keep the film stretched into tubular form when extended. Small miniature coaxial cable is another possibility.

Further studies in greater detail are required to solve the mast, location, extension method, and transmission line construction problem. Required are more detailed information about the vehicle, the stowage and rigidity requirements, and other design limitations.

VHF Antenna for SLRV

Description

The antenna proposed for operation at 120 Mc and 150 Mc on the SLRV consists of a vertical monopole fed against a ground plane of four horizontal wires extending radially from the base of the monopole. These ground wires and the monopole are approximately one-quarter wave in length at the midband frequency of 135 Mc. The monopole is made of two wires forming a "Vee" similar to half of the dipole element employed in the Surveyor array. It is expected that the broadbanding effected by this single "Vee" monopole will be sufficient to cover both the transmitting and receiving bands with a VSWR of 1.5:1 or less. The antenna gain will be approximately 2.0 db with respect to an isotropic source.

Mechanical Design

This antenna, less mast, is estimated to weight 0.5 pound. Figure II.2-71 shows an oblique view of it.

---

*DeHavilland Aircraft of Canada, Ltd., Malton, Ont.
STEM: Storable Tubular Extendable Member

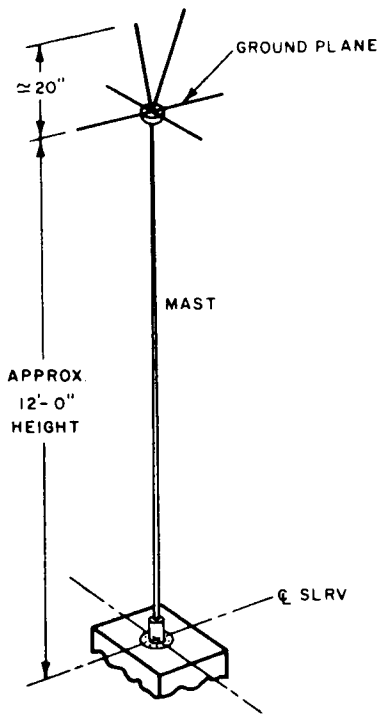

Figure II.2-71. VHF Antenna Design Proposed for Location on SLRV

Here, as in the Surveyor VHF antenna, the problem with the mast is compatibility and weight. There are several alternatives possible as far as the mast design is concerned. These are:

1) Telescoping mast with a cold gas ejector bottle. The weight of this type can be estimated from the booms for the Radiation Detector and Geophysical Experiment on Surveyor. This will probably be the heaviest solution to the problem, but it has the advantage of compactness when in the restricted position. The antenna and ground-plane elements would be made of beryllium spring tape, slightly dished, or spring wire, both of which will spring out into position when released.

2) A STEM device to extend a coiled tape which forms a tube as it unreels. It can be driven with a spring motor, or D.C. motor designed for a single extension or operation.

3) A whip mast which bends enough to go within the payload compartment of Surveyor, and which springs erect as the SLRV is dropped free onto the Lunar surface. This would probably be the lightest design, provided that a mast can be designed to bend within the available space, and be rigid enough when erect to meet the requirements of the system. It must not snag on the Surveyor as the SLRV is dropped free.

4) An articulated mast composed of short tubular sections joined with spring-loaded hinges which snap open and lock as the mast erects. There are other possibilities which come to mind, the feasibility of which, along with those mentioned, can only be shown after more detailed study and design. The whip seems to offer the best solution, based on present knowledge.

The feed line problem is somewhat dependent on the type of mast. For example, if a metal whip mast is selected, the feed line center conductor could be run up the center of the mast in a coaxial arrangement. If a Fiberglass mast proved to be feasible, this and other feed designs may be possible. For example, the outside surface could be coated with a metallic film making a coaxial arrangement, or parallel lines could be printed on the surface of the plastic.

The final design of mast will depend on the rigidity, stowage, and weight requirements, and these will become available in a later phase of the program. The feed line design can be integrated into the mast design after these parameters are known and design concept settled.

Transmission Lines

Two types of transmission lines are considered for this application: unbalanced coaxial lines, and balanced, open-wire lines.

Coaxial lines have the advantage of being completely shielded, and thus introduce no electrical problems caused by proximity to metallic structures, etc. On the other hand, the feed network circuitry has a simpler design and broader bandwidth when constructed of balanced transmission line sections. In addition, no baluns are required at the dipole terminals. Hence, at this stage of the antenna design, an open-wire transmission line is preferred to conventional coaxial lines. A very light-weight line can be made by two parallel aluminum strips to a Mylar ribbon. If subsequent design of the terminal equipment requires coaxial inputs, baluns may be employed to convert the balanced lines to unbalanced terminals.

Preliminary estimates of line losses are 0.5 db to 1.0 db for the Surveyor array at a height of 18 feet, and 0.5 db for the SLRV antenna at a height of 12 feet.

F. PHYSICAL CHARACTERISTICS OF S-BAND AND VHF COMMUNICATIONS CONFIGURATIONS

This discussion contains tabulations and plots of physical characteristics of both S-band (for "Direct" Earth/SLRV/Earth routing) and VHF (for SLRV/Surveyor/SLRV relay routing) communication equipments. The data are grouped as follows:

1. Data Used for Tradeoff Studies

Table II. 2-13: Tabulation of S-Band Transmitter and Receiver Physical Characteristics.

Fig. II. 2-72: S-Band Transmitter Characteristics

Note: This is a plot of the transmitter data contained in Table II. 2-13.

Fig. II.2-73: Weight versus Frequency for VHF Transmitters of various Output Power Levels.

Fig. II. 2-74: Power Input versus Frequency for VHF Transmitters of various Output Power Levels.

2. Physical Characteristics "Direct" (S-Band) and "Indirect" or Relay (VHF) Configurations

Table II. 2-14: Physical Characteristics for Representative S-Band "Direct" Configuration on SLRV.

Table II. 2-15: Physical Characteristics for Individual Units of Recommended VHF Relay Configuration.

Table II. 2-16: Physical Characteristics for Total Surveyor and SLRV sections of Recommended VHF Relay Configuration.

TABLE II. 2-13

S-BAND TRANSMITTER AND RECEIVER PHYSICAL CHARACTERISTICS*

UNIT	Power Output[1] (Watts)	Power Amplifier Tube		Solid State Driver Output (Watts)	Weight[2], [5] (Lbs)	Volume[3] (Cu. In.)	Dimensions (Inches)	Operate Power[4] (Watts)	Standby Power (Watts)
		Type	Gain						
TRANSMITTERS	20	Amplitron	20 db	0.25	10.0	270	4.5 x 6 x 10	65	4
	10	Amplitron	20 db	0.12	9.5	255	4.25 x 6 x 10	40	4
	10	Triode	13 db	0.60	10.0	270	4.5 x 6 x 10	100	5
	10	TWT	30 db	0.012	10.0	270	4.5 x 6 x 10	75	2
	5.0	Triode	13 db	0.30	9.0	255	4.25 x 6 x 10	60	5
	2.0	Triode	10 db	0.25	4.7	140	4.5 x 5 x 6	25	4
	1.7	Solid State	--	2.00	4.5	135	4.5 x 5 x 6	47	-
	1.0	Solid State	--	1.20	4.2	135	4.5 x 5 x 6	28	-
	1.0	Triode	10 db	1.20	4.2	135	4.5 x 5 x 6	13.5	4
	0.50	Solid State	--	0.60	3.7	96	3 x 5 x 6	10.5	-
	0.25	Solid State	--	0.30	3.6	96	3 x 5 x 6	5.5	-
RECEIVERS		Coherent			5	144	4 x 6 x 6	3.5	
		Non-coherent			4	120	4 x 5 x 6	2.5	
		Balanced Mixer Front End — 11-db Noise Figure for either receiver.							

Notes:
(1) Power output is power to antenna (includes diplexer loss of 0.75 db).
(2) Xmtr. weight includes diplexer of 24 oz.
(3) Xmtr. volume includes diplexer of 40 cu. in.
(4) Data assumes power supply of 24 VDC ±5%.
(5) For dual power level outputs, add 0.75 lb. for diode switch and control.

*RCA Design Data

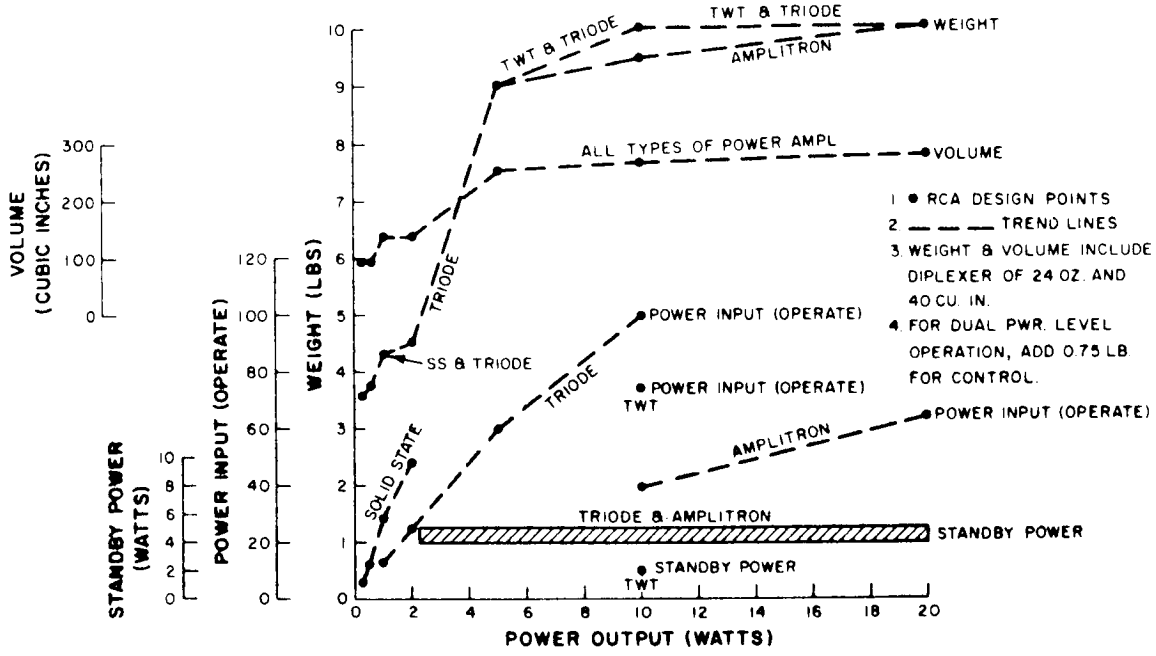

Figure II. 2-72. S-Band Transmitter Characteristics (RCA Design Data)

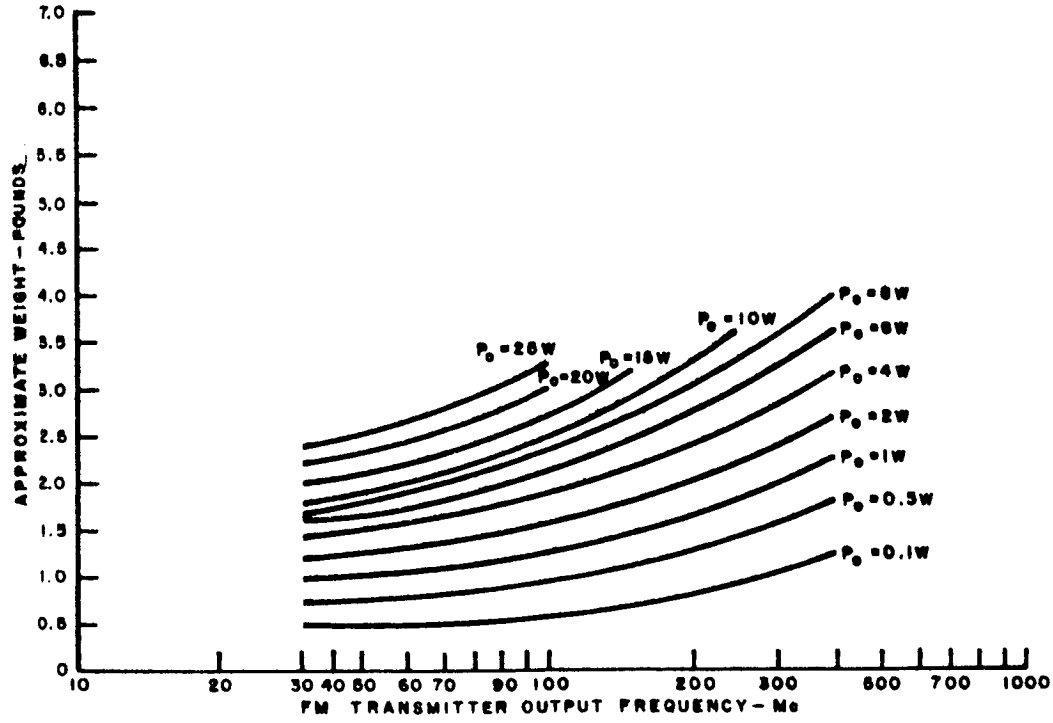

Figure II. 2-73. Approximate Weight versus Frequency for Various Output Power Levels

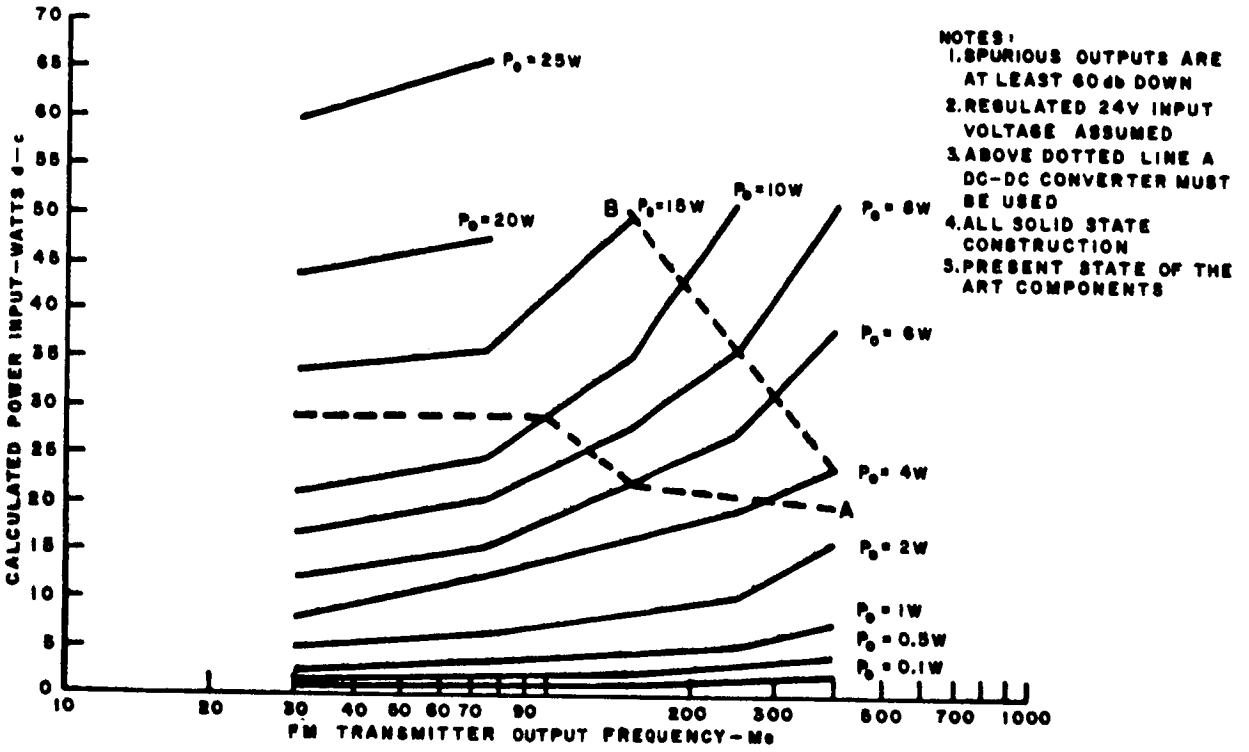

Figure II. 2-74. Calculated Input Power versus Frequency for Various Output Power Levels

TABLE II. 2-14

PHYSICAL CHARACTERISTICS FOR REPRESENTATIVE S-BAND "DIRECT" CONFIGURATION ON SLRV

Unit	Weight (lbs)	Power (watts)		Volume (cu. in)
		Operate	Standby	
S-Band Transmitter (1-watt Triode Amplifier) (including Diplexer)	3.2	13.5	4 (1)	100
S-Band Receiver (Non-Coherent)	4.0	2.5	2.5 (2)	120
Diplexer	1.5	--	--	40
S-Band Omni Antenna (For reception of commands)	0.5	--	--	-- (3)
S-Band Directional Antenna (15 db)	5 to 8 (4)	5 to 10 (5)	1 to 2	-- (3)
Communication Central Control	0.5	0.1	0.1	27
Range and Bearing Provisions	Not included			
TOTALS	14.7 to 17.7	21.1 to 26.1	7.6 to 8.6	287

(1) Tube filaments must be kept on to avoid warm-up time when transmission is required.
(2) Must be kept "on" to receive commands sent at random intervals.
(3) Volume not included for externally mounted assemblies.
(4) Weight includes gimbal and drive system.
(5) Power includes that for drive system.

TABLE II. 2-15

PHYSICAL CHARACTERISTICS FOR INVIDUAL UNITS OF RECOMMENDED VHF RELAY CONFIGURATION

Equipment	Weight (lbs)	Power (watts)		Volume (cu. in.)
		Operate	Standby	
Units aboard Surveyor				
VHF Transmitter	2.0		0.1	40
2-watt mode		8.0		
0.2-watt mode		1.5		
VHF Dual Receiver	1.2	1.4 or 2.4 [1]	0.1	24
VHF Triplexer	1.3	--	--	32
VHF Antenna & Feed [2]	1.0	-- [3]	--	--
Range & Bearing Unit	0.5	0 or 0.9		34
S/SLRV Selector	0.1	0.1		<1
S/E Selector	0.5	1.3		12
TOTALS	6.6	Varies per modes	0.2	6 x 6 x 6 package
Units aboard SLRV				
VHF Transmitter	2.0		0.1	40
2-watt mode		8.0		
0.2-watt mode		1.5		
VHF Receiver	0.6	1.0	1.0	12
VHF Diplexer	1.0	--		24
Antenna and Feed [2]	0.5	--		
Input Selector	0.4	0.8		8
DIBSI Multiplexer	0.5	0.2		8
TOTALS	5.0	10 or 3.5 [4]	1.1	4 x 5 x 6 package

Notes:
(1) 1.4 watts for all modes except Bearing; 2.4 watts during Bearing as second section of receiver required.
(2) Antenna weights exclude any devices for extending same.
(3) 0 during all modes except Ranging and Bearing; 0.9 watts during such modes.
(4) 10-watts during 2-watt transmitter operation; 3.5 during 0.2-watt transmitter operation.

TABLE II. 2-16

PHYSICAL CHARACTERISTICS REQUIREMENTS FOR COMMUNICATIONS SUBSYSTEM

Item	Section Aboard Surveyor				Section Aboard SLRV				Total Communications Subsystem			
Weight (lbs.) [1] Requirement	6.6				5.0				11.6			
Volume (Cu. In.) [4]	216				120				336			
Dimensions (In.) [4]	6 x 6 x 6				4 x 5 x 6				---			
	Operate or TV Mode with Trans. period of			Charge or Hibernate Mode	Operate or TV Mode with Trans. period of			Charge or Hibernate Mode	Operate or TV Mode with Trans. period of			Charge or Hibernate Mode
	High Pwr.	Low Pwr.	Stand-by		High Pwr.	Low Pwr.	Stand-by		High Pwr.	Low Pwr.	Stand-by	
Input Power (Watts) Surveyor Sources												
+29 V Reg.	10.8 [2]	4.3 [2]	0.2	---	--	--	--	---				
SLRV Sources									20.8 [2]	7.8 [2]	1.3	1.0 [3]
+24 V Reg.	--	--	--	---	10	3.5	1.1	1.0 [3]				
Power Dissipation (Watts)	8.8 [2]	4.1 [2]	0.2	---	8	3.3	1.1	1.0 [3]	16.8 [2]	7.4 [2]	1.3	1.0 [3]

NOTES:
(1) Excludes any device required for extending VHF antenna.
(2) Add 0.90 watts for period when Range measurement takes place, or add 2.0 watts for period when Bearing measurement takes place.
(3) VHF Receiver on to receive commands.
(4) Less antenna and any devices for extending same.

G. SIGNAL DEGRADATION DUE TO NOISE BUILDUP IN RELAY OPERATION

When radio signal energy is transferred between two terminals by means of an intervening relay device, noise energy is introduced at the relay location, which contaminates the signal energy beyond that which would have occurred if the signal energy had been transferred directly (without the intervening relay). This contamination is permanently introduced in non-coherent detection processes and will partially contaminate coherent processes. The residue degradation will either produce inferior data quality at the final terminal, or must be compensated by increases of the system gains in the link between the initial transmitter and the relaying device. The amount of increase that would be required is dependent upon the equivalent carrier-to-noise ratio at the final receiving terminal, which would provide the desired performance quality for a direct link.

To derive the parametric compensation that would be required in the communications between the SLRV and the DSIF terminals when the Surveyor is used as a relaying device, the model shown in Fig. II.2-75 is used as the starting point. Since the solution will be provided in parametric form, the direction of signal transfer is immaterial and will be introduced by the appropriate selection of the desired C/N ratio at the receiving terminal. For general simplification, the following assumptions will be made as illustrated in Figure II. 2-75.

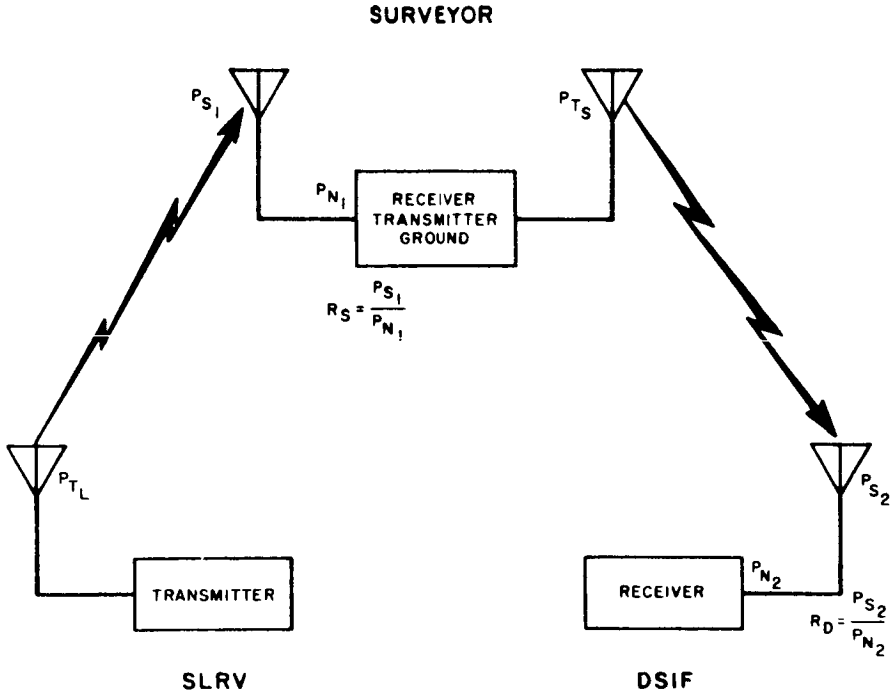

Figure II.2-75. Basic Relay Model

(1) Direction of traffic flow is from the SLRV to the DSIF, whether the transfer is through the Surveyor as a relay or not.

(2) The range between the SLRV and DSIF is identical to that of the Surveyor to DSIF, in the first approximation.

(3) Frequency of operation will be identical for both SLRV and Surveyor in the first approximation.

(4) The transmission spectrum at the output of the Surveyor transmitter is identical to that of the transmitter at the SLRV, although additional baseband noise is present.

The above set of assumptions is intended to normalize the characteristics of the relay link to those of the direct link, such that the incremental increase of power output for the SLRV transmitter due only to the relaying process can be evaluated. Actual power levels must be computed on the basis of the specific links, without the restrictive assumptions necessary for the case of the relay model.

Analysis of the basic relay model shown in Fig. II. 2-75 indicates that the signal energy received at the input terminals of the Surveyor due to the output power, P_{T_L}, of the transmitter at the SLRV (accounting for the link gains and losses) is identified as P_{S_1}. However, due to the noise susceptability of the Surveyor receiver, noise energy, P_{N_1}, is also received. Thus, the power output of the Surveyor transmitter will be the result of the composite signal and noise energy and the overall gain characteristic of the Surveyor receiver and transmitter as a relay device, G_r. This output can be expressed as:

$$P_{T_S} = P_{S_S} + \alpha P_{N_S} \qquad 0 < \alpha \ll 1 \qquad \text{(II.2-109)}$$

where P_{T_S} output power of the Surveyor transmitter,

$P_{S_S} = G_r P_{S_1}$ = amplified signal energy at the output of the Surveyor transmitter,

$P_{N_S} = G_r P_{N_1}$ = amplified noise energy at the output of the Surveyor transmitter, and

α = the noise improvement factor attained by the detection process in the Surveyor receiver.

If the ratio of input signal energy to total input energy is defined as β, then

$$\beta = \frac{P_{S_1}}{P_{N_1} + P_{S_1}} \qquad \text{(II.2-110)}$$

Then,

$$\beta = \frac{P_{S1}/P_{N1}}{1 + P_{S1}/P_{N1}} = \frac{R_S}{1 + R_S} \qquad \text{(II.2-111)}$$

and the components of signal and noise energy in the output of the Surveyor transmitter can be expressed as:

$$P_{Ss} = \frac{R_s G_s}{1 + R_s} (P_{S_1} + P_{N_1}) = R_S G_S P_{N1} \qquad \text{(II.2-112)}$$

and

$$P_{Ns} = \frac{\alpha G_S}{1 + R_S} (P_{S_1} + P_{N_1}) = \alpha G_S P_{N1} \qquad \text{(II.2-113)}$$

Equation (II.2-109) can be rewritten as:

$$P_{TS} = G_S (R_S + \alpha) P_{N1} \qquad \text{(II.2-114)}$$

At the input terminals of the DSIF receiver, the carrier-to-noise ratio can be expressed as:

$$R_d = \frac{P_{S2}}{P_{N2}} = \frac{m P_{TS}}{P_{N2}} , \qquad \text{(II.2-115)}$$

where m is the proportionate part of the Surveyor output power that appears across the terminals of the DSIF receiver, due to the link gains and losses.

If the energy of P_{TS} were the result of a pure signal ($R_s = \infty$), R_d would be the resultant carrier-to-noise ratio, and this would be the equivalent of a non-relayed link. However, for the relayed use, P_{TS} is not pure signal, but a composite of signal and noise energy. Thus, the equivalent carrier-to-noise ratio at the DSIF receiver can be expressed as:

$$R_{d_{eq}} = \frac{P'_{S2}}{P'_{N2}} \qquad \text{(II.2-116)}$$

where $P'_{S2} = m P_{Ss} = m R_S G_S P_{N1} = \frac{m R_S}{R_S + \alpha} P_{TS}$

$$P'_{N2} = m P_{NS} + P_{N2} = m \alpha G_S P_{N1} + P_{N2}$$

$$= m \frac{\alpha}{R_S + \alpha} P_{TS} + P_{N2}$$

By substituting these into equation (II.2-116),

$$R_{d_{eq.}} = \frac{m P_{TS} \frac{R_S}{R_S + \alpha}}{m P_{TS} \frac{\alpha}{R_S + \alpha} + P_{N2}} = \frac{R_d R_S}{\alpha R_d + R_S + \alpha} \qquad \text{(II.2-117)}$$

from which

$$R_d = \frac{R_{d_{eq}} (R_S + \alpha)}{R_S - \alpha R_{d_{eq}}} \qquad \text{(II.2-118)}$$

$$= \frac{R_{d_{eq}} (R'_S + 1)}{R'_S - R_{d_{eq.}}} \qquad \text{(II.2-119)}$$

where $R'_S = R_S \alpha$.

Equation (II.7-10a) can be interpreted as the relationship between the carrier-to-noise ratio required at the DSIF receiver (R_d), when the relay mode is used to the carrier-to-noise ratio at the DSIF receiver (R_{deq}) if the relay mode were not used, in terms of the adjusted carrier-to-noise ratio at the Surveyor receiver (R_s). This adjusted carrier-to-noise ratio is that value which would be present if the Surveyor receiver had no detection process to provide baseband noise improvement.

The values pertinent to the relationship of equation (II.2-119) are plotted in Figure II. 2-76. Several characteristics are apparent from equation (II.2-119) or Figure II. 2-76:

(1) $R_d = R_{deq}$ only when $R'_s =$ ∞

(2) R'_s R_{deq}

(3) For any value of R_{deq}, $(R_d)(R'_s)$ is minimum when R'_s $2 R_{deq}$

The first condition is a reiteration of the non-relay condition, while the second indicates the permanent trait of the noise contamination. However, the third one indicates that the total power requirement for the combined SLRV and Surveyor can be minimized if the carrier-to-noise ratio at the DSIF is used to dictate the design level for the carrier-to-noise ratio at the Surveyor by a +3-db differential.

Fig. II. 2-77 is a replotting of Fig. II. 2-76 to illustrate the degradation of the C/N ratio at the DSIF, unless the SLRV transmitter power is proportionately increased to compensate for this action.

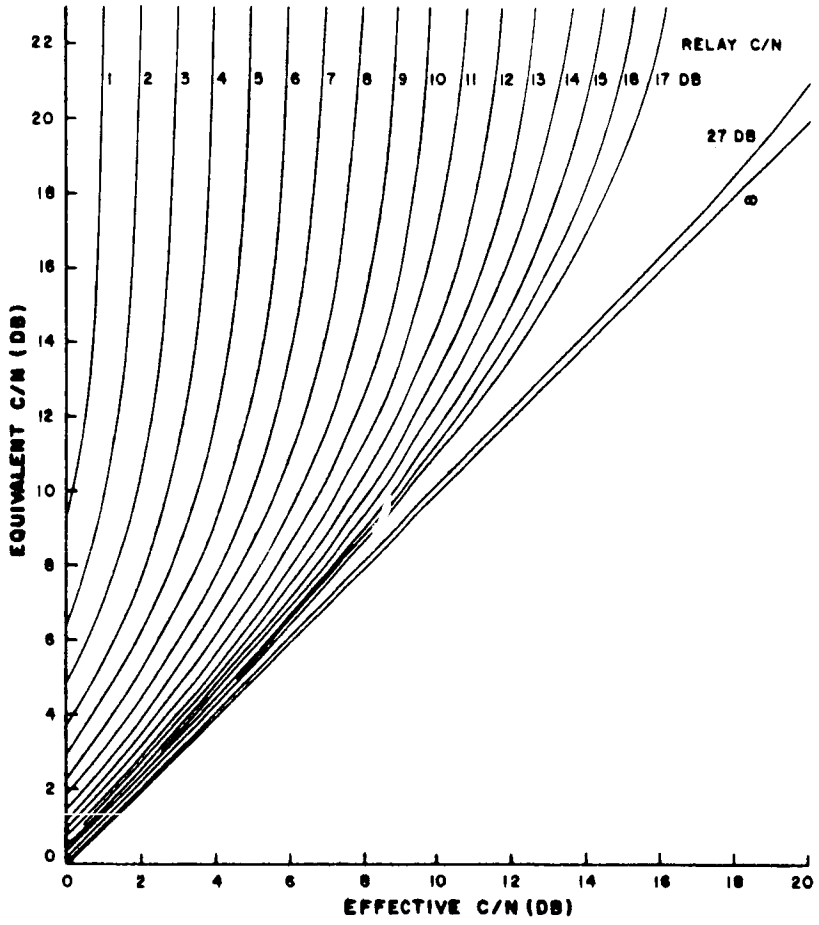

Figure II. 2-76. Relationship Between Effective and Equivalent C/N Due to Intermediary Relay C/N

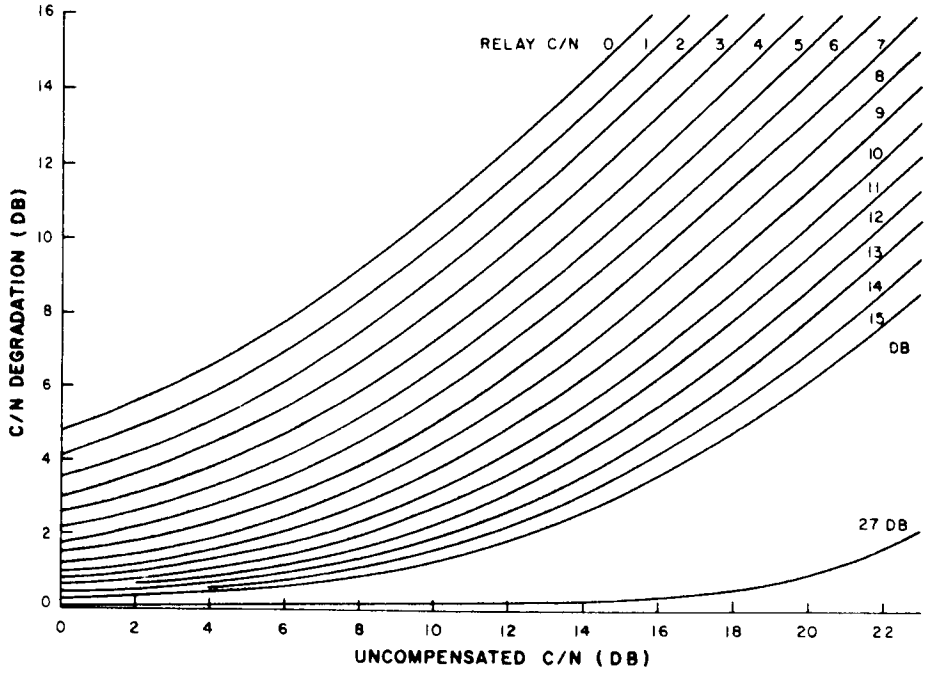

Figure II. 2-77. Degradation in C/N Due to Intermediary Relay

H. VHF DIRECT EARTH/SLRV/EARTH BACKUP CONSIDERATIONS

Ignoring the frequency allocation/interference problem, the possibilities of backup VHF direct Earth/SLRV/Earth communications is worthy of consideration.

1. Earth/SLRV Commands

If the Surveyor S-band receiver or VHF transmitter were to fail, a backup 150 Mc link direct Earth/SLRV could be employed to send commands to SLRV. Performance of such a link would approximate that of the S-band Earth/SLRV link discussed in Section II. 2 by using the same DSIF 85-foot parabolic dish. That is, the reduction in antenna gain at the lower frequency would be compensated for by the reduced space loss, since these functions both vary as the square of the carrier frequency. A gain over the S-band link would be 7 db due to lower receiver noise figure, but losses would include a 10-db C/N ratio requirement and wider IF due to instabilities. These losses about nullify the 7-db noise figure improvement, so performance would remain close to the 10^{-5} BEP (bit error probability) given in Paragraph B.

2. SLRV/Earth Communications

In spite of the path-loss/antenna-gain cancellation, the performance of this link would be inferior to the S-band because of the increase in system noise temperature as contrasted to use of the maser. Also, if a conventional FM receiver (limiter/discriminator detection) were used rather than phase-lock demodulation, a higher C/N ratio would be required. If phase-lock demodulation is employed, the noise figure differential would be about 4 db.

Thus, as contrasted to the results of Paragraph B, an antenna gain on SLRV of about 19 db would be required with a 2-watt VHF transmitter, in order to achieve threshold in the DSIF receiver (3. 3-Mc bandwidth) for 90% of the time, assuming the 210-foot dish case. Since only pseudo-omni-type antennas are proposed for SLRV, this additional 19 db would have to be achieved on the ground, if video reception were a requirement. Since the 210-foot dish represents a gain of 36 db at 120 Mc, we would need a gain of 55 db for the video (TV) case. This requires a structure over 1600 feet in diameter.

If we neglect additional antenna provisions, the 210-foot dish will permit the thresholding of a VHF receiver of noise bandwidth equal to 19 db less than 3. 3 Mc, or about 40 kc. This shows that the telemetry data and narrowband video could be received if such an alternate TV capability were provided on SLRV. (In this respect it is worth noting that Surveyor has an emergency narrowband video of only 1. 2 kc, for which a 4. 4-kc noise bandwidth is provided in the DSIF receiver).

APPENDIX III
POWER SUPPLY SUBSYSTEM

APPENDIX III
POWER SUPPLY SUBSYSTEM

A. INTRODUCTION

This appendix represents the detailed analyses which were used to arrive at conclusions and preliminary designs.

B. MODUS OPERAND I FOR THE SLRV POWER SUBSYSTEM STUDY

1. Selection of Generators

A study was conducted of existing power sources which could be applied to the program. It was apparent that the only feasible types for this mission were

- Solar Array
- Radioisotopic Thermoelectric Generator (RTE)
- Radioisotopic Thermionic Generator (RTI)

Effort was concentrated solely in these areas.

2. Establishment of Power Requirements

In the next step, initial power requirements were established for mission performance in three cases. These were:

(1) Indirect

In this method, the Surveyor is used as an intermediary (up-link as well as down-link) in communicating with the SLRV.

(2) Direct

Communication with the SLRV is direct from the earth ground station (the Surveyor does not participate).

(3) Hybrid

Up-link communication with the SLRV is direct; down-link communication with the SLRV is indirect (via Surveyor).

3. Preliminary Power Duty Cycles

Preliminary power duty cycles for the indirect link were established for two surface conditions: a relatively rough moon and a relatively smooth moon. Duty cycles for the direct and hybrid links could be readily obtained by providing for the increased communication requirements.

4. Parametric Curves

With establishment of the power duty cycles, it was then possible to establish the range of loads presented to the power subsystem.

It was readily apparent that parametric curves would be required at this point. This was due to the following reasons:

(1) The load requirements of the subsystems were still being refined.

(2) The mission profiles were constantly being reviewed as a function of the power duty cycles, reliability aspects, earth contact time, hibernation, etc.

(3) The power duty cycle obviously would influence the size and type of power source selected.

(4) The power subsystem itself was in a state of flux. It was not only dependent on items (1) through (3), above, but also on performance parameters of subsystem elements as well as the system design.

In short, because of the interdependence of these items, parametric curves would indicate the direction of further study, as well as the necessary tradeoffs of performance and weight.

Parametrics were generated for RTE specific power output of 1.0, 1.5, and 2.0 watts per pound (including converter). An orientable solar-array subsystem was compared with the RTE on the same tradeoff basis. For the orientable array, it was assumed that operation was effected solely from the storage battery. The solar array was oriented normal to the sunline, to recharge the battery during non-operation (charge) intervals.

It was expected that realistic tradeoffs could be made before a preliminary design of the final system was completed. Although the final design could vary as much as 10 or 15 percent from the parametric study, this would not affect conclusions reached in comparing the various systems.

These studies were conducted for both Goldstone and World-Wide Coverage, and for three different cases of load requirements. The latter covered the range of interest.

5. Vendor Data and Specification Approval

In the meantime, the following specifications were released:

(1) To JPL, an RTE specification to meet specified power and weight requirements, for review and recommendation.

(2) To RTE vendors, requests for parametric data.

(3) To battery vendors specifications for silver-zinc and silver-cadmium batteries to facilitate a tradeoff comparison both for "state-of-the-art" and projected mission requirements.

(4) To solar cell vendors, specifications for "state-of-the-art" and projected solar-cell data.

6. Subsystem Improvements

In order to further reduce the over-all weight of all the power subsystems, a number of refinements were made. These included:

(1) The Multiple-Cycle Approach

By increasing the number of operational cycles, the battery could be smaller. While the integrated operational energy would still be the same, the smaller duty cycle requires less energy storage from the battery. Limiting conditions here are battery-cycle lifetimes, and increase in both charge and discharge rates.

(2) Change to World-Wide Contact

By changing to World-Wide contact, another weight saving resulted. The limiting "charge rate" could be averaged over 24 hours rather than the 12-hour contact provided by Goldstone. Moreover, the over-all mission time-interval would be shortened. It might be possible to complete the mission in one lunar day, or at worst in approximately 1.5 lunar days. Thus, hibernation survival would at most be required for one lunar night only, with a large portion of the mission already accomplished.

7. Final Power Duty Cycle

Final power duty cycles were generated for a "smooth" and a "rough" moon. These were based upon final requirements of all the subsystems and selected mission profiles.

8. Final Configuration of a Fixed Solar Array and RTG* Design

By the time the vehicle stowage had been configured into the straddle mode, it not only met the c.g. constraints required for the Surveyor, but also provided more latitude for the power-generator configuration. The RTG thermal rejection problem was considerably simplified. Moreover, it was possible to use a fixed solar array which could provide power during operation. This affected a further reduction in system weight.

*RTG (Radioisotopic Generator is a generic term including both the RTE and RTI)

9. Preliminary Design Stage

(1) Fixed Solar Array

Several fixed arrays were reviewed and the best of these were selected.

(2) RTE

Two RTE's were developed for SLRV: one ("state-of-the-art") using lead-telluride thermocouples, and the other (next generation) using silicon-germanium. The maximum power capability of each was determined for operation in the configuration envelope.

(3) Both General Atomics and Martin-Marietta contended that the RTI was impractical for this mission, because of delivery requirements. Therefore, this system was discarded.

Final inputs were received from the vendors on the specifications originally submitted. As a result of these inputs, it was necessary to adjust performance parameters.

C. GENERAL DISCUSSION OF POWER SUBSYSTEMS

An initial study was conducted into various power subsystems and conversion techniques, in order to highlight those best suited to the SLRV mission. Table II.3-1 lists the power subsystems considered and the major disadvantages of each. The conclusion reached is that the three most likely power subsystems are photovoltaic (solar) cells, radioisotope thermoelectric generators (RTE), and radioisotope thermionic generators (RTI). The study effort, therefore, was concentrated on these systems.

TABLE II .3-1

POTENTIAL POWER SUPPLY SUBSYSTEMS FOR THE SLRV

Energy Source	Energy Storage	Conversion Technique	Comments Relevant to SLRV Power Supply Subsystem
Nuclear Fission	Not Required	Dynamic	Minimum reactor weight is much too heavy for mission.
		Thermionic	Minimum reactor weight is much too heavy for mission.
		Thermoelectric	Minimum reactor weight is much too heavy for mission.
Radio-Isotope	Secondary Batteries or Thermal Storage	Dynamic	Disadvantages: complexity, unavailability, and possible weight penalty.
		Thermionic	Disadvantages: Low output voltage, high converter weight, schedule problems.
		Thermoelectric	Disadvantages: Requires large radiator.
Solar	Secondary Batteries or Thermal Storage	Dynamic	Requires precise orientation of solar collector, heavier than solar photovoltaic for low power levels.
		Thermionic	Requires precise orientation of solar collector, heavier than solar photovoltaic for low power levels.
		Thermoelectric	Requires precise orientation of solar collector, heavier than solar photovoltaic for low power levels.
		Photovoltaic	Main disadvantages of system is lack of growth potential.

TABLE II.3-1 (Continued)

POTENTIAL POWER SUPPLY SUBSYSTEMS FOR THE SLRV

Energy Source	Energy Storage	Conversion Technique	Comments Relevant to SLRV Power Supply Subsystem
Chemical	Fuel Tanks	Dynamic	Weight of storage and conversion apparatus too heavy.
		Fuel Cell	Too heavy for the total mission energy requirements.
	Primary Batteries		Too heavy for the total mission energy requirements.

D. ORIENTABLE SOLAR ARRAY

In the initial phase of the study, consideration was given to a rolled-up stowage mode for the SLRV aboard the Surveyor. A feasible configuration for this stowage mode is a single planar array mounted on the rear axle.

Conservatively, it assumed that no power is generated during locomotion. To prepare for charge, the vehicle is turned so that the vehicle axis is coplanar with the sunline. Then the array is elevated so that it is normal to the sunline. To prepare for operation, the array is retracted so that it is vertical. In this state, power will be generated only when the sun illuminates the array from the rear. However, this effect is difficult to assess, since it is dependent upon the vehicle path in relation to the sun, as well as the sun elevation angle. Hence, this effect was neglected in the estimation of required subsystem weight.

For the orientable array, the array area was restricted to about 4 square feet projected in order to meet SLRV stowage requirements within the Surveyor as well as vehicle clarances.

This type of array requires a relatively heavy battery, since all energy during operation is obtained solely from the battery. The multiple-cycle approach and world-wide coverage were used to reduce the battery weight. However the resultant battery weight is still so heavy that the desired mission cannot be met with the allocated system weight. However, the analyses performed for the fixed array in the following sections indicate how the mission may yet be met.

E. SOLAR-CELL DATA

A study has been made of the photovoltaic devices available for this mission. Figure II.3-1 illustrates the variations of efficiency versus temperature for three types of glass-covered solar-cell shingles, namely, silicon P-on-N, silicon N-on-P, and gallium arsenide. The cell efficiencies chosen represent cells which are readily available at a reasonable cost. This choice will serve for the purpose of illustration. Table II.3-2 lists the efficiencies and efficiency-degradation of the three cell types. It should be recognized that some discrepancies exist for the degradation factor in source literature, depending upon the method of measurement; however, the values used are substantially correct.

Figure II.3-1 indicates that gallium arsenide can only be considered if its air-mass-zero efficiency at 25°C is within approximately 1 percent of the silicon cells. Considering that higher efficiency silicon cells are available and the current state-of-the-art of gallium-arsenide cells, the latter cannot compete.

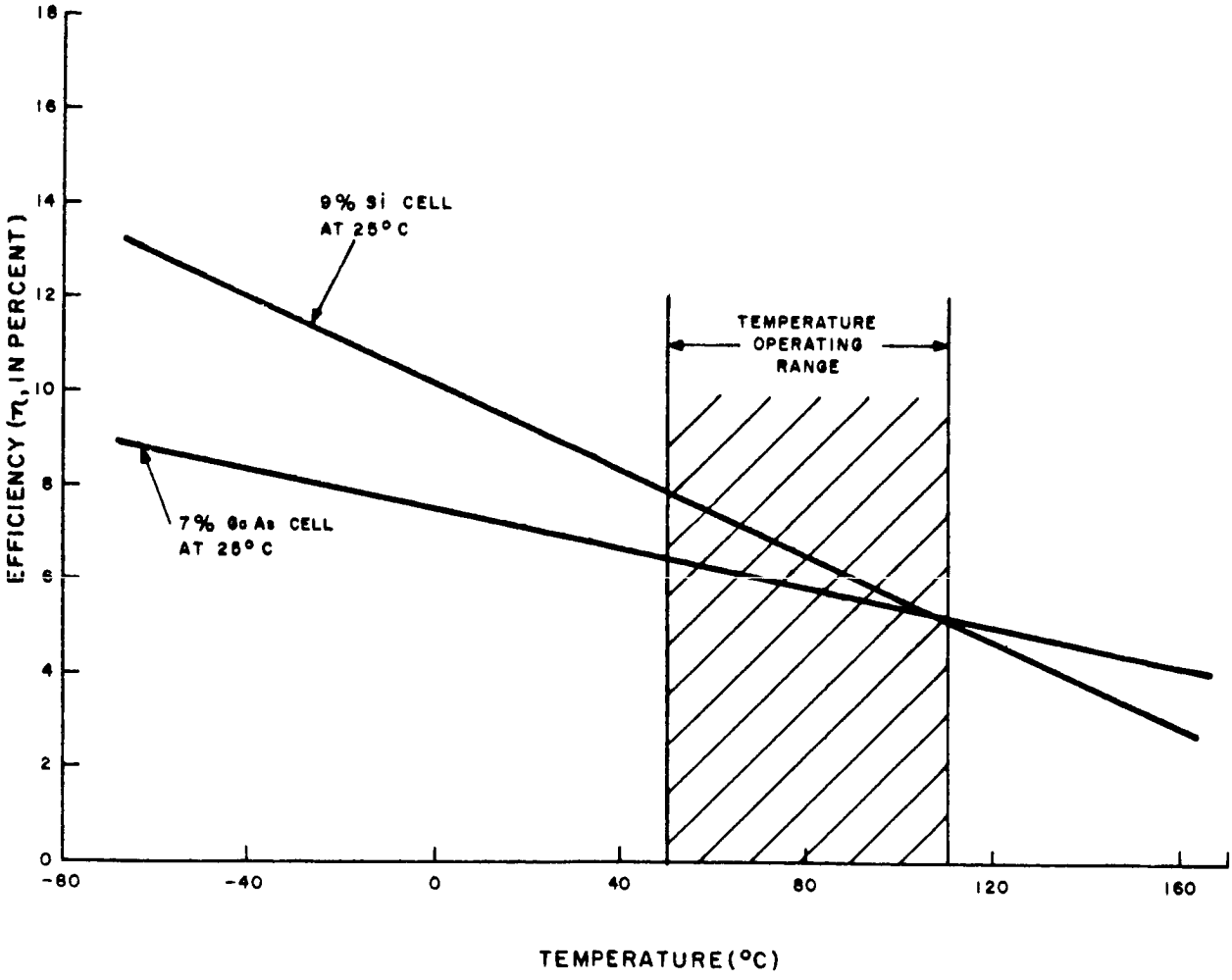

Figure II.3-1. Efficiency versus Temperature for Silicon and Gallium Arsenide Glass-Covered Solar-Cell Shingles

TABLE II.3-2

EFFICIENCY AND DEGRADATION OF SOLAR CELLS

Cell Type	Efficiency of glass-covered shingle at 25°C and air-mass zero (percent)	Efficiency Degradation factor (%/°C)
Silicon P-on-N	9	0.50
Silicon N-on-P	9	0.50
Gallium Arsenide	7	0.29*

*Technical Documentary Report No. ASD-TDR-63-516, Volume II, dated December, 1963. Contract No. AF33(657)8493

Thin-film cadmium-sulfide cells have also been investigated. The power-to-weight ratio obtained with this cell is considerably higher than is possible with single-crystal silicon or gallium arsenide. A ratio as high as 30 watts per pound has been obtained from single cells. However, these cells have not undergone any flight testing to date. Moreover, the low efficiency of these cells requires a substantial area, which makes the use of this cell impractical for the SLRV design. For this reason, thin-film cadmium-sulfide will not be considered for this mission.

1. Further Investigation of Solar-Cell Efficiencies

It was apparent that an increase in operating time could be obtained with an increase in solar-cell efficiency. In order to establish the availability of solar cells of various efficiencies, a survey of the industry was conducted involving five solar-cell vendors. The five vendors were asked to give cost estimates for five cell shingles covered by a 0.006-inch fused silica, with anti-reflective coating and a blue-red filter. (A five-cell, 1 x 2-cm shingle was chosen as the basis for the estimates, because this configuration is one with which all vendors are familiar). The information provided by the five vendors has been evaluated and adjusted in accordance with AED experience with each vendor on other programs. The results are shown in Table II.3-3. The costs have been normalized to the highest cost quoted for a shingle having an efficiency of 10%.

The estimate at this time indicates that minimum efficiencies of 10 percent P/N or N/P from the solar-cell shingle can be obtained without entering the region of very high costs.

2. Temperature Effects

The temperature dependence of solar-cell current-voltage curves is generally expressed in terms of the temperature dependence open-circuit voltage and short-circuit current.

TABLE II.3-3

RELATIVE COSTS OF SOLAR CELL SHINGLES OF VARIOUS EFFICIENCIES

Vendor Designation	Efficiency*		
	9.5%	10.0%	***10.5%
A	0.70	0.88	
B	0.84	1.00**	1.93
C	0.77	0.85	

*Efficiencies are for air-mass zero, 25°C, 139.6 mw/cm² sunlight. Shingles have 6-mil cover glass, blue-red filter.

**Costs are arbitrarily normalized at the vendor, B, 10% quote. For example, the price quoted by vendor C for a 10% efficient shingle is 85% of the price quoted by vendor B for a 10% shingle.

***N/P only

The range of open-circuit voltage and short-circuit current temperature coefficients presented by various solar cell manufacturers and by AED measurements is shown in Table II.3-4. It is significant that these values were determined under various light conditions, with different types of cells, and over different temperature ranges.

The numbers selected for projection of current-voltage (I-V) curves to various temperatures are: -2.2 mv/°C and +0.025 ma/°C, at open-circuit voltage and short-tions. This is particularly significant in the case of current-temperature relationship because the current is spectrally sensitive.

3. Current-Voltage Curves

The curve shape which was used to represent the 10-percent efficient shingle was determined from an average of current-voltage curves of modules used on the Nimbus program. This curve was adjusted to indicate a shingle efficiency of 10 percent at 25°C, air mass zero, and at an incidence of 139.6 mw/cm². The translation of the curve to represent the shingle output at temperatures other than 25°C was performed using the temperature coefficient discussed above. The I-V curve was translated laterally and vertically to the new short circuit voltage points. The shape of the curve was maintained.

TABLE II.3-4

TEMPERATURE COEFFICIENTS

Vendor Designation	$\frac{\Delta Voc}{\Delta T}^{*}$ (mv/°C)	$\frac{\Delta Isc}{\Delta T}^{**}$ (ma/°C)
A	-2.29	----
B	-1.78	----
C	-2.20	+.025
D	-2.05	+.048
E	-2.26	+.035

$^{*}\frac{\Delta Voc}{\Delta T}$ = $\frac{\text{change in open-circuit voltage (mv)}}{\text{change in temperature (°C)}}$

$^{**}\frac{\Delta Isc}{\Delta T}$ = $\frac{\text{change in short-circuit current (ma)}}{\text{change in temperature (°C)}}$

4. Radiation Considerations

Document EPD-98, Revision 1, indicates that expected radiation damage is not considered significant. However, a brief study was conducted into the possible effects of radiation encountered in the mission.

Radiation encountered by SLRV can be described as follows:

- Electrons and protons encountered during transit through the radiation belts;
- Protons encountered during the period of travel from ten earth radii to the lunar surface; and
- Protons encountered as a result of a solar wind occurring during the lunar lifetime.

The total 1 Mev equivalent electron flux is calculated in Table II.3-5.

Cell Degradation

Solar-cell degradation due to radiation is estimated to be approximately 7.5 percent, based on data available on RCA-Mountaintop N-on-P solar cells (see Figure II.3-2). As shown below, sputtering effects can reduce solar-cell output by an additional 3 percent, thus increasing the total loss to 10.5 percent. Also, the loss is time-dependent; hence, the 10.5-percent total loss represents the maximum ("worst-case") degradation. Although P-on-N cells have been selected for the Surveyor, it is probable that N-on-P cells will be selected for SLRV, in order to take advantage of their superior radiation-resistance characteristics.

The cover glass recommended is Corning 0211 microsheet, which has a significant price advantage over fused silica, and does not materially compromise the radiation resistance characteristics for a vehicle having a relatively short mission lifetime such as SLRV. This will be further reviewed in the Phase II program.

Coatings on the cover glass will be anti-reflective on the top surface and blue-red on the bottom. The anti-reflection coating on the top surface of the cover glass will reduce surface reflections and thus effectively increase transmission by about 3 percent. The blue-red filter has an optical transmission from approximately 400 millimicrons to approximately 1100 millimicrons. This filter gives the solar array lower α/ϵ ratio than a blue filter, thus permitting the array to operate at a lower temperature and increasing the effective power output. Blue-red filters have been used on the Nimbus solar modules and have been subjected to extensive thermal testing from -80°C to +66°C.

TABLE II.3-5

RADIATION ENCOUNTERED BY SLRV

Irradiation Type	Equivalent 1-Mev Electron Flux in electrons/cm
Electrons encountered in radiation belts	1.34×10^{12}
Protons encountered in radiation belts	4.1×10^{12}
Solar flare protons	14.0×10^{12}
Solar wind protons	low energy (negligible)
Total	19.44×10^{12}

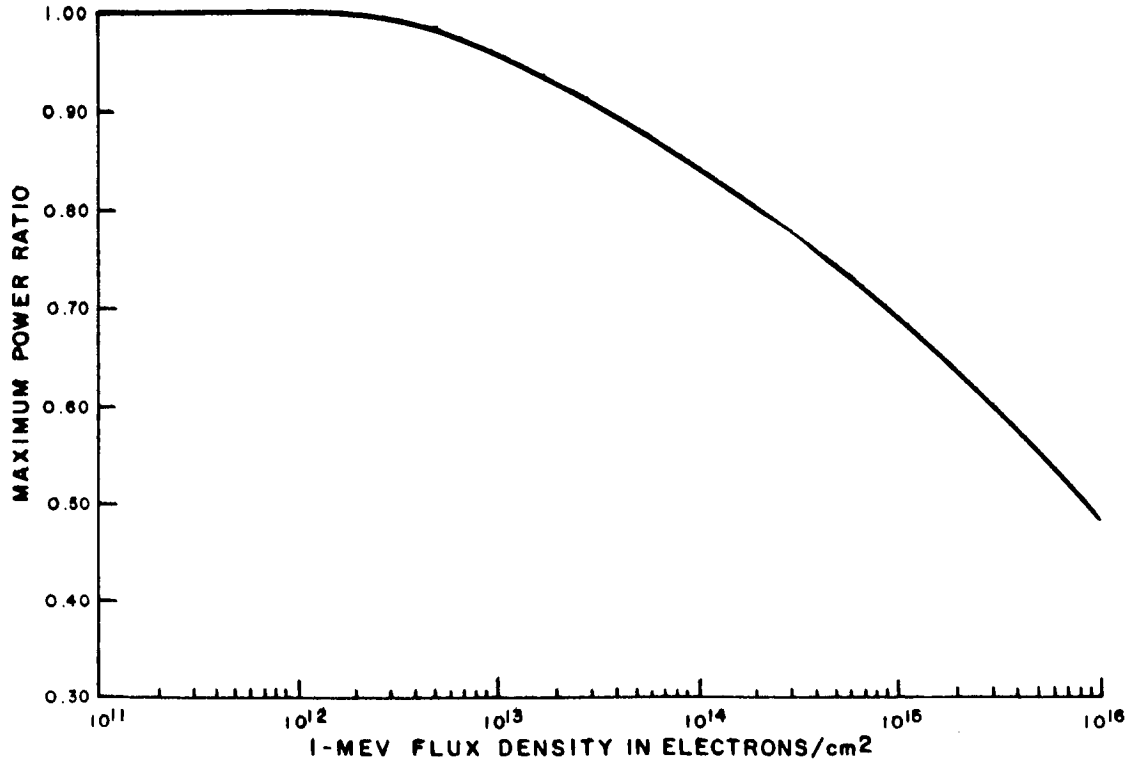

Figure II.3-2. Solar-Cell Degradation in the Radiation Environment

Adhesive for the bonding of cover glasses to the solar cells will be Furane 15E or an equivalent. Furane 15E* has been used successfully on other space vehicles and shows no appreciable radiation degradation for the radiation levels calculated in Table II.3-5

Sputtering

Impact of the solar-wind particles (assumed to be low-energy ions) may cause the surface material to wear away. The rate of removal of microsheet or for fused silica is given by

$$L = \frac{(mv)\,\theta\,A}{Ne}$$

where

L is the rate of removal of a layer of material (cm/sec);

m is the particle density ($\frac{particles}{cm^3}$ $x\ 10^5$) ;

v is the particle velocity (1.5×10^6 cm/sec);

θ is the sputtering coefficient, equal to 0.03;

A is the atomic weight of fused silica (28g)

N is Avogadro's Number, equal to 6.02×10^{23}; and

e is the density of fused silica (2.3 g/cm^3).

From this formula,

$$L = 7.08 \times 10^{-5}\ cm\ .$$

or, $L = 0.00007$ cm removed by sputtering. This corresponds to an 0.46 percent loss of cover-glass thickness. This could reduce transmission by about 3 percent due to the loss of the anti-reflection coating on the upper surface of the cover glass. Also affected by a sputtering process would be any anti-static coating on the cover-glass surface.

Assumptions

(1) Travel time through the earth radiation belts is approximately 3.5 hours.

*Furane 15E bonded cover glasses have been thermally cycled between -80°C and +60°C in excess of 1000 times, with only minor (less than 3%) degradation in solar-cell output. Deterioration due to particle radiation is insignificant below 10^{16} electrons/cm^2 exposure.

(2) Solar cells are N-on-P with 0.006-inch thick fused silica (for calculation purposes only) covers.

(3) Low-energy protons will be stopped by the glass covers (6-mil glass effectively stops 5-Mev protons).

(4) Solar flare of one-week duration occurs during the flight of SLRV or while it is operating on the lunar surface.

(5) Solar wind occurs during a solar flare.

(6) Solar wind particles are either low-energy protons or low-energy ions.

Approximately seventy percent of the equivalent 1-Mev radiation encountered (See Table II.3-6) results from a solar flare, which could occur at any time during the vehicle's operational period or not occur at all. If it occurs early in the operational period, most of the degradation due to radiation will take place then, and the array output will be reduced for the duration of the mission.

The sputtering (wearing away) effect will occur only if a solar wind occurs, and then only if the wind is composed of ions rather than low-energy protons.

5. Shingle Qualification

Because the temperature extremes expected on the solar-cell arrays are -130°C to +100°C, a thermal cycle qualification test for shingles must be conducted during Phase II of the program. This test will extend the temperature limits to -140°C and +110°C. The dwell times present in the lunar temperature cycle will not necessarily be reproduced, but the number of cycles will be increased to include the maximum number of cycles that flight arrays would receive during ground tests and the lunar mission. Tests of this nature have been performed successfully on the Surveyor panel and on other programs,* although the temperature range for most of these have not been as extensive.

Tests performed on the Surveyor panel indicate that cracked cover glasses may result from exposure to lunar night. This is not expected to degrade the cell output by more than 5 percent.

6. Dust Protection

Current theories concerning lunar surface composition were explored. The theories vary from one which considers the surface to be composed of a one-hundred-foot-layer of fine particles to a theory which says that the smallest particle is the size of a baseball.

---

*At RCA, this includes Tiros, Relay and Nimbus.

Assuming that some provisions must be made to protect against dust, investigations have been made of techniques for keeping camera lenses free of dust. Indications are that the dust buildup will be due to electrostatic attraction, which can be reduced by coating the surface with an anti-static coating. This is a conductive coating (usually tin oxide) through which a current may be passed to break down the static attraction. (This approach may not be suitable for this application). The effect of anti-static coatings on optical transmission is currently being investigated. The use of anti-static coatings which do not require the passage of an electrical current is a possibility. However, there is no evidence that such techniques have proven feasible.

The entire dust protection program needs further study, in the definition of the dust environment, the minimizing of associated problems and the means necessary to meet these requirements.

7. Configuration

It has been proposed that the SLRV solar-cell array consist of five-cell (1 cm x 2 cm) solar cell shingles. Because of the unusual shape of the array, it may be possible to cover a larger area with unit areas of 2 cm^2, than with an array made up of larger cells. Investigations will be conducted during the Phase II program to determine the feasibility of using configurations other than the five-cell shingle, as well as reducing the thickness of the cells as a weight-saving measure.

8. Shingle Weight Reduction

Based on limited data it appears that a reduction in shingle weight is now a practical accomplishment. RCA-Mountaintop has fabricated quantities of 14-mil thick cells, both with and without a solder backing (on the P side). The following table compares weights of the 14-mil and conventional 17-mil wafer.

Wafer Thickness - mils (1 x 2 cm cells)	Weight With Solder Backing-gms	Weight Without Solder Backing-gms
17	0.242	0.187
14	0.199	0.144

A shingle composed of five (1 x 2 cm) 17-mil wafers with connecting tabs, but without glass filter, weighs 1.52 grams. Use of the 14-mil wafer with solder backs reduces the shingle weight to 1.30 grams. Shingle weight based on the use of solderless 14-mil wafers is 1.03 grams.

This latter weight is optimistic because solder is required to shingle the cells together and this is not included in the 1.03 gram weight. It is estimated that the additional weight for solder is 0.15 grams, yielding a total of 1.18 grams.

The table below shows the weight of completed shingles:

Wafer Thickness (mils)	Weight of Completed Shingle with 6-mil glass (gm)
17 (with solder back)	1.82
14 (with solder back)	1.60
14 (no solder back; solder added as needed)	1.48

The figures stated herein are based on a limited quantity of cell weight data and should be regarded only as design goals. It is anticipated that within the next few months increased 14-mil wafer production will yield statistically significant weight information.

F. ARRAY SUBSTRATE AND MATERIALS

1. Substrate for Orientable Array

A preliminary investigation was performed to determine the material and section details of the solar-array structural panel to be used for this program. A tentative selection was made of titanium-alloy 75A honeycomb-sandwich panel, with resistance-welded core and skin brazed to core. This appeared to be the lightest of the group investigated. The total weight for this type panel is 2.21 pounds, based on an assumed square panel of 4 square feet, which was originally developed for the orientable array. Fabrication dimensions are as follows:

Total depth of section,	0.375 inch;
Thickness of skin,	0.007 inch;
Thickness of core foil,	0.002 inch; and
size of core cell,	0.1875 inch.

These dimensions were based upon the following additional assumptions:

- Area of panel, 24 inches square maximum surface area;
- Manner of support, hinged on the top;
- Location of panel, plane of panel normal to the longitudinal axis of the spacecraft;
- Vibratory amplification factor, 20; and
- Loading conditions;
  10 g longitudinal at launch vibration, and
  25 g lunar impact.

Table II.3-7 lists various type of alloys, their core and skin sizes, allowable stresses, margins of safety at launch condition, and weight per panel. Impact and mechanical maneuverability conditions on the lunar surface are not critical, and thus they are not listed. Molybdenum alloy was included in this investigation because its coefficient of expansion is fairly close to that of silicon solar cells. From the standpoint of the thermal stress developed, this combination seems to reduce the stresses. However, it is uncertain whether this alloy can be satisfactorily fabricated into a honeycomb panel. Table II.3-8 lists the thermal coefficients of expansion and specific weight of the various materials considered.

Till now, the investigation has been confined largely to the strength requirements, brazed versus bonded type of panel construction, material availability for fabrication, and strength-to weight ratio comparisons. It should be noted that the bonded-type panel

TABLE II.3-7

HONEYCOMB PANEL WEIGHT SUMMARY FOR SLRV

		Skin Material & Gage	Cell Material Gage & Size	Allowable Skin Stress	Section Depth Inch	Margin of Safety	Weights (lbs)				Remarks
							Skin	Cell	Skin Adhesive	Total	
Bonded Core & Skins	1	Alum. Alloy 5052 - H38 0.010"	Alum. Alloy 0.001" 3/8"	25,000 PSI Fatigue Str @ 10^6 cyc.	1/2	-0.20	1.15	0.26	0.48**	1.89	Not satisfactory (Low M.S.)
									0.80***	2.21	
	2	Alum.Alloy 5052 - H38 0.010"	Alum. Alloy 0.001" 3/8"	25,000 PSI Fatigue Str @ 10^5 cyc.	5/8	+0.01	1.15	0.32	0.48	1.95	Marginal
									0.80	2.27	
	3	T1 Alloy 75A 0.007"	T1 Alloy 0.001" 3/16"	67,600 PSI Buckling	3/8	+0.14	1.32	0.45	0.48	2.25	Weighs more than brazed panel
									0.80	2.57	
	4	Molybdenum Alloy 0.007"	Alum.Alloy 0.001" 3/16"	*86,500 PSI Fatigue Str @ 10^5 cyc.	3/8	+0.05	2.94	1.58	0.48	5.00	Alloy might not be suitable for honeycomb fabrication
									0.80	5.32	
Brazed Core & Skins	1	Alum. Alloy 6951 0.010"	Alum.Alloy 0.008" 1/4"	31,000 PSI Fatigue Str @ 10^5 cyc.	1/2	-0.01	1.15	2.10	---	3.25	Marginal
	2	Alum. Alloy 6951 0.010"	Alum.Alloy 0.008" 1/4"	31,000 PSI Fatigue Str @ 10^5 cyc.	5/8	+0.25	1.15	2.64	---	3.79	Not desirable (High M.S.)
	3	T1 Alloy 75A 0.007"	T1 Alloy 0.002" 3/16"	67,600 PSI Buckling	3/8	+0.14	1.32	0.89	---	2.21	Higher Str/Wt ratio & higher fabrication cost than Alum.
	4	Molybdenum Alloy 0.007"	Alum.Alloy 0.008" 1/4"	86,500 PSI Fatigue Str @ 10^5 cyc.	3/8	+0.05	2.94	1.58	---	4.52	Alloy might not be suitable for honeycomb fabrication

MINIMUM SKIN TH'K & CORE GAGE FOR BRAZED ALLOYS

1. Alum Alloy
   Bridgeport Brass Co.
   Rep. J. J. Dore: 9-12-63

   Skin: .010"
   Core: .008"
   Cell size: 1/4"

2. Titanium Alloy
   Honcor Corp.
   Rep. W. B. Haynie: 9-17-63

   Skin: .005"
   Core: .002"
   Cell size: 3/16"

*Assumed fatigue str. @ 10^5 cyc. is approx. 75% of F_{ty}
**HT-424 Adhesive
***EPON-422 Adhesive

TABLE II.3-8

THERMAL COEFFICIENTS AND SPECIFIC WEIGHTS OF MATERIALS FOR SOLAR ARRAY

Material	Coefficient of Thermal Expansion per °C at 20°C	Specific Wt., Lb/in^3
Silicon Cells	4.2×10^{-6}	0.089
Aluminum	24×10^{-6}	0.098
Titanium	9×10^{-6}	0.165
Molybdenum	6×10^{-6}	0.37

permits a reduction in skin thickness due to fabrication techniques. The various metals selected for this investigation are aluminum, titanium, and molybdenum.

Because of the interacting thermal stresses (transient and steady state) in the adhesive for the specified temperature profile, interface problems of solar cells bonded to the honeycomb panel will probably require a large effort in the development program of the solar array.

2. Solar Array Bonding Materials

An investigation has been made into the bonding materials required for a solar array which will mechanically withstand its intended environment and still perform its intended function. Some possible materials which show promise are shown in Table II.3-9. These materials will be further investigated and tested in phase II.

3. Substrate for Fixed Array

A study was made to determine the total weight of the solar array substrate for the fixed array shown in Figure II.3-3. Computations were made on the basis of a bonded honeycomb panel with titanium alloy skins (0.002") and aluminum alloy core. Table II.3-10 lists calculations for 75g, 100g, and 150g response. These data were then plotted on a normalized basis (see Figure III.6-2), with the abscissa as the dynamic load equal to the product of η (the response g-loading) and Q (the applied load in lbs/ft^2); the ordinate is the weight of the substrate including the skins and honeycomb panel only.

In using this curve for determining the total weight of the solar array substrates, a trial weight of the solar array substrates must be assumed, at the beginning, since

TABLE II.3-9

ADHESIVE, INSULATING, AND STAKING MATERIALS
FOR USE ON SOLAR ARRAY

Material	Use
G.E. LTV-602 - G.E. RTV-108 Dow Corning Silastic 140 Furane Epocast 15E	Cover Glass to Solar Cell Adhesive
G.E. RTV-560 - G.E. RTV-511 Dow Corning Silastic 140 Conap Conathane 1520/AH-5 Conap Conathane 1921/048	Solar Cell to Insulation Coating Adhesive
Conap 1132 Union Carbide R-620	Electrical Insulation Coating
Normco 2030-85, 506, and 570 Emerson and Cumings Stycast 3070, 1090, and 2850 G.T. Conap 1921/048 - DuPont Adiprene/Moca L-100	Staking Material
Pittsburgh Plate Glass - Plymaster ACG-2009-20 *Bloomingdale Rubber Co. HT424 Shell Chemical Co. - Epon 422 AF 300	Substrate Adhesive
"Lithafrax" Powder 2121 "Lithafrax" Powder 2123	Fillers

* It should be noted that Bloomingdale Rubber Co. HT424 has passed preliminary tests conducted by Ryan Aeronautical Company.

the substrate weight is a function of the unknown total weight. For clarification of the use of the curve, an example calculation is illustrated as follows for the array in question.

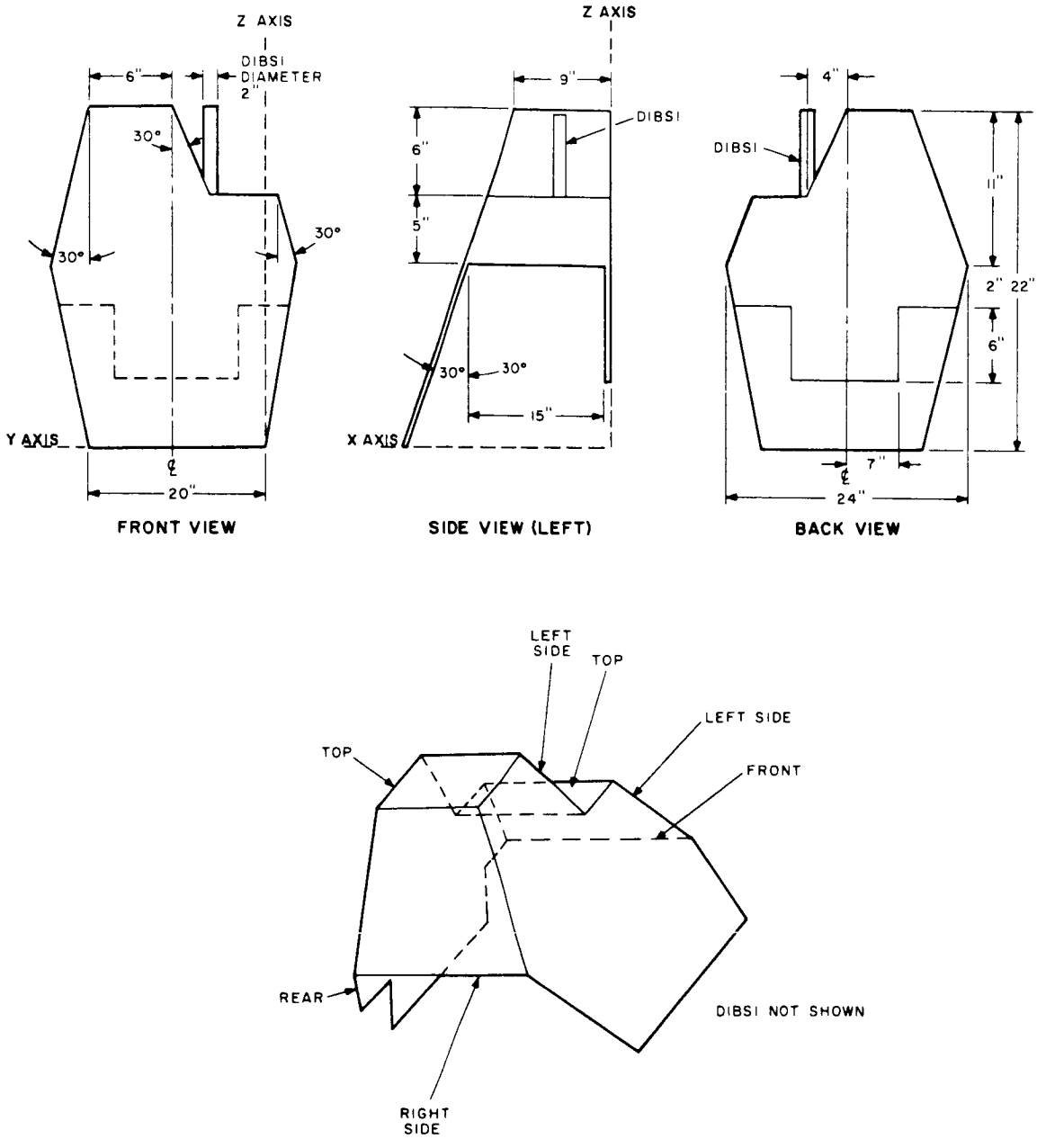

Figure II.3-3. Pictorial View of Fixed Array (DIBSI Not Shown)

TABLE II.3-10

TABULATION OF CALCULATIONS FOR VARIOUS "g" RESPONSES

Panel	Area (In^2)	Panel Depth	Skin Gage	Cell Size	Core Density	Bending Stress	Buckling Allowable	M.S.	Weight in lbs.		
									Core	Skin	Total
75 g Response											
A	308	.250	.002	1/4	2.30	9,600	9,850	+.02	.104	.213	.317
B	150	.250	.002	3/8	1.60	5,050	5,300	+.05	.034	.104	.138
C	480	.500	.002	3/16	3.10	11,200	15,100	+.35	.424	.332	.756
D	64	.250	.002	3/8	1.60	2,360	5,300	Amp	.015	.044	.059
E	49	.250	.002	3/8	1.60	1,290	5,300	Amp	.012	.034	.046
F	88	.250	.002	3/8	1.60	3,040	5,300	+.74	.020	.061	.081
G	99	.250	.002	3/8	1.60	3,640	5,300	+.45	.023	.069	.092
											1.489
100 g Response											
A	308	.250	.002	3/16	3.10 #/ft^3	12,800	15,100	+.18	.140	.213	.353
B	150	.250	.002	1/4	2.30 #/ft^3	6,700	9,850	+.47	.049	.104	.153
C	480	.500	.002	3/16	3.10 #/ft^3	14,900	15,100	+.01	.424	.332	.756
D	64	.250	.002	3/8	1.60 #/ft^3	3,150	5,300	+.68	.015	.044	.059
E	49	.250	.002	3/8	1.60 #/ft^3	1,720	5,300	Ample	.012	.034	.046
F	88	.250	.002	3/8	1.60 #/ft^3	4,050	5,300	+.30	.020	.061	.081
G	99	.250	.002	3/8	1.60 #/ft^3	4,850	5,300	+.10	.023	.069	.092
											1.540
150 g Response											
A	308	.500	.002	1/4	2.30 #/ft^3	9,600	9,850	+.03	.210	.213	.423
B	150	.250	.002	3/16	3.10 #/ft^3	10,000	15,100	+.51	.066	.104	.170
C	480	.500	.003	3/16	3.10 #/ft^3	22,500	27,600	+.22	.424	.498	.922
D	64	.250	.002	3/8	1.60 #/ft^3	4,750	5,300	+.12	.015	.044	.059
E	49	.250	.002	3/8	1.60 #/ft^3	2,580	5,300	Amp	.012	.034	.046
F	88	.250	.002	1/4	2.30 #/ft^3	6,100	9,850	+.61	.029	.061	.090
G	99	.250	.002	1/4	2.30 #/ft^3	7,250	9,850	+.36	.033	.069	.102
											1.812

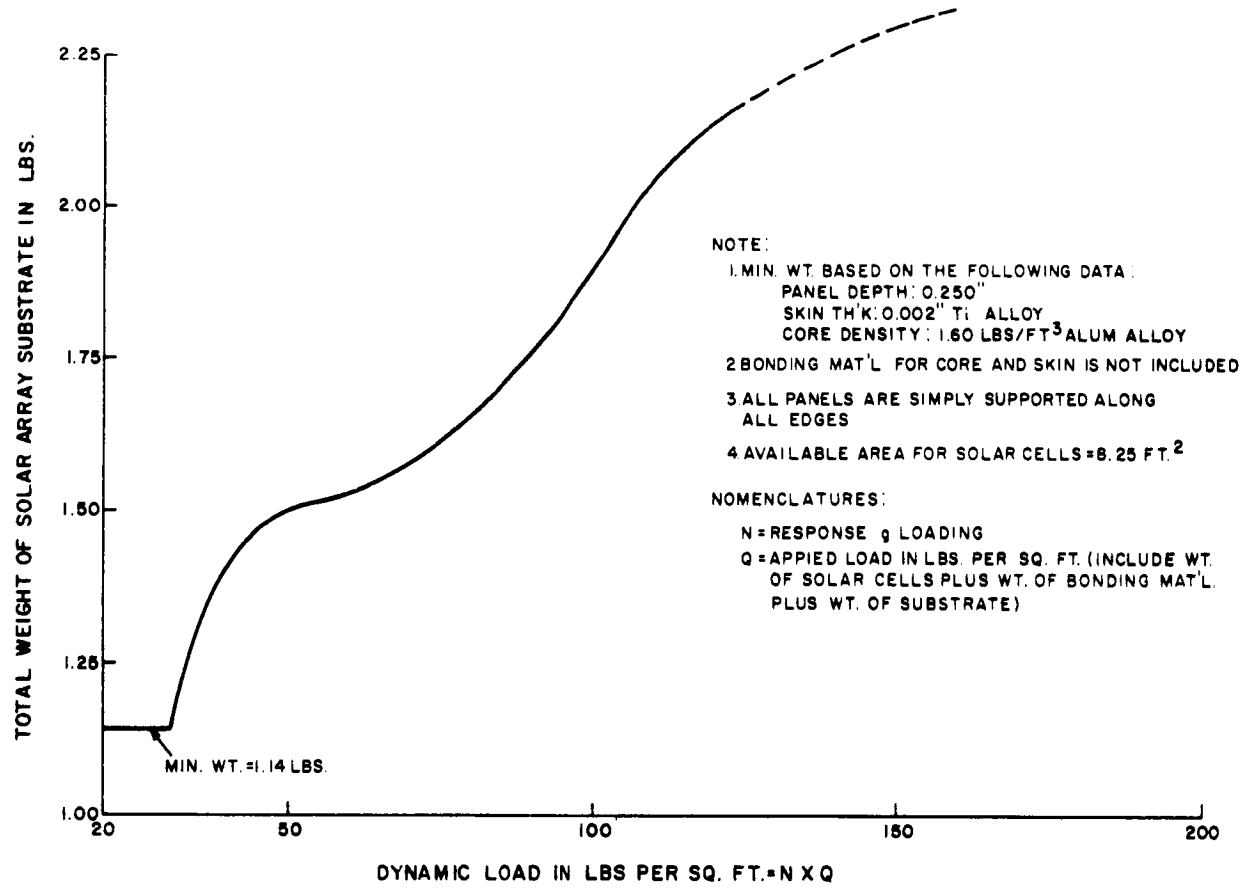

Figure II.3-4. SLRV-Solar Array Substrates Weight vs. Dynamic Load

$$q = \frac{7.80\ lbs}{*8.25\ ft^2} = .945\ lbs/ft^2$$

A dynamic response of 75 g's are assumed. A usual amplification factor of 10 is obtained in testing spacecraft with a longitudinal vibration of 10 g input. However, a number of panels are vertical or almost vertical. Thus, amplification for these panels would not be as large. Furthermore, the array can be fabricated as one assembly providing greater rigidity and reducing weight. Computations to determine the amplification factor require an analysis of the actual array, structural support, rear axle, etc. which is a function of the actual design. For the dynamic response of 75 g then, the dynamic loading $\eta q = .945 \times 75 = 71$. From the curve the total substrate weight = 1.60 lbs.

The center of gravity of the panel was computed based on this 75 g response loading (see Table II.3-11). The fundamental frequency of the largest panel (panel C) is approximately 400 cps.

* See Table II.3-1

TABLE II.3-11

CALCULATION OF C.G. BASED ON 75g RESPONSE

Panel	W	Z	Y	X	WZ	WY	WX
A	.317	9.25	12.37	0	2.93	3.92	0
B	.138	13.05	21.25	6.11	1.80	2.93	.845
C	.756	7.07	12.19	15.52	5.35	9.22	11.730
D	.059	15.86	7.00	5.36	.94	.413	.316
E	.046	13.00	5.00	6.14	.60	.230	.282
F	.081	10.41	1.53	6.35	.84	.124	.514
G	.092	19.00	12.50	4.50	1.75	1.150	.414
Σ	1.487				14.21	17.99	14.101

$$Z_c = \frac{\Sigma WZ}{\Sigma W} = \frac{14.21}{1.487} = 9.55$$

$$Y_c = \frac{\Sigma WY}{\Sigma W} = \frac{17.99}{1.487} = 12.05$$

$$X_c = \frac{\Sigma WX}{\Sigma W} = \frac{14.101}{1.487} = 9.50$$

Sample Calculation:

714 5 - 1x2 cm shingles @ 1.52 gm/shingle		2.40 lbs
6 mil glass, 0.3 gm/shingle		0.50 lb
Adhesives, diodes, wiring, RTV @ 1.40 gm/shingle (approximately)		2.20 lbs
	Total	5.10 lbs
Weight of substrate bonding material Bloomingdale (HT-424)		1.10 lbs
Assumed weight of substrate		1.60 lbs
	Total Weight	7.80 lbs

This calculation was based on the following conservative assumptions:

1. Response g loading is normal to the plane of every panel.
2. All panels are simply supported along all edges by a structural frame which transmits the panel load to the rear axle.
3. The solar array will be mounted in the stowage position to avoid impact between the array and the adjoining Surveyor structure.
4. Differential thermal expansion between panels and their supporting structures are assumed small.

4. Preliminary Testing of a Sample Panel

In order to determine the effect of temperature extremes on a Titanium faced aluminum core bonded sandwich, Ryan Aeronautical Co. conducted thermal cycling tests suggested by RCA. The procedure and results are outlined below.

The sandwich specimen consisted of .010 Ti-75 facings bonded with Bloomingdale Rubber Co. HT424 epoxy-phenolic adhesive to perforated Hexcel aluminum core of 1/4" hex and .004 3003 H18 foil of 7.9 #/ft^3 density. The facings were prepared for bonding by immersion in a solution of Bloomingdale's Prebond 700. The core was cleaned with aliphatic naptha. The sandwich was cured by gradually raising the temperature to 335° F. in 40 minutes and then holding at 335° F. for one hour under 50 psi pressure in a laboratory hydraulic press. The sandwich was cut into four 3" x 12" specimens.

In order to thermally cycle the specimen within the capabilities of the equipment available at Ryan, a departure was made from the requirements stated by RCA.* The stated requirement was that the sandwich withstand a thermal shock from -160°C to +40°C (-256°F to +104°F) in 15 minutes for 25 cycles. This is equivalent to the shock sustained by a plane array during sunrise.* The test was conducted by heating the specimen to +40°C in an oven and then completely immersing it in liquid argon at -185°C. (-302°F). Total cycle time was eight minutes. This was accomplished 25 times. It can be seen that the thermal shock to the panel was more severe than the stated requirements.

In order to determine the effect of the thermal cycling on the integrity of the sandwich, a flexure test was made on a specimen that was not thermally cycled, and the same test conducted on the specimen that was thermally cycled. The specimens were simply supported on a 10" span and the load applied at two quarter points. The specimens failed by a compression buckling of the skins between the load application points. The facing stress developed by the uncycled specimen was 111,000 psi and a shear stress

* Requirements determined from thermal analysis.

in the glue line between the reaction and load points of 427 psi. This test confirmed the fact that the thermal cycling had no adverse effect on the strength of the sandwich or on the adhesive.

The gage combinations and temperature cycling were not exactly as suggested, but since the tests were more rigorous than the requirements, the Titanium skin and aluminum honeycomb core approach is valid for consideration as solar panel substrate for the SLRV program.

G. SLRV SOLAR ARRAY THERMAL ANALYSIS

The solar array configurations investigated in the study were:

(1) A single hinged panel enabling sun orientation at all times during the lunar day;

(2) A single fixed panel at 0, 30, 45, 60 and 90 degree inclinations to the local horizontal;

(3) A fixed multi-panel array consisting of five panels joined in a polyhedral arrangement. (Fixed array).

All analyses below are based on an assumed Nimbus-type panel.

1. Theory and Equations

The following equations are written for a fixed array consisting of "n" panels. (Case 3, above).

The direct solar input (Q_S) to the panels is

$$Q_s = \alpha_n' A_{n_p} S$$

The lunar radiation (Q_M) absorbed by the panels is

$$Q_M = (0.81 \sin\theta + 0.015 \cos\theta)(\epsilon_n \psi_n + \epsilon_{n_i} \psi_{n_i}) A_n$$

The albedo input (Q_R) to the panels is

$$Q_R = 0.10\, S \sin\theta\, (\alpha_n \psi_n + \alpha_{n_i} \psi\, n_i)\, A_n$$

The temperature of each panel is calculated by solving simultaneously energy balances of the form:

$$\alpha_n' A_{n_p} S + .10\, S \sin\theta\, (\alpha_n \psi_n + \alpha_{n_i} \psi_{n_i})\, A_n$$

$$+ (.81 \sin\theta + .015 \cos\theta)(\epsilon_n \psi_n + \epsilon_{n_i} \psi_{n_i})\, A_n$$

$$+ \sum^{N} R_{n-N}\, \sigma\, T_N^4 = (\epsilon_n + \epsilon_{n_i})\, A_n\, \sigma\, T_n^4$$

where

a'_n = the effective solar absorptivity of the external surface of the nth panel.

NOTE:

$$a_n = p\,a_c + (1-p)\,a_R$$

$$a'_n = a_n - p\,\eta$$

$$\epsilon_n = p\,\epsilon_c + (1-p)\,\epsilon_R$$

a'_{n_i} = the solar absorptivity of the internal surface of the nth panel.

$\epsilon_n, \epsilon_{n_i}$ = the effective emissivity of the external and internal surfaces of the nth panel, respectively.

ψ_n, ψ_{n_i} = the fractions of energy that leave the external and internal surfaces of the nth panel, respectively, and fall upon the moon.

A_{n_p} = the projected area of the nth panel, to the sun, in square inches.

A_n = the area of one side of the nth panel, in square inches.

θ = the elevation angle, or, the angle that the sun vector makes with the local horizontal.

S = solar constant = 0.9 watt/in^2

R_{n-N} = radiative coupling factor between body n and each of the N bodies to which it is coupled, in square inches.

T_n, T_N = the temperatures of bodies n and N respectively, in °K.

σ = Stefan-Boltzmann constant.

p = packing factor

η = solar cell efficiency

The transient response of the panels can be calculated by solving equations of the form:

$$mc\,\frac{dT_n}{dt} = Q_s + Q_M + Q_R - (\epsilon_n + \epsilon_{n_i})\,A_n\,\sigma\,T_n^4 + \sum^{N} R_{n-N}\,\sigma\,T_N^4$$

where:

mc = the thermal mass of the solar-cell panels, in watt-sec per degree K.

For the simpler array configurations in which the array consists of single flat panels (as in Cases 1 and 2, above), the energy balance is the same except that there are no terms which represent the heat transfer between panels ($\sum^{N} R_{n-N} \sigma T_N^4$). Therefore, for a simple flat array, it is not necessary to solve simultaneous equations to calculate the temperature of the array.

2. Parameters Used in the Analyses

The following properties of the solar-cell panels and lunar surface were assumed in the analyses:

Single Panel Array (Cases 1 and 2)

Cell Side

$\alpha_c = 0.76$
$\epsilon_c = 0.85$
} Nimbus type cells with blue-red filters.

Back Side

$\alpha_i = 0.2$

$\epsilon_i = 0.85$

$p = 1.0$

$\eta = 0$

Multi-Panel Array (Case 3)

Cell Side

$\alpha_c = 0.76$
$\epsilon_c = 0.85$
} Nimbus type cells with blue-red filters.

$\alpha_R = 0.2$
$\epsilon_R = 0.86$
} Rokide A

Back Side

$$\alpha_{n_i} = 0.2$$

$$\epsilon_{n_i} = 0.90$$

$$p = 0.80$$

$$\eta = 0.06$$

Lunar Surface

emissivity = 0.9

absorptivity = 0.9

albedo = 0.1

3. Analysis of the Single Panel Array

The single panel configurations were investigated for the cases in which the back of the panels were (1) insulated and, (2) uninsulated. It was assumed that the panels were oriented in azimuth at all times. This is a reasonable design condition while the vehicle is parked for battery recharge. (Orientable Array*)

The analysis showed that insulation on the panel backs causes excessive temperature excursions; therefore, it is recommended that the back surfaces of the solar array not be insulated. The results which follow are all based on the panels being uninsulated.

The results are given in Figure II.3-5. This figure presents the ratio of projected area to the sun vector to total area versus angle from the subsolar point (β) for various panel orientations (ϕ). The solar cell panel temperature for each condition is also given. The line $\phi = \beta$ represents the hinged panel positioned for maximum power.

The direct solar input (Q_S) to the panels is given by:

$$Q_s = \alpha_n' A \cos(\beta - \phi) S$$

where: $\beta = 90 - \theta$

*See Paragraph D.

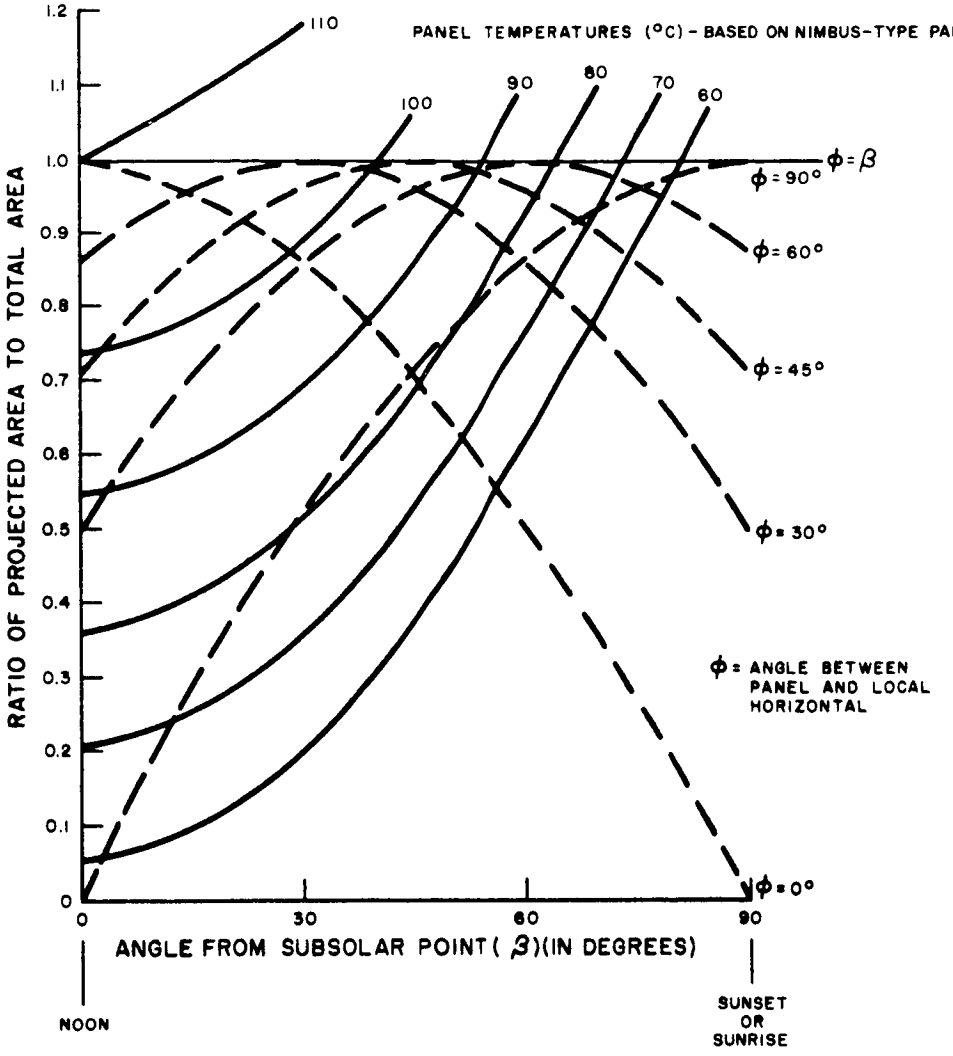

Figure II.3-5. Temperatures for Various Ratios of Projected Area of Solar Panels Normal to the Sun Vector to Total Area versus Angle from the Subsolar Point for Various Panel Orientations

The other inputs to the panels are as previously defined.

In the case where the panels are always sun-oriented ($\phi = \beta$), the direct solar input is

$$Q_s = \alpha_n' \, A \, S$$

Temperatures for the uninsulated hinged single solar-cell panel were also determined for three lunar-surface configurations. This was done to determine the effect of operation in a valley. The configurations considered were:

Infinite flat plane;

Flat plane connected to a 15-degree inclined plane, both extending to infinity; and

Two 15-degree inclined planes both extending to infinity.

Figure II.3-6 shows the panel temperature versus angle from the subsolar point. These results indicate that the maximum temperature occurs for the two inclined plane conditions. The maximum temperature is approximately 116°C at an angle of 35 degrees from the subsolar point. This maximum is only 5°C above the flat plane maximum temperature of 111°C. The major effects of the lunar surface geometry are to shift the point of maximum temperature and to shorten the lunar day by shadowing the vehicle.

In addition to the steady-state panel temperature during the lunar day and night, the transient response at sunrise and sunset was determined. The effect of the vehicle was neglected. The temperature response versus time from sunset or sunrise is shown in Figure II.3-7. Since the vehicle has a time constant larger than the panel, the effect of the vehicle will be to reduce the slope of the temperature-time profile. The results in Figure II.3-7 are, therefore, conservative estimates.

During the lunar night, the unprotected solar-cell panel will reach a minimum temperature of minus 152°C. Methods of raising this temperature have been examined. The most practical approach would be to cover the panel with an insulating shutter during the lunar night. With only a shutter, the panel temperature can be raised to minus 125°C. With the addition of a 10-watt heat source in the shutter (i.e., radioactive pellet), the temperature can be increased to minus 75°C.

However test results appear to indicate that the panel should be able to survive the temperature range encountered with minimum degradation.

Analysis of the Fixed Array (Polyhedral

The fixed array considered in the study is shown in Figure II.3-8. The array was made symmetrical to simplify the analysis for this phase, (i.e. the cutout was neglected).

(1) The panels were assumed to be coupled radiatively only. Conduction transfer between the panels was neglected. In a real array, the temperature differences between panels would be less than those calculated due to conductive paths.

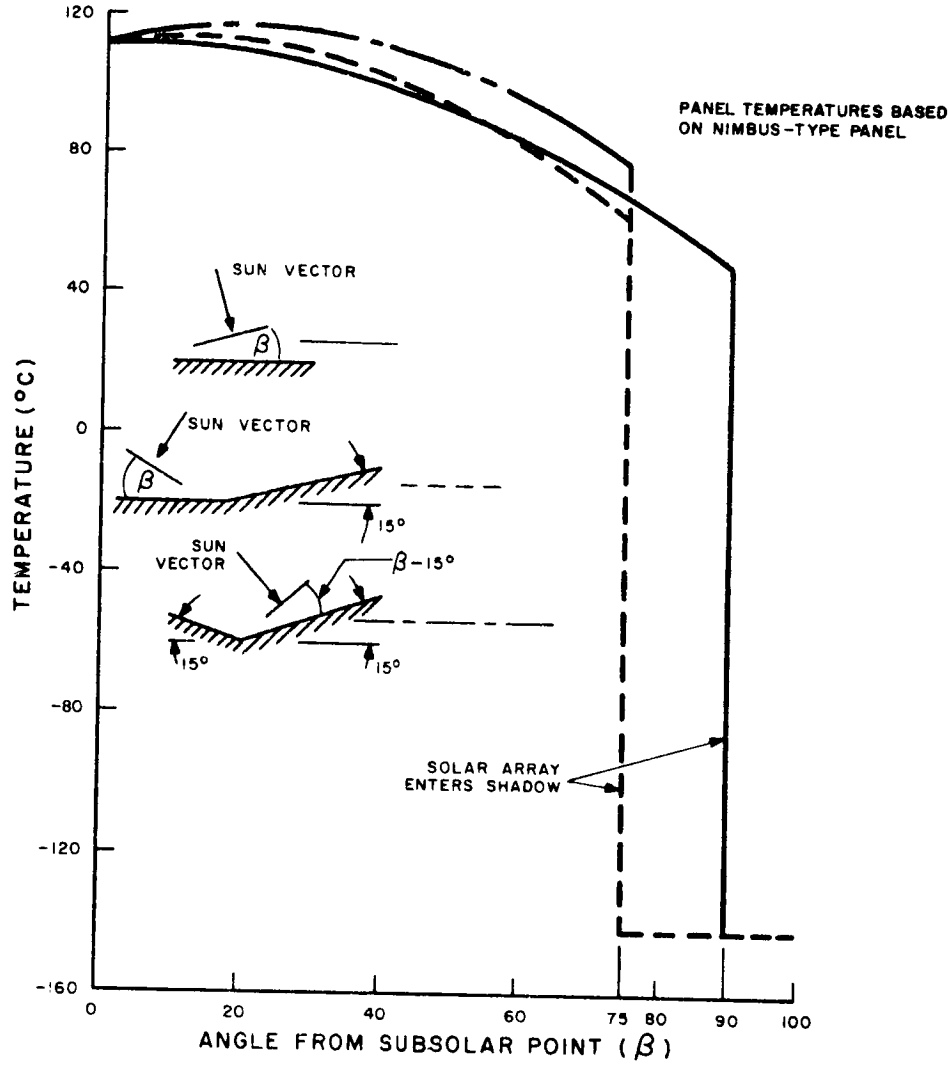

Figure II.3-6. Temperature of Solar Panels versus Angle from the Subsolar Point for three Lunar Surface Configurations

(2) Heat transfer between the array and the remainder of the vehicle was not considered. If this were considered, the array would run at lower temperatures than those predicted at high elevation angles and higher temperatures than those predicted at low elevation angles. The temperature of each of the array panels was calculated for azimuth angles of 0, 30, 60, 90, 120, 150 and 180° at elevation angles of 0, 30, 60 and 90°. It was not necessary to go beyond 180° azimuth as the array is symmetrical beyond this angle.

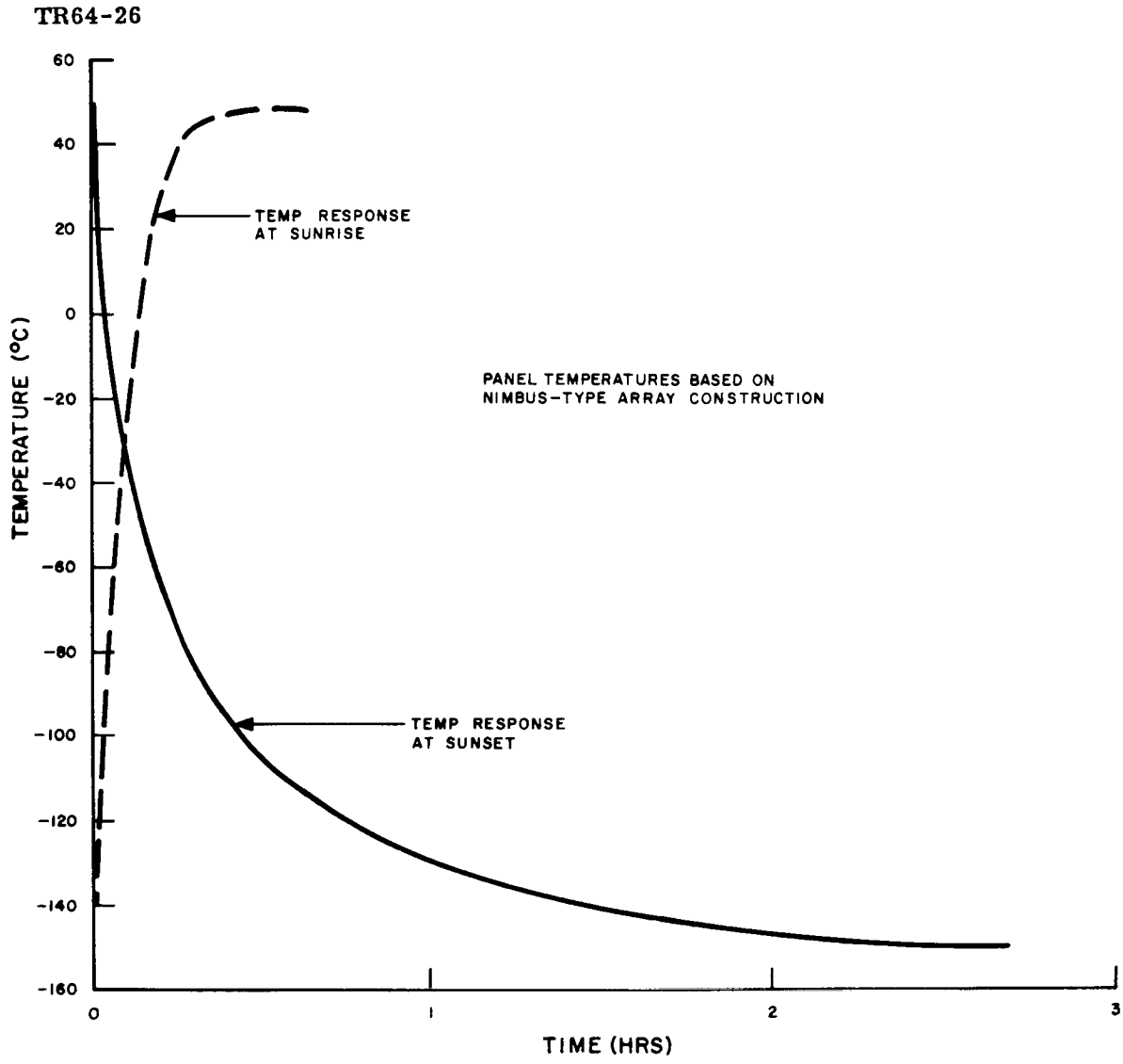

Figure II.3-7. Temperature Response of Solar Panels at Sunrise and Sunset

Figures II.3-9 thru II.3-12 show the panel temperatures versus azimuth angle for the constant elevation angles of 0, 30, 60 and 90°. Figures II.3-13 thru II.3-17 show temperatures of each panel versus azimuth angle for varying elevation angles. It is seen that the maximum temperature reached by any panel in any orientation is 100°C (Panels C and EG). Considering all orientations, all of the panels will at one time be at a temperature between 90-100°C. Panel C reaches a maximum temperature at an elevation angle close to 60° (more calculations for additional elevation angles are necessary to determine the exact elevation angle at which the temperature peaks). Although the sun is not normal to Panel C at this elevation angle, the combination of lunar inputs and direct solar input are close to a maximum at that point. The average temperature of the array at night will be approximately -152°C.

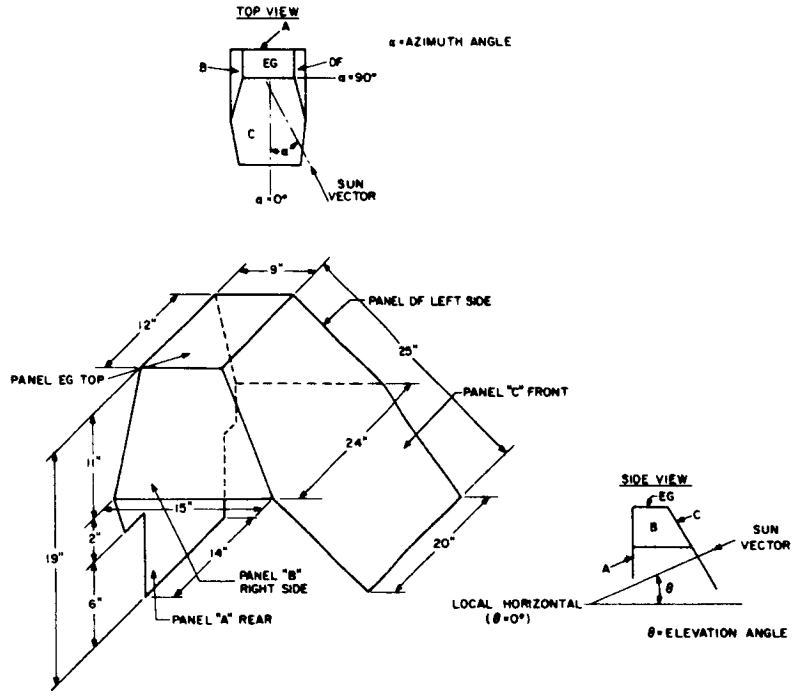

Figure II.3-8. SLRV Fixed Panel Solar Array Configuration

TR64-26

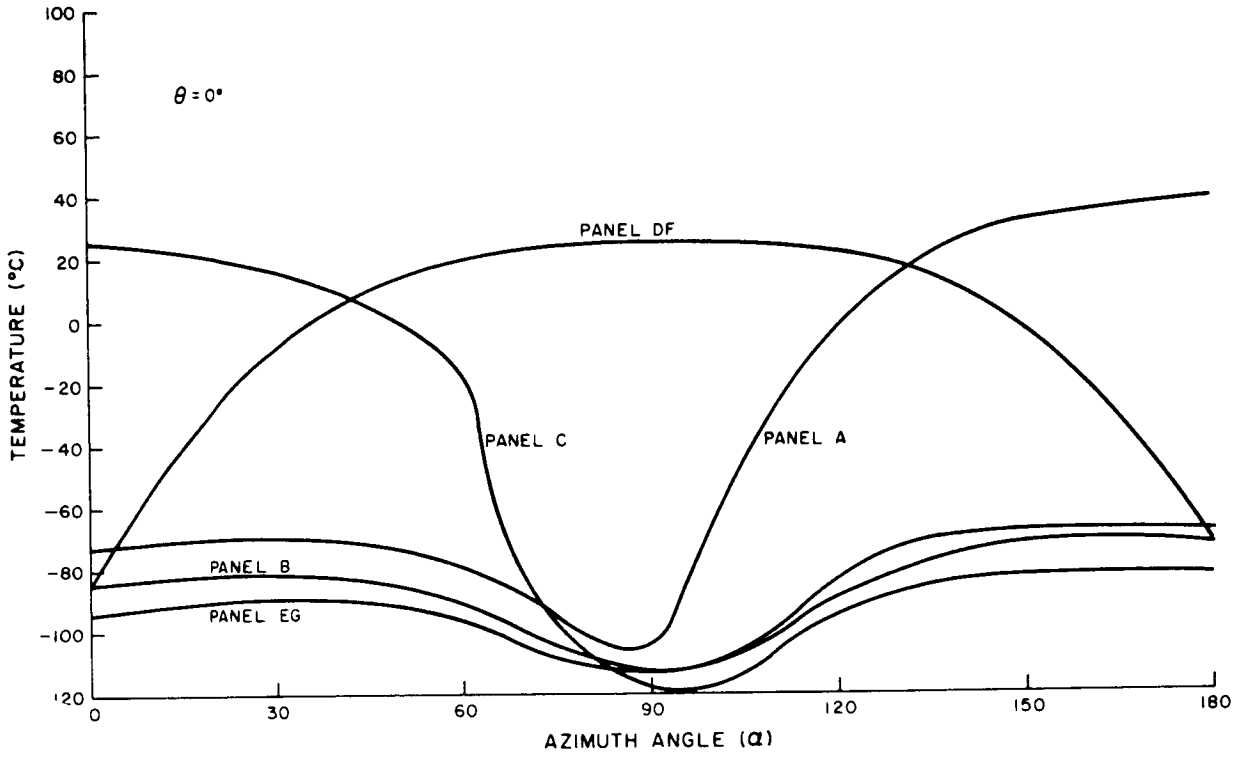

Figure II.3-9. SLRV Panel Temperature vs. Azimuth Angle for an Elevation Angle (θ) of 0° (Fixed Array)

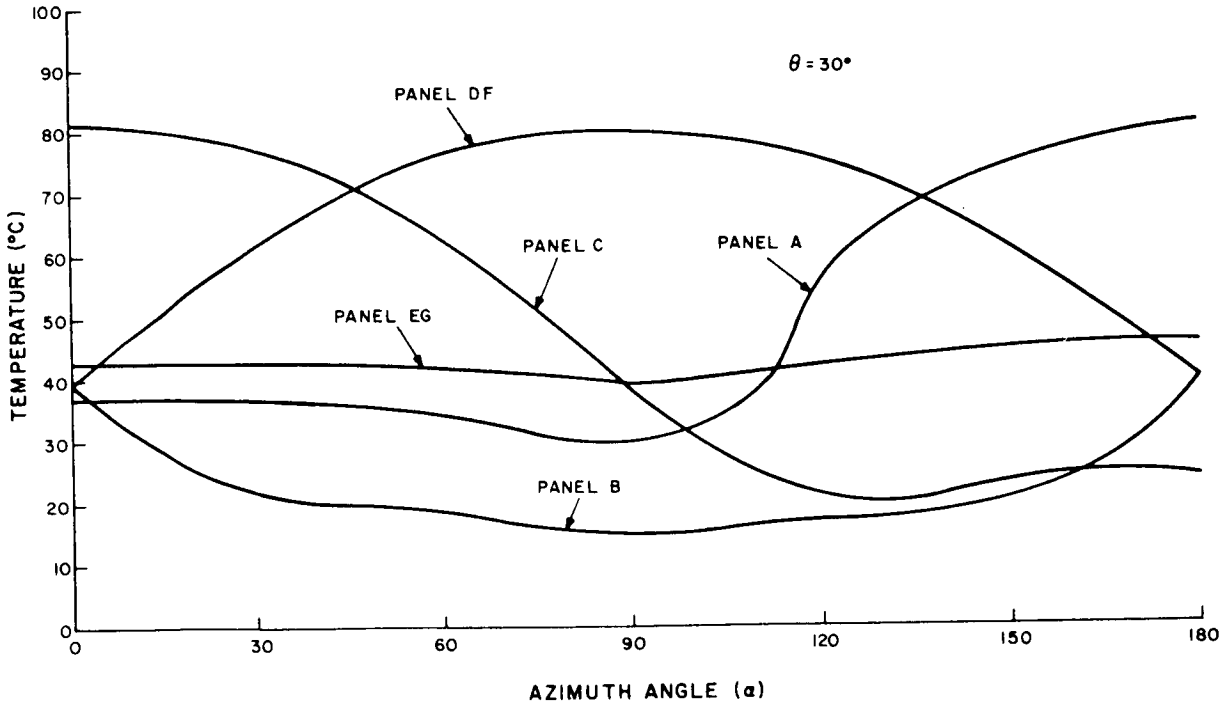

Figure II.3-10. SLRV Solar Panel Temperature vs. Azimuth Angle for an Elevation Angle (θ) of 30° (Fixed Array)

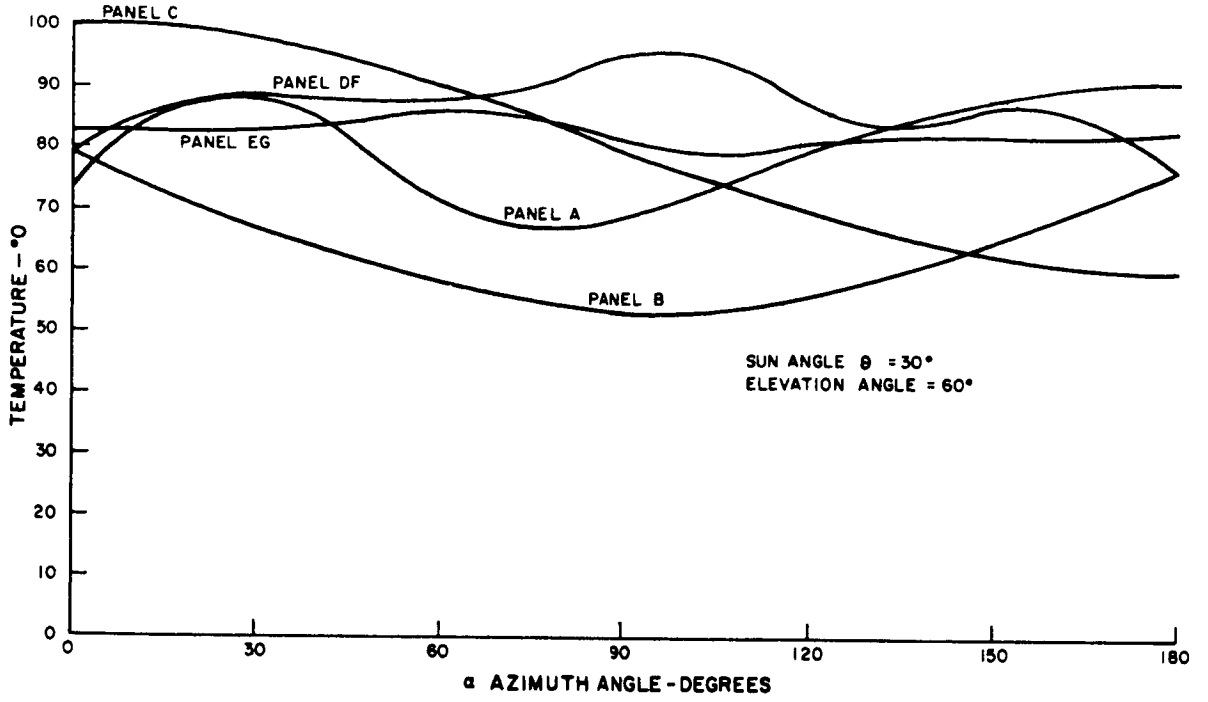

Figure II.3-11. SLRV Solar Panel Temperature vs. Azimuth Angle

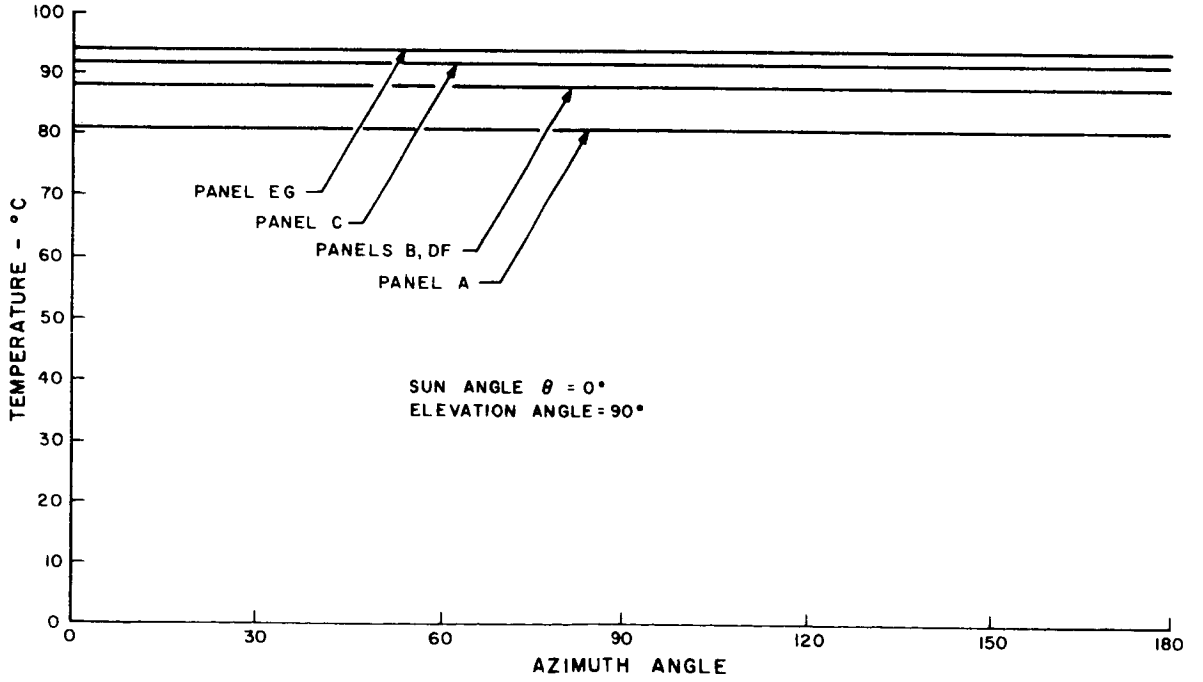

Figure II.3-12. SLRV Solar Panel Temperature vs. Azimuth Angle

TR64-26

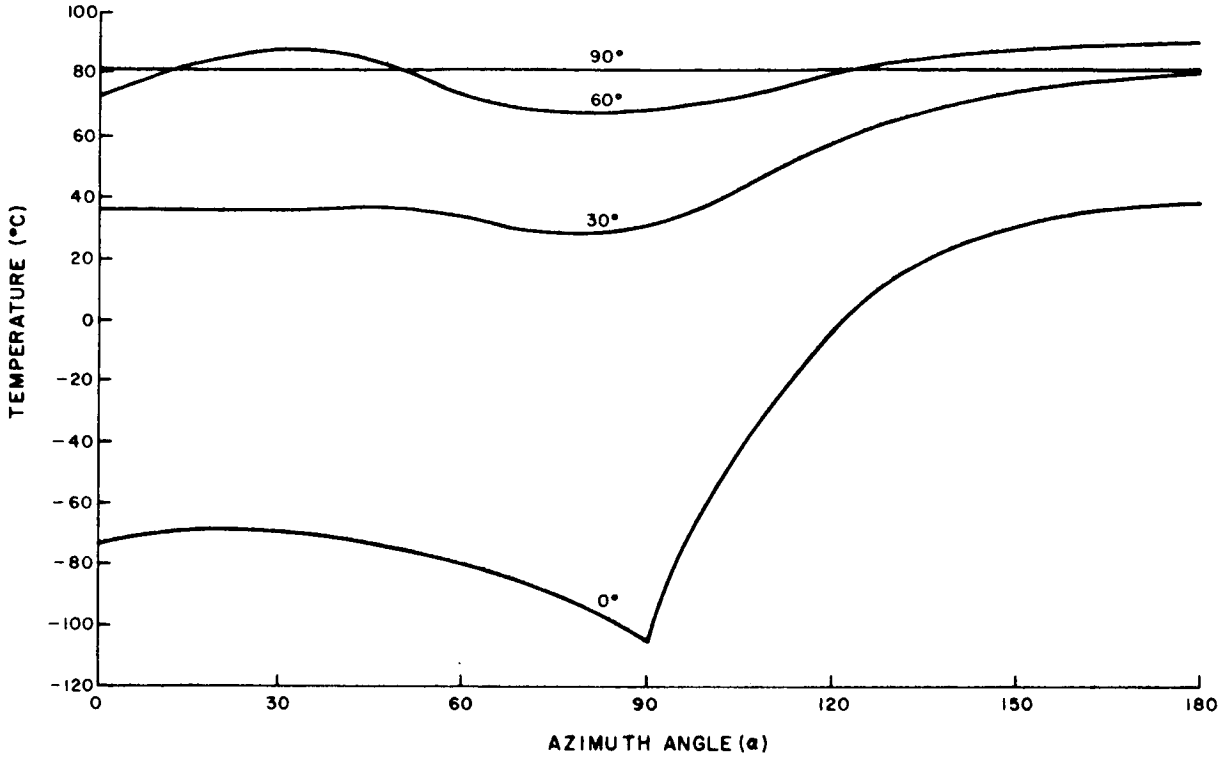

Figure II.3-13. Panel "A" Temperature vs. Azimuth Angle for Various Elevation Angles (Fixed Array)

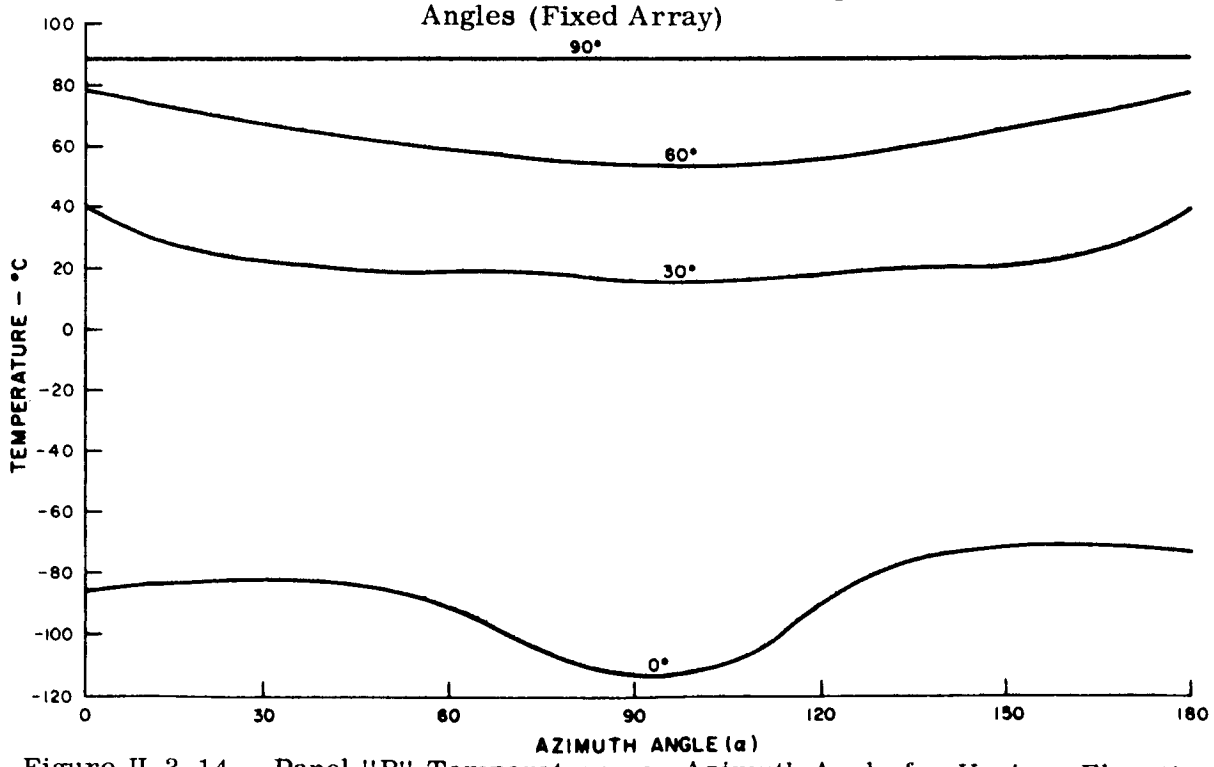

Figure II.3-14. Panel "B" Temperature vs. Azimuth Angle for Various Elevation Angles (Fixed Array)

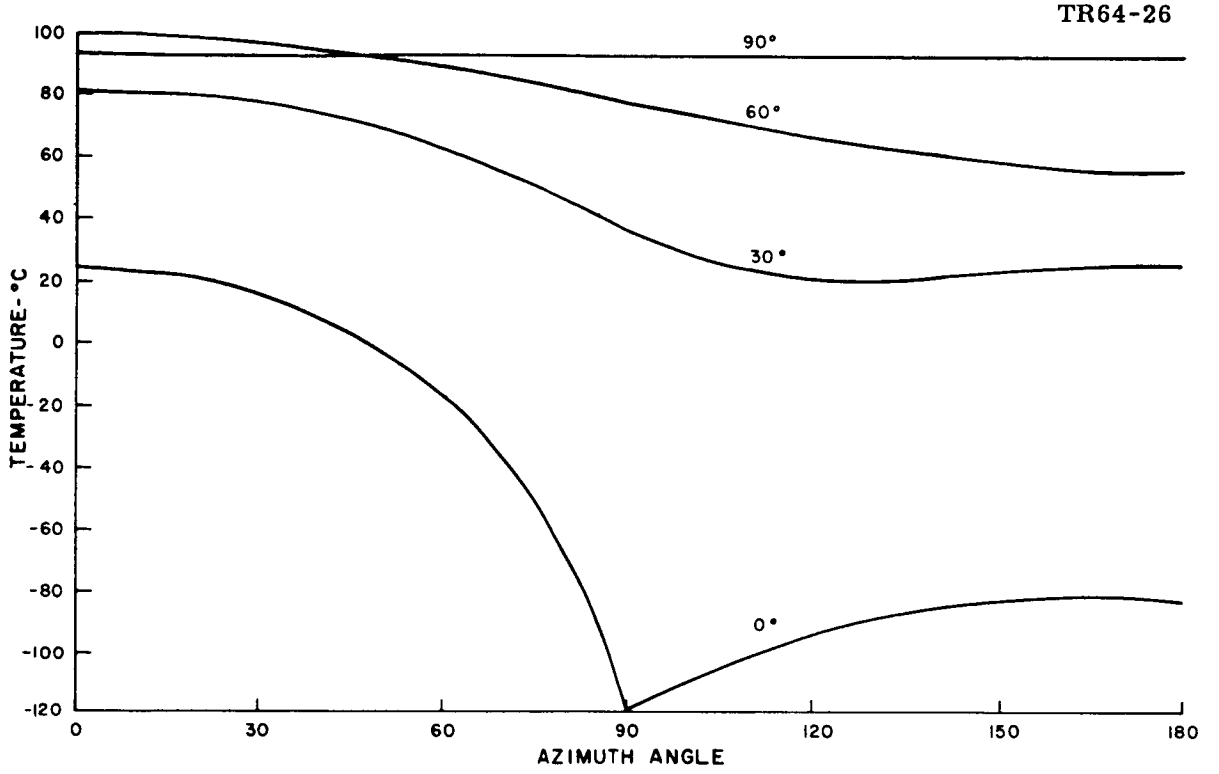

Figure II.3-15. Panel "C" Temperature vs. Azimuth Angle for Various Elevation Angles (Fixed Array)

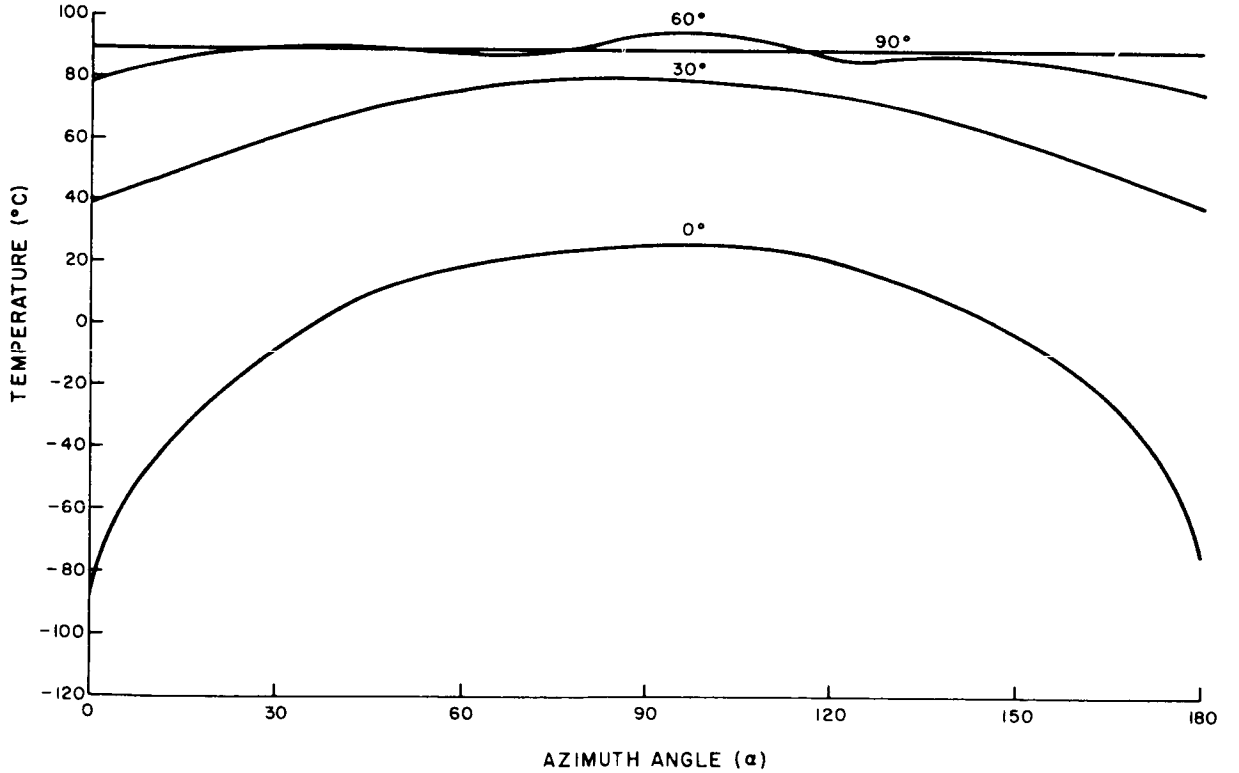

Figure II.3-16. Panel "DF" Temperature vs. Azimuth Angle for Various Elevation Angles (Fixed Array)

TR64-26

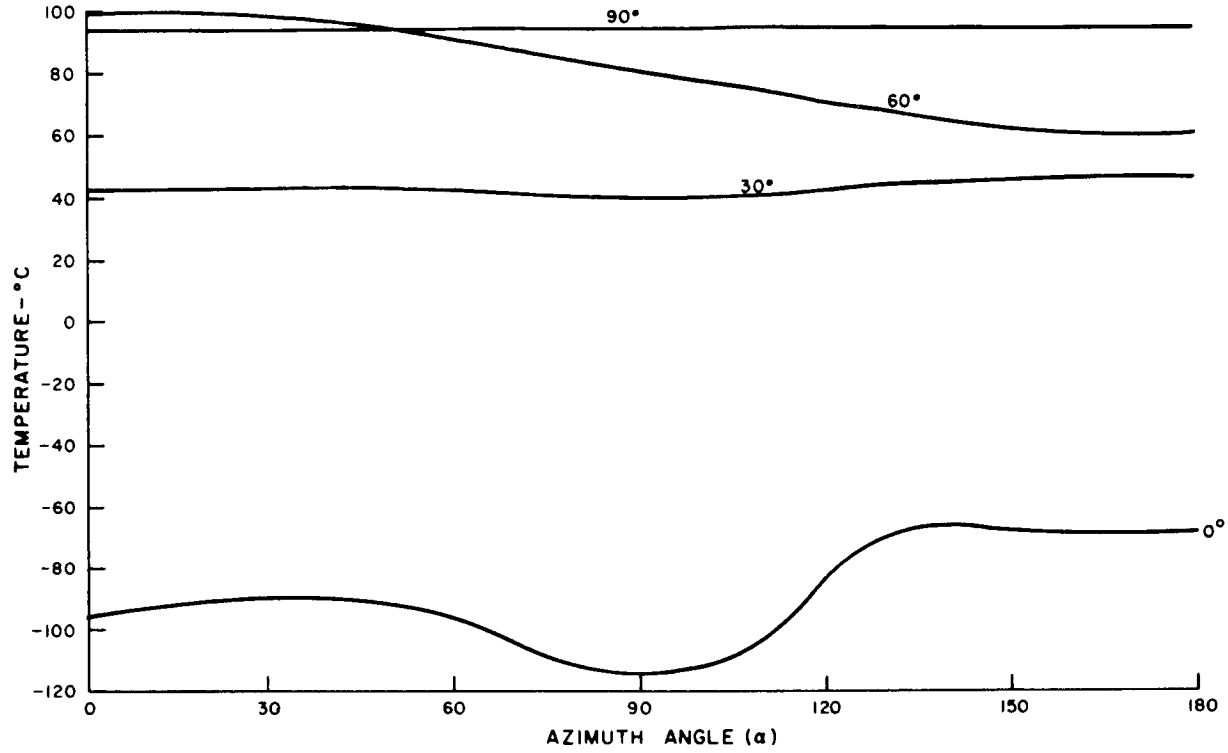

Figure II.3-17. Panel "EG" Temperature vs. Azimuth Angle for Various Elevation Angles (Fixed Array)

It should be noted that the azimuth angle will be a function of the vehicle path in relation to the sun line. The plots generated assumed travel in one direction. The effect of varying the azimuth angle would tend to average out fluctuations for each of the panel curves.

The Phase II Thermal Effort

The Phase II effort will include an analysis which accounts for conductive as well as radiative coupling between the solar panels. Heat transfer between the array and the vehicle will be included as the vehicle configuration firms up. The transient response of the array as it moves in azimuth will be investigated. A program of measurements of the solar absorptivities and infrared emissivities of all finishes used on the array surfaces will be performed. Further attention will be given to the effect of a lunar slope or valley on the thermal response of the array. A model of the array will be constructed and tested in order to verify the thermal design.

H. BATTERIES

1. Battery Requirements

Basically, three conditions affect the electrical size of the battery in the SLRV power subsystem:

(a) Minimum acceptable time to operate per cycle. It is assumed that the total current drain in operate (I_o) is constant and independent of the operate time per cycle, and that the average array current during operate (i_s) is variable. Then from Figure II.3-18 the greatest average battery discharge current (which is equal to the difference current $I_o - i_s$) will occur when i_s is the smallest. Given a battery capacity C ampere-hours and a maximum depth of discharge of 50%, the minimum per-cycle operate time is

$$\Delta t_{o\ min.} = \frac{0.5\ C}{(I_o - i_{s\ min.})} \qquad \text{(II.3-1)}$$

(b) Relative recharge capability. Figure II.3-18 contains a plot of the battery recharge current I_{ch}, defined as $I_s - I_c$. Since I_c is constant, I_{ch} is maximum when I_s is maximum. Hours maximum recharge rate is thus

$$Hours\ chge\ rate = \frac{C}{I_{ch_{max}}} \qquad \text{(II.3-2)}$$

(c) Total anticipated cycle life. A modification of eq. (II.3-1) yields the following relationship:

$$\Delta t_{o_{ave}} = \frac{0.5\ C}{(1.48 - i_{s_{ave}})} \qquad \text{(II.3-3)}$$

The average array current $i_{s_{ave}}$ in the operate mode over the elevation angle range, is judged to be approximately 0.6 amperes Figure II.3-18. Thus it can be said that, on the average, the per-cycle operate time is determined by the battery capacity C and the selected maximum depth of discharge of 50% in eq. II.3-3.

The minimum total operate time on the moon is approximately 100 hours. Thus, division of II.3-3 into 100 will yield the total no. operate cycles. It will be assumed, that, in addition to the moon-operate cycles, fifteen ground test cycles will be required. The total required cycle life "f" is thus.

$$f = 15 + \frac{200\ (I_o - i_{s_{ave}})}{C} \qquad \text{(II.3-4)}$$

Figure II.3-18 is a plot of the relationships of eq. II.3-1, 3-2 and 3-3.

It is clear that, for any reasonable battery capacity, the cycle life is marginal at best in regard to Silver-Zinc batteries. The latter type batteries are light weight, but are not intended primarily for cycling. Little if any reliable data exists at this time to justify recommendation of a silver-zinc battery for a cycle life of the order of magnitude in question. State-of-the-art knowledge points to the fact that such batteries, if built reliably to withstand a relatively large number of cycles, would no longer possess an inherent weight advantage over Silver-Cadmium (AgCd) batteries. The latter are known to have undergone successful tests for hundreds of cycles. Results of an investigation made to determine the applicability of either type battery to this mission are given in paragraph 2, below.

Best present-day estimate of the specific energy (whrs per pound) of the AgCd type batteries is plotted in Figure II.3-18. Since the plot is intended to show realistic package weights, it is clear that batteries consisting of physically smaller cells have lower specific energies. The total battery weight plotted is based on the estimated specific energy and a total on-board watt-hours capacity defined by C on the abscissa and an average discharge voltage of 26 volts.

Figure II.3-18 shows that by decreasing capacity, C, the minimum per-cycle operate time decreases and the total required cycle life increases. The weight of the battery also decreases with increasing C, but the relative charge rate is increased as the weight is lowered.

It can be stated that an acceptable lower limit on the operate time duration is about one hour. Then the required battery capacity, C, is 2 ahrs, with a battery weight of 3.7 lbs, a cycle life required of roughly 100 cycles, and a relative recharge rate of C/2. Within the limits of feasibility, therefore, the recommended battery for the SLRV mission is a 2 Ahr, Ag-Cd battery, weighing 3.7 pounds. It will consist of 24 series-connected cells to meet system requirements.

2. Comparison of Ag–Cd and Ag–Zn Sealed Batteries as Applicable to the SLRV Mission

In comparing the Ag-Cd and Ag-Zn sealed battery systems, importance was placed on both the relative reliabilities of the two systems and the energy to weight ratios. The energy to weight ratio information was determined from several inquiries placed with the following firms: The Electro-Storage Battery Company (Missile Battery Division), Yardney Corporation, Gulton Industries, and Eagle Picher. Although data released by these companies vary to an extent, the watt-hours per pound ratio for a packaged silver zinc system is approximately 28 watt-hours per pound for the electrical size in question, and in the case of the silver cadmium system, it is approximately 15 watt hours per pound. The relative reliability has been determined on a basis of 25% depth of discharge for silver zinc batteries, and a 50% discharge depth for Ag-Cd to obtain a valid comparison.

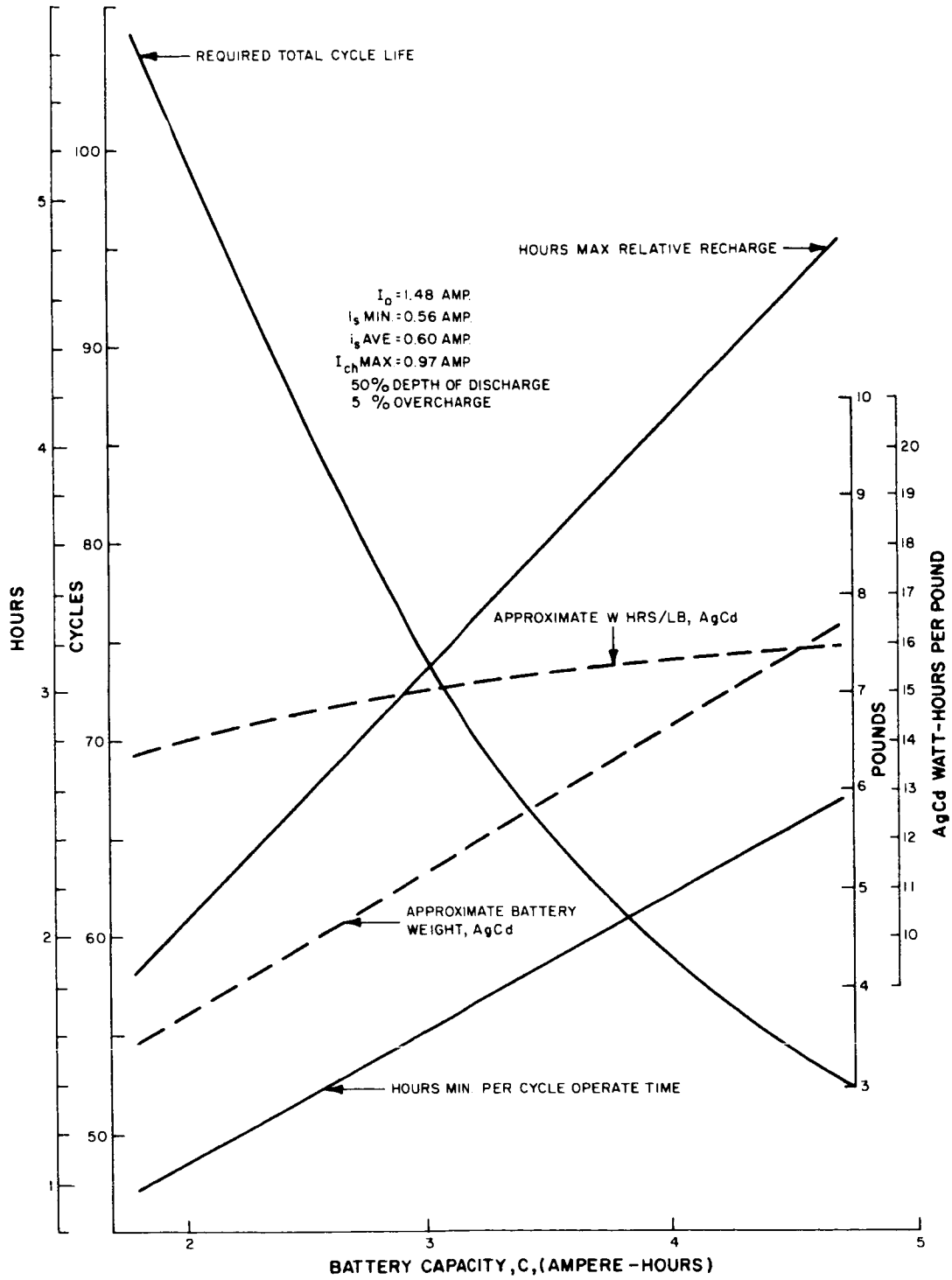

Figure II.3-18. Battery Requirements

TR64-26

The only known information available in data form suitable for comparing both systems is from the work done by The Inland Test Laboratories, Cook Electric Company, Dayton, Ohio, on an Air Force Project No. 8173, Task No. 817304 and found in the technical documentary report No. ASD-TDR-63-394, April, 1963, entitled "Alkaline Battery Evaluation". Under this contract, the Inland Test Laboratories cycled both sealed silver zinc and sealed silver cadmium batteries composed of an eight-cell series string under a two hour orbit condition in which the batteries were discharged for 35 minutes at various discharge depths and temperatures.

An analysis of data for the battery types, based upon the 2-hour orbit data, yields the following:

Ag-Zn at 25% Depth of Discharge

Mean Cycles to failure	(μ)	=	232
Variance	(σ^2)	=	14,400
Standard Deviation	(σ)	=	120

Ag-Cd at 50% Depth of Discharge

μ	=	600
σ^2	=	43,600
σ	=	208

The 2-hour orbit reflects a 35 minute discharge interval followed by an 85 minute charge interval. From the values of μ and σ for the two battery types, assuming the mean cycles to failure is normally distributed, the following probabilities have been generated for each eight-cell series string.

Probability of Survival for a 50-cycle mission:

Ag-Zn = 0.9356

Ag-Cd = 0.9958

Probability of Survival for a 100-cycle mission:

Ag-Zn = 0.8643

Ag-Cd = 0.9918

It was indicated earlier in this discussion that a battery composed of 24 series-connected silver cadmium cells is recommended. This is equivalent to three eight-cell series strings; a silver zinc battery would require two eight-cell series strings to supply the approximately equivalent voltage. The probabilities of survival of the two types of series strings are now compared.

The probability of picking one faining Ag-Zn series string from the lot of those in the 50-cycle mission equals (1-0.9356) or 0.0644. Assuming a lot of sufficient quantity, the probability of selecting another failing string also equals 0.0644. Thus, there is a 2 x 6.44% or 12.88% of choosing an Ag-Zn two-battery string not capable of lasting 50 cycles. This gives a probability of survival of 0.8712. For the Ag-Cd series string, the probability for failure in less than 50 cycles is substantially 3 (1-0.9958) or 1.26%. Thus, the probability for survival is 0.9874. The same analysis applies for the 100-cycle mission. The results are tabulated below.

Probability of Survival for a 50-cycle mission:

Ag-Zn = 0.8712

Ag-Cd = 0.9874

Probability of Survival for a 100-cycle mission:

Ag-Zn = 0.7286

Ag-Cd = 0.9754

It is apparent from the data given that the Ag-Cd battery has a significantly higher survival probability than can be expected from the Ag-Zn battery. Also, it might be well to state at this point that the Ag-Cd data is pessimistic in that the μ and σ values were computed from batteries still operating with the actual testing not completed. On the other hand, the Ag-Zn data is based strictly upon cycles to failure.

Figures II.3-19 and II.3-20 represent a graphical presentation of the battery data for the two types.

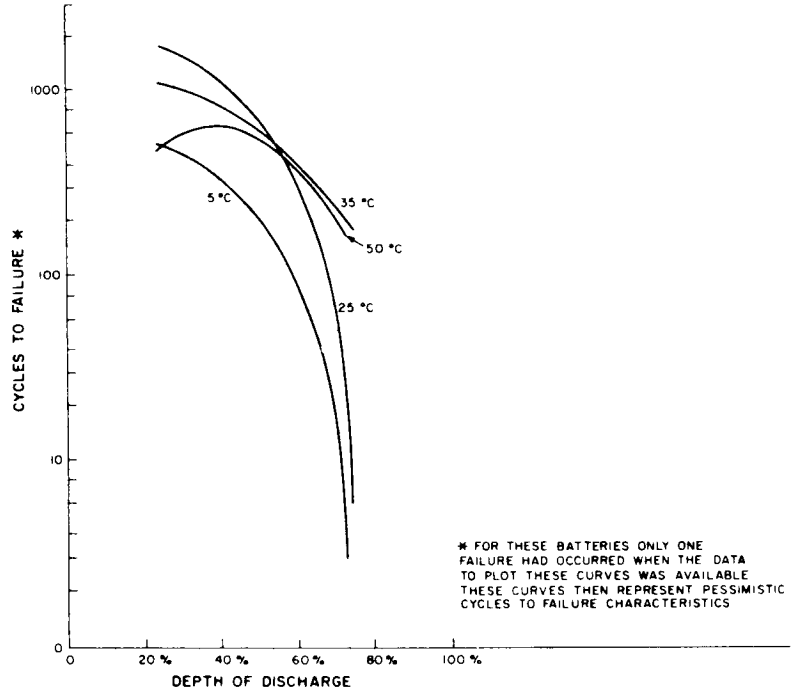

Figure II.3-19. Data for Ag-Cd Batteries (8-cell packs)

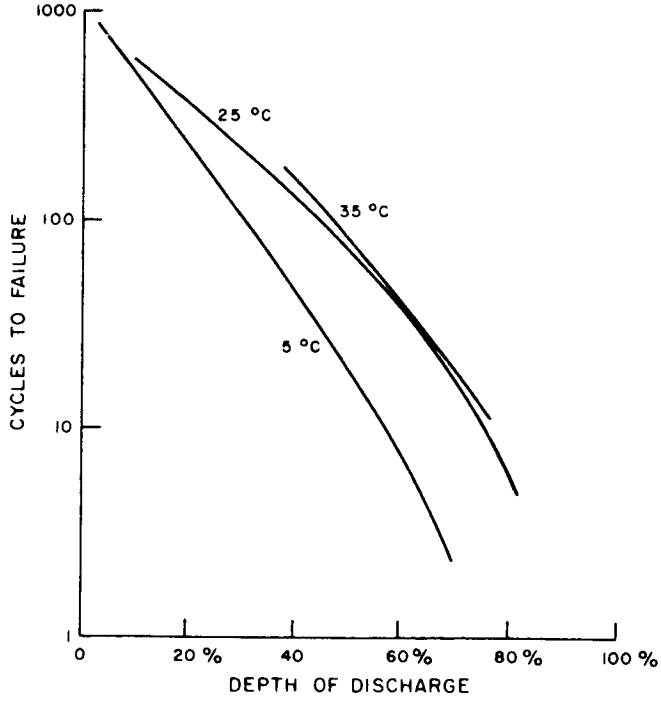

Figure II.3-20. Data for Ag-Zn Batteries (8-cell packs)

J. SOLAR CELL SHINGLE POWER CALCULATIONS

For a solar shingle which is made up of five 1 x 2 cm cells in series, I-V curves were made and are shown in Figure II.3-21. The I-V characteristics were obtained by extending known curves and data for a 9% shingle to the required 10.5% shingle.* The variation of I-V characteristics with temperature was made with 25°C characteristics as the base. The high temperature cut-off (110°C) was based upon the thermal analysis for an orientable array.

For an efficiency of 10.5% based on Air-mass zero and 25°C the maximum power output is as follows:

$$P_{o_{max}} = N \times A \times P_s \times \eta$$

where

N = number of cells

A = active area of each cell, 1.8 cm²

P_S = solar constant at air mass zero, 140 mw/cm²

η = cell efficiency at air mass zero and 25°C, 10.5%

$P_{o_{max}}$ = power output of shingle at air mass zero & 25°C, mw

$P_{o_{max}} = 5 \times 1.8 \times 140 \times .105 = 132.2$ mw/shingle

The available power per shingle was found as a function of temperature (see Figure II.3-22 for various shingle voltages.

1. Optimum Shingle Voltage

The energy delivered per shingle at a fixed shingle voltage was found by summing power per shingle over the temperature-time profile (See Figure II.3-23.) This is equivalent to:

$$W = \int_o^t P(t)\, dt$$

which is the total energy output per shingle per lunar day (See Figure II.3-24.) The peak in the energy-vs-operating voltage in the optimum voltage point. It should be noted that the power output curve is fairly flat over a relatively wide voltage range.

*See paragraph E.3.

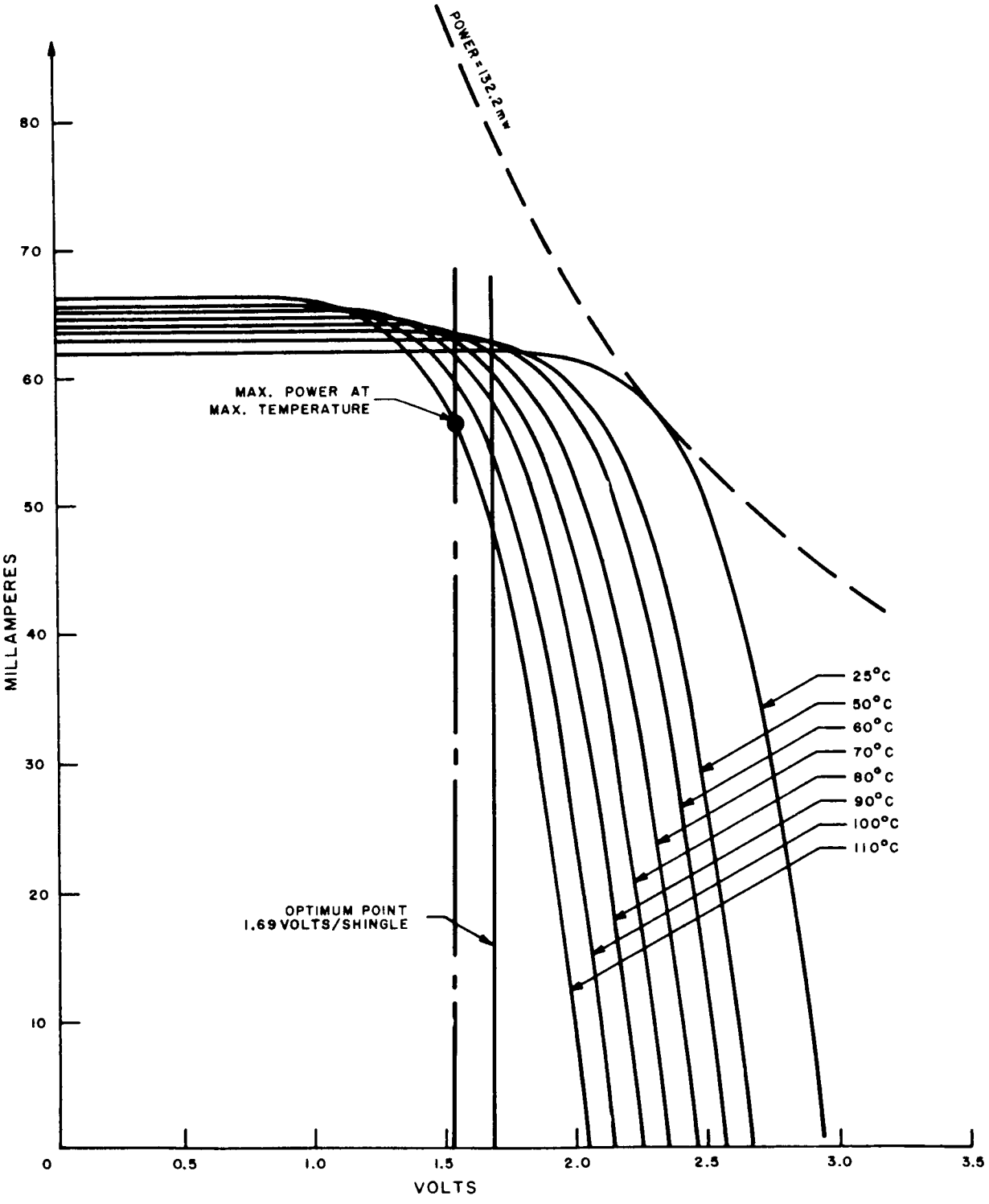

Figure II.3-21. Solar Shingle I-V Characteristics

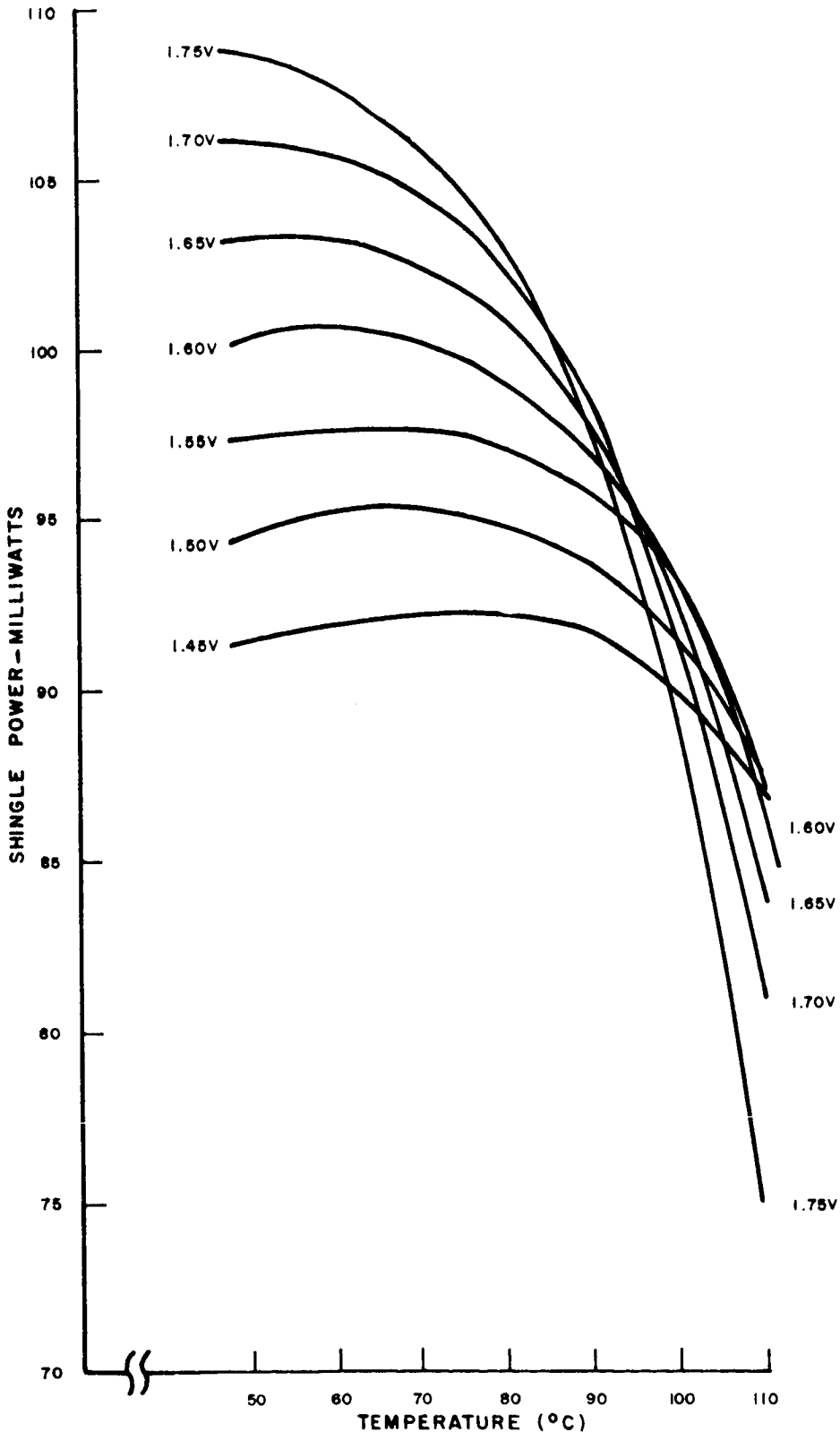

Figure II.3-22. Shingle Power Output as a Function of Temperature

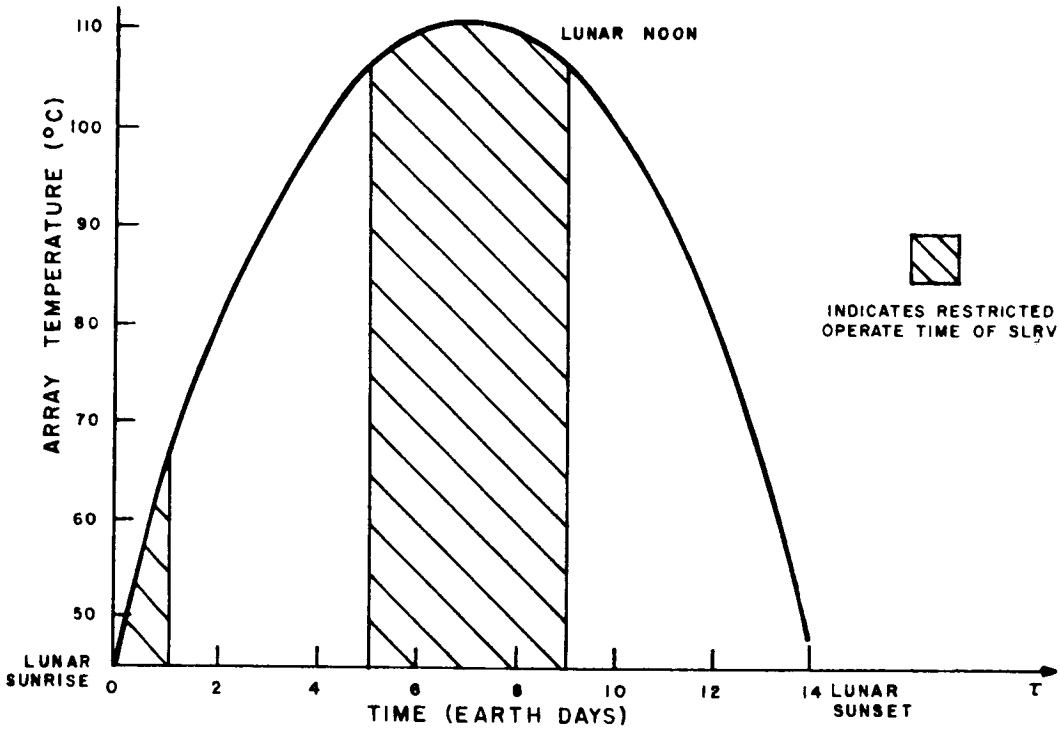

Figure II.3-23. SLRV Solar-Cell Shingle Temperature-Time Profile

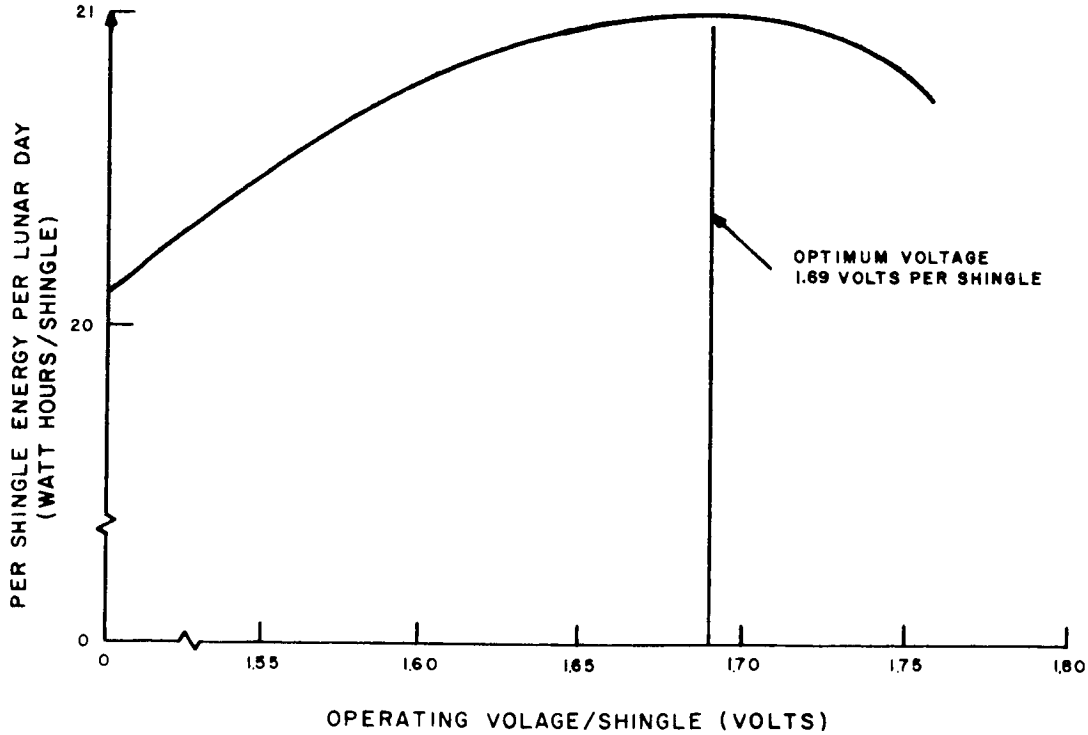

Figure II.3-24. Energy Per Shingle for Temperature and Operation as in Figure III.9-3.

The optimum operating point was found to be at 1.69 volts per shingle. An array whose shingles operate at this voltage will provide the maximum energy under the temperature conditions assumed. This might be compared to operation at the maximum power point at maximum temperature (at 110°C). From Figures III.9-3 and III.9.4 this corresponds to 1.55 volts. The energy delivered, per shingle, at the optimum voltage (1.69 volts) is approximately 2.5% greater than the energy delivered, per shingle, at the maximum power voltage (1.55 volts). Of course battery temperatures, battery and solar array tolerances must be taken into account in finally establishing the optimum voltage.

2. Tracking Array Maximum Power Point

An investigation was made to determine the effect of tracking the maximum power point of the array for all combination of temperature and sun angle. This requires a converter to be interposed between the array and the battery.

The calculation of the energy output for fixed point as opposed to tracking the maximum power point showed a slight gain in the latter. Energy output when tracking was 21.6 watt-hours. The gain was 3.25% over the fixed-point energy of 20.9 watt-hours.

When losses in the tracking system, added complexity, added weight, and accuracy of tracking are considered, it is certain that the advantage of the 3.25% gain will be lost.

TR64-26

K. POWER SUPPLY PARAMETRIC CALCULATIONS

Parametric calculations were made for Solar Cell (Orientable Array) and RTE power systems. The purpose of these calculations was to determine the effect of Goldstone and World-Wide coverage on system weight, modes of operation, power levels and to ultimately compare a solar cell orientable array with an RTE power system.

For Goldstone coverage mode 2 operation was analyzed. For World-Wide coverage modes 3A & 4A were analyzed. (For mode description see Figure II.3-25.)

Three power levels for each of the modes of operation were calculated as follows:

	P_{LR1}	P_{LR2}	P_{LU}
Case I	14 watts	2	6
Case II	24 watts	2	6
Case III	34 watts	2	6

where P_{LR1} is the average regulated power to load during operation, watts

P_{LR2} is the average regulated power to load during charge, watts

P_{LU} is the average unregulated power to load during operation, watts.

1. Solar Cell-Battery Power Supply Parametric Calculations (Orientable Array)

For the purpose of demonstrating the analytical approach to the parametric analysis, the case of the solar cell-battery power supply will be presented in detail. This same approach was used for an RTE system and where applicable the constants used were the same.

The block diagram for the solar cell battery power supply is shown in Figure II.3-26.

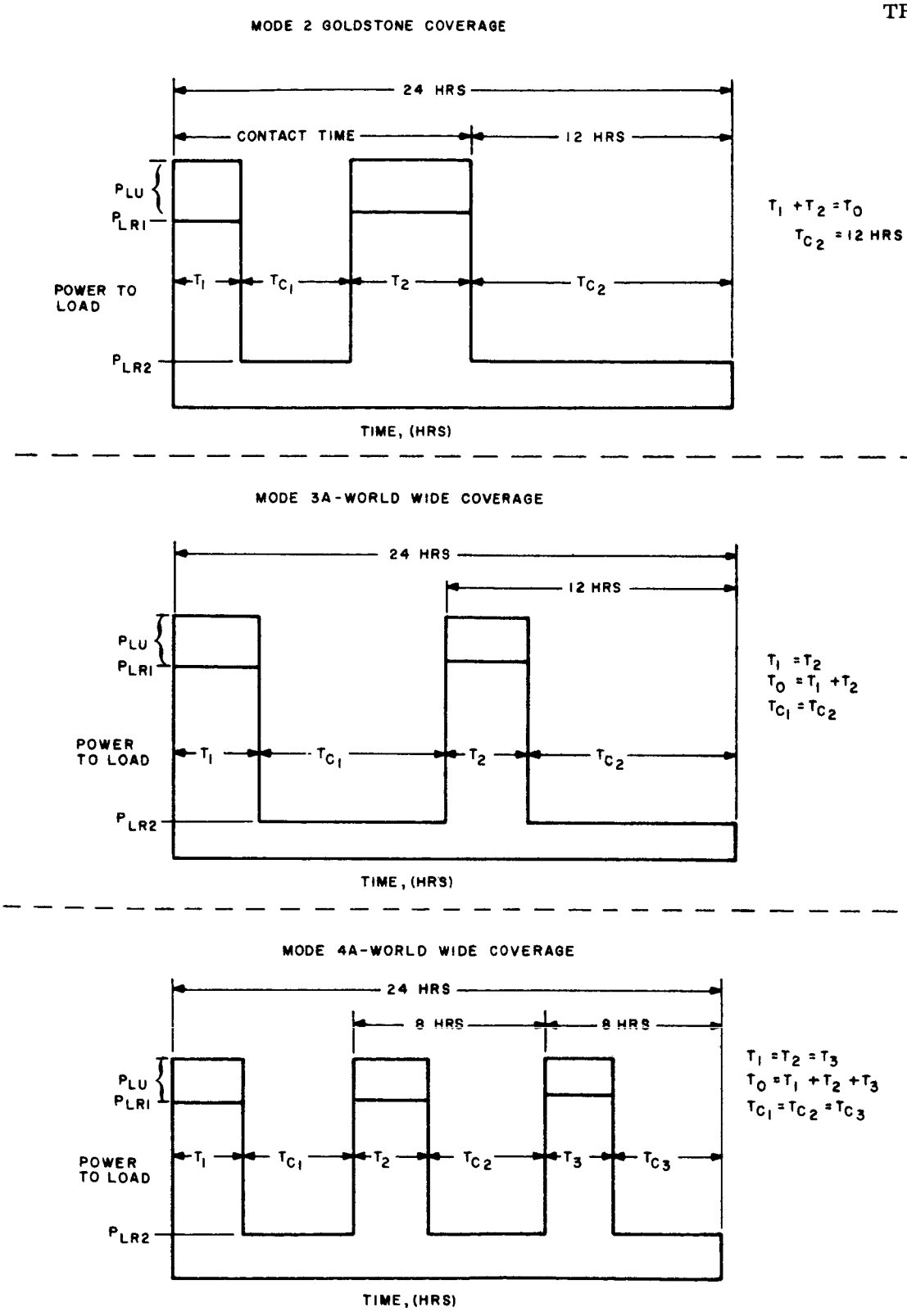

Figure II.3-25. Description of Modes of Operation

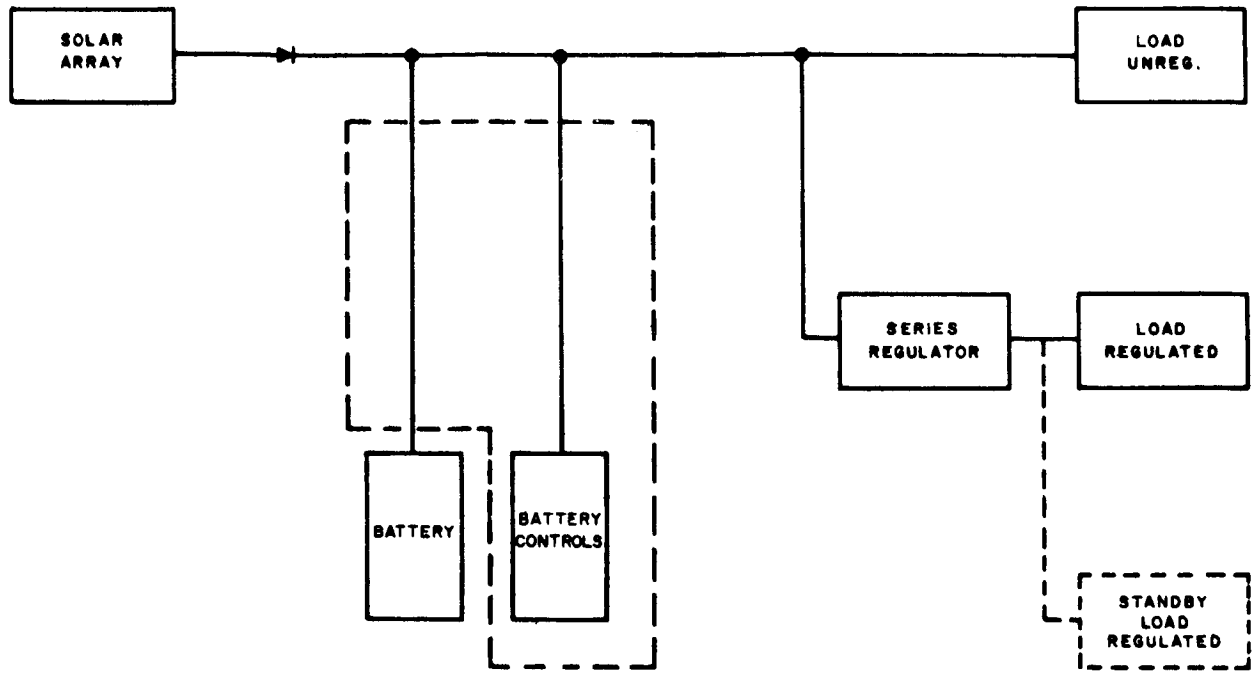

Figure II.3-26. Solar Cell/Battery Schematic Block Diagram

Definition of Symbols:

P_{SA} - Power* delivered by solar array during non-operate times (T_{C1}, T_{C2}, T_{C3});

P_B - Power* delivered by battery during operate times (T_1, T_2, T_3);

P_{LU} - Power* delivered to loads using unregulated voltage (occurs only during operate times);

P_{LR1} - Power* delivered to loads using regulated voltage during operate times;

P_{LR2} - Power* delivered to loads using regulated voltage during non-operate times (i.e. charge);

P_R - Raw power output from the RTE generator;

V_D - Battery discharge voltage;

*average power

B_{A-H} - Battery capacity, ampere-hours;

E_B - Total Battery capacity, watt-hours;

T_1, T_2, T_3 - Operate times - portion of cycle when SLRV mission is being performed;

T_{C1}, T_{C2}, T_{C3} - Non-Operate times - portion of cycle when mission is not performed and power is taken from the array to re-charge the battery and operate standby load;

T_o - $T_1 + T_2 + T_3$ Total operate time;

T_C - $T_{C1} + T_{C2} + T_{C3}$ Total charge time;

η_B - Battery watt-hour efficiency which is defined by (energy output)/(energy input); $\eta_B = 0.67$

η_D - Factor to reflect loss in diodes and has an efficiency; $\eta_D = 0.93$

η_{RC} - Efficiency of voltage regulator when only standby load (P_{LR2}) is being used; $\eta_{RC} = 0.60$

η_{RO} - Efficiency of voltage regulator when operate load (P_{LR1}) is being used; $\eta_{RO} = 0.85$

η_C - Converter efficiency for an RTE; $\eta_C = 0.87$

Charge Mode

The charge mode is shown in the block diagram in Figure III.10-3.

Assume Battery Controls consumes no power.

For Goldstone $T_{c_1} + T_{c_2} = T_c$

$$P_{SA}\, T_c \eta_D = \frac{P_B T_o}{\eta_B} + \frac{P_{LR2}\, T_C}{\eta_{RC}} \qquad \text{(II.3-5)}$$

TR64-26

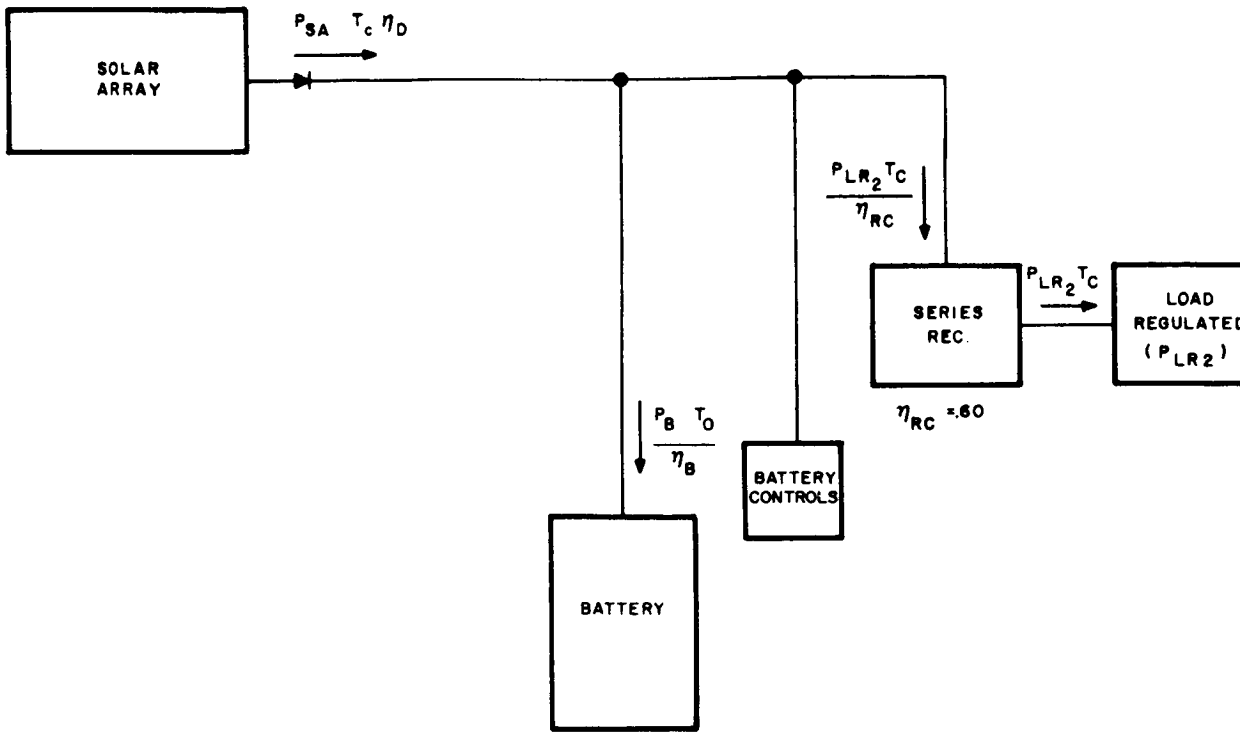

Figure II.3-27. Block Diagram of the Charge Mode

$$P_{SA}\eta_D = \frac{P_B}{\eta_B}\frac{T_o}{T_C} + \frac{P_{LR2}}{\eta_{RC}} \qquad \text{(II.3-6)}$$

$$P_{SA} = \frac{P_B}{\eta_D \eta_B}\frac{T_o}{T_C} + \frac{P_{LR2}}{\eta_D \eta_{RC}} \qquad \text{(II.3-7)}$$

$$T_C = 24 - T_o$$

$$P_{SA} = \frac{P_B T_o}{\eta_D \eta_B (24 - T_o)} + \frac{P_{LR2}}{\eta_D \eta_{RC}} \qquad \text{(II.3-8)}$$

Operate Period

The block diagram for the operate mode is shown in Figure II.3-28.

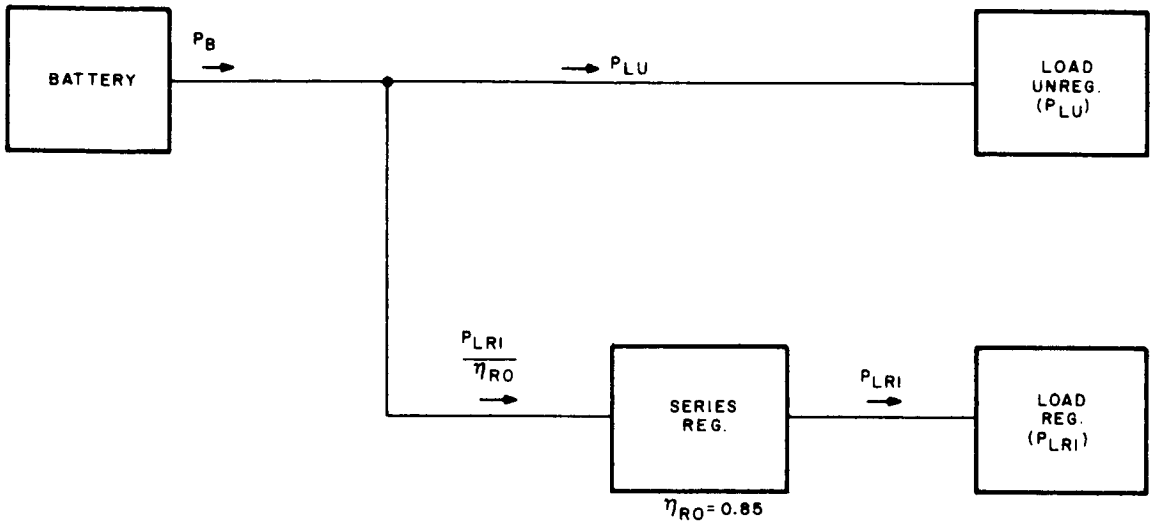

Figure II.3-28. Block Diagram of the Operate Period

$$P_B = + \frac{P_{LRI}}{\eta_{Ro}} + P_{LU} \qquad \text{(II.3-9)}$$

The maximum depth of discharge is 50% (this occurs at the 12-hour point).

Then, from equation (II.3-9).

$$\left(P_{SA} - \frac{P_{LR2}}{\eta_D \eta_{RC}} \right) \eta_D \eta_B T_{C2} = 0.50 E_B \qquad \text{(II.3-10)}$$

where $0.50 = Depth\ of\ Discharge$

For this parametric analysis, a silver-zinc battery system has been used throughout.

$$\beta_{A\text{-}H} = \frac{E_B}{V_D}$$

The following constants were developed for 10.5% Air Mass 0, sningles covered with 6-mil fused silica on a substrate which weighs 0.5 lbs/ft^2, and a packing factor of 85%.

$$A = Array\ Area = \frac{P_{SA}}{5.9\ watts/ft^2}$$

$$W_a = Array\ Weight = \frac{P_{SA}}{5.9\ watts/lb.}$$

The same analytical approach was extended to cover World-Wide operation and Modes 3A and 4A.

The results of this analysis are graphically shown in Figures II.3-29, 30 & 31.

Additional assumptions used for the calculations were as follows.

(1) Charging occurs during non-operational period only.

(2) A silver-zinc battery (no redundancy) using a max. depth of discharge = 50%.

(3) Battery charge rate not to exceed C/4 rate.

(4) Battery discharge rate not to exceed C/1.3 rate.

(5) No degrading of specific energy of the battery as a function of charge or discharge rates.

(6) Minimum battery weight is established as 2 lbs.

(7) Weight of electronics equals 1.7 lbs. (1 lb. for line regulator and 0.7 lbs. for charge electronics).

(8) Battery discharge voltage equal 24 volts average.

(9) Silicon N-on-P cells having an air mass zero efficiency of 10.5% (including glass, filter, and adhesive), were used.

(10) Weight of array of 1 lb/ft^2.

(11) Packing factor for the array of 85% was used.

(12) Weight of orientable array drive equals 1.5 lbs.

2. Results

For the orientable solar array a direct comparison for a specific case is shown in Table II.3-12. This table shows the weight advantage of World-Wide coverage over Goldstone coverage and the advantage of mode 4A (3 cycles) over mode 3A (2 cycles). The difference in system weight is due solely to battery weight. It is possible that further weight advantage may be gained by increasing the number of cycles per day. The Limitation here is cycle life versus charge and discharge rates.

Note, also that the array exceeds the 4 ft^2 area for the roll-up mode at 10 hours operate time.

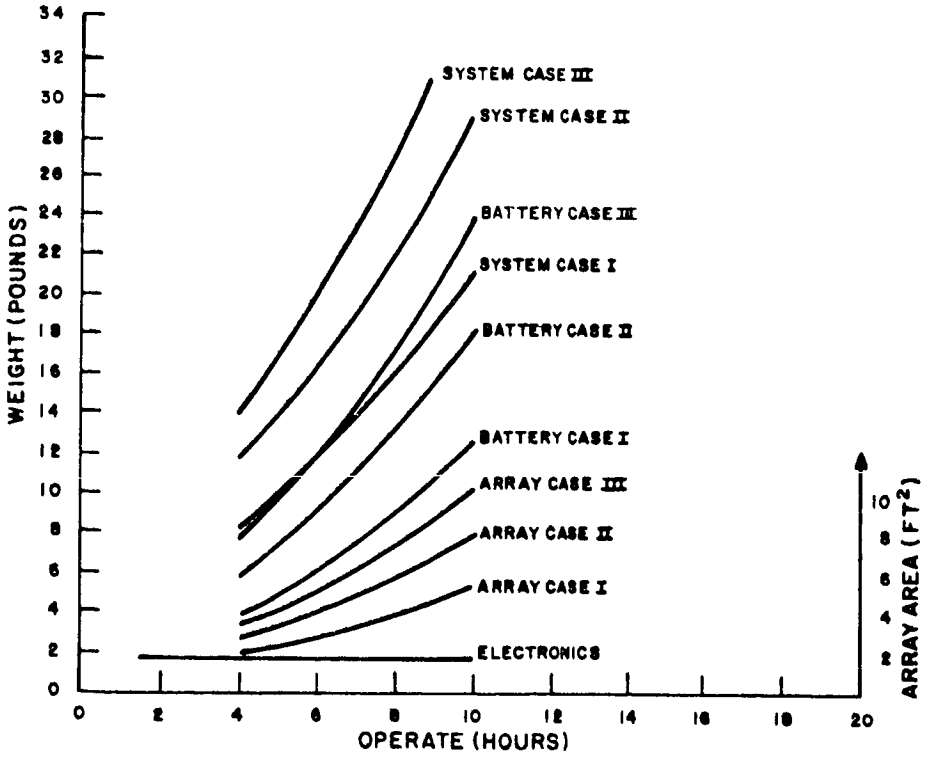

Figure II.3-29. Power System Weight for Goldstone Coverage (Mode 2)

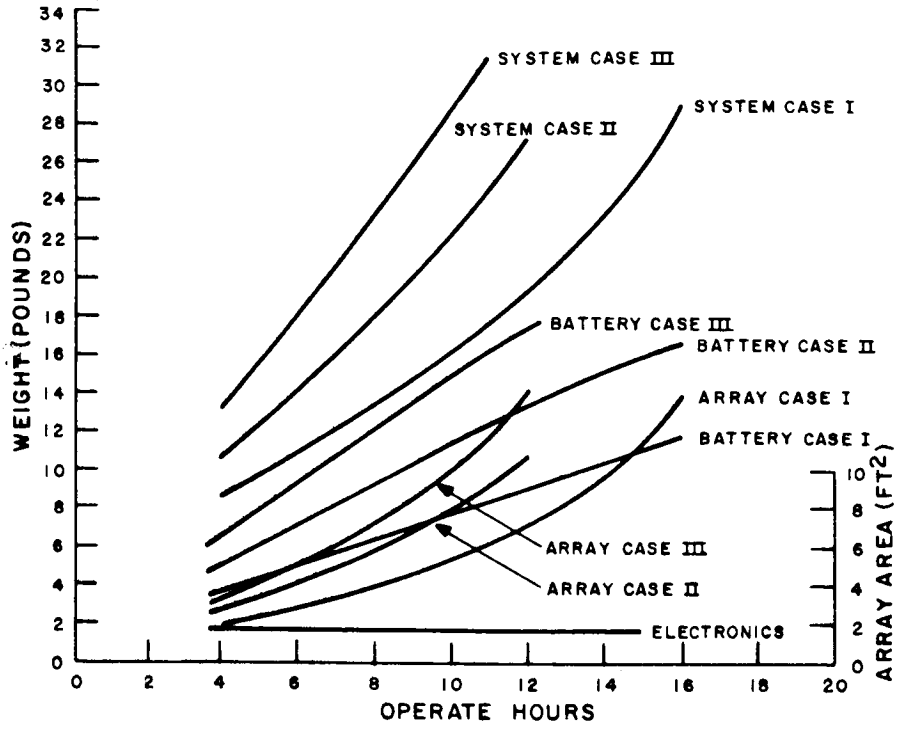

Figure II.3-30. Power System Weight for World Wide Coverage (Mode 3A)

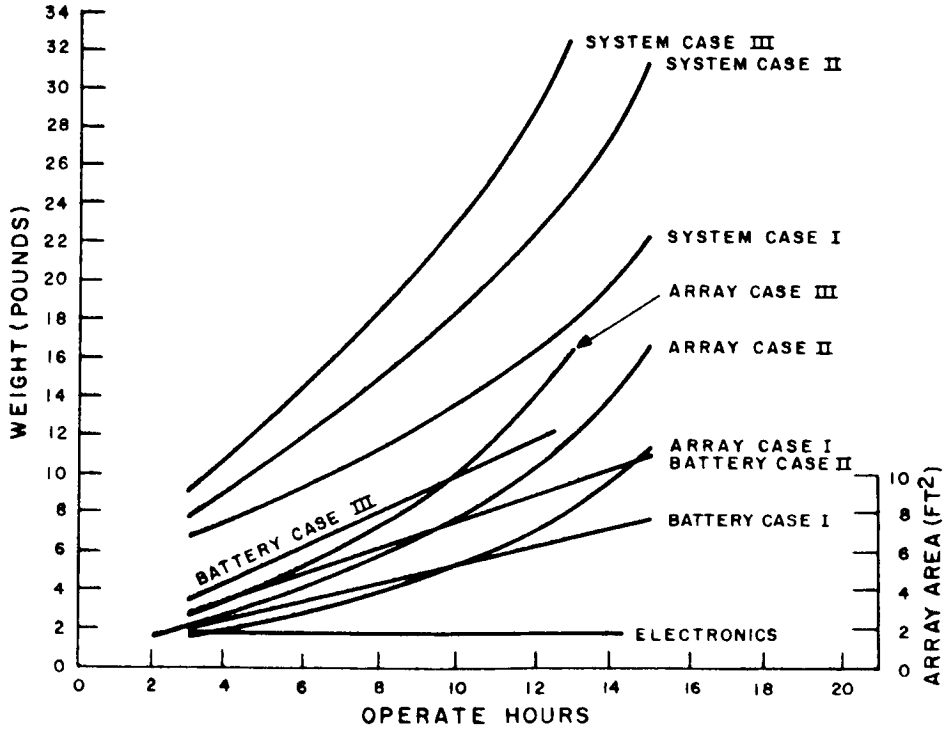

Figure II.3-31. Power System Weight for World Wide Coverage (Mode 4A)

TABLE II.3-12

SYSTEM WEIGHT COMPARISON ORIENTABLE SOLAR ARRAY

Coverage	Mode	Power Level	Operate Time/24 hrs.	System Weight
Goldstone	2	Case II	10 hours	28.5 lbs.
World Wide	3A	Case II	10 hours	22 lbs.
World Wide	4A	Case II	10 hours	18.5 lbs.

3. **RTE Power Supply**

As stated previously, the approach for the parametric study for an RTE supply was the same as that used for the solar cell-battery supply. The Mode description, power levels, and coverage are identical to those defined previously with the exception that during operate time the RTE does deliver power to the load. The symbol used for this power output is $P_R \eta_c$ where:

P_R = Raw power output for RTE, (watts)

η_C = Converter efficiency at 87%.

The power delivered by the RTE as a function of operate time is shown in Figure II.3-32. The block diagram for the RTE supply is shown in Figure II.3-33.

Also, 1.0, 1.5, and 2.0 watts/lb ratios of RTE output were used as a parameter. For this ratio, the power is taken at the output of the converter and the weight includes that of the RTE and converter combination. This point is indicated by a double arrow in Figure II.3-33.

The basic equation derived by the conservation of energy approach is indicated below:

$$P_R \eta_C = \frac{T_o \left[\frac{P_{LR1}}{\eta_B \eta_{RO}} + \frac{P_{LU}}{\eta_B} - \frac{P_{LR2}}{\eta_{RC}} \right] + \frac{24 P_{LR2}}{\eta_{RC}}}{\left(24 - T_o + \frac{T_o}{\eta_B} \right)}$$

The terms in this equation are defined previously.

The assumptions used for the calculations are as stated previously.

The parametric curves resulting from this study are shown in Figures II.3-34 through II.3-42.

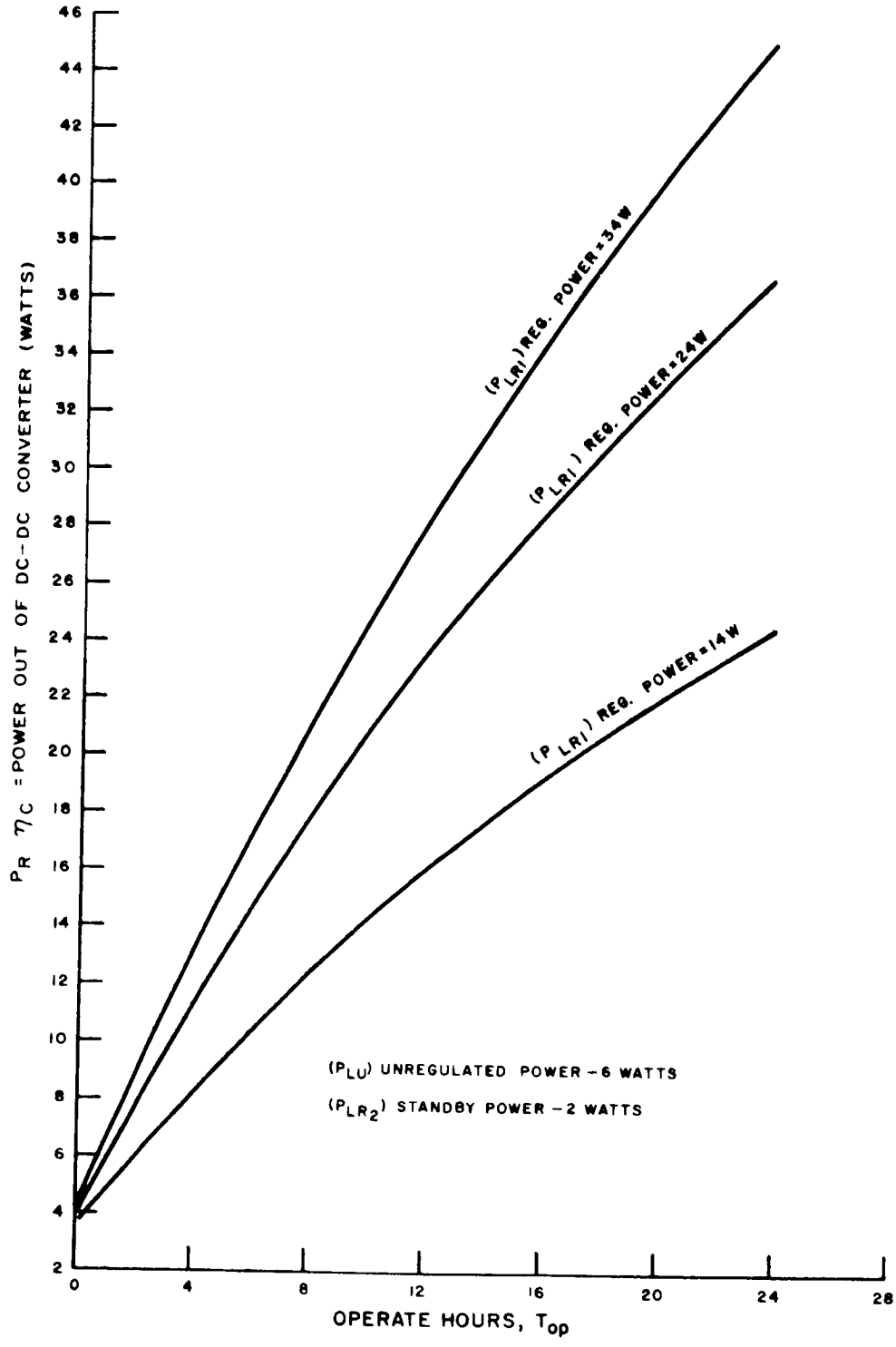

Figure II.3-32. Power Delivered by RTE as a Function of Operate Hours

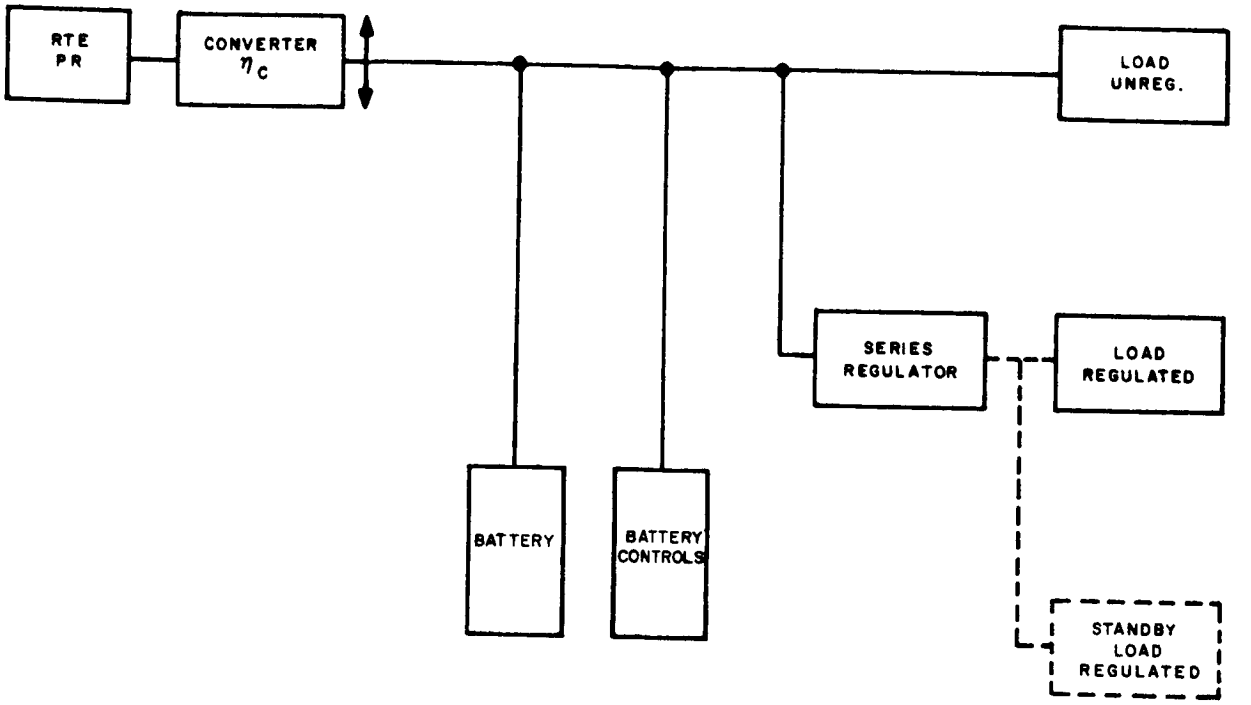

Figure II.3-33. Block Diagram for RTE Supply Single Battery (No Redundancy)

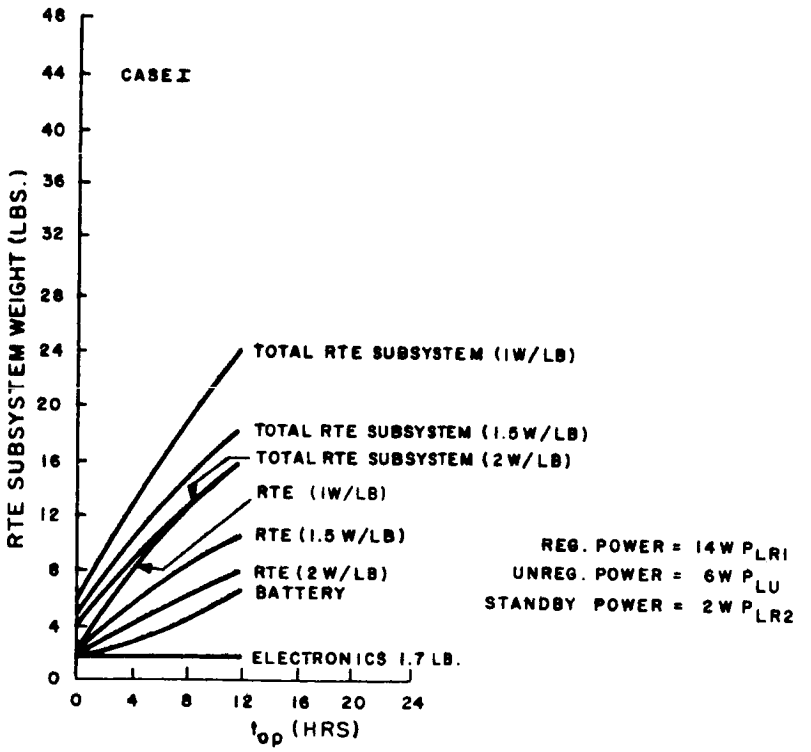

*Figure II.3-34. Subsystem Weight versus Operating Time Goldstone - Mode 2, Case I

*See II.3-27

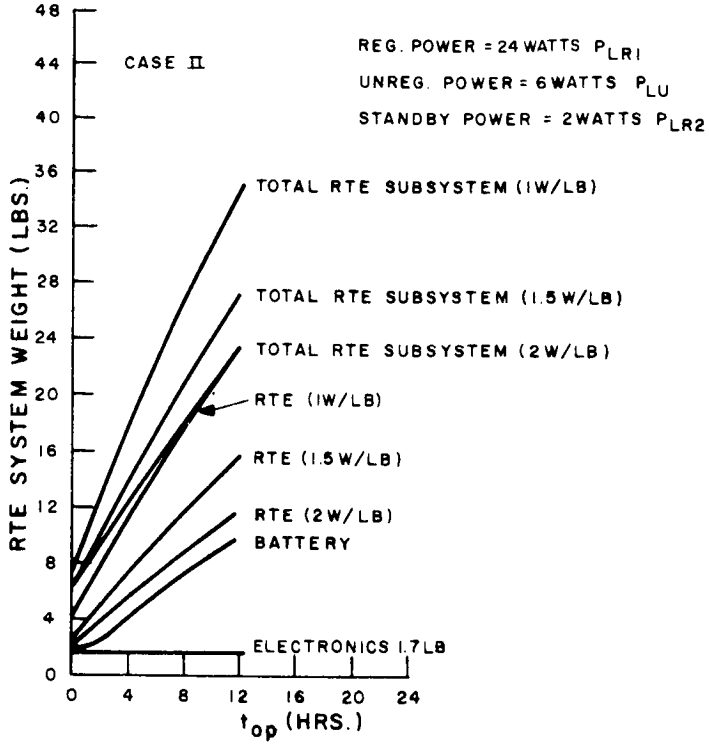

*Figure II.3-35. Power Subsystem Weight versus Operating Time Goldstone Mode 2, Case II

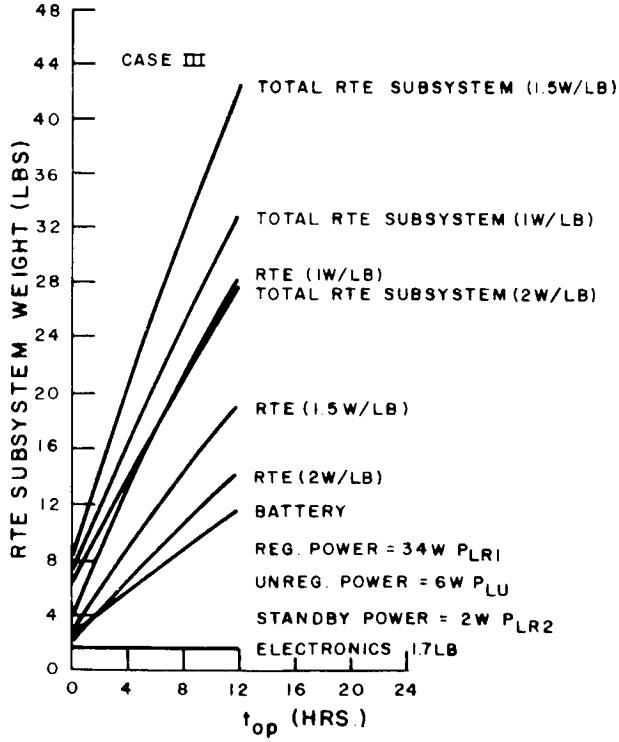

*Figure II.3-36. Power Subsystem Weight versus Operating Time Goldstone Mode 2, Case III

*See II.3-27

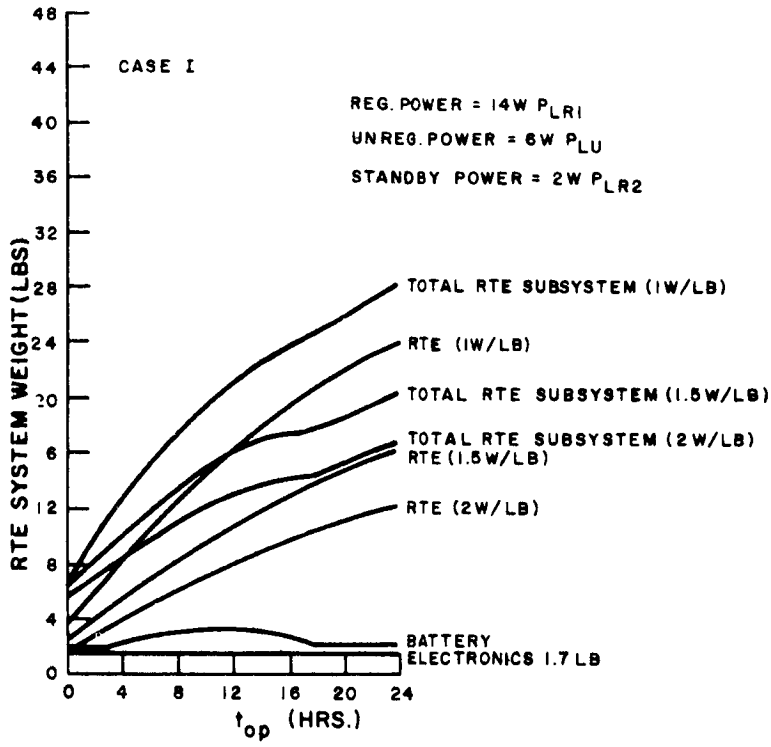

*Figure II.3-37. Power Subsystem Weight Versus Operating Time World-Wide Mode 3A, Case I

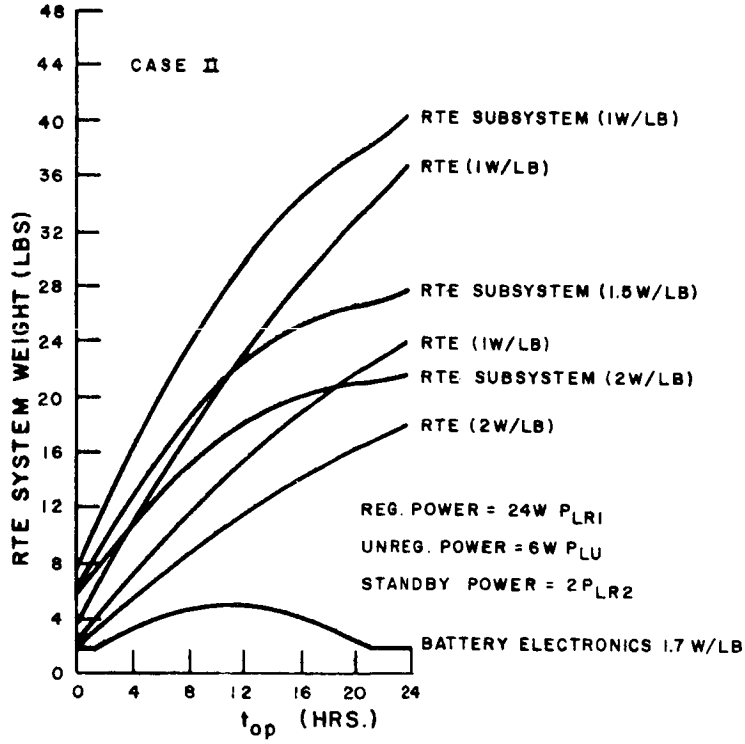

Figure II.3-38. Power Subsystem Weight versus Operating Time World-Wide Mode 3A, Case II

*See II.3-27

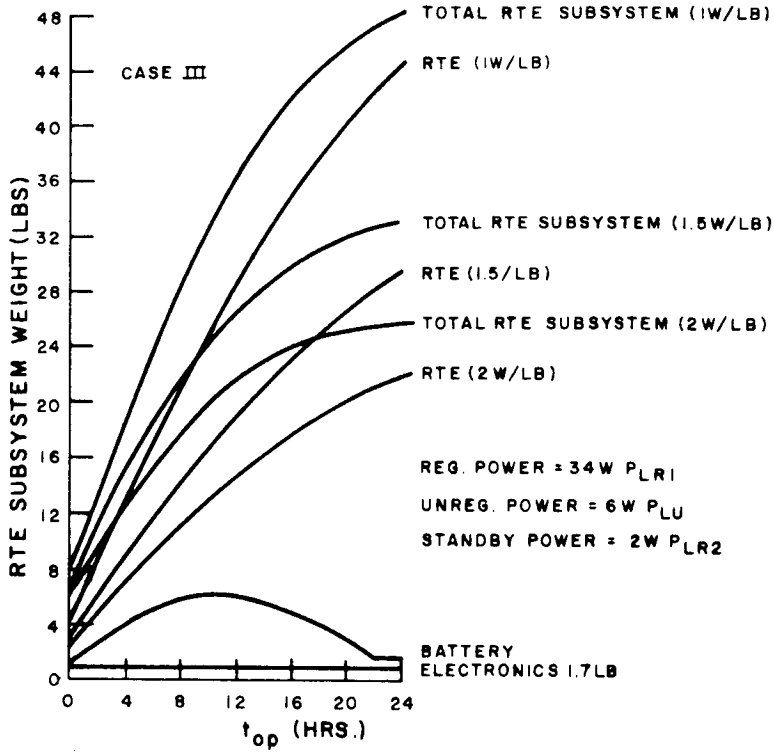

*Figure II.3-39. Power Subsystem Weight versus Operating Time World-Wide Mode 3A, Case III

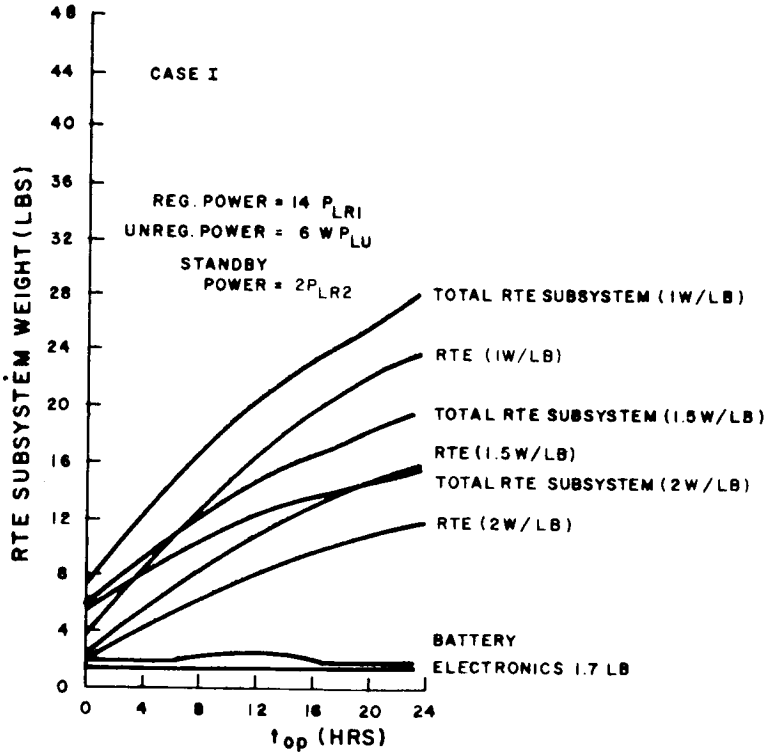

*Figure II.3-40. Power Subsystem Weight versus Operating Time World-Wide Mode 4A, Case I

*See II.3-27

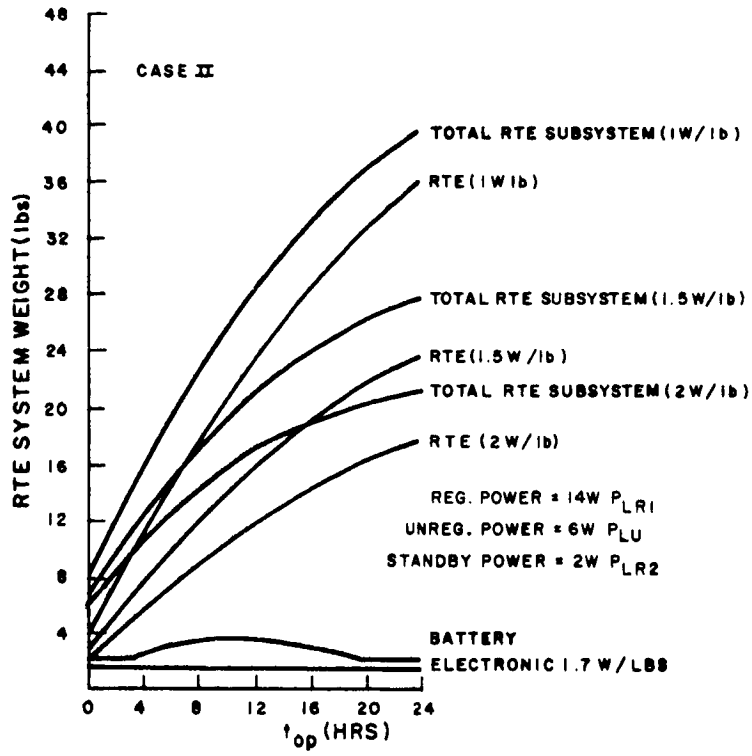

*Figure II.3-41. Power Subsystem Weight versus Operating Time World-Wide Mode 4A, Case II

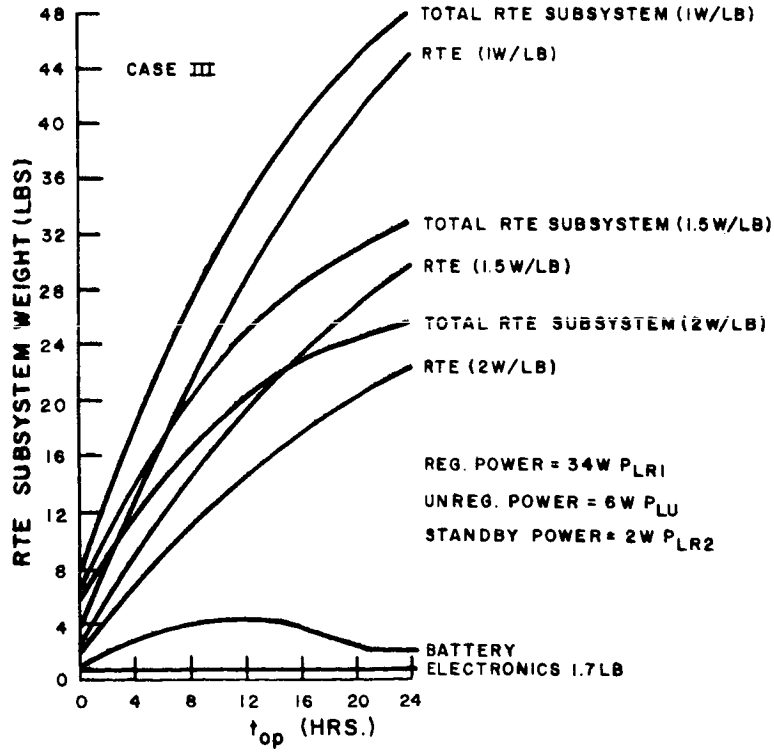

*Figure II.3-42. Power Subsystem Weight versus Operating Time World-Wide Mode 4A, Case III

*See II.3-27

4. Results

For the RTE a direct comparison for a specific case is shown in Table II.3-13. This table shows clearly the weight advantage of World Wide coverage over Goldstone and the advantage of mode 4A. For this power system further weight reduction may be gained by increasing the number of cycles per day.

TABLE II.3-13

SYSTEM WEIGHT COMPARISON

Coverage	Mode	*Specific Wt.	Power Level	Operate Time/24 hrs.	System Wt.
Goldstone	2	1.5 watt/lb.	Case II	10 hrs.	25 lbs.
World Wide	3A	1.5 watt/lb.	Case II	10 hrs.	22 lbs.
World Wide	4A	1.5 watt/lb.	Case II	10 hrs.	19.5 lbs.

*The specific weight includes the weight of the RTE plus converter and the power assumed to be available from the converter.

L. FIXED ARRAY ANALYSIS

1. Analytical Approach

The solar array configuration shown in Figure II.3-43 was analyzed for projected area and power output. The effective and average area and power are shown in Figures II.3-44 and II.3-45.

The panel areas were computed using Figure II.3-43 . For projection calculations, a reference frame was established (Figure II.3-46). Any vector in this system may be represented in the form:

$$\bar{A} = A(\cos\gamma\cos\beta\,\hat{i} + \cos\gamma\sin\beta\,\hat{j} + \sin\gamma\,\hat{k}) \qquad \text{(II.3-11)}$$

If two vectors are established, then the angle between them may be found from the vector dot product.

If we let the unit vector $\bar{N}$ represent the normal to the panel and the unit vector $\bar{S}$ represent the sun vector, then:

$$\bar{N} \cdot \bar{S} = |N| \cdot |S| \cos\theta = \cos\theta \qquad \text{(II.3-12)}$$

where: $|N| = |S| = 1$ *since* $\bar{N}$ *and* $\bar{S}$ *are taken as unit vectors*

θ is the angle between $\bar{N}$ and $\bar{S}$.

To include all possible panels we assign β_1 and γ_1 to the panel vector and β_2 and γ_2 to the sun vector.

Thus the dot product is:

$$\bar{N} \cdot \bar{S} = N(\cos\gamma_1\cos\beta_1\,\hat{i} + \cos\gamma_1\sin\beta_1\,\hat{j} + \sin_{\gamma 1}\hat{k}) \cdot S(\cos\gamma_2\cos\beta_2\,\hat{i} + \cos\gamma_2\sin\beta_2\,\hat{j} + \sin\gamma_2\,\hat{k}) \qquad \text{(II.3-13)}$$

$$\cos\theta = \sin\gamma_1\sin\gamma_2 + \cos\gamma_1\cos\gamma_2\cos(\beta_1 - \beta_2) \qquad \text{(II.3-14)}$$

This relation was used to project panel areas as the array rotated in azimuth and the sun increased in elevation.

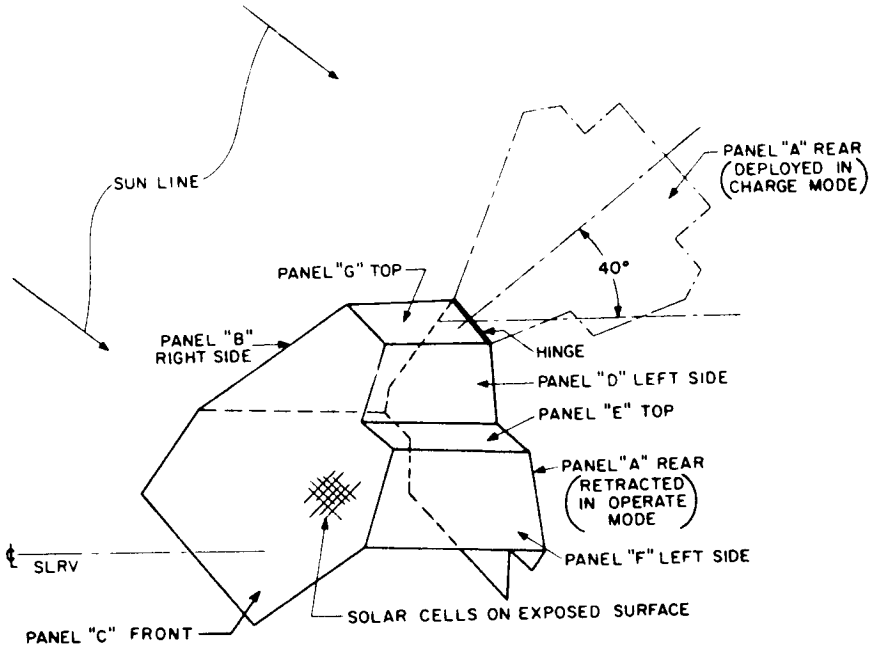

Figure II.3-43. Pictorial View of Fixed Array (DIBSI Not Shown)

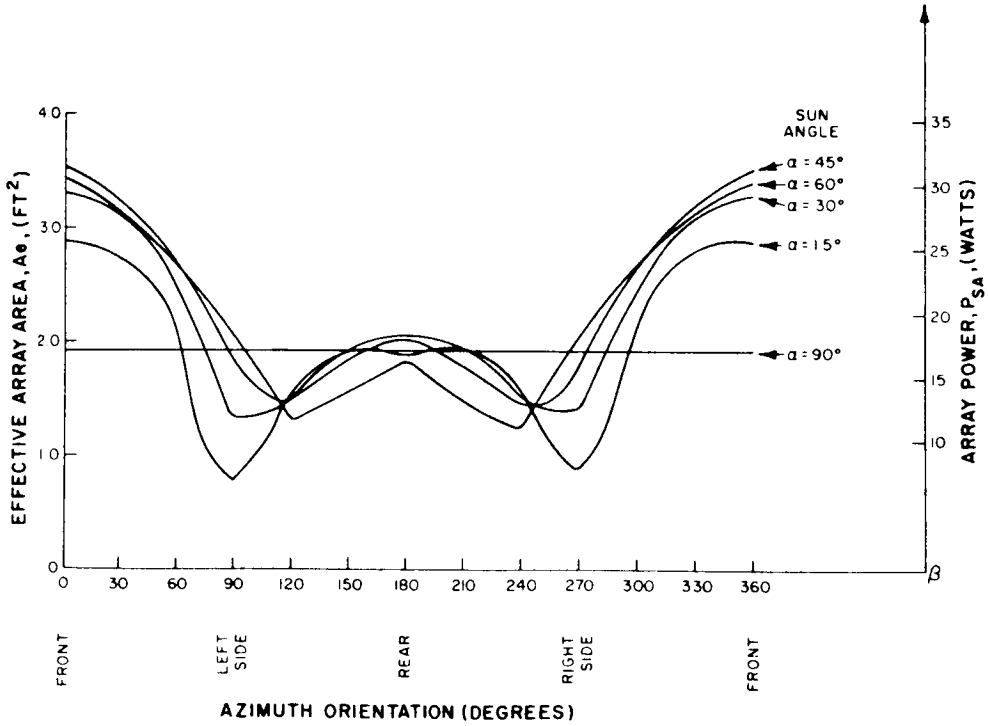

Figure II.3-44. Effective Array Area and Power Output vs. Azimuth and Sun Angle (For Fixed Array)

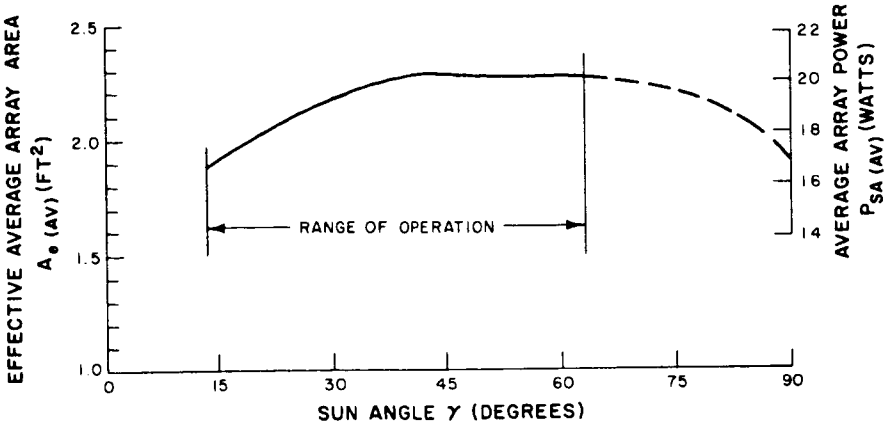

Figure II.3-45. Average Array Area and Power vs. Sun Angle (For Fixed Array)

2. Angle Effect

When solar cells are illuminated by light incident at an angle θ with respect to the cell's normal, the power output may be expressed as

$$P_S = P_{SN} \cos\theta \, F(\theta) \qquad \text{(II.3-15)}$$

where P_S is power out with non-normally incident light

P_{SN} is power out with normally incident light.

θ is the angle between the light vector and the normal vector

$F(\theta)$ is a function of θ (Figure III.11-5) which adjusts the power output to account for the difference between actual cell performance and that implied by a pure cosine relationship

3. Packing Factors and Effective Panel Area

An approximate packing factor was computed for each surface by finding the number of series strings of 5-cell (1cm x 2cm) shingles which could be fitted on each.

To illustrate the procedure, the calculation for the front panel will be shown.

Shingle Area (Five 1x2cm cells)	$A_S = 1.43\ in^2$
Intershingle Packing Factor	$p.f. = 0.9$
Required area for each shingle	$A_{se} = 1.43/.9 = 1.6\ in^2$
Area of front panel	$Ap = 463\ in^2$

TR64-26

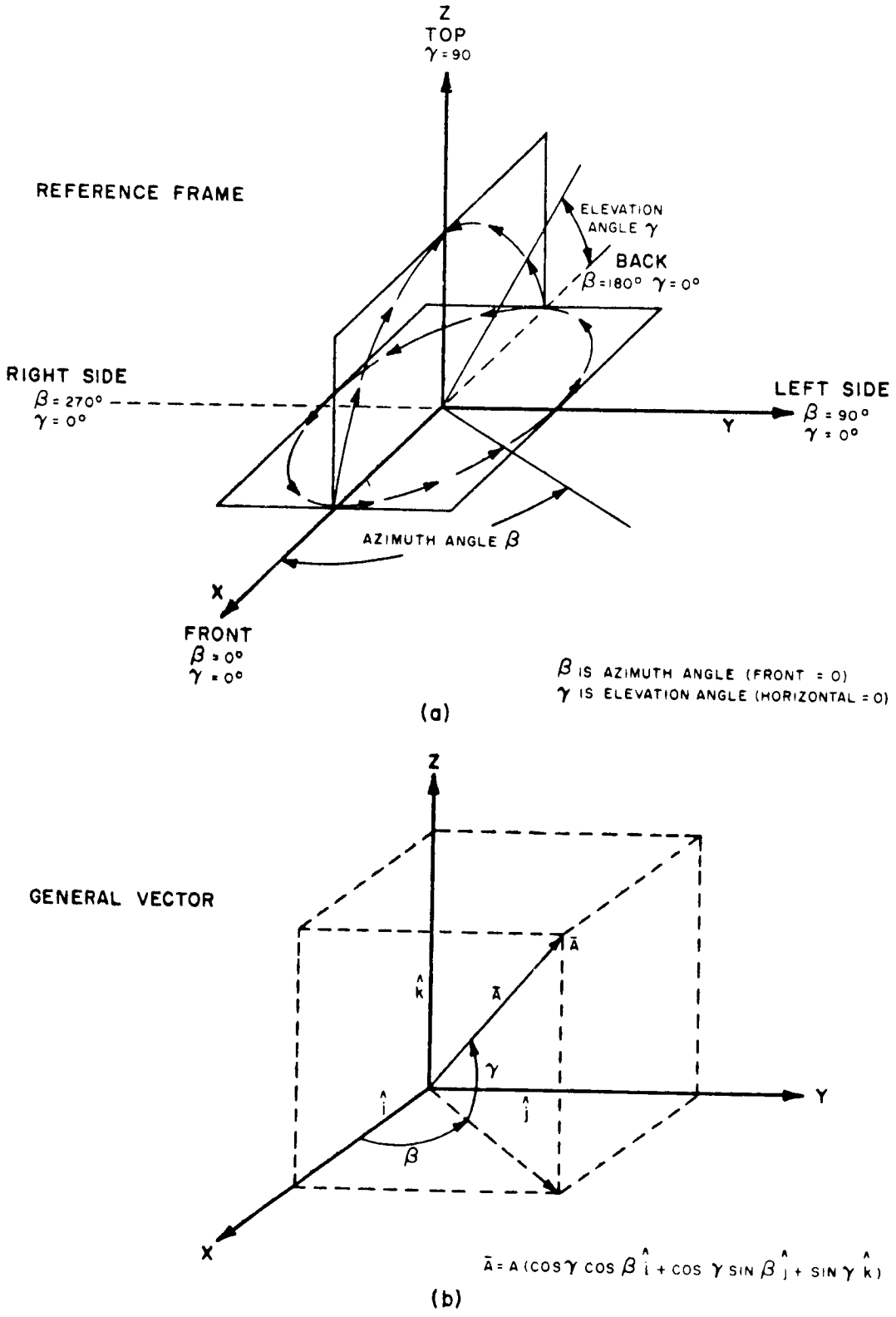

Figure II.3-46. Reference Frame Definition and General Vector $\bar{A}$

Number of shingles	NOS	$A_p \; A_{se}$ 463 1.6 = 290 shingles
Number of series strings, assuming 20 series shingles per string required.	NSS	$NOS \; 20$ 14.5 = 14 series strings
Packing Factor	$P.F.$	$(0.9) \frac{20 \; NSS}{NOS}$ = 0.87

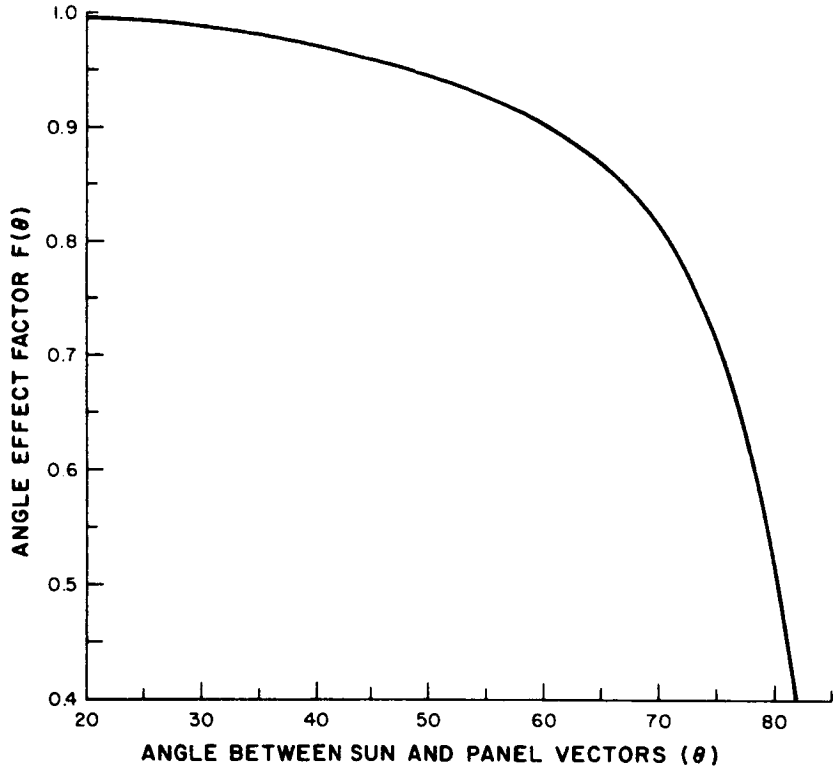

Figure II.3-47. Angle Effect Factor vs. Angle

The effective area of a panel is defined as the product of the area and the packing factor. For the front panel:

$$\text{Effective Area} = A_e = A_p \times P.F. \qquad = 402 \; in^2 = 2.8 \; ft.^2$$

Table II.3-14 is a tabulation of panel area, packing factor, and effective area. It will be noted that the effective area was reduced for the left side and top panels because of DIBSI shadow.

TABLE II.3-14

SLRV SOLAR PANEL STATISTICS

Panel	Area	Packing Factor	Effective Area	Comments
Front (C)	463 in^2	.87	402 in^2 = 2.8 ft^2	14 Series Strings
Left Side (D&F)	155 in^2	.75	86 in^2 = .6 ft^2	Assume DIBSI always shadows one of four series strings
Rear (A)	295 in^2	.88	259 in^2 = 1.8 ft^2	9 Series Strings
Right Side (B)	151 in^2	.77	106 in^2 = .74 ft^2	4 Series Strings
Top (E&G)	118 in^2	.73	86 in^2 = .6 ft^2	3 Series Strings $0^o < \beta < 180^o$
			58 in^2 = .4 ft^2	2 Series Strings (one shadowed) $180^o < \beta < 360^o$
Total Area = 8.25 ft^2				

The effective area includes the effects of packing factor, shadowing, angle of incidence, and angle effect. This area can then be analyzed as the area of an equivalent solar array.

4. Array Power Density

The array power density (watts/ft^2) is calculated for 10.5% efficiency shingles. The power output for each shingle is:

$$P_o = 97.3 \text{ milliwatts/shingle}$$

This number is the per-shingle output corresponding to a temperature of +92°C which is assumed to be the weighted average temperature for which the array is to be designed. Actual maximum operating temperature is slightly higher.

The power/ft^2 can be found from

$$\text{Power Density} = P.D. = P_o ND$$

where: P_o is power per shingle

N is the number of shingles per ft^2 of effective area as in Table II.3-14

$$N = \frac{144\ in^2/ft^2}{1.43\ in^2/shingle} = 100\ \frac{Shingles}{ft^2}$$

Noting that packing factors, shadowing and angle effect were taken into account in the effective area calculations,

D is combined degradation including

wiring losses	$d_w = 0.96$	$D = 0.91$
seasonal solar constant variation	$d_s = 0.97$	
off optimum operation	$d_o = 0.98$	

The array power density is

$$P.D. = (97.3\ mw)\ (100)\ (0.91) = 8.86\ watts/ft^2\ of\ actual\ corrected\ cell\ area.$$

The array power is the product of the array power density and the effective array area.

The effective array area and power -vs-degrees azimuth, and the average effective array area and power integrated over 360° azimuth are shown in Figures II.3-44 and II.3-45. These plots apply to the Operate Mode where any azimuth orientation of the vehicle with respect to the sun vector is possible.

5. Array During Charge

During the charge mode, in order to expose maximum area to the sun, the rear panel will be rotated on a hinge at its top edge so that it faces towards the front of the vehicle. Its normal is oriented to a fixed angle of $\gamma_1 = 40°$ to minimize variations from normal for the operational window of sun angle between 12° and 66°. The fixed angle simplifies the elevation mechanism drive. The effective area and power during charge is shown in Figure II.3-48.

6. Approximations

The analysis herein presented is approximate to the extent that an actual shingle layout has not been performed. However, it may be possible to use smaller shingles (2 or 3-cell, for instance) to achieve or exceed the packing factors estimated.

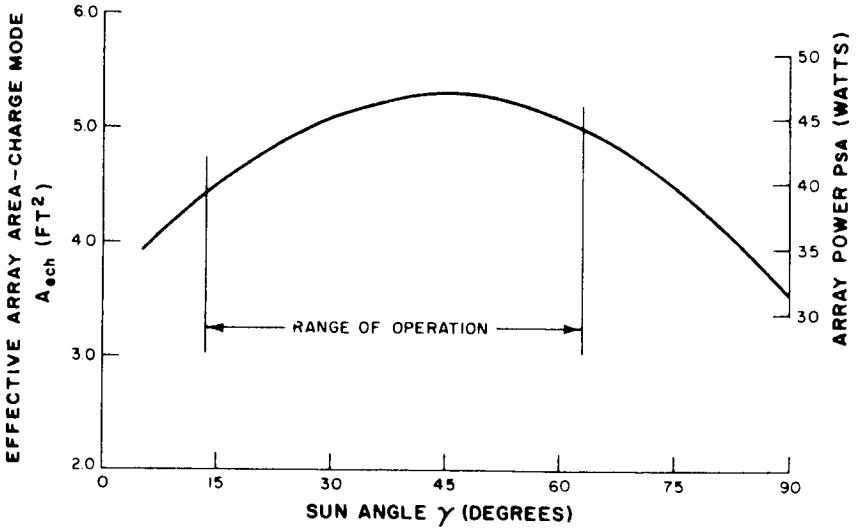

Figure II.3-48. Array During Charge vs. Sun Angle (Fixed Array)

The temperature-time profiles of the SLRV fixed array configuration are not precisely known at this time; a previously calculated temperature range for an oriented single plane* has been used as a matter of a worst-case approach.

Other factors such as design safety factors, radiation effects, lunar night time exposure are not treated here. They are suitably covered in Paragraph E.

Pending a detailed array analysis based on valid temperature, packing efficiency, and radiation damage assumptions, a 15% safety factor will be applied to the power output numbers presented.

7. Lunar Power Regulatory Electronics

General

Five regulated DC voltage levels are required for operation of the Rover Vehicle. Two +24V regulated levels are indicated, one obtained through series regulation, and the other through the regulated converter. A block diagram of the system is shown in Vol. I, Summary, Figure 3.1-13. The solar cell array mainly supplies battery charge current during the charge mode, in addition to approximately 2.3 watts (plus associated losses). The individual array panels are connected to the unregulated bus through blocking diodes. A silver cadmium battery, shown in Figure 3.1-13, supplies the majority of power during the operate time.

*See Paragraph G.

A state-of-charge monitor is included and performs the following functions:

(1) It senses the current flowing in the battery;

(2) Performs integration of the current time product (Ampere-Hours);

(3) Converts the signal to digital form (8 bits), and this information is telemetered to earth.

With the ampere-hour monitor it is possible to know the state of charge of the battery accurately at any time, and coupled with other telemetry data, provide insight into the actual battery performance.

A series regulator is connected through a relay contact to the unregulated bus, and supplies loads up to 16.2 watts at a regulated 24.0 volt ± 2% level during the operate mode. During the charge mode the relay (see Figure 3.1-13) disconnects the series regulator from the unregulated bus.

The converter provides four regulated voltages (see Figure 3.1-13). It is a driven, duty-cycle regulated converter. Duty-cycle regulation is obtained through a small self-saturating magnetic amplifier, controlled from the 24V output tap.

Regulated Converter

A schematic diagram of the regulated converter is shown in Figure II.3-49. It supplies DC voltage levels of +24 volts, +4 volts, -12 volts, and -6.3 volts, all regulated to within 2% (line, load, and temperature).

The +24 volt output from the converter supplies a continuous 1 watt load, whereas the +24 volt output from the series regulator supplies various loads, ranging from 3.7 watts to 16.2 watts. In order to supply a regulated power of 16.2 watts, the series regulator must therefore be relatively inefficient at lower power levels. In fact, at a 1 watt power level during charge, the series regulator would be approximately 50% efficient. Hence, during the charge mode, the series regulator is disconnected by a relay and the 1 watt required at the +24 volt level is supplied by the converter. The converter efficiency at this output voltage level is relatively high (at least 80%). A substantial portion of the converter losses are rectifer losses at the low voltage taps, and other relatively fixed losses (not a function of load).

Referring to the schematic in Figure II.3-49, the operation of the converter is as follows:

1. Sliding frequency oscillator -

   The sliding frequency oscillator is an inverter, the output of which is a square wave voltage varying in amplitude proportional

TR64-26

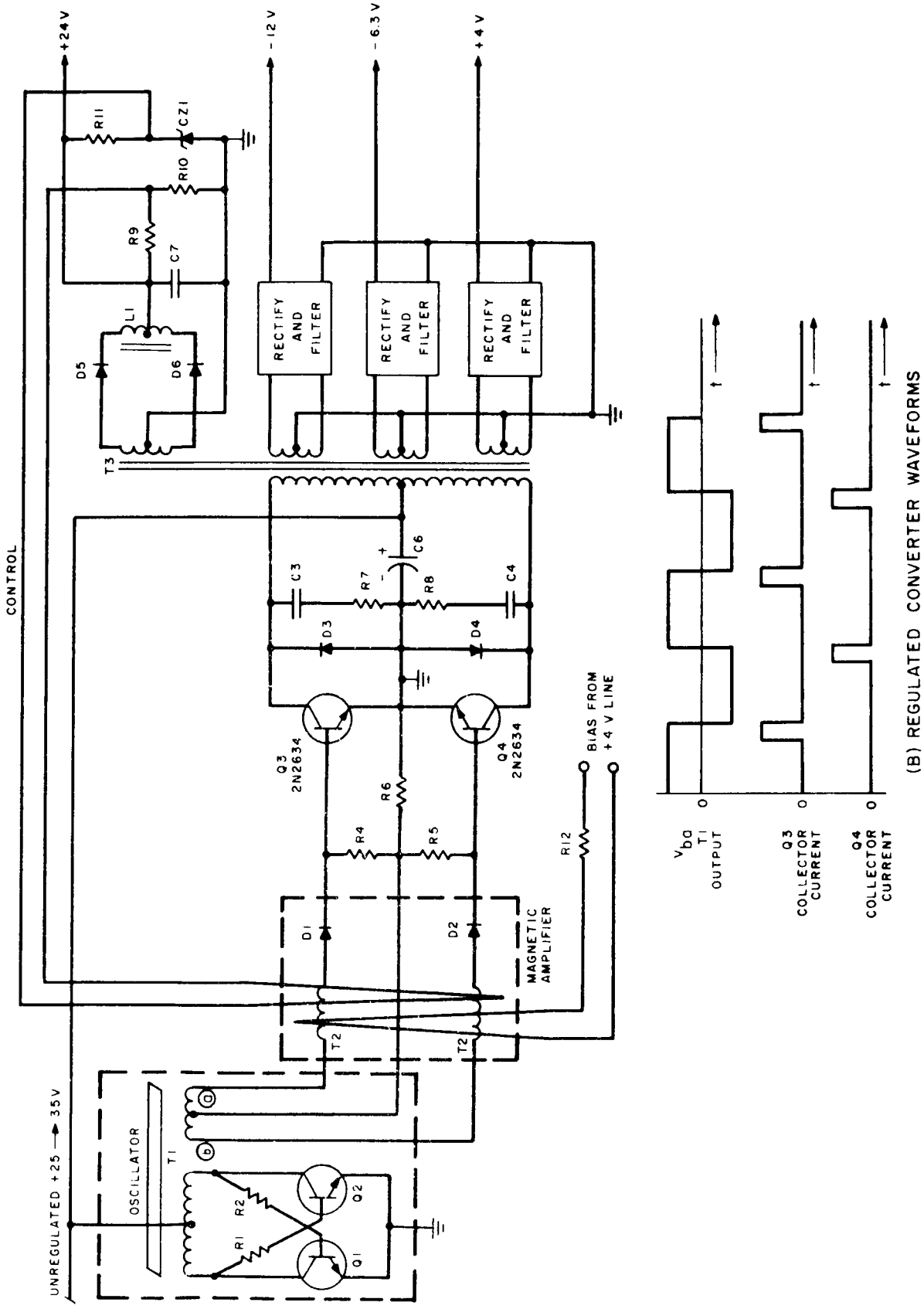

Figure II.3-49. Regulated Converter

to the unregulated bus voltage level. Its output is coupled through transformer T_1 to the reactors of the magnetic amplifier T_2;

2. Magnetic Amplifier -

The self-saturating magnetic amplifier is constructed of two matched square hysteresis loop tape wound toroidal cores, each progressively wound to form separate reactors, and then stacked. A control winding and a bias winding is looped through both cores, and the resulting assembly encapsulated in light weight epoxy. Each reactor of the magnetic amplifier blocks the square wave (voltage from transformer T_1) until saturation occurs. At this time the pulse turns on the associated converter transistor for the remainder of the half cycle. On the alternate half cycle the second reactor performs the same function in regard to the second converter transistor. The resulting duty cycle modulated wave form appears at the primary and secondaries of transformer T_3 (step-down to the proper level), and is shown in Figure II.3-49. The outputs at each secondary are four-way rectified and filtered. The control winding of the magnetic amplifier is connected between the balance terminals of a sensing bridge made up of resistors R9 through R11, and zener diode CZ1, which applies a voltage to the control winding proportional to the error voltage existing at the converter +24V bus. The control winding is wound over each of the cores in such a direction to reduce the error (negative feedback). It does this by biasing the reactor cores, thereby varying the volt seconds required to saturate each reactor.

3. Primary Circuit -

The primary circuit of the converter is composed of switching transistors Q3 and Q4, commutating rectifiers D3 and D4, capacitors C3, C4, and C6, resistors R7 and R8, and transformer T3. Transistors Q3 and Q4 are triple-diffused, planar, passivated NPN silicon power transistors having low saturation resistance and high breakdown voltage levels (BV_{CEO} is approximately 100 volts). Rectifiers D3 and D4 commutate primary current (reflected from the secondaries) when both Q3 and Q4 are non-conducting. Capacitors C3 and C4, and associated resistors R7 and R8 improve the dynamic load lines of Q3 and Q4, respectively, as well as dissipating spike energy which may exist due to leakage reactance in transformer T3. Transformer T3 is constructed with a non-saturating tape wound toroidal core, exhibiting approximately 92% efficiency at 600 cycles per second and full load. Capacitor C6 provides a low impedance at the converter

input and attenuates high frequency current components which would otherwise exist in the converter supply line.

4. Output Rectifiers and Filters -

The four output windings of transformer T3 terminate in full wave center tapped rectifier connections, the outputs of which are filtered by LC sections (such as L1 and C7 in Figure II.3-49). The inductors are the flux reversing type resulting in minimal size and weight. They are designed for greater than critical inductance over the operating load ranges. The rectifiers incorporated in the +4 volt and -6.3 volt windings will be either low loss germanium rectifiers, or driven low saturation resistance silicon medium power transistors. Low rectifier voltage drops are required for the +4 volt and -6.3 volt levels in order to remain within the ±2% regulation band, and to maximize efficiency.

Series Regulator

The series regulator must provide 3.7 watts to 16.2 watts load power during the operate time, at a regulated voltage level of +24 volts ±2%. During the charge mode, the series regulator is disconnected from the unregulated bus by a relay contact. A schematic diagram of the series regulator is shown in Figure II.3-50. Transistor Q4, zener diode CZ1, diode CR1, and resistors R5 through R9 comprise a temperature stable error amplifier which compares the regulated bus voltage level with the zener diode CZ1 voltage level, and provides base drive to transistor Q3, which in turn supplies base current to Q2, the driver of pass transistor Q1. Resistor R1 and diode CR2 allow the regulator to turn on under load, and diode CR1 provides temperature compensation for transistor Q4.

State-of-Charge Monitor

The battery state-of-charge monitor provides eight bits of binary information, containing the ampere-hour (effective coulombs) capacity of the battery, for the telemetry subsystem. The telemetered information is an indication of the state of charge of the battery at any given time. This feature minimizes the usual necessity to oversize the battery to make all charge rates safe. Referring to the block diagram in Figure II.3-51 , operation of the state-of-charge monitor is as follows: the battery charge current, I, is passed through a one-turn control winding of a magnetic amplifier, which in turn develops two proportional voltage signals ($-K_2 I$ and $+K_1 I$) which are applied to an "or" gate, the output of which is connected to a voltage sensitive VFO (variable frequency oscillator), and the resulting signal converted into a train of clock pulses. The number of clock pulses per unit time is proportional to battery current. Discharge current sets the reversible counter to count forward; charge current reverses the count. Thus given the initial conditions of a

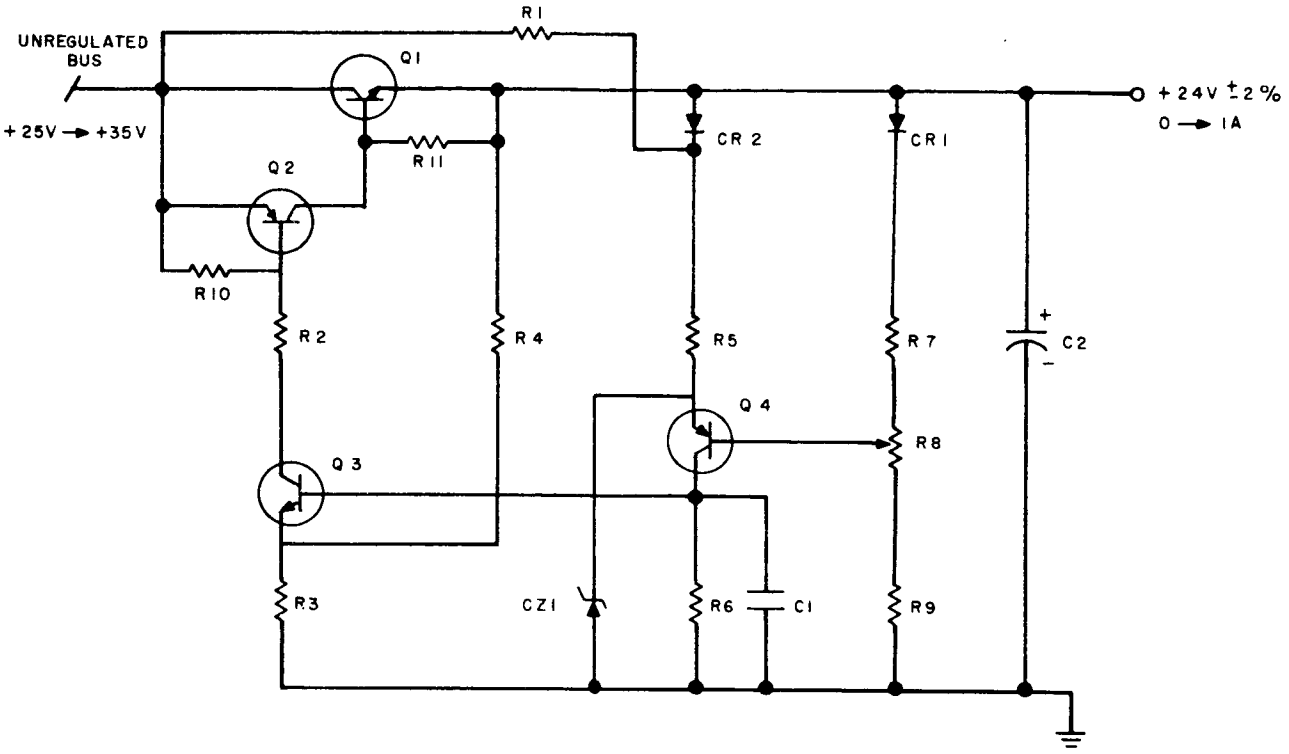

Figure II.3-50. Series Regulator

fully charged battery and a zero count, clock pulses stored in the counter are proportional to ampere-minutes discharge. The charge and discharge scale factors (K1 and K2) are chosen to reflect the battery efficiency and may be adjusted prior to launch. A detection of zero count indicates that the number of effective ampere-minutes charge (ampere-minutes charge times battery efficiency factor) just equals the number of ampere-minutes discharge. A battery is assumed to be recharged and the Operate signal is initiated. A total ampere-hours equalling total battery capacity may be stored in the counter, and is reflected in eight binary bits for telemetry processing.

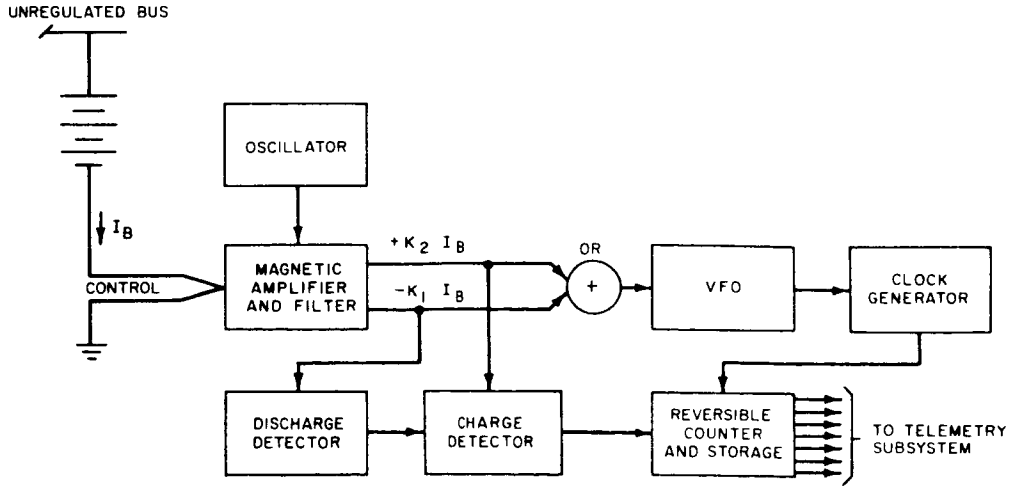

Figure II.3-51. State of Charge Monitor

8. Telemetry

The telemetry required and appropriate transducer circuitry is specified for the SLRV system configuration previously shown.

The circuitry will have nominal outputs of 0 to +5 volts working into the telemetry subsystem minimum input impedance of 1 megohm.

The analog switch back current is specified as less than 0.25 microamperes which affects the transducer output impedance. To minimize the loading of the transducers and eliminate the effect of switch back current, the maximum output impedance will be less than 0.5% of the telemetry input impedance.

$$Z\ (out) \leq 0.5\%\ Z\ (input) = (0.005)\ (1 \times 10^{6}\ ohms)$$

$$Z\ (out) \leq 5 \times 10^{3}\ ohms$$

This makes the loading current equal to 0.5% of the effective current in the transducer output.

The effect of switchback current (I_{SB}) on the transducer output voltage can now be computed --

$$\Delta V\ (output)\ max. = (I_{SB})_{max.}\ Z\ (out)_{max.}$$

$$= (0.25 \times 10^{-6}\ amps)\ (5 \times 10^{3}\ ohms)$$

$$= 1.25\ millivolts$$

This is 0.025% of the 5 volt nominal transducer output.

The power subsystem requires 21 telemetry points, (18 analog and three digital) as given in Table II.3-15.

Voltage telemetry will be taken for the array, battery, and regulated bus voltages.

If the transducer is to indicate the voltage measured from zero to its maximum value, then a simple voltage divider (Figure II.3-52) will be used.

For some telemetry points, it may be advantageous to have the transducer indicate a range of voltages where the lower limit is not zero (i.e. expanded scale). This can be accomplished by providing a voltage offset.

TABLE II.3-15

LUNAR ROVING VEHICLE - ROVER SUBSYSTEM TELEMETRY

Item	Function	Units Measured	Range Measured	Form of Output	Expected Output Voltage	Source Impedance	Transducer Accuracy	Location of Measured Quantity	Location of Transducer
1	Array/Battery Voltage	Volts	20 - 36	Analog	1 - 5V	5K	±2%	Axles 2 & 3	Axle 2
2	Voltage of 2 Cells	Volts	2 - 4	Analog	2 - 4V	5K	±1%	Axle 2	Axle 2
3	24V Regulated Bus	Volts	20 - 28	Analog	3 - 5V	5K	±1%	Axle 2	Axle 2
4	Solar Array Current	Amperes	0 - 2	Analog	0 - 5V	5K	±2%	Axles 2 & 3	Axle 2
5	Battery Current	Amperes	0 - 3	Analog	0 - 5V	5K	±2%	Axle 2	Axle 2
6	Battery State-of-Charge	Amp-Hrs.	0 - 6	8-Bit Digital	To Be Determined	5K	±4%	Axle 2	Axle 2
7-8	Battery Temp (2)	°C	-10° to +60°	Analog	0 - 5V	5K	±2%	Axle 2	Axle 2
9-15	Solar Array Temp. (7 Panels)	°C	20 to +110	Analog	0 - 5V	5K	±2%	Axle 3	Axle 2
16	+24V Converter Output	Volts	20 - 28	Analog	3 - 5V	5K	±1%	Axle 2	Axle 2
17	-12V Converter Output	Volts	8 - 16V	Analog	2 - 5V	5K	±1%	Axle 2	Axle 2
18	-6.3V Converter Output	Volts	3 - 9V	Analog	2 - 5V	5K	±1%	Axle 2	Axle 2
19	+4.0V Converter Output	Volts	3 - 5V	Analog	0 - 5V	5K	±1%	Axle 2	Axle 2
20	Array Stowed	-	-	Digital (1 Bit)	0 - 4V	5K	-	Axle 3	Axle 3
21	Array Deployed	-	-	Digital (1 Bit)	0 - 4V	5K	-	Axle 3	Axle 3

Battery voltage is to be telemetered at more than one point, so that cell short may be detected.

Following is a brief description of the telemetry circuitry required, with the exception of the Battery State-of-Charge Monitor discussed in another section.

- Unregulated Voltage

  The circuit shown in Figure II.3-53, will be used for expanded range monitoring. This circuit will have sufficient accuracy and resolution so that it will be possible to detect a shorted cell when information derived from this telemetry point is used in conjunction with telemetered voltage across two cells.

- Voltage across Two Storage Cells

  It is desired to determine whether all storage cells placed in series are sound. If a cell does short, careful ground command sequence would have to be followed to maintain regulated bus voltage at series regulator output.

  The telemetry point in question yields information concerning per-cell voltage, which is compared with the Unregulated Voltage; the latter should equal the per-cell voltage times the total number of storage cells in series, if all cells are operating properly.

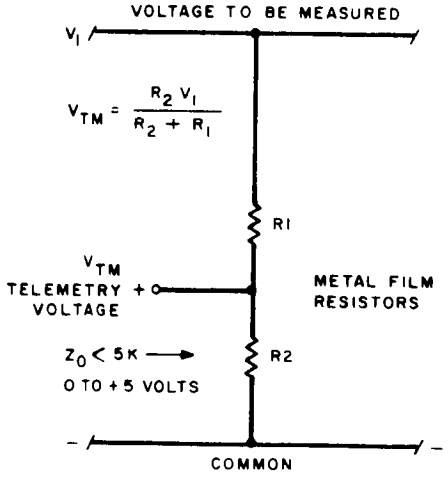

Figure II.3-52. Full Scale Voltage Telemetry Circuit

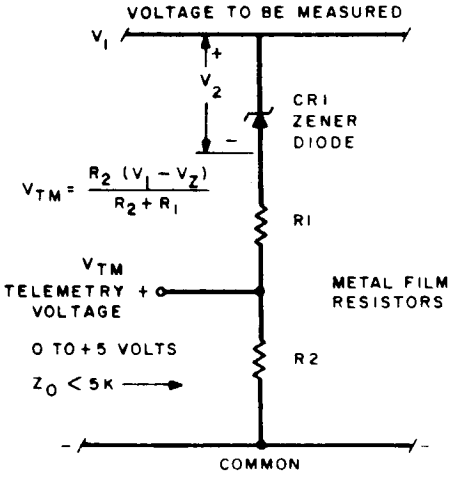

Figure II.3-53. Expanded Range (Offset) Voltage Telemetry Circuit

Since the voltage variations across 2 cells are within the required output voltage limits, they will be monitored directly. A resistor is used and is physically located

close to the battery to prevent catastrophic loss of these two cells in case the conductor to the telemetry input becomes shorted to ground. The maximum value for this resistor can be roughly 1% of the input impedance (i.e. 10K), commensurate with accuracy desired.

- Regulated Bus Voltages

  Expanded scale transducers may be required for the regulated bus voltages since it is desired to measure voltage over a relatively narrow range.

  The circuit of Figure II.3-53 is suitable for this application. It will give the desired accuracy if the range of voltages is narrow. It may be temperature compensated, if necessary.

- Solar Array Current Telemetry

  The Solar Array current will be telemetered by measuring and amplifying the voltage developed across a sensing resistor. Appropriate circuitry is shown in Figure II.3-54.

  This circuit has been operated in a similar application with temperature drift (worst case) of 3.2 mv/°C and expected 1 year drift (worst-case) of 2.2%. Typical temperature stability to be expected is 1.8 mv/°C. Linearity is typically ±2% (including effects of array voltage variations) and can be reduced to about 1% if required.

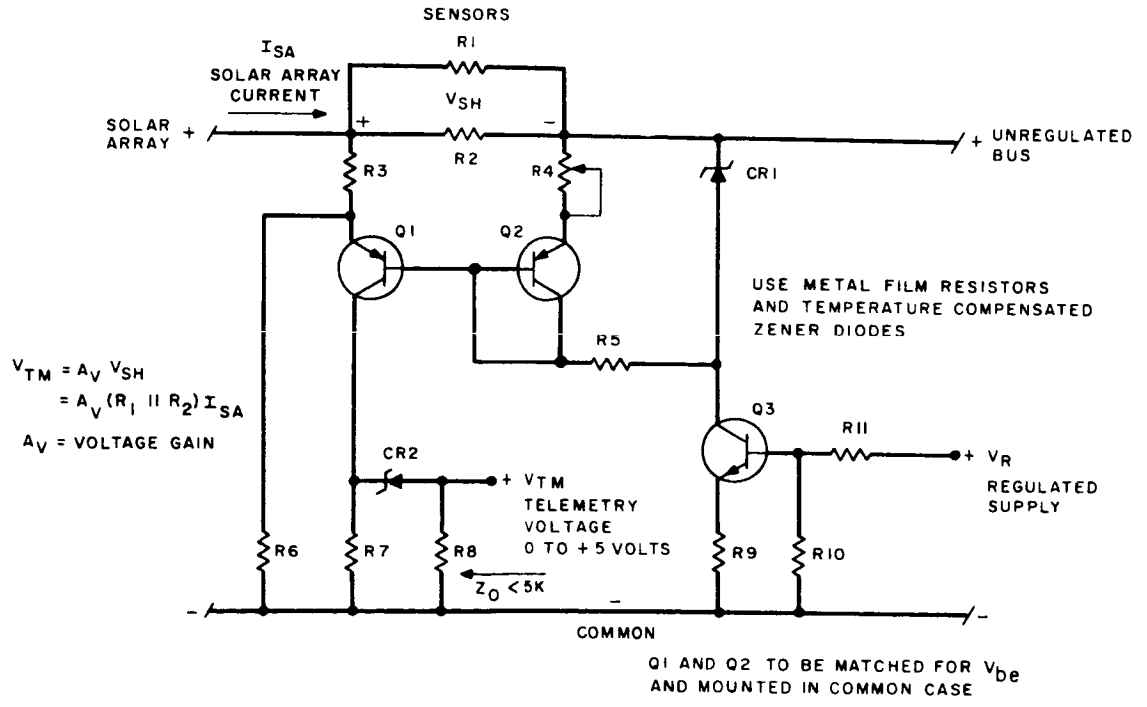

Figure II.3-54. Solar Array Current Telemetry

- Battery Current and Battery State-of-Charge

  These points will be determined by the Battery State-of-Charge Monitor. The ampere-hours state of charge information applied to the Telemetry Subsystem will be in the 8-bit digital form. Amperes battery current will be an analog voltage.

- Temperature Telemetry

  Temperature telemetry will be taken on the battery and solar array. The circuit of Figure II.3-55 will provide the nominal voltage output for the temperatures ranges encountered.

  Component values depend on the temperature range and voltage available. An offsetting circuit can be added, if the temperature range is small and expanded scale is desired.

- Rear Panel Erection Telemetry

  Limit switches will be provided to monitor position of the rear panel at either extreme (folded and erected).

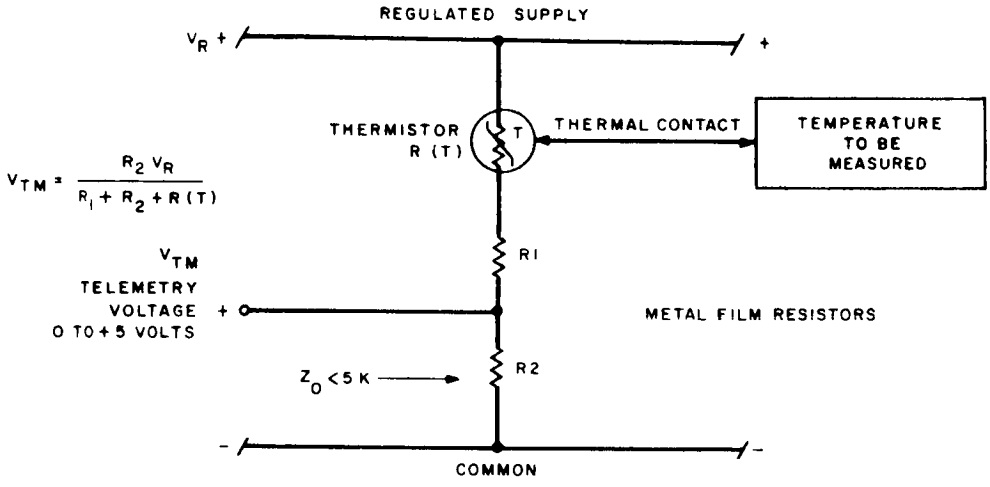

Figure II.3-55. Temperature Telemetry

9. Power Profile Analysis

Power Requirements

A. Charge Mode

Load to other S/S in Chge. Mode:	1.00 watts
	1.10 watts
	0.20 watts
	2.30 watts
plus state-of-charge Monitor	+0.105 watts
Telemetry (one point at each of 4 buses)	+0.046 watts
Total watts @ conv. output in charge	2.451 watts
Total standby loss in converter when in chge.	+2.170 watts
Total watts input to converter in "charge,"	4.621 watts
(Note that converter efficiency in Charge $\frac{2.451}{4.621}$ 100 = 53%)	
4.62w. @ +35V. Unreg. Bus Level,	0.132 a.
Telemetry other than conv. output voltages	0.041 a.
	0.173 amp.

B. Operate Mode

a. Standby

In addition to Charge Mode power of 2.451 watts, there are these outputs required @ converter:

	3.300 watts
	3.000 watts
	1.110 watts
	1.500 watts
	0.900 watts
	0.300 watts
Total converter output when in Operate,	12.561 watts
@ 75% converter off when in Operate,	16.750 watts

	Total pwr required @ series reg. in standby:	0.100 watts
		1.590 watts
		2.000 watts
	Total pwr to all required inputs, less series reg. T/M and series reg. shunt loss, when in Operate Standby	20.44 watts
	Assume that battery is in Discharge whenever in Operate; @ +25V, battery voltage,	0.819 amp.
	Series reg. shunt loss	0.025
	T/M other than conv. output voltages	0.041
	Total Sys. Current Drain when in Standby Op:	0.885 amp.
b.	Locomotion	
	20 watts @ +25V unreg.	0.8 amp.
	Standby Operate current	0.885 amp.
	Total Drain when in Locomotion	1.685 amp
c.	Steering	
	5.4 watts @ +25V unreg.	0.216 amp.
		+0.885 amp.
	Total when in Steering	1.101 amp.
d.	DIBSI	
	as before,	0.885 amp.
	plus: 0.5 w. @ +4V @ 75% off.	0.03 amp.
	5.0 w. @ +25V unreg	0.20 amp.
	Total	1.115 amp.
e.	TV	
	as before,	0.885 amp.
	plus: 12.5 w. @ +24V	0.521 amp.
	ave. of Az. Head and Sun Shield Peaks	0.450 amp.
	Total Drain when in TV	1.855 amp.

Operate Mode Profiles

Reference: pg VIII-5, 2nd Lunar Rover Monthly Progress Report

A. Guidance Step

a. Smooth Moon Integrated Profile

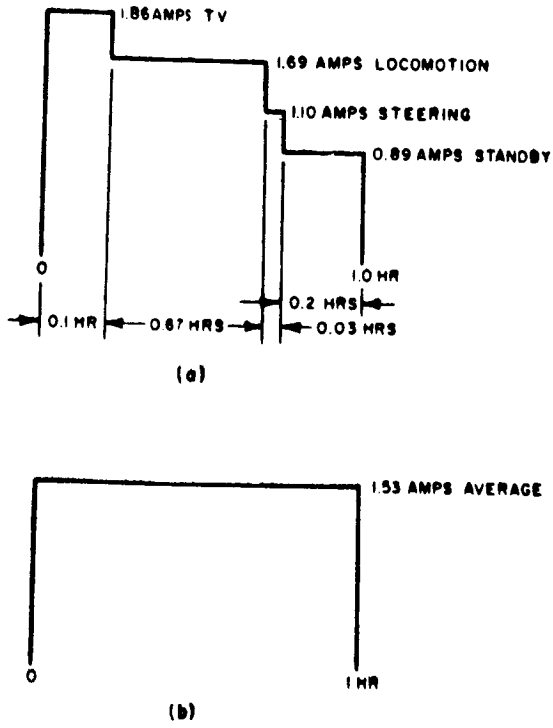

Figure II.3-56

b. Rough Moon Integrated Profile

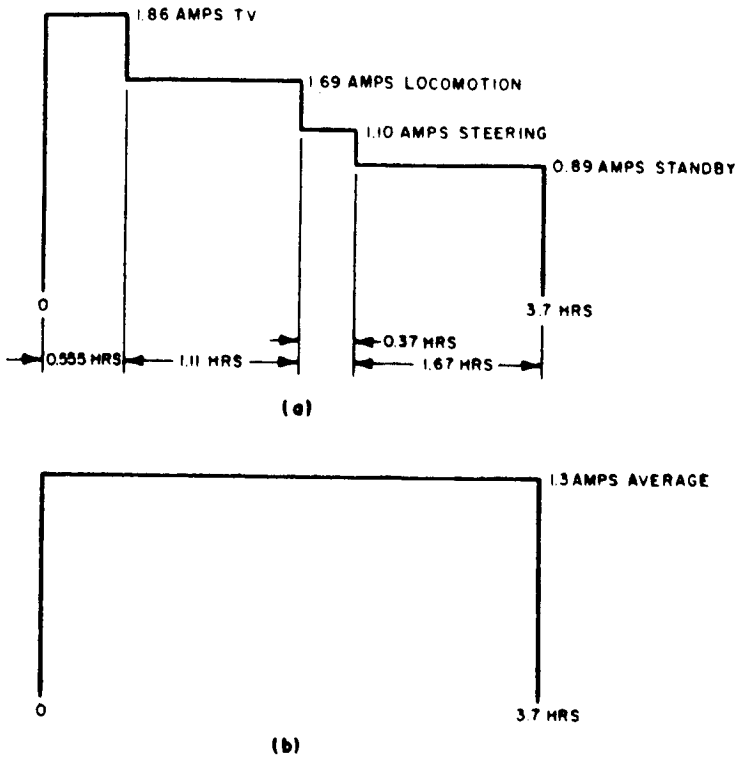

Figure II.3-57

c. Contour Mapping Step

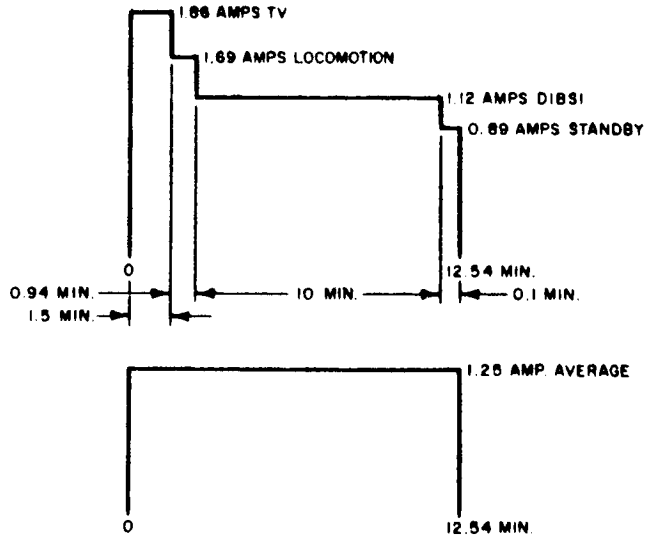

Figure II.3-58

Operation is assumed to consist of alternating Guidance and Contour Mapping Steps.

Smooth Moon Operate are current I_o:

$$\frac{1.53(60) + 1.25\ (12.54)}{60 + 12.54} = 1.48 \text{ amp.}$$

Rough Moon Operate are current I_o:

$$\frac{1.3(3.7)60 - 1.25(12.54)}{3.7(60) - 12.54} = 1.30 \text{ amp.}$$

10. Solar Array Capability and its Effect on Operate Time

During Charge, the Rover Vehicle will be oriented so as to expose maximum solar cell area to the sun; during operate, the exposed area will be an average over 360° azimuth rotation. The array output during Operate will be less than during Charge.

Figure II.3-59 shows the relationships between array outputs for both conditions and the Operate time duty cycle.

Let I_o = current drain when in Operate; this is 1.48 amp., Smooth Moon Ave. case.

I_c = current drain during charge or 0.173 amp.

i_s = ave. array current during Operate.

I_s = Array current during Charge.

T = Total hrs. Operate time per 24 hrs.

e_b = battery Ahr. charge-discharge efficiency factor (e_b = 0.95)

Condition of Amp-Hour Balance is defined by the following equation:

$$(I_o - i_s)T = (I_S - I_c)(24-T)\, e_b \qquad \text{(II.3-16)}$$

Solving for T,

$$T = \frac{24}{\dfrac{I_o - i_s}{(I_S - I_c)\, e_b} + 1} \qquad \text{(II.3-17)}$$

$$a \triangleq \frac{i_s}{I_S}$$

Substituting that and the numerical values into equation II.3-17.

$$T = \frac{24}{\frac{1.48 - a I_s}{(I_s - 0.173)0.95} + 1}$$

The last equation is plotted in Figure II.3-59 . The Operate time vs. elevation angle is plotted in Fig. II.3-60 ; it is based on the array capability only. Using plots of

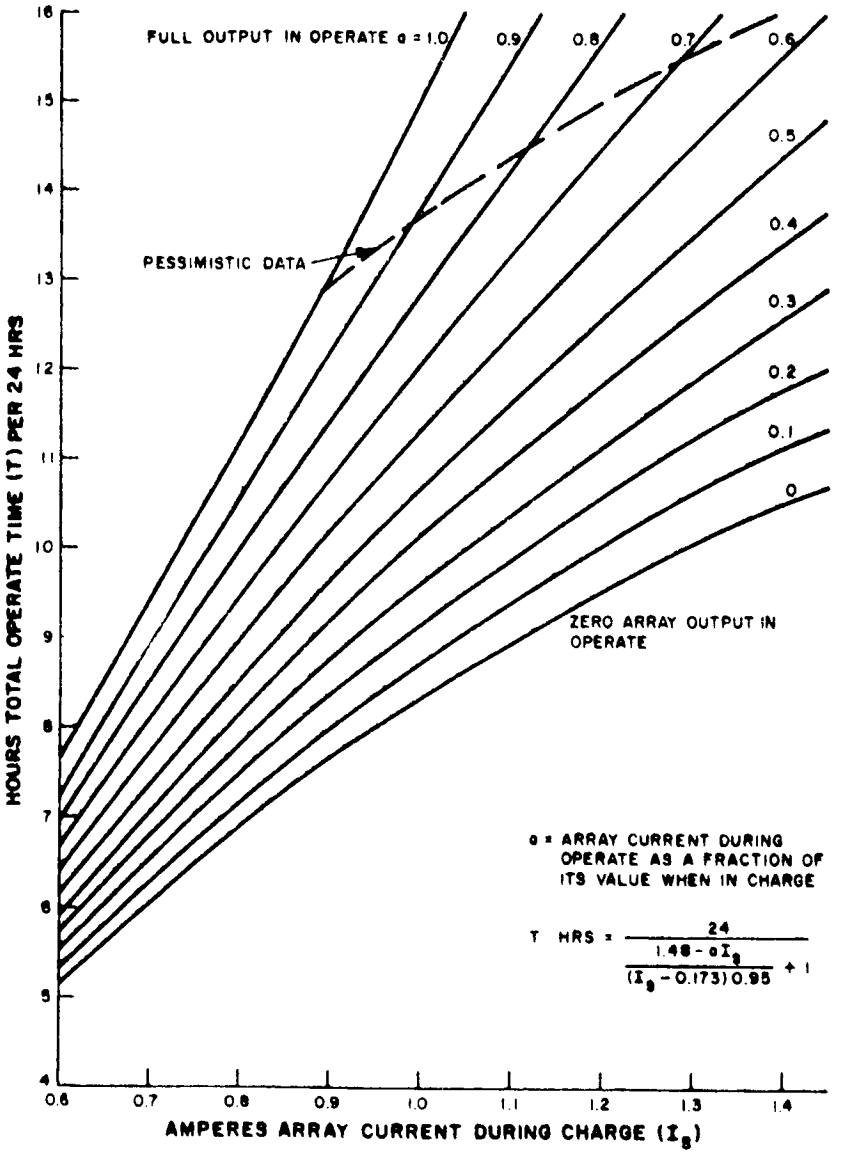

Figure II.3-59. Relationship Between Operate Time and Solar Array Capability

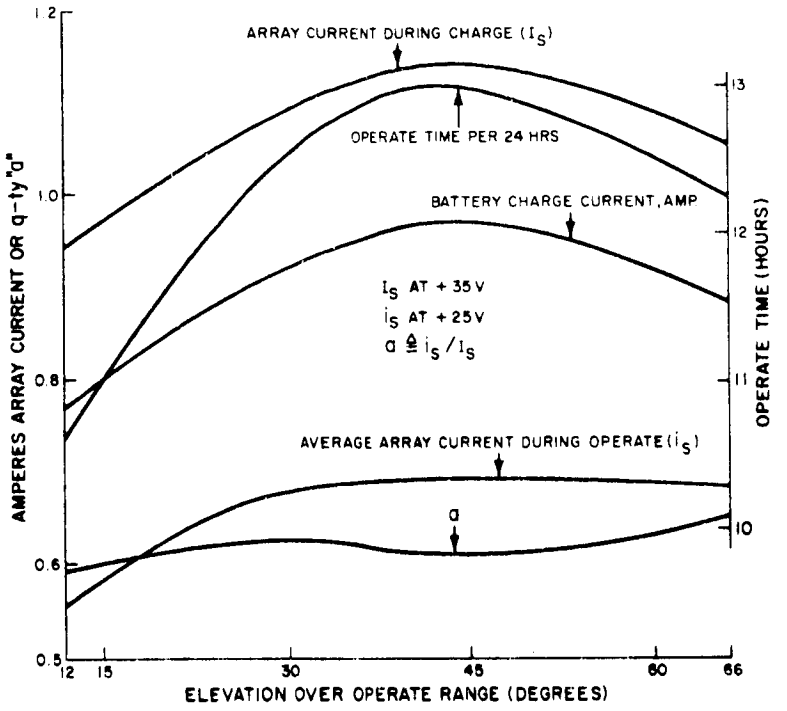

Figure II.3-60. Operate Time Duty Cycle and Array Output Current, SLRV

array output power included in Paragraph L.1, array current during charge and during Operate was computed. Following that, the current values were multiplied by a factor of 0.85 to include a 15% safety factor to account for the uncertainties discussed in an earlier section. The resulting array current values were plotted over the 12° to 66° working range of elevation angles.

This information and that of Figure II.3-59 permitted construction of a plot of Operate time (total per 24 hrs.) vs. the elevation angle. The battery capacity is not affected by either the total or the per-day operate time; operate time is a function only of the load requirements and the array capability.

It is evident from Figure II.3-60 that the fixed array configuration investigated has a capability of greater than ten hours Operate time per day. In fact, the plot of Operate time in Figure II.3-60 permits an estimate of the Operate time on a day-by-day basis as follows: (state of "1st day" is at sun elevation angle of 12°; a day is equivalent to 12° change in sun vector)

1st day	11.3 hrs Operate
2nd	12.4
3rd	12.9
4th	12.7
1/2-day following	6.2

Total Operate time possible first 4.5 days, 12° to 66° elev. angle 55.5 hours.

This amounts to 12.3 hrs. average per-day Operate time possible.

11. Phase II Program

The phase II effort will encompass the final and optimum design of the power system. Areas of anticipated investigation are briefly discussed below.

- Array Optimization

  The array will be designed following a search of the best array configuration for the mission. The present configuration is not necessarily an optimal one.

The interactions between the many facets of the array performance will be evaluated and optimized. The effects of layout (i.e. packing factor) on the thermal analysis will be found and these results used to further improve the layout.

A similar interdependence exists with the substrate, structure and solar cell problems. Indications are that some savings in weight can be effected in areas such as the substrate, cover glass weight, shingles, etc.

The investigation and analysis of all the individual and combined effects and problems will result in the optimum solar array from the standpoint of configuration, output, weight, and thermal considerations.

- Shingle Operating Voltage

  In the operation of a system employing a fixed solar array, many problems not applicable to an oriented configuration may arise. Two basic analytical approaches are to be considered.

  a) Maximum energy approach.

     The evaluation of the maximum energy output for a solar shingle becomes further complicated in this case by the different layouts for each solar panel, the different temperature-time profiles for each panel, the orientations of each panel, and the angle effect of non-normally incident solar illumination.

     It is within the realm of possibility that this approach will not result in an optimum or even workable system due to the many complicating factors which were not experienced in the straight-forward analysis of the orientable array.

  b) Tracking Maximum Power

     The analysis and evaluation of a device which tracks the solar-array-maximum-power point is also complicated by the fixed array configuration.

Investigations will be performed to determine the advantages (or disadvantages) of using a maximum-power-point-tracker during the charge-time and operate-time.

M. GENERAL

The information presented concerning the use of and general characteristics of an RTE takes due regard of the specific information presented by the Martin-Marietta Corp. In addition, their cooperation in providing this general information is appreciated.

1. Fuel

In view of the mission life, a short half-life isotope is suitable for this application. An isotope with a high thermal watt to weight ratio must be used if the weight of a radioisotope generator is to be competitive with other power systems (solar cells) and if it is to fit within the envelope dimensions dictated by the SLRV-Surveyor combination. For this generator either Polonium 210 or Curium 242 is suitable for the mission. Curium 242 is the first choice but Polonium 210 would be the back-up fuel in the event that unanticipated problems such as availability, high temperature problems, etc. occur. The reason Curium 242 is the first choice is that it has a half life somewhat greater than Polonium 210, 0.45 years compared to 0.38 years respectively.

2. Safety and Isotope Containment

To date all space flights which have used RTE power supply used an α emmiting isotope as the heat source. The capsule containing the isotope was inserted in the generator at the contractors' facility prior to shipment of the generator to the launch site. Hence, no special remote handling equipment or additional shielding other than that afforded by the capsule was required at the launch site.

The governing philosophy with regard to earth reentry for these flights was isotope burn-up. However, the fuel used for these flights was PU 238 which has a half life of 86 years.

For the SLRV mission the accepted philosophy, as stated by the Martin-Marietta Corp., is one of lunar containment and earth reentry containment. The capsule must be designed to contain the isotope in the event that the capsule impacts the moon's surface at a speed of approximately 7000 ft/sec. This velocity would occur if the Surveyor retro rocket failed to perform. It is this philosophy which governs at this time.

Safety testing is a continuing program and has no definite final performance characteristics associated with it. As such a cut-off time cannot be defined for this aspect of an RTE program. However, it is anticipated that minimum safety criteria will be met in time to meet the mission schedule.

Systems incorporating lead telluride conversion elements have been successfully tested for its safety aspects and as a result have been launched. However, a more attractive system incorporates silicon germanium conversion elements. This system requires

higher hot junction and capsule temperatures than lead telluride. These silicon-germanium RTE systems have not been safety tested nor have they been launched. However, the Nuclear Division of Martin-Marietta has been developing higher temperature capsules on the Snap 11 and SR-90 programs. This effort can be useful in developing a capsule to work with silicon-germanium conversion elements.

It is entirely possible to reduce the capsule temperature during earth-moon transit by several approaches. The use of multi-foil insulation in conjunction with an inert gas will reduce the capsule temperature from launch pad to lunar landing. RCA-AED is now developing an RTE which incorporates a multi-foil insulating technique which is a first step to this goal. Another approach is to provide additional radiator surface during transit which would be disconnected following lunar landing. Either of these approaches will reduce the capsule temperature during the non-operating part of the program. Hence, the time and effort required for capsule safety testing can be reduced.

3. Physical Characteristics

The envelope dimension within which the RTE unit must fit has been established by the SLRV-Surveyor constraints for stowage and lunar mobility. For this envelope the maximum size RTE which can be accomodated is one which has a raw power output of 30 watts for a lead telluride system and 50 watts for a silicon-germanium system. Associated with each of these systems is a heat rejection temperature of 350°F for lead telluride and 500°F for silicon-germanium system. The hot junction temperature is 1000°F and 1500°F respectively. The limitation on output is due to the radiator required to meet the SLRV-Surveyor envelope constraint. With a modification of DIBSI on the rear axle it may be possible to increase the maximum raw power output of an RTE by another 10%.

The weights of various parts of the RTE are summarized in Tables II.3-16, -17, -18 for different containment philosophies. These data have been supplied by Martin-Marietta, Nuclear Division. A summary of this information appears in Table II.3-19

The physical size and component weights of the RTE were based on electrical power output versus time shown in Figure II.3-61. The power flattening is accomplished by a heat dump door, whose opening is controlled by the hot junction temperature of the conversion elements.

As presently conceived sufficient isotopes will be provided to permit a 30-day slip of the launch window and permit sufficient time for checkout procedures.

TABLE II.3-16*

EARTH RE-ENTRY CONTAINMENT, LUNAR CONTAINMENT PHILOSOPHY

Parts	PbTe (30 watts)	SiGe (30 watts)	SiGe (50 watts)
Lunar impact protection	6.25 lbs	6.25 lbs	7.50 lbs
Ablative material	3.25	3.25	4.50
Radiator fins	4.00	3.00	4.00
Heat dump mechanism	1.50	1.50	1.50
Basic generator	5.50	5.00	5.50
Total	20.5 lbs	19.0 lbs	23.0 lbs

TABLE II.3-17 *

EARTH RE-ENTRY CONTAINMENT,
NO LUNAR RE-ENTRY CONTAINMENT PHILOSOPHY

Parts	PbTe (30 watts)	SiGe (30 watts)	SiGe (50 watts)
Lunar impact protection	1.0 lbs	1.0 lbs	1.25 lbs
Ablative material	2.0 lbs	2.0 lbs	2.5 lbs
Radiator	4.0 lbs	3.0 lbs	4.0 lbs
Heat dump mechanism	1.5 lbs	1.5 lbs	1.5 lbs
Basic generator	5.5 lbs	5.0 lbs	5.5 lbs
Total	14.0 lbs	12.5 lbs	14.8 lbs

* Does not include other Power Subsystem elements

TABLE II.3-18*

EARTH BURN-UP, NO LUNAR RE-ENTRY CONTAINMENT PHILOSOPHY

Parts	PbTe (30 watts)	SiGe (30 watts)	SiGe (50 watts)
Lunar inpact protection	0.5 lbs	0.5 lbs	0.75 lbs
Ablative material	0.5 lbs	0.5 lbs	1.0 lbs
Radiator	4.0 lbs	3.0 lbs	4.0 lbs
Heat dump mechanism	1.5 lbs	1.5 lbs	1.5 lbs
Basic generator	5.5 lbs	5.0 lbs	5.5 lbs
Total	12.0 lbs	10.5 lbs	12.3 lbs

TABLE II.3-19**

SUMMARY OF CONTAINMENT PHILOSOPHY

Containment Philosophy	PbTe (30 watts)	SiGe (30 watts)	SiGe (50 watts)
1 — Presently accepted philosophy (Earth containment, lunar containment)	1.4 watts/lb	1.55 watts/lb	2.1 watts/lb
2 — EARTH containment, no lunar containment	2.1 watts/lb	2.4 watts/lb	3.35 watts/lb
3 — EARTH burn-up, no lunar containment	2.5 watts/lb	2.85 watts/lb	4.0 watts/lb

* Does not include other Power Subsystem elements.

** Specific power on raw power output basis.

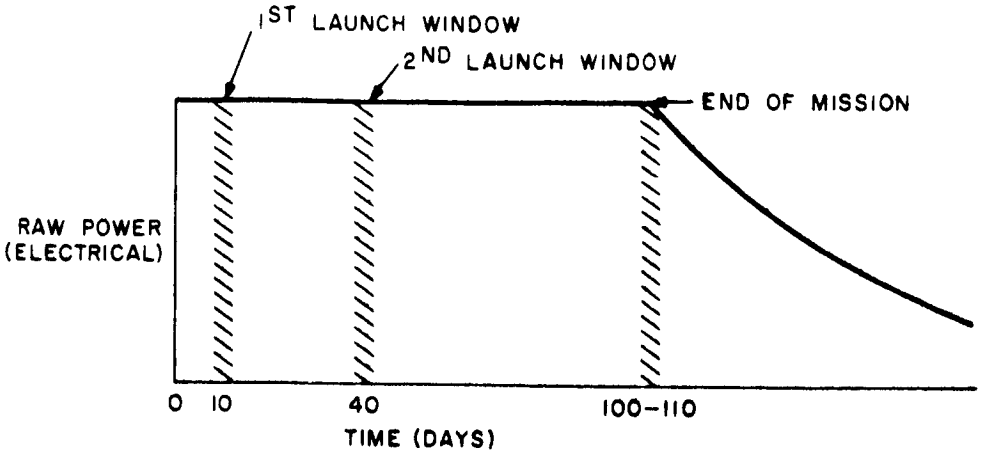

Figure II.3-61. Electrical Power Output vs. Time (RTE)

4. **Integration of an RTE**

An RTE power supply can be readily integrated into the SLRV vehicle. Its location on the rear axle will satisfy the dimensional envelope constraints imposed by stowage requirements on the SLRV for earth-moon transit and will satisfy lunar locomotion requirements imposed by the vehicle. Figure II.3-62 shows conceptually the RTE installation on the vehicle's rear axle.

During earth-moon transit the heat dump door will be in the open position viewing space. A thermal shield must be added to prevent heat rejection to the rear of the vehicle. If mounted on the SLRV, this shield must be removed prior to operation of the vehicle; if mounted on the surveyor, it may remain if it doesn't interfere with the surveyor operation. This will be investigated in Phase II.

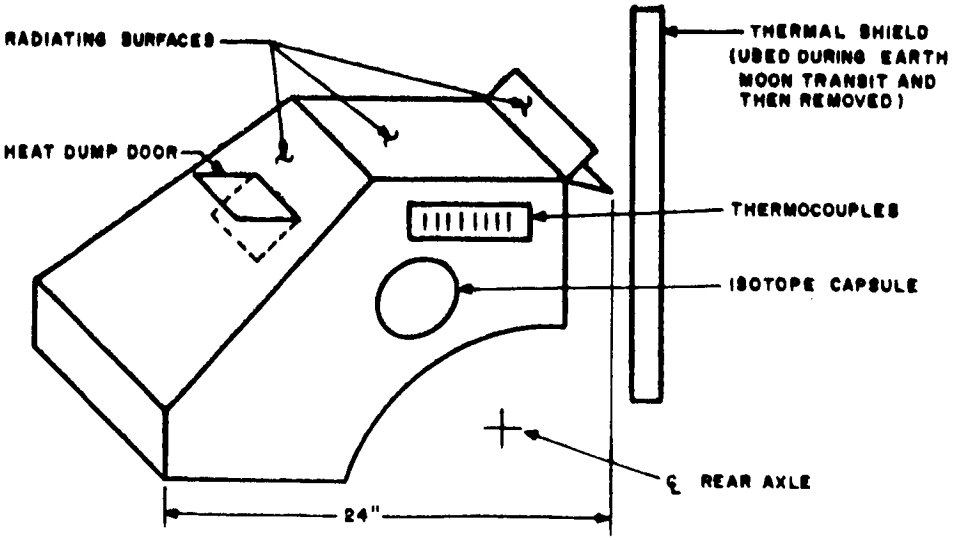

Figure II.3-62. Conceptual Configuration of an RTE

5. Schedule

An electrically heated prototype using a PbTe conversion system with a raw power output of 30 watts could be built and be ready for qualifications testing by September, 1965 if work started on this device by July, 1964.* The technology for this system is well advanced and as such the probability of meeting the required schedule is high.

An RTE incorporating a SiGe conversion system up to a 50-watt level could also be built and be ready for qualification testing by September, 1965 if work started by July, 1964. However, the technology for this system is not as far advanced as is the PbTe system due to the higher temperatures involved and to the limited experience on a SiGe conversion system. In view of this, a higher risk in meeting early launch schedules is involved than in the PbTe system. Reducing the capsule temperature during earth-moon transit (see Paragraph 2) will help to reduce the schedule risk.

6. Conclusions

In spite of the greater schedule risk which is involved by the use of SiGe thermocouples it is concluded that an RTE should incorporate this type of conversion device. The weight of such a unit will be less than one incorporating PbTe conversion elements and growth potential (to 50 watts) is available. This conclusion does not include cost as a factor.

III.12.7 Preliminary Requirements for an RTE

A document was prepared stating the preliminary requirements for an RTG. These requirements resulted from a study comparing solar-cell battery power supply performance with an RTE power supply. This document appears at the end of this section. The document has been issued to JPL in order to determine the feasibility for developing an RTE with the characteristics described within the time schedule of interest.

* The September 1965 date was derived from a scheduled launch date of early 1966.

N. PRELIMINARY REQUIREMENTS FOR AN RTE

1. General

Component Parts

For this document, the component parts of an RTE consist of the fuel (radioisotope), capsule, shielding (if required), thermocouple modules, insulation, radiator and the necessary structural members required to assemble the component parts into a single operating power source subsystem.

Operational Concept

The RTE will supply the power and energy required to a power conditioning subsystem, a storage subsystem, a power distribution subsystem and loads.

2. Power Output

Average Power

The average power developed by the RTE at the design voltage, V_D, and for the duration of the mission is shown as a function of weight in Figure II.3-63.

Power Profile

The output power profile for the RTE is permitted to vary during the mission life in a manner shown in Figure II.3-64, Curve A or may be an essentially constant power output as shown in Figure II.3-64, Curve B. The output power shown in Figure II.3-64 is at the design voltage, V_D, which corresponds to points 1, 2, and 3 on the I-V curves shown in Figure II.3-65.

Design Voltage

The design voltage, V_D, is specified as the voltage at the maximum power point at mid-life. For the purpose of this preliminary specification, mid-life occurs at the end of 1 month of mission life. The design voltage is shown on the I-V curves

of Figure II.3-65. These I-V curves correspond to the variations expected for Curve A, Figure II.3-64.

3. Weight

For an average power output from the RTE a corresponding weight is shown in the graph of Figure II.3-63. The weight of the RTE must include all component parts itemized in paragraph 1.

4. Volume

The size of an RTE unit must fit into the envelope dimensions shown in Figure II.3-66. The horizontal projected area is nominally 400 in^2.

5. Life Requirements

The mission life shall be 2 months. Due to considerations of capsule loading, launch pad time requirements and transit time approximately 1.5 months shall be added to mission life to establish the life requirements of the RTE. This is a total of 3.5 months.

6. Mission Constraints

Temperature Tolerance

For operating conditions, the radiating surface and direction of radiation of the RTE is shown in Figure II.3-67. It is not expected that the temperature of the radiating surface will adversely affect SLRV components if the rejected heat is dissipated as shown.

During the transit phase to the moon, additional radiating surfaces can be added to the operational RTE radiator to maintain a safe temperature for the RTE components.

A suitable means can be developed to maintain a safe temperature for the RTE components on the launch pad.

Nuclear Radiation Tolerance

The maximum permitted dosage at Surface A in Figure 5 shall be 10^6 rads over the life requirements of the SLRV. It can be assumed that 1/16 of aluminum will be used to enclose the electronic components in its compartment.

Environmental Requirements

The vibration and shock loads for the RTE are as specified by the Surveyor Spacecraft.(1) It is expected that the radioisotope capsule safety test program will subject the capsule to conditions well in excess of the loads imposed on the RTE by the SLRV mission. The remaining components of the RTE will be tested in accordance to the referenced document.(1)

Lunar operation will impose on the RTE shock and vibration loads below that which is imposed on the RTE by the Surveyor Spacecraft.

Lunar-Night Operation

It is not anticipated that the rejected heat from the RTE will be used as a heat source during lunar night. However, the electrical power which can be generated by the RTE may be used for compartment heating. This requirement is of secondary importance.

7. Schedule

The number of RTE units required and delivery dates are outlined below.

4 Engineering test models (unqualified — April 1965)

°2 mechanical models

---

(1) Hughes Aircraft Company, Specification No. 239503, Rev. C, Surveyor Basic Bus (2100 pounds) Payload Interface Requirements and Spacecraft Description, 20 November 1963.

*1 Electrical model

*1 Thermal model

*2 Prototypes - September 1965

1 Flight Model - April 1966

Remaining Flight Models at 2 months intervals

to a maximum of 12 total flight units.

*Electrically heated capsules are required for these items.

°No electrical power output is required for these items.

Units and components required for safety program, reliability testing and spares are not included in the above listing at this time.

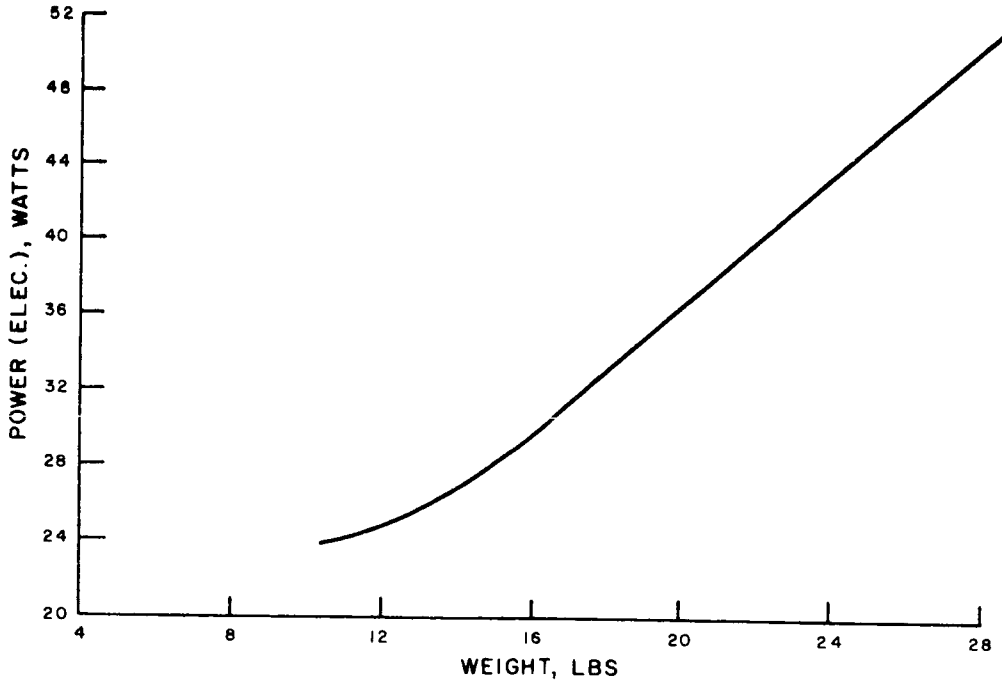

Figure II.3-63. RTE Electrical Power Output vs weight

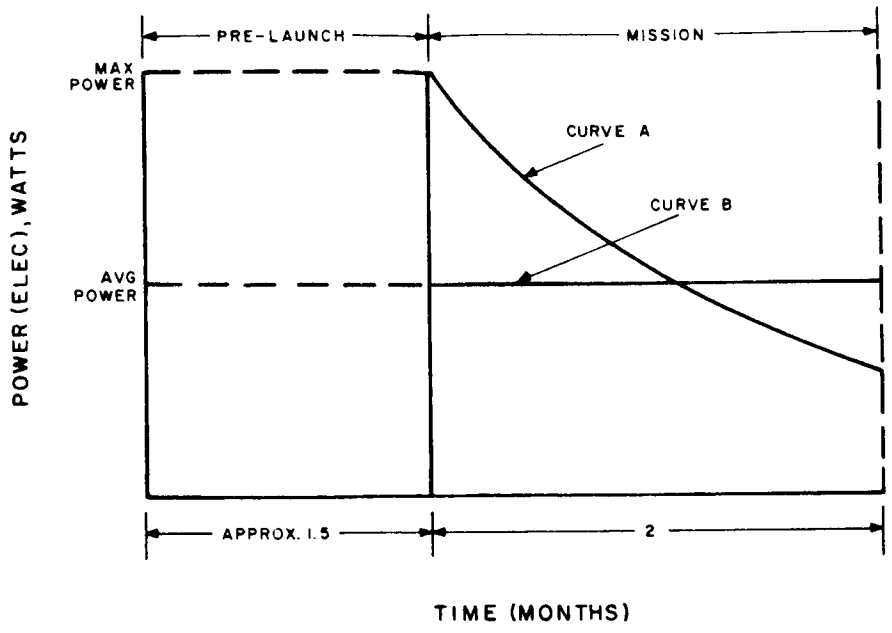

Figure II.3-64. Electrical Power Output vs weight

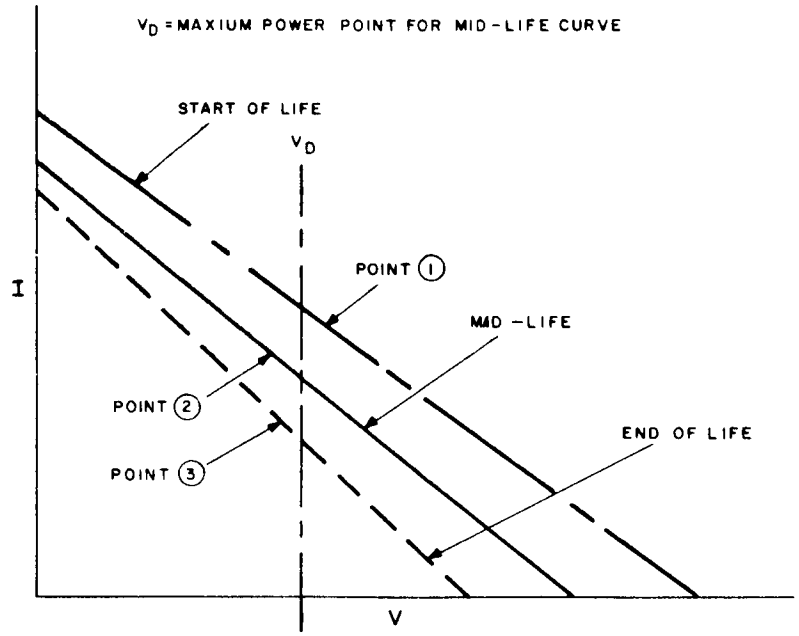

Figure II.3-65. I-V Curves where Power Output Varies with Time

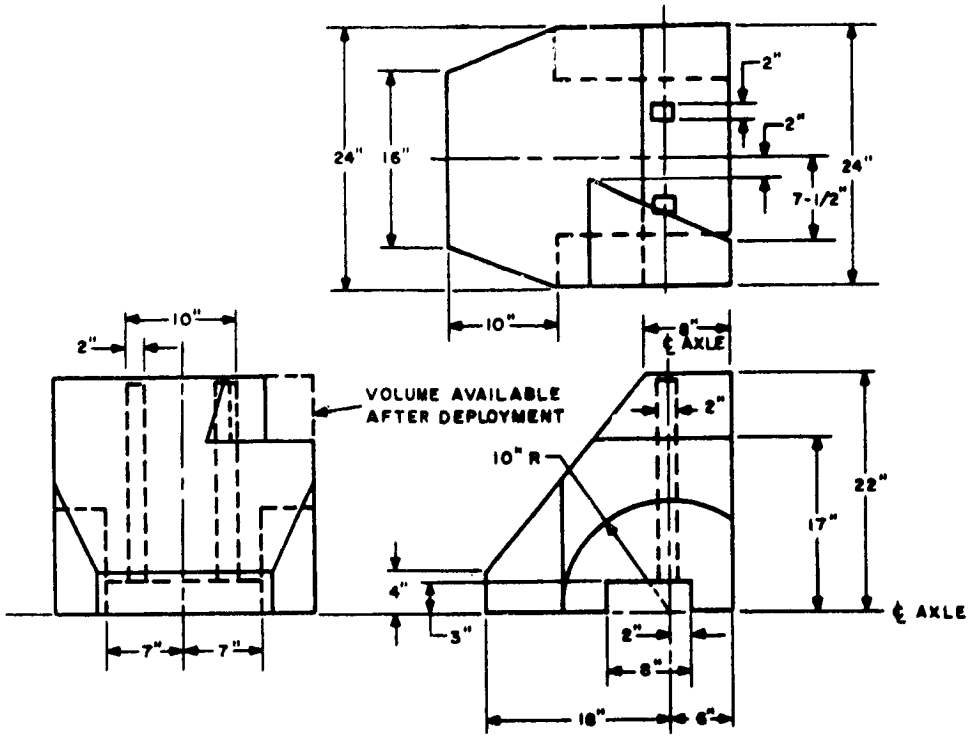

Figure II.3-66. RTE Envelope Dimensions

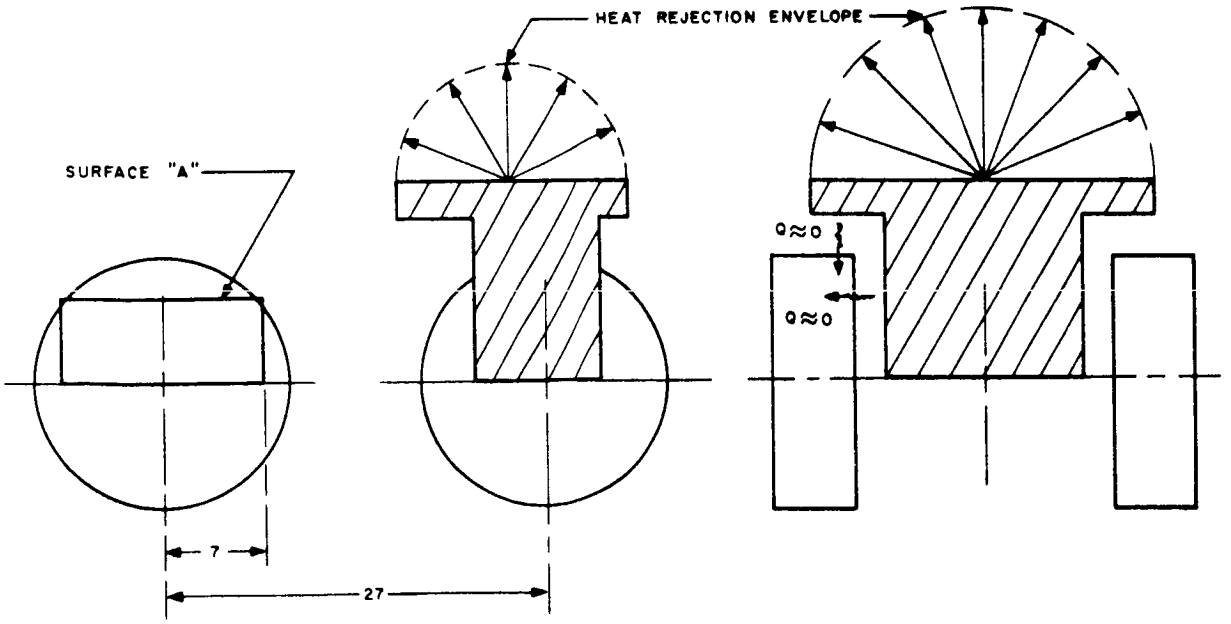

Figure II.3-67. Pictoral Representation of an RTE

TR64-26

O. RTI

A review of power supplies for the SLRV mission indicated that an RTI system is worthy of study. On the surface, it has many advantages which look very attractive. It is inherently a low weight and small volume device and the high temperature associated with its operation requires a comparatively small radiator. However, the associated equipment required, such as the DC to DC converter may weigh as much as 12 lbs for reasonable efficiency (70%) at the power levels required by the SLRV mission. In addition its high-temperature operation, normally an advantage, creates many problems with regard to isotope, capsule, and materials. The experience on the SNAP 13A device bears this out.

A number of vendors namely, Martin-Marietta Corp. and General Atomics were contacted to supply specific information with regard to operating characteristics, physical characteristics and schedules for an RTI. In both cases, the opinion was that there is no advantage to this system over an RTE on a weight basis and it does not look promising on a system basis at these power levels. Further, it is out of the question with regard to the time schedules of interest.

As a result of this investigation it is recommended that this system be discarded for this mission.

APPENDIX IV
TELEMETRY SUBSYSTEM

APPENDIX IV
TELEMETRY SUBSYSTEM

A. TELEMETRY DATA REQUIREMENTS

The telemetry data requirements for the SLRV have been finalized. These requirements have been distributed among the three axles and detailed listings are shown in Tables II.4-1, II.4-2 and II.4-3 for the front, center, and rear axles respectively.

TABLE II.4-1

AXLE NO. 1 (FRONT)

Item	Function	Units	Range	Form	*Expected Volts To Telemetry	Required Sampling Rate	Required Accuracy	Bits Per Sample Required	Analog Channels	Digital Bits	Remarks
A1	Drive Motor #1 Current	amps.	0-500ma	analog	0-5V	1 per 2 sec.	±20%	3-4	1	---	Possible transducer problem due to high current requirement. Signal processor required. Low priority.
A2	Wheel Housing #1 Pressure	psi	0-5psi	digital	0-4V	extremely low	presence	---	---	1	High priority - questionable as to where pressure threshold will be set.
A3	Wheel Housing #1 Temperature	°C	100°C - 200°C	analog	0-5V	1 per 2 sec.	±10%	4-5	1	---	Temperature range may present a transducer problem.
A4	Drive Motor #2 Current	amps.	0-500ma	analog	0-5V	1 per 2 sec.	±20%	3-4	1	---	Possible transducer problem due to high current requirement. Signal processor required. Low priority.
A5	Wheel Housing #2 Pressure	psi	0-5psi	digital	0-4V	extremely low	presence	---	---	1	High priority - questionable as to where pressure threshold will be set.
A6	Wheel Housing #2 Temperature	°C	100°C - 200°C	analog	0-5V	1 per 2 sec.	±10%	4-5	1	---	Temperature range may present a transducer problem.
A7	Radioisotope Heating Pellet Position (Electronics Compartment)	in or out	---	digital	0-4V	extremely low	---	---	---	1	Importance depends on power supply choice. If RTG is used, a heater resistor may be required.
A8	Axle #1 Steering Position	deg.	-30° to +30°	analog	0-5V	1 per 2 sec.	discrete steps at 7.5° per step	4-5	1	---	Desirable for operator display. Could be simultaneously displayed or telemetered with rear axle steering.
A9	Steering Motor Pressure	psi	0-5psi	digital	0-4V	extremely low	presence	---	---	1	High priority - questionable as to where pressure threshold will be set.
A10	Steering Motor Temperature	°C	100°C - 200°C	analog	0-5V	1 per 2 sec.	±10%	4-5	1	---	Temperature range may present a transducer problem.
A11	Clinometer Data (Roll)	deg.	-45° to +45°	digital	0-4V	1 per 2 sec.	±0.1%	---	---	20	High precision - low response when stopped. Low precision - high response in motion. High priority - information necessary when TV pictures are taken.

TABLE II. 4-1 (Continued)

AXLE NO. 1 (FRONT)

Item	Function	Units	Range	Form	*Expected Volts To Telemetry	Required Sampling Rate	Required Accuracy	Bits Per Sample Required	Analog Channels	Digital Bits	Remarks
A12	Clinometer Data (Pitch)	deg.	-45° to +45°	digital	0-4V	1 per 2 sec.	±0.1%	---	---	20	Same as above for A11.
A13	Sun Azimuth Angle	deg.	0-120° (on each of three sensors)	digital	0-4V	1 per 2 sec.	0.1 to 0.5°	---	---	10	Operator display desirable. Should be sampled at same time as clinometer and odometer. Part of TV telemetry. Only sampled when stopped.
A14	Vidicon Faceplate Temperature	°C	0-100° C	analog	0-5V	greater than 10 sec.	±5%	5-6	1	---	Engineer display for sensing dangerous condition.
A15	TV Regulated Voltage Input	volts	24V ±1%	analog	0-5V	low	±1.0%	10	1	---	Low priority - may be monitored on output of power supply regulator.
A16	TV System Current Drain	ma.	0-500ma	analog	0-5V	low	±10%	4-5	1	---	High priority. TV only.
A17	TV Camera Azimuth Angle	deg.	0-360°	analog	0-5V	low	±1%	6-7	1	---	High priority - may be monitored digitally if steps are discrete. TV only.
A18	TV Camera Sun Shutter	aper. size	0-1 inch	digital	0-4V	low	--	3-4	---	5	Questionable as to the type of iris control used. TV only.
A19	Vidicon High Voltage	volts	0-500V	analog	0-5V	low	±10%	4-5	1	---	Necessary - TV only.
A20	Vidicon Incident Light	foot lamberts	100 - 2400	analog	0-5V	low	±10%	4-5	1	---	Not determined to be in system yet. TV only.
A21	Axle #1 Compartment Temperature (A)	°C	0-100° C	analog	0-5V	low	±5%	5-6	1	---	Necessary.
A22	Axle #1 Compartment Temperature (B)	°C	0-100° C	analog	0-5V	low	±5%	5-6	1	---	Same as above in A21.
A23	Axle #1 Compartment Temperature (C)	°C	0-100°C	analog	0-5V	low	±5%	5-6	1	---	Same as above in A21.

*If voltage inputs are less than shown in this column, some degradation in transfer accuracy will result.

TABLE II. 4-1 (Continued)

AXLE NO. 1 (FRONT)

Item	Function	Units	Range	Form	*Expected Volts To Telemetry	Required Sampling Rate	Required Accuracy	Bits Per Sample Required	Analog Channels	Digital Bits	Remarks
A24	Command Verification	---	---	digital	0-4V	1 per 1/2 sec	---	---	---	20	The number of digital bits shown is a maximum. Desirable for operator display.
A25	TV Camera Elevation	up or down	---	digital	0-4V	low	---	---	---	1	Low priority - TV only.
A26	Vidicon Filament Voltage	volts	0-10V	analog	0-5V	low	±10%	4-5	1	---	Necessary.
A27	Thermal Controller Switches	open or closed	---	digital	0-4V	low	---	---	---	4	Low priority - number of the thermal switches to be established.
A28	TV Mast Limit Switch	on or off	---	digital	0-4V	low	---	---	---	1	

*If voltage inputs are less than shown in this column, some degradation in transfer accuracy will result.

TABLE II. 4-2

AXLE NO. 2 (CENTRAL)

Item	Function	Units	Range	Form	*Expected Volts To Telemetry	Required Sampling Rate	Required Accuracy	Bits Per Sample Required	Analog Channels	Digital Bits	Remarks
B1	Drive Motor #3 Current	amps.	0-500ma	analog	0-5V	1 per 2 sec.	±20%	3-4	1	---	Possible transducer problem due to high current requirement. Signal processor required. Low priority.
B2	Wheel Housing #3 Pressure	psi	0-5psi	digital	0-4V	extremely low	presence	---	---	1	High priority - questionable as to where pressure threshold will be set.
B3	Wheel Housing #3 Temperature	°C	100°C - 200°C	analog	0-5V	1 per 2 sec.	±10%	4-5	1	---	Temperature range may present a transducer problem.
B4	Drive Motor #4 Current	amps.	0-500ma	analog	0-5V	1 per 2 sec.	±20%	3-4	1	---	Possible transducer problem due to high current requirement. Signal processor required. Low priority.
B5	Wheel Housing #4 Temperature	°C	100°C - 200°C	analog	0-5V	1 per 2 sec.	±10%	4-5	1	---	Temperature range may present a transducer problem.
B6	Wheel Housing #4 Pressure	psi	0-5psi	digital	0-4V	extremely low	presence	---	---	1	High priority - questionable as to where pressure threshold will be set.
B7	Wheel #3 Clutch Position	in or out	---	digital	0-4V	low	---	---	---	1	Necessary.
B8	Wheel #4 Clutch Position	in or out	---	digital	0-4V	low	---	---	---	1	Necessary.
B9	Wheel #3 Rotation	revo-lutions	---	digital	0-4V	low	---	---	---	1	May require a counter for more accurate resolution.
B10	Wheel #4 Rotation	revo-lutions	---	digital	0-4V	low	---	---	---	1	Same as above in B9.
B11	Zero Volts Telemetry Calibration	volts	0V	analog	0V	low	0.5%	10	1	---	Necessary for data reduction.
B12	Full Scale Telemetry Calibration	volts	5V	analog	5V	low	0.5%	10	1	---	Necessary for data reduction.
B13	Radioisotope Heating Pellet Position (Electronics Compartment)	in or out	---	digital	0-4V	extremely low	---	---	---	1	Importance depends on power supply choice. If RTG is used, a heater resistor may be required.

*If voltage inputs are less than shown in this column, some degradation in transfer accuracy will result.

TABLE II. 4-2 (Continued)

AXLE NO. 2 (CENTRAL)

Item	Function	Units	Range	Form	*Expected Volts To Telemetry	Required Sampling Rate	Required Accuracy	Bits Per Sample Required	Analog Channels	Digital Bits	Remarks
B14	Axle No. 2 Compartment Temperature (A)	°C	0-100°C	analog	0-5V	low	±5%	5-6	1	---	Necessary.
B15	Axle #2 Compartment Temperature (B)	°C	0-100°C	analog	0-5V	low	±5%	5-6	1	---	Same as above in B14.
B16	Axle #2 Compartment Temperature (C)	°C	0-100°C	analog	0-5V	low	±5%	5-6	1	---	Same as above in B14.
B17	Receiver AGC (VHF)	volts	0-1V	analog	0-5V	low	±5%	5-6	1	---	High priority.
B18	Transmitter P.A. Voltage (VHF)	volts	0-300V	analog	0-5V	low	±5%	5-6	1	---	Low priority.
B19	Transmitter Output Power (VHF)	watts	0-2W	analog	0-5V	low	±20%	3-4	1	---	Necessary.
B20	Battery Temperature	°C	0-50°C	analog	0-5V	low	±5%	5-6	1	---	There is a possibility that more channels will be required for this measurement. High priority.
B21	Battery Voltage	volts	22 - 30V	analog	0-5V	low	±5%	5-6	1	---	High priority.
B22	Battery Charge Current	amps.	0-1.5 amp.	analog	0-5V	low	±5%	5-6	1	---	High priority.
B23	Battery Pressure	psi	0-10psi	analog	0-5V	low	±5%	5-6	1	---	High priority.
B24	Total Battery Current Drain	amps.	0-5 a	analog	0-5V	low	±5%	5-6	1	---	High priority
B25	Command Verification	---	---	digital	0-4V	1 per 1/2 sec.	---	---	---	44	Number of bits shown is a maximum and includes center and rear axle commands.
B26	Total Regulated Current	amps.	0-2a	analog	0-5V	low	±5%	5-6	1	---	High priority.
B27	DC to DC Converter for RTG	---	---	analog	0-5V	low	(?)	(?)	3	---	Not necessary if solar panels are used.
B28	Thermal Controller Switches	open or closed	---	digital	0-4V	low	---	---	---	6	Low priority.

*If voltage inputs are less than shown in this column, some degradation in transfer accuracy will result.

TABLE II. 4-1 (Continued)

AXLE NO. 2 (CENTRAL)

Item	Function	Units	Range	Form	*Expected Volts To Telemetry	Required Sampling Rate	Required Accuracy	Bits Per Sample Required	Analog Channels	Digital Bits	Remarks
B29	Instruction Error Flip Flop	set or reset	---	digital	0-4V	1 per 1/2 sec.	---	---	---	1	Low priority.
B30	Emergency Stop Flip Flop	set or reset	---	digital	0-4V	1 per 1/2 sec.	---	---	---	2	Low priority.
B31	Address Storage Flip Flop	set or reset	---	digital	0-4V	1 per 1/2 sec.	---	---	---	1	Low priority.
B32	Instruction Register	---	---	digital	0-4V	1 per 1/2 sec.	---	---	---	5	Low priority.
B33	Instruction Bit Counter	---	---	digital	0-4V	1 per 1/2 sec.	---	---	---	5	Low priority.
B34	SLRV Identification	---	---	digital	0-4V	1 per 1/2 sec.	---	---	---	1	Low priority.
B35	Regulated Voltage Output	volts	23-25V	analog	0-5V	low	±0.5%	8-9	1	---	High priority.
B36	Regulated Voltage Output	volts	(6-7V) pos.	analog	0-5V	low	±0.5%	8-9	1	---	High priority.
B37	Regulated Voltage Output	volts	(6-7V) neg.	analog	0-5V	low	±0.5%	8-9	1	---	High priority.
B38	VHF Antenna Erected and Locked	---	---	digital	0-4V	low	---	---	---	1	Low priority.

*If voltage inputs are less than shown in this column, some degradation in transfer accuracy will result.

TABLE II.4-3

AXLE NO. 3 (REAR)

Item	Function	Units	Range	Form	*Expected Volts To Telemetry	Required Sampling Rate	Required Accuracy	Bits Per Sample Required	Analog Channels	Digital Bits	Remarks
C1	Drive Motor #5 Current	amps.	0-500ma	analog	0-5V	1 per 2 sec.	±20%	3-4	1	---	Possible transducer problem due to** high current requirements. Special processor required. Low priority.
C2	Wheel Housing #5 Pressure	psi.	0-5psi	digital	0-4V	extremely low	presence	---	---	1	High priority - questionable as to where pressure threshold will be set.
C3	Wheel Housing #5 Temperature	°C	100°C - 200°C	analog	0-5V	1 per 2 sec.	±10%	4-5	1	---	Temperature range may present a transducer problem.
C4	Drive Motor #6 Current	amps.	0-500ma	analog	0-5V	1 per 2 sec.	±20%	3-4	1	---	Possible transducer problem due to** high current requirements. Signal processor required. Low priority.
C5	Wheel Housing #6 Pressure	psi	0-5psi	digital	0-4V	extremely low	presence	---	---	1	High priority - questionable as to where pressure threshold will be set.
C6	Wheel Housing #6 Temperature	°C	100°C - 200°C	analog	0-5V	1 per 2 sec.	±10%	4-5	1	---	Temperature range may present a transducer problem.
C7	Axle #3 Steering Position	deg.	-30° to +30°	analog	0-5V	1 per 2 sec.	discrete steps at 7.5° per step	4-5	1	---	Desirable for operator display. Could be simultaneously displayed or telemetered with front axle steering.
C8	Steering Motor Temperature	°C	100°C - 200°C	analog	0-5V	1 per 2 sec.	±10%	4-5	1	---	Temperature range may present a transducer problem.
C9	Steering Motor Pressure	psi	0-5psi	digital	0-4V	extremely low	presence	---	---	1	High priority - questionable as to where pressure threshold will be set.
C10	Solar Panel Temperature (A) or Radiator Temperature on RTG	°C	(?)	analog	0-5V	low	±10%	4-5	1	---	Temperature range may present a transducer problem.
C11	Solar Panel Temperature (B) or Radiator Temperature on RTG	°C	(?)	analog	0-5V	low	±10%	4-5	1	---	Same as above in C10.
C12	Solar panel elevation	deg.	0-90	analog	0-5V	low	±10%	4-5	1	---	Not needed if RTG is used.

*If voltage inputs are less than shown in this column, some degradation in transfer accuracy will result.
**Denotes could be monitored on central axle.

TABLE II.4-3 (Continued)

AXLE NO. 3 (REAR)

Item	Function	Units	Range	Form	Expected Volts To Telemetry	* Expected Sampling Rate	Required Accuracy	Bits Per Sample Required	Analog Channels	Digital Bits	Remarks
C13	DIBSI drive motor current	amps.	0-250ma	analog	0-5V	1 per 2 sec.	±20%	3-4	1	---	Will be monitored on central** axle for both motors. DIBSI only.
C14	DIBSI displacement (A)	cm	0-50cm	analog	0-5V	( )	±5%	5-6	1	---	Necessary - DIBSI only.
C15	DIBSI displacement (B)	cm	0-50cm	analog	0-5V	( )	±5%	5-6	1	---	Necessary - DIBSI only.
C16	DIBSI temperature (A)	°C	-100° to +250° C	analog	0-5V	low	±5%	5-6	1	---	Necessary for transducer calibration - May present transducer problem. DIBSI only
C17	DIBSI temperature (B)	°C	-100° to +250° C	analog	0-5V	low	±5%	5-6	1	---	Necessary for transducer calibration - May present transducer problem. DIBSI only
C18	DIBSI limit switch (A)	on or off	(?)	digital	0-4V	low	---	---	---	1	Low priority - may be in emergency stop operation. DIBSI only.
C19	DIBSI limit switch (B)	on or off	(?)	digital	0-4V	low	---	---	---	1	Low priority - may be in emergency stop operation. DIBSI only.

*If voltage inputs are less than shown in this column, some degradation in transducer accuracy will result.
**Denotes could be monitored on central axle.

TR64-26

B. SUMMARY OF TELEMETRY REQUIREMENTS

A summary of the telemetry requirements for the SLRV are shown in Table II.4-4.

TABLE II.4-4

SUMMARY OF TELEMETRY REQUIREMENTS

(Exclusive of DIBSI Force and Acceleration Experiments)*

Analog Channels		Digital Bits	
Axle No. 1	16	Axle No. 1	85
Axle No. 2	24	Axle No. 2	73
Axle No. 3	14	Axle No. 3	5
Total	54	Total	163

Interaxle Telemetry Wiring Requirements

No electronics compartment on 3rd axle				With electronics compartment on 3rd axle	
Axle No. 1 to Axle No. 2		Axle No. 2 to Axle No. 3			
Power for Telemetry	5 leads	Telemetry data	16 leads	Telemetry data	2
Timing for Telemetry	2	Ground lead	1	Timing	2
Telemetry Serial Output	3	Prime DIBSI Exp.	2	DIBSI Output (Prime)	2
				Power	5
Total	10 leads	Total	19 leads	Total	11

*DIBSI force and acceleration experiments will be transmitted separately on two subcarriers; one subcarrier for force and one for acceleration. The number of subcarriers may be reduced to one by placing the force experiment directly on baseband.

C. DATA-FRAME FORMAT

The data-frame format for the SLRV Telemetry Subsystem has been determined. The format for the "TV-Data", "DIBSI-Data", and "Routine-Data" Modes is shown in Tables II.4-5, II.4-6 and II.4-7 respectively.

TABLE II.4-5. DATA FRAME FORMAT FOR "TV DATA" MODE

Data Points	Analog Channel Requirements	
	Analog Words	Axle
TV Regulated Voltage Input	1	Front
TV System Current Drain	1	
TV Camera Azimuth Angle	1	
Vidicon High Voltage	1	
Vidicon Incident Light	1	
Spares	5 (max)	
Zero Volts Telemetry Calibration	1	Center
Full-Scale Telemetry Calibration	1	
Spares	2 (max)	
	Digital Channel Requirements	
	Bits	Axle
Clinometer Data (Roll)	20	Front
Clinometer Data (pitch)	20	
Sun Azimuth Angle	10	
TV Camera Sun Shutter	5	
TV Mast Limit Switch	1	
Spares	10	
Spares	10	Center
Frame Synchronization	33 (max)	
Mode Identification	2	

TABLE II.4-6. DATA FRAME FORMAT FOR "DIBSI DATA" MODE

Data Points	Analog Channel Requirements	
	Analog Words	Axle
Zero Volts Telemetry Calibration	1	Center
Full-Scale Telemetry Calibration	1	
Battery Voltage	1	
Total Battery Current Drain	1	
Total Regulated Current	1	
Regulated Output Voltage (23 to 25v)	1	
Regulated Output Voltage (6 to 7v pos)	1	
Regulated Output Voltage (6 to 7v neg)	1	
Spares	3 (max)	
DIBSI Drive Motor Current	1	Rear
DIBSI Displacement (A)	1	
DIBSI Displacement (B)	1	
DIBSI Temperature (A)	1	
DIBSI Temperature (B)	1	
Spares	3 (max)	
	Digital Channel Requirements	
	Bits	Axle
Diagnostic and Control Verification	18 (max)	Front
Diagnostic and Control Verification	65 (max)	Center
DIBSI Limit Switch (A)	1	
DIBSI Limit Switch (B)	1	
Spares	10 (max)	Front
Spares	10 (max)	Center
Frame Synchronization	33 (max)	-
Mode Identification	2	

TABLE II.4-7. DATA FRAME FORMAT FOR "ROUTINE DATA" MODE

Data Points	Analog Channel Requirements	
	Analog Words	Axle
Drive Motor #1 Current	1	Front
Wheel Housing #1 Temperature	1	
Drive Motor #2 Current	1	
Wheel Housing #2 Temperature	1	
Front Axle Steering Position	1	
Steering-Motor Temperature	1	
Vidicon Faceplate Temperature	1	
Vidicon Incident Light	1	
Front Axle Compartment Temperature (A)	1	
Center Axle Compartment Temperature (B)	1	
Rear Axle Compartment Temperature (C)	1	
Vidicon Filament Voltage	1	
Spares	2 (max)	
Drive Motor #3 Current	1	Center
Wheel Housing #3 Temperature	1	
Drive Motor #4 Current	1	
Wheel Housing #4 Temperature	1	
Zero Volts Telemetry Calibration	1	
Full-Scale Telemetry Calibration	1	
Center Axle Compartment Temperature (A)	1	
Center Axle Compartment Temperature (B)	1	
Center Axle Compartment Temperature (C)	1	
Receiver AGC (VHF)	1	
Transmitter PA Voltage (VHF)	1	
Transmitter Output Power (VHF)	1	
Battery Temperature	1	
Battery Voltage	1	
Battery Charge Current	1	
Battery Pressure	1	
Total Battery Current Drain	1	
Total Regulated Current	1	
DC to DC Converter for RTG	3	

TABLE II.4-7. DATA FRAME FORMAT FOR "ROUTINE DATA" MODE (Continued)

Data Points	Analog Channel Requirements	
	Analog Words	Axle
Regulated Voltage Output (23 to 25v)	1	Center
Regulated Output Voltage (6 to 7v pos)	1	
Regulated Output Voltage (6 to 7v neg)	1	
Spares	3 (max)	
Drive Motor #5 Current	1	Rear
Wheel Housing #5 Temperature	1	
Drive Motor #6 Current	1	
Wheel Housing #6 Temperature	1	
Rear Axle Steering Position	1	
Steering-Motor Temperature	1	
Solar-Panel Temperature (A) or Radiator Temperature on RTG	1	
Solar-Panel Temperature (B) or Radiator Temperature on RTG	1	
Solar-Panel Elevation	1	
Spares	2 (max)	
	Digital Channel Requirements	
	Bits	Axle
Wheel Housing #1 Pressure	1	Front
Wheel Housing #2 Pressure	1	
Radioisotope Heating Pellet Position	1	
Steering-Motor Pressure	1	
Clinometer Data (Roll)	20	
Clinometer Data (Pitch)	20	
Sun Azimuth Angle	10	
TV Camera Sun Shutter	5	
Diagnostic and Control Verification	18	
Thermal Controller Switches	4	
Spares	10 (max)	
Wheel Housing #3 Pressure	1	Center
Wheel Housing #4 Pressure	1	
Wheel #3 Clutch Position	1	
Wheel #4 Clutch Position	1	
Wheel #3 Rotation	1	
Wheel #4 Rotation	1	
Radioisotope Heating Pellet Position	1	
Diagnostic and Control Verification	65	

TABLE II. 4-7. DATA FRAME FORMAT FOR "ROUTINE DATA" MODE (Continued)

Data Points	Digital Channel Requirements	
	Bits	Axle
Thermal Controller Switches	6	Center
SLRV Identification	1	
VHF Antenna Erected and Locked	1	
Wheel Housing #5 Pressure	1	Rear
Wheel Housing #6 Pressure	1	
Steering-Motor Pressure	1	
Spares	20 (max)	
Frame Synchronization	33 (max)	-
Mode Identification	2	

APPENDIX V

COMMAND AND CONTROL SUBSYSTEM

APPENDIX V
COMMAND AND CONTROL SUBSYSTEM

A. FUNCTIONAL DESCRIPTION

The Command and Control Subsystem will provide the necessary synchronizing control, timing control, accumulation registers, command decoding, error checking and emergency controls to allow the operator at the DSIF to command the SLRV with a high degree of reliability and confidence.

The subsystem logic will be physically separated according to the areas where different subsystem control is required; this will provide a limit on the number of wires between the axles of the vehicle. The Vehicle Central Decoder (VCD), which takes the data output from the Communications Subsystem, accumulates the serially received instruction bits, checks for transmission errors, identifies the SLRV commands, generates subsystem timing, and transfers a portion of the instruction word to the Vehicle Subsystem Decoders (VSD's) if SLRV identification has been made. The VSD's, of which there are two, will decode the data bits and produce a signal for the control device of the particular subsystem for which the command was intended.

1. Instruction Format & Coding

The SLRV Command and Control Subsystem will be compatible with the existing Surveyor Instruction Format and Instruction Coding, which are defined as follows:

- Instruction Format: Bit order in instruction word.
- Instruction Coding: How the instruction word is broken up for transmission.

The Surveyor Instruction Format comprises the following data in the sequence shown:

(a) Four bits of Word Synchronization data

(b) Five bits of Address Complement data

(c) Five bits of Address True data

(d) Five bits of Order Complement data

(e) Five bits of Order True data

The instruction bit rate for serial data transmission from Earth to Surveyor is 48 bits per second on a 2.3-kc subcarrier. This same rate will be used for relaying the instruction word to the SLRV on the Indirect Link. This rate requires

0.5 second for the transmission of a complete instruction word. The Instruction Coding for transmission of Surveyor instruction words utilizes a form of split-phase Non-Return to Zero (NRZ) as shown in Figure II.5-1.

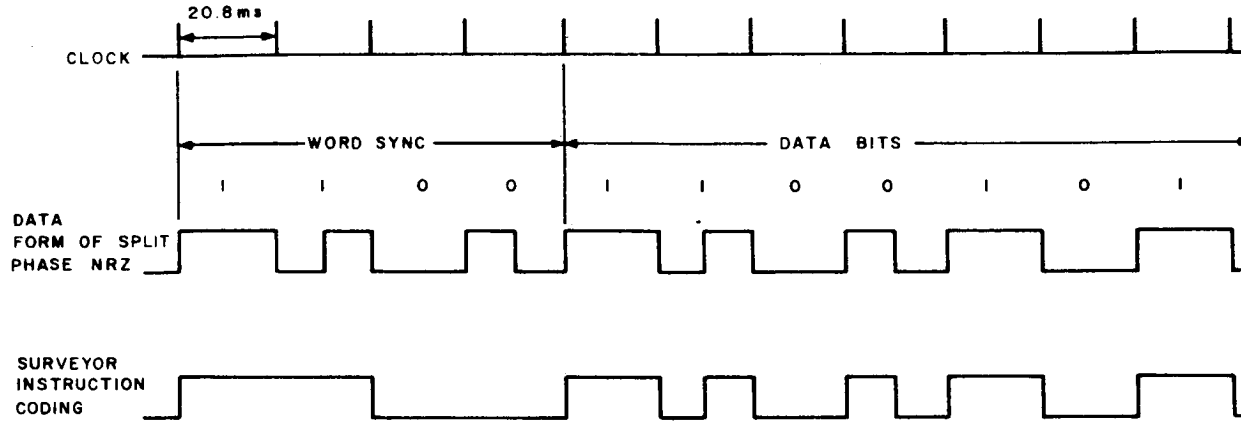

Figure II.5-1. Surveyor Instruction Code

The Surveyor Instruction Code requires:

(1) The Word-Sync data be contained in two clock periods at an uninterrupted logical "1" level followed by two clock periods at an uninterrupted logical "0" level.

(2) A level transition occurring at the start of each clock period during the time the data bits are to be transmitted.

(3) The second half of each clock period to be at the logical level specified by the particular data bit to be transmitted.

The SLRV Command and Control Subsystem derives the Word-Sync, data bit timing, and data information from the information contained in the items listed above. This function will be accomplished in the VCD.

2. Command Requirements

Tables II.5-1 through 5-3 are the lists of commands required for controlling the various subsystems of SLRV. The commands listed in Tables II.5-1 and III.5-2 are addressed to SLRV; the commands listed in Table II.5-3 are addressed to Surveyor.

TABLE II.5-1

NON-LOCOMOTION COMMAND LIST (MODAL SYSTEM)

To Front and Center Compartments for Front and Center Axles
1. CLEAR 2. CHARGE MODE 3. OPERATE MODE 4. TV MODE 5. COMPARTMENT HEAT ON 6. COMPARTMENT HEAT OFF
To Front Compartment for Front Axle
7. TV STANDBY 8. TV ON 9. TV OFF 10. TV AZIMUTH STEP CLOCKWISE 11. TV AZIMUTH STEP COUNTERCLOCKWISE 12. TV HEIGHT STEP 13. TV SUN SENSOR OVERRIDE 14. TV PICTURE SEQUENCE
To Center Compartment for Center Axle
15. HIBERNATE MODE SELECT 16. HIBERNATE MODE ALERT 17. HIBERNATE MODE EXECUTE 18. XMTR LOW POWER 19. XMTR HIGH POWER 20. XMTR OFF 21. XMTR HIGH POWER SELECT 22. RANGE MEASUREMENT ON 23. RANGE MEASUREMENT OFF 24. TLM ON 25. TLM OFF 26. VSD ON 27. VSD OFF 28. ERROR OVERRIDE 29. EMERGENCY STOP OVERRIDE

To Center Compartment for Rear Axle
30. DIBSI SELECT
31. DIBSI DEPLOY
32. DIBSI RETRACT
33. DIBSI START
34. DIBSI STOP
35. SOLAR PANEL STEP UP
36. SOLAR PANEL STEP DOWN

TABLE II.5-2

LOCOMOTION AND STEERING COMMANDS

To Front and Center Compartments for All Axles
37. LOCOMOTION FORWARD
38. LOCOMOTION REVERSE
To Front and Center Compartments for Front and Rear Axles
39. STEER CENTER
40. STEER STEP RIGHT
41. STEER STEP LEFT
42. STEER HARD RIGHT
43. STEER HARD LEFT
44. WHEEL DISCONNECT ALERT
45. WHEEL DISCONNECT EXECUTE
To Front Compartment for Front Axle
46. WHEEL DISCONNECT SELECT FRONT RIGHT
47. WHEEL DISCONNECT SELECT FRONT LEFT
48. STEERING INHIBIT FRONT
To Center Compartment for Rear Axle
49. WHEEL DISCONNECT SELECT REAR RIGHT
50. WHEEL DISCONNECT SELECT REAR LEFT
51. STEERING INHIBIT REAR
To Center Compartment for Center Axle
52. WHEEL CLUTCH DISENGAGE CENTER RIGHT
53. WHEEL CLUTCH DISENGAGE CENTER LEFT
54. WHEEL CLUTCHES ENGAGE CENTER RIGHT AND LEFT
55. LOCOMOTION CONTINUOUS SELECT
56. LOCOMOTION STOP SELECT RIGHT
57. LOCOMOTION STOP SELECT LEFT

TABLE II.5-3

SURVEYOR-BASED SLRV EQUIPMENT COMMANDS

Command Number	Command
1.	CLEAR
2.	SLRV DEPLOY SELECT STEP ONE
3.	SLRV DEPLOY SELECT STEP TWO
4.	SLRV DEPLOY SELECT STEP THREE
5.	SLRV DEPLOY ALERT
6.	SLRV DEPLOY EXECUTE
7.	VHF XMTR LOW POWER
8.	VHF XMTR HIGH POWER
9.	VHF XMTR OFF
10.	VHF RCVR ZERO NARROW BAND
11.	VHF RCVR ZERO WIDE BAND
12.	VHF RCVR ZERO OFF
13.	VHF RCVR ONE NARROW BAND
14.	VHF RCVR ONE WIDE BAND
15.	VHF RCVR ONE OFF
16.	RANGE MEASUREMENT
17.	BEARING MEASUREMENT

All commands which elicit controls performing irreversible functions have the following requirements.

(1) Associated controls must be verified by the ground-console operator before the function is performed.

(2) The actual command which causes the function to be performed must be a dual command wherein an Alert command is followed by an Execute command within a specified time period.

(3) If there are several similar functions from which to select, the choice will be effected by separate Select commands. (These will also serve for the requisite ground verification mentioned above).

These rules give rise to the Select-Alert-Execute command sequences appearing on the command lists.

Non-Locomotion Commands

The commands listed in Table II.5-1 cause the following actions to occur.

- CLEAR

  This command resets the functions of Error-Storage, Error-Override, Emergency-Stop-Storage, Emergency-Stop Override, Steering-Inhibit, Hibernate-Mode-Select, Wheel-Disconnect-Select, TV-Sun-Sensor-Override. This command also serves as an emergency command to stop locomotion, steering, DIBSI deployment and retraction, and DIBSI operation.

- HIBERNATE MODE SELECT
- HIBERNATE MODE ALERT
- HIBERNATE MODE EXECUTE

  The first of these three commands prepares the SLRV for entering hibernation. Then, sending the second and third commands as a dual command, turns off power to the Television and Telemetry Subsystems, to the transmitter and to the VSD, and puts the Power Subsystem in the charge configuration. After a short time delay, the Power Subsystem is put in the hibernate configuration.

- CHARGE MODE

  This command turns off power to the Television and Telemetry Subsystems, and to the transmitter and the VSD; it puts the Power Subsystem in the charge configuration.

- OPERATE MODE

  This command turns on power to the Television and Telemetry Subsystems, and to the transmitter and the VSD. It puts the Power Subsystem in the normally operating configuration, the Television Subsystem in a standby state, and selects transmitter low power.

- TV MODE

  This command turns on power to the Television and Telemetry Subsystems, and to the transmitter and the VSD. It puts the Power Subsystem in the normally operating configuration, turns on high power to the Television Subsystem, and selects "TV Input" for the Telemetry Subsystem. If the TV-Picture Mode is entered from the Operate Mode, and if the command XMTR HIGH POWER SELECT has been sent, then the command TV MODE selects transmitter high power.

- TV STANDBY

  This command turns on power to the Television Subsystem, turns off television high power, and selects transmitter low power.

- TV ON

  This command turns on power to the Television Subsystem, turns on television high power, selects "TV Input" for the Telemetry Subsystem, and selects transmitter high power if the command XMTR HIGH POWER SELECT has been sent.

- TV OFF

  This command turns off television high power, turns off power to the Television Subsystem, and selects transmitter low power.

- TV AZIMUTH STEP CLOCKWISE
- TV AZIMUTH STEP COUNTERCLOCKWISE

  These commands rotate the television mast one step in the appropriate direction.

- TV HEIGHT STEP

  This command alternately raises and lowers the television mast.

- TV PICTURE SEQUENCE

  This command starts the television-picture sequence to produce one video frame.

- TV SUN-SENSOR OVERRIDE

  This command overrides the automatic operation of the sun shutter.

- XMTR LOW POWER

  This command turns on power to the transmitter and selects transmitter low power; it resets the XMTR High-Power Select storage function.

- XMTR HIGH POWER

  This command turns on power to the transmitter and selects transmitter high power.

- XMTR OFF

  This command selects transmitter low power, and turns off power to the transmitter.

- XMTR HIGH POWER SELECT

  This command sets the XMTR High-Power Select storage function so that transmitter high power is selected automatically during the operations of television, ranging, and DIBSI.

- RANGE MEASUREMENT ON

  This command selects "Range Input" for the Transmitter, selects transmitter high power if the command XMTR HIGH POWER SELECT has been sent, and selects "Wide Band" for the receiver.

- RANGE MEASUREMENT OFF

  This command selects transmitter low power, selects "Narrow Band" for the receiver, and removes the "Range Input" selection for the transmitter.

- TLM ON
- TLM OFF

  These commands control power to the Telemetry Subsystem.

- VSD ON
- VSD OFF

  These commands control power to the VSD.

- ERROR OVERRIDE

  This command overrides the authority of the error checking function, thus allowing commands to be "active" regardless of instruction errors.

- EMERGENCY STOP OVERRIDE

  This command overrides the authority of the emergency-stop function, thus allowing locomotion, steering, and DIBSI functions to continue in spite of having received an emergency-stop signal.

- DIBSI SELECT

  This command alternately selects the right and the left DIBSI unit for response to the other DIBSI commands, and selects the corresponding data channel.

- DIBSI DEPLOY

  This command deploys the selected DIBSI unit, selects "DIBSI Input" for both the Telemetry Subsystem and the transmitter. Selects

- transmitter high power if the command XMTR HIGH POWER SELECT has been sent, and provides for the transmitter to receive calibration voltages on the DIBSI data lines.

- DIBSI RETRACT

  This command retracts the DIBSI unit. When the unit becomes fully retracted, transmitter low power is selected and the "DIBSI Input" selection for both the Telemetry Subsystem and the transmitter is removed.

- DIBSI START

  This command starts the automatic operation of the DIBSI experiment and the transmitter receives force and acceleration data on the DIBSI data lines.

- DIBSI STOP

  This command stops operation of the DIBSI experiment, and the transmitter receives calibration voltages on the DIBSI data lines.

- SOLAR PANEL STEP UP

- SOLAR PANEL STEP DOWN

  These commands rotate the solar panel one step in the appropriate direction.

- COMPARTMENT HEAT ON

- COMPARTMENT HEAT OFF

  These commands, respectively, move the heating pellets in and out of the electronics compartments.

Locomotion and Steering Commands

The commands listed in Table V. 1-2 cause the following actions to occur.

- LOCOMOTION FORWARD

- LOCOMOTION REVERSE

  These commands start vehicle locomotion in the appropriate direction. If command No. 55 (see Table II.5-2) was given prior to these commands, then these commands must be terminated by commands No. 56 or 57 (see Table II. 5-2).

- LOCOMOTION STOP SELECT RIGHT

- LOCOMOTION STOP SELECT LEFT

  These commands select the odometer switch that will stop locomotion after one wheel revolution.

- LOCOMOTION CONTINUOUS SELECT

  This command allows locomotion, once started, to continue without being stopped by an odometer switch.

- WHEEL CLUTCH DISENGAGE CENTER RIGHT
- WHEEL CLUTCH DISENGAGE CENTER LEFT
- WHEEL CLUTCHES ENGAGE CENTER RIGHT AND LEFT

  These three commands control the mechanical coupling of locomotion drive power to the center wheels.

- WHEEL DISCONNECT SELECT FRONT RIGHT
- WHEEL DISCONNECT SELECT FRONT LEFT
- WHEEL DISCONNECT SELECT REAR RIGHT
- WHEEL DISCONNECT SELECT REAR LEFT
- WHEEL DISCONNECT ALERT
- WHEEL DISCONNECT EXECUTE

  Of these six commands, the first four commands select a wheel. Then, sending the last two commands as a dual command causes the mechanical coupling of locomotion drive power to the selected wheel to be irreversibly removed via an explosive squib.

- STEER CENTER
- STEER STEP RIGHT
- STEER STEP LEFT
- STEER HARD RIGHT
- STEER HARD LEFT

  These five commands yaw the front and rear axles to steer the vehicle.

- STEERING INHIBIT FRONT
- STEERING INHIBIT REAR

  These commands allow single-axle vehicle steering.

Surveyor-Based SLRV Equipment Commands

The commands listed in Table II.5-3 cause the following actions to occur on board Surveyor.

- CLEAR

  This command resets the SLRV deployment selectors and the range measurement and bearing measurement controls.

- SLRV DEPLOY SELECT STEP ONE
- SLRV DEPLOY SELECT STEP TWO
- SLRV DEPLOY SELECT STEP THREE
- SLRV DEPLOY ALERT
- SLRV DEPLOY EXECUTE

  These five commands deploy the SLRV from the Surveyor spacecraft. The first Select command is sent and then verified on the ground console via Surveyor telemetry. Then the Alert-Execute dual command is sent causing the Select command to be carried out. Then the first Select command is cleared and the second Select command is sent, and the entire cycle is repeated. The same is done for the third Select command.

- VHF XMTR LOW POWER

  This command turns on power to the VHF transmitter and selects transmitter low power.

- VHF XMTR HIGH POWER

  This command turns on power to the VHF transmitter and selects transmitter high power.

- VHF XMTR OFF

  This command turns off power to the VHF transmitter and selects low power.

- VHF RCVR ZERO NARROW BAND

  This command turns on power to the first VHF receiver and selects narrow band response.

- VHF RCVR ZERO WIDE BAND

  This command turns on power to the first VHF receiver and selects wide band response.

- VHF RCVR ZERO OFF

  This command turns off power to the VHF receiver.

- VHF RCVR ONE NARROW BAND
- VHF RCVR ONE WIDE BAND
- VHF RCVR ONE OFF

  These three commands are similar to the three previous ones but are for the second VHF receiver. Two receivers are required for the bearing measurement; but, for relaying SLRV data back to Earth, one receiver serves as a back-up for the other.

- RANGE MEASUREMENT

  This command sets the range measurement configuration and the configuration is reset by the CLEAR command.

- BEARING MEASUREMENT

  This command sets the bearing measurement configuration and this configuration is reset by the CLEAR command.

Mode Transitions

For the convenience of the earth-based operator and for command redundancy purposes, mode commands have been included in the command list. The mode diagram in Figure II.5-2 shows the permissible mode transitions and the subsystem states brought about by each mode command. The following operations will be normally performed in the Operate Mode.

(1) Locomotion

(2) Steering

(3) DIBSI experiment

(4) Solar panel motion

(5) Range and bearing measurements

(6) Compartment heat control

However, these can also be performed in the TV Mode. Note from the diagram that the TV-Picture mode can be entered directly from the Charge Mode; this capability was included for redundancy purposes and for design simplicity, but in normal operation this mode transition will probably not be used. Note also that the Hibernate Mode can be entered from any other mode. Note also that the Hibernate Mode can be entered from any other mode; this was done for design simplicity, and does not represent a hazard since a sequence of three commands is required to effect this mode transition; however, in normal operation this transition will probably be made from the Charge Mode. When the transmitter is on, it will normally be at the low power level. However, if the command XMTR HIGH POWER SELECT is sent, subsequent operations of television, ranging , or DIBSI will automatically switch the transmitter to the high power level for the duration of the operation.

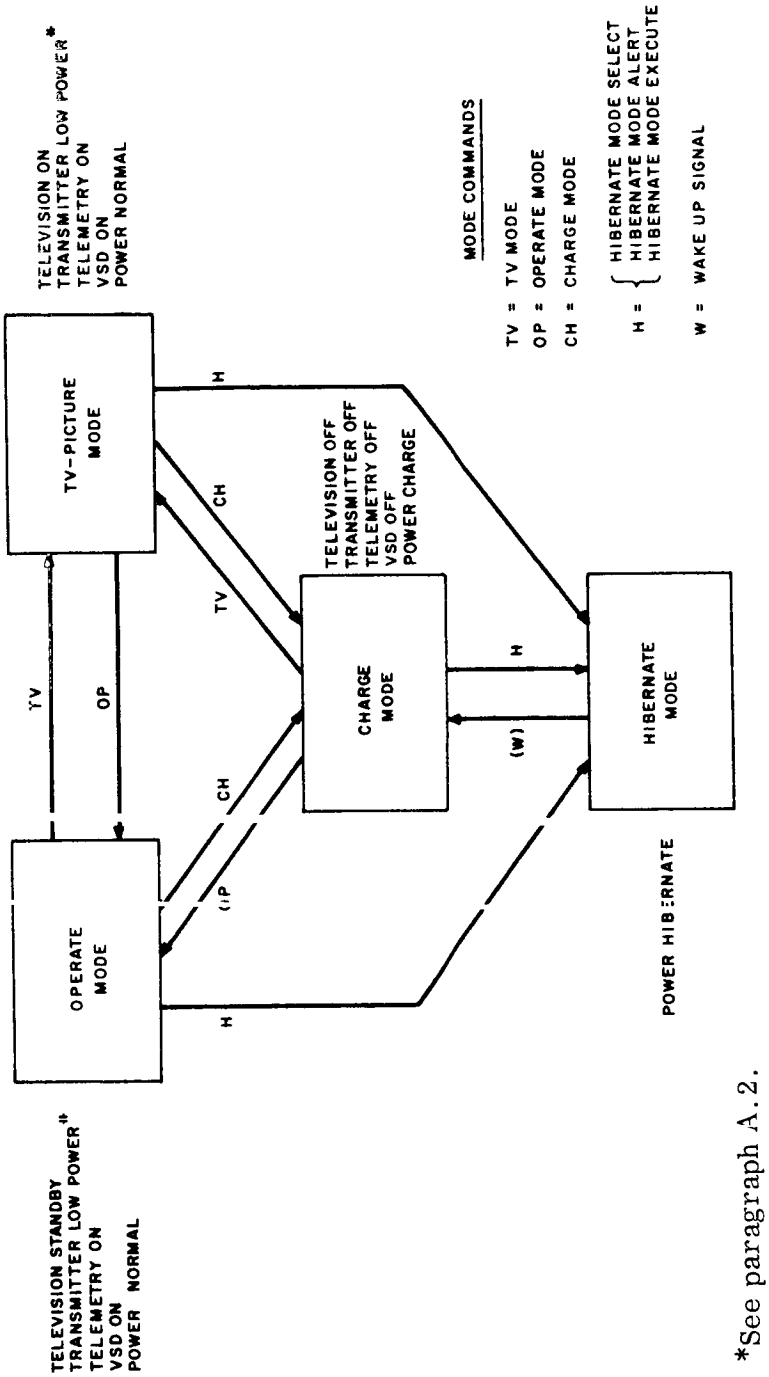

*See paragraph A.2.

NOTE: THE SUBSYSTEM STATES LISTED NEXT TO EACH MODE ARE BROUGHT ABOUT BY THE CORRESPONDING MODE COMMAND. THE RECEIVER AND VCO ARE OFF ONLY IN THE HIBERNATE MODE.

Figure II.5-2. Mode Diagram

3. Telemetry Points

Telemetry Points in the SLRV

The list of command and control subsystem telemetry sampling points is divided into three sections and these are tabulated in Tables II.5-4, 5-5, 5-6. The three sections consist of the following:

(1) VCD (in center compartment);

(2) VSD_1 (in front compartment);

(3) VSD_2 (in center compartment).

The entries in each section are subdivided into the two categories of either "Verification" or "Diagnostic".

The Verification entries are intended to confirm controls elicited in response to commands received and, thus, represent a complete feedback around the system command loop from ground-operator intent to ground-operator verification (except for those controls which are pulsed and, therefore, not telemetered). For the cases where several controls are elicited by a single command, each of these controls is listed separately. In order to include the situation where commands only cause responses in functions internal to the Command and Control Subsystem, these internal functions are included in the Verification category. The Verification category also includes SLRV-originated signals whose status should be known to the ground operator. (It is anticipated that each Verification signal will light a lamp on the SLRV operating console to facilitate verification.)

The Diagnostic entries are intended for use only in cases where malfunction is suspected. All entries in the telemetry list in Tables II.5-4, 5-5, 5-6, represent digital signals requiring one sampling bit each.

In summary, there are a total of 89 telemetry sampling points in the SLRV Command and Control Subsystem; 18 are located in the front compartment and 71 are located in the center compartment. Of the 89 points, 49 are Verification telemetry points and 40 are Diagnostic telemetry points. The detailed distribution appears in Table II.5-7.

Telemetry Points in the Surveyor Spacecraft

The telemetry sampling points associated with the Surveyor-based SLRV Command and Control Subsystem are listed below. All entries are in the Verification category and all represent digital signals

TABLE II.5-4

COMMAND AND CONTROL SUBSYSTEM TELEMETRY LIST FOR VCD

Verification	Diagnostic	In Center Compartment
	x	Shift Register Stage One
	x	Shift Register Stage Two
	x	Shift Register Stage Three
	x	Shift Register Stage Four
	x	Shift Register Stage Five
	x	Counter Stage One
	x	Counter Stage Two
	x	Counter Stage Three
	x	Counter Stage Four
	x	Counter Stage Five
	x	Half Period Blanking
	x	Address Bit
	x	SLRV Address
	x	Check
	x	Error
x		Error Storage
x		Error Override
x		Emergency Stop
x		Emergency Stop Override
x		Bump
x		Tilt
x		Fade
x		Hibernate Select

TABLE II.5-5

COMMAND AND CONTROL SUBSYSTEM TELEMETRY LIST FOR VSD_1

Verification	Diagnostic	In Front Compartment
	x	Locomotion Power Front
x		Locomotion Motor Power Front, Forward
x		Locomotion Motor Power Front, Reverse
x		Wheel Disconnect Select Front Right
x		Wheel Disconnect Select Front Left
	x	Steering Limit Right (front axle)
	x	Steering Limit Left (front axle)
	x	Steering Sector Right (front axle)
	x	Steering Sector Center (front axle)
	x	Steering Sector Left (front axle)
x		Steering Inhibit Front
	x	Steer Step (front axle)
	x	Steer Center (front axle)
	x	Steering Power Front
x		Steering Motor Power Front, Right
x		Steering Motor Power Front, Left
x		TV Power
x		TV High Power Control

TABLE II.5-6

COMMAND AND CONTROL SUBSYSTEM TELEMETRY LIST FOR VSD_2

Verification	Diagnostic	In Center Compartment
	x	Locomotion Power Center
x		Locomotion Motor Power Center, Forward
x		Locomotion Motor Power Center, Reverse
	x	Locomotion Power Rear
x		Locomotion Motor Power Rear, Forward
x		Locomotion Motor Power Rear, Reverse
x		Stop Selector Right
x		Stop Selector Left
	x	Wheel Switch Right
	x	Wheel Switch Left
x		Odometer Right Wheel
x		Odometer Left Wheel
x		Wheel Disconnect Select Rear Right
x		Wheel Disconnect Select Rear Left
	x	Steering Limit Right (rear axle)
	x	Steering Limit Left (rear axle)
	x	Steering Sector Right (rear axle)
	x	Steering Sector Center (rear axle)
	x	Steering Sector Left (rear axle)
x		Steering Inhibit Rear
	x	Steer Step (rear axle)
	x	Steer Center (rear axle)
	x	Steering Power Rear
x		Steering Motor Power Rear, Right
x		Steering Motor Power Rear, Left
x		VSD Power
x		XMTR Power
x		XMTR High Power Control
x		XMTR High Power Select
x		XMTR Range Input

TABLE II.5-6

COMMAND AND CONTROL SUBSYSTEM TELEMETRY LIST FOR VSD_2 (Continued)

Verification	Diagnostic	In Center Compartment
x		XMTR DIBSI Input
x		TLM DIBSI Input
x		DIBSI Select Right
x		DIBSI Select Left
	x	DIBSI Deploy/Retract Power Right
	x	DIBSI Deploy/Retract Power Left
x		DIBSI Deploy/Retract Motor Power Right, Deploy
x		DIBSI Deploy/Retract Motor Power Right Retract
x		DIBSI Deploy/Retract Motor Power Left, Deploy
x		DIBSI Deploy/Retract Motor Power Left, Retract
x		DIBSI Operate Motor Power Right
x		DIBSI Operate Motor Power Left
x		DIBSI Calibrate
x		DIBSI Data
x		DIBSI Data Select Right
x		DIBSI Data Select Left
	x	DIBSI Both Retracted
	x	DIBSI Deployment Interlock

Note: "XMTR TV Input" and "TLM TV Input" will be telemetered from the transmitter and the Telemetry Subsystem respectively.

TABLE II.5-7

TELEMETRY POINT DISTRIBUTION

Section	Verification	Diagnostic	Total
VCD	8	15	23
VSD_1	9	9	18
VSD_2	32	16	48
Front Compartment	9	9	18
Center Compartment	40	31	71
Total	49	40	89

requiring one sampling bit each. These signals will be sampled and telemetered by the Surveyor telemetry subsystem.

SLRV Deploy Select Step One

SLRV Deploy Select Step Two

SLRV Deploy Select Step Three

VHF XMTR Power

VHF XMTR High Power Control

VHF RCVR ZERO Power

VHF RCVR ZERO Wide Band Control

VHF RCVR ONE Power

VHF RCVR ONE Wide Band Control

Range Measurement

Bearing Measurement

B. FUNCTIONAL AND STRUCTURAL CONFIGURATION

The SLRV basic vehicle configuration requires that a Command and Control Subsystem interface be provided as close as possible to the location of each of the other subsystems. The interface with subsystems on the front and center axles will be accomplished from the VSD located on the appropriate axle. The interface with subsystems mounted on the rear axle will be accomplished from the VSD located on the center axle because no thermally controlled compartment will exist on the rear axle.

The VCD, which accepts the instruction word to be operated upon, is located in the center compartment on the center axle. The VCD derives the word-sync, data-bit timing, and the data bits from data received from the Communications Subsystem. The VCD then operates on the data and transfers the appropriate data to both VSD_1 and VSD_2 for generating the appropriate subsystem controls.

1. Vehicle Central Decoder – VCD

Figures II.5-3 through 5-6 collectively, constitute a block diagram of the VCD. Figure II.5-3 shows the word-sync and bit-timing detectors. The input waveform from the receiver is passed through a noise integrator to remove transitions relatively short as compared to the actual data transitions. The waveform is then shaped by a Schmitt trigger and passed on to the word-sync and bit-timing detectors.

The word-sync detector consists of a ramp integrator, a threshold Schmitt trigger, and a pulse amplifier. The ramp integrator continually integrates the input waveform and produces linear ramps of positive and negative slopes according to the polarity of the input data. When two clock periods of uninterrupted logical "ones" are received, the output ramp reaches the threshold required to change the state of the Schmitt trigger. The following two clock periods of uninterrupted logical 0's produce a linear ramp of negative slope. When the recover threshold is reached, the Schmitt trigger returns to its quiescent state. The output of the Schmitt trigger is amplified and used as the word-sync signal for the VCD logic. During the transmission of the data bits, the output of the ramp integrator never reaches the threshold required to change the state of the Schmitt trigger.

The bit-timing detector operates as follows. Two one-shot multivibrators trigger on the positive and negative transitions of the input waveform. The outputs of the one-shot multivibrators are OR'ed together to produce a string of short pulses corresponding to the input transitions. The pulse corresponding to the transition that occurs during word-sync time is inhibited from producing bit timing in the AND GATE. The AND GATE, in conjunction with the half-period blanking flip-flop prevents the pulses corresponding to the transitions that occur at the middle of the clock period from being recognized. The output of the AND GATE triggers a 15.6 millisecond delay

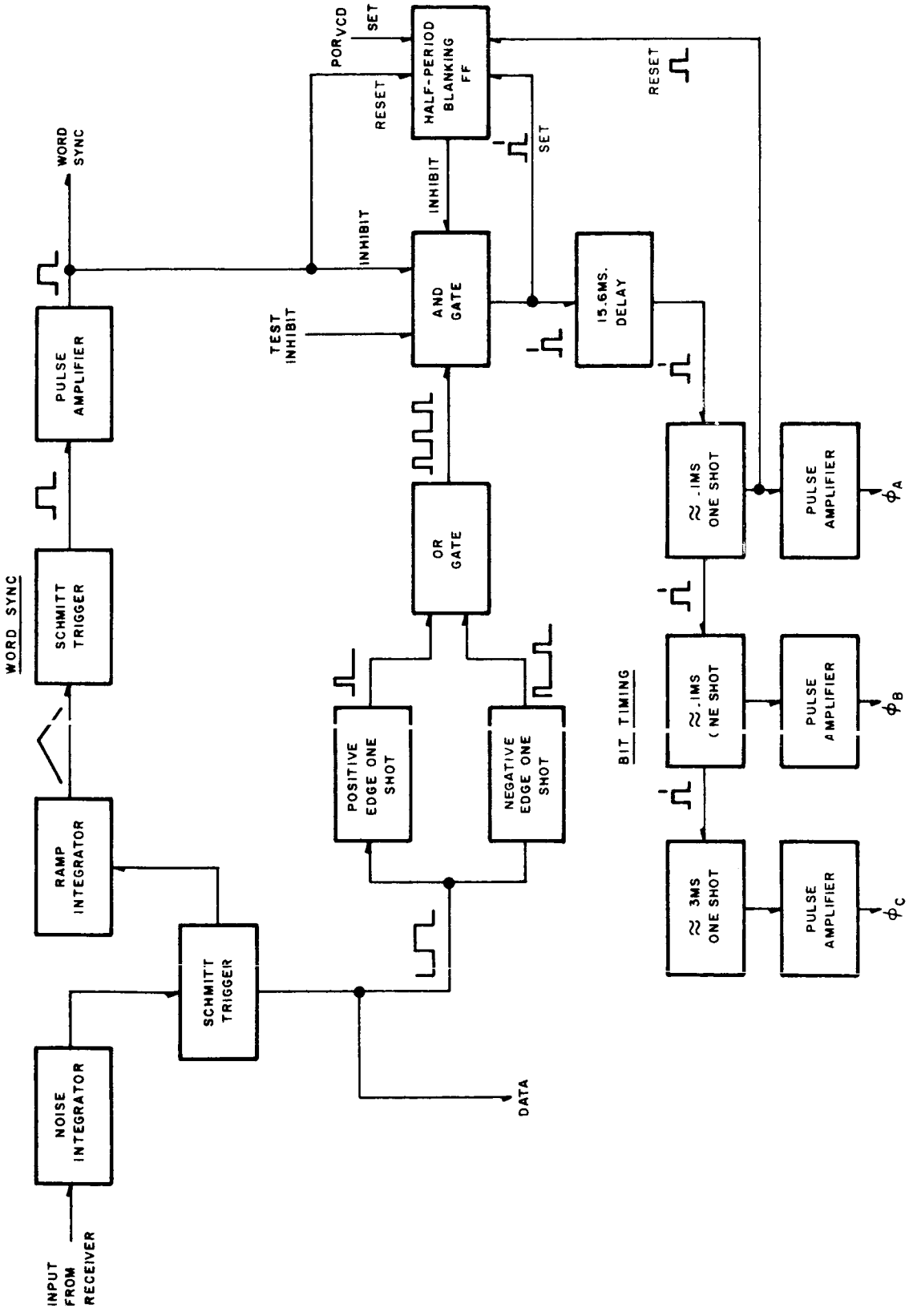

Figure II.5-3. Word-Sync and Bit-Timing Detectors, Block Diagram

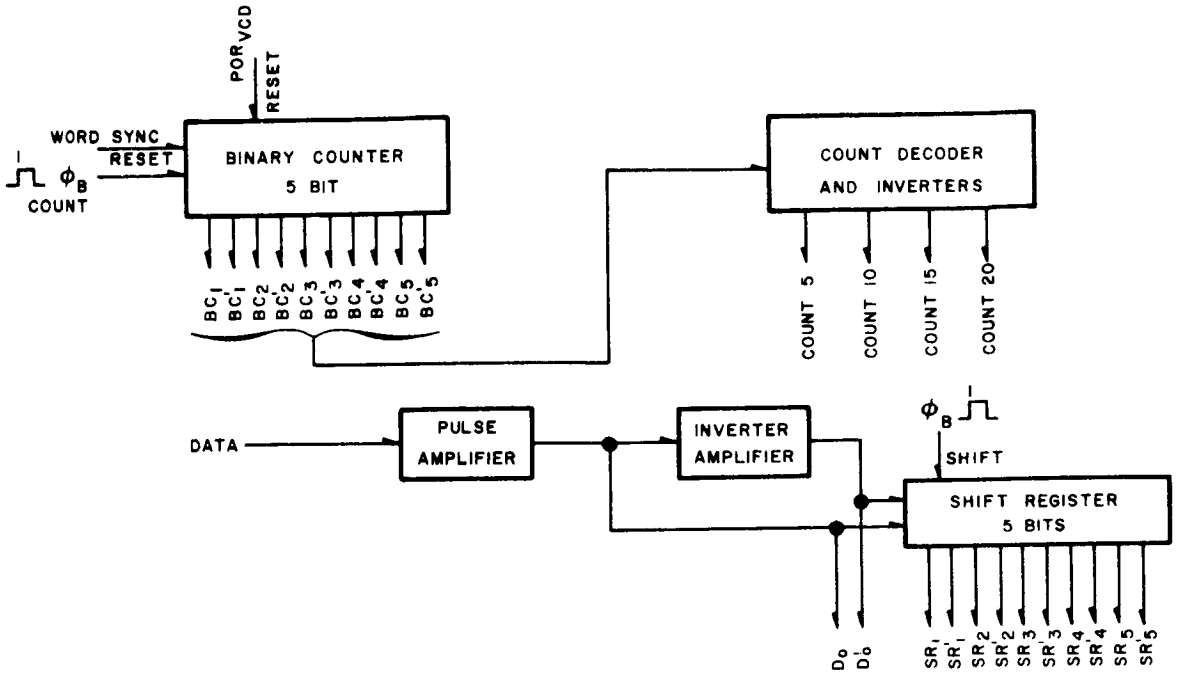

Figure II.5-4. Bit-Timing Binary Counter, Count Decoder, and Data-Shift Register, Block Diagram

one-shot multivibrator to provide the three timing control pulses, ϕ_A, ϕ_B and ϕ_C, where ϕ_A is the pulse used for error checking; ϕ_B is the pulse used for triggering the binary counter; and ϕ_C is the pulse used for operating on the stored data bits. These timing pulses start 15.6 milliseconds after the beginning of each clock period with ϕ_B starting at the trailing edge of ϕ_A, and ϕ_C starting at the trailing edge of ϕ_B. The Power-On Reset signal (POR_{VCD}) is generated as a result of the VCD power being turned on. The POR_{VCD} sets the half-period blanking flip-flop and this prevents any timing control pulses from being generated by the input data until the first word-sync occurs. Thus, initial partial-words cannot cause spurious responses.

Figure II.5-4 shows the binary counter, count decoder, and the data-shift register. The binary counter is reset by word-sync and is triggered by the leading edge of pulse ϕ_B. The POR_{VCD} resets the binary counter to zero and this condition is maintained until after the first word-sync occurs. The leading edge of pulse ϕ_B also advances the shift register. Remembering that pulse ϕ_B occurs approximately 15.7 milliseconds after the start of a clock period, or in the middle of the second half of the clock period, this pulse will cause the data appearing at the input of the register to be stored. Simultaneously, pulse ϕ_B advances the stored data by one stage.

Figure II.5-5 shows the temporary-bit store, the SLRV command identification, gated drivers, and strobe generators. Four of the five bits of address-true data

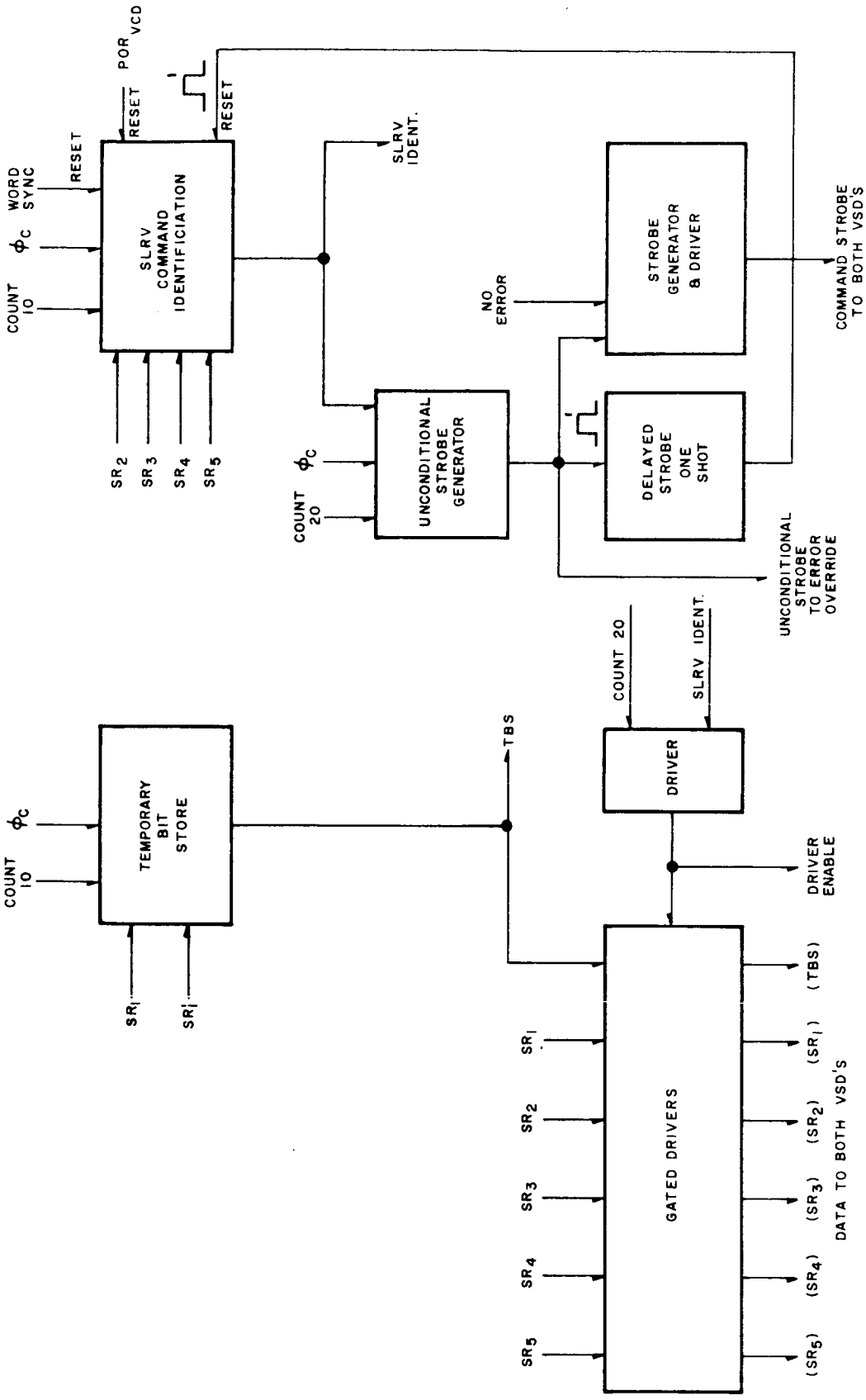

Figure II.5-5. Temporary Bit Store, SLRV Command Identification, Gated Drivers, and Strobe Generators, Block Diagram

from the Surveyor instruction format are used to determine whether the received command is an SLRV command. SLRV command identification is made from the contents of four stages of the shift register; this identification is triggered by the tenth ϕ_c pulse. At the same time, the contents of the fifth stage of the shift register are placed into a temporary-bit store for later use with the five order-bits of the instruction word. The gated drivers transfer the contents of the shift register and the temporary-bit store to the VSD's when the binary counter contains a count of 20; this transfer occurs only when an SLRV command identification has been made. These drivers are gated to stay in a low-power condition except for a few milliseconds out of a 0.5-second period. The driver-enable signals are used in the drivers of the VSD's for the same purpose.

Two different strobes are required by the VCD and VSD logic. A command strobe is generated for use by the VSD's on the twentieth ϕ_c pulse if: (1) SLRV command identification has been made; and (2) no error was encountered in receiving the instruction word. A second strobe, generated on the twentieth ϕ_c pulse if an SLRV command identification has been made independent of error conditions, is necessary for controlling the error-override logic. The second strobe signal also triggers a delay which removes the SLRV identification signal and shuts off the driver-enable signal. This arrangement is necessary because, if the data transmission is interrupted, it is possible for the binary counter to stay at a count of 20 and for the SLRV identification function to remain set (resulting in the gated drivers being kept in their high-power state).

Figure II.5-6 shows the error-check control, error-detector, emergency-stop control, and the VSD power control. The error-check control establishes the two periods in each word during which an error check will be performed. The first period begins with the fifth ϕ_c pulse and ends with the tenth ϕ_c pulse; the second period begins with the fifteenth ϕ_c pulse and ends with the twentieth ϕ_c pulse. The error detector, during the ϕ_A pulse, compares the shift-register input data with the contents of the fifth stage of the shift register; the two items compared must be complements of each other during the checking interval established by the error-check control function. A non-complement comparison will set the Error flip-flop; each word-sync resets it. The error-override control allows the no-error signal to be maintained in spite of the detection of errors. The CLEAR command removes the override.

The emergency-stop control receives signals from other subsystems indicating that the SLRV either encountered an obstacle, or has developed an excessive roll or pitch angle, or that the RF signal strength from Surveyor has become dangerously low. These occurences are stored and, OR'ed together, constitute the stop signal. The Emergency-Stop Override control allows the stop signal to be inhibited in spite of the existence of stored emergency stop signals. The CLEAR command removes the override, as well as resetting the storage unless the received signal persists.

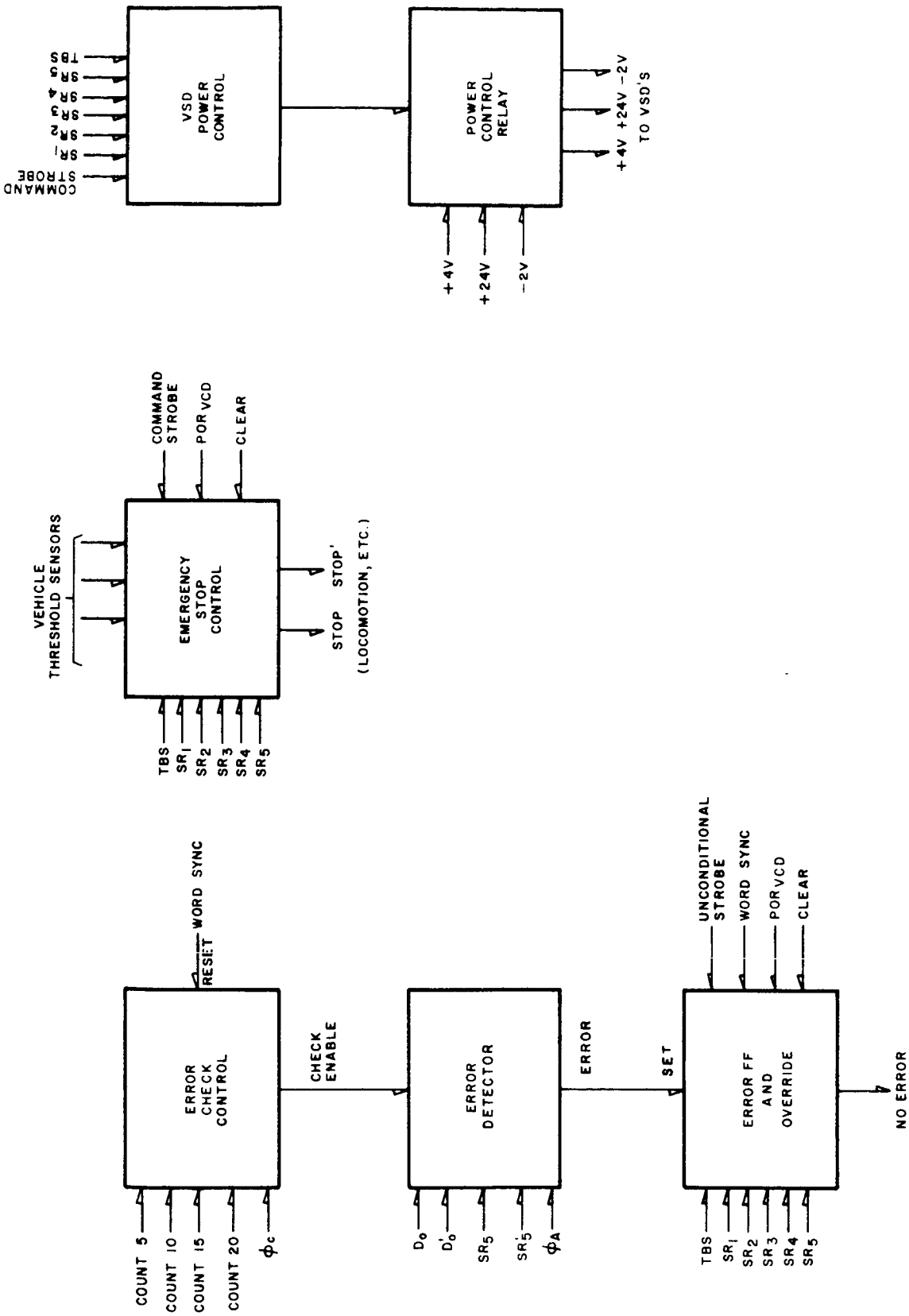

Figure II.5-6. Error Check, Emergency Stop Control and VSD Power Control, Block Diagram

The command strobe, when gated by the no-stop signal, constitute a new strobe which is used by locomotion, steering, and DIBSI controls. Thus, a stop condition can prevent these controls from responding to commands.

The VSD Power Control allows the earth-based operator to turn the VSD's on and off upon command.

2. Vehicle Subsystem Decoders – (VSD)

Both VSD's simultaneously receive six bits of data on parallel lines from the VCD. Each VSD decodes those commands which it requires for the generation of its control functions. The decoded command generates a control-drive signal for use by the appropriate subsystem.

The VSD in the front compartment, VSD_1, controls locomotion, steering, television, and compartment heat, as related to the front compartment and front axle. The VSD in the center compartment, VSD_2 controls locomotion, transmitter, telemetry, and compartment heat, as related to the center compartment and center axle; VSD_2 also controls locomotion, steering, DIBSI, and solar panel, as related to the rear axle.

The detailed logic design for converting the decoded commands into control-drive signals is individually suited to each recipient subsystem. The basis of locomotion control is a pair of latching relays: the first relay controls the application of electrical motor power thus determines whether locomotion will occur; the second relay controls the polarity of the applied power and thus determines whether locomotion will be forward or reverse. Odometer switches stop locomotion by resetting the first relay.

The basis of steering control is similar to that for locomotion: the first relay determines whether a change of steering direction will occur; the second relay determines whether the change of direction will be to the right or to the left. In addition to these relays, limit switches and direction switches are also required. The limit switches prevent the application of electrical motor power if such application would tend to cause the steering direction to exceed the direction limits. The direction switches provide the necessary information for determining when to reset the first relay in order to stop the steering motors. These switches also provide information for determining which way to turn in order to steer center.

DIBSI-deployment control is basically similar to steering control. However, since there are only two positions (deploy and retract), DIBSI-deployment control needs no position switches; the limit switches determine when to stop the deploy/retract motor. The second relay determines whether DIBSI will deploy or will retract. The first relay allows immediate interruption of electrical motor power in response to either an emergency stop condition or to a ground command; this feature also exists in locomotion control, steering control, and DIBSI-operation control.

DIBSI-operation control is simpler than that of locomotion, steering, or DIBSI-deployment because the motor turns in one direction only. Therefore, the first relay is required (to control application of electrical motor power) but not the second.

TV azimuth and mast height, as well as solar panel direction, are controlled by stepping motors; these require only a pulse in order to actuate them. The center-wheel clutches and the compartment heaters are solenoid-actuated, and require only a pulse to operate them. The control circuitry for a pulse-actuated device consists of little more than a pulse fattener and a power driver. Similarly, this applies for the explosive squibs associated with the front and rear wheels; however in this case, additional circuitry is necessary in order to provide for dual-command recognition.

Power for television, transmitter, and telemetery is supplied via individual latching relays. Television high-power switching and transmitter high/low power selection are flip-flop controlled, as is the establishing of the transponder configuration for ranging. Input line selection for transmitter and telemetry are flip-flop controlled, although not all of these flip-flops are in the Command and Control Subsystem.

3. Subsystem Circuit Considerations

Integrated circuits are presently being considered as the basic circuit configuration to be used by the Command and Control Subsystem. The weight, size, and power constraints applied to all subsystems of the SLRV dictate a packaging technique which is comparable with the state of the art.

The latest indications are that the manufacturing problems of the vendors involved are being overcome thus enabling them to meet delivery requirements. The delivery problem has been the major factor for not considering integrated circuits prior to this time.

Special consideration is warranted in the following circuit areas:

(1) the noise integrator, ramp integrator, and 15.6-millisecond one-shot multivibrator in the VCD;

(2) the power-on reset circuits used in the VCD and both VSD's;

(3) the prevention of actuating irreversible functions when power is turned on.

APPENDIX VI
TELEVISION SUBSYSTEM

APPENDIX VI
TELEVISION SUBSYSTEM

A. GENERAL

The mission requirements for the TV subsystem are as follows:

- Provide images suitable for navigating the SLRV over the lunar surface.
- Provide images over a 360° azimuth field for use in mapping the lunar surface.
- Provide narrow-baseline stereoscopy without the necessity for locomotion.
- Be capable of providing to the DSIF stations data which can be processed for the navigation and mapping functions.

Several TV camera subsystems with their associated optical and mechanical equipment have been studied as possibilities for accomplishing the dual functions of providing visual imagery for vehicle guidance and lunar survey. It has been concluded that a single 1-inch vidicon camera with an SPS surface and an F/4, 13-mm-focal-length lens mounted on the top of a 20-inch mast and depressed 13-1/2° with respect to the normal to the mast provides the optimum configuration to satisfy the mission requirements. Short-baseline stereoscopy is provided by a 6-inch or greater vertical movement of the camera and mast on command.

In this appendix, the alternative systems and configurations studied are discussed in detail. Thermal, power, weight, and performance characteristics are given for the preferred configuration.

B. SUBSYSTEM DESIGN CONSTRAINTS

The primary constraint on the TV subsystem is the requirement for sufficient reliability to satisfy an extended mission life in the order of 3 months. Coupled with the reliability requirement are constraints to minimize the mission time and the weight and power required. The weight and power constraints prevent the use of redundancy. Hence, the reliability of the TV subsystem must be based primarily on simplicity rather than redundancy. The vidicon camera, which is fundamentally a simple assembly, is considered to be the only suitable device for this mission. The performance characteristics of the TV mapping function are detailed in JPL "Requirement for a Rover Vehicle for the Surveyor Spacecraft, Engineering Planning Document No. 98 Revision 1".

In summary, the four basic criteria in establishing a TV subsystem to perform the mission are reliability, mission time, power, and weight. The design factors which affect these four criteria are:

- Range and Field of View
- Frame Rate and Transmission Bandwidth
- Dynamic Range and Sensitivity
- Resolution Capability
- Availability of Flight-Proven Hardware
- Choice of Photoconductor
- Duty Cycle
- Maximum Repetition Rate
- Residual Image
- Optical Configuration
- Mechanical Configuration
- Environment

These factors are discussed in detail in the following sections of this appendix.

1. Range and Field of View

It is essential to elevate the camera above the vehicle to obtain a useful field of view. The range as a function of mast height is shown in Figure II.6-1 The constraints on the height of the mast are: (1) the requirement to fold up the vehicle for transportation on Surveyor; (2) the requirement for maintaining a suitable operating and storage temperature on the components isolated on the mast; and (3) the requirement for a low center of gravity to maintain high vehicle mobility (not more than 3 inches above the axle when the vehicle is locomoting).

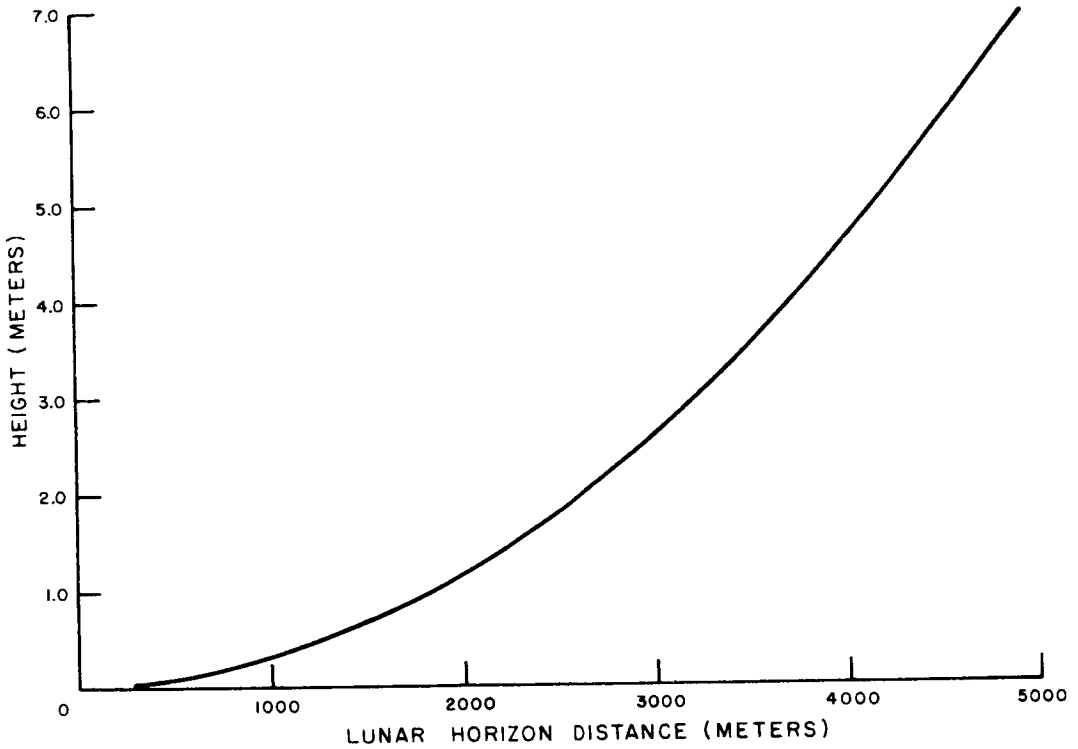

Figure II.6-1 Lunar Horizon Distance versus Camera Height

For mapping, both a long range and a large field of view are advantageous; navigation can be accomplished with a smaller field of view. The limitations on the mapping mission are: (1) the resolution of the sensor and (2) the feasibility of manufacturing high-performance wide-angle optical systems.

2. Frame Rate and Transmission Bandwidth

The time required to perform the navigation and mapping functions represents a significant part of the total mission time, if the power required for azimuth and elevation motion of the TV camera and video transmission is to be limited to a value which can be supported by the primary power supply. Trade-off studies performed to optimize the video-data transmission system indicate the desirability of operating indirectly via Surveyor. With an available bandwidth of 220 Kc and a horizontal and vertical resolution of 500 lines, the maximum frame rate for analog data transmission was derived from the relationship:

$$\text{Frame Time} = \frac{(\text{TV Resolution Lines})^2}{2(\text{Bandwidth}) \times (\text{Kell Factor}) \times (\% \text{ Active Horizontal Lines})}$$

$$T_F = \frac{500^2}{2 \times 220 \times 10^3 \times 0.7 \times 0.9} = 9.05 \text{ seconds}$$

Analysis of a digital transmission system indicated that it would not result in a significant increase in frame rate. No further work was undertaken on a digital system because of its added complexity.

Direct transmission with a base bandwidth of 40 Kc would require a frame time of 5 seconds. This would necessitate the use of a storage vidicon with an ASOS (antimony sulfi-oxy-sulphide) or selenium photoconductive surface with shutter and aperture control, which is discussed in Paragraph 6.

With the selected frame rate of 0.9 second, indirect or direct transmission with reduced resolution (~200 lines) can still be achieved with a base bandwidth of 40 Kc in the event of failure of the 220 Kc indirect link. The low-resolution mode would require that the horizontal line rate of the TV camera be reduced from 716 scan lines to 300 scan lines. A comparable change would be necessary in the ground-station video recording equipment.

3. Dynamic Range and Sensitivity as a Function of Lunar Illumination

The dynamic range and sensitivity of the TV system directly affect the mission time by establishing the acceptable light level, and hence the time of the lunar day during which high-quality pictures can be produced.

Variations in solar elevation and azimuth relative to the optical axis of the camera system are expected to cause changes in highlight brightness from a maximum of about 2200 foot-lamberts down to one-hundredth of this value. The TV subsystem is required to resolve picture detail over this range of highlight brightness and should ideally be able also to resolve contrast changes in the range from 22 to 2.2 foot-lamberts. For an F/4 lens, this corresponds to a variation in faceplate illumination from 34 to 0.0156 foot-candles, assuming no aperture control.

Since any form of aperture control must inevitably add to the complexity of the system, it is proposed to make use of the phenomenon peculiar to vidicons known as "line storage". As explained in Paragraph 10 , it has been established by RCA that there are three modes of storage in a photoconductive surface. By operating in both the frame-storage and line-storage regime, the dynamic range of a vidicon operated in the open-shutter mode can be extended significantly (1000:1).

The sensitivity of the SPS vidicon is sufficient to achieve a peak-to-peak video/rms noise ratio of 36 db down to a faceplate illumination of 1.1 foot-candles.

4. Resolution Capability

A significant factor in determining the mission time, and hence the reliability of SLRV, is the resolution of the TV subsystem, since this determines the useful range of the camera. This useful range in turn establishes the number of pictures which must be taken, thereby affecting the mission time.

A maximum resolution of 800 TV lines is currently achievable with 1-inch vidicons utilizing electromagnetic focusing and deflection. The resolution is reduced to between 500 and 600 TV lines using a hybrid vidicon with electrostatic focusing and electromagnetic deflection. There is, however, a reduction of 1.5 pounds in weight and about 2 watts in power if a hybrid vidicon is used. It is concluded that the reductions in weight and power justify the use of a hybrid vidicon, because the useful range of the camera is limited by mast height, which in turn depends upon the weight of the camera as shown in Paragraph 8.

5. Availability of Flight-Proven Equipment

Data on qualified spacecraft TV cameras was collected and is tabulated in Table II.6-1. It was concluded that weight and power restrictions were such that a hybrid vidicon having electrostatic focus and electromagnetic deflection would best fulfill the mission requirements.

6. Choice of Photoconductor

As further background for the trade-off studies, testing and evaluation of selected vidicons was performed. Three photoconductive surfaces were investigated: (1) antimony trisulphide, solid-porous-solid (SPS); (2) antimony sulphi-oxy-sulphide; and (3) selenium. For each surface, the mode of operation, dynamic range, resolution, maximum frame times, and temperature sensitivity were examined. From this trade-off study, which is summarized in Table II.6-2 , it was concluded that an SPS surface, as used in the Apollo camera presently under development at RCA, offered the best compromise among wide dynamic range, simplicity, and short duty cycle. Because of the limitation on maximum frame time, optimum resolution could only be achieved via an indirect (220 Kc) transmission link.

For operation over a direct link with maximum resolution, a storage vidicon making use of an ASOS or selenium photoconductive surface and having a slower readout capability similar to the Ranger camera would be required. Shuttered operation and iris control would also be required. The ASOS surface, as used in the Ranger and NIMBUS cameras, was not studied further because of the difficulty in reducing the residual image below 5% in a reasonably short time. Temperature control during hibernation was also considered to be a problem within this surface. The results of a comparison of SPS and selenium surfaces are summarized in Table II.6-3. The selenium tubes were tested with a shutter at 1-second frame times. Experience from other programs indicates that much longer frame times are possible without any deterioration in image quality.

In considering the effect of the lunar environment on the camera, it was established from other space programs that selenium surfaces deteriorate during operation at 50°C. RCA's experience with selenium indicates that the surface deterioration is a function of the time during which the surface is exposed to elevated temperatures (above 35°C).

TABLE II.6-1

DATA ASSEMBLED FOR VIDEO ASSEMBLY TRADE-OFF STUDIES

CAMERA NAME	NIMBUS AVCS	APT	TIROS	RANGER (F)	RANGER (P)	RANGER (3,4,5)	OAO	APOLLO
TYPE OF VIDICON	ELECTROMAGNETIC DEFLECTION AND FOCUS - ASOS 1" VIDICON	1" VIDICON ELECTRO-MAGNETIC DEFLECTION AND FOCUS - ASOS	0.5" VIDICON ELECTROMAGNETIC DEFLECTION AND FOCUS - ASOS	1" VIDICON ASOS, E-M DEFLECTION AND FOCUS	1" VIDICON ASOS, E-M DEFLECTION AND FOCUS	1" VIDICON ASOS ELECTROSTATIC DEFLECTION AND FOCUS	1" VIDICON ASOS ELECTROSTATIC DEFLECTION AND FOCUS	1" VIDICON-HYBRID SPS, E-M DEFLECTION ELECTROSTATIC FOCUS
RESOLUTION (T V LINES)	800 HORIZ 600 VERT	700 HORIZ 550-600 VERT	400 HORIZ 350 VERT	700 HORIZ 700 VERT	200 HORIZ 200 VERT	200 HORIZ 150 VERT	350 HORIZ 300 VERT	220 HORIZ 220 VERT
FRAME TIME (SECONDS)	6.5	2.0	2.0	2.56	0.2	10.0	-	0.1
BANDWIDTH (K C.)	80.0	1.6	62.5	200.0	200.0	2.0	60.0	500
DYNAMIC RANGE	8.0 40 TO 0.004 (FT CAND SEC.)	0.7 TO 0.01 (FT CAND SEC.)	1.0 TO .01 (FT CAND SEC.)	0.68 TO .004 (FT CAND SEC.)	0.27 TO .003 (FT CAND SEC.)	3 TO .01 (FT CAND SEC.)	2ND TO 7TH MAGNITUDE STAR	005 TO 30.0 (FT CAND SEC.)
SIGNAL / NOISE (DB) (PEAK SIGNAL) / (PEAK TO PEAK NOISE)	30	17	34	30	29	23	29	38
ERASE AND PREPARE TIME (SECONDS)	26	8	28/8	2.56	0.64	5	0	0
REPETITION RATE (SECONDS)	9.1	208	30/10	5.12	0.84	13	CONT READ	CONT READ
RESIDUAL IMAGE (PER CENT)	5	5	2/10	3	10	10	N/A	20 PER CENT AFTER SECOND SCAN
HIGHLIGHT BRIGHTNESS (FT LAMBERTS)	11,800	11,800	8,500	650/2700	650/2700	2,400	2 ND MAGNITUDE STAR	480
LENS FOCAL LENGTH (MM); APERTURE	17 MM F/4 TO F/16 (VARIABLE IRIS)	5.7 MM F/1.1 888	5 MM F/1.5	25 MM / 76 MM F/1, F/2	25 MM / 76 MM F/1, F/2	40 INCH F/5.6	76 MM F/2.8 "	9 MM F/1.8
EXPOSURE TIME (MILLISECONDS)	4.0	4.0	1.5	5	2	20	NO SHUTTER	NO SHUTTER
ACTIVE LINES	833	800	500	1150	300	200	350	312
IMAGE FORMAT (INCHES)	0.44 X 0.44	0.44 X 0.44	0.25 X 0.25	0.44 X 0.44	0.11 X 0.11	0.44 X 0.44	0.44 X 0.44	0.43 X 0.30
HORIZ. LINE TIME (MILLISECONDS)	7.5 MS	250 MS	4.0 MS	2.22 MS	0.666 MS	50 MS	2.86 MS	3.12 MS
WEIGHT PER CAMERA (LBS)								
SENSOR ASS	9.1	10.23	6.5 (3 LB LENS)	6.9	6.1	(NO LENS OR SHUTTER)		(NO LENS)
ELECTRONICS	6.8	9.75	3.9	7.8	7.8	CAMERA AND CONTROL = 6.0	12.5 (LENS = 4 LBS)	
CONTROLS	2.3		3.9	2.7	2.7		8.5	
TOTAL	18.2	19.98	14.3	17.4	16.6		21.0	EST 50 LBS
POWER PER CAMERA (WATTS)								
CAMERA	19.0		9.4	21.0	22.8			
CONTROLS	2.0		2.2	9.7	9.7			
TOTAL	21.0	18.0	11.6	30.7	32.5	5.2	9.0	6.5 (EST.)
VOLUME (CU IN.)								
SENSOR ASS	135	215	139	93	87	POWER MOD = 72	175	
ELECTRONICS	156	312	112	350	350	CAMERA ELEC = 199	385	
CONTROLS	104	0	86	91	91	TOTAL 271	0	
TOTAL	400	527	337	534	528		560	88.8

TABLE II.6-2

COMPARISON OF PHOTOCONDUCTIVE SURFACES

	Antimony Trisulphide (SPS)	Antimony Sulphi-Oxy-Sulphide (ASOS)	Selenium
Mode of operation	Open shutter	Shuttered	Shuttered
Dynamic Range (foot-candle-sec.)	70 to 0.01	0.4 to 0.004	0.075 to 0.00075
Horizontal Resolution (% at 600 TV lines)	12	Not measured	15
Max. Frame Time	1 to 2 sec.	10 sec.	10 sec.
Operating Temp. Range	-10° to +55°C	-10° to +50°C	-10° to +35°C
Storage Temp. Range	-150° to +90°C	-?* to +70°C	-150° to +35°C

*Not known, but significantly worse than for homogeneous surfaces.

TABLE II.6-3

VIDICON DATA CHARACTERISTIC OF TUBES TESTED

Parameter	S.P.S.* Open Shutter (RCA)		Selenium Shuttered Westinghouse		Selenium Shuttered GEC	
Tube Number	N79	F539	3-8-805	3-7-727	2938931	2938979
Read Scan Time	1 sec	1 sec	1 sec	1 sec	1 sec	1 sec
Horizontal Resolution (% at 600 TV lines)	9	12	15	No Data	No Data	No Data
Signal-to-noise (Highlight)	36/1	40/1	80/1	75/1	30/1	110/1
Vidicon Highlight	70 ft.-candles	70 ft.-candles	0.075 ft.-candles sec.	0.075 ft.-candles sec.	0.3 ft.-candles sec.	0.3 ft.-candles sec.
Dynamic Range (Faceplate Illumination)	*70 to 0.01 ft.-candles	*70 to 0.01 ft.-candles	0.075 to 0.00075 ft.-candles sec.	0.075 to 0.00075 ft.-candles sec.	0.3 to 0.01 ft.-candles sec.	0.3 to 0.002 ft.-candles sec.
Duty Cycle (%)	50	50	50	50	50	50
Repetition Rate (sec.)	3	3	2	2	2	2
Residual Image (%)	5	5	2	2	4	5

*At light levels of 20 foot-candles and greater some deterioration of vertical resolution is apparent.

The SPS surface is the least susceptible to degradation from temperature changes during operation and storage.

7. Duty Cycle, Repetition Rate, and Residual Image

Duty cycle and repetition rate have a direct bearing on the power requirement and the time necessary to complete the mission. The constraints on the duty cycle and repetition rate are residual image and photoconductor leakage (which require that the tube be erased and prepared between active frames). In determining the duty cycle and repetition rate for the various surfaces, a residual image of 5% or less was established as a necessary performance factor. Duty cycle has been defined as the ratio of active readout time to total operating time; repetition rate is defined as the minimum interval between active frames.

Typical power profiles obtained with the various tubes are shown in Figure II.6-2 , and a mission operation is shown in Figure II.6-3 .

8. Alternative Mounting Configurations for the Camera and Lens

General

To satisfy the requirements of JPL - EDP98, Revision 1, it was concluded that a mast-mounted TV camera and optics at a minimum height of 18 inches above the front-axle center line would be necessary to accomplish the mission. Alternatives considered included the following:

- 1-inch vidicon fixed in upper part of mast with mirror in object space.

  Narrow-angle (20°) lens.

  Mirror rotating about azimuth and elevation axes.

- 1-inch vidicon fixed in lower part of mast with optical relay or fiber optics and mirror in object space.

  Narrow-angle (20°) lens.

  Mirror rotating about azimuth and elevation axes.

- 1-inch vidicon attached to head of mast.

  Wide-angle (45°) lens.

  Camera and mast rotating about azimuth axis.

  Elevation traverse of 6 inches for short-baseline stereoscopy.

- Two 1/2-inch vidicons mounted at head of mast.

These configurations are listed in Table II.6-4 . In order to satisfy the center-of-gravity requirements while maintaining the simplest and most reliable configuration,

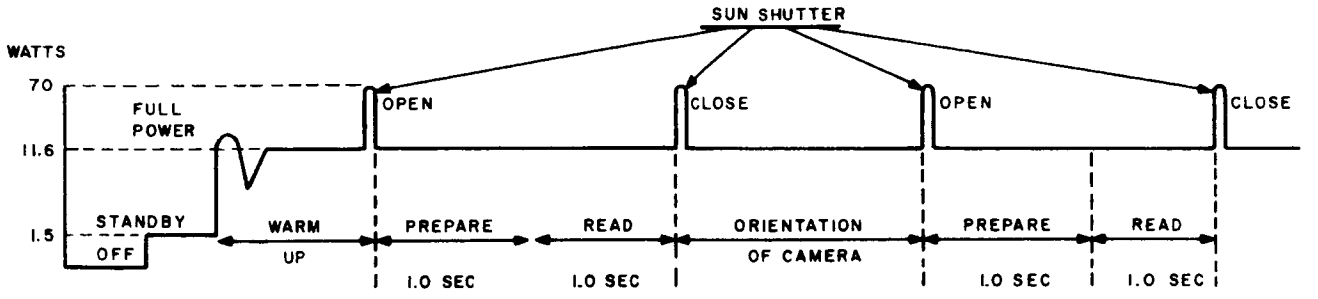

S.P.S. SURFACE (RCA)

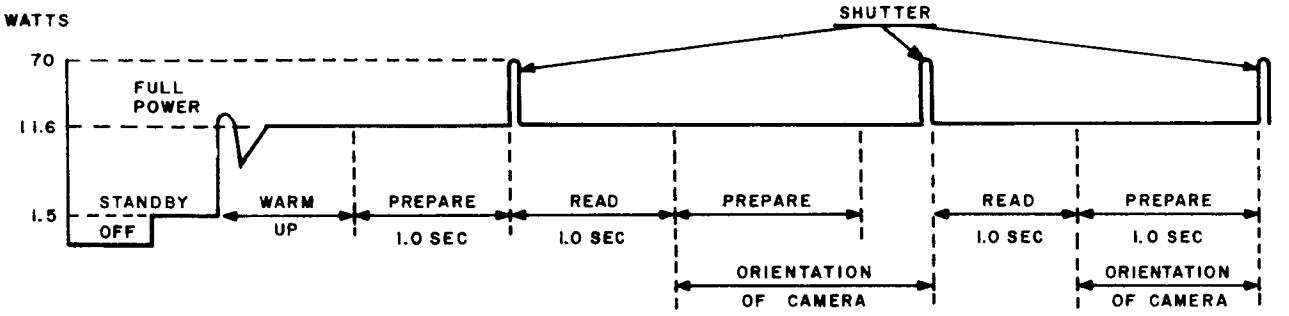

SELENIUM SURFACE (G.E.C.-WESTINGHOUSE)

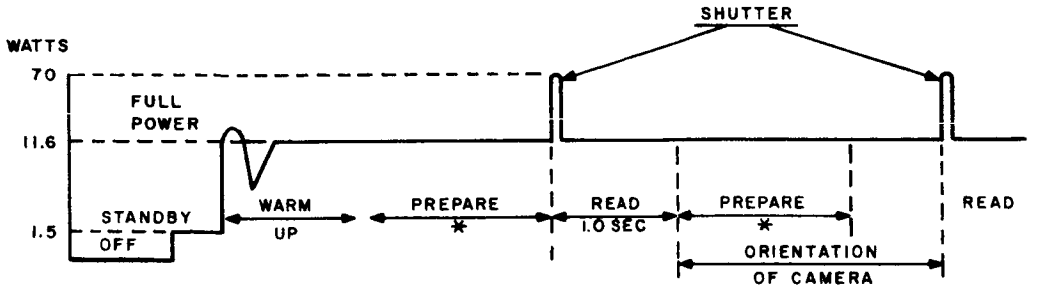

* MINIMUM PREPARE TIME FOR AN ELECTROMAGNETIC 1" VIDICON: 2.5 SEC

ASOS SURFACE (RCA)

Figure II.6-2. Power Profiles Observed from Selected TV Systems
Bandwidth: 220KC Frame Rate: 1.0 sec
Vidicon: One Inch Hybrid — 500 TV Lines

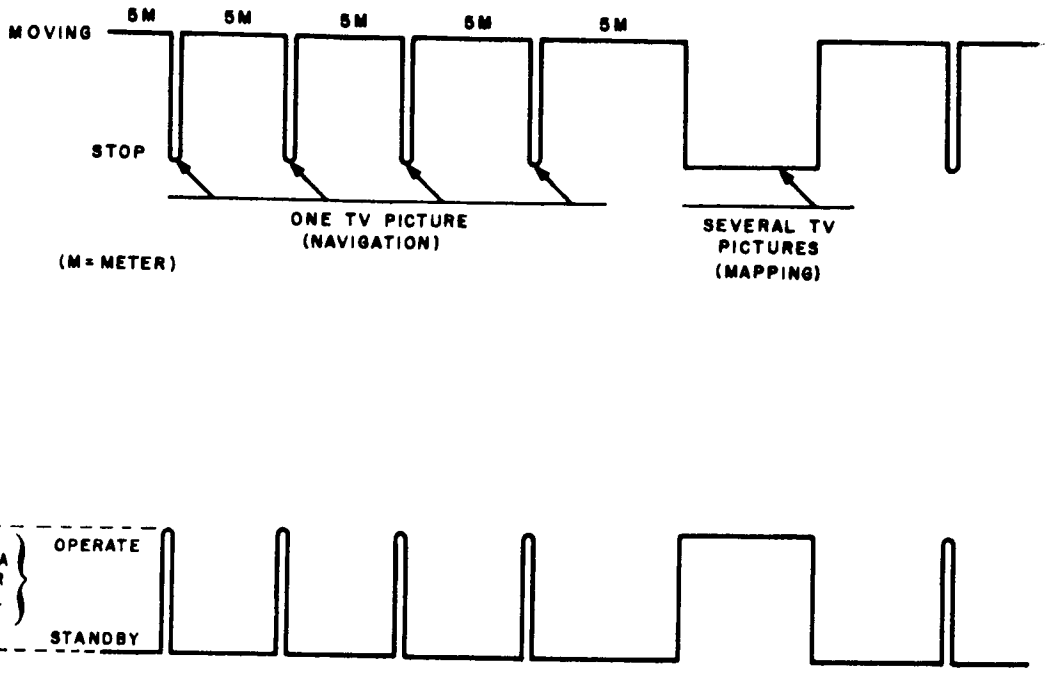

Figure II.6-3. Typical Mission (No Shutter)

TABLE II.6-4

COMPARISON OF MOUNTING CONFIGURATIONS

Configuration	Maximum Mast Height* (in.)	Thermal Problems	Optical Performance
1-inch vidicon in upper part of mast Azimuth/Elevation Mirror	12.5	Vidicon, Az/El. Drive	Good
1-inch vidicon in lower part of mast Relay optics Azimuth/Elevation Mirror	24	Vidicon, Relay Optics, Az/El. Drive	High transmission loss. Degraded aperture response.
1-inch vidicon at head of mast	18.7	Vidicon	Excellent
Two 1/2-inch vidicons at head of mast	15	Vidicon	Lower resolution

*Predicated on requirement for over-all center of gravity located 3 inches above axle center line.

it is proposed that a single 1-inch vidicon camera and lens assembly be mounted directly on the mast head, depressed 13.5° from the normal to the mast to provide near-field coverage for vehicle navigation. The camera electronics, excluding the video preamplifier, are to be mounted in the thermally controlled compartment on the front axle. The connection between the camera and the thermal compartment is to be by flexible cable band.

Mast Height Versus Center of Gravity

Calculations of maximum mast height for the three mounting configurations studied are given in the following paragraphs. The weights assumed in the calculations are as follows:

GM Vehicle	Weight (lb)	Center of Gravity
Steering	1.0	0.5" below axle
Wheels & Drive	5.8	0.0" below axle
Structure	5.8	0.0" below axle
Frame	0.4	2.5" below axle
	13.0	0.12

Payload (without mast)	Weight (lb)	Center of Gravity (below axle)
Command & Control Telemetry (Including Sun-Aspect Sensor)	3.20	Not defined
Camera Electronics (including aximuth drive)	4.75	Not defined
	7.95	2.3" (assumed)
Subtotals	20.25 lb	1.0" below axle

Mast	Weight (lb)
Azimuth drive	1.45
2.5" mast	0.084 lb/inch
Camera	1.50
Sun Shields Sensor	1.30
Optics (simple lens)	0.5
Relay Optics	4.0
Mirror	1.00

TR64-26

Camera Mounted in Upper Part of Mast (Figure II.6-4)

30-mm Lens - Weight 0.5 lb

5-inch mirror and window - Weight 1.25 lb

Azimuth drive at top of mast

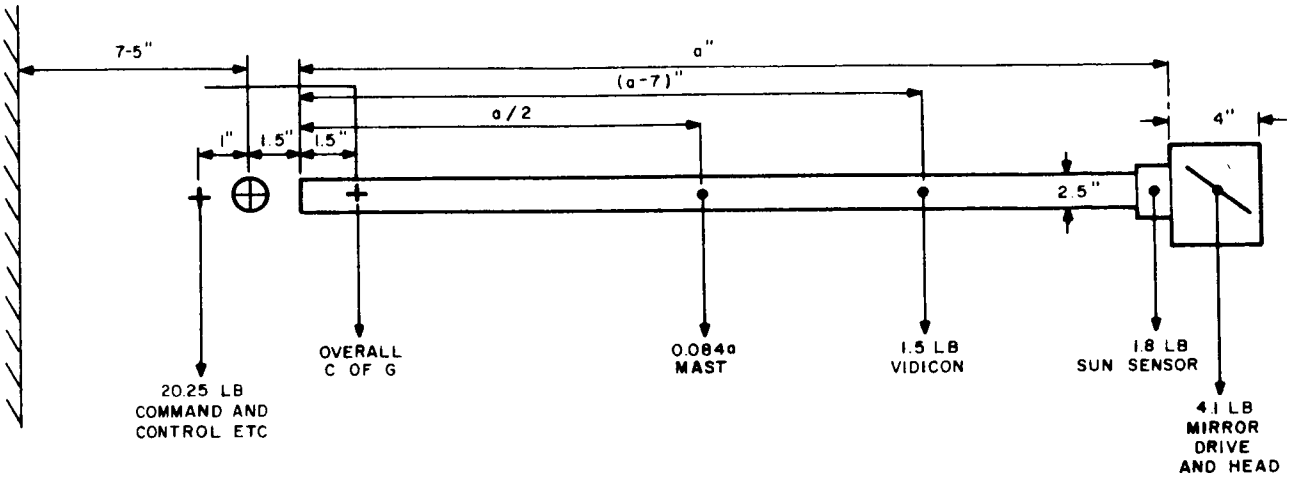

Figure II.6-4. Sketch of TV Mast with Camera Mounted in Upper Part of Mast

$$4(20.25) = (a+2-1.5)\,(4.1) + (a-1.5)\,(1.8) + (a-7-1.5)\,1.5 + \left(\frac{a}{2} - 1.5\right)(0.084a)$$

$$4(20.25) = (4.1)a + (0.5)4.1 + (1.8)a - (1.5)\,(1.8) + (1.5)a - (8.5)\,(1.5) + (0.042)a^2 - (1.5)\,(0.084)a$$

$$4(20.25) = (.042)a^2 + (4.1+1.8+1.5-(1.5)\,(.084))a + (0.5)4.1 - (1.5)\,(1.8) - (8.5)\,(1.5)$$

$$81 = (0.042)a^2 + 7.27\,a - 13.4$$

$$a = \frac{-7.27 + \sqrt{(7.27)^2 + 4(.042)\,94.4}}{0.084} =$$

$$a = \frac{-7.27 + \sqrt{53.9 + 15.8}}{0.084} = \frac{-7.27 + \sqrt{69.7}}{0.084}$$

$$a = \frac{-7.27 + 8.35}{0.084} = \frac{1.08}{0.84} = 12.5$$

Results:

Mast height = 12.5"

Optical axis height = 23.8"

Camera Weight:

4.75	Electronics
1.07	Mast
1.50	Camera
1.80	Lens, shutter, sensor
4.10	Head, Mirror
13.22	lb

Camera Mounted in Base of Mast (Figure II.6-5)

Relay Optics - weight 4.0 lb

Azimuth drive at top of mast

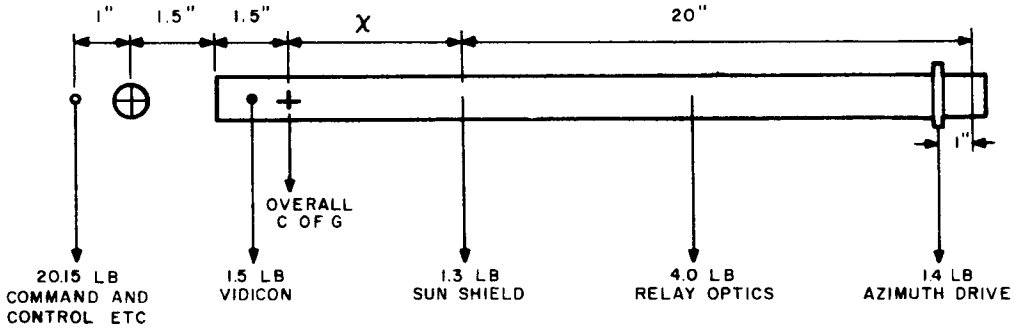

Figure II.6-5. Sketch of TV Mast with Camera Mounted in Base of Mast

Camera Mounted at Head of Mast (Figure II.6-6).

If

$x = 2.5$

Mast height = 24 inches

Optical axis height = 33 inches

Total camera weight = 13.7 lb

Camera Mounted at Head of Mast (Figure II.6-6)

14.5-mm, F/3.5 Lens; weight, 0.3 lb

No mirror

Azimuth drive at bottom of mast

Twist wire

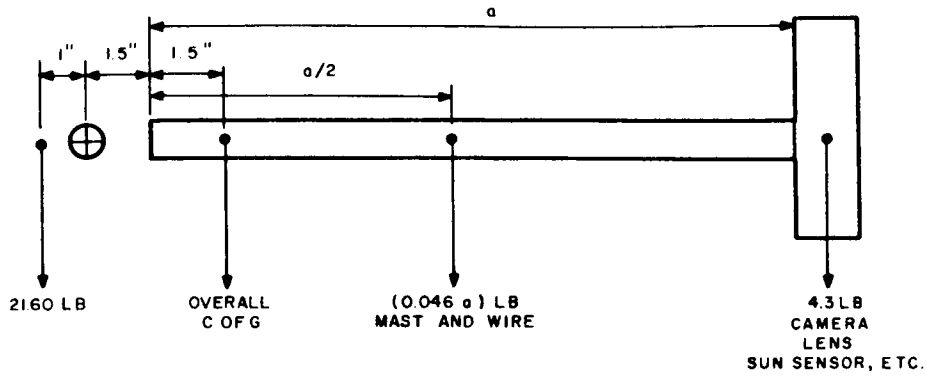

Figure II.6-6. Sketch of TV Mast with Camera Mounted at Head of Mast

$$22.25(4) = (a+1.3-1.5)\ 4.1 + (\frac{a}{2} - 1.5)\ (0.046)a$$

$$22.25(4) = (a-0.2)\ (4.1) + (0.023)a^2 - 1.5\ (0.046)a$$

$$89 = (4.1)a - (0.2)\ (4.1) = (0.023)a^2 - (1.5)\ (0.046)a$$

$$89 = (0.023)a^2 + (4.1 - 0.069)a - 0.82$$

$$0 = (0.023)a^2 + (4.03)a - 89.9$$

$$a = \frac{-4.03 + \sqrt{(4.03)^2 + 4(0.023)(89.9)}}{0.046} = \frac{-4.03 + \sqrt{16 + 8.28}}{0.046}$$

$$a = \frac{-4.03 + \sqrt{24.28}}{0.046} = \frac{-4.03 + 4.92}{0.046} = \frac{0.89}{0.046}$$

$$a = 19.35 \text{ inches.}$$

Results:

Mast height = 19.35 inches

Optical axis = 29.0 inches

Total Camera Weight = 11.9 lbs

Optical Performance Good

9. Environment

The TV subsystem is required to survive:

- Launch
- Separation
- Cruise
- Landing
- Locomotion
- Lunar Night

The subsystem must operate when SLRV is stationary during the lunar day.

Survival

In order to ensure survival during the launch, separation, and landing phases of the mission, the TV camera and mast will be restrained in flight by clamps, with vibration/shock isolation if found necessary during development.

Flight assemblies, including associated electronic units mounted in the thermal compartment on the front axle of SLRV, will be qualified by being subjected to the following vibration tests:

Frequency (cps)	Vibration Level	Duration
100-1500	2.0 G (rms) white gaussian noise	11 minutes
100-1500	4.5 G (rms) white gaussian noise	5 minutes
1-1500	Sine wave	2 minutes/oct.

The cruise and locomotion phases of the mission are not expected to impose significant vibration and shock loads on the TV subsystem.

Survival of the camera during lunar night is dependent upon the choice of photoconductive surface. Although not yet tested for extended periods of time at temperatures approaching those of the lunar night (-190°C), it is known that homogeneous surfaces such as SPS (antimony tri-sulphide) and selenium are less likely to separate from the faceplate than are more complex photoconductive layers.

Operation

During the lunar day, temperatures in excess of +100°C may be attained by objects on the lunar surface. The SPS surface is capable of being stored at +90°C. For optimum performance, the vidicon must be maintained at a temperature between +10°C and +45°C. With some degradation in performance, the vidicon may be operated at temperatures between -10°C and +55°C. Thermal analysis has shown that the vidicon can be maintained within these temperature limits for solar-elevation-angle limits of 12° to 66° by passive thermal control.

Electrostatic attraction of dust (if present on the lunar surface) would seriously impair the performance of the TV subsystem. Theoretical calculations indicate that photo-recombination effects will limit the daytime potential of the SLRV to a few volts. During the lunar night when there is no photo-recombination, the potential of the vehicle may rise to a very high value. Further investigation of this problem is required during Phase II of the study. It is proposed that a 100-mil cover glass be placed at the front of the lens assembly and coated with a transparent metallic surface to facilitate discharge of dust particles which may adhere to the surface. Disposal of dust particles will be facilitated by the downward-pointing aspect of the camera assembly.

To resist the effect of sub-atomic particles created by solar flares, the cover glass is to be made "non-browning" by the use of a cerium-oxide glass.

Image Smear

In order to limit image smear to less than 1/2 TV line, the motion of the mast must not exceed 2 minutes of arc. Damping of the suspension between the front and center axles will be required to ensure that the angular rate of movement of the mast does not exceed 0.03°/second during the "TV Picture" cycle.

Thermal Control

The thermal-control configuration investigated considered the vidicon to be mounted horizontally in a housing 12 inches long and 2.5 inches in diameter. The housing is mounted on a 1-inch-diameter mast approximately 19 inches long. It was desired to maintain the vidicon faceplate between +10°C and +45°C during operating periods. During storage periods, the vidicon temperature can vary between -150°C and +90°C. The preliminary analysis did not consider any radiative or conductive heat transfer between the vidicon housing and the remainder of the vehicle.

The temperature history of the vidicon housing is calculated by solving the energy balance:

$$Q + a_B A_B S \sin\theta + a_T A_{TP} S \cos\theta$$

$$+ 0.10 S \cos\theta (a_B \psi_B A_B + a_T \psi_T A_T + a_F \psi_F A_F)$$

$$+ (0.81 \cos\theta + 0.015 \sin\theta)(\epsilon_B \psi_B A_B + \epsilon_T \psi_T A_T + \epsilon_F \psi_F A_F)$$

$$- (\epsilon_B A_B + \epsilon_T A_T + \epsilon_F A_F) \sigma T^4 = mc \frac{dT}{dt},$$

where

a_B, a_T, a_F = the absorptivity of the back, top, and front of the vidicon housing, respectively;

ϵ_B, ϵ_T, ϵ_F = the emissivity of the back, top, and front of the vidicon housing, respectively;

S = solar constant = 0.9 watt/in^2;

ψ_B, ψ_T, ψ_F = the fractions of energy that leave the back, top, and front of the vidicon housing, respectively, and fall upon the moon;

Q = internal power dissipation, in watts;

θ = the angular displacement of the vehicle from the sub-solar point;

A_B, A_F = the area of the back and front of the vidicon housing, respectively, in square inches;

A_{TP} = the projected area to the sun of the top surface of the vidicon housing;

T = the temperature of the vidicon housing, in °K;

mc = the thermal mass of the vidicon housing, in watt-seconds per degree K;

t = time, in seconds; and

σ = Stefan-Boltzmann constant.

The bottom half of the circumferential area of the vidicon housing was assumed to be insulated sufficiently so that it could be considered an essentially adiabatic surface. This can be accomplished in practice by using some type of super-insulation, such as alternating layers of aluminized Mylar and micro-fiber mat. The exposed surfaces were assumed to have the following properties in the analysis:

Back End:

$$\alpha_B = 0.99$$

$$\epsilon_B = 0.67$$

Top:

$$\alpha_T = 0.2$$

$$\epsilon_T = 0.9$$

Front End (Lens End):

$$\alpha_F = 1.0 \text{ (due to cavity effect)}$$

$$\epsilon_F = 1.0$$

The analysis considered the vidicon housing to be at the steady-state temperature at any point on the lunar surface. The analysis did not consider the effect of the SLRV operating in a lunar valley or on a lunar slope.

Two configurations for controlling the temperature of the vidicon housing were investigated. The configurations were identical except for the addition of a 0.25-inch fin on one end of the vidicon housing in one of the configurations (Figure II.6-7). This is the more efficient arrangement since it provides an additional direct solar input to the vidicon housing, which is especially helpful near the terminator plane.

Figure II.6-7 shows that, one earth day after emerging from lunar night ($\theta = 77.8°$), the vidicon housing temperature is -8.2° with no internal dissipation. For the finless configuration shown in Figure II.6-8, the vidicon housing temperature is -20°C with $\theta = 77.8°$ and no internal dissipation. For both configurations, the maximum temperature of the vidicon housing with 1 watt of internal dissipation is approximately +38°C.

In either case, it will be necessary to supply from 0.3 to 0.5 watts to the vidicon housing during lunar night in order to maintain the faceplate at or above -150°C. Three possible ways of supplying this power are the following:

(1) Direct conduction of heat from the vehicle through the mast and into the vidicon housing.

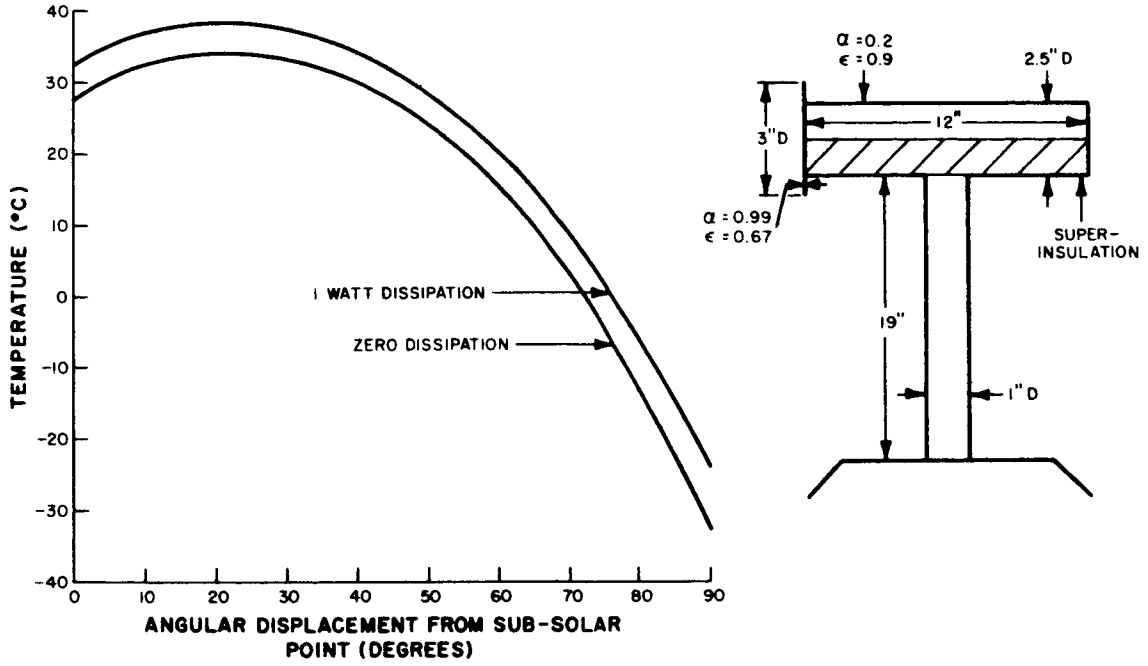

Figure II.6-7. Vidicon Housing Steady-State Temperatures As a Function of SLRV Angular Displacement from the Sub-solar Point Configuration 1

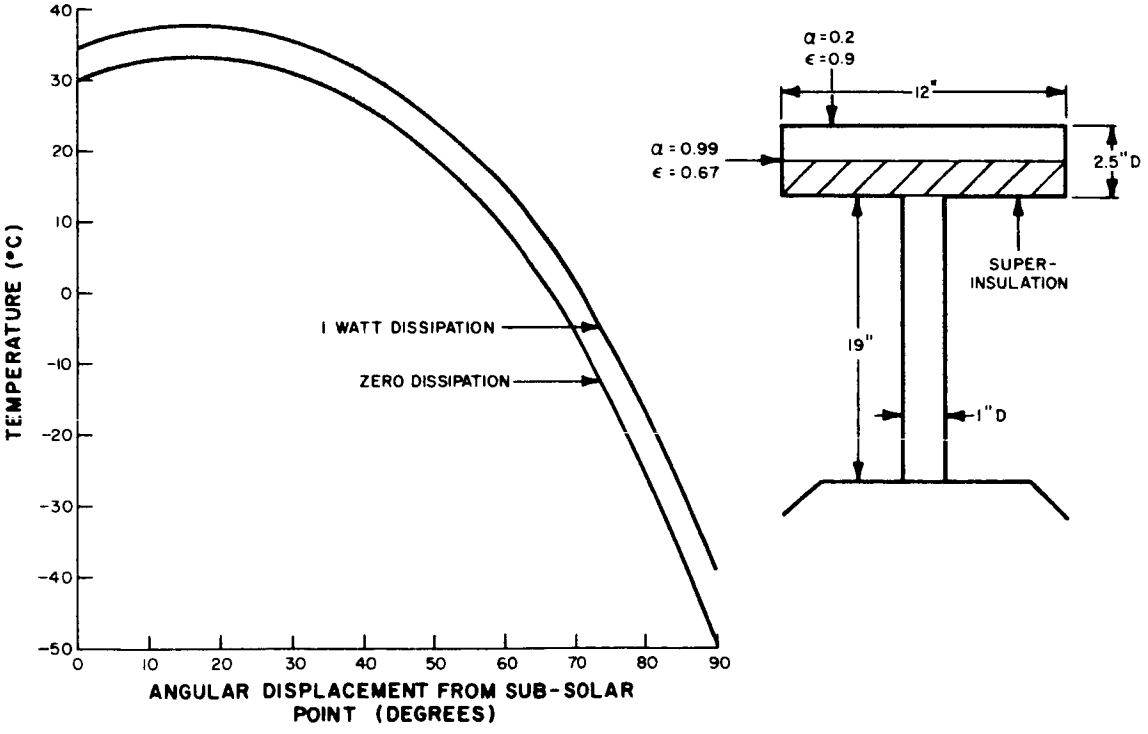

Figure II.6-8 Vidicon Housing Steady-State Temperatures As a Function of SLRV Angular Displacement from the Sub-solar Point Configuration 2

(2) Placing radioactive pellets in the vidicon housing.

(3) Draining a small amount of current from the batteries to the vidicon during lunar night.

The Phase I investigation indicates that the vidicon can be held within specified temperature limits by applying proper finishes and insulation to the vidicon housing. The statement that these temperature limits can be met is predicated on the assumption that the vidicon will not be required to operate within 1 earth day after emerging from lunar night.

10. Modes of Operation of SPS Vidicon with Open Shutter

The vidicon proposed for the SLRV will deliver a usable signal-to-noise ratio over an incident light range of > 1000 to 1. At low light levels (< 1 foot-candle-second at faceplate) the vidicon operates in the Frame Storage Mode. At intermediate light levels (between 1 and 50 foot-candle-seconds) such as are expected to be encountered at the lunar surface, the vidicon operates in the line-storage mode. Finally, at high light levels (> 50 foot-candle-seconds), the vidicon operates in the spot-storage mode.

Frame-Storage Mode - When operating in the frame-storage mode (i.e., the normal mode of operation for low light levels or shuttered operation), an element of the target can be represented by a small capacitance in parallel with a high resistance. During the "Prepare" cycle, each elemental capacitance is charged to target potential (Figure II.6-9). Exposure to light lowers the resistance of the photoconductor, causing the

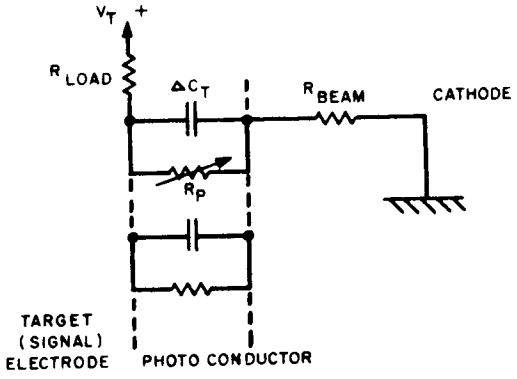

Figure II.6-9. Equivalent Circuit of Vidicon Picture Element

target capacitance to discharge partially. The change in potential, and hence the signal current required during readout to restore the charge on the target capacitance, is a linear function of the integrated light flux for small changes in potential. Conventionally, the change in potential at the target is kept to a few volts only in order to minimize beam landing errors. The potential on the electron-gun side of the photoconductor is shown in Figure II.6-10.

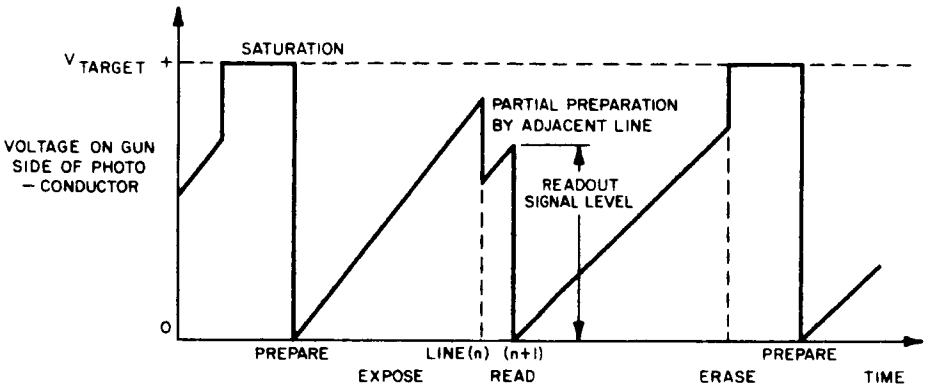

Figure II.6-10. Frame-Storage Operation with Open Shutter

Line-Storage Mode* - If the incident light between "Prepare" and "Read" is sufficient to cause complete discharge of the target capacitance, the target is effectively saturated. Under these conditions, the only a-c component in the signal current is that due to the phenomenon known as line storage. Line storage occurs because the spread of the beam under saturation conditions is sufficient to cause limited charging of target elements in adjacent lines, resulting in line-by-line preparation. The time interval between "line preparation" and "line read" is short enough at all but the highest light levels to prevent complete saturation of these elements following line preparation. The resultant signal current therefore consists of a large d-c component on which is superimposed the a-c signal information. The potential on the electron-gun side of a photoconductor element is shown in Figure II.6-11.

Spot-Storage Mode - At very high incident light levels, an element will saturate between line scans. Under these conditions, partial preparation occurs during readout from the immediately preceding elements in the same line. Under these conditions, the signal current contains a very large d-c component with a much smaller signal component corresponding to the saturated highlight.

*"Pickup Tube Performance With Slow Scanning Rates", Shelton, Charles T. and Steward, N. W., July 1958, Journal of the SMPTE

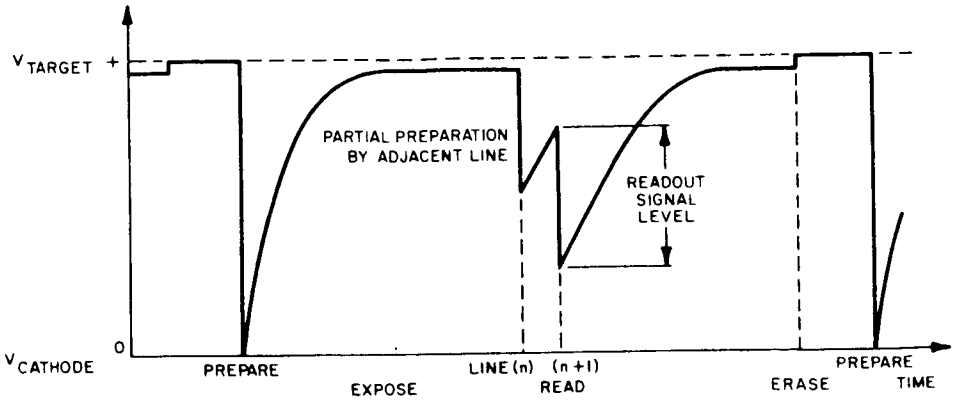

Figure II.6-11. Line-Storage Operation with Open Shutter

Experimental verification of the above phenomena has confirmed the fact that a vidicon operating under open-shutter conditions is capable of accepting an incident light variation of > 1000:1, and this is illustrated in Figure II.6-12. Because of these effects, absolute determination or estimation of the light levels at the lunar surface will not be possible.

VIDICON #F538
TYPE C74098 (S.P.S.)
(RCA-8134)

$E_{g1,}$ — -40V
$E_{g2,}$ — +300V
$E_{g3\&g6,}$ — +450V
$E_{g4,}$ — +80V (FOCUS)
$E_{g5,}$ — +300V
$E_{TAR,}$ — +15V

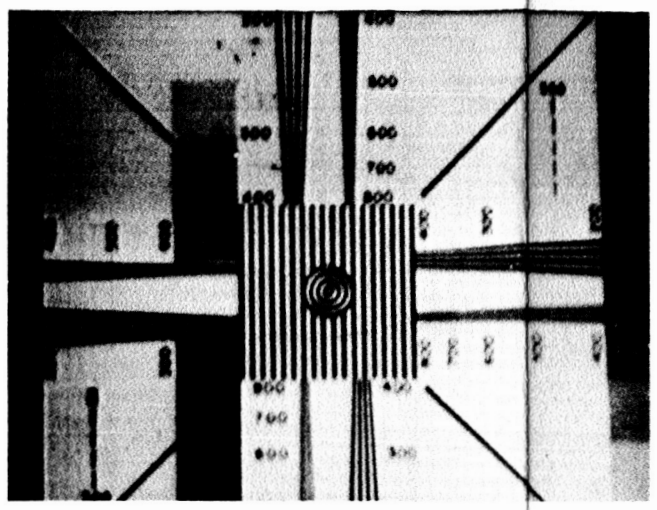

F/28

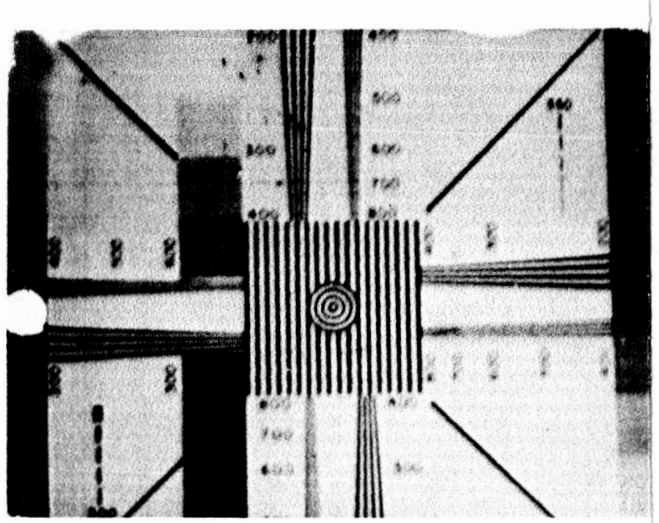

F/4

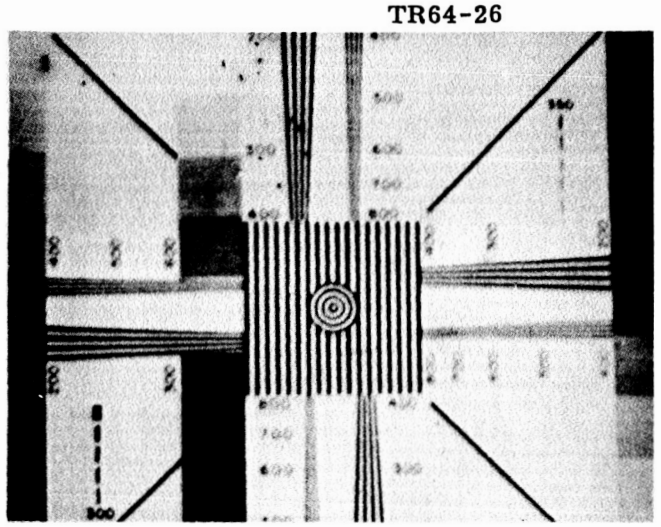

F/5.6

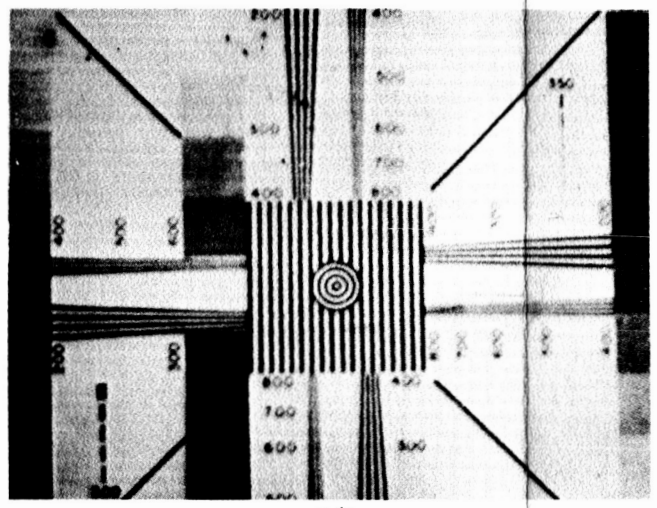

F/8

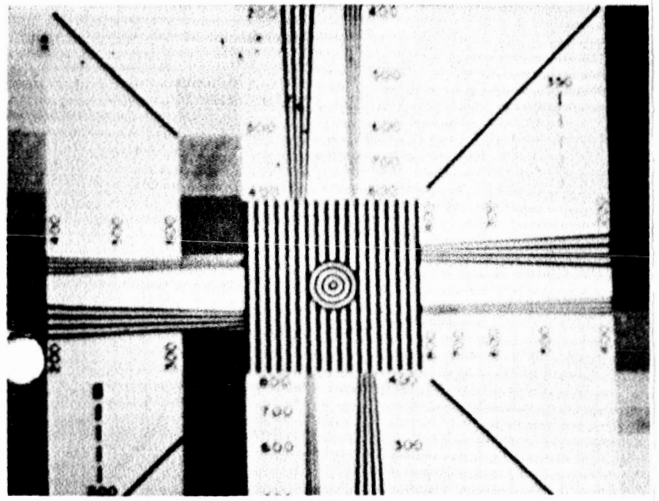

F/11

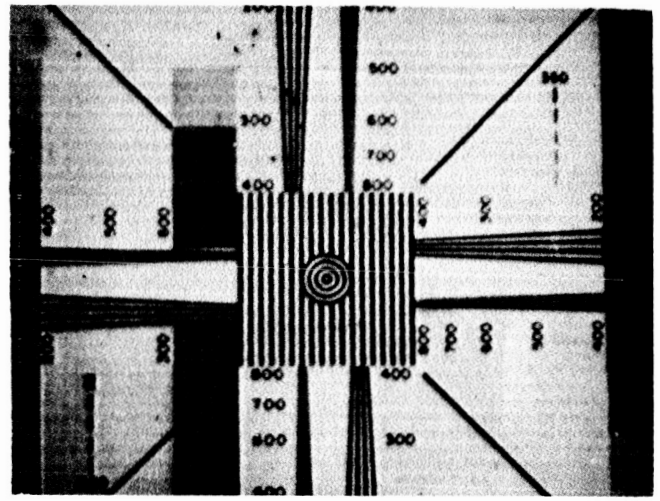

F/16

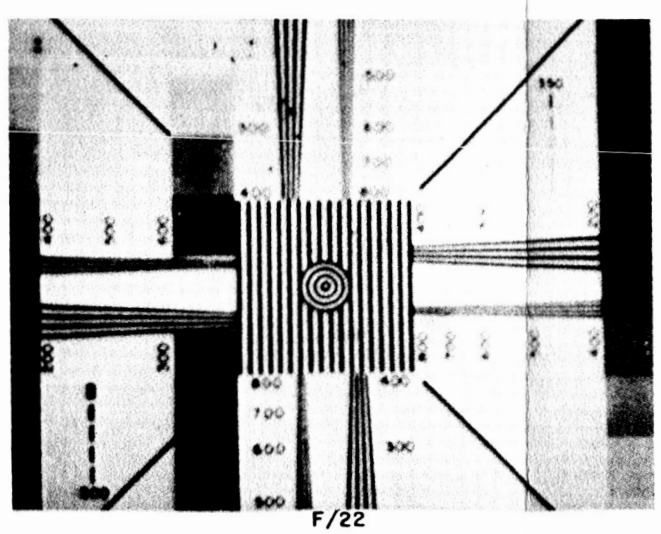

F/22

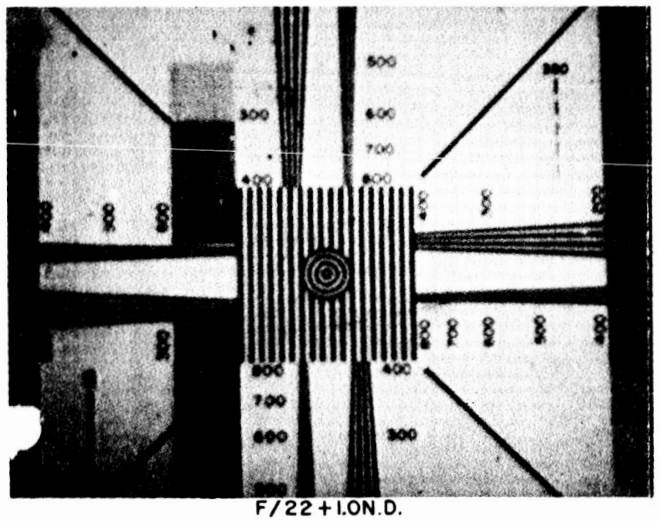

F/22 + I.ON.D.

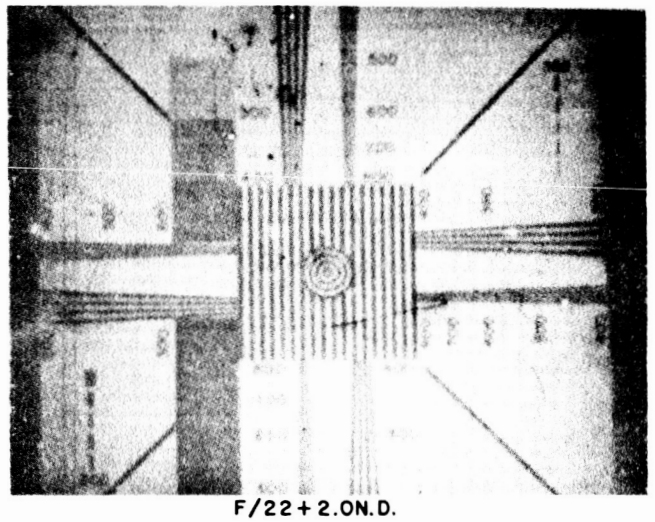

F/22 + 2.ON.D.

Figure II.6-12. Polaroid Prints of RETMA Test Chart taken at F/2.8 with No Filter and F/22 with 1.0 Neutral Density Filter (i.e., x10 Attenuation)

C. OPTICS

1. Introduction

This section outlines the factors and technical features related to the optics. Optical systems of a number of different camera configurations have been studied in conjunction with the requirements dictated by the over-all TV subsystem design. A short summary of the analysis of the optical parameters which determine the choice and final over-all performance of the optical system is presented.

The main optical characteristics in each case which required study in conjunction with particular optical configurations studied are as follows:

(1) Optical performance with reference to modulation transfer factors.

(2) Illumination over the field (and over-all light transmission).

(3) Physical and mechanical limitations.

(4) Depth-of-field limitations.

The over-all TV subsystem was to be defined with respect to the known trade-off factors. The primary optical configurations considered during Phase I are as follows:

(1) Optical systems which image directly onto the vidicon — The study indicated one of two basic systems. In one, an inclined mirror (at approximately 45°) was used to turn the incident light through 90° into the lens system, where the lens and vidicon axes were coincident, being located in the upper part of a mast. Rotation of the mirror in azimuth about the lens axis permitted a full 360° scanning field, while mounting of the mirror in different elevations allowed control of the horizontal viewing angle of the optical system. In the second, both the vidicon and the optics (whose axes were again coincident) were mounted directly on top of the mast to view the field without the aid of a mirror. The optical axis was parallel to the ground and perpendicular to the mast of the SLRV. Rotation of the whole vidicon plus optical assembly (or the mast) permitted a full 360° azimuth to be scanned. No elevation facility was planned with this configuration.

(2) Optical system which incorporates an image transfer system — This system enables the vidicon to be located in the base of the mast or lower compartment, the viewing optics (entrance pupil) being at the top of the mast as in a periscope. A number of different approaches were initially examined, and the most promising was studied in detail. The approaches considered were as follows:

(a) A primary imaging lens together with relay lens (one or more) to relay the image down the mast.

(b) A compound optical periscope-type system with built-in azimuthal scanning mirror at the upper end and imaging directly onto the vidicon at the lower end. A periscope-type system of about 20 inches was envisaged.

(c) Fiber optics unit.

For each optical configuration, the optical characteristics mentioned previously were examined in detail. The trade-off studies associated with the main SLRV system design established the determining factors for the optical configurations. Weight, size, mast configuration and shape, and center of gravity were clearly limiting factors with regard to the optical system and were the deciding criteria of the feasibility of a given system. The selection of field of view for the optics was determined by the mission requirements resulting from the systems analysis study and the optical performance obtained. In turn, the field of view established the focal length. Different fields of view were considered according to the over-all system configuration.

2. Optical Constraints

The optics must be selected on the basis of the performance quality of different designs, the weight and size of the system, and the functional requirements. The best performance will be obtained by the simplest system with a single (compound) lens system. The weight, size, and optical performance are interrelated with both the stop number and the field of view. Further constraints on the field of view arise in the case of an azimuthal scanning mirror and elevation-depression head. Choice of field of view depends initially on the focal length, which in turn must be selected according to the limiting resolution required at the various ranges of interest. Good resolution characteristics at long ranges are achieved only by long-focal-length optics with a narrow field of view; hence, a limited area coverage is possible at near ranges. Good resolution at near ranges using short-focal-length, wide-angular-field lenses is readily obtained at the expense of poor long-range resolution. Thus, the final selection of the optics configuration becomes a matter of trade-offs among all of the parameters mentioned above.

The optics for a stereoscopic system can be expected to involve duplicate cameras, or alternatively single mirror systems having a limited field of view. The base line is limited in both cases, although longer base lines with wider fields of view are possible with two cameras at the expense of greater weight.

The constraints on the F/number are mainly determined by the optical performance, while the illumination sensitivity of the vidicon is a secondary factor. A fixed F/number of approximately F/4 has therefore been adopted. In high-quality lenses, the thickness of the vidicon faceplate must also be taken into account, particularly at large field angles.

Modification of the distortion characteristics of a lens over the field, independently of the other optical properties of the lens, is not readily accomplished. Certain special types of lenses (e.g., torroidal) have unusual distortion characteristics, but their optical performance is not very good.

3. Discussion of Optical Systems

In the direct-imaging system mentioned, a search was made for commercially available lenses having fields of view between 20° and 30°. The azimuthal mirror size depended on the angular field and the effective diameter of the lens according to the formula:

$$\textit{Mirror dimensions: } L = D/\{\cos\theta \sin(45^\circ - \theta)[1 - \tan\theta]\},$$

where θ is the total angular field, D is the effective lens diameter, and L is the long dimension of the mirror. This is plotted for a series of D values in the Figure II.6-13. The value of D depends on the lens, the location of its nodal points, and the mechanical construction. Except for small angular fields, it was found that large-size mirrors would be required.

A number of lenses were found suitable to cover fields up to 34 degrees, incorporating a reasonably sized mirror. Figures II.6-14 through II.6-16 show the corresponding

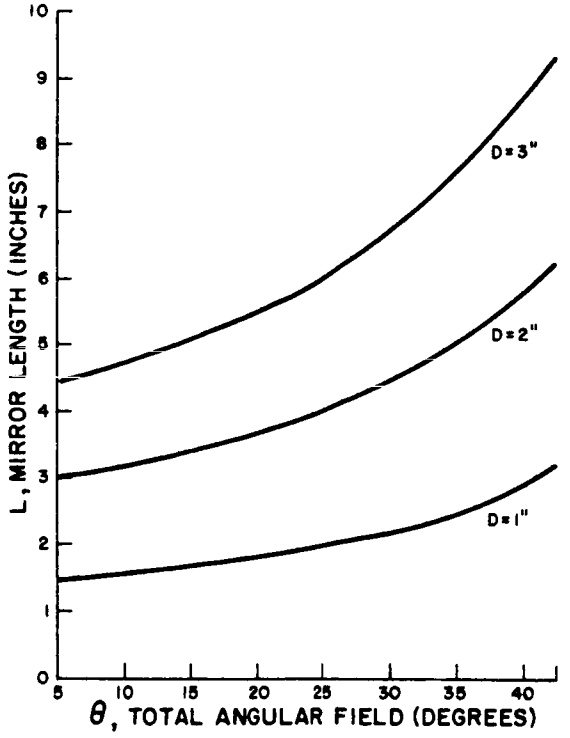

Figure II.6-13. Mirror Size for Azimuthal Scanning Head

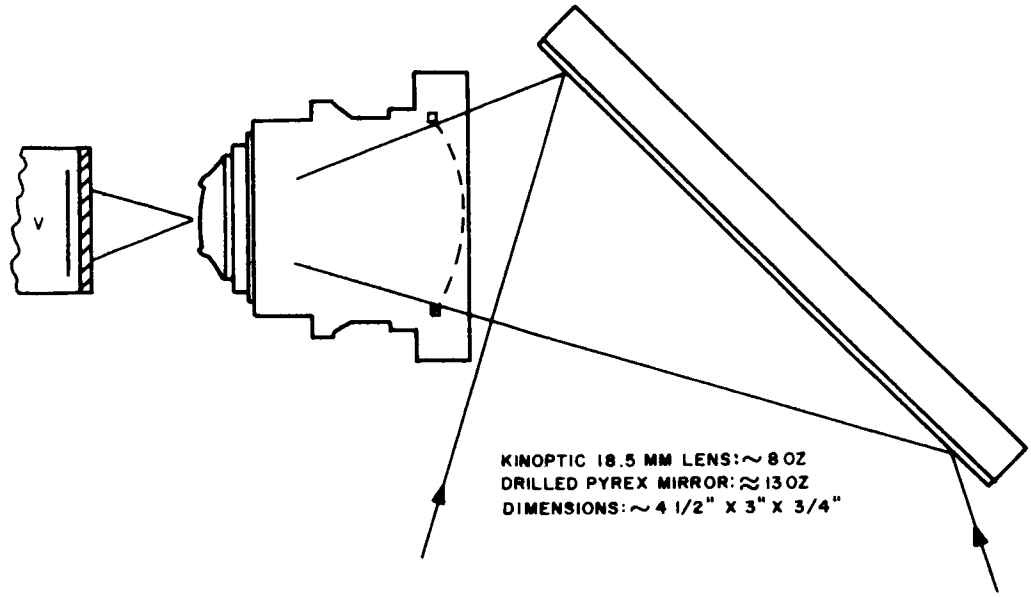

Figure II.6-14. Kinoptic Epochromat 18.5mm f/2 - Mirror Geometry
Rectangular Field of View: 34°

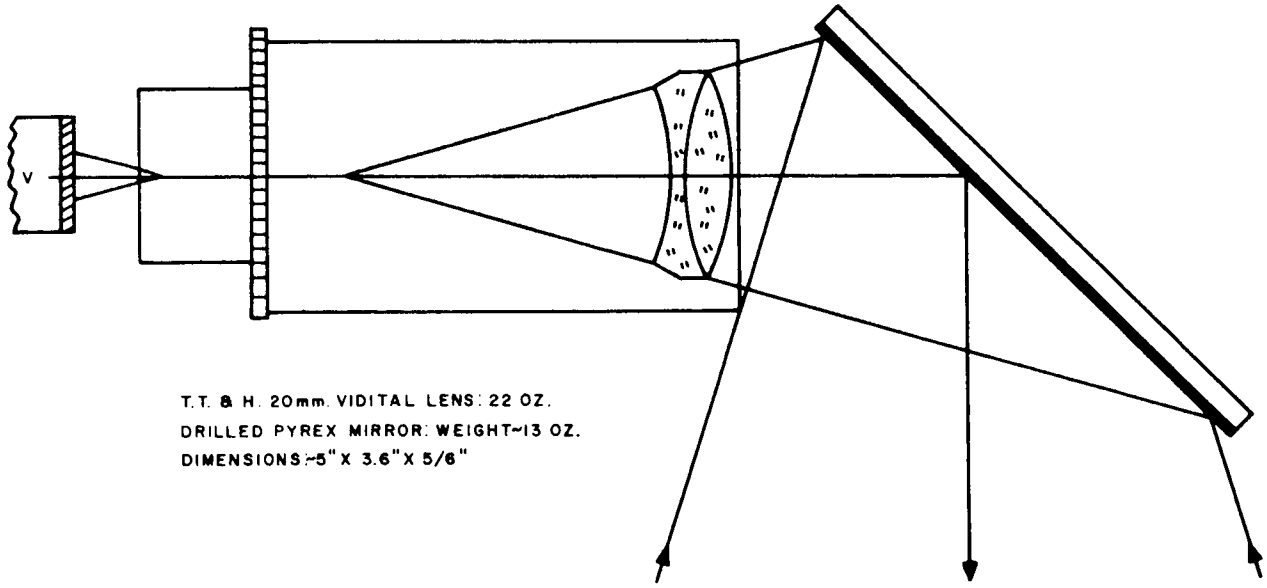

Figure II.6-15. Vidital Lens. 20mm f/1.9 - Mirror Geometry
Rectangular Field of View: 30°

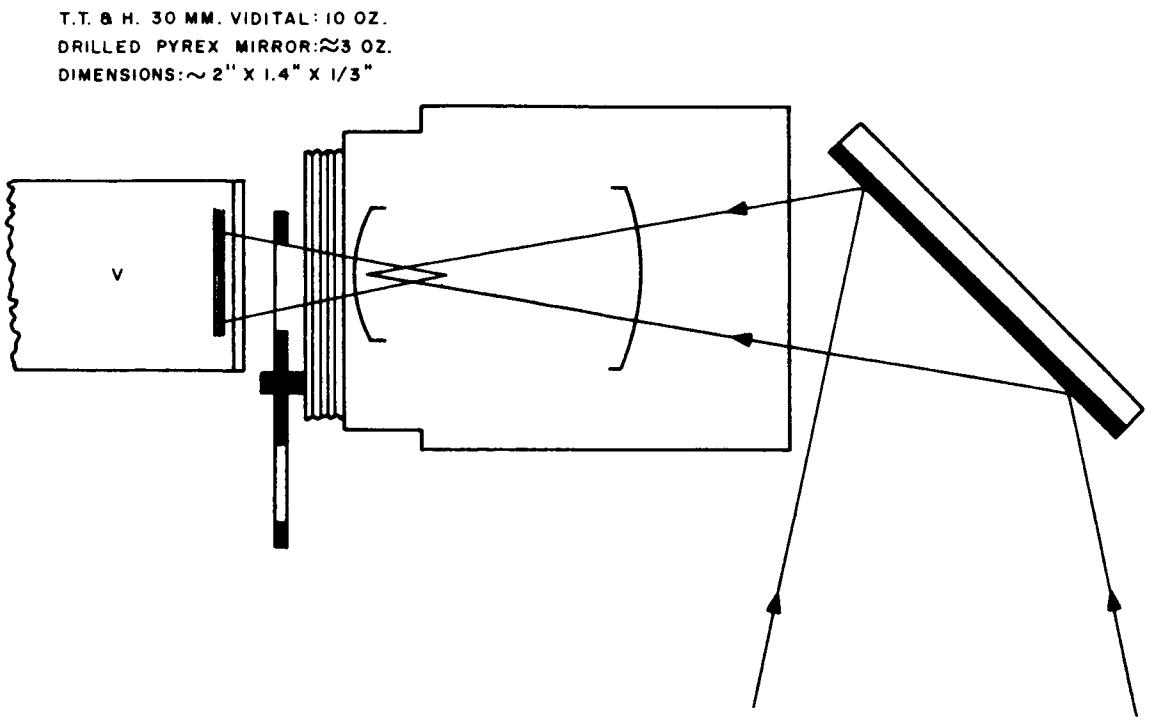

Figure II.6-16. TT&H Vidital Lens 30mm T/1.5 - Mirror Geometry Rectangular Field of View 21°

mirror arrangement and dimensions for those particular lenses. Three lenses had the best optical performance of those considered. The mirror weights and dimensions are as indicated on each figure. In practice, there is no accurate means for relating mirror size to lens focal length and field of view. Each lens must be considered in turn, knowing its optical principal points and its dimensions. The mirror itself would be lightweight, either of Beryllium or aluminized pyrex blank, the pyrex being drilled to lighten the mirror (or possibly a honeycomb blank being a structure which would be ceramically fused to a glass blank). It was tentatively decided that the drilled pyrex would be most suitable.

The optical performance of these lenses was evaluated in terms of their optical modulation transfer function over the field, and curves of this function measured experimentally at RCA are shown in Figures II.6-17 through II.6-19 at different apertures out to spatial frequencies of 27 cycles/mm (54 TV lines/mm).

At least two other lenses (Angenieux 24 mm, F/2.2; and 28 mm, F/1.8) were also acceptable from the weight viewpoint and mirror dimension, but their optical performance was not expected to be as good over the field as that of the three lenses mentioned previously.

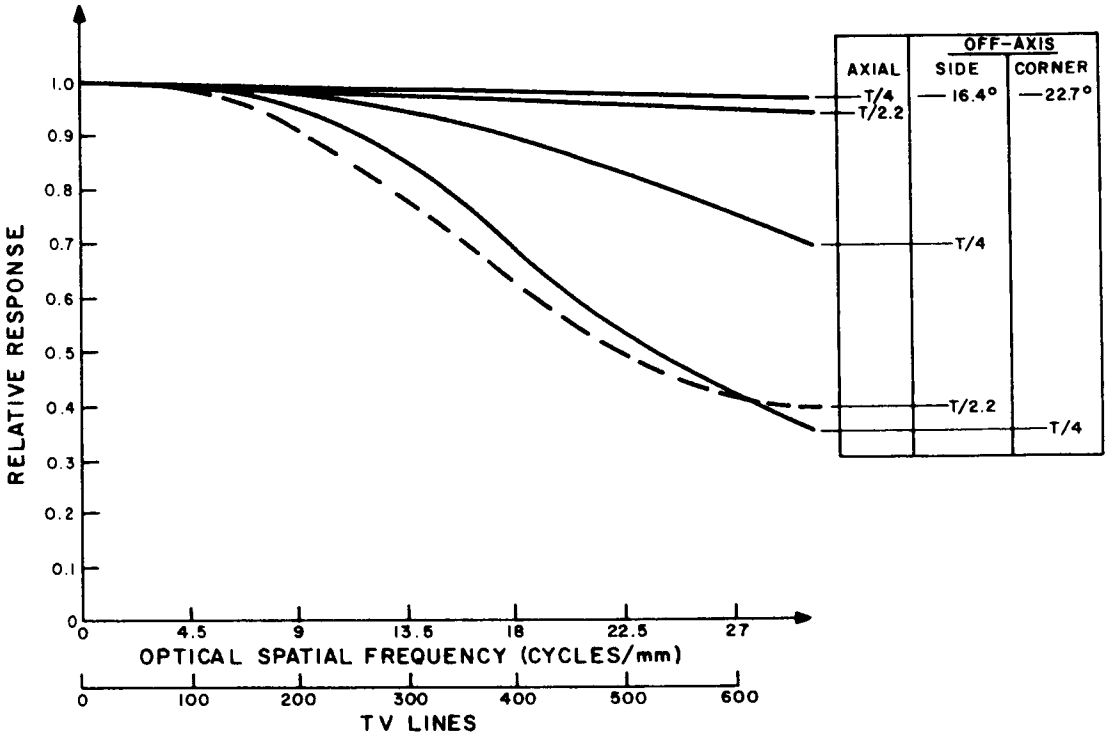

Figure II.6-17. Contrast Modulation Function (Sine Wave Response) 18.5mm f/2 Kinoptic Apochromat

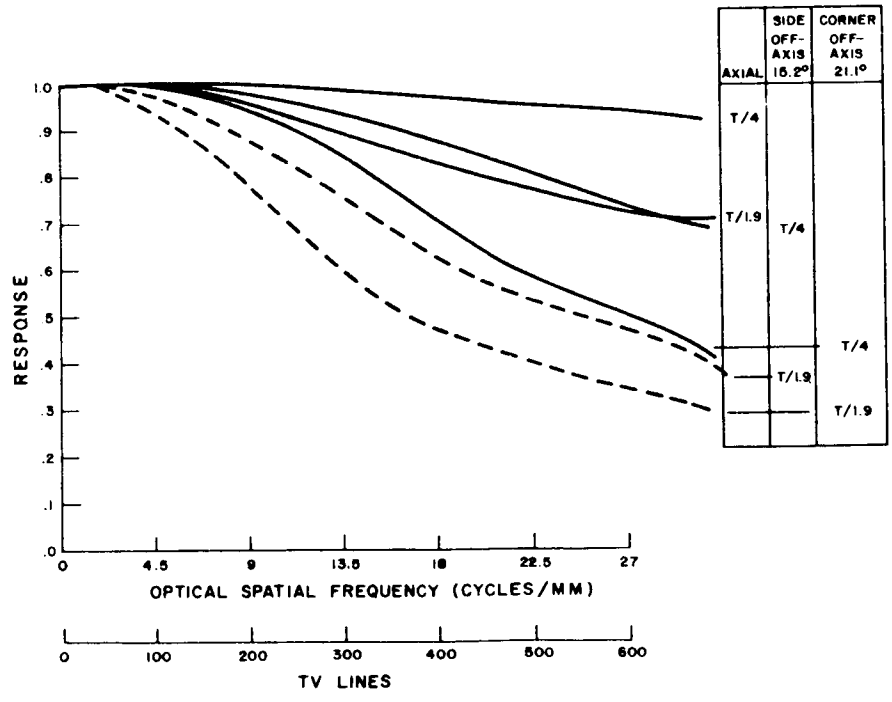

Figure II.6-18. Contrast Modulation Function (Sine Wave Response) 20mm T/1.9 Vidital (T.T.&H) Lens

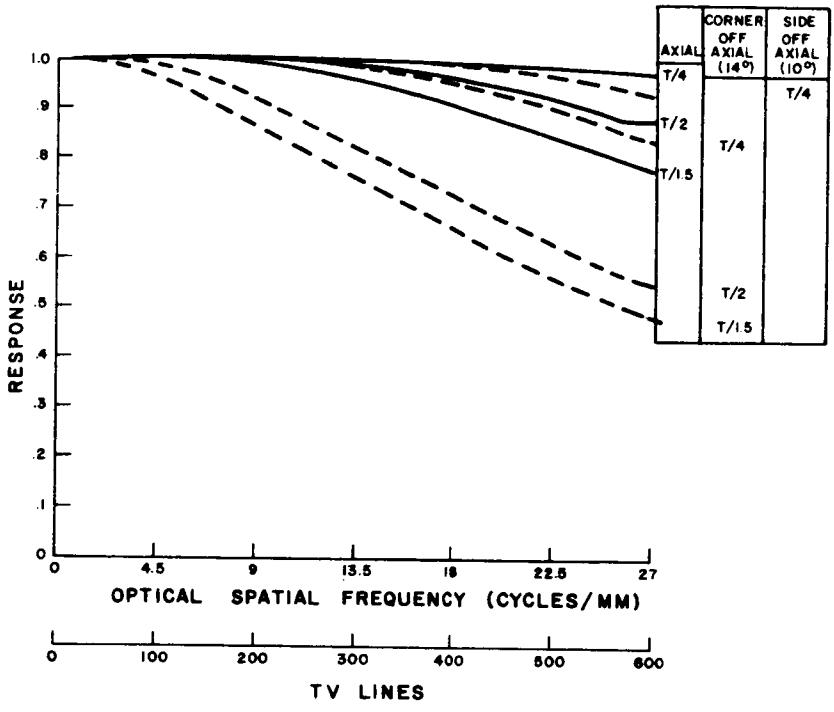

Figure II.6-19. Contrast Modulation Function (Sine Wave Response) 30mm T/1.5 T.T.&H Vidital Lens

In addition to the main mast supporting the optical unit and the necessary drive units, a fairly lightweight mechanically operated filter and sun shield were envisaged as simply combined in a disc rotated between the lens and vidicon. An approximate weight breakdown of the mechanical structure was thus as follows:

	Weight (lb)
Mirror mount of azimuthal scan head	0.75
Drive and gears for driving head	1.25
Mast and supports	1.5
Filter/sun shield wheel and drive	1.0
TOTAL WEIGHT	4.5

This total weight is increased by the optical system and vidicon unit.

In the second arrangement with the optics on top of the mast, no mirror was used. The center of gravity of the whole system in this case may be appreciably raised for a given mast height, providing a corresponding reduction in the optical and vidicon weight can be achieved. The main advantage appears in the much wider angular field

possible because of the absence of a mirror. Only the optical properties of the lens limit the field angle. The following two major effects at wide angles are significant:

(a) Optical performance decreases rapidly at wide angular fields. The wider the field, the more complex the optical design and hence the heavier the lens (in order to maintain performance). In general, a lightweight lens covering a wide angular field will not have high performance characteristics.

(b) Illumination over the field falls off approximately according to a fourth-power law:

$$I = I_o \cos^4 \theta,$$

where θ is the field angle. Thus, at a field angle of 30 degrees the illumination will fall by nearly 50% (in practice the lens aberrations modify the above relationship to a certain extent).

Consequently, the over-all performance is likely to be compromised in wide-angle systems. The system requirements now called for a 45 degree rectangular field (and hence a 62° diagonal) on a 500-TV-line (27 cycles/mm) system. The most suitable lens commercially available lens appeared to be an Angenieux F/3.5, 14.5-mm-focal-length system from both weight and optical performance standpoints. This lens will provide a 42° angular field of view (59° on the diagonal). It weighs 4 ounces and will cover up to an 85° field. Resolution tests on this lens indicate that it has fairly good performance over the whole field. Modulation transfer function (sine-wave response) curves have been measured on axis only (because of limitations in the measuring equipment), and a response of more than 70% is obtained out to spatial frequencies of 27 cycles/mm. No suitable commercial lens comparable to the Angenieux has been found. A loss resulting from fall-off in illumination will certainly occur because of the cosine fourth law, but no vignetting in this lens occurs to cause further losses. Field curvature in this lens is also small and should not produce a serious degradation of response.

In order to reduce the center of gravity of the SLRV, designs in which the vidicon tube was located in the lower compartment were examined, a mast approximately 20 inches high being considered. An optical transfer system in the mast would enable the viewing lens to be located at the top of the mast (a rotatable mirror being necessary to turn the light beams through 90° and to scan through an azimuth of 360°).

Initially, the simple extension of the lens-vidicon distance by placing a simple relay lens between the viewing lens (on top of the mast) and the vidicon (in the lower compartment) was examined. A suitable high-quality lens designed for unit magnification and with a focal length of about 4 inches would be required. A number of suitable lenses are readily available. However, cascading two optical systems inevitably

means loss of performance. It is essential to include a field lens at the first aerial image position, increasing the over-all weight. The performance of such a compound system built up from the separate units would be very poor off the axis because of field curvature, chromatic aberration, and off-axial aberrations. Only by stringent optical design and subsequent modification of one or more of the components could high performance over the field be achieved. It was finally concluded that only a rigorous optical ray trace through the entire system would be likely to enable modifications to be made to produce a good optical performance. Other systems involving telescopic systems were, for the same reason, rejected. In fact, no high-performance system was likely to evolve from this approach. Such a cascaded arrangement of ready-made optics would only yield a heavy and inferior-performance system with respect to the 30° field (or larger) required.

It was essential to have a system designed as a composite unit including the azimuthal scanning mirror, the image lens, and the transfer lenses as one single compund optical system. Only by established optical design techniques could an acceptable periscopic-type system be obtained. In the first instance, an investigation of the feasibility of suitable designs, together with an estimate of their performance over the field from center to corner, was requested from a number of optical firms able to accomplish this. Only initial concept and feasibility analyses were obtained.

Provisional technical specifications for the optical mast were decided upon, and these are listed in Table II.6-5 , which was forwarded to the optical firms.

A very rough indication of two types of system that were proposed are represented in the Figure II.6-20. The optical firms approached believed that they could meet the performance specifications, but a more definite evaluation can only be obtained after a complete design study program. The transmission losses in the periscope system are not expected to be high (probably of the order of 20%). Uniformity of illumination would be fairly good over the field envisaged, but no figures are yet available.

Imaging of the object field onto a fiber bundle may be carried out at the top of the mast and the image relayed by the fiber optics to the faceplate of the vidicon located some distance away in the lower compartment. The weight of the quartz or glass bundle in such a system would be fairly low (less than 0.5 lb), but a number of disadvantages and problems have precluded its use for the present purpose.

Coupling of the fiber bundle and vidicon faceplate (which must be a fiber faceplate) inevitably causes a loss in light and optical performance because of random mismatching of the individual fibers. This effectively causes a degradation of the modulation transfer function response. The performance of fiber optics at the present time is limited compared to optical systems, and a high loss in response would occur over the spatial frequency range of the vidicon. In addition, the transmission losses are high (in a 20-inch length, well over 50% loss is expected to occur in the fiber bundle). Cascaded with the primary imaging lens, poor over-all performance can be expected.

TABLE II.6-5

PROVISIONAL TECHNICAL SPECIFICATIONS - OPTICAL MAST

Mirror: (38.75° to horizontal):	Optical axis elevation depressed 12.50°. To rotate through 360° in azimuth; dimensions and weight to be as small as possible.
Mast length:	20 inches.
Mast diameter:	Not critical (say 1 inch to 3 inches).
Mast weight (total):	Preferably less than 2 lbs.
Mast center of gravity:	As close to vidicon as possible
Environment:	Rugged to withstand launch acceleration (30g for 11m. secs). Temperature variations + 400°K to + 100°K. Hard vacuum (10^{-12} mm Hg).
Optical Specifications	
Focal length:	Approximately 15 mm.
Field of view:	Approximately 40° (55° diagonal).
Aperture:	F/4.
1 inch vidicon:	500 TV line system. 11.2 mm square format.
Performance required:	High contrast (at least 50% response), from center to corner of field over zero to 22.5 cycles/millimeter (contrast means modulation transfer factor).
Spectral characteristics:	Sensor - Vidicon (with antimony trisulphide face). Source - sunlight. Flare and scattered light in the system must be low.

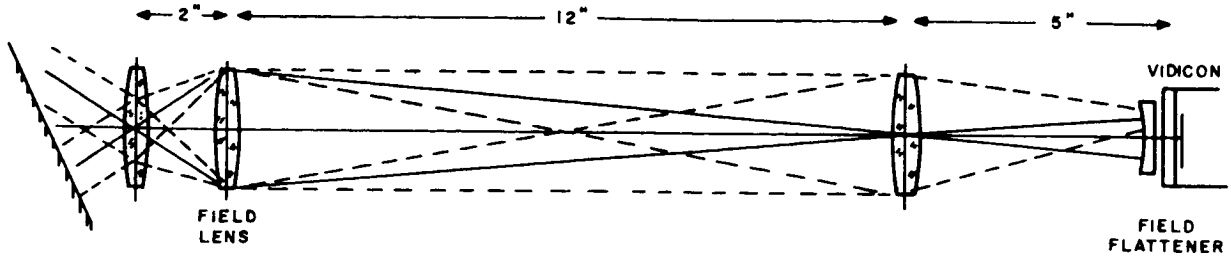

(a) ITEK AZIMUTHAL SCANNING PERISCOPE.

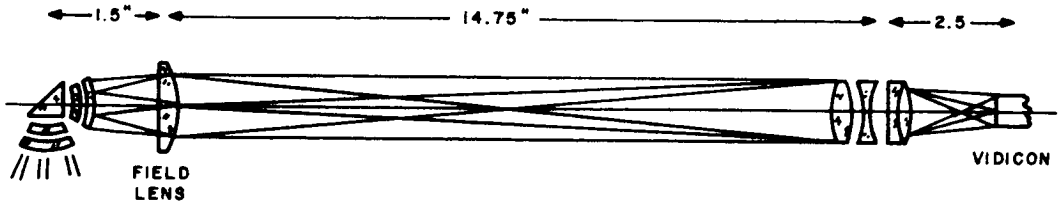

(b) AMERICAN OPTICAL (J.W. FECKER) —OPTICAL TRANSFER SYSTEM

(METROGON UNIT) (EFFECTIVE FOCAL LENGTH≈15MM.)

Figure II.6-20. Schematic Optical Designs for Periscope-Type Mast of 20 Inches

The preceding discussion has presented only an outline of the main optical considerations. A detailed study of environmental constraints has not been accomplished. Non-browning glass on special order could probably be used in the manufacture of most of the above systems if a radiation risk is thought to exist. Protection of the optics against dust intrusion would necessitate a sealed system, and a window having a metalized antistatic film may be used to minimize electrostatic attraction.

Investigation of means to minimize the effects of micrometeorite and microscopic-particle bombardment has yet to be carried out, but the inclusion of a special window (of sapphire, for example) may provide effective protection.

4. Depth-of-Field Analysis

It is possible to assess the depth of field and the nearest distance at which good optical performance is obtained. In the present case, this can be estimated in terms of the loss of response (i.e., fall-off of the modulation transfer function or sine-wave response) that can be allowed without seriously degrading the image. The following theoretical expressions have been worked out from which the near field (μ_1) and the far field (μ_2) can be calculated. The lens is arranged to be focused at a distance $\bar{\mu}$

Near field:

$$\mu_1 = \mu_2 \Big/ \left\{ 1 + \frac{2\Delta z}{f^2} \mu_2 \right\}$$

Lens focused at:

$$\bar{\mu} = \frac{2\mu_1 \mu_2}{\mu_1 + \mu_2}$$

and

$$\Delta Z = \frac{F^2 \, 8n\lambda}{\pi},$$

where

f is the focal length of the lens,

F = lens aperture (or focal ratio),

λ = mean wavelength of light (taken as 5.5×10^{-5} cm),

and n is an integer whose value must be determined from sine-wave response curves for defect of focus of a lens for a particular lens aperture.

As an example, the near and far field of the 14.5 mm Angenieux F/3.5 lens has been calculated. It is first decided that, at the highest spatial frequence of interest (22.5 cycles/mm), no more than a 10% drop in response is to occur due to imaging objects at different object distances (the lens focal distance being fixed).

The corresponding n-value can be found from the defect of focus sine-wave response curves for a particular lens aperture (say F/4), since these are well established.

For the 10% tolerance chosen, the n-value in this case is approximately n = 3. From this, the factor Δz is found to be $\Delta z = 6.7 \times 10^{-3}$. For a range of far-field values μ_2, the respective near distance for the lens can be found from the expression given above, the lens being focused accurately at some intermediate distance $\bar{\mu}$. Table II.6-6 shows a series of values for the near and far fields.

The lens will give satisfactory images within the near and far fields quoted, but outside these distances the image quality will deteriorate rapidly (because of an effective fall in sine-wave response). The figures evaluated are those for a high-quality (aberration-free) lens, but will also be representative of high-quality lenses in practice. All lenses are influenced by their aberrational characteristics and a small modification of the effective depth of field may arise. This analysis is meant to provide specific limits on the near and far fields and to allow the performance to be described with reference to sine-wave response characteristics.

TABLE II.6-6

VALUES FOR NEAR AND FAR FIELDS

Far Field μ_2(meters)	Near Field μ_1 (meters)	Lens Focusing Distance $\bar{\mu}$ (meters)
∞	1.56	3.12
100	1.56	3.03
50	1.52	2.94
10	1.35	2.38

APPENDIX VII

SYSTEM ENGINEERING

APPENDIX VII
SYSTEM ENGINEERING

A. OVER-ALL SYSTEM

The over-all block diagram for the SLRV electronic system is shown in Figure II.7-1: At this stage in the program, it is not possible to present all the logic and interlock circuits associated with the complex control structure. Instead, the symbolic control and switch functions are identified by the commands that actuate them. The commands are designated by numbers as noted in Tables II.5-1 and II.5-2 (Appendix V) of this report.

B. PHYSICAL CHARACTERISTICS OF THE ELECTRONIC SYSTEM

1. Weight

The weight breakdown of the electronic system is shown in Table II.7-1. The total weight of approximately 52.0 pounds has been derived as well within the state-of-the-art. Table II.7-2 is a comparative breakdown of the communications and power subsystems for the direct and indirect links. (Subsystems other than power and communications are the same for the two links.) The basic direct system is some 22 pounds heavier than its indirect equivalent. The fact that an RTG power subsystem for the direct link is compared with a solar-array power subsystem for the indirect link is quite realistic. The power demands of the direct link system (approximately 40 watts) are such as to preclude use of the solar array, because of the volume limitations of the Surveyor stowage envelope.

2. Power

Table II.7-3 lists the power dissipations of the various subsystems, so defined that thermal design problems within individual compartments can be evaluated when related to power duty cycles. In pertinent cases, power dissipations are shown in various modes of vehicle operation. This is elaborated in Table II.7-4, which shows which subsystems are operative in any particular mode of operation. Using this table it is possible to evaluate the average power requirements for various hypothetical missions.

During the course of the study several different standardized missions were examined. The main usefulness of this standardized approach was in the ability to compare power and time requirements of the direct and indirect systems. It is noteworthy that even for missions of significantly different emphasis, the average power to be supplied to the load always turns out to be of the order of 30 watts for the indirect link and on the order of 42 watts for the direct link. Lunar surface roughness variations appear to contribute more to changes in average power than do the sequences of steps used in the standardized mission chosen. Typical standardized missions and power profiles are discussed elsewhere in this report.

3. Volume

Table II.7-5 lists those component volumes which are pertinent to packaging requirements.

TABLE II.7-1 WEIGHT BREAKDOWN FOR SLRV ELECTRONICS SYSTEM, INDIRECT LINK (WEIGHT IN POUNDS)

Subsystem	Axle 1 Inside Thermal Comp.	Axle 1 Outside Thermal Comp.	Axle 2 Inside Thermal Comp.	Axle 2 Outside Thermal Comp.	Axle 3	SLRV Totals	Surveyor
Communications							
SLRV: VHF Transmitter 2 Watt Mode / 0.2 Watt Mode			2.0	—			
SLRV: VHF Receiver (100-200 Mc)			0.6	—			
SLRV: VHF Diplexer			1.0	—			
SLRV: VHF Antenna & Feed*			—	0.5			
SLRV: Input Selector			0.4	—			
SLRV: DIBSI Multiplexer			0.5	—			
Surveyor: VHF Transmitter 2 Watt Mode / 0.2 Watt Mode							2.0
Surveyor: VHF Dual Receiver							1.2
Surveyor: VHF Triplexer							1.3
Surveyor: VHF Antenna & Feed*							1.0
Surveyor: Range & Bearing							0.5
Surveyor: Input Selectors							0.6
Subtotals			4.5	0.5		5.0	6.6
Television							
Basic Micromodular Camera							
Vidicon & Plug		0.2					
Light and Target Ring		0.1					
Preamplifier		0.25				1.5	
Deflection Coil and Shield		0.40 (1.5)					
Decoupling		0.35					
Alignment Coils		0.20					
Electronics	4.25					4.25	
Sun Shutter		1.3				1.3	
Sun Sensor							
Optics							
Lens (14.7mm Angenieux)		0.5				.5	
Mount & Filter							
Structure							
18-inch Mast & Camera Housing		2.0				5.8	
Azimuth Motor & Drive	2.5 (3.8)						
Elevation Drive	1.3						
Subtotals	8.05	5.3				13.35	
Telemetry							
Central Data Processor			1.0 (1.7)				
Data Pre-Processor			0.7				
Data Pre-Processor	0.7						
Subtotals	0.7		1.7			2.4	
Power							
Solar-Cell Array							
Solar Cells, Glass Covers					2.4		
Glass					0.5 (7.8)		
Adhesive					2.3		
Substrate					2.6		
Battery (Silver Cad.)			3.70				
Charge, Discharge, and Regulation Electronics			3.00				
Drive Motor					1.0		
Subtotals			6.70		8.8	15.5	
Command and Control							
Vehicle Central Decoder (VCD)			0.9 (3.3)				
Vehicle Sub-Decoder (VSD_1)	0.9						
Vehicle Sub-Decoder (VSD_2)			2.4				
SLRV Control Unit							0.8
Subtotals	0.9		3.3			4.2	0.8
Other							
Control Relays	0.45		1.25			1.7	
Solar Azimuth Indicator		1.5				1.5	
Control & Test Control Unit	1.0		1.0			2.0	
Subtotal	1.45	1.5	2.25			5.2	
Totals	11.10	6.8	18.45	0.5	8.8	45.65	7.4

*No provision for extending antennas is included in antenna weight estimates.

TABLE II.7-2

ELECTRONIC SYSTEM WEIGHT COMPARISON-DIRECT VERSUS INDIRECT LINK

Direct Link		Indirect Link	
Subsystem	Weight (pounds)	Subsystem	Weight (pounds)
Communications		**Communications**	
SLRV: "S"-Band Transmitter	3.2	SLRV: VHF Transmitter (2-Watt Mode / 0.2-Watt Mode)	2.0
SLRV: "S"-Band Receiver	4.0	SLRV: VHF Receiver	0.6
SLRV: "S"-Band Diplexer	1.5	SLRV: VHF Diplexer	1.0
SLRV: "S"-Band Omni Antenna	0.5	SLRV: VHF Antenna & Feed(1)	0.5
SLRV: "S"-Band Directional Antenna	6.5	SLRV: Input Selector	0.4
SLRV: Central Communications Control	0.5	SLRV: DIBSI Multiplexer	0.5
SLRV: VHF Transmitter (R&B)	2.0		5.0
SLRV: VHF Receiver (R&B)	0.6		
	18.8		
Surveyor: VHF Transmitter (R&B)	2.0	Surveyor: VHF Transmitter (2-Watt Mode / 0.2-Watt Mode)	2.0
Surveyor: VHF Receiver (R&B)	0.6	Surveyor: VHF Receiver	1.2
Surveyor: VHF Omni Directional Antenna	0.5	Surveyor: VHF Triplexer	1.3
	3.1	Surveyor: VHF Antenna & Feed(1)	1.0
		Surveyor: Range and Bearing	0.5
		Surveyor: Input Selectors	0.6
			6.6
Subtotal	21.9	Subtotal	11.6
Power		**Power**	
Assuming: 10-12 hrs. operation per 24-hr. day; 34 Watts Regulated, 6 Watts Unregulated		**Solar-Cell Array**	
Battery	4.0	Solar Cells, Glass Covers	2.4
Electronics	3.0	Glass	0.5
RTE Generator & Converter	21.0(2)	Adhesive	2.3
		Substrate	2.6
			7.8
		Battery	3.7
		Charge, Discharge & Regulation Electronics	3.0
		Drive Motor	1.0
Subtotal	28.0(3)	Subtotal	15.5
		Difference(4) 49.9-27.1	=22.8

(1) No provision for extending antennas is included in weight estimate.

(2) Assuming 1.5 to 1.7 watts/pound.

(3) An approximation of the right order of magnitude; actually a function of the RTE earth and lunar containment philosophy.

(4) The other subsystems retain same weight for both Direct and Indirect Links.

Subsystem	Axle 1		Axle 2		Axle 3	SLRV Totals		Surveyor
	Inside Thermal Comp.	Outside Thermal Comp.	Inside Thermal Comp.	Outside Thermal Comp.				
			Charge Mode	Operate Mode		Charge Mode	Operate Mode	Operate Mode
Communications								
SLRV: VHF Transmitter								
2-Watt Mode			—	8.0				
0.2-Watt Mode			0.1	1.5				
SLRV: VHF Receiver (100-200 Mc)			1.0	1.0				
SLRV: VHF Diplexer			—	—				
SLRV: VHF Antenna & Feed			—	—				
SLRV: Input Selector			—	0.8				
SLRV: DIBSI Multiplexer			—	0.2				
Surveyor: VHF Transmitter								
2-Watt Mode								8.0
0.2-Watt Mode								1.5
Surveyor: VHF Dual Receiver								1.4 or 2.4[1]
Surveyor: VHF Triplexer								—
Surveyor: VHF Antenna & Feed								—
Surveyor: Range & Bearing Unit								0 or 0.9[2]
Surveyor: Input Selectors								1.4
Subtotals			1.1	10.0/3.5		1.1	10.0/3.5	

	Axle 1		Axle 2		Axle 3	SLRV Totals		Surveyor
	Operate Mode	TV Mode	Operate Mode	TV Mode				
Television								
Basic Camera								
Vidicon & Plug			0.68	0.93				
Light and Target Ring				0.25				
Preamplifier				0.25				
Deflection Coil & Shield				0.05				
Decoupling				—				
Alignment Coils				0.05				
Electronics	0.75	10.05						

TABLE II.7-3

TR64-26

POWER DISSIPATIONS (WATTS) FOR THE INDIRECT LINK

Sun Shutter				2.5 Watt-Sec. per Oper.								
Sun Sensor			0.07	0.07								
Optics												
Lens (14.7-mm Angenieux)												
Structure												
18-inch Mast & Camera Housing												
Azimuth Motor & Drive				25.0 Watt-Sec. per Oper.								
Elevation Drive				30.0 Watt-Sec. per Step.	4.1(3)						14.16	
Subtotals	0.75	10.05	0.75									
Telemetry												
Central Data Processor												
Data Pre-Processor #2							1.6					
Data Pre-Processor #1	0.8											
Subtotals	0.8						1.6				2.4	
Power												
Solar Cell Array												
Solar Cells, Glass Covers												
Glass												
Adhesive												
Substrate												
Battery (Silver Cad.)												
Regulation, Charge & Discharge Electronics							6.0					
Drive Motor												
Subtotals							6.0				6.0	
								Charge	Operate			
Command & Control												
Vehicle Central Decoder (VCD)								1.3	1.3			
Vehicle Sub-Decoder (VSD_1)	—	1.17										
Vehicle Sub-Decoder (VSD_2)								—	2.54			
SLRV Control Unit										0.9		
Subtotals	—	1.17						1.3	3.84		5.01	0.9
Other												
Instrumentation (Including Solar Azimuth Indicator, Thermistors, etc.)	2.0						1.0					
Subtotals	2.0						1.0				3.0	

Note (1) For use in bearing measurement - both receivers used.
(2) Zero during all modes except range and bearing.
(3) Does not include elevation and azimuth drives.

#2

TABLE II.7-4

POWER USAGES IN THE MAJOR MODES, INDIRECT LINK

Mode	Power (Watts) Reg.	Unreg.
Charge Mode		
Receiver - On	1.0	
Part VCD - On	1.3	
	2.3	
Regulated Converter @ 53% efficiency		2.2
Total Power	4.5	
Television Mode		
Television - On	14.1	
Telemetry - On	2.4	
VCD - On	1.3	
VSD - On	3.7	
Receiver - On	1.0	
Instruments	3.0	
Either: (a) Transmitter in Low-Power Mode	1.5	
or		
(b) Transmitter in High-Power Mode	8.0	
Subtotal		
(a) With Transmitter in Low-Power Mode	27.0	
(b) With Transmitter in High-Power Mode	33.5	
Regulator @ 75% efficiency		
(a) With Transmitter in Low-Power Mode		9.0
(b) With Transmitter in High-Power Mode		11.2
Total Power	(a) 36.0	
	(b) 44.7	

Mode	Power (Watts) Reg.	Unreg.
Operate Mode		
Television - Standby	1.5	
Transmitter - Low Power	1.5	
Telemetry - On	2.4	
VCD - On	1.3	
VSD - On	3.7	
Receiver - On	1.0	
Instruments (Solar azimuth, Clinometer, etc.)	3.0	
Regulator @ 75% efficiency		4.8
Total Power	19.2	

Powers Used in Conjunction with Operate Mode

Range

No increase in SLRV power dissipation during this activity.

Bearing

No increase in SLRV power dissipation during this activity.

Locomotion

16.5 Watts (unreg.)/wheel max. at intermittent stall, lasting for 30 sec. max.

19.5 watts (unreg.) total in locomotion.

Steer

7.5 watts (unreg.) max. at stall, lasting for 30 sec. max.

2.5 watts (unreg.) max. at nominal steering speed.

DIBSI

7.1 watts (unreg.) average lasting up to 220 sec.

Subsystem		Axle 1 Inside Thermal Compartment	Axle 2 Inside Thermal Compartment	Surveyor
Communications				
SLRV: VHF Transmitter			40.	
SLRV: 2-watt mode				
SLRV: 0.2-watt mode				
SLRV: VHF Receiver			12.	
SLRV: (100-200 Mc)				
SLRV: VHF Diplexer			24.	
SLRV: VHF Antenna and Feed	(a)			
SLRV: Input Selector			8.	
SLRV: DIBSI Multiplexer			8.	
Surveyor: VHF Transmitter				40.
Surveyor: 2-watt mode				
Surveyor: 0.2-watt mode				
Surveyor: VHF Dual Receiver				24.
Surveyor: VHF Triplexer				32.
Surveyor: VHF Antenna and Feed	(a)			
Surveyor: Range and Bearing				34.
Surveyor: Input Selector				12.
Subtotals			92.0	142.0
Television				
Basic Camera: Vidicon and Plug	(a)			
Basic Camera: Light and Target Ring	(a)			
Basic Camera: Preamplifier	(a)			
Basic Camera: Deflection Coil and Shield	(a)			
Basic Camera: Decoupling	(a)			
Basic Camera: Alignment Coils	(a)			
Basic Camera: Electronics		60.		
Sun Shutter	(a)			
Sun Sensor	(a)			
Optics: Lens (14.7 mm Angenieux)	(a)			
Structure: 18-inch Mast and Camera Housing	(a)			
Azimuth Motor and Drive		70.		
Elevation Drive		70.		
Subtotals		200.0		
Telemetry				
Central Data Processor			40.	
Data Pre-Processor #2				
Data Pre-Processor #1		20.		
Subtotals		20.	40.	
Power				
Solar-Cell Array: Solar Cells, Glass Covers	(a)			
Solar-Cell Array: Glass	(a)			
Solar-Cell Array: Adhesive	(a)			
Solar-Cell Array: Substrate	(a)			
Battery (Silver Cad.)			60.	
Charge, Discharge and Regulation Electronics			50.	
Drive Motor	(a)			
Subtotals			110.0	
Command & Control				
Vehicle Central Decoder (VCD)			26.	
Vehicle Sub-Decoder (VSD)		32.		
Vehicle Sub-Decoder (VSD_2)			64.	
SLRV Control Unit				32.0
Subtotals		32.0	90.0	32.0
Other				
Solar Azimuth Indicator		70.		
Control and Test Control		20.	20.	
Subtotals		90.0	20.0	
Totals		342.0	352.0	174.0

(a) Volumes not indicated for items outside thermal compartment.

TABLE II.7-5 TR64-26

VOLUME OF ELECTRONICS INSIDE THERMAL COMPARTMENTS AND SURVEYOR (VOLUMES IN CUBIC INCHES)

C. THERMAL CONSIDERATIONS

A preliminary transient analysis has now been completed on the electronic components of Thermal Compartments Nos. 1 and 2 of the SLRV. It has been calculated that if the components were on continuously, with no inactive periods for charging of the batteries, the operating temperature of the electronics would strongly depend upon the average power dissipated during the guidance steps. Because of the thermal mass of the components in each unit, transient conditions during the contour and DIPSI modes are slight. The maximum change of temperatures during these latter two modes was found to be only ±5°C from the guidance step average.

In view of the above, the first step in obtaining a transient analysis is to calculate the average equilibrium temperatures during the guidance step as functions of the position on the lunar surface. For these calculations, several assumptions had to be made. It was first assumed that the vehicle always faced towards the sun (this gives a maximum heat condition.) It was further assumed that the thermal switches respond in such a manner as to prevent the component from dropping below -10°C during the daylight period.

Using the above assumptions, the power profile as described elsewhere in this report, and the data of Tables II.7-3 and II.7-4, it is possible to obtain the equilibrium temperature of the components in Compartments Nos. 1 and 2 during the guidance step (Figure II.7-1. In Compartment 2, six thermal switches are used. However, it has been found that as the average power dissipation of Compartment 1 is much less than that of Compartment 2, only one thermal switch is needed on Compartment 1 if the radiator area is kept approximately equal to 200 inch^2. This situation has been assumed to derive the temperature curves for compartment 1.

Next, the equilibrium temperature during the inactive charging mode is needed. If the internal dissipation of the batteries during charging is 3.5 watts, then the two dotted curves of Figure II.7-1 represent this equilibrium temperature (making the assumptions noted above).

The temperatures are now bracketed between the appropriate two curves for Compartment Nos. 1 and 2 of Figure II.7-1. However, the actual temperature at any time is dependent upon the duty cycle of the units. Therefore, a transient analysis was performed for the following duty cycle: 3.3 hours on 4.7 hours off for charging of batteries; 3.3 hours on, 13.7 hours off for charging of batteries. The results of this analysis show that because of the thermal mass of the components and Compartment 2, at no position on the moon's surface will the temperature reach the maximum equilibrium temperature. Because of the longer charge cycle experienced during inactive modes, the inactive equilibrium temperature will be reached. Because of its smaller mass, equilibrium is reached in both modes for Compartment 1. The results for both Compartments 1 and 2 are presented in Figure II.7-2 with angular position from the sub-solar point as a parameter.

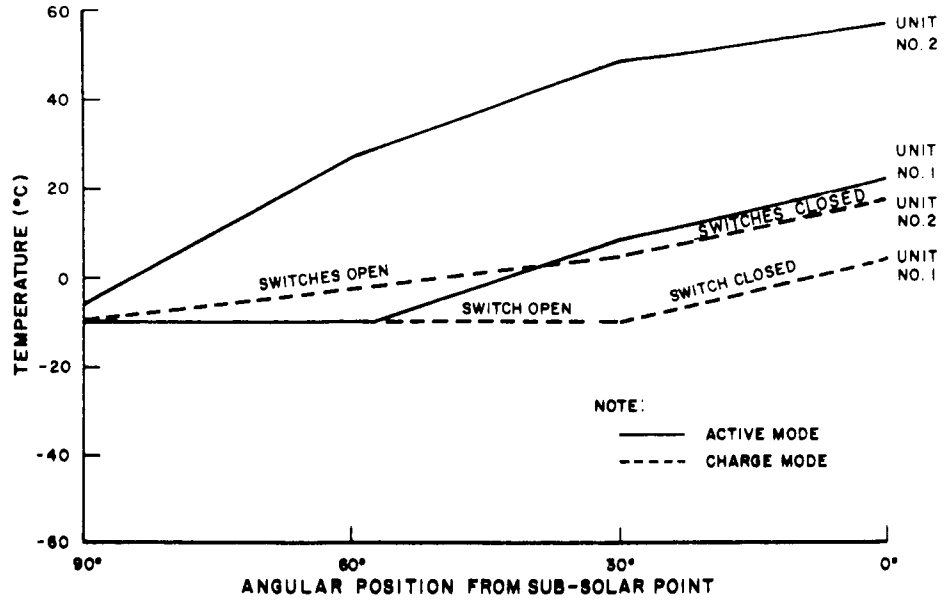

Figure II.7-1. Equilibrium Temperatures for Active and Inactive (Charged Modes)

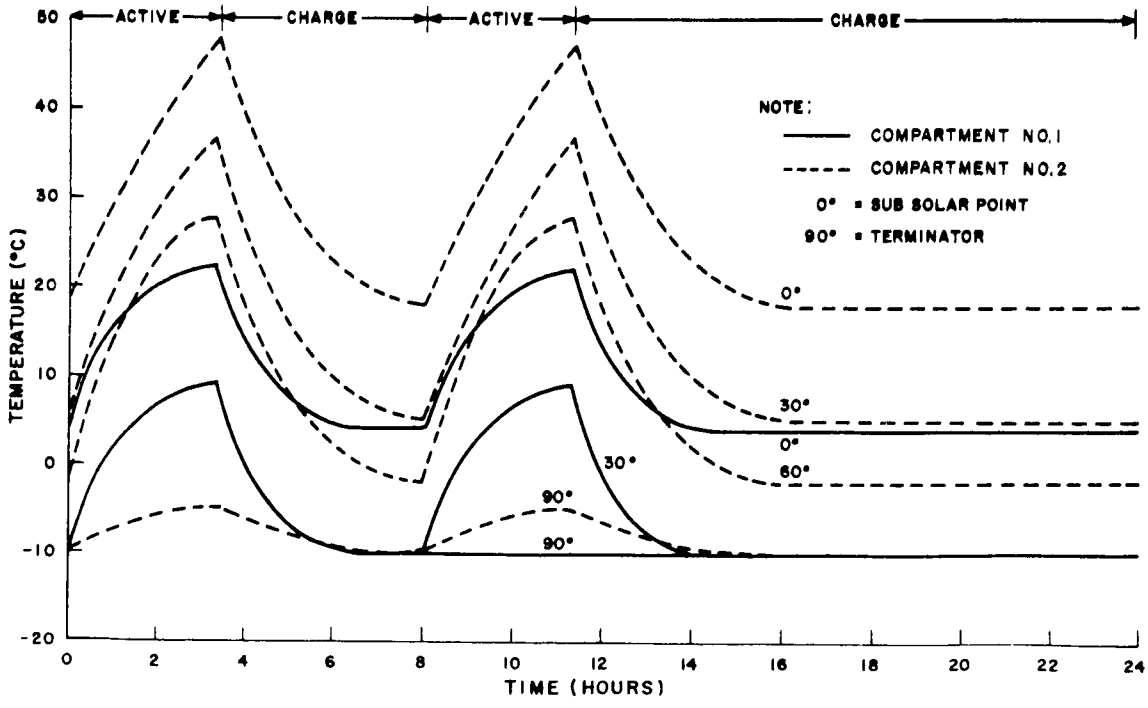

Figure II.7-2. Transient Response of Internal Components of Unit No. 1 and Unit No. 2

The results of the transient analysis as represented by the Figures indicate that, for the duty cycle proposed, no adverse temperatures will result at any position on the surface of the moon during the sunlit period. If the duty cycle is different from that used above, the temperature of Compartment 2 still can be determined approximately from the data presented. A good rule of thumb is to calculate the maximum by the relation that if the active period is less than 4 hours, $\Delta T_{max}/\Delta Time = 10°C/hr.$, and

$$T_{max} = T_{min} + \frac{\Delta T_{max}}{\Delta Time} \times t$$

where T_{min} = equilibrium temperature of the charge mode and t = duration of the active mode.

If the active cycles are greater than 4 hours, then T_{max} is approximately the equilibrium temperature of the active mode and T_{min} is the equilibrium temperature of charging mode. T_{min} will only occur during the 12-hour period when the SLRV is out of contact with Goldstone. In any condition, the range of temperatures during the lunar day for the SLRV electronics is from -10°C to +57°C.

D. ENVIRONMENTAL CONSIDERATIONS

In general, it has been assumed throughout the study that factors which have an environmental context would be considered on the basis of data derived for Surveyo This meant that until better data were available, vibration input levels were to be assumed at eight times the forcing levels at the Centaur attachment points, to allow for the unknown magnification factors involved.

Some reservation must be made before adopting the above philosophy. That is, it is difficult to accept a thesis which neither allows for attenuation at higher frequencies nor recognizes that the magnification factor will itself be a variable. A factor of 8 normally applies to a point of resonance and lies in the frequency band 20 to 100 cps. In normal circumstances, slight overdesign can be tolerated. In the case of the SLR care must be taken to ensure that no weight penalty is incurred. Before a testing pr gram is implemented this should be resolved.

E. THE ENGINEERING CONCEPT

The 'airplane' design concept of making a structure and building separate 'black boxes' that fit inside it is quite inexcusable in principle and unacceptable in practice. From the outset, recognition has been given to the concept that subsystems have individual identities only insofar as required to logically assist test and replacement. The electronics assembly in each of the thermal compartments will be designed as an integrated package, minimizing over-all weight and volume.